Geochemical Signatures of Native Gold Alloys as a Tool for Understanding Auriferous Ore Deposits

Carl Peter Spence-Jones

Submitted in accordance with the requirements for the degree of
Doctorate in Philosophy

The University of Leeds
Institute of Applied Geosciences
School of Earth and Environment

October, 2021

The candidate confirms that the work submitted is his own and that appropriate credit has been given where reference has been made to the work of others.

This copy has been supplied on the understanding that it is copyright material and that no quotation from the thesis may be published without proper acknowledgement.

The right of Carl Peter Spence-Jones to be identified as Author of this work has been asserted by him in accordance with the Copyright, Designs and Patents Act 1988.

Acknowledgements

I would like to thank my supervisors Dr Robert Chapman, Dr David Banks and Dr Graham McLeod for their individual support and insights into my research. In particular I want to thank Rob for his invaluable supervisions and infectious passion for gold studies, including getting properly hands on, very wet and gloriously muddy when panning. Without Rob sharing so much hard-won panning experience a lot less gold would have been collected. I would also like to acknowledge my excellent supervisory team for allowing me, occasionally rather stubbornly, to find my own direction for the project. Additionally, I would like to express gratitude to the faculty in the department, many of whom have offered advice and support. There are many people who have contributed professional expertise and in particular I would like to thank Dr Richard Walshaw, John 'Harry' Wyn Williams and Gary Keech for assisting with sample preparation, analysis and creating a friendly atmosphere in the department.

The project was funded by the University of Leeds, and I would like to extend my gratitude to the Faculty of Environment for giving me the opportunity to undertake my part time PhD alongside a teaching position in the School of Earth and Environment. Further funding was provided though a Graduate Student Fellowship grant from the Society of Economic Geologists, who are an exemplary, altruistic professional society and have made so much of this project possible. I would like to express my gratitude for the support I have had from the gold mining industry. In particular I wish to thank, Scotgold PLC and Dalradian Gold, the operators of the two UK mines studied. The Atlin part of the project owes much to Jeff Kyba, Fionnuala Devine, Mitch Mihalynuk, Alex Zagorevski, and the Atlin placer miners, including Peter Shorts, whose geological knowledge, humbly shared alongside incredible hospitality, made the fieldwork and Atlin study possible.

I would like to thank my friends, especially to Matt, Tom, Hugh and Georgian in the Ores group. Thank you to many people in the University of Leeds Speleological Association (ULSA) for all the weekend caving fun over the years and to Emma for keeping me on track during the challenges of the pandemic in the final year.

I would like to thank my family, especially my mother Dr Maureen Birch for her unwavering support throughout my academic career and

struggles with dyslexia. A special thank you goes to my sister, Dr Helen Spence-Jones, for kindly drawing the chapter illustrations during her own PhD writeup period. Finally, I would have never believed a PhD was possible without the encouragement and the dedicated efforts of Jana Kodicek. I still cherish the results of her patience, persistence and tutoring and my gratitude to her cannot be adequately expressed.

Abstract

Studies of native gold sampled from drainages are an important exploration tool and an increasing number of studies have evaluated the characteristics of detrital gold to understand gold camps and the deposits within them. This thesis focuses on the compositional analysis of the native gold sampled from drainages. By sampling the detrital gold eroded out from a gold deposit, the gold particles can be compared to in situ gold particles, thereby allowing correlation with knowledge gained from traditional mineralogy and an assessment of the gold on a deposit (macro) scale. This provides a novel assessment of how variable a deposits' mineralisation might be which can provide useful context to micro scale observations.

To develop, investigate and test correlative uses of detrital gold samples with traditional mineralogy, three different studies were conducted at the Cononish Mine (Scotland), Curraghinalt Mine (Northern Ireland) and the Atlin Gold Camp (British Columbia).

This work demonstrates that populations of gold particles sampled directly from mines differ from detrital populations obtained from drainages. Detrital populations are considered more representative of the mineralisation within a deposit, as they are the residual lags resultant from the erosion of a huge volume of material. Correlation between gold particles in ore and in detrital population provides a context to the compositions in ore on a deposit/ system scale. By identifying the importance of specific gold compositions within the deposit observations of the ore assemblages associated with gold events can be examined in a deposit scale context which would otherwise not be possible. This allows temporal and spatial differences between ore samples to be evaluated for significance. This provides a contextual framework for observed changes in the ore assemblages, and therefore mineralising fluids. This work presents a method for relating micro to macro scale characterisations of a gold mineralisation using gold compositions. It demonstrates that detrital gold studies can improve the understanding of gold mineralisation and, critically, can provide a context for the gold mineralisation across multiple scales within a deposit, which through traditional mineralogy alone is difficult to achieve.

Table of Contents

List of Tables

List of Figures

The imagination of nature is far, far greater than the imagination of man

– Richard Feynman

Chapter 1 Introduction

Native gold has been a part of humanity and its cultures for over 5000 years. Gold is found both as a native metal and as metallic minerals in a wide variety of tectonic settings and ore deposits (Boyle, 1987). Native gold has been sought after due to its scarcity alongside desirable properties such as its chemical inertness, malleability, reflectance and more recently electrical conductivity. This made it an ideal currency, a use that still persists in modern commerce, alongside its uses in aesthetic jewellery and in industry.

Native gold is an alloy containing variable proportions of gold and silver, other metals may also be present, which are completely miscible (Palyanova, 2020). The proportions of gold (or silver) in alloy is commonly referred to as fineness, calculated using the proportions of gold and silver: $Fineness = (Au \times 1000)/(Au + Ag)$ (Morrison et al., 1991). A complete solid solution is observed in natural gold alloys from pure gold particles (native gold) to pure silver particles (native silver) (Fisher, 1945, Morrison et al., 1991, Gammons and Williams-Jones, 1995). In geological studies the term electrum is often used for Au/Ag ratios between 0.2-0.8 (Gammons and Williams-Jones, 1995, Chapman et al., 2021). However, in this work the term 'gold alloy' is used instead and is defined here as a gold particle containing between 0 to 80 %wt. Ag. The use of 'gold alloy' follows the rationale of Chapman et al. (2021) who advocate that this is a preferable term to use for gold as it avoids confusion when populations contain both native gold and electrum by removing the arbitrary division between the two minerals.

The controls on the composition of gold alloys in geological systems was first described by Gammons and Williams-Jones (1995) who presented models relating gold composition to physiochemical parameters of idealised hydrothermal ore fluids, thereby providing the foundation for current transport models (Hannington et al., 2016, Goldfarb and Groves, 2015, Garofalo and Ridley, 2014, Pokrovski et al., 2014). The modelled parameters critical to gold composition are the temperature and pressure, along with a number of important chemical properties of the fluids (Gammons and Williams-Jones, 1995). The chemical parameters are the pH and oxidation/redox potential of the fluid along with the activity of ligands that act as solvents for gold and silver in hydrothermal fluids (Gammons and Williams-Jones, 1995, Pokrovski et al., 2014, Pokrovski et al., 2009). The principal solvents responsible for the solvation of gold and silver observed in geological fluids are widely accepted to be sulphur and chlorine complexes (Gammons and Williams-Jones, 1995, Pokrovski et al., 2014, Pokrovski et al., 2009) although recently transport as

gold colloids has been shown to occur in several hydrothermal systems (Hannington et al., 2016, Petrella et al., 2020).

In recent years the number of studies that describe gold alloys in natural occurrences has been increasing, including a growing discussion on the use of detrital gold as an indicator mineral (Pochon et al., 2021, Chapman et al., 2021). Detrital gold has been used as an indicator of hard rock mineralisation since the early history of mining with gold panning used to track gold back towards its source(s). More recently, the ability of analytical techniques to determine mineral chemistries has led to the development of indicator mineral techniques to distinguish between mineralised/fertile and un-mineralised magmatic systems for both diamond bearing kimberlites and porphyry systems (Bouzari et al., 2011, McClenaghan, 2011).

The potential to develop detrital gold exploration tools using mineral chemistry is an attractive prospect as the composition of gold alloys relates directly to the physiochemical conditions it was deposited in. Morrison et al. (1991) documented both finesses of gold particles and smelted doré bars, semi-pure bars of gold and silver, from different deposit types by investigating differences between the deposits. Subsequent studies by Chapman et al. (2021) and Liu and Beaudoin (2021) examined 39,832 and 710 gold particles respectively, taken from 526 and 51 localities and reported some promising results although they document significant problems in using the simple metric of average alloy composition.

The problem with using gold alloy compositions is that, while differences in gold composition are reported between different deposits, the observed gold alloy populations are not mutually exclusive between gold formed in different deposit styles. Using data published by Chapman et al. (2021), the differences as well as overlaps can be seen between different deposits and different deposit types, Figure 1.1.

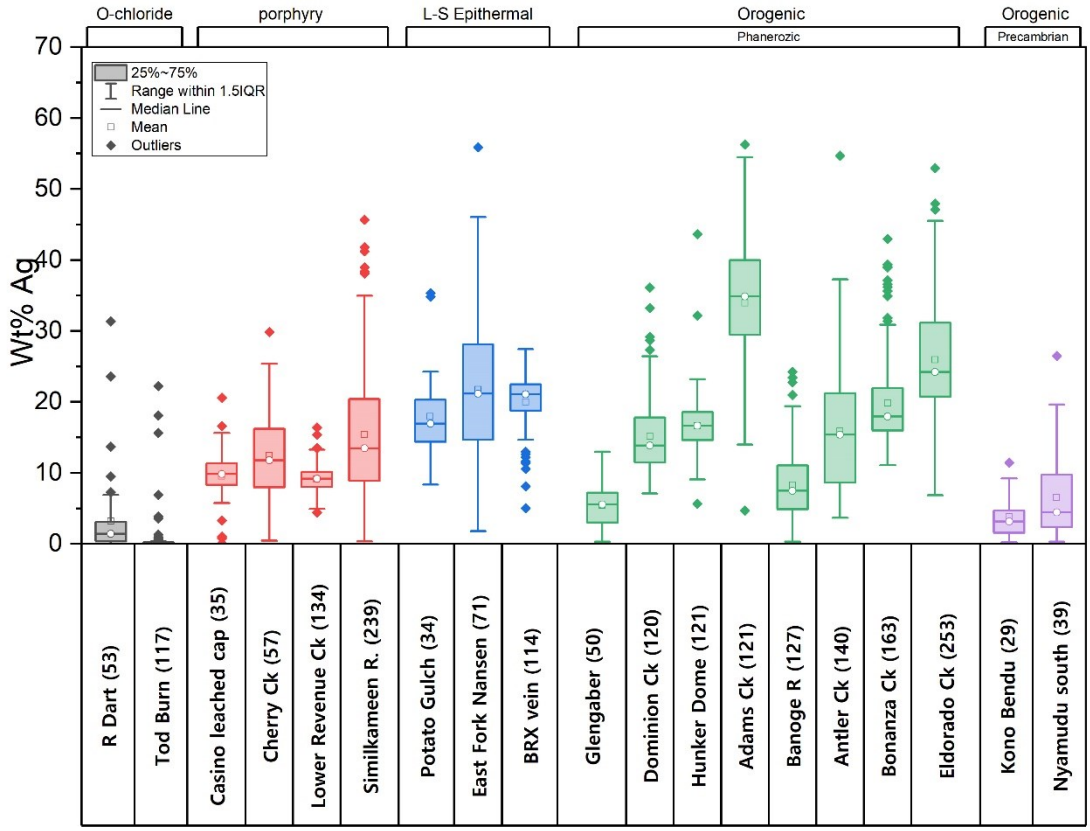

Figure 1.1 – Box plot of silver component of the detrital gold particles sampled from 5 different deposit types. Plot shows the samples, those available with all particle's compositions, taken from the digital supplementary material of Chapman et al. (2021).

Despite overlaps in the alloy compositions between deposit types, when data is compiled from many deposits into a single 'signature' some interesting observations and trends are observable in the data of Chapman et al. (2021), Figure 1.2. The most distinctive signature is observed in the gold from low temperature oxidising chloride auriferous systems (OCAS) which have significant palladium (± mercury) alongside low (<10 wt%) silver particle populations combined with selenium-, tellurium-, and platinum group-bearing associated mineral inclusions (Olivo et al., 1995, Chapman et al., 2021).

In addition to the distinctiveness of OCAS, Precambrian (Archean) gold deposits are generally noted to have lower silver compositions than younger orogenic systems, which have a large range of gold alloy compositions observed and make up the majority of samples (Chapman et al., 2021, Morrison et al., 1991, Utter, 1979, Oberthur et al., 1997). A similar trend of higher (and larger ranges of) silver enrichment is generally seen in epithermal systems compared to porphyry systems when broadly comparing deposits.

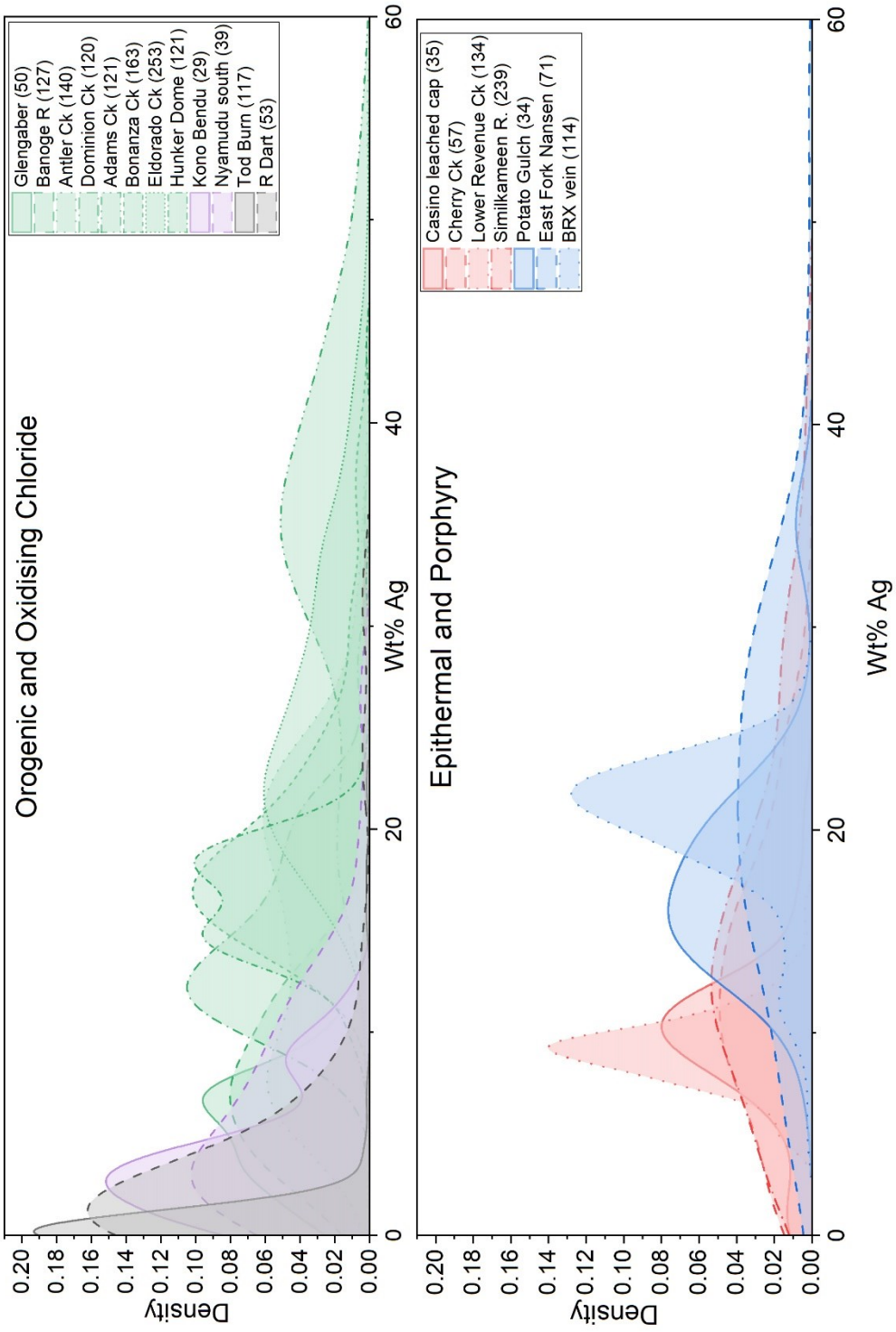

Figure 1.2 – Distribution plots of Ag concentrations of samples (shown in figure 1.1) from Chapman et al. (2021). coloured by type; green are phanerozoic orogenic deposits, purple are precambrian orogenic deposits, grey are oxidizing chloride deposits, red are porphyry deposits and blue are Epithermal deposits.

The differences between the complied data grouped by deposit types are considered to represent the differences in the physicochemical conditions characteristic of the different deposit types. For example, porphyry systems generally have higher temperatures and pressure than epithermal systems (Heinrich, 2005) which is reflected in the gold alloys. Due to the multitude of variables which influence ore genesis and the wide spectrum of deposits, the general trends between deposit types do not hold when comparing individual systems with significant overlap present. Therefore, Chapman et al. (2021) states that the average gold fineness is a poor indicator of deposit type and ore genesis, due to the significant overlaps observed.

To overcome the difficulties in defining deposits many workers have 'proposed incorporating further variables in addition to the silver content of the gold alloy. In the literature the two most common approaches are the use of mineral inclusion suites and additional trace element geochemistry (Chapman et al., 2021).

Inclusion suites, which are assemblages of minerals which were enclosed within the gold particle as it formed, are observed within sectioned gold grains (Chapman et al., 2018, Chapman et al., 2017, Chapman et al., 2009). These suites are then used in combination with alloy compositions in order to differentiate between gold from different sources. Because different deposit styles have distinctly different ore and gangue mineral assemblages that accompany the gold, through inclusion suites it is possible to differentiate between two different systems that may have similar alloy composition. However, there are a number of problems which hinder development of a generic classification of deposits due to the amount of data needed to develop robust signatures (Chapman et al., 2021). A large number of gold particles are required to develop a suite because a range of different minerals are observed along with the fact that inclusions are only observed in a small proportion of sectioned gold particles (Chapman et al., 2021, Chapman et al., 2010). Because of sample size problems the interpretations of inclusion suites are commonly based on the observation of a few rare minerals within a large sample of gold particles which may or may not be sourced from a single source, although recent approaches to sample collection have endeavoured to collect sufficient gold particles to provide robust data sets.

Additional mineralogical information is typically obtained through methods such as Laser Ablation Inductively Coupled Plasma Mass Spectrometry (LA-ICP-MS) which can measure trace element concentrations in gold to a few parts

per million (ppm) with higher sample throughput than other methods (Banks et al., 2018, Pochon et al., 2021, Liu and Beaudoin, 2021, Liu et al., 2021). Results from a LA quadrupole and a time-of-flight mass spectrometer LA system (which measures all selected elements simultaneously) have shown that only a small number of elements are homogenously distributed in Au alloy (Banks et al., 2018). In addition to Ag, elements observed in minor amounts and considered to be in solid solution are Cu, S and Hg in proportions that vary with the conditions of formation (Banks et al., 2018, Ozoliņš et al., 1998b, Boyle, 1979, Ozoliņš et al., 1998a, Terakura et al., 1987). Additional elements (Si, Al, S, Ti, V, Cr, Mn, Fe, Co, Ni, Cu, Zn, Ga, Ge, As, Se, Y, Nb, Mo, Rh, Pd, Ag, Cd, In, Ir, Sn, Sb, Te, La, W, Pt, Au, Hg, Pb, Bi, Th and U) are observed in trace amounts., figure 1.3, and are present either as local/heterogeneous concentrations likely to represent inclusions of minerals, often too small to observe by conventional methods (Liu and Beaudoin, 2021, Liu et al., 2021, Banks et al., 2018, Gas'kov, 2017).

On the basis of current understanding the use of additional elements concentrations in the gold alloy for fingerprinting is restricted to a small number which are observed to be homogeneously distributed within gold alloys (Au, Ag, Cu, Hg and Sb) (Banks et al., 2018). This is because most chalcophile (Ag, Cu, Zn, Bi, Sb, Pb, As, and Sn), siderophile (Pd, Fe, Co, Ni, and Mo) and lithophile (Mg, Al, Ca, and Si) elements are present as inclusions of gangue minerals, they present complex or limited uses as discriminants for fingerprinting the alloy.

Although the potential of alloy trace element fingerprinting is constrained to four minor elements, LA-ICP-MS analysis does provide potential data on very small heterogeneous concentrations or mineral inclusions within the alloy which can be combined with inclusion suite analysis if a time-of-flight (TOF) mass spectrometer system is used (Banks et al., 2018). The need for a TOF system is because the transient chemical signature produced by a small or micro inclusion mineral is too short a time to allow a conventional quadrupole mass spectrometer to cycle through the required number of elemental masses required (Banks et al., 2018)

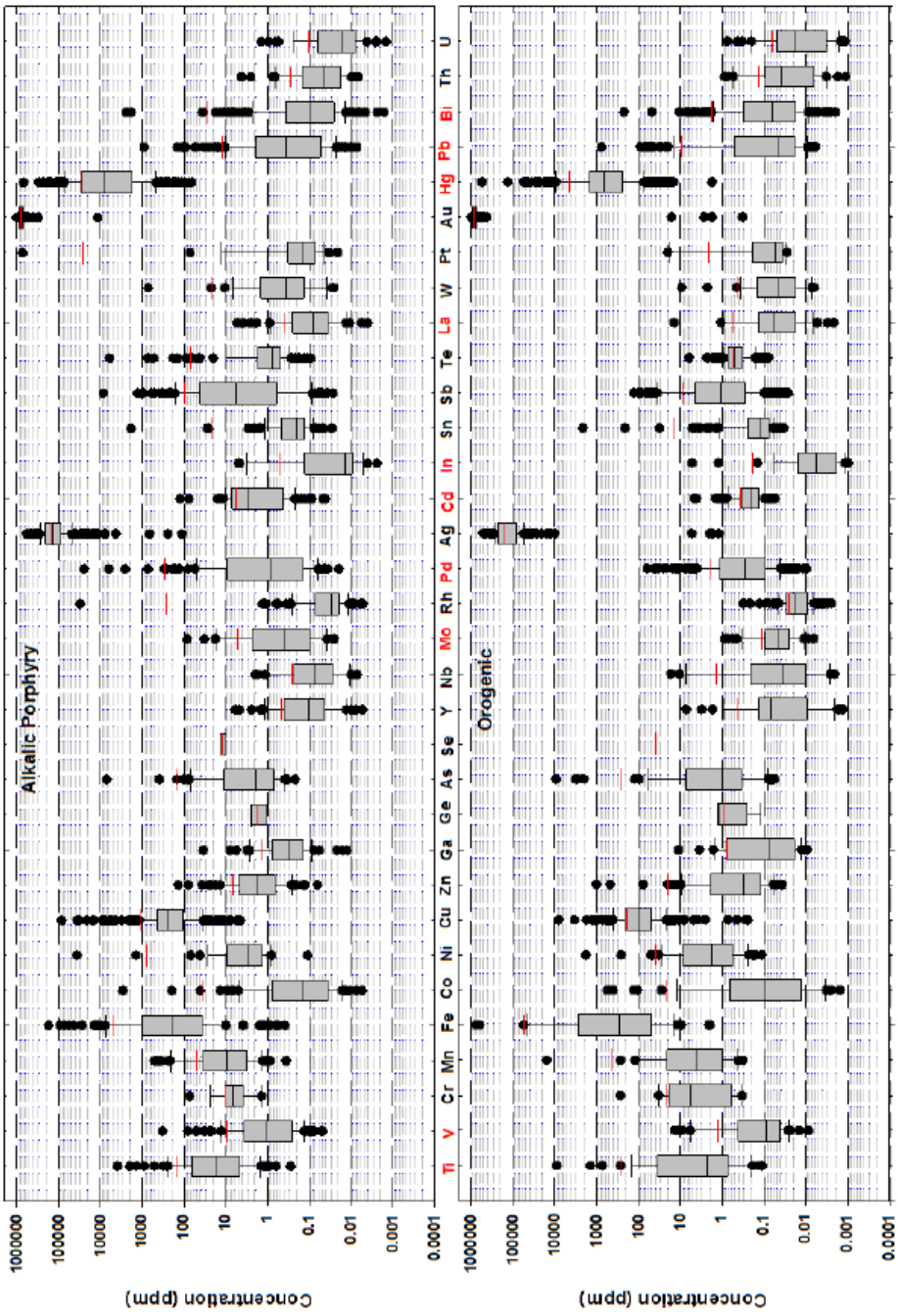

Figure 1.3 – Box (25th and 75th percentile) and whisker (5th and 95th percentile) plots showing ranges of concentrations observed in gold particles from LA-ICP-MS analysis of over 800 gold particles taken from Banks et al. (2018). Horizontal black line is the median value and the red line the mean value.

Studies of gold particles in detrital (placer) samples reveal that populations of natural gold are complex, containing variable proportions of gold alloys that have of different compositions. Knight et al. (1999) reported comparable distributions in lode and detrital samples in the Klondike mining district. However, limited studies have explored the specifics of the variation in gold compositions, especially in relation to lode systems. Recently the number of studies that apply models of Au/Ag in hydrothermal fluids first championed by Gammons and Williams-Jones (1995) to detrital gold studies has been increasing. For example, recent studies interpreting spatial differences in detrital gold particles in the context of the thermodynamic models of Gammons and Williams-Jones (1995) have been published by (Chapman et al. (2010), Omang et al. (2015) and Dongmo et al. (2019). These studies compare detrital populations however they rarely link specific veins/deposit or paragenetic stages to the detrital analysis and were limited by the number of (or access to) potential lode sources.

The most detailed knowledge of gold compositions in relation to the physiochemical controls on ore formation result from mineralogical studies on lode systems and experimental work undertaken in attempts to replicate natural systems using a range of different autoclave apparatus (Gammons and Williams-Jones, 1995, Hannington et al., 2016, Pokrovski et al., 2014). Auriferous ore systems are well documented to change temporally, with mineral assemblages typically interpreted into stages which are presented as paragenetic sequences to reflect the general temporal changes in the mineralisation. Where a gold composition is reported alongside the paragenetic mineral assemblages, it is observed that the later stages show increased Ag concentrations in relation to early stages (Spence-Jones, 2013, Large and Maslennikov, 2020, Wilkinson et al., 1999).

Despite abundant knowledge on the mineralogy of ore deposits and the properties of gold in the detrital environment, studies bridging the gap by examining both detrital populations and the nature of gold particles in a detailed paragenesis are conspicuously absent. This thesis examines this gap in the literature through studies which aim to relate compositional characteristics of detrital gold populations with traditional mineralogical studies of deposits. The project examines 3 localities which each provide a different level of knowledge of the in-situ gold mineralisation alongside large samples of detrital gold.

The reason for examining the different localities was to demonstrate how combined detrital lode gold studies could benefit commercial deposits at

different stages of the mining life cycle. The Cononish deposit, Scotland, presented in chapters 3 and 4, represents a developed in production mine where exposure of significant mineralisation along with ore processing is available. The Curraghinalt deposit in Northern Ireland, Chapter 5, represents an exploration target which has limited drill samples of the mineralisation with more extensive knowledge of the in-situ mineralisation still in development. The Atlin District in British Columbia, Chapter 6, was chosen to represent an exploration district, where no economic lode deposits have been identified but abundant detrital gold is present.

References

BANKS, D. A., CHAPMAN, R. & SPENCE-JONES, C. 2018. Detrital gold as a deposit-specific indicator mineral by LAICP-MS analysis. *Geoscience BC Report (project 2016-006).*

BOUZARI, F., HART, C., BARKER, S. & BISSIG, T. 2011. Porphyry indicator minerals (PIMS): A new exploration tool for concealed deposits in south-central British Columbia. *Geoscience BC Report,* 17**,** 1-31.

BOYLE, R. W. 1979. The geochemistry of gold and its deposits (together with a chapter on geochemical prospecting for the element). *Geological Survey of Canada, Bulletin,* 280.

BOYLE, R. W. 1987.Gold History and Genesis of Deposits, 1st edition. Springer US, New York.

CHAPMAN, R., BANKS, D. A. & SPENCE-JONES, C. 2017. Detrital gold as a deposit-specific indicator mineral, British Columbia: analysis by laser-ablation inductively coupled plasma–mass spectrometry. *Geoscience BC Summary of Activities 2016.* Geoscience BC.

CHAPMAN, R. J., ALLAN, M. M., MORTENSEN, J. K., WRIGHTON, T. M. & GRIMSHAW, M. R. 2018. A new indicator mineral methodology based on a generic Bi-Pb-Te-S mineral inclusion signature in detrital gold from porphyry and low/intermediate sulfidation epithermal environments in Yukon Territory, Canada. *Mineralium Deposita,* 53**,** 815-834.

CHAPMAN, R. J., BANKS, D. A., STYLES, M. T., WALSHAW, R. D., PIAZOLO, S., MORGAN, D. J., GRIMSHAW, M. R., SPENCE-JONES, C. P., MATTHEWS, T. J. & BOROVINSKAYA, O. 2021. Chemical and physical heterogeneity within native gold: implications for the design of gold particle studies. *Mineralium Deposita*.

CHAPMAN, R. J., LEAKE, R. C., BOND, D. P. G., STEDRA, V. & FAIRGRIEVE, B. 2009. Chemical and Mineralogical Signatures of Gold Formed in Oxidizing Chloride Hydrothermal Systems and their Significance within Populations of Placer Gold Grains Collected during Reconnaissance. *Economic Geology,* 104**,** 563-585.

CHAPMAN, R. J., MORTENSEN, J. K., CRAWFORD, E. C. & LEBARGE, W. 2010. Microchemical Studies of Placer and Lode Gold in the Klondike District, Yukon, Canada: 1. Evidence for a Small, Gold-Rich, Orogenic Hydrothermal System in the Bonanza and Eldorado Creek Area. *Economic Geology,* 105**,** 1369-1392.

DOMGMO, F. W. CHAPMAN, R. J. BOLARINWA, A. T. YONGUE, R. F. BANKS, D. A. OLAJIDE-KAYODE, J. O. Microchemical characterization of placer gold grains from the Meyos-Essabikoula area, Ntem complex, southern Cameroon. Journal of African Earth Sciences. 2019 Mar 1;151:189-201.

FISHER, N. H. 1945. The fineness of gold, with special reference to the Morobe gold field, New Guinea. *Economic Geology,* 40**,** 449-495.

GAMMONS, C. H. & WILLIAMS-JONES, A. E. 1995. Hydrothermal Geochemistry of Electrum - Thermodynamic Constraints. *Economic Geology and the Bulletin of the Society of Economic Geologists,* 90**,** 420-432.

GAROFALO, P. S. & RIDLEY, J. R. 2014. Gold-transporting hydrothermal fluids in the Earth's crust: an introduction. *Geological Society, London, Special Publications,* 402**,** 1-7.

GAS'KOV, I. V. 2017. Major impurity elements in native gold and their association with gold mineralization settings in deposits of Asian folded areas. *Russian Geology and Geophysics,* 58**,** 1080-1092.

GOLDFARB, R. J. & GROVES, D. I. 2015. Orogenic gold: Common or evolving fluid and metal sources through time. *Lithos,* 233**,** 2-26.

HANNINGTON, M., HARÐARDÓTTIR, V., GARBE-SCHÖNBERG, D. & BROWN, K. L. 2016. Gold enrichment in active geothermal systems by accumulating colloidal suspensions. *Nature Geoscience,* 9**,** 299-302.

HEINRICH, C. 2005. The physical and chemical evolution of low-salinity magmatic fluids at the porphyry to epithermal transition: a thermodynamic study. *Mineralium Deposita,* 39**,** 864-889.

KNIGHT, J. B., MORTENSEN, J. K. & MORISON, S. R. 1999. Lode and placer gold composition in the Klondike district, Yukon Territory Canada: Implications for the nature and genesis of Klondike placer and lode gold deposits. *Economic Geology and the Bulletin of the Society of Economic Geologists,* 94**,** 649-664.

LARGE, R. & MASLENNIKOV, V. 2020. Invisible Gold Paragenesis and Geochemistry in Pyrite from Orogenic and Sediment-Hosted Gold Deposits. *Minerals,* 10**,** 339.

LEAKE, R. C., CHAPMAN, R. J., BLAND, D. J., STONE, P., CAMERON, D. G. & STYLES, M. T. 1998. The origin of alluvial gold in the Leadhills area of Scotland: evidence from interpretation of internal chemical characteristics. *Journal of Geochemical Exploration,* 63**,** 7-36.

LIU, H. & BEAUDOIN, G. 2021. Geochemical signatures in native gold derived from Au-bearing ore deposits. *Ore Geology Reviews,* 132**,** 104066.

LIU, H., BEAUDOIN, G., MAKVANDI, S., JACKSON, S. E. & HUANG, X. 2021. Multivariate statistical analysis of trace element compositions of native gold from orogenic gold deposits: Implication for mineral exploration. *Ore Geology Reviews,* 131**,** 104061.

MCCLENAGHAN, M. B. 2011. Overview of common processing methods for recovery of indicator minerals from sediment and bedrock in mineral exploration. *Geochemistry-Exploration Environment Analysis,* 11**,** 265-278.

MORRISON, G. W., ROSE, W. J. & JAIRETH, S. 1991. Geological and geochemical controls on the silver content (fineness) of gold in gold-silver deposits. *Ore Geology Reviews,* 6**,** 333-364.

OBERTHUR, T., WEISER, T., AMANOR, J. A. & CHRYSSOULIS, S. L. 1997. Mineralogical siting and distribution of gold in quartz veins and sulfide ores of the Ashanti mine and other deposits in the Ashanti belt of Ghana: Genetic implications. *Mineralium Deposita,* 32**,** 2-15.

OLIVO, G. R., GAUTHIER, M., BARDOUX, M., LEAO DE SA, E., FONSECA, J. T. F. & SANTANA, F. C. 1995. Palladium-bearing gold deposit hosted by Proterozoic lake superior-type iron-formation at the Caue iron mine, Itabira District, southern Sao Francisco Craton, Brazil; geologic and structural controls. *Economic Geology,* 90**,** 118-134.

OMANG, B. O., SUH, C. E., LEHMANN, B., VISHITI, A., CHOMBONG, N. N., FON, A. N., EGBE, J. A. & SHEMANG, E. M. 2015. Microchemical signature of alluvial gold from two contrasting terrains in Cameroon. *Journal of African Earth Sciences,* 112**,** 1-14.

OZOLIŅŠ, V., WOLVERTON, C. & ZUNGER, A. 1998a. Cu-Au, Ag-Au, Cu-Ag, and Ni-Au intermetallics: First-principles study of temperature-composition phase diagrams and structures. *Physical Review B,* 57**,** 6427-6443.

OZOLIŅŠ, V., WOLVERTON, C. & ZUNGER, A. 1998b. First-principles theory of vibrational effects on the phase stability of Cu-Au compounds and alloys. *Physical Review B,* 58**,** R5897-R5900.

PALYANOVA, G. A. 2020. Gold and Silver Minerals in Sulfide Ore. *Geology of Ore Deposits,* 62**,** 383-406.

PETRELLA, L., THÉBAUD, N., FOUGEROUSE, D., EVANS, K., QUADIR, Z. & LAFLAMME, C. 2020. Colloidal gold transport: a key to high-grade gold mineralization? *Mineralium Deposita,* 55**,** 1247-1254.

POCHON, A., DESAULTY, A.-M., BAILLY, L. & LACH, P. 2021. Challenging the traceability of natural gold by combining geochemical methods: French Guiana example. *Applied Geochemistry,* 129**,** 104952.

POKROVSKI, G. S., AKINFIEV, N. N., BORISOVA, A. Y., ZOTOV, A. V. & KOUZMANOV, K. 2014. Gold speciation and transport in geological fluids: insights from experiments and physical-chemical modelling. *Geological Society, London, Special Publications,* 402.

POKROVSKI, G. S., TAGIROV, B. R., SCHOTT, J., BAZARKINA, E. F., HAZERMANN, J. L. & PROUX, O. 2009. An in situ X-ray absorption spectroscopy study of gold-chloride complexing in hydrothermal fluids. *Chemical Geology,* 259**,** 17-29.

SPENCE-JONES, C. 2013. *Metallurgical Investigation of the Ore at the Cononish Gold Mine, Scotland.* MGeol Masters, Univeristy of Leicester.

TERAKURA, K., OGUCHI, T., MOHRI, T. & WATANABE, K. 1987. Electronic theory of the alloy phase stability of Cu-Ag, Cu-Au, and Ag-Au systems. *Physical Review B,* 35**,** 2169-2173.

UTTER, T. 1979. The morphology and silver content of gold from the Upper Witwatersrand and Ventersdorp Systems of the Klerksdorp gold field, South Africa. *Economic Geology,* 74**,** 27-44.

WILKINSON, J., BOYCE, A., EARLS, G. & FALLICK, A. 1999. Gold remobilization by low-temperature brines; evidence from the Curraghinalt gold deposit, Northern Ireland. *Economic Geology,* 94**,** 289-296.

Chapter 2 Literature review and discussion of compositional data in the study of detrital gold particles and populations.

Summary

This chapter reviews and discusses statistical approaches to the study of populations of detrital gold particles, especially the interpretation of compositional data. The chapter first reviews the genesis of detrital gold deposits (pre-sampling factors), before discussing sampling protocols and the limitations related to field collection. Finally, a review and discussion of analytical approaches for the characterization of gold populations is presented with suggested new approaches presented to improve studies.

Very limited literature exists which includes in-depth discussions of the statistical methods used in detrital gold studies (Pochon et al., 2021). Because of the focus of much the literature on applied geological and observational studies this chapter seeks to draw upon specialist statistical literature. The pure statistical literature is combined with geological knowledge with the aim of presenting insights that could improve the interpretations in detrital gold studies, specifically the quantification of unknowns, caveats and limitations of the studies.

2.1 Introduction

The physical transport of gold particles away from in situ ore by surficial processes means that detrital populations, defined as the set of gold particles from a specific sampling location, are allochthonous. The modern position of the sample is known, however the original source location (or locations) of the gold particles will have been obfuscated by multiple processes such as sediment transport and surficial geological processes. If detrital populations are to be characterised to provide information about the original in situ auriferous ore deposits and their formation, then the allochthonous, displaced and detrital nature of the deposits must be a principal consideration in studies. Therefore, a solid understanding of the surficial history of the environment that a detrital gold sample was collected within, provides context and caveats within which all samples and observations should be interpreted.

Due to the chemical properties of gold, the core composition of gold particles is preserved during erosion and transport processes, despite changes in the physical morphology and external surface of the particle (Townley et al., 2003, Chapman et al., 2010, Crawford, 2007). The knowledge that gold composition is preserved presents an opportunity to investigate the compositional features of gold particles formed within the bedrock. However, the combined effects of erosion, transport, physical concentration and sampling of gold particles from sediments obscures geographical relationships between the bedrock source and the sampled detrital gold particles. Therefore, quantification of the erosion, transport, physical concentration and sampling processes are necessary if detrital gold compositions are to be used to improve the understanding of the chemical nature of gold from the auriferous mineralisation within the bedrock.

Compositional analysis of the gold particles in a sample population has become a principal tool for comparison between detrital gold populations, along with the morphology, chemical heterogeneity and mineralogy of inclusions (Chapman et al., 2021). Leake et al. (1998) proposed that these methods are combined to produce a “microchemical characterization” or signature of a gold population which has been widely adopted in the literature (Alam et al., 2019, Knight et al., 1999b, Leake and Bland, 1992, Leake et al., 1997, Leake et al., 1998). Compositional differences between gold particles taken from different sample populations are inferred to represent evidence of different hypogene sources of the detrital gold, and bimodal populations in a single sample are often taken as evidence of mixing of gold from two sources (Leake et al., 1997, Chapman et al., 2021). There has however been little

discussion on the statistical significance of results in published comparisons between samples and many studies present subjective visual comparisons of the data to support interpretations of compositional populations.

This chapter reviews known sources of uncertainty relevant to compositional and detrital gold studies with the aim of reducing the subjectivity of analyses of compositional data from detrital gold samples. The literature review of possible sources of uncertainty is divided into three sections discussed in chronological order. Firstly, pre-sampling factors are discussed including consideration of the source & processes involved in the formation of the gold including erosional & surficial transport processes. Secondly, sampling methods are discussed focusing on the causes of uncertainty and errors that may affect later analysis. Finally, the analysis and interpretation of the data obtained is discussed in detail including the effects of sample size, comparisons between continuous distributions and examples of how statistical methods can be applied to quantify and test hypotheses.

2.2 Review and Discussion of compositional gold studies

The term ‘source’ must first be clearly defined in relation to detrital gold studies before further discussion of detrital or placer gold studies. The term ‘source’ in this context is taken to define a physical volume from which the gold particles originated from within bedrock. However, the physical location from which a gold particle originates is unknown as ore deposits typically consist of many individual ‘volumes’ which can differ from one another. To address this problem practically the ‘source’ needs be defined as a mineralising auriferous ‘system’ present on a large scale (which is determined by the catchment area of a detrital sample site), not as an individual part, vein or portion of the system. The source region is considered to have undergone a series of geological events to produce populations of gold particles that have definable ranges of properties.

The term ‘source’ as used in this study is in contrast to many deposits scale studies, which often consider the ‘source’ as the location within the hard rock deposit that a single gold particle or particle(s) came from. The reason that source is taken here to represent a volume is because gold deposits/systems deposit particles of different compositions in different parts of the system/deposit (see sections 2.2.2 and 2.2.3). Therefore, the broader less specific definition the ‘source’ is required to enable the gold particles to be considered as populations not as individual particles.

A gold particle must undergo weathering and erosion to release it from a rock volume before transport and deposition into a sediment before it can be collected during sampling. Considering each of these processes individually the following section reviews the possible influence of processes occurring at each stage of the journey to being incorporated in a sediment. It focuses specifically on processes that could result in separation of gold particles based on physical or chemical properties. Any differential processes in the surficial environment would conceivably produce a physical separation of particles that would be problematic for studies of detrital gold particles. If a process is demonstrated to affect all the gold particles equally, it can be assumed to have no effect on the properties of the population of gold particles and therefore does not need to be considered in subsequent analysis.

2.2.1 Erosional and surficial transport processes

The nature of the erosional processes responsible for liberating gold particles from the rock volume containing the gold will depend on the composition of the

rocks and climatic conditions. Generally, if erosion removes a large volume of rock there should be very little differential effects on gold particles. However, a potential source of differential treatment of gold particles could be produced by different locations/ minerals hosting gold within a vein. For example, gold which is found as inclusions within chemically unstable minerals (such as a sulphide) may be very rapidly released during erosion. However, if some of the gold particles are hosted as inclusions within a resistate mineral (such as quartz) it will not be released as free gold until the mineral hosting it has physically broken down. This can result in gold particles being transported before they are released into the surficial environment as free particles. This is generally referred to as ‘armouring’ in the literature (Boyle, 1987). At the collection site, armoured gold particles are likely to have shorter transport distances as free gold particles after liberation from their armouring minerals, compared to particles that are quickly liberated from the host rock matrix. The contribution of an ‘armouring effect’ to the transport history of a gold particle is dependent on the stability and characteristics of the specific mineral(s) hosting the gold particle. This is an important consideration when sampling a specific sediment volume downslope/downstream in detrital gold studies (Wrighton, 2013, Knight et al., 1999a).

The physical transport of gold particles and sediments is a predictable process, with all except glacial transport, moving material in a down slope direction. Gold particles liberated from a defined volume of rock can be considered to experience comparable transport mechanisms, if armouring of particles is not a significant factor. Mass transport processes will move material locally down slopes until reaching a valley or local depression where fluvial stream and rivers will tend to dominate transport and move material further down the gully or valley. Using the assumption that material moves downhill constrains the potential catchment that gold in sediments could have been sourced from. This is a fundamental principle when panning or using detrital gold particles for mineral exploration.

Particles of gold are typically transported in fluvial systems by saltation within the bed load of sediment (Goldfarb, 2007). The density of gold/silver alloys, figure 2.1, result in gold particles requiring moderate to high flow velocities to mobilise and transport, and as such they behave hydrodynamically equivalent to less dense particles of significantly larger diameters. The limited experimental work conducted on gold particles in flume tanks has used pure gold particles and therefore potentially may not accurately replicate the range of densities that natural gold alloys possess (James and Minter, 1999, Carling

and Breakspear, 2006). Because silver is less dense Ag-rich alloy particles could potentially be transported further downstream that pure Au, all other factors being equal. Field studies such as those by Crawford (2007) which provide data on gold composition in the context of transport distance are limited, and often such data is not the primary focus of the work. However, from the limited data where repeat sampling has been conducted along individual drainages, no systematic change to the core compositions of gold particles in collected populations has been reported to occur (such as: Leake et al. (1997), Chapman et al. (2000), Chapman and Mortensen (2016), Chapman et al. (2010)).

Wrighton, (2013) related particle morphology to long (10's Km) transport distances in drainages with significant potential of multiple gold particle inputs. He required sample populations to be compositionally comparable when performing analysis of morphology. This study, along with other published studies, provides significant evidence that the distribution of compositions in a detrital gold population is independent of the transport distance of the particles. Importantly this indicates that the transport of different composition gold particles does not result in fractionation of different compositions. Because the physical morphology and size of the gold particles controls the hydrodynamics of a gold particle during fluvial transport, a further implication is that the shape and size of gold particles is not correlatively coupled to gold alloy composition.

The statement that; no fractionation of different compositions of gold particles occurs with increasing fluvial transport, only holds when sectioned gold particles are analysed to report the composition in the core of the gold particle. Studies of gold grains which examine the surface of gold particles document that compositions of particles can change with increasing transport. This is due to the progressive development of gold rich (> 98 wt.% Au) rims and/or overgrowths typically between 2–10 μm in thickness on the surface of gold particles during surficial transport (Utter, 1979, Chapman et al., 2021, Craw et al., 2017). Therefore, care must be taken to analysis the core compositions of the gold particles avoiding surficial rims (which may be problematic for very small or flat particles which have a cross section of less than 20 microns in width).

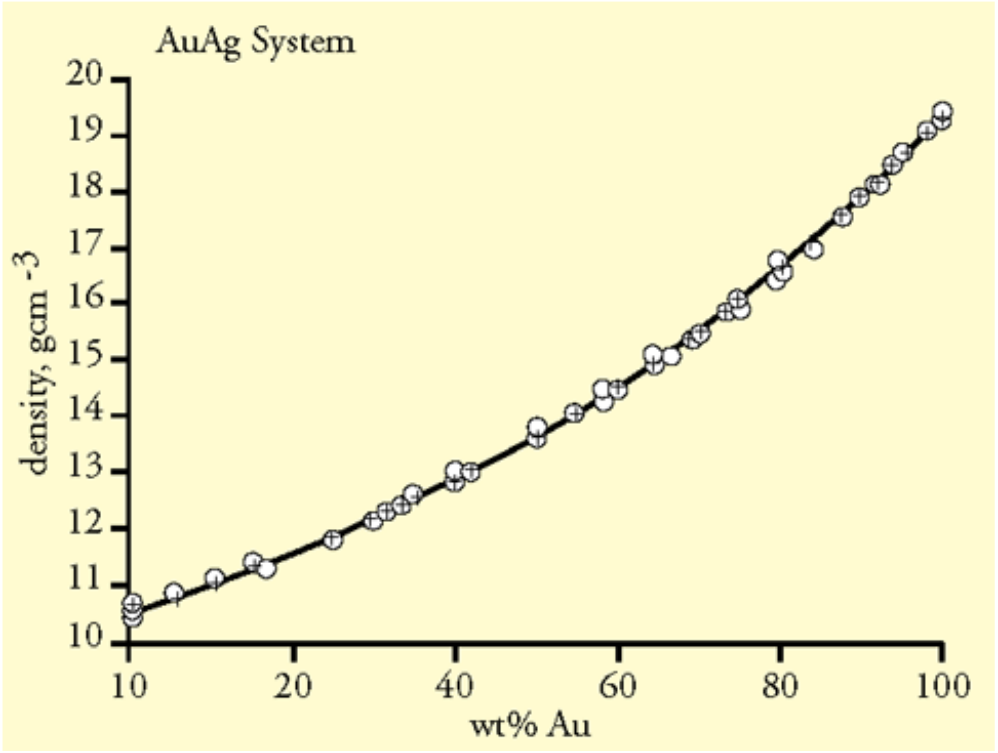

Figure 2.1 – Density of gold/silver alloys dependent on composition (Kraut and Stern, 2000).

The transport mechanisms of gold particles which are responsible for placer accumulations have been investigated through sedimentological examinations of the host sediments (Goldfarb, 2007) and provide insights as to why significant differential transport due to density differences of different composition gold particles is not observed in studies. Sedimentological investigations of placer sediments have observed high concentrations of gold particles on scour surfaces, at the bedrock interface, within the matrix of coarse conglomerates and at the base of channel ways (Boyle, 1979, Eyles and Kocsis, 1989, Goldfarb, 2007). In a review of placer formation mechanisms Carling and Breakspear (2006) highlighted that many gold placers are formed by processes that result in the winnowing of lighter sediment from coarse, poorly sorted, conglomeratic sediments which are deposited during rapidly varying flows, such as occur during flood events. Considering these flow regimes, the density difference between high and low Ag gold potentially has minimal effect on transport. This is because all the gold particles irrespective of density will be mobile and saltated in the bedload during a high energy flood event and are deposited en masse before later processes remove lighter sediment to form auriferous lags. Therefore, if the flow removing lighter sediment during the winnowing phase cannot transport the lightest gold (Ag rich), then no differentiation of gold by density would occur.

2.2.2 Sampling of detrital gold particles

It is important to consider the sampling techniques, the methodologies and specifically how they influence the data collected when conducting a detrital gold study. This is because a sample of detrital gold particles can only be a sub-sample of the population of gold within the sediments. Samples are typically collected using in the field gravity separation, such as sluicing and gold panning; see Leake et al. (1997) for details of techniques. This allows large volumes of loose sediment to be processed efficiently maximising the number of gold particles that can be collected from a sample location.

In an ideal sampling method, the probability of sampling any individual gold particle from the total population of gold particles in the sediment, here termed the 'master sediment population', would be equivalent. The greater the number of particles that are collected in a sub sample, the more the population will asymptotically converge towards reproducing the 'master sediment population'. In real world conditions however, small gold particles can be harder to recover with standard gravity concentration methods. However, this is not generally considered an issue. As long as the method is consistent, it can be assumed that for each size of gold particle, the chance of sampling would be equivalent when comparing samples from different sites.

As only a tiny proportion of the gold particles that are assumed to be present within the sediment are usually collected, the size of the sub-sample must be considered carefully so that it represents the characteristics of an unknown 'master population' with sufficient precision to address the research hypotheses. The determination of how many gold particles are sufficient when collecting a gold sub-sample is a contentious non-trivial problem, however it is accepted that a larger sample size is always superior as this will converge towards the properties of the master population with increasing sample size.

There has been a general trend towards collecting larger number of gold particles in a sample over time (Chapman et al., 2021). Modern studies advocate samples of at least 100 in order to obtain data on gold inclusions, which are, at present, favoured as a discriminant between systems over a compositional assessment of a population (Chapman et al., 2010, Chapman et al., 2021, Pochon et al., 2021, Girard et al., 2021). This thesis considers the question of the required sample size in considerable detail as part of the data analysis process and demonstrates methods for assessing the effect of sample size on empirical datasets of gold particle compositions.

Detrital gold particles are typically collected using a variety of traditional sluicing and panning methods which have been used for hundreds of years, though the exact scale and physical arrangement of equipment varies (Leake et al., 1997). These methods are a remarkably efficient and reliable tool for the concentration of heavy minerals (Theobald Jr, 1957) as long as the gold has been fully liberated from lighter minerals/armouring and the size of the particles are sufficient - typically found to be >50μm for gold alloys (Chapman et al., 2009). In studies of the efficiency of panning, the recovery of dense minerals (percent of total minerals retained in the first pan vs total present in the sample) is observed to increase as the targeted mineral density increases (Theobald Jr, 1957). All the gold particles over >50 μm in a sediment are potentially recoverable in the first panning of a sample. The author has observed that all the gold particles of this size are recovered in the first panning of a sediment by skilled panners through a check procedure conducted by re-panning the tailings.

It is fundamental to detrital gold studies that sampling methods are unbiased and produce reproducible samples. This can be checked using field duplicates from two sediment samples obtained close to each other in the drainage. In addition, as panning is a skilled task, sampling programs should consider the skill level of the samplers and quality assurance procedures such as re-panning of tailings by a different sampler should be undertaken to demonstrate correct procedures and proficiency of the person conducting the sampling. The nature of heavy mineral distributions in a drainage system means that different panners have ‘favourite’ types of target areas and so may target different sediment environments (traps). Problematically, no published study testing the equivalence of gold particle populations, taken systematically from different sediment environments within a drainage system is known to the author. However, the reproducibility of sampling has been demonstrated through comparison of the compositional signatures of duplicate field samples as part of published studies, see figure 2.2 (Chapman et al., 2009, Chapman et al., 2000, Chapman et al., 2010).

The observation that comparable data is obtainable when collecting field duplicates, which may or may not have been taken from variable sedimentary environments within in a single drainage, tentatively confirms two assumptions of detrital gold sampling methods: Firstly, that the sampling techniques are appropriate and secondly, that the local sedimentary processes in the stream do not significantly affect the compositional signature of the populations, with no apparent variation in the populations of duplicates. This is significant as it

provides evidence in support of the assumption that, on a local scale, the population of gold particles in the drainage has a consistent distribution of gold composition on a 10s to 100's meter scale (excluding situations where additional bedrock sources add additional particles). It is concluded that no differentiation of gold particles of different compositions is produced due to sedimentary and fluvial processes locally.

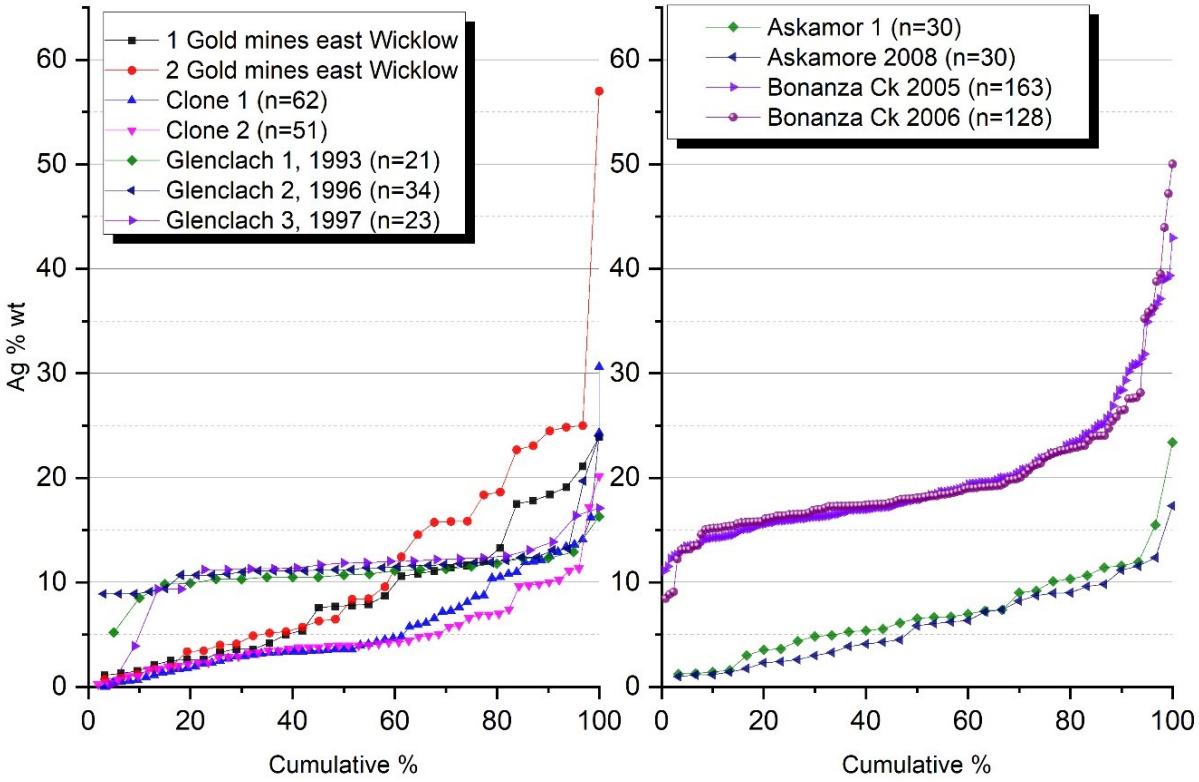

Figure 2.2 – Cumulative plot (see page 25 for discussion of plot style) of multiple samples taken from close to each other within a single drainage (duplicate samples) that have been published in the literature. The plot shows good repeatability of the compositional distributions obtained from the samples. Samples from the following sources; Clone and Askamore samples from Moles and Chapman (2019). Lone star, Boulder lode, Bonanza Creek samples after Chapman et al. (2010) Glenclach after Chapman et al. (2000).

2.2.3 Analysis and interpretation of detrital gold compositional data

This section reviews methods for comparing populations of gold particles and presents proposed improvements which could provide more accurate quantification and communication of comparisons in detrital studies. Before examining the methods used in published studies, it is important to understand the question that the detrital gold studies seek to answer. Published studies can be broadly separated into two categories:

Spatial studies: These aim to identify/understand the dispersal of gold from a lode source in the surficial environment. For example, studies on morphological relationships with transport distances such as Knight et al. (1999a), Melchiorre and Henderson (2019), Wrighton (2013) or focused placer-lode relationship studies such as Chapman et al. (2016).

Comparative studies: These aim to compare characteristics of gold particle populations taken from multiple localities or drainages, which are typically spatially separated such that the gold must be sourced from different hard rock occurrences. These are the most common type of study in the detrital gold literature as the findings are directly applicable to commercial exploration projects. The aim of such studies is to develop characterizations or signatures of detrital gold samples in order to develop predictive tools which could identify the features of the source mineralisation from the detrital gold. For example, regional/camp scale comparisons between drainages such as Pochon et al. (2021) Chapman et al. (2011). Leake et al. 1997) Molese et al. (2013) or studies which compare between different deposit styles (such as Liu and Beaudoin, (2021) Liu et al. (2021) Chapman et al. (2021).

Both these types of studies require comparison of differences, or consistencies, between the measured properties of gold particles in two or more sample populations (that can be of different sizes). This is problematic because two different sized sub-samples taken from a population which has large ranges of gold composition can appear to be different when plotted and visually compared. In many cases differences in the populations of two or more samples are not clear cut and a judgment must be made if the difference between two samples is significant, or due to random variability in sub-sampling of a single population? This question must be resolved to correctly interpret the data.

To compare between compositional signatures of samples detrital gold studies commonly use graphical cumulative frequency (CF) plots to present this data and then interpret the results using visual comparisons between the plots of the distributions to address research hypotheses (Leake et al., 1997, Chapman et al., 2000). A good example of a study which illustrates how early detrital gold studies used visual comparisons to assess multiple sample populations is Leake et al. (1998). This study is ideal as it has 12 samples along a single drainage, Shortcleuch Water; see figure 2.3, which have similar but subtly different compositional signatures of the sample populations, figures 2.4 and 2.5. This data set is a perfect example of ambiguous data that required the authors to make comparative judgments on how significant differences were between sample populations. The Leake et al. (1998) dataset will therefore be used to illustrate concepts and ideas throughout subsequent parts of this chapter's discussions.

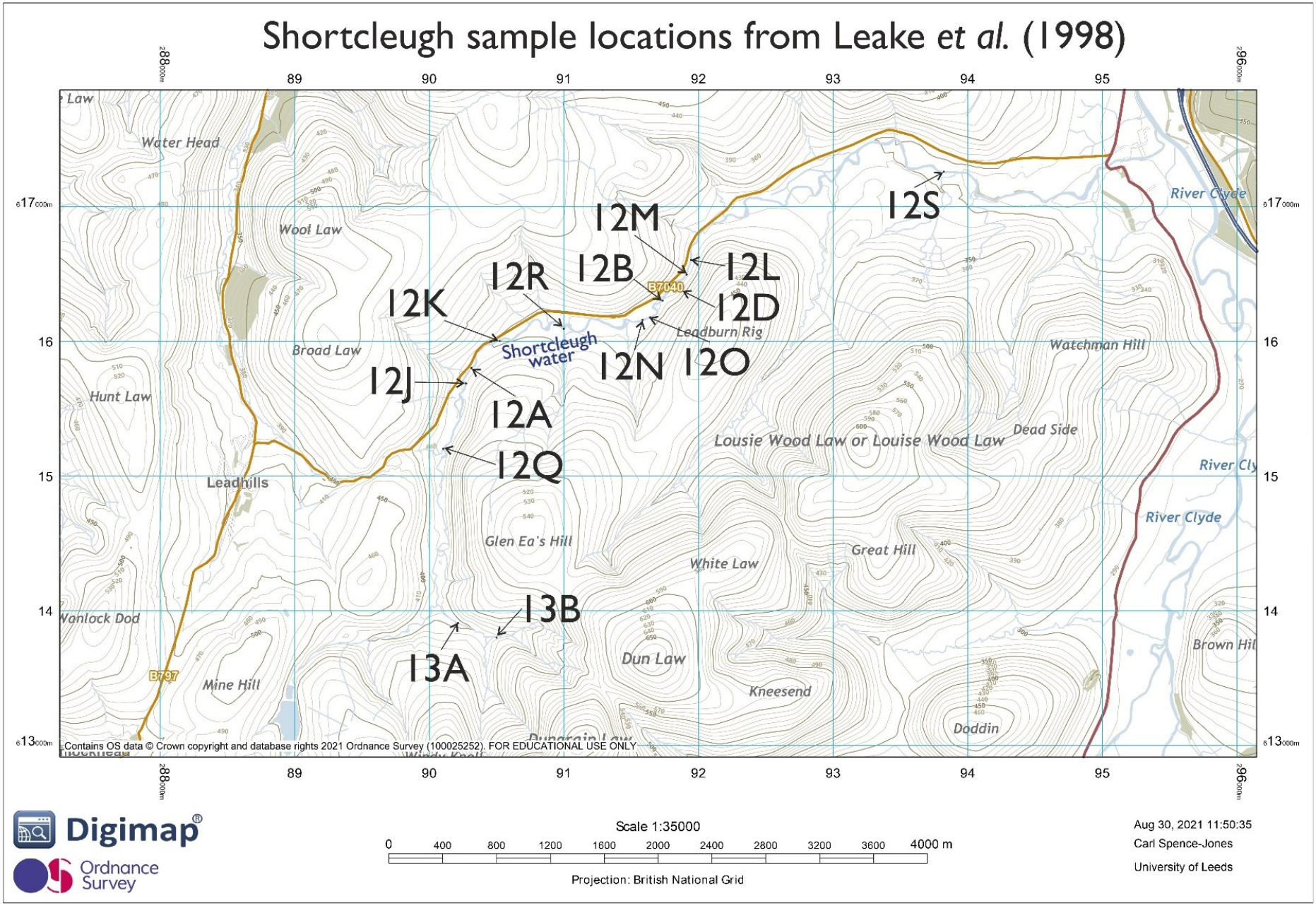

Figure 2.3 – A sample map showing sample locations along Shortcleuch Water, Leadhills, Scotland. Taken from (Leake et al, 1998)

Figure 2.4 – Cumulative frequency plot of the Ag composition of 12 sample populations from Shortcleuch water (Leake et al, 1998).

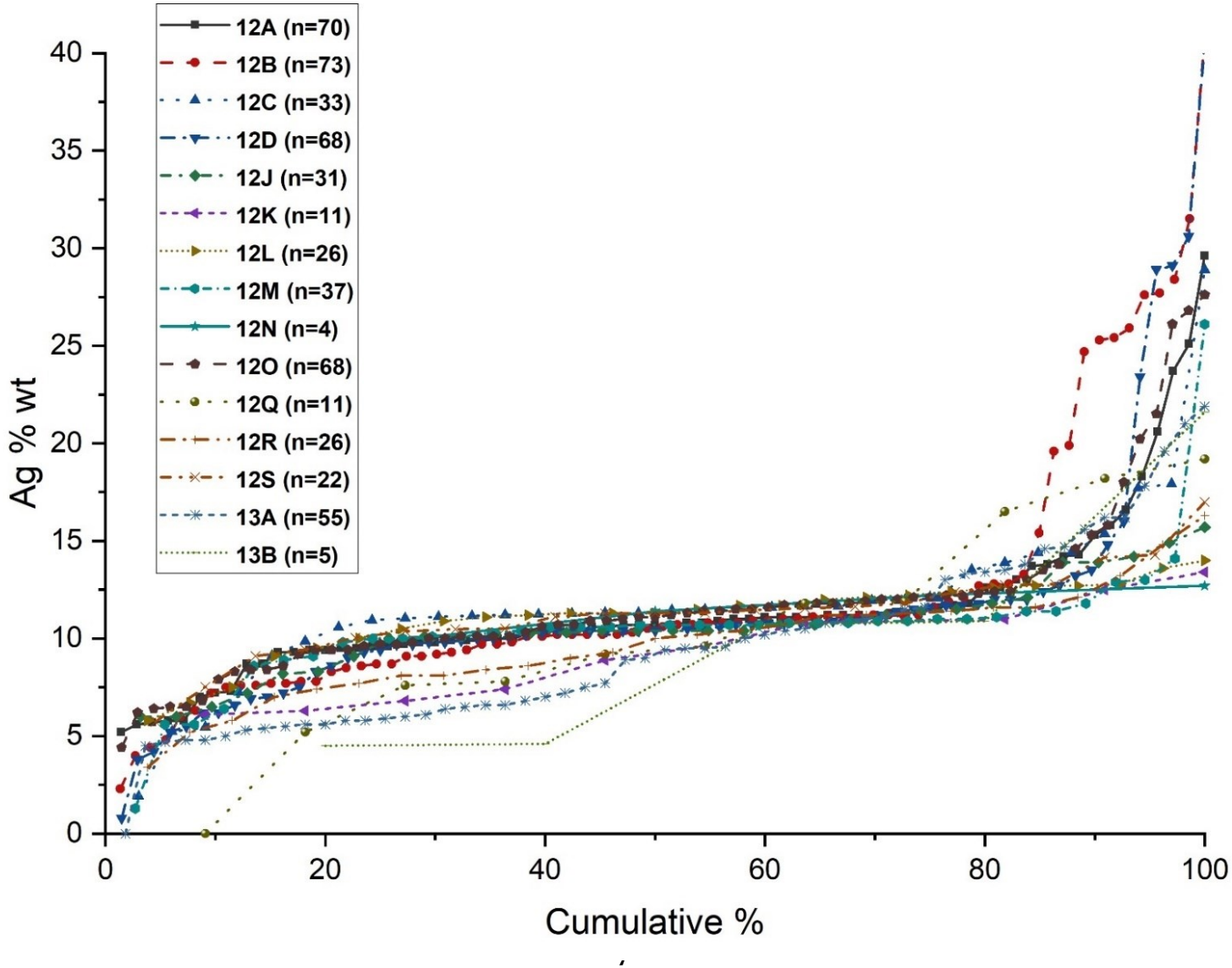

Figure 2.5 – Individual cumulative frequency plots of the Ag composition of 12 sample populations from Shortcleuch water presented in the format of the original paper (Leake et al, 1998)

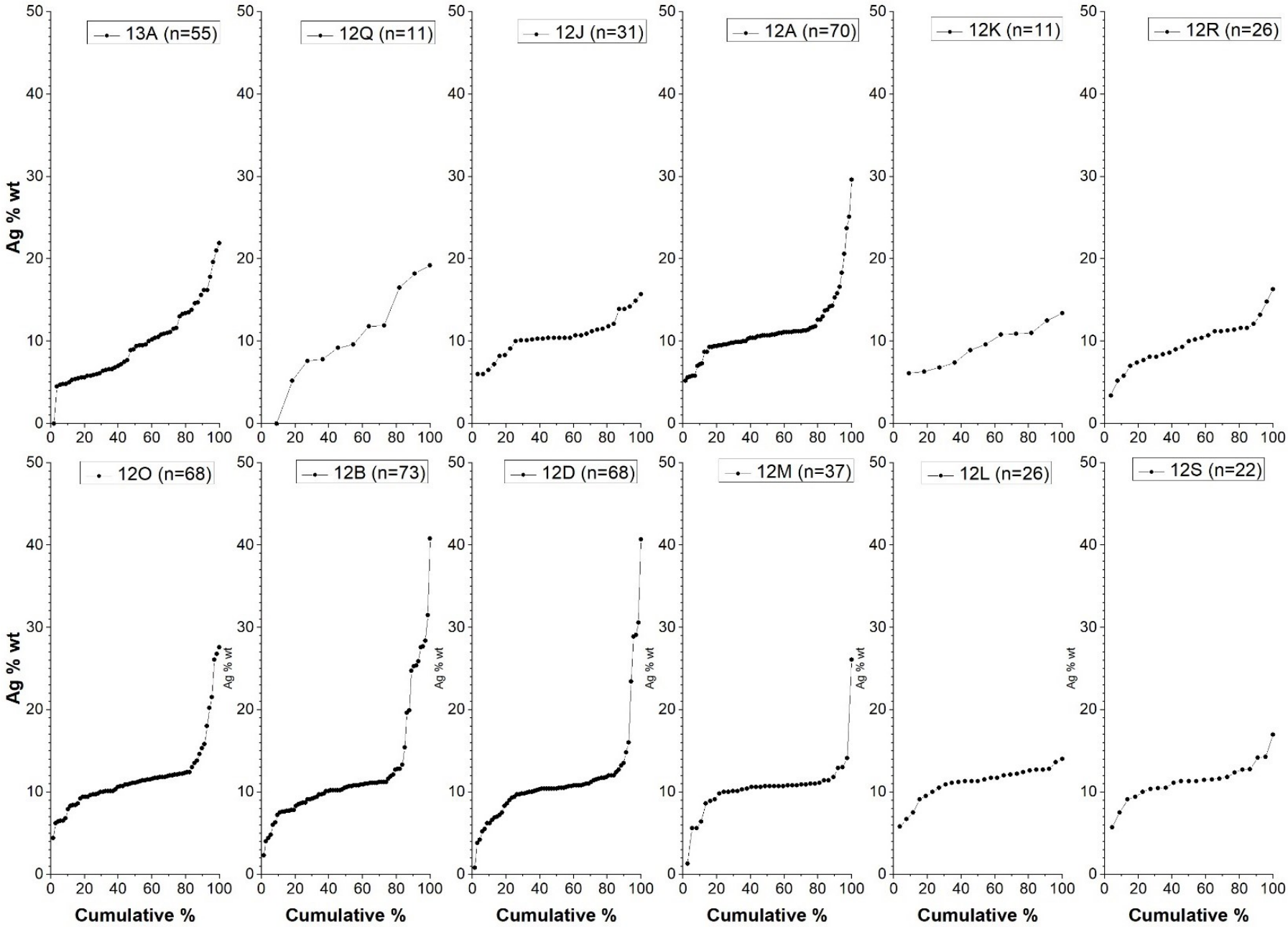

cumulative frequency plots

The justification for the visual examination of cumulative plots is that simple statistical parameters such as the mean, median or interquartile range are problematic as they do not retain all the actual data values within a population. This is important because placer populations may be derived from multiple sources. Therefore, a visual comparison of cumulative frequency plots displays all the data and also allows comparison of samples of different size (Chapman et al., 2000). The visual appraisal of the graphical data relies on the discretion of the analyst, so the result is a subjective interpretation of the plot resulting in an uncertain level of confidence in the interpretation (Chapman et al., 2000, Buja et al., 2009) Additionally, a well-documented phenomenon is that individuals conducting visual analysis of data generally tend towards over-interpretation of patterns (Buja et al., 2009, Wickham et al., 2010). Explicit discussion of methods to calibrate the visual comparative processes are lacking in the gold literature despite the subjectivity being a known issue. Sometimes publications present supplementary or alternative lines of evidence, such as inclusions or trace elements, to avoid using potentially subjective compositional data in studies.

However, not all studies have relied on visual comparisons to analyse compositional populations. Two studies by Utter (1979) and Pochon et al. (2021), used Kolmogorov-Smirnov tests, a statistical method used to compare between sample populations quantifiably, which could be better tool for comparison between gold populations. In order evaluate comparative methods the sources of uncertainty must be carefully evaluated. The following sections break down specific aspects of studies in relation to the data analysis challenges faced.

2.2.3.1 The effect of sample size on compositional distributions

As discussed previously there has been a general trend towards larger numbers of gold particles collected in a sample and there is a consensus that the larger the number of particles sampled the more representative a sample is obtained (Leake et al., 1998, Chapman et al., 2010). Some literature suggests that as few as 16 particles or less can be used to characterise the general nature of an observed populations (Leake et al., 1998). However, this is not adequate to capture features of some sample populations, specifically high and low silver tails or samples with a large range of compositions. Samples of at least 100 particles are advocated by Chapman et al. (2021). Chapman et al. (2010) advocates larger samples to both produce adequate

compositional data for comparisons and to collect sufficient inclusions in the alloy for inclusion characterisations. However, inclusions may not be common is some populations (an aspect of detrital gold studies that will not be addressed in detail in this chapter).

The effect of sample size on the compositional signature must be evaluated and understood if interpretations of the data are to have value. Detrital gold studies do not collect equal samples of equal sizes from all locations as the numbers of particles is determined by the abundance of gold in an area and the time available to sample. Larger samples are often obtainable in specific drainages known to be prospective, which is often the initial attraction for exploration in an area. However, if a study seeks to investigate gold occurrences spatially in an area or camp, then samples are needed from as many catchments and drainages as possible. These are often of very variable nature, in terms of the gold enrichment, sedimentary environment, and ease of access/sampling. This means that the highest abundance of detrital gold found during sampling does not necessarily correlate, as one might expect, with the best hard rock gold source deposits.

A simple check to see if there may be any systematic problems that relate to sample sizes is to plot samples in size order. For example, this is done in figure 2.6 for the Shortcleuch samples which clearly shows a pattern where the largest samples all have high silver tails to the distributions not seen in smaller samples. This raises the question ‘Is the presence of a high silver tail a function of sample size?’ or a real change in the compositional signature due to a different local source (examined statistically in section 2.2.4.2). An additional source could affect both the compositional signature and abundance with the following logical argument: If additional gold from a second source is combined to a consistent ‘background’ regional population, it would increase the abundance of gold available to sample locally. This would result in easier sampling and naturally larger samples being obtained if similar ‘effort’ goes into all collection at all the sample sites as well as effecting the compositional signature.

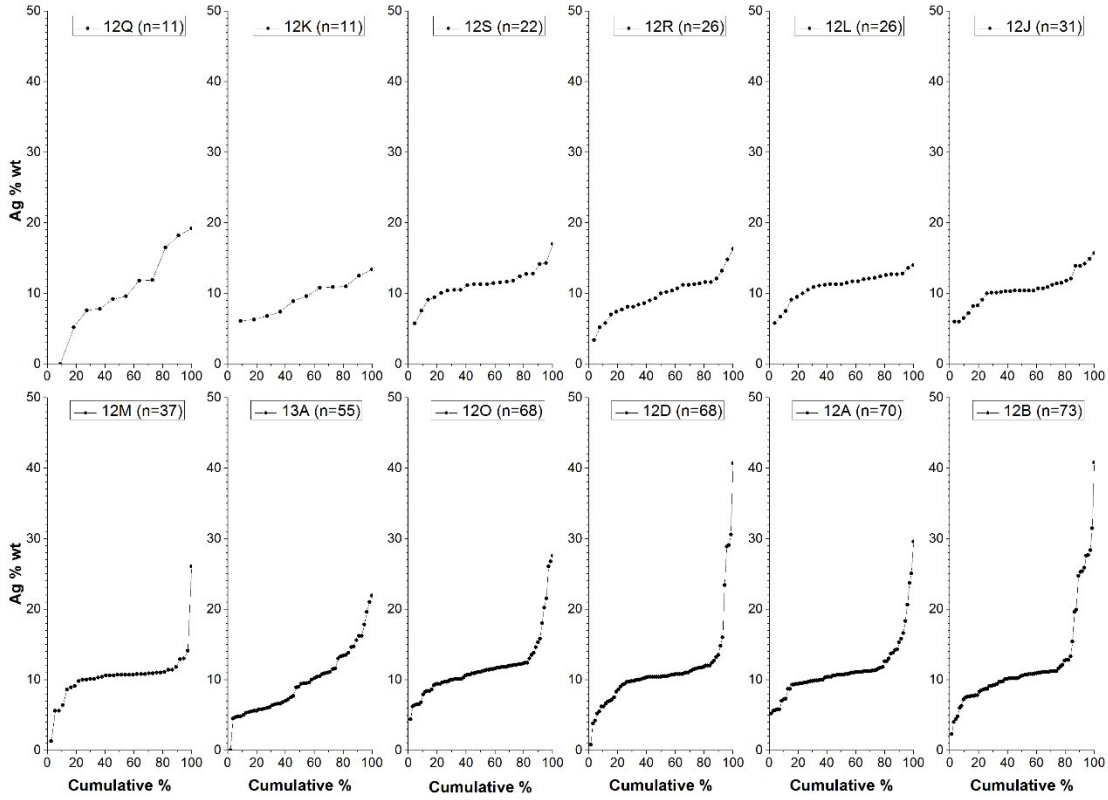

Figure 2.6 – Individual sample sites for Shortcleuch from Leake et al. (1998) rearranged into sample size order.

As the examples from Shortcleuch show, it is not easy to draw conclusions on the significance of a co-variation of abundance and compositions. To further explore the problem of relying on abundance and ease of obtaining a large detrital gold sample, consider a theoretical example of two 1-meter quartz veins each with equal dimensions. One vein carries gold at 1 gram per ton the other at 100 gram per ton but in every other aspect these are identical. If we then consider two identical streams with equal geometries, A^1 and A^2 in figure 2.5, that run over these veins eroding, transporting and depositing gold in the sediment, then the amount of gold particles correlates with the abundance in the veins. However, when the geometries of the streams are different, B^1 and B^2 in figure 2.7, then the lower abundance vein quartz vein could create a more persistent and higher abundance of gold. Therefore, if there is a larger stream vein interaction with the vein parallel to the stream, then greater amounts of the vein material will be eroded by the stream compared to a high-grade vein crosscutting the stream at 90 degrees. In conclusion placer-lode source geometric relationships can result in decoupled abundances between the lode sources and placer accumulations, even without the additional influence of

hydrology and processes of placer formation which will produce additional unevenness in abundances in the streams.

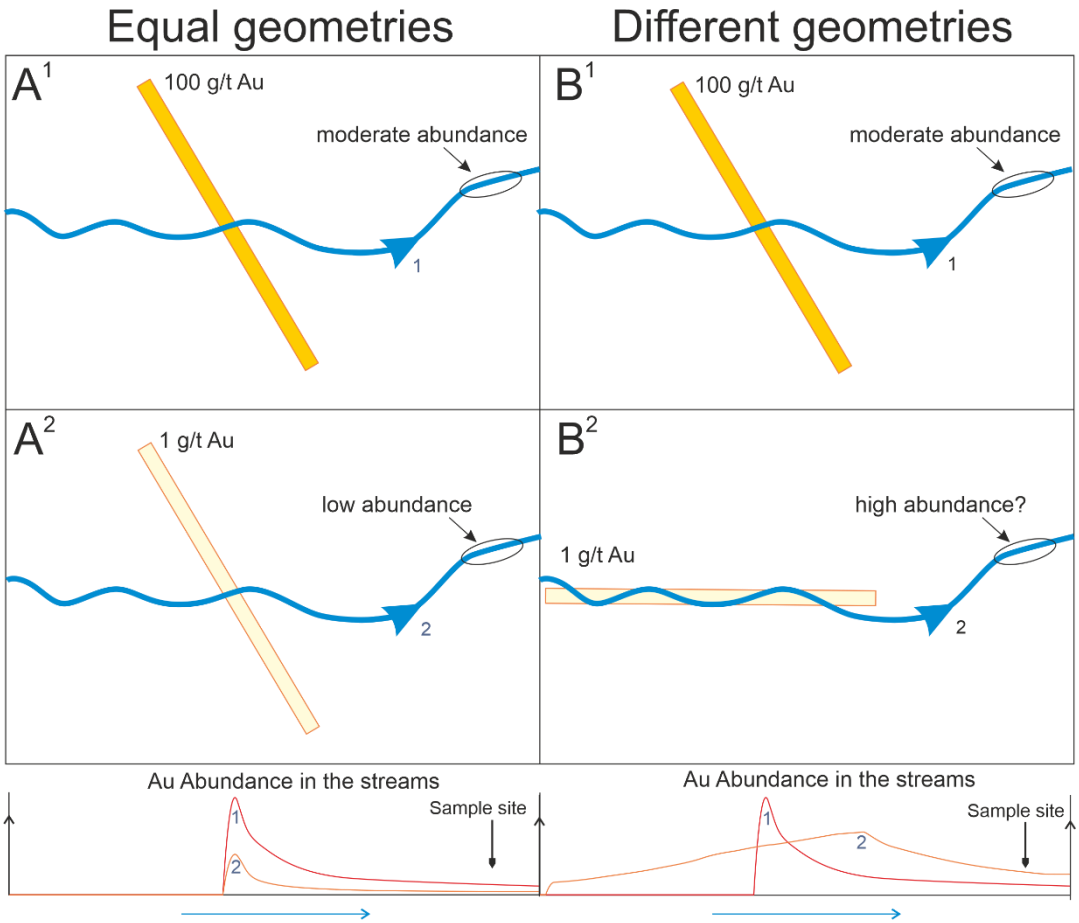

Figure 2.7 – Conceptual diagram to illustrate how hard rock deposits may not necessarily correlate with detrital gold particle abundance in the sediments.

Two separate statistical explorations of the effects of sample size are undertaken bellow to allow discussion of two different problems that relate to small sample sizes. First the probability of sub-sampling gold of a defined composition from a master population in the drainage is explored using the binomial sampling probability calculation. This quantifies the probability that a gold particle from a distinct (defined) compositional range might be collected or missed in a sample population of a given size. It therefore can be used determine the random chances inherent when sub-sampling detrital gold particle populations. Secondly, the problem of how to compare between samples of different sizes while accounting for the uncertainties inherent to the data is addressed by comparisons between continuous distributions.

To calibrate the inference that small sample sizes would not reproduce small numbers of extreme compositions (for example a small number of high silver

gold particles “high silver tails” of the distributions in figure 2.6) it is important to consider the assumption, discussed above, that all gold particles within the volume of sediment sampled have an equal chance of being collected. If this assumption is accepted, a probabilistic approach can be used to appraise the chance of collecting a specified proportion of the gold compositional range using the general probability formula for binomial sampling, *equation 2.1* (Andersen, 2005). The equation uses only two inputs to calculate a probability; the sub-sample size (n) to be collected and the proportion of the compositional range in relation to the master population.

$$P_{n_i=0} = (1 - X_i)^n$$

Equation 2.1 – where $P_{n_i=0}$ is the probability of not collecting any gold particles from the *i* ‘th population in a sample of size (n) particles, dependent on the proportion of the gold belonging to the *i* ‘th population out of the total gold population (Xi).

The equation for predicting the probability that particles belonging to a sub population are not collected can be used for any sample size and the results of doing this are shown graphically in figure 2.8, which can be used as a quick reference for the effects of sample size if a small sub-population is suspected in some of the samples in a dataset. In addition to data evaluation, the probabilistic estimation of sampling probability can also be used to design detrital gold surveys and inform the sample size needed.

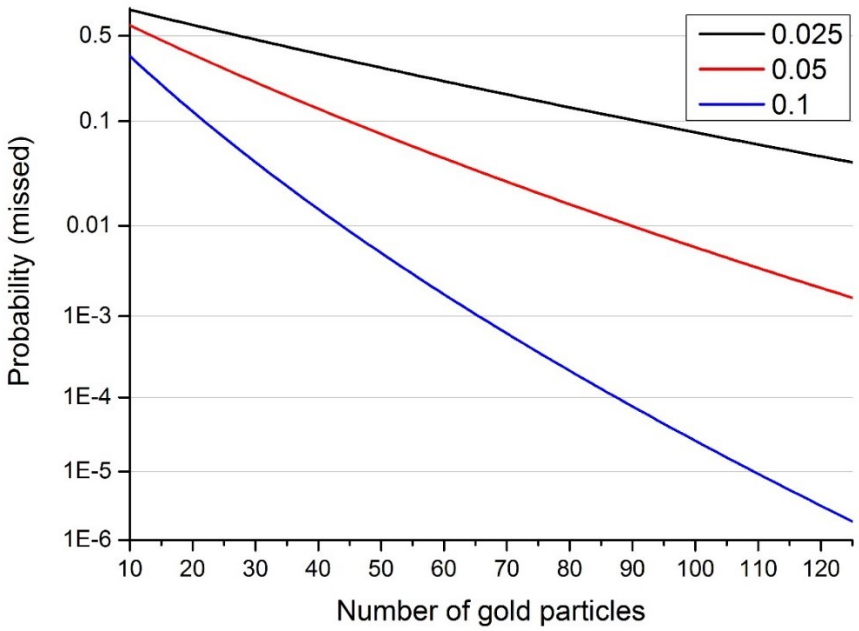

Figure 2.8 – Relationship between sample size and the probability then particles belonging to a sub population are not collected. Shown for sub populations that make up 10%, 5% and 2.5% of the total population (X_i = 0.1, 0.05 and 0.025) of gold particles in the master population (sediment) that the sample will be collected from.

Each individual sample from the example Shortcleuch Water dataset is assessed for the probability that the field sub-sample would not contain any high silver gold particles >16 wt% Ag. (Defined as local type 2 source by Leake et al. (1998)). For these calculations a key variable is the proportion of the >16 wt% Ag. gold in the master population (all gold particles in the sediment). To estimate this proportion the proportion of a subgroup, the field samples can be used as a guide to estimate the proportion. Considering the Shortcleuch dataset the highest proportion of >16 %wt. Ag gold observed is 9% (Sample 12O), excluding sample 13A (11%) which is believed by Leake et al. (1998) to possibly have a separate source. As such, three proportions of 10%, 5% and 1% of particles being >16 %Ag wt. gold has been chosen and the binomial sampling probability calculated for sample sizes equal to the empirical field samples, table 2.1.

Table 2.1 – Calculated probabilities that a sub-type of gold particle would not be collected in 3 scenarios where the sub type 2 (>16 %Ag wt.) is present as 10%, 5% and 1% of all gold in the master population.

		Probability type 2 missed		
Sample	N	10% Type 2	5% Type 2	1% Type 2
12A	70	0.001	0.028	0.495
12B	73	0.000	0.024	0.480
12C	33	0.031	0.184	0.718
12D	69	0.001	0.029	0.500
12J	31	0.038	0.204	0.732
12K	11	0.314	0.569	0.895
12L	26	0.065	0.264	0.770
12M	37	0.020	0.150	0.689
12O	68	0.001	0.031	0.505
12Q	11	0.314	0.569	0.895
12R	26	0.065	0.264	0.770
12S	22	0.098	0.324	0.802
13A	55	0.003	0.060	0.575

Using the calculated probabilities, shown in table 2.1, for the 6 samples which did not contain a high silver tail (>16 %Ag wt gold) in the Shortcleuch dataset (12C, D J, K, L and Q), the probability is negligible that the entire set recorded a false negative; i.e. that they have all been sampled from a population containing high silver gold but all do not have a >16 %Ag wt gold particle in the sample. To illustrate this the probability can be calculated; the probability that 6 samples all did not sample a >16 %Ag wt gold particle when the master population contained a 5% proportion of >16 %Ag wt gold is:

$$0.184 * 0.029 * .204 * 0.569 * 0.264 * 0.569 = \ 0.000093$$

This means that it is highly improbable that all the samples could have been collected from sediment which did actually contain a high silver gold subpopulation (in a proportion of 5% or higher of the total gold inventory). This supports the inference, stated by Leake et al. (1998), that the high silver gold is not ubiquitously present in the detrital populations in Shortcleuch Water in a quantitative way. By using and presenting a probabilistic approach improved communication of the uncertainty can be presented based on clear criteria. For the Shortcleuch data, the original interpretation of the authors was likely to be correct but the authors presented little information on uncertainty in this conclusion.

The use of binomial sampling probability calculations poses a significant problem in detrital gold studies, in that it requires the population to be divided into discreet sub-populations which have well-defined compositional limits. This is problematic as 'typical' gold sample population has a continuous

distribution of gold compositions over a discreet range of values. They are therefore are not easy to divide into clear sub-populations, which is an essential requisite of the binomial calculation. In addition, it is likely that the compositional ranges from two sources overlap partially or totally making an estimated division between sub populations challenging or meaningless to adopt.

The problems with overlapping populations are evident when published samples are examined. Consider the three samples shown in figure 2.9, two of which cover a very similar range from 0 to 30% Ag and a third that partially overlaps from 11 to 30 % Ag. When comparing these geographically unrelated samples (used here as examples of populations), it is clear that Bonanza Creek and Clone River compositional signatures cannot be differentiated by defining a sub population with a specific Ag composition as they have the same compositional range, and therefore only analysis of the full distributions of compositions can differentiate between the two samples.

In the case where a partial overlap between the compositions of two populations exists, it is only possible to use compositions outside of the overlapping range. This means that the probability method discussed above would only be able to detect a second population in cases where a substantial part of a population is outside the range of the dominant population range. For example, using the data shown in figure 2.9, consider a situation where Bonanza Creek was the dominant population and Shortcleuch Water composite gold was in the minority. In this case the probability method could be used. However, if the situation was reversed the probability method could not be used, as the addition of a second (different) population could only be recognised through analysis of the shape of the distribution. This is discussed at length in the next section (2.2.4).

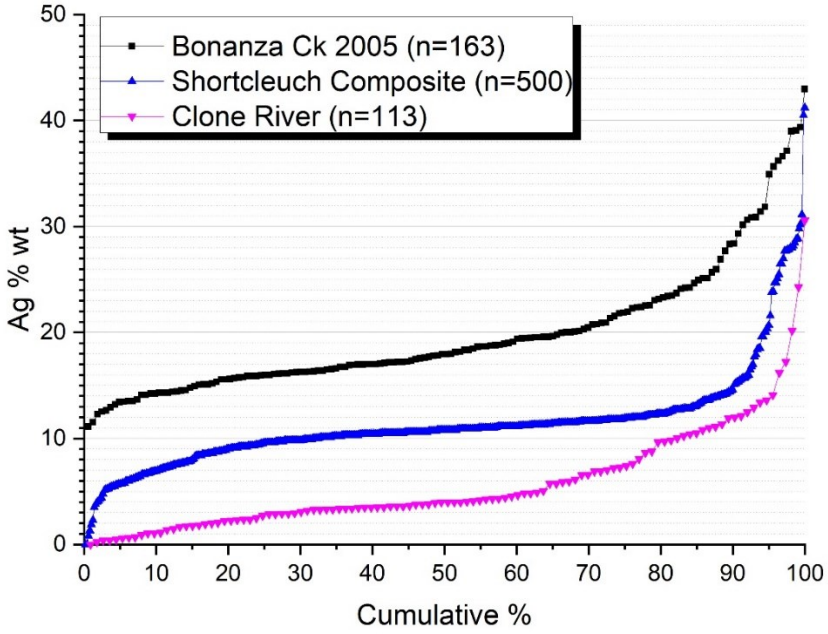

Figure 2.9 – Examples of different compositional distributions taken from the literature. Bonanza Creek after Chapman et al. (2010). Shortcleuch combined data after Leake et al. (1998). Clone River after Moles and Chapman (2019).

2.2.4 Comparisons between continuous distributions

The tools used to compare the shapes of compositional distributions (compositional signature) for detrital gold samples are of critical importance in detailed gold studies. It is necessary to account for the effects of sub-sample sizes, which produces variability in populations, in order to evaluate if two distributions are significantly different. While this has been done visually by experienced workers, it is desirable to develop statistical methods that are capable of impartially evaluating if the differences between two compositional signatures are significant, with a reportable certainty.

To illustrate the challenges that may be encountered when examining distributions from multiple samples, three distributions from published samples have been taken from the literature and mixed together in different combinations in a fictional arrangement of streams. This allows an illustration of the difficulties in an example which has known, and ideal, mixing of the distributions into multicomponent compiled populations, figure 2.10.

The results of sample mixing shown in figure 2.10 illustrate the complexity and difficulties encountered in discerning the relationships between sample populations in multiple samples. The distributions of the samples are shown in the bottom right of the figure for 6 fictional sample sites. The sites are shown by the stars on the map. Sample sites 1 to 3 are samples each sourced from a single deposit and represent the different compositional distributions of the three sources. Sample sites 4 and 5 represent mixing of two populations of gold particles from two different deposits to create a composite population. Sample site 6 represents mixing of sample sites 4 and 5 originating from all 3 deposits.

Comparing the results of simulated mixing of populations in the fictional example several key features are observed. Firstly, that mixing gold particles with compositions that fully overlap in compositional range produces subtle changes to the curves. This is shown in sample 4 where 163 gold particles of the Bonanza sample are added to the 500 particles of the Shortcleuch composite sample. In this case the gradient of the distribution is affected due to the smaller compositional range of the smaller sample, Bonanza Creek sample (10 - 40 % Ag), but otherwise has minimal effect. It is key to note that although the number of gold particles from the two deposits are disparate (500 vs 163) the compositional ranges are similar. In this situation a bimodal population is not clearly observed (i.e.no clear ‘step’ in the plot), and so identification of the change in distribution would require careful comparison and high-quality sampling (ideally multiple/ duplicates along a single drainage).

In cases where two populations are mixed in approximately equal proportions, as in the case of sample 5 in figure 2.10, the cumulative frequency plot displays a clearly bimodal distribution with a clear stepped curve observed. This is the classic pattern which published studies describe as indicating a mixed sample from multiple sources (Chapman et al., 2021). However, as further mixing of samples occurs, shown by sample 6 in figure 2.10 (which combines sample 4 and 5) the curves become smoothed and inflections and steps due to mixing of populations become subtle and difficult to distinguish.

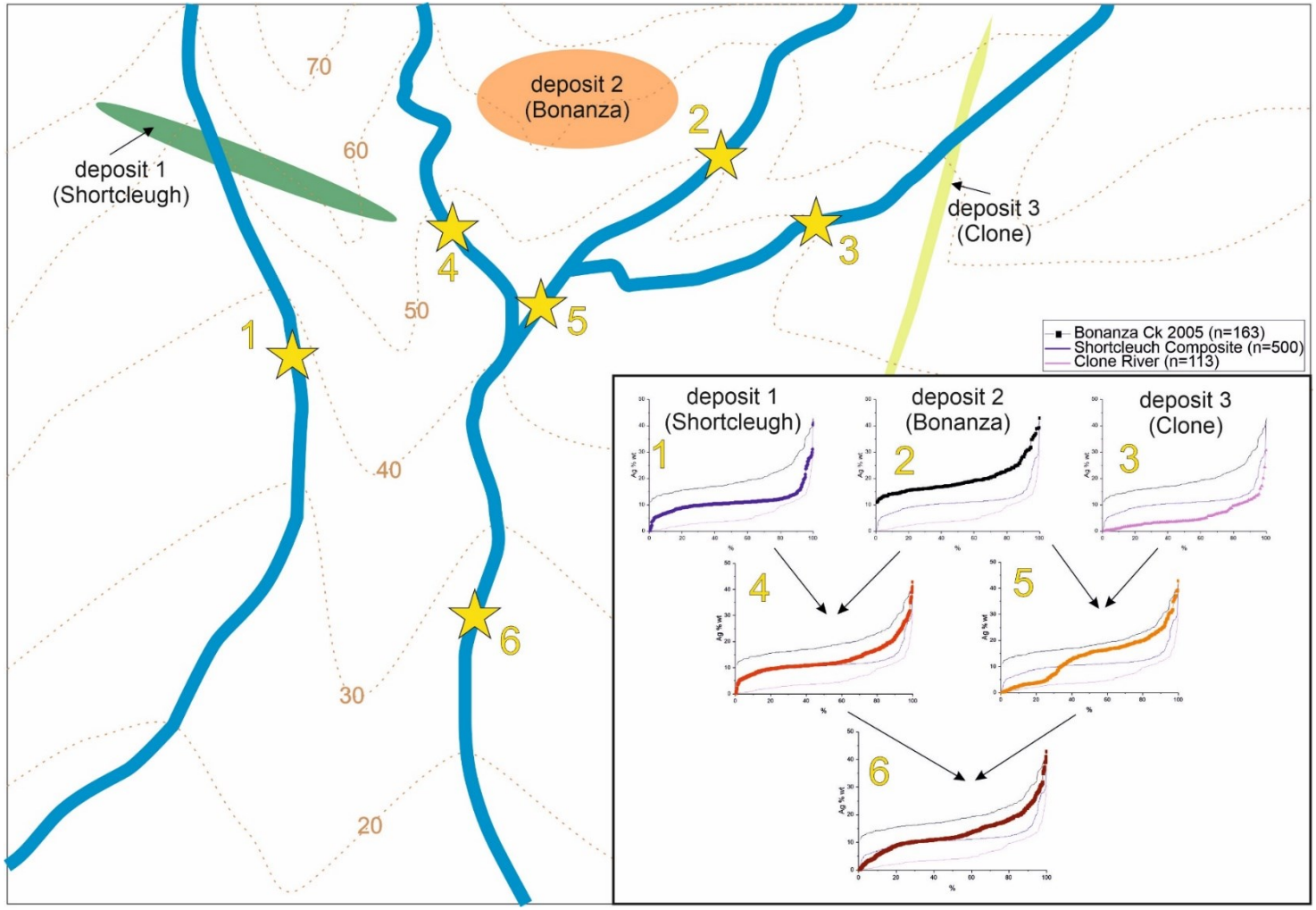

Figure 2.10 – Fictional example of a gold bearing area using three published gold populations to illustrate the challenges of identifying mixed populations. The three samples were mixed together simply by combining the gold particles of multiple samples together to create a new sample.

2.2.4.1 ‘Line-up’ method of visual comparison

If two samples are visually similar when compared to each other it can be suggested that the differences between them result from the random variance introduced by the sampling processes. The probability that the differences between two samples are due to random chance when sub-sampling cannot be quantified through simple comparative methods on a single plot. To address this problem, we can apply the methods of Buja et al. (2009) to remove bias from the visual comparison of samples by comparing the real data to synthetic populations. An example line up is shown in figure 2.11. In this method the real sample is compared to synthetic ‘decoy’ populations (of the same size) sub-sampled from a single population created by combining the two (or more) populations suspected of being not significantly different from each other. The test (null) hypothesis is that the two samples under test are the result of subsampling a single master population. If the real data cannot be consistently selected as standing out from the random synthetic data by multiple observers, it can be considered as consistent with the expected variation produced by random chance during sub-sampling.

A p-value, which is the probability of obtaining results at least as extreme as the observed results of a statistical hypothesis test, can be calculated for this method and is dependent on the number of decoys presented. For example, if 19 synthetic ‘decoy’ populations are shown alongside the real data there is a 1/20 chance of the viewer randomly picking the real data even if the null hypothesis is true, as all distributions are equivalent. This method can be repeated multiple times using independent observers and by recording the guesses of each observer a greater robustness in the p-value is obtained. It is important to note that the test protocol cannot be self-administered by the data analyst unless they somehow produce the plot of the real data among the 19 null plots randomly i.e., in such a way that the location of the real data is not known and has not been seen by the analyst before. If the data analyst has previously seen a plot of the real data, then this may bias the results due to memory of any of its idiosyncrasies.

In the example shown in figure 2.11 (taken from the Shortcleuch dataset), the real data is on plot F, second plot on the second row, and is sample 13A from Leake et al. (1998) which was identified as having a different compositional signature from all the others, by the original authors. However, they did not state the confidence of this interpretation. The real data is then compared against synthetic ‘decoy’ samples which were taken from a composite sample

of gold particles (n=500) created by combining all the samples from Shortcleuch Water (figure 2.11). If sample 13A (plot F on 2.11) is consistently selected by observers as being the most ‘different’ plot from the line-up, it can be stated that it is statistically different with a p-value of 0.05.

In order for the results to be meaningful the synthetic ‘decoy’ populations must be relevant to the hypothesis tested. This can be achieved by using a subsampling (bootstrapping) methodology which simulates field sampling and thus the variance in distributions produced by random sub-sampling from a single (selected) ‘master’ population of gold particles. This is achieved by using “sampling with replacement” and is done by randomly selecting each data point so each value in the master population is given equal chance of being selected (Efron, 1992). This replicates the fact that there is a near infinite population of gold particles in the sediment, which have a continuous distribution of compositions, thus the sampling of a single gold particle does not affect the probability of collecting other gold particles.

When creating the additional subsamples, the variable that must be controlled carefully is the nature of the ‘master’ population from which synthetic sampling will be conducted. The analyst has a choice about how to define/create a master population; either the field samples suspected of being similar are combined together and then the new sub-samples drawn from the pooled data, or the sub-samples are drawn from the largest single field sample population in the comparison set.

The decision on combining samples or not depends on the hypothesis to be tested and the quality of the samples. If the samples are being tested to see if they are drawn from a single population (a common test for detrital gold data), and no samples are of poor quality or have suspected bias, then the samples should be combined. This is because if the hypothesis is true then both samples would be drawn from a single population, the “true” (unknowable) master population of gold in the sediment, with each field sample deviation from this distribution only due to sub-sampling induced variance. As such, as the variance observed in each individual sample is random, the difference in a sample will tend to “cancel out” variance observed in other samples when they are combined into a master population. If an increasing number of samples were combined to produce the pooled data, then the variance from the master population distribution will become asymptotically small and thus become a more accurate representation of the “true” distribution of the population of gold particles in the sediment.

An example of a line-up is shown in figure 2.11, using cumulative frequency plots in contrast to the histograms used by Buja et al. (2009). Due to the geometric difficulties of comparing multiple curves plotted separately as cumulative frequency plots, the test sample and decoy samples are all shown with a referenced population. The reference population chosen is the ‘master’ population used to create the bootstrap sub samples and this allows for finer distinctions to be visually recognised between graphs.

The visual line up method has several advantages over simple decision making by a single analyst. The main advantage is that by presenting the data to impartial observers, bias is removed as preconceptions about the results are unable to influence the result.

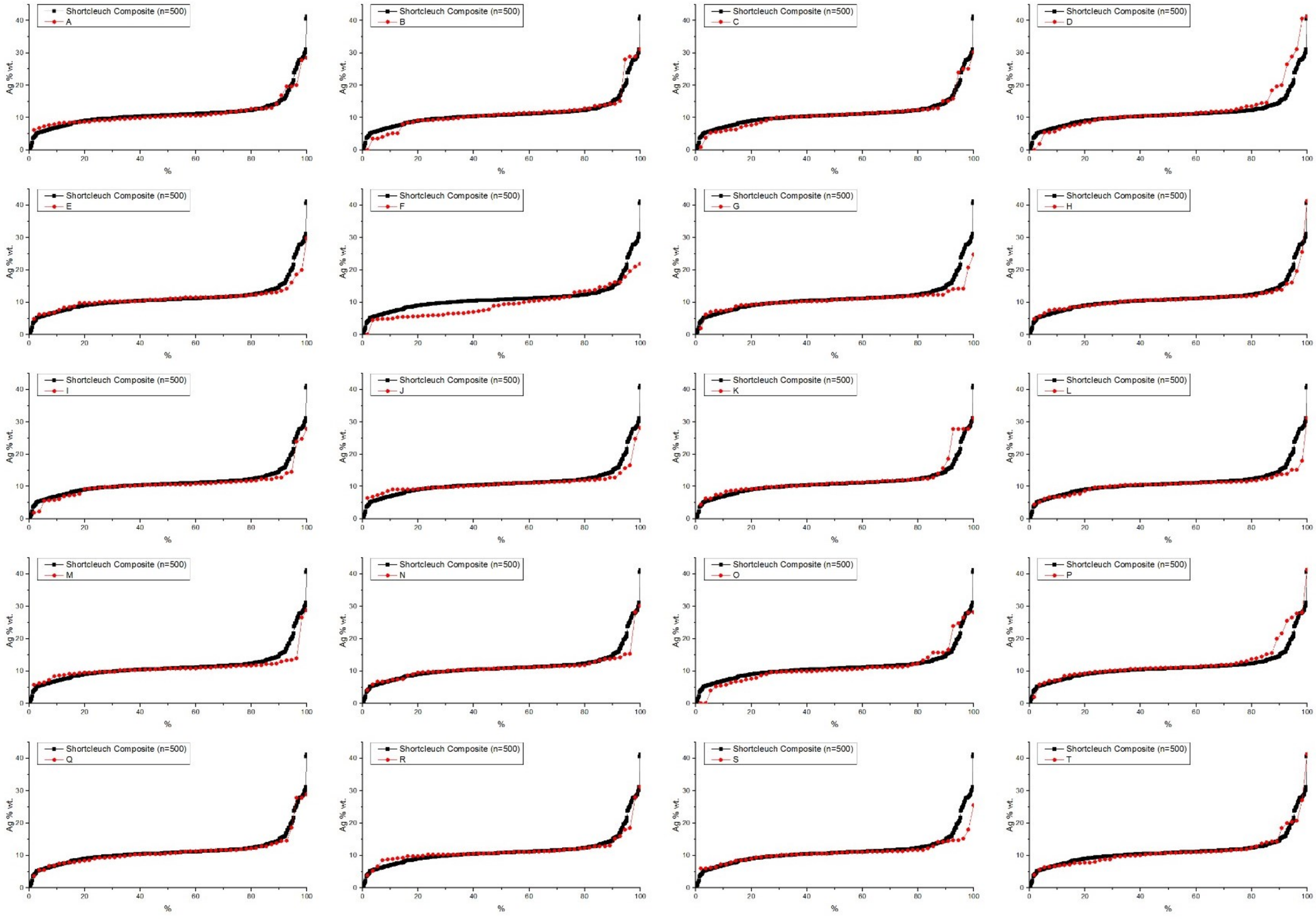

Figure 2.11 – A example of a Line up test using data from Leake, et al. (1998).

The question asked of the viewer is: Which sample (red line) is the most different from the black line and why? The black line is present in all the plots to allow comparisons accurately when viewing multiple plots. It is the population from which the synthetic samples were created.

2.2.4.2 Non-parametric tests

A different approach to test if two populations could be both drawn from a single master distribution is to use non-parametric mathematical tests which are designed to test statistical hypotheses. Non-parametric methods are appropriate as they do not require any assumption to be made about the distribution of the data during analyses. The Kolmogorov–Smirnov (K-S) test has been previously used for gold particle populations data by Pochon et al. (2021) and Utter (1979).

Two widely used non-parametric tests; the Mann–Whitney U (Mann-W) test and Kolmogorov–Smirnov (K-S) test, were selected to analyse the similarity between pairs of samples (Massey, 1951, Fagerland and Sandvik, 2009, Mann and Whitney, 1947). The null hypothesis for both of these tests is that; the observed variability between samples is the result of random sub-sampling of both populations from a single 'master' distribution of Ag values.

Both the tests measure the differences between populations using different statistical parameters. The principle of each test is described below and is applied to example data drawn from the literature to allow for discussion of the suitability of each test to detrital gold work. Both tests were conducted using the OroginPro statistical software package (version 9.1.0). The results from both the Mann-W and K-S tests are reported as p-values, thus they indicate the probability of obtaining test results at least as extreme as the results actually observed, assuming that the null hypothesis is correct. Therefore, the larger the p-value the greater the confidence in the null hypothesis being correct that the two populations could be produced from subsampling a single distribution.

The Mann–Whitney U test

This is a test that compares samples of unequal size and non-normal distributions by comparing the Mann-Whitney U statistic, which is derived from equation 2.2. The Mann-Whitney test is regarded as an effective test to identify significant differences in the mean, or medians, between non-normal populations, however it is documented that the robustness of the test decreases with increasing sample size differences, especially when the degree of skewness of the population is strong (Fagerland and Sandvik, 2009).

$$U = \sum_{i=1}^{n_1} r_{1i} - \frac{n_1(n_1+1)}{2}$$

Equation 2.2. Where: r_{1i} is the rank assigned to data in a sample (x_i) for $x_i = 1,2,\ldots\ldots,x_i$.

The Kolmogorov–Smirnov test

The Kolmogorov–Smirnov test compares a pair of samples through the quantification of the maximum distance (D) between the two cumulative frequency distributions of the samples. This is shown in figure 2.12, where the test statistic (D) is the separation distance in the X axis proportion of the population (given as a number, 0 to 1). The probability (p-value) is calculated by comparing the test statistic to the D values expected if the null hypothesis is true. Thus, the calculated p-value is the probability of generating a value of D as large as that observed through random chance, assuming the null hypothesis holds. The test is sensitive to differences in both location and shape of the empirical data within the cumulative distribution function and it has the advantage that the test can be simply understood, especially if the analyst is familiar with cumulative frequency distributions.

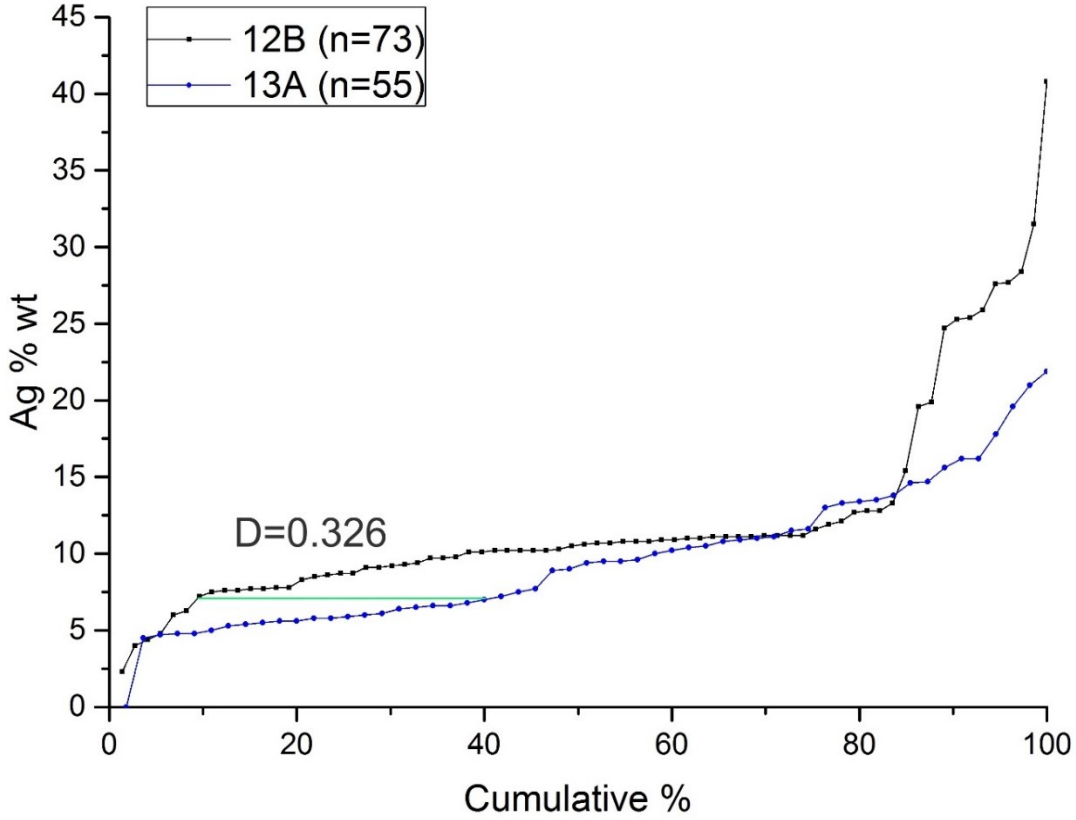

Figure 2.12 – Cumulative frequency plot of a pair of samples taken from Shortcleuch Leake et al. (1998) demonstrating how the K-S test D value can be visually displayed.

Pochon, et al. (2021) and Utter (1979) both used the K-S test on empirical datasets to compare between empirical distribution of elements in the alloy for populations of gold particles. The work by Pochon, et al. (2021) used a modified form the K-S testing from Gabler, et al. (2017) which uses multiple element comparisons simultaneously to test the origin of gold sourced from different mines to identify providence. They demonstrated their methods' effectiveness at discriminating between samples from different sources within French Guiana and presented it as a tool to identify suspect populations in the supply chain.

The modified K-S method of Gabler, et al. (2017) will not be used in this thesis as it relies on multiple elements in addition to the Au and Ag content. This has an advantage as it reports a critical D value which provides a better quantified assessment of how 'fit for purpose' a sample size is (Pochon et al., 2021). While Cu, S and Hg are observed in solid solution in gold alloys the low concentrations require impractical count times when collecting data on large numbers of particles using an electron microprobe (EMPA) (Banks et al.,

2018). Therefore, additional elements are best obtained by LA-ICP-MS analysis and because the majority of data, both published in the literature and generated in this project, is collected using EMPA, the uncertainties with additional minor traces makes the modified K-S method of Gabler, et al. (2017) impossible to robustly use.

2.2.4.2.3 Applying non-parametric tests to published empirical data

The use of empirical data is important as it provides an opportunity to present an example of how explorative data evaluation can be conducted using non-parametric testing. It is important to note that the statistical testing is a tool which must be used appropriately on good quality data and best practice would utilise it alongside other geological methods. It is to be noted that the original work by Leake, et al. (1997) used extensive geological knowledge of the area alongside other gold particle data, such as inclusions assemblages, to formulate their conclusions. To avoid complicating the example presented below, some aspects of the original work are not fully incorporated in this discussion. Therefore, the following discussion should be taken as an example of using statistical methods in an explorative data evaluation. It is not a review, or full re-evaluation, geologically of the study presented by Leake et al. (1997).

To assess and evaluate the comparative Mann-Whitney (Mann-W) and Kolmogorov–Smirnov (K-S) tests they are applied to an exemplar dataset from Shortcleuch Water. The results are shown in matrices, tables 2.2 and 2.3, which display the p-values between a pairs of field samples in a single table. A significance level of 0.05 was used for the testing and the table is coloured with cells highlighted red if the p-value was below this value.

Examining the results, the same overall patterns and relationships are seen in both the Mann-W and K-S tables although there are some differences. This demonstrates that differences in the tests does result in measurable differences in results for empirical gold particle compositional signature data. As was previously discussed above, the K-S test is sensitive to differences in both location and shape of the distributions whereas the Mann-W test is more sensitive to changes in mean or median values of the populations. The results support the statement that the K-S test, which has been used by Pochon et al. (2021), is more suitable than the Mann-W test for detrital gold studies because it more constantly provides rejection or acceptance of the null hypothesis when considering multiple pairs of samples.

Because the non-parametric tests only report a simplistic statistical result comparing the distribution of a parameter between two sample populations it

is important to consider the context of the samples geologically. The geological reasoning as to why two samples are tested to see if they contain comparable distributions must be considered. Because geological mineralization is complex two samples being different is only one piece of evidence which could contribute to the understanding of a study area.

Considering the results of the K-S tests on the Shortcleuch Water all these samples are from a single valley. So, comparing all the samples to see if they are comparable tests a geological hypothesis that they all contain gold from a single ‘system’. Examining the results of the Mann-W and K-S tests, tables 2.2, 2.3 and 2.4, it can be seen that the results of 8 samples indicate that they are not significantly different from each other, thus the null hypothesis cannot be rejected between any combination of the 8 samples. This, internally consistent, group of samples, which we will term the ‘main Shortcleuch (Sc) group’ contains samples 12A, 12B, 12D ,12J, 12K, 12M, 12Q and 12R. This group has distributions of gold particle composition which have variation (as measured by the K-S test between pairs) that is lower than would be expected in 95% of random sub-samples (of their individual size) taken from a single master distribution (a confidence level of 0.05).

Table 2.2 – Mann-Whitney test pairs matrix comparison, red cells indicate P value bellow 0.05.

Mann-W	12A (70)	12B (73)	12D (68)	12J (31)	12K (11)	12L (26)	12M (37)	12O (68)	12Q (11)	12R (26)	12S (22)	13A (55)
12A (70)												
12B (73)	0.531											
12D (68)	0.452	0.867										
12J (31)	0.624	0.966	0.994									
12K (11)	0.144	0.243	0.387	0.352								
12L (26)	0.119	0.076	0.035	0.097	0.039							
12M (37)	0.485	0.912	0.846	0.926	0.446	0.017						
12O (68)	0.317	0.168	0.117	0.242	0.068	0.540	0.098					
12Q (11)	0.615	0.662	0.804	0.875	0.577	0.561	0.873	0.440				
12R (26)	0.143	0.330	0.354	0.344	0.690	0.026	0.442	0.030	0.642			
12S (22)	0.198	0.130	0.096	0.141	0.054	0.909	0.061	0.739	0.606	0.040		
13A (55)	0.010	0.022	0.057	0.079	0.705	0.018	0.117	0.003	0.419	0.433	0.023	

Table 2.3 – Kolmogorov-Smirnov test pairs matrix comparisons. Red cells indicate P value bellow 0.05. For all sample (top) and the main group of 8 samples only (bottom).

K-S	12A (70)	12B (73)	12D (68)	12J (31)	12K (11)	12L (26)	12M (37)	12O (68)	12Q (11)	12R (26)	12S (22)	13A (55)
12A (70)												
12B (73)	0.288											
12D (68)	0.683	0.941										
12J (31)	0.636	0.637	0.971									
12K (11)	0.255	0.417	0.308	0.310								
12L (26)	0.035	0.011	0.005	0.264	0.023							
12M (37)	0.253	0.448	0.465	0.424	0.180	0.001						
12O (68)	0.107	0.046	0.073	0.208	0.159	0.632	0.013					
12Q (11)	0.255	0.680	0.308	0.310	0.833	0.227	0.180	0.257				
12R (26)	0.065	0.622	0.245	0.313	0.826	0.089	0.166	0.075	0.401			
12S (22)	0.094	0.037	0.043	0.124	0.087	0.931	0.005	0.758	0.271	0.112		
13A (55)	0.001	0.002	0.004	0.016	0.456	0.007	0.003	0.000	0.544	0.130	0.010	

K-S	12A (70)	12B (73)	12D (68)	12J (31)	12K (11)	12M (37)	12Q (11)	12R (26)
12A (70)								
12B (73)	0.288							
12D (68)	0.683	0.941						
12J (31)	0.636	0.637	0.971					
12K (11)	0.255	0.417	0.308	0.310				
12M (37)	0.253	0.448	0.465	0.424	0.180			
12Q (11)	0.255	0.680	0.308	0.310	0.833	0.180		
12R (26)	0.065	0.622	0.245	0.313	0.826	0.166	0.401	

Table 2.4 – Matrix of samples showing pairs the were identified as significantly different by one (or both) non-parametric tests

	12A (70)	12B (73)	12D (68)	12J (31)	12K (11)	12L (26)	12M (37)	12O (68)	12Q (11)	12R (26)	12S (22)	13A (55)
12A (70)												
12B (73)												
12D (68)												
12J (31)												
12K (11)												
12L (26)	KS	KS	BOTH	KS	BOTH							
12M (37)						BOTH						
12O (68)		KS					KS					
12Q (11)												
12R (26)						MW		MW				
12S (22)		KS	KS				KS			MW		
13A (55)	BOTH	BOTH	KS	KS		BOTH	KS	BOTH			BOTH	

The main Sc group of samples is shown visually in figure 2.13 in comparison to each other and to a composite population of all the gold particles in the 'main group' of samples. This produces a continuous distribution covering a wide range of composition from 0 to 40 % wt. Ag with a clear majority of the gold particles between 8-12% Ag and significant low and high silver tails to the distribution.

The remaining samples, samples 12L, 12O, 12S and 12A, from Shortcleuch Water are identified by the K-S testing as significantly different to the main Sc group of 8 samples. However, it is important to note that the comparative K-S testing of the 4 samples against the main group of samples is not definitive and interpretation whilst also considering the geology is required. The comparisons of sample 12L and 12O illustrate how the results require interpretation and is presented as an example in the following paragraph.

The sample 12L is determined to be different to 6 out the 8 samples in the core Sc group. This means that 12L cannot be stated as significantly different to two of the samples in the main group of samples, samples 12Q and 12R. If all the samples in the main group are considered to be sourced from a single master population, the question is how can the signature of 12L be comparable to some of the group and not others? The answer is that the K-S testing result between samples is conducted in a way that intrinsically adjusts the comparison in relation to the sample sizes. When the sizes of the samples are considered, it is noted that 12L (26 particles) is not significantly different from samples 12 Q (11 particles) and 12R (26 particles). Therefore, the result of the K-S test (that the differences between the samples are not significantly larger than the expected variation which could be expected if both samples were subsampled from a single population) can be interpreted as showing that the sample size is too small to enable meaningful comparisons. In other words, a sample which contains such a small number of gold particles is expected to be affected strongly by random chance and if repeat samples of such a size were collected, they would show noticeable variation in the signatures.

Sample 12O is one of the largest samples (containing 68 particles) so the result that it may be significantly different must be given careful consideration geologically as sample size issues are unlikely to be the reason. Presenting the results in a matrix format allows multiple samples to be compared to each other and stochastic interrelationships between all samples considered in borderline cases. When this is done it is noted that of the K-S results for three out of the four samples (12O, 12S and 12L) that are different from the main Sc

group, form a second internally consistent group which cannot be determined as significantly different from each other, See tables 2.4, 2.5 and figure 2.15. If these samples were spatially linked and related it could be concluded that they represent a different source, however they are not spatially related and occur interspersed with the other samples. Therefore, a different geologically appropriate explanation is needed. This could either be due to local changes or variations in the mineralising system that produced the main group, or due to a minor addition of separate gold sources to the signature of the main Sc group.

The only sample in the Shortcleuch data which can be identified as individually unique and having a different distribution from all the other samples is sample 13A, figure 2.14. Sample 13A is the highest sample upstream from the others, therefore being different from the others is geologically plausible and can be explained by being outside the catchment of the system that formed the main Sc group signature (Leake et al., 1998).

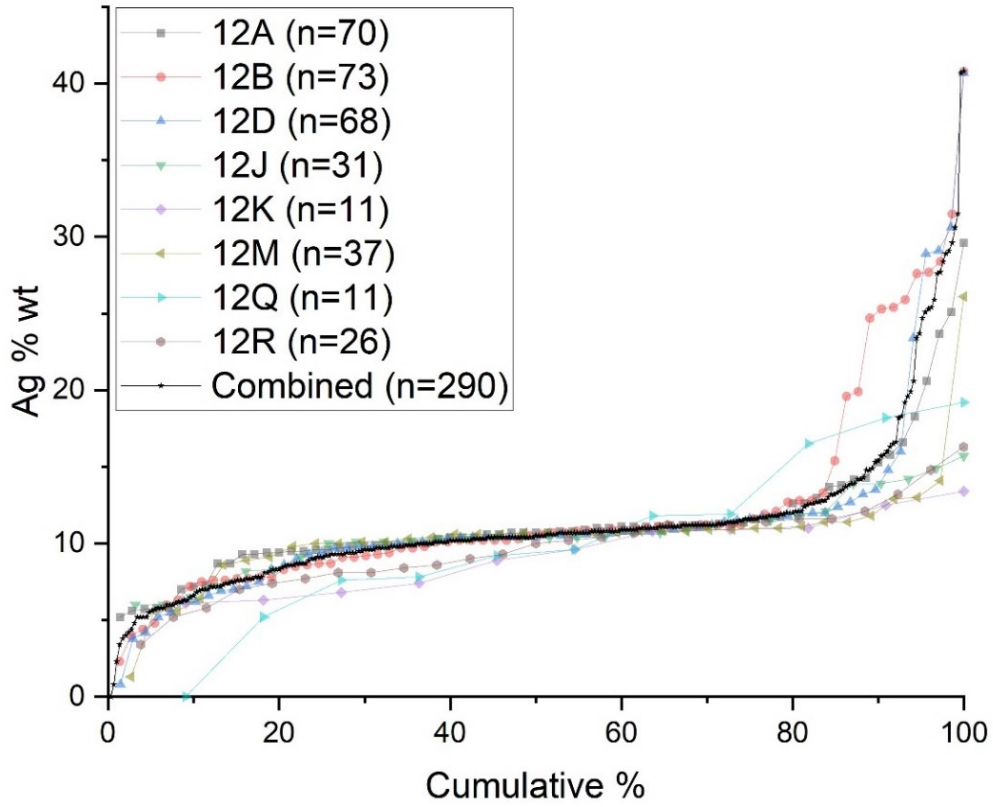

Figure 2.13 – Main group of 8 samples identified as not significantly different plotted with the distribution of the composite population created by combining all the gold particles in the 8 field samples in the main group.

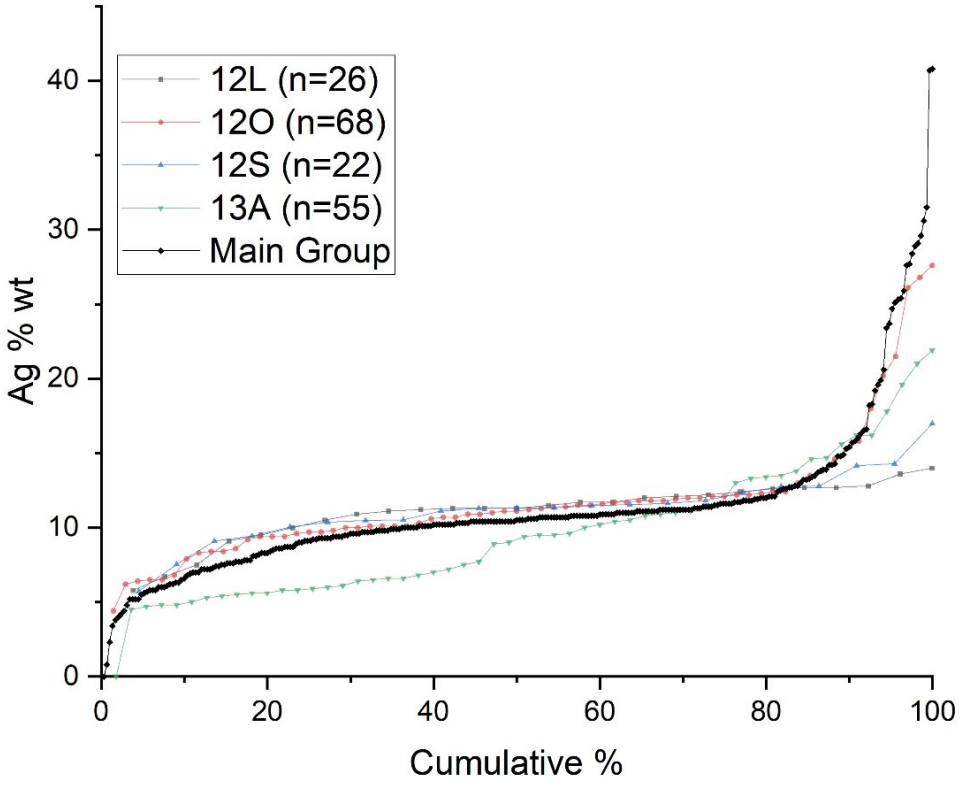

Figure 2.14 – The composition main group of samples compared to the 4 samples which were identified as significantly different by the K-S tests.

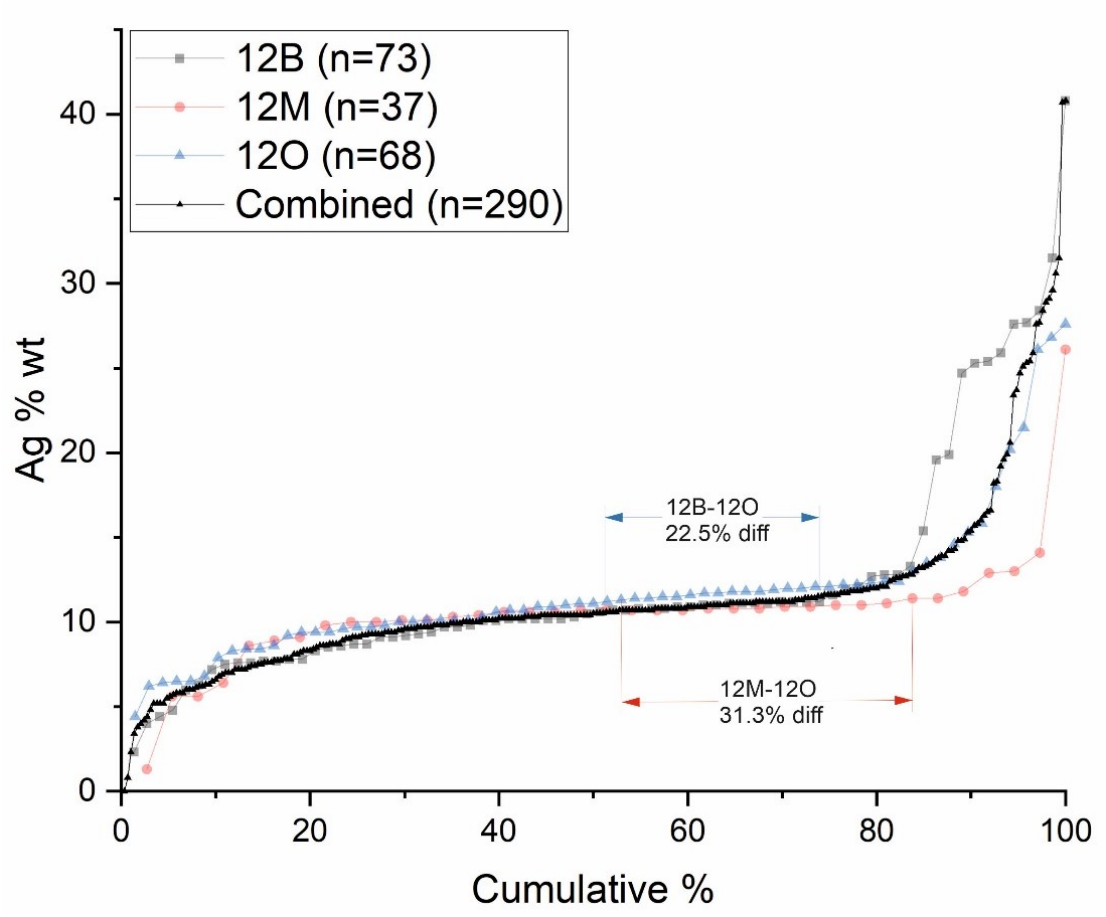

Figure 2.15 – A Cumulative frequency plot visualising the K-S test metric between sample 12O and the two "main group samples" it is identified as significantly different from. The K-S test measure (largest proportional distance difference between the curves a constant Ag) is shown for both the 12B-12O and 12M-12O pairs.

Table 2.5 — A matrix plot of the K-S test pairs P-values

	12L (26)	12O (68)	12S (22)	13A (55)
12L (26)				
12O (68)	0.632			
12S (22)	0.931	0.758		
13A (55)	0.007	0.000	0.010	

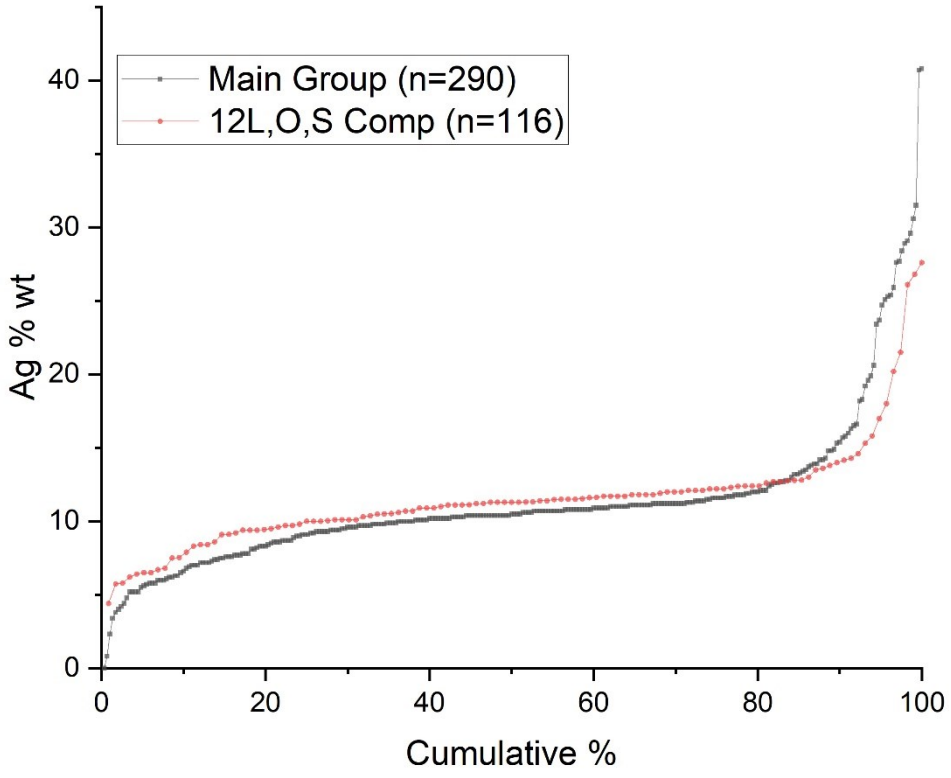

Figure 2.16 – Cumulative frequency plots of the two composite samples created from the Shortcleuch Water samples set.

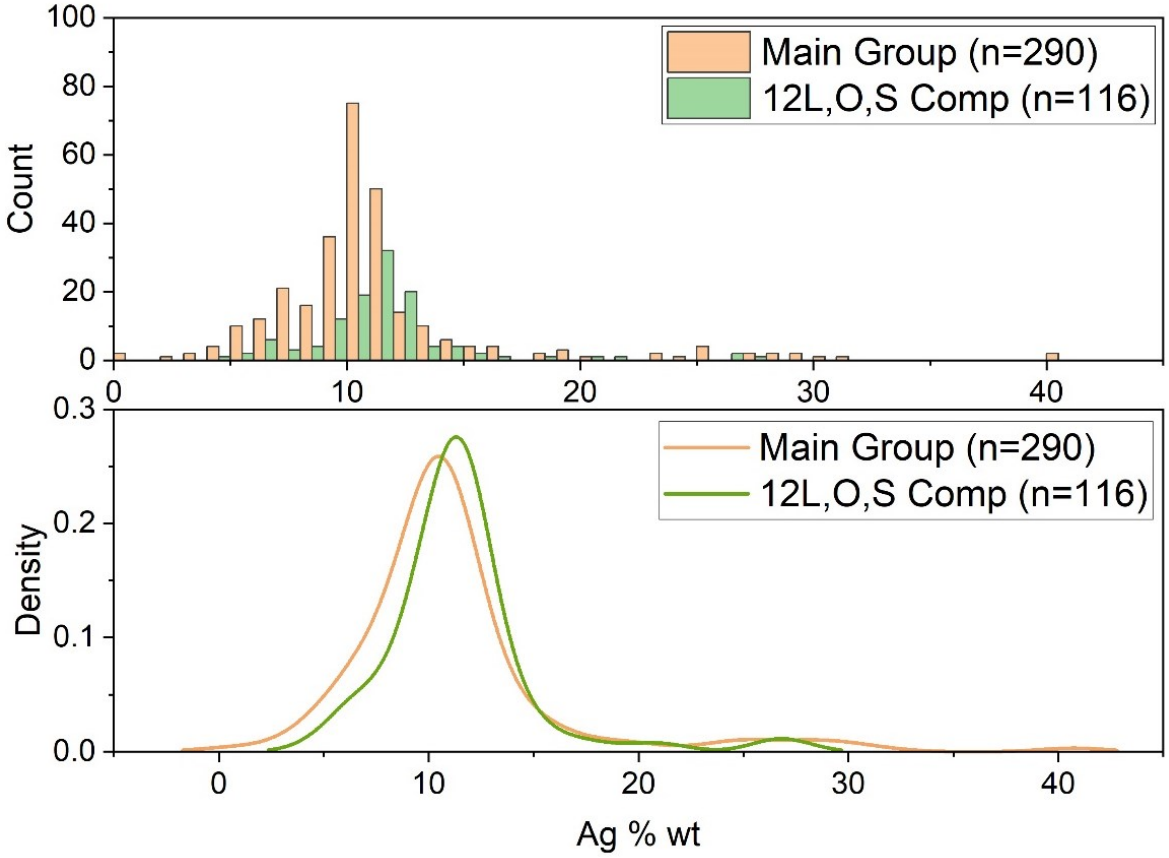

Figure 2.17 – Histograms (top) and normalised distributional curves (bottom) of the two composite samples created from the Shortcleuch Water samples. Using 1% bins.

2.5 Conclusions

A review of published literature of compositional signatures of detrital gold has considered the sources of error and uncertainty in detrital gold studies. The available evidence suggests that differentiation of gold particles due to their composition is not significant in surficial transport and sample collection (see discussions in chapter 1). Therefore, the observed compositional signature of gold particle populations should reflect the compositions of gold particles eroded into the catchment volume corresponding to a sample location.

The application of non-parametric statistical tests, specifically the Kolmogorov–Smirnov test, has significant advantages in data appraisal for detrital gold studies over current methods, and is simple to implement on large datasets. This is in agreement with the work of Pochon, et al. (2021) who advocated using K-S tests as part of a holistic comparison of the properties of gold from different mines in French Guiana.

Work applying the K-S test to empirical data shows that the statistical methods factor in sample size issues when testing the hypothesis; that two samples could have been sub-sampled from a single master population. Because of this, bigger differences between two sample's distributions are needed for smaller samples than for larger samples in order to identify, statistically significantly (i.e. having a very low probability of the difference occurring due to random chance), that two populations are not sourced from a single master population. Because the K-S test hypothesises that the samples are sourced from a comparable master population, care must be taken when applying it to empirical data because inappropriately small sample sizes will always result in the K-S test returning a result that there is a statistical chance they are sampled from a single master population. If the sample size is not taken into account, it is possible that inappropriate conclusions may be drawn from this K-S test result. This is especially problematic if undue weighting is given to the statistical test (because it produces a clear, easy to understand result) above additional information, observations and geological constraints, during the formulation of interpretations and conclusions.

The uses of non-parametric statistical methods therefore require suitably large sample sizes to address a specific research question. If the sample size is large enough, then these methods are a highly effective tool for robustly comparing two detrital gold populations without inherent bias. Therefore K-S testing will

be used alongside other traditional methods in this study to investigate and contrast between empirical compositional data sets.

Having a robust methodology to analyse the alloy compositions of gold particles in sample populations is important as other techniques such as inclusion assemblages, or trace elements in the alloy are not always possible because they may not be present or practical to measure. The composition of Au and Ag in a gold particles's alloy is reliable, repeatable and obtainable for any gold particle and so can be used on any gold particle sample. Therefore, understanding the Au/Ag ratio of golds alloy, and especially the distribution of Au/Ag alloy ratios in natural populations, has the potential to impact a wide range of detrital gold and mineralisation studies.

References

ALAM, M., LI, S.-R., SANTOSH, M. & YUAN, M.-W. 2019. Morphology and chemistry of placer gold in the Bagrote and Dainter streams, northern Pakistan: Implications for provenance and exploration. *Geological Journal,* 54**,** 1672-1687.

ANDERSEN, T. 2005. Detrital zircons as tracers of sedimentary provenance: limiting conditions from statistics and numerical simulation. *Chemical Geology,* 216**,** 249-270.

BANKS, D. A., CHAPMAN, R. & SPENCE-JONES, C. 2018. Detrital gold as a deposit-specific indicator mineral by LAICP-MS analysis. *Geoscience BC Report (project 2016-006).*

BOUZARI, F., HART, C., BARKER, S. & BISSIG, T. 2011. Porphyry indicator minerals (PIMS): A new exploration tool for concealed deposits in south-central British Columbia. *Geoscience BC Report,* 17**,** 1-31.

BOYLE, R. W. 1979. The geochemistry of gold and its deposits (together with a chapter on geochemical prospecting for the element). *Geological Survey of Canada, Bulletin,* 280.

BUJA, A., COOK, D., HOFMANN, H., LAWRENCE, M., LEE, E. K., SWAYNE, D. F. & WICKHAM, H. 2009. Statistical inference for exploratory data analysis and model diagnostics. *Philos Trans A Math Phys Eng Sci,* 367**,** 4361-83.

CARLING, P. A. & BREAKSPEAR, R. M. D. 2006. Placer formation in gravel-bedded rivers: A review. *Ore Geology Reviews,* 28**,** 377-401.

CHAPMAN, R., BANKS, D. A. & SPENCE-JONES, C. 2017. Detrital gold as a deposit-specific indicator mineral, British Columbia: analysis by laser-ablation inductively coupled plasma–mass spectrometry. *Geoscience BC Summary of Activities 2016.* Geoscience BC.

CHAPMAN, R., COOK, M., GRIMSHAW, M. & MYLES, S. 2016. Placer-lode gold relationships in the Nansen placer district, Yukon. *Yukon Exploration and Geology*.

CHAPMAN, R. J., ALLAN, M. M., MORTENSEN, J. K., WRIGHTON, T. M. & GRIMSHAW, M. R. 2018. A new indicator mineral methodology based on a generic Bi-Pb-Te-S mineral inclusion signature in detrital gold from porphyry and low/intermediate sulfidation epithermal environments in Yukon Territory, Canada. *Mineralium Deposita,* 53**,** 815-834.

CHAPMAN, R. J., BANKS, D. A., STYLES, M. T., WALSHAW, R. D., PIAZOLO, S., MORGAN, D. J., GRIMSHAW, M. R., SPENCE-JONES, C. P., MATTHEWS, T. J. & BOROVINSKAYA, O. 2021. Chemical and physical heterogeneity within native gold: implications for the design of gold particle studies. *Mineralium Deposita*.

CHAPMAN, R. J., LEAKE, R. C., BOND, D. P. G., STEDRA, V. & FAIRGRIEVE, B. 2009. Chemical and Mineralogical Signatures of Gold Formed in Oxidizing Chloride Hydrothermal Systems and their Significance within Populations of Placer Gold Grains Collected during Reconnaissance. *Economic Geology,* 104**,** 563-585.

CHAPMAN, R. J., LEAKE, R. C. & MOLES, N. R. 2000. The use of microchemical analysis of alluvial gold grains in mineral exploration: experiences in Britain and Ireland. *Journal of Geochemical Exploration,* 71**,** 241-268.

CHAPMAN, R. J. & MORTENSEN, J. K. 2016. Characterization of Gold Mineralization in the Northern Cariboo Gold District, British Columbia, Canada, Through Integration of Compositional Studies of Lode and Detrital Gold with Historical Placer Production: A Template for Evaluation of Orogenic Gold. *Economic Geology,* 111**,** 1321-1345.

CHAPMAN, R. J., MORTENSEN, J. K., CRAWFORD, E. C. & LEBARGE, W. 2010. Microchemical Studies of Placer and Lode Gold in the Klondike District, Yukon, Canada: 1. Evidence for a Small, Gold-Rich, Orogenic Hydrothermal System in the Bonanza and Eldorado Creek Area. *Economic Geology,* 105**,** 1369-1392.

CRAW, D., HESSON, M. & KERR, G. 2017. Morphological evolution of gold nuggets in proximal sedimentary environments, southern New Zealand. *Ore Geology Reviews,* 80**,** 784-799.

CRAWFORD, E. C. 2007. *Klondike placer gold : new tools for examining morphology, composition and crystallinity.* Text.
DOMGMO, F. W. CHAPMAN, R. J. BOLARINWA, A. T. YONGUE, R. F. BANKS, D. A. OLAJIDE-KAYODE, J. O. Microchemical characterization of placer gold grains from the Meyos-Essabikoula area, Ntem complex, southern Cameroon. Journal of African Earth Sciences. 2019 Mar 1;151:189-201.
EFRON, B. 1992. Bootstrap Methods: Another Look at the Jackknife. *In:* KOTZ, S. & JOHNSON, N. L. (eds.) *Breakthroughs in Statistics: Methodology and Distribution.* New York, NY: Springer New York.
EYLES, N. & KOCSIS, S. P. 1989. Sedimentological controls on gold in a late Pleistocene glacial placer deposit, Cariboo Mining District, British Columbia, Canada. *Sedimentary Geology,* 65**,** 45-68.
FAGERLAND, M. W. & SANDVIK, L. 2009. The Wilcoxon-Mann-Whitney test under scrutiny. *Stat Med,* 28**,** 1487-97.
FISHER, N. H. 1945. The fineness of gold, with special reference to the Morobe gold field, New Guinea. *Economic Geology,* 40**,** 449-495.
GABLER, H. E., SCHINK, W., GOLDMANN, S., BAHR, A. & GAWRONSKI, T. 2017. Analytical Fingerprint of Wolframite Ore Concentrates. J Forensic Sci, 62, 881-888.
GAMMONS, C. H. & WILLIAMS-JONES, A. E. 1995. Hydrothermal Geochemistry of Electrum - Thermodynamic Constraints. *Economic Geology and the Bulletin of the Society of Economic Geologists,* 90**,** 420-432.
GAROFALO, P. S. & RIDLEY, J. R. 2014. Gold-transporting hydrothermal fluids in the Earth's crust: an introduction. *Geological Society, London, Special Publications,* 402**,** 1-7.
GAS'KOV, I. V. 2017. Major impurity elements in native gold and their association with gold mineralization settings in deposits of Asian folded areas. *Russian Geology and Geophysics,* 58**,** 1080-1092.
GIRARD, R., TREMBLAY, J., NÉRON, A. & LONGUÉPÉE, H. 2021. Automated Gold Grain Counting. Part 1: Why Counts Matter! *Minerals,* 11**,** 337.
GOLDFARB, R. J. & GROVES, D. I. 2015. Orogenic gold: Common or evolving fluid and metal sources through time. *Lithos,* 233**,** 2-26.
GOLDFARB, Y. I. 2007. Dynamic classification of alluvial gold placers in the northeast of Russia. *Geology of Ore Deposits,* 49**,** 241-270.
HANNINGTON, M., HARÐARDÓTTIR, V., GARBE-SCHÖNBERG, D. & BROWN, K. L. 2016. Gold enrichment in active geothermal systems by accumulating colloidal suspensions. *Nature Geoscience,* 9**,** 299-302.
HEINRICH, C. 2005. The physical and chemical evolution of low-salinity magmatic fluids at the porphyry to epithermal transition: a thermodynamic study. *Mineralium Deposita,* 39**,** 864-889.
JAMES, C. S. & MINTER, W. E. L. 1999. Experimental flume study of the deposition of heavy minerals in a simulated Witwatersrand sandstone unconformity. *Economic Geology,* 94**,** 671-688.
KNIGHT, J. B., MORISON, S. R. & MORTENSEN, J. K. 1999a. The relationship between placer gold particle shape, rimming, and distance of fluvial transport as exemplified by gold from the Klondike district, Yukon Territory Canada. *Economic Geology and the Bulletin of the Society of Economic Geologists,* 94**,** 635-648.
KNIGHT, J. B., MORTENSEN, J. K. & MORISON, S. R. 1999b. Lode and placer gold composition in the Klondike district, Yukon Territory Canada: Implications for the nature and genesis of Klondike placer and lode gold deposits. *Economic Geology and the Bulletin of the Society of Economic Geologists,* 94**,** 649-664.
KRAUT, J. C. & STERN, W. B. 2000. The density of gold-silver-copper alloys and its calculation from the chemical composition. *Gold Bulletin,* 33**,** 52-55.
LARGE, R. & MASLENNIKOV, V. 2020. Invisible Gold Paragenesis and Geochemistry in Pyrite from Orogenic and Sediment-Hosted Gold Deposits. *Minerals,* 10**,** 339.

LEAKE, R. C. & BLAND, D. J. 1992. Internal compositional variation and mineral inclusions within gold as a means of source characterisation. *British Geological Survey Technical Report WG/92/47*.

LEAKE, R. C., CHAPMAN, R. J., BLAND, D. J., CONDLIFFE, E. & STYLES, M. T. 1997. Microchemical characterization of alluvial gold from Scotland. *Transactions of the Institution of Mining and Metallurgy Section B-Applied Earth Science,* 106**,** B85-B98.

LEAKE, R. C., CHAPMAN, R. J., BLAND, D. J., STONE, P., CAMERON, D. G. & STYLES, M. T. 1998. The origin of alluvial gold in the Leadhills area of Scotland: evidence from interpretation of internal chemical characteristics. *Journal of Geochemical Exploration,* 63**,** 7-36.

LIU, H. & BEAUDOIN, G. 2021. Geochemical signatures in native gold derived from Au-bearing ore deposits. *Ore Geology Reviews,* 132**,** 104066.

LIU, H., BEAUDOIN, G., MAKVANDI, S., JACKSON, S. E. & HUANG, X. 2021. Multivariate statistical analysis of trace element compositions of native gold from orogenic gold deposits: Implication for mineral exploration. *Ore Geology Reviews,* 131**,** 104061.

MANN, H. B. & WHITNEY, D. R. 1947. On a Test of Whether one of Two Random Variables is Stochastically Larger than the Other. *The Annals of Mathematical Statistics,* 18**,** 50-60.

MASSEY, F. J. 1951. The Kolmogorov-Smirnov Test for Goodness of Fit. *Journal of the American Statistical Association,* 46**,** 68-78.

MCCLENAGHAN, M. B. 2011. Overview of common processing methods for recovery of indicator minerals from sediment and bedrock in mineral exploration. *Geochemistry-Exploration Environment Analysis,* 11**,** 265-278.

MELCHIORRE, E. B. & HENDERSON, J. 2019. Topographic gradients and lode gold sourcing recorded by placer gold morphology, geochemistry, and mineral inclusions in the east fork San Gabriel River, California, U.S.A. *Ore Geology Reviews,* 109**,** 348-357.

MOLES, N. R. & CHAPMAN, R. J. 2019. Integration of Detrital Gold Microchemistry, Heavy Mineral Distribution, and Sediment Geochemistry to Clarify Regional Metallogeny in Glaciated Terrains: Application in the Caledonides of Southeast Ireland. Economic Geology, 114, 207-232.

MORRISON, G. W., ROSE, W. J. & JAIRETH, S. 1991. Geological and geochemical controls on the silver content (fineness) of gold in gold-silver deposits. *Ore Geology Reviews,* 6**,** 333-364.

OBERTHUR, T., WEISER, T., AMANOR, J. A. & CHRYSSOULIS, S. L. 1997. Mineralogical siting and distribution of gold in quartz veins and sulfide ores of the Ashanti mine and other deposits in the Ashanti belt of Ghana: Genetic implications. *Mineralium Deposita,* 32**,** 2-15.

OLIVO, G. R., GAUTHIER, M., BARDOUX, M., LEAO DE SA, E., FONSECA, J. T. F. & SANTANA, F. C. 1995. Palladium-bearing gold deposit hosted by Proterozoic lake superior-type iron-formation at the Caue iron mine, Itabira District, southern Sao Francisco Craton, Brazil; geologic and structural controls. *Economic Geology,* 90**,** 118-134.

OMANG, B. O., SUH, C. E., LEHMANN, B., VISHITI, A., CHOMBONG, N. N., FON, A. N., EGBE, J. A. & SHEMANG, E. M. 2015. Microchemical signature of alluvial gold from two contrasting terrains in Cameroon. *Journal of African Earth Sciences,* 112**,** 1-14.

OZOLIŅŠ, V., WOLVERTON, C. & ZUNGER, A. 1998a. Cu-Au, Ag-Au, Cu-Ag, and Ni-Au intermetallics: First-principles study of temperature-composition phase diagrams and structures. *Physical Review B,* 57**,** 6427-6443.

OZOLIŅŠ, V., WOLVERTON, C. & ZUNGER, A. 1998b. First-principles theory of vibrational effects on the phase stability of Cu-Au compounds and alloys. *Physical Review B,* 58**,** R5897-R5900.

PALYANOVA, G. A. 2020. Gold and Silver Minerals in Sulfide Ore. *Geology of Ore Deposits,* 62**,** 383-406.
PETRELLA, L., THÉBAUD, N., FOUGEROUSE, D., EVANS, K., QUADIR, Z. & LAFLAMME, C. 2020. Colloidal gold transport: a key to high-grade gold mineralization? *Mineralium Deposita,* 55**,** 1247-1254.
POCHON, A., DESAULTY, A.-M., BAILLY, L. & LACH, P. 2021. Challenging the traceability of natural gold by combining geochemical methods: French Guiana example. *Applied Geochemistry,* 129**,** 104952.
POKROVSKI, G. S., AKINFIEV, N. N., BORISOVA, A. Y., ZOTOV, A. V. & KOUZMANOV, K. 2014. Gold speciation and transport in geological fluids: insights from experiments and physical-chemical modelling. *Geological Society, London, Special Publications,* 402.
POKROVSKI, G. S., TAGIROV, B. R., SCHOTT, J., BAZARKINA, E. F., HAZERMANN, J. L. & PROUX, O. 2009. An in situ X-ray absorption spectroscopy study of gold-chloride complexing in hydrothermal fluids. *Chemical Geology,* 259**,** 17-29.
SPENCE-JONES, C. 2013. *Metallurgical Investigation of the Ore at the Cononish Gold Mine, Scotland.* MGeol Masters, Univeristy of Leicester.
TERAKURA, K., OGUCHI, T., MOHRI, T. & WATANABE, K. 1987. Electronic theory of the alloy phase stability of Cu-Ag, Cu-Au, and Ag-Au systems. *Physical Review B,* 35**,** 2169-2173.
THEOBALD JR, P. K. 1957. The gold pan as a quantitative geologic tool. *Bulletin.* - ed.
TOWNLEY, B. K., HÉRAIL, G., MAKSAEV, V., PALACIOS, C., PARSEVAL, P. D., SEPULVEDA, F., ORELLANA, R., RIVAS, P. & ULLOA, C. 2003. Gold grain morphology and composition as an exploration tool: application to gold exploration in covered areas. *Geochemistry: Exploration, Environment, Analysis,* 3**,** 29-38.
UTTER, T. 1979. The morphology and silver content of gold from the Upper Witwatersrand and Ventersdorp Systems of the Klerksdorp gold field, South Africa. *Economic Geology,* 74**,** 27-44.
WICKHAM, H., COOK, D., HOFMANN, H. & BUJA, A. 2010. Graphical inference for infovis. *IEEE Transactions on Visualization and Computer Graphics,* 16**,** 973-979.
WILKINSON, J., BOYCE, A., EARLS, G. & FALLICK, A. 1999. Gold remobilization by low-temperature brines; evidence from the Curraghinalt gold deposit, Northern Ireland. *Economic Geology,* 94**,** 289-296.
WRIGHTON, T. M. 2013. *Placer gold microchemical characterization and shape analysis applied as an exploration tool in western Yukon.* Msc, Univeristy of British Columbia.

Chapter 3
Mineralisation at the Cononish gold mine, Scotland

Summary

This chapter presents a characterisation of lode gold vein deposit to facilitate a comparison between gold particles within a deposit and detrital populations (which will be presented in chapter 4.) Observations are focused on linking vein mineralogy, textures and relationships to the chemical properties of gold particles in the deposit volume.

A synthesis of published studies of the Cononish deposit with observations taken as part of this PhD project is presented. These further develop the known characterisation of the deposit, specifically the interpreted paragenesis, by providing additional observations and cathode-luminescence techniques, which have not previously been used to investigate the ore deposit. This provides the best possible characterisation of the veins in the deposit and a correlation between the paragenesis and gold particles which indicates evolving geochemical conditions of the mineralising system.

Additionally, it presents the results from a sample of free gold particles taken from the gravity concentration tables of the processing plant at the mine. This sample represents a sub sample of gold particles in the ore which provides a characterisation of the population of gold particles in the ore system. This is combined with the paragenesis work to provide an estimate of the proportion of gold particles derived from individual vein stages of the paragenesis, thereby allowing identification of the premier auriferous vein stages.

3.1 Introduction

This chapter presents work undertaken at the Cononish gold mine in Scotland. The aim of the study was to review and expand on the knowledge of the auriferous mineralisation that forms the Cononish deposit. This provides a characterisation of the in-situ mineralisation enabling subsequent examination of the relationship between the lode gold and the detrital gold population.

In general, paragenetic diagrams present generalisations of veins and bodies of rock to separate and define mineral assemblages in a few very simplified groupings. These often group generations of a vein development into a single assemblage, with sub-divisions created where sharp boundaries or crosscutting relationships can be observed. As such, many deposits have very simple paragenetic diagrams (if they exist at all) which typically represent major events effecting the primary 'host' lithologies and major time periods when epigenetic processes (such as ore precipitation, or secondary weathering) occurred (eg.Kamilli, 1998).

Simple parageneses are typically presented on a deposit scale. Many examples are published in reviews and classifications of orogenic gold deposits where a deposit is represented by a single mineral assemblage (Mueller and Groves, 1991, Vearncombe, 1993, Robert and Poulsen, 1997, Goldfarb et al., 2001, Groves et al., 2003, Phillips and Powell, 2015). While these can be used for broad distinctions between very different systems, they lack the temporal complexity and detail that has been documented within many mesothermal auriferous systems. The lack of mineralogical detail and the over-simplification of auriferous systems (which does not consider them as unstable or evolving events) are potentially critical hurdles in interpreting the fundamental underlying processes in the formation of ore systems and developing predictive models.

Studies examining finer temporal relationships (such as the work of Large and Maslennikov (2020) which reported gold deportment within the growth bands of single pyrite crystals), demonstrate the power to resolve changes in the chemical and physical conditions of ore fluid on the scale of a single depositional event down to the scale of a single crystal. However, the long-standing challenge within the geosciences is to integrate observations over a wide range of scales. The aim is to develop the ability to extrapolate over many orders of magnitude from outcrop or smaller scale observations. However, at present analytical technologies focused on microscale observations, such as mineralogical observations of ores in thin section, have outpaced larger scale

(whole deposit) studies. This has created a significant gap between our knowledge of gold deposits on a millimetre scale and our knowledge of the same systems on a deposit scale. The extrapolation of such highly detailed millimetre scale paragenesis to deposit/ore system scale offers significant potential for advancement and could result in greater understanding of the chemical (in)stability of ore deposition from fluids in mineralising systems.

3.2 The Cononish gold deposit

In order to understand the deposit and allow discussion of processes that contributed to the formation of the Cononish deposit, the following section introduces the geological background and setting of the deposit. It includes a summary of the geological units, structures and tectonic setting of the Cononish deposit which are published in the literature.

3.2.1 Deposit Geological setting

The Cononish mine is located in the Grampian terrane of Scotland 3km west of the village of Tyndrum. The Grampian terrane, part of the Appalachian-Caledonian orogenic belt, consists of Neoproterozoic Dalradian Supergroup metasediments and is divided, from the base upwards, into the Grampian, Appin, Argyll, Southern Highland and Trossachs groups (Tanner, 2012, Stephenson et al., 2013b). The Dalradian supergroup was deposited in a shallow to deep marine setting during the formation of the Iapetus Ocean between >750Ma to approximately 512 Ma, though uncertainties exist about the exact timing of deposition (Rooney et al., 2011).

In the Tyndrum area Neoproterozoic Dalradian Supergroup metasediments, see figure 3.1, were subjected to multiple metamorphic events. These are summarised in figure 3.2. The peak metamorphism occurred at approximately 470 Ma and subjected the sequence to amphibolite–grade as part of the Grampian Orogeny (Stephenson et al., 2013a). This event produced extensive deformation (D_1–D_4) which produced nappe structures, locally overturning large areas of the stratigraphy, with the Cononish deposit located on the upper limb of Beinn Chuirn Anticline (one of the large nappe structures). The nappes are dissected by later major NE–trending sinistral faults which are documented to have early sinistral and later normal component of displacement (Tanner, 2012, Stephenson et al., 2013b). A geological map of the area shows the

spatial relationship of these features, figure 3.1, and the geological history of the area is summarised in figure 3.2 and figure 3.3.

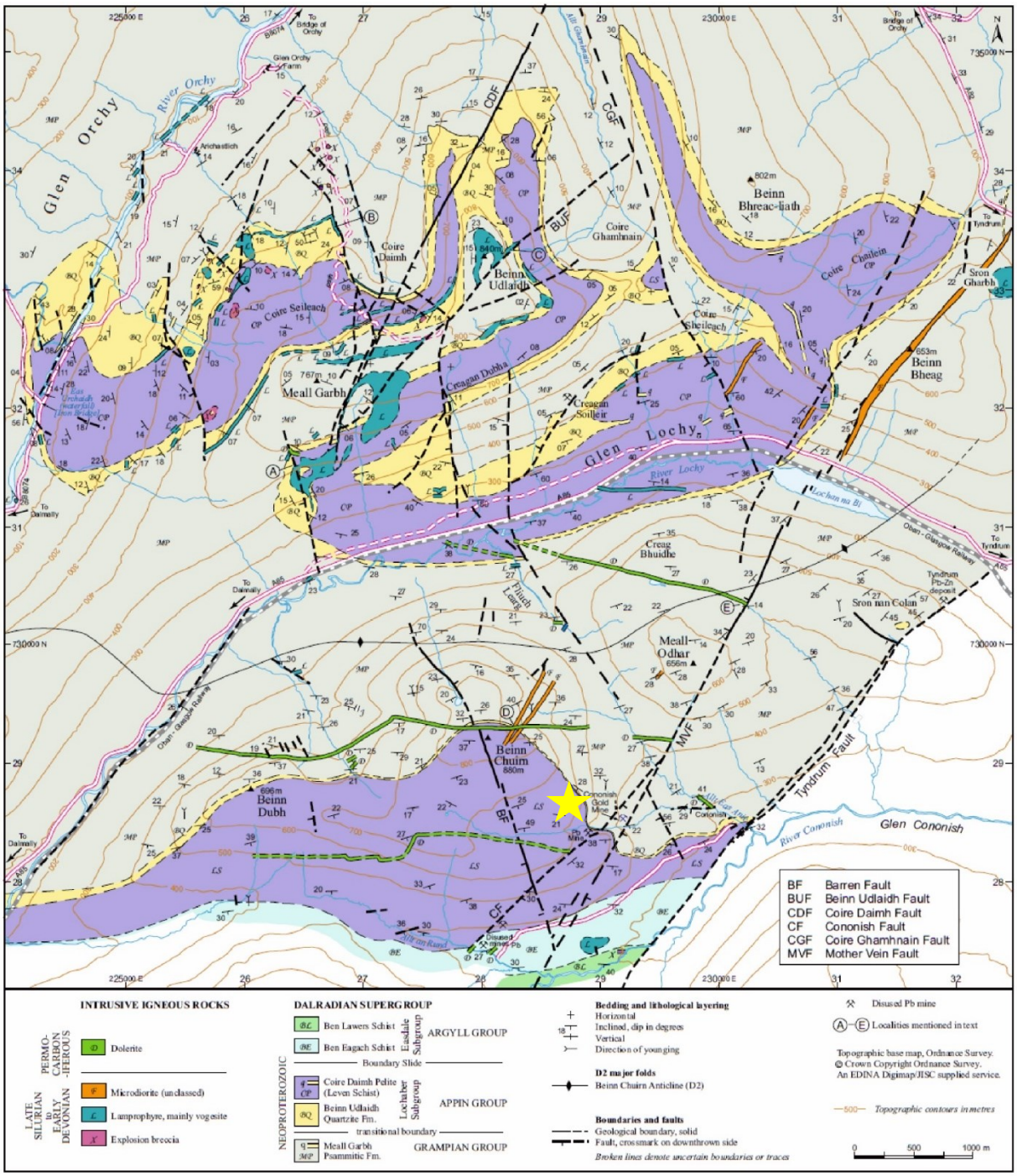

Figure 3.1 – Geological map of the Tyndrum area reproduced from (Tanner, 2012). The Cononish deposit (yellow star) is hosted within the Cononish fault (CF), subparallel to the Tyndrum fault at the bottom of the mapped area. There are notable large "barren" quartz veins named the Mother Vein (MVF) and Barren Fault (BF) which are emplaced along minor faults in the vicinity of the mine.

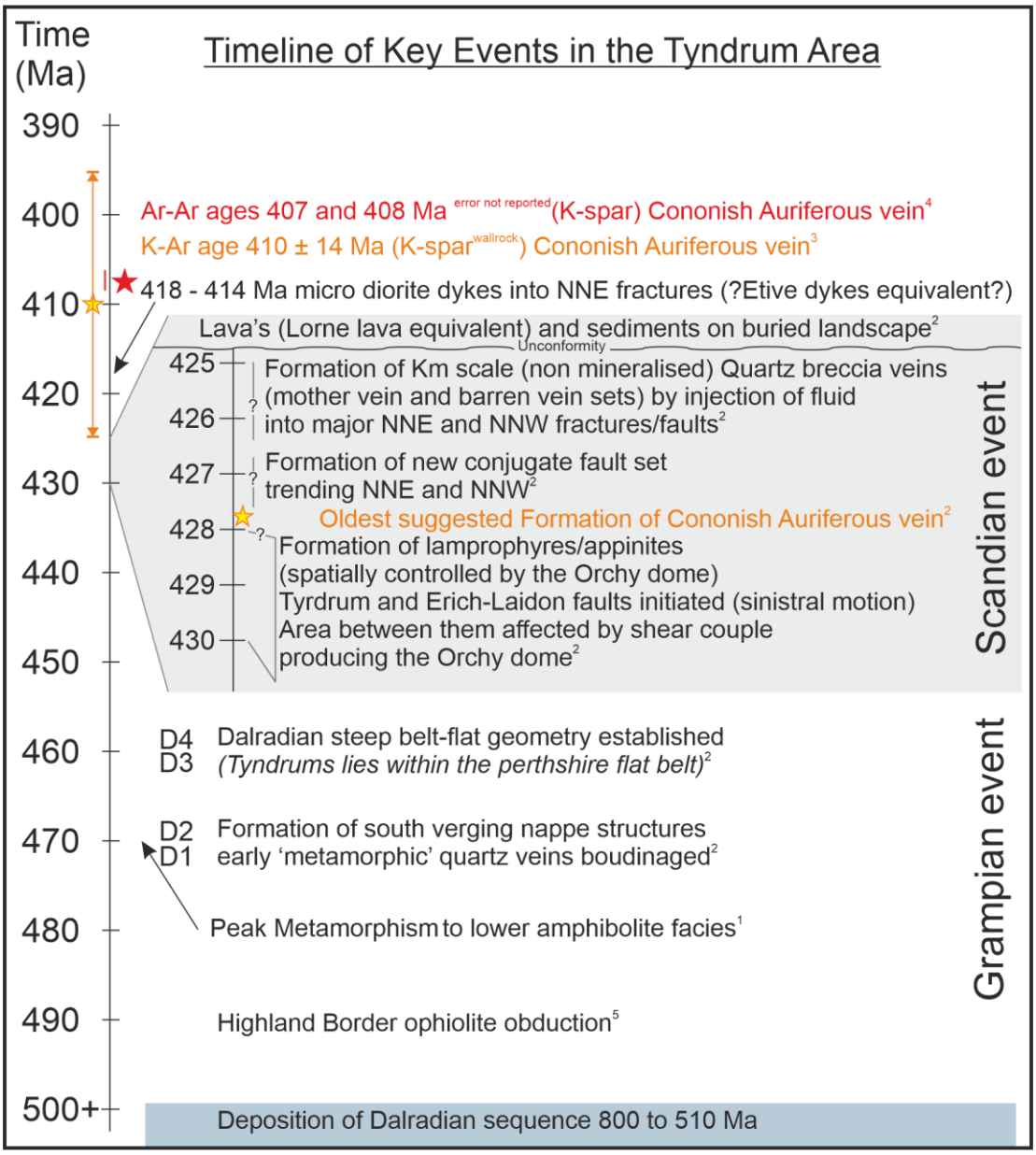

Figure 3.2 — Time line of important events in the Tyndrum area modified after Tanner (2012) and Hill et al. (2013). Subscript numbers refer to the following sources: [1] Stephenson et al. (2013a), [2] Tanner (2012), [3] Treagus et al. (1999), [4] Rice et al. (2012), [5] Chew et al. (2010).

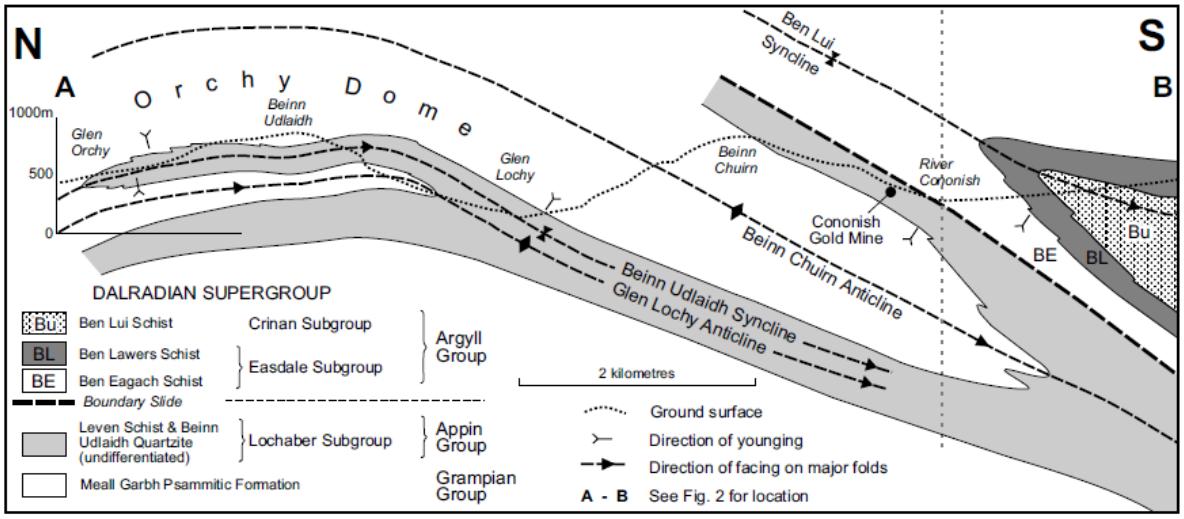

Figure 3.3 – Diagrammatic N-S cross section of the Cononish/ Glen Orchy area showing the structural and stratigraphic position of the Cononish mine on the upper (right way up) limb of the Beinn Chuirn Anticline (Tanner, 2012)

3.2.2 The Cononish gold deposit

The Cononish deposit was identified by Ennex International Plc and is located at GR: NN 29160 28575 on the slopes of the Beinn Chuirn within Glen Cononish, Figure 3.1. The deposit is a single sub vertical vein up to 6m wide within a fault striking 040°. The early history of discovery is reported in Earls et al. (1992) and summarised in the following two paragraphs.

The potential for a deposit was identified due to the discovery of auriferous float at Eas Anie in 1984. At the site two pre-existing adits existed, driven along lead bearing quartz veins (termed “B-min” vein by Earls et al. (1992)), in the Eas Anie cliff face. These were investigated but found to not host the styles of mineralisation observed in the float. Subsequent trenching on the hill above the cliff undertaken in 1985 identified auriferous outcrops of a vein (termed “A-min” vein by Earls et al. (1992)) over a 250m strike length which was drilled in an initial 10-hole program.

Following additional prospecting work, in 1986 the company, identified a sub parallel auriferous quartz sulphide vein, within 30m to the east of the lead mining adits. This was targeted with a larger drill program (46 holes) in 1987 and 1988 and followed up with the driving of a test adit along the vein structure to define a resource. This defined the early resource of 750,000t grading 7.99 g/t Au (Earls et al., 1992). The mine has been through several companies’ ownership and is currently operated by Scotgold Resources Plc. The resource

of the deposit is reported to be 617,000t grading 13.4g/t Au and 55.3g/t Ag (Scotgold Resources Limited, 2015)

'The deposit is hosted by metasediments of the Grampian and Appin Groups which are the correct way up (Figure 3.3). The succession observed to host the mineralisation is reported by Earls et al. (1992) and Hill et al. (2013) and a summary is shown in table 3.1 and figure 3.1. Three distinct alteration zones are identified by Earls et al. (1992) who interpreted the alteration to have developed early in the veining sequence:

1. Outer zone of chloritized garnet and biotite (up to 15 m from vein)

2. Bleached middle zone, typically buff coloured, caused by sericitization of chlorite (up to 5m from vein)

3. Reddened inner zone, often silicified and occasionally containing fine disseminated pyrite. The red colour varies from salmon pink to brick red created by haematite within altered feldspars (up to 2m from the vein)

The vein has been described by multiple authors in the academic literature and in company reports and has been studied mineralogically (Spence-Jones, 2013, Earls et al., 1992, Spence-Jones et al., 2018), for fluid inclusions (Pattrick et al., 1988) and structural setting (Tanner, 2012, Tanner, 2014). Treagus et al. (1999), Tanner and Thomas (2010). Tanner (2012) and Tanner (2014) have examined the structural relationships including folding and faulting in the development of veins and mineralisation in the Tyndrum area. These studies along with the work of Treagus et al. (1999), and Tanner and Thomas (2010), provide a detailed account of and framework for the development of faults and veining of the local area in the context of the regional tectonics. They also present structural observations and several differing models for the timing and formation of the auriferous veins observed in the area. A review of the Cononish auriferous vein and its relationship to the structures is presented in this chapter, following additional observations presented in the results. The observations and conclusions of the above published studies are introduced as appropriate in the discussion section.

Table 3.1 – Description of the succession of metasediments that host the Cononish deposit after Earls et al. (1992)

Mine classification (Earls et al., 1992)	**Description taken from Earls et al. (1992)**	**Established name**
Portal psammite (25m to 30m thick)	Poorly laminated medium to coarse quartzofeldspathic psammite with thin pelitic partings (first 400m of development underground is in this unit, see figure 3.1)	Meall Garb Psammite (Eilde Flags)
Lower adit psammite (25m to 30m thick)	Laminated psammite with 5-10cm thick beds of variably pure and impure psammite	Benn Udlaidh quartzite (Glen Coe Quartzite)
Calcareous member (8m to 25m thick)	Biotite (or chlorite) pelite with contorted carbonate veinlets up to 0.5m in width)	Leven schist
Upper adit member (15m-30m thick)	Well laminated fine to medium psammite with subsidiary pelites (<25%)	Leven schist
Mixed member (10m to 20m thick)	Interbedded psammites (1m thick) and petlite (up to 50%)	Leven schist
Cliff Pelite member (45m to 50m thick)	Alternating pelites and semipelites with some amphibolite units and rare psammite. Chloritic and garnetiferous units common.	Leven schist
Hickey formation	Quartz semipelite characterised by thin beds containing 1-2mm quartz particles with stratiform amphibolites.	Dallmally quartzite

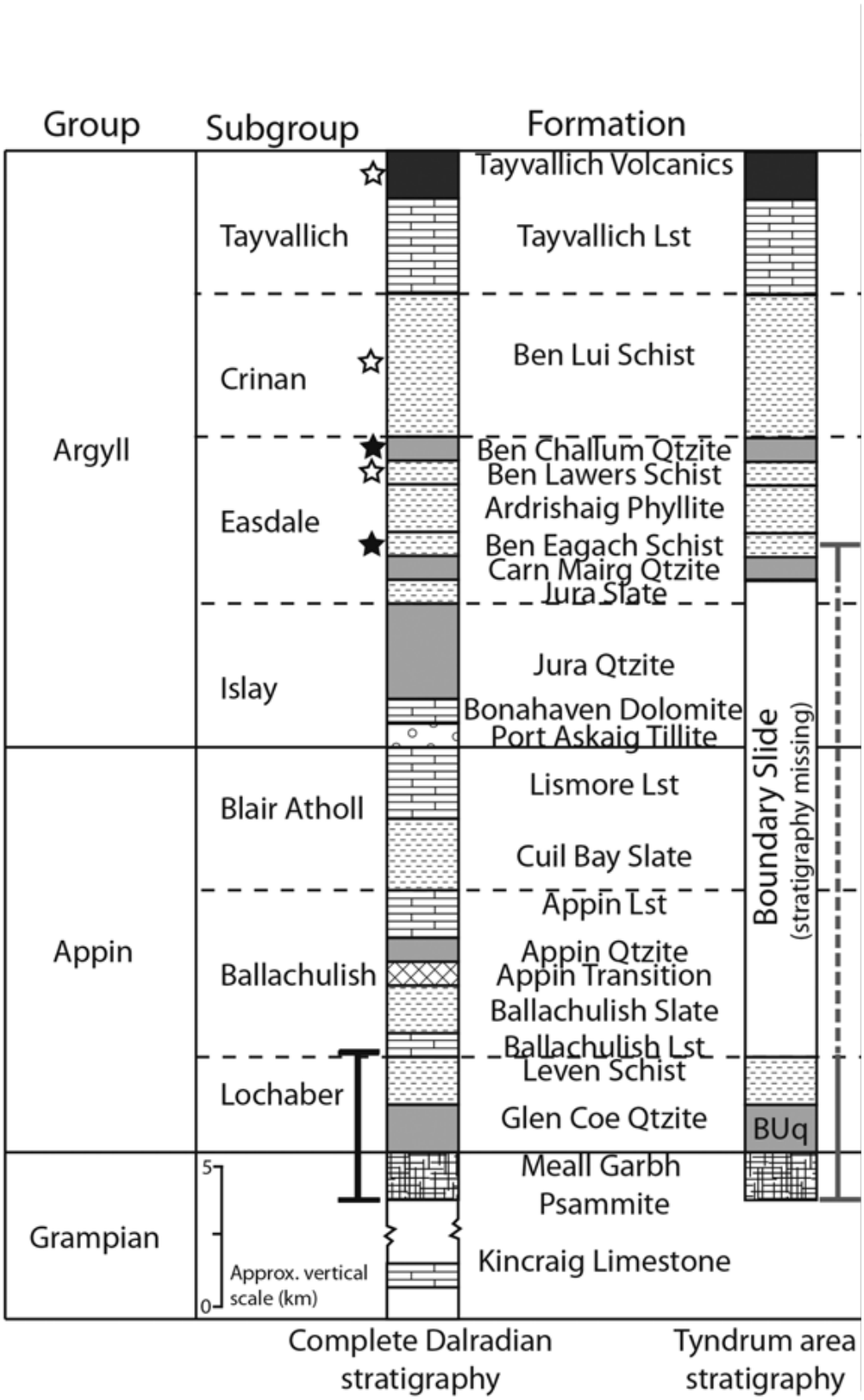

Figure 3.4 – Stratigraphy of the host sequence after Hill et al. (2013). Open Stars indicate volcanogenic sulphide horizons; solid stars indicate syn-sedimentary stratabound SEDEX horizons. BUq is the Beinn Udlaidh Quartzite which is equivalent to the Glen Coe Quartzite.

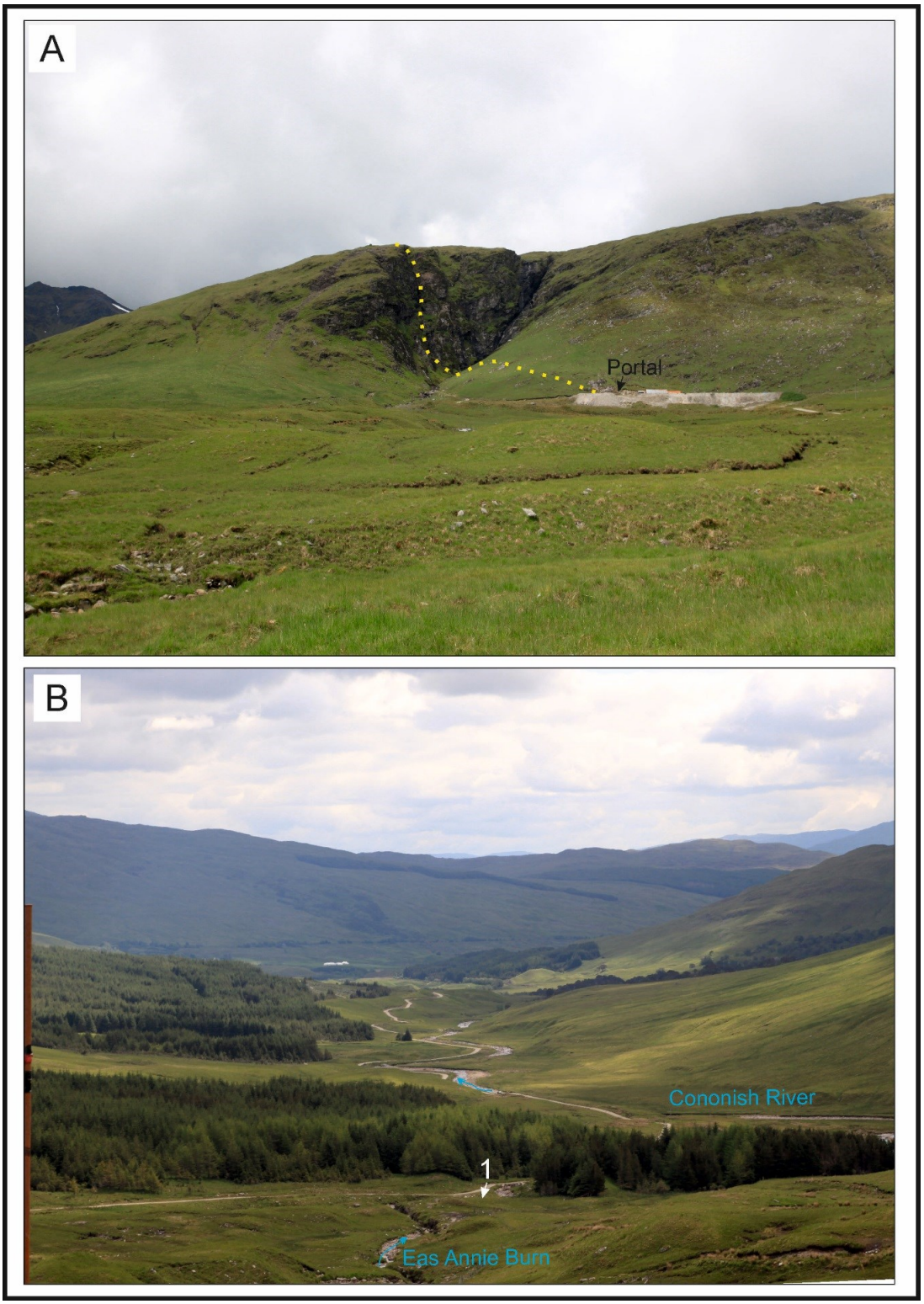

Figure 3.5 – Photographs of Glen Cononish taken in 2012. A. photo looking west towards the mine site from the Cononish farm showing the surface expression of the Eas Anie vein in yellow. B. Photo taken from the mine site looking east down the valley showing Eas Anie Burn and the Cononish River.

3.3 Methods

A previous Masters research project (MGeol) on the Cononish gold deposit by the author, conducted prior to this work, constrained the gold composition of individual stages within an interpreted paragenetic framework (Spence-Jones, 2013). To improve upon the existing work, field observations and further sampling was undertaken during a visit to the Cononish mine site in 2015 & subsequently polished thin sections and sulphur isotope samples were prepared.

3.3.1 Sample collection

Samples used in this work come from two sources, primary field work and re-sampling of an existing sample set held at the University of Leicester (collected by the author during the MGeol research project). The location of all the samples is shown in table 3.2 and the locations displayed on a geology map of the exposure, figure 3.6. The primary field work and sampling were conducted during a visit to the underground exploration adit on the 4th May 2016, facilitated by Scotgold Resources PLC. A total of 10 hand specimen samples were collected along with observations and photographs of the exposures.

3.3.1 Sample preparation

Petrographic sections, both polished block and polished thin sections, were prepared from hand specimens using the facilities at the University of Leeds. Samples were cut to size using diamond lapidary saws and grinding was achieved using Buehler Motopol rotating grinding wheels with 40µm and 10µm diamond-impregnated disks. The 30µm thicknesses of the polished sections was achieved by hand lapping and optical estimation using the birefringence of quartz. Final polishing was performed using the Buehler Automat 250 polishing system with sequentially finer diamond paste and the final finish achieved using 0.5µm diamond suspension or Gamma alumina as needed.

Table 3.2 – Location of rock samples taken from the Cononish mine, with details of sections made from them.

Sample ID	distence allong Adit	Mine plan X	Mine plan Y	OS_X	OS_Y	Description	Thin section	S Isotope
CSJ_CON_001				228632	728085	Taken from 1.5m+ wide Cononish vein sample with course sulphides and sulphide rich late shears.		
CSJ_CON_002				228632	728085	Taken from 1.5m+ wide Cononish vein sample with course sulphides and sulphide rich late shears.	C002	Yes
CSJ_CON_003				228632	728085	Sample of late sulphide rich shear zone in massive white quartz.	C0031,C0032,C0033	Yes
CSJ_CON_004				228632	728085	Taken from 1.5m+ wide Cononish vein sample with course sulphides and sulphide rich late shears.		
CSJ_CON_005				228770	728194	Vein sample from narrow late sulphide rich shear near crosscutting B min vein		
CSJ_CON_006				228770	728194	Vein sample from narrow late sulphide rich shear near crosscutting B min vein		
CSJ_CON_007				228840	728264	Cononish main vein bulk representative sample at location		
CSJ_CON_008				228840	728264	Cononish main vein bulk representative sample at location		
CSJ_CON_009				228840	728264	Cononish main vein bulk representative sample at location		
CSJ_CON_010				228778	728198	B min sample taken from parallel structure to mineralised vein in adit		
CSJ_CON_011				228690	728154	Stockwork developed in footwall		
CSJ_CON_012				228671	728114	Footwall sample 1m from main Qz vein		
CSJ_CON_013				228543	728021	Vein breccia		Yes
CSJ_CON_014				229086	728542	Offshoot veinlet with redeanded clasts and a suphpide rich core to the vein		
CSJ_CON_015				228809	728238	Contact and margin of the dyke in the adit.		
CSJ_CON_1601	NA	NA	NA			Mother vein sample		
CSJ_CON_1602	NA	NA	NA			Footwall host rocks	67181	
CSJ_CON_1603	No value	11497	10969			Footwall psammite to " portal vein	67190	
CSJ_CON_1604	754m	10852	10972			Early vein sample	(1604), (1604), 67186, 67186, 67186, 67186	
CSJ_CON_1605	no value	11495	10968			Portal vein east sample	67184	
CSJ_CON_1606	456.8	11120	10947			Cononish main vein bulk representative sample at location	1606A, 67182, 67183	
CSJ_CON_1607	456.8	11120	10947			Cononish main vein bulk representative sample at location	1607, 67187	
CSJ_CON_1608	548	11023	10947			Vein in footwall of main vein/fault zone	(1608B), 67196	
CSJ_CON_1609	548	11023	10947			Cononish main vein bulk representative sample at location	(1609B), (1609A) 67197, 67197,	
CSJ_CON_1610A	565	11015	10949			Hanging wall host rocks	67188	
CSJ_CON_1610B+C	500	11078	10955			Mineralised psammite footwall	67189	

3.3.1 Analytical Procedures

Light microscopy and reference maps of samples

Reconnaissance transmitted and reflected light microscopy was conducted using a James Swift MP3502 microscope with a trilocular head to which a Canon 550D digital camera was attached using an Olympus phototube. Additional higher quality images and petrography was also conducted using an Olympus BH2 microscope with the 550D camera attached.

To achieve wide fields of view and present petrographic contexts on a larger scale than low power objectives can achieve, multiple images were taken of an area and digitally stitched into a single image using Kolor autopano giga (v4) software. This software stiches images using automated geometric analysis and allows for additional manual correlation of points on image pairs (if stitching is not satisfactory using the automated algorithm).

To facilitate accurate recording of sites of interest and features for later analysis maps of the samples were created. For polished blocks maps were created of the sample in reflected light using Kolor autopano giga (v4) software. For thin sections maps were created using desktop scanners, with two polarising films allowing XPL imaging if required. These were then annotated and used as references for observations and analytical work.

Scanning electron microscopy

Scanning electron microscopy was conducted using a TESCAN VEGA3 XM (Tungsten source) SEM, equipped with X-max 150 SDD EDS and Aztec 3.3 software and fitted with a TESCAN RGB filtered CL imaging system at the Leeds Electron Microscopy and Spectroscopy Centre (LEMAS) Facility.

For general petrographic analysis using BSE and EDS, a 20KV accelerating voltage and beam intensity set between 15 to 18 (but generally set at 15) was used. Working distances were between 12-18mm from the sample surface depending on mountings used.

For cathodoluminescence imaging different SEM parameters were used from BSE/EDX work to achieve brighter luminescence from the quartz. A high beam intensity of 19 (occasionally 20) was used with a 20Kv accelerating voltage. These parameters give spot sizes of around 750 to 900nm (dependent on working distance). The majority of images were captured as automated panoramas using the image snapper feature of the Tescan control software. For these panoramas dwell times of 32µs (scan speed 6) were generally found

to capture good quality images while keeping scan time reasonable. Working distances between 18mm (optimum recommended for the CL detector geometry of the instrument) and 25mm were used, with the larger working distances used to allow larger fields of view for CL scans of whole sections within reasonable timeframes (overnight runs with approximately 5 to 9 hours per section).

Electron Microprobe

Quantitative analysis of chemical compositions of individual mineral phases was conducted using a JEOL 8320 electron microprobe. An accelerating voltage of 20kV with a beam current of 200nA and a peak count time totalling 90 seconds with 30 seconds off peak was used for gold alloy analysis.

The CL maps of samples from the Cononish gold vein were examined to investigate if the multiple generations of veining (paragenetic sequence interpreted from petrology) could be identified and distinguished by differences in the luminescence of the quartz. This work focused on the gold mineralisation with only one sample containing quartz belonging to the Pb-Zn vein. These vein types are easily distinguished in situ and the veins are typically spatially separated, forming in different structures within the adit, thereby facilitating targeted sampling of the Au veins. The colour of the luminescence of the quartz is consistent with published investigations of hydrothermal quartz (Götze, 2009) and other hydrothermal gold bearing quartz veins (Wertich et al., 2018). Hot Cathode luminescence images of the sections from the veins show quartz that displays a blue florescence, as seen in figure 3.10 (and in places blue green luminescing veinlets).

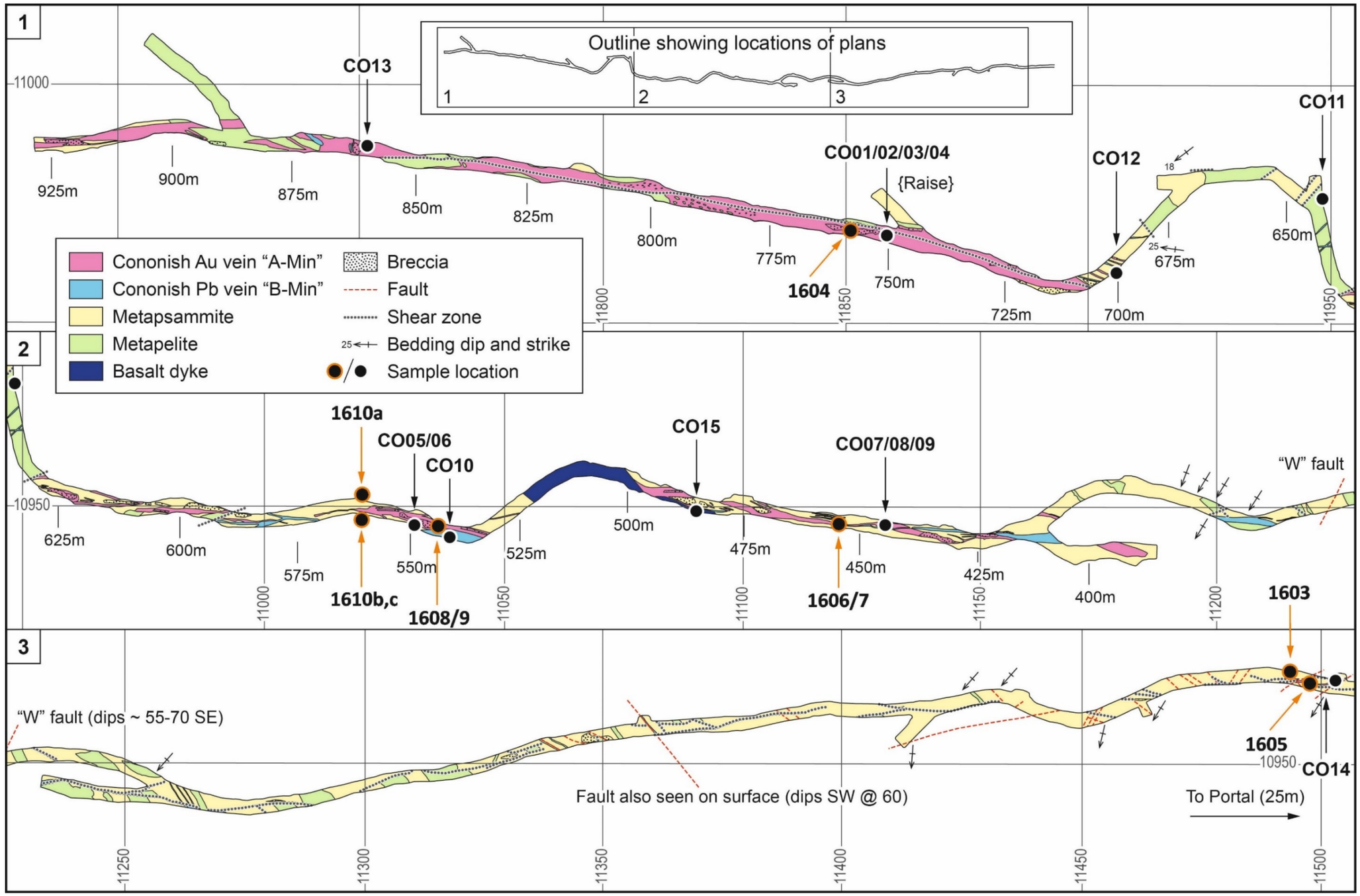

Figure 3.6 – Simplified mine plan of the 400mL underground development of Spence-Jones (2013) showing sample locations from the MGeol project (black dots) and this work (orange ringed dots).

3.4 Results

3.4.1 Mineralogy and paragenesis

The two vein systems, lead (Pb) vein and auriferous veins, are present in the Cononish mine and these are distinct both structurally and texturally and were formed in independent mineralising events (Earls et al., 1992, Tanner, 2012, Spence-Jones et al., 2018). The two systems are coincident in a few places in the underground exposure, shown in figure 3.6. Most of the sampling and data collections were targeted on the auriferous veins. Due to the coincident nature of the two systems in places, a brief description of the Pb vein is presented at the end of the results section to illustrate the sharp contrast in vein style with the auriferous vein.

3.4.1.1 The auriferous Cononish vein

The complete paragenesis, figure 3.8, represents the synthesis of observations and samples collected during a Masters level project (MGeol) and PhD research by the author. Where observations, samples and results were obtained as part of the Masters project, they are referenced to the Master's thesis (Spence-Jones, 2013).

The Cononish vein was observed and sampled underground during the PhD project on 18/04/2016. (The gold bearing vein is observed in outcrop to be predominantly comprised of massive milky white quartz, with clear multiple generations that brecciate and crosscut the host rock and early vein stages. The textures are observed to be variable, with different styles of brecciation, and degrees of crosscutting by vein generations observed in the exposure of the vein in the underground workings.) The following section reports the results of the field, mineralogical and geochemical work undertaken.

3.4.1.1.1 General character of the underground exposure of the mineralisation

The Cononish Au vein (termed A – Min by Earls et al. (1992)) is poorly exposed on the surface; however, the unlined exploration adit allows access to examine the vein in outcrop. Overall, the Cononish Au vein is predominantly formed from massive milky white quartz, produced by multiple, sub–millimetre to cm wide vein generations with minor pyrite, chalcopyrite, and galena. The width of

the largest quartz-sulphide vein sections was observed to be variable, ranging from the full width of the adit (3m) down to sections as narrow as 0.5m. However, the true width of the mineralised zone is difficult to identify in outcrop as the vein anastomoses, forms a breccia zone, and replaces wall rock to a variable degree, along the trend of the Eas Anie fault, figure 3.6.

In areas where a significant quartz vein is exposed, the local host rocks are observed to be brecciated and occur as rotated clasts within a matrix supported hydrothermal quartz breccia. This quartz breccia is crosscut by later quartz and sulphide veining/fracturing: figure 3.7 and 3.9.

The latest sulphide rich veinlets are developed strongly in proximity to a fault plane (the Eas Anie fault), which crosscuts all the veining observed in the adit. The majority of the mineralisation is developed in the foot wall, although the position of the fault plane varies in relation to the mineralisation, with mineralisation developed in both the foot wall and hanging wall, shown in figure 3.9.

The petrographic investigation of the vein allows division of the mineralisation and veins into temporally constrained paragenetic stages developed by Spence-Jones (2013). Through examining cross-cutting relationships, textures, and mineral associations, measurable differences and variations can be seen in the veining style and mineralogy. The detailed paragenesis which provides a simplified model of the temporal and mineralogical genesis of the mineralisation presented by Spence-Jones (2013) remains unchanged, figure 3.8. However, further details of the identified generations of veining from field observations, hand specimens and microscopy which are presented below are primary observations (unless otherwise stated) undertaken during this research to refine the characterisation of the vein, check the previous published work and provide a solid observational foundation for later interpretations. The further observations, descriptions and characterisation of the vein are presented below in chronological (paragenetic) order.

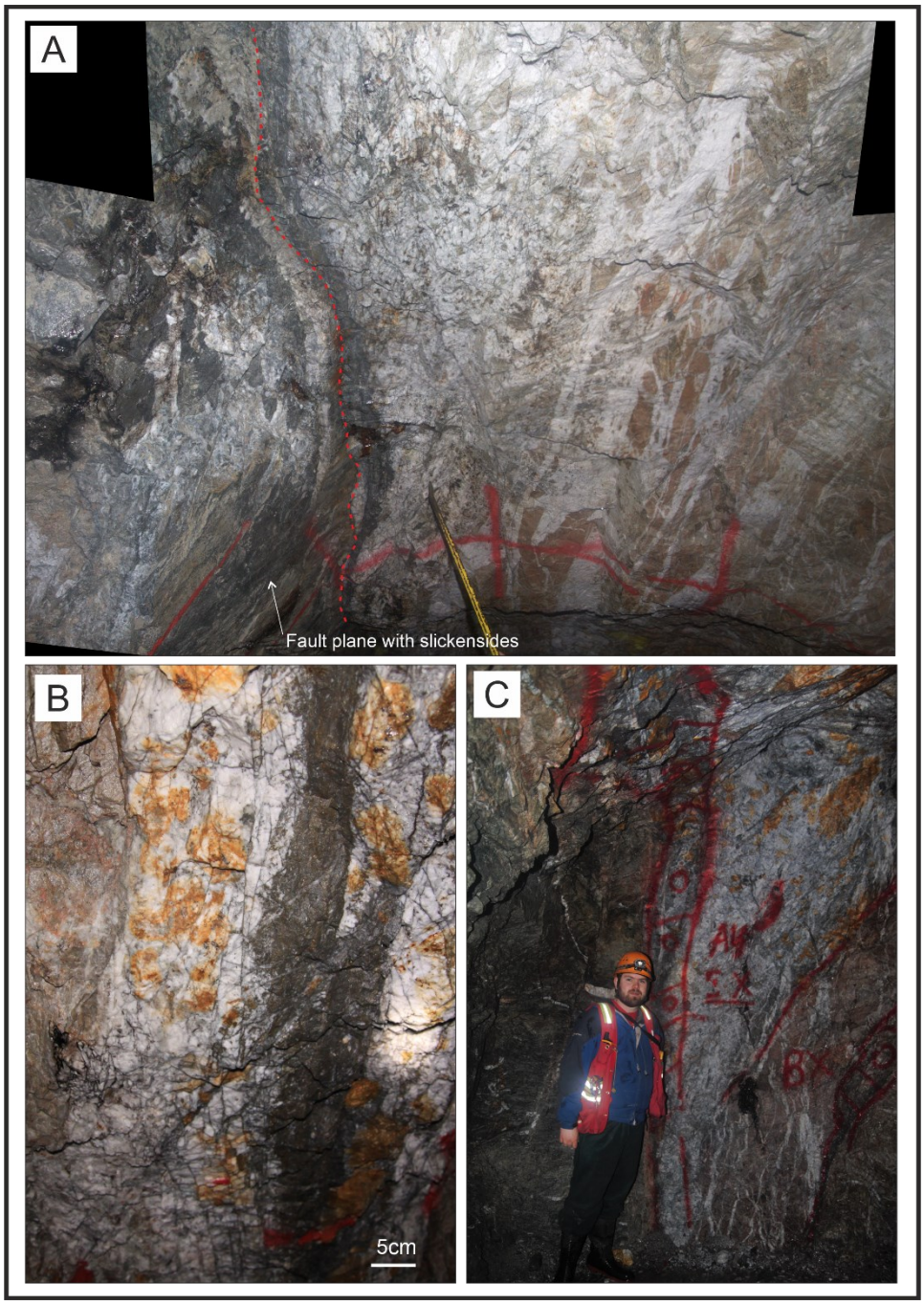

Figure 3.7 – Photographs of the Cononish Adit taken in 2016.

A) Photograph of the back (roof) and west rib taken looking north towards the portal. The Eas Anie fault can be seen (red) surrounded by dark sulphide rich veinlets. Distal to this, a quartz dominated breccia with tabular clasts of wall rock within the multigenerational hydrothermal quartz containing minor sulphides. B) Photograph of a well-developed 5-15cm sulphide vein within earlier quartz as an example of what is observed close to the fault in A above. C) Photograph of the end of the exploration adit in 2016 (looking south) showing the variability in the width of the vein going from 3m+ to 0.4m over a vertical distance of 4m. This location is a good example of where the largest vein widths are developed in the hanging wall of the fault.

3.4.1.1.2 Vein Stages

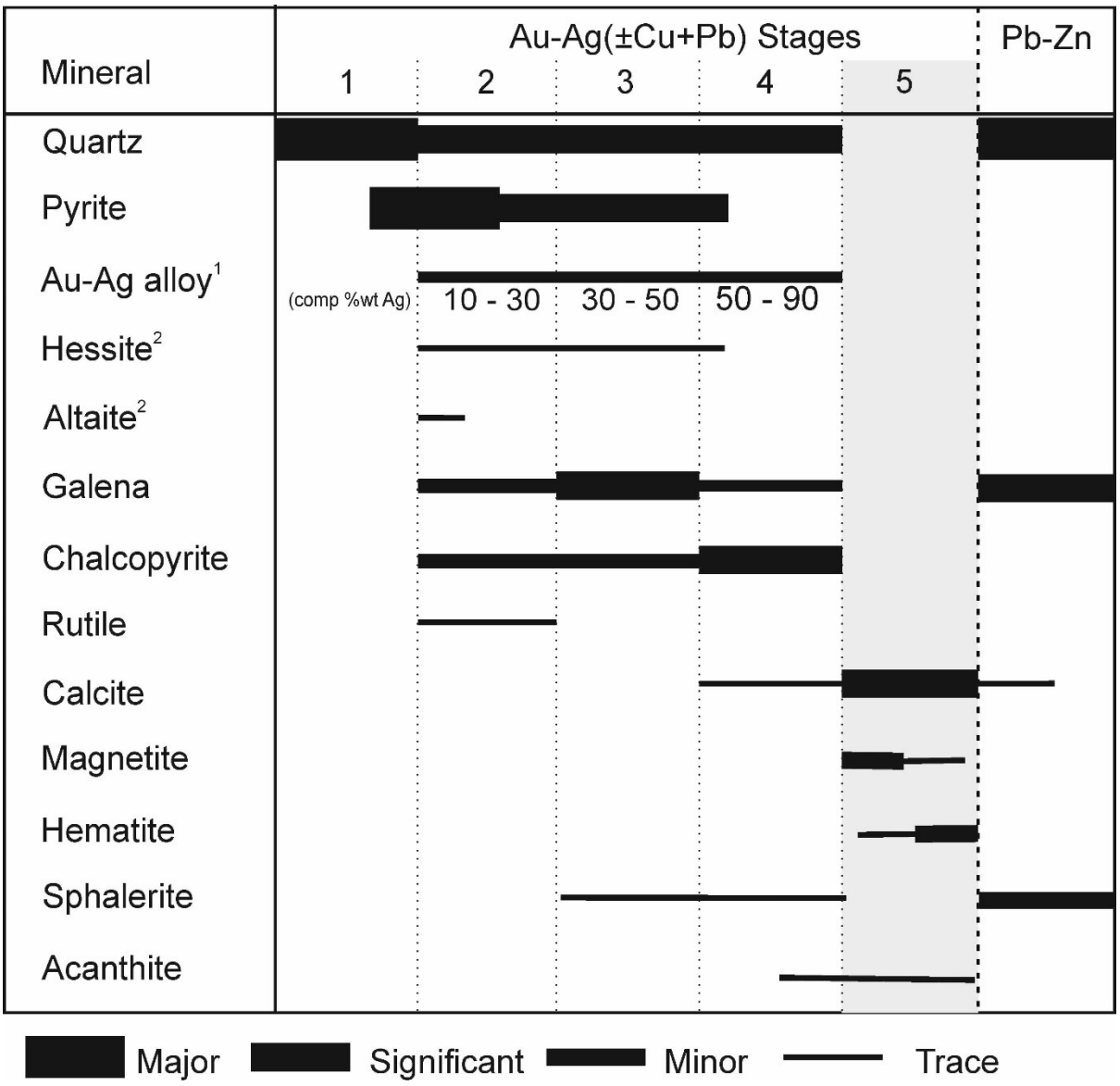

Figure 3.8 – Paragenesis of the Cononish Au vein modified after Spence-Jones (2013). [1] aproximate Au-Ag alloy composition (as wt.% Ag) for each stages is shown under the bar. [2] telluride minerals: hessite ($AgTe_2$) and altaite (PbTe). The highlighted stage 5 event is of uncertain origin and its genetic relation to either the earlier Au or later Pb mineralisation is unknown.

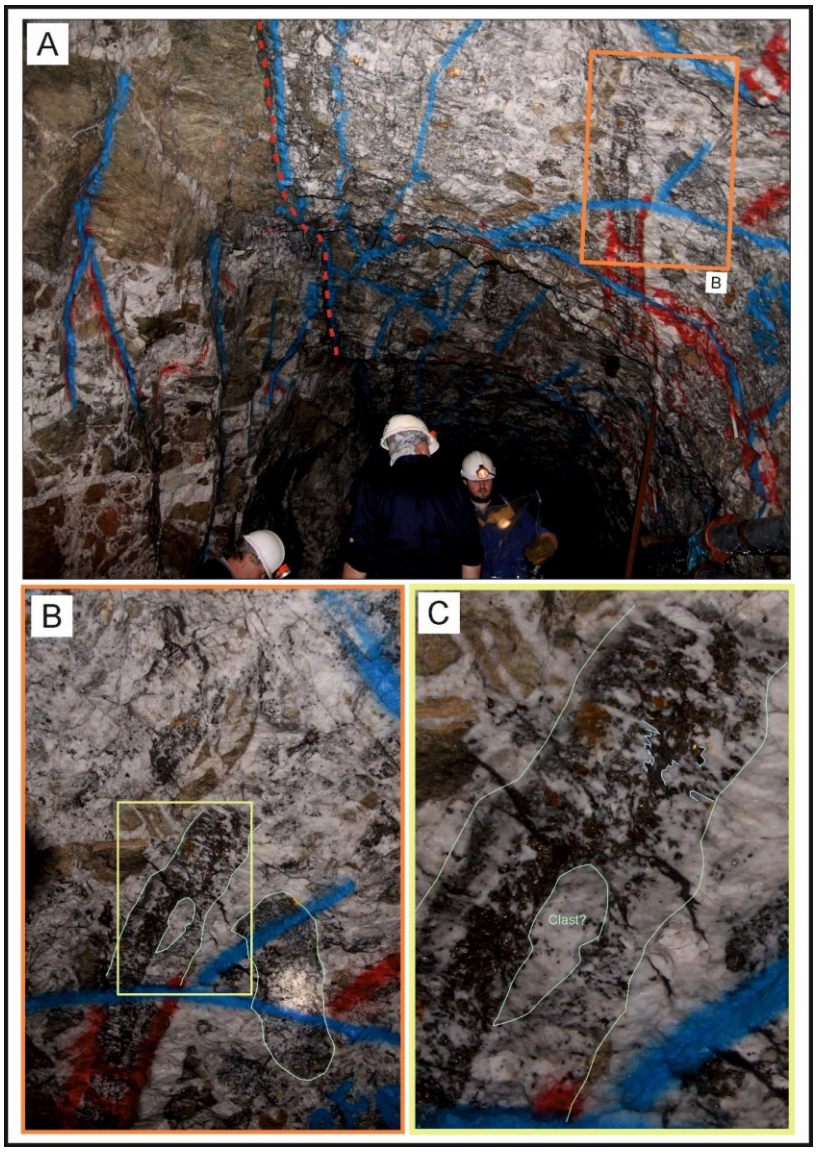

Figure 3.9 – Photographs of the Cononish Adit taken in 2016.

A) photograph looking towards the portal (north) of the gold vein along the Eas Anie fault 750m from the adit entrance. In the left rib (wall) (hanging wall of the fault) the country rock had been brecciated by milky white quartz with little sulphide present (stage 1). The main vein is developed in the footwall of the fault (red) and forms the entire roof of the adit. In the roof this can be seen crosscutting veins of early cockscomb quartz-sulphide veining of stage 2 mineralisation (shown with the margins highlighted in area/image B). In addition to the stage 2 sulphides, late veining is most intensely developed around the fault plane (red) as fine (mm to cm scale sulphide rich veinlets (stage 3/4) along fractures, which heavily fracture the early vein stages. Images B and C progressively enlarge a section of the vein showing the texture of stage 2 mineralisation. In C, cockscomb quartz terminations are highlighted for a small section of the stage 2 vein in light blue. The space between the cockscomb quartz is infilled with pyrite which highlights the form of the quartz in the vein.

Stage 1 – Early quartz veining

Visually the majority (an estimated 70–80% by volume) of the multigenerational vein is a milky white quartz-dominated matrix–supported breccia and is classified as the first vein development within the Eas Anie structure (stage 1). In the adit this early hydrothermal breccia is principally developed in the footwall of the Eas Anie fault. This is clearly seen in a section of the 'main' vein in the exploration adit (440mL) between 650m and 750m (see figures 3.6 and 3.9). In this area the early 'milky' quartz breccia is up to 3m wide and rare euhedral coarse quartz crystals and sub veins are observed within it. Very few sulphides are observed associated with this stage. The vein textures indicate that it formed as a result of critical fracturing, with multiple fluid assisted opening events producing local hydraulic fracturing of previous vein material (Jébrak, 1997).

The clasts of the early quartz breccia (up to ~80 cm) are angular fragments of altered (silicified, sericitized and reddened (K feldspar)) local host lithologies and parts of earlier quartz vein. The relic cleavage observed in pelitic and psammitic clasts indicate that there is significant rotation of these fabrics during brecciation as can be seen in figures 3.7 and 3.9. This further supports significant opening potential indicating hydrostatic pressures exceeded lithostatic during formation.

The milky quartz vein (matrix) is formed of coarse 1-2 cm crystals cut by a multitude of fine 50–1000 μm stringer veins. In thin section the fine quartz stringers that crosscut the coarse crystals are observed to be in optical continuity with the larger crystal that they crosscut, indicating that the vein quartz crystallised as epitaxial overgrowths on earlier quartz crystals. Cathode luminescence imaging reveals that coarse euhedral crystals are more common than visually indicated in outcrop or in thin section observations. The earliest quartz has clear oscillatory growth bands (often only preserved as fragments within later vein complexes). Overprinting the growth bands is pervasive fracturing, with (relatively) dark luminescence quartz observed within the fractures. The barren quartz (stage 1) and Stage 2 quartz appear to be nearly identical with the only differences being macroscopic textural (cross cutting relationships) and the different mineral assemblage of the two stages. The evolution from stage 1 to stage 2 style veins is a continuous process as both share very similar textures, structures and styles of veining.

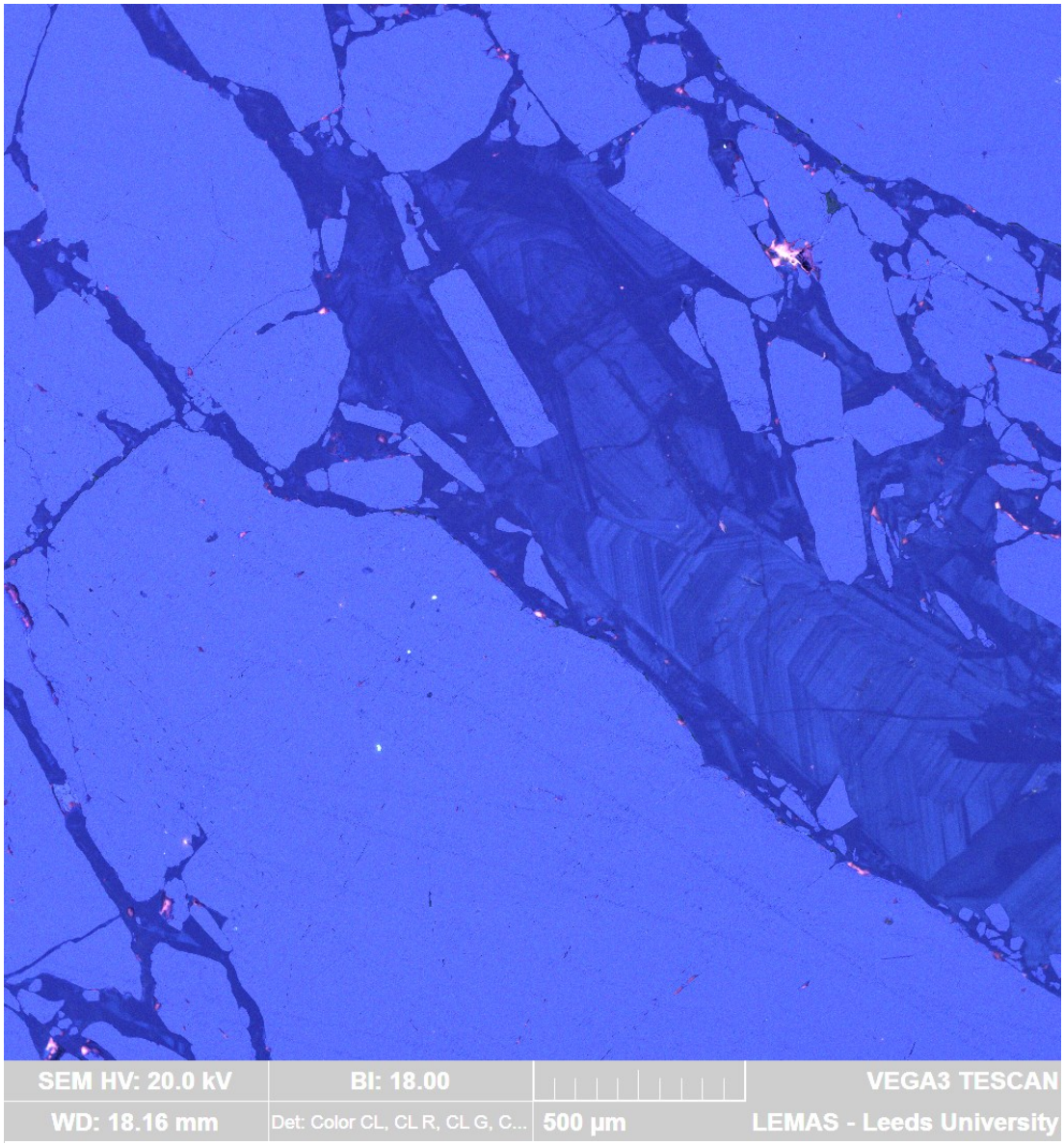

Figure 3.10 – CL colour image (brightness enhanced) showing the complexity of the early stage 1/2 veining. Note 50+ growth bands within a single quartz crystal (right) surrounded by coarse pyrite. The late dark quartz appears to crosscut the early quartz and is in contact/hosts the pyrite and associated Au and sulphide stages. Polished Block 02D. The brightness of the pyrite is due to the BSE detector being in the inserted position. This was discovered to interfere with the CL imaging, particularly when imaging high reflectance opaque phases making them appear to luminesce (interpreted to be reflecting light from the luminescing BSE detector into the CL detector tube.)

Stage 2 – Early Au–Ag mineralisation

Crosscutting the early quartz is a later swarm of quartz veinlets, with coarse pyrite veins, which are similar in character to the early quartz breccia but distinctly include coarse pyrite as part of the matrix. As such this sub-stage of early veining is identifiable within the large vein structure by the presence of the coarse pyrite, which defines it as a vein stage.

The pyrite occurs in tabular bodies/pods and is disseminated with quartz. The tabular bodies/pods of pyrite range in size from 1 cm up to 30 cm, figures 3.7, 3.9 and 3.11. In rare places, the massive pyrite is observed to form the core to cockscomb veinlets, infilling the centre of the structure between coarse euhedral quartz crystals, shown in figure 3.9. The pyrite within the pods is coarse with crystals up to 0.5cm observable and is often heavily fractured, especially where later development of veining has occurred, figures 3.9, 3.11 and 3.12.

Multiple generations of euhedral quartz, with pyrite in the centre of the veinlets, are observed to crosscut each other. This produces complex, chaotic hydrothermal breccia textures. The 100's of individual vein openings appear to be responsible for the substantial width of the vein. This is consistent with other mesothermal gold vein systems which are documented to represent a considerable number of depositional events within a single structure (Yardley, 1996, Cox and Ruming, 2004, Bons et al., 2012).

The quartz in this stage is very hard to distinguish from stage 1 quartz, and it is only separable by identifying zones where quartz + pyrite is observed on a macroscopic scale. Examples of this can be seen in figure 3.9C, where the stage 2 vein is clearly identifiable as a discrete parallel sided sulphide rich tabular structure. This can be compared to the vein in figure 3.11A, where the vein structure is more chaotic and forms a complex breccia with clasts of early quartz pyrite in later quartz cement, making delineation of early quartz pyrite vein structures very challenging visually to follow though the outcrop.

Microscopy reveals that the coarse pyrite crystals of this vein stage host the earliest Au–Ag (±Cu, Pb) mineralisation. The earliest gold alloy is observed within fractures, and as trails of inclusions (figure 3.12), in the early pyrite seen in figures 3.11, and 3.7. The gold is observed to be associated with the assemblage hessite (Ag2Te) + Au–Ag alloy + galena ± altaite (PbTe) ± chalcopyrite which are all found as inclusions, trails of inclusions and veinlets within the coarse pyrite, figure 3.12 and 3.13. The trails of inclusions are interpreted to be the result of recrystallisation of the pyrite crystals after the

formation of these mineralised crosscutting veinlets. This interpretation is supported by the discovery of a pyrite crystal that appears to have undergoing partial recrystallization, shown in figure 3.13. It is observed that in half of this pyrite crystal a trail of inclusions appears to be the extension of an intact veinlet, which is observed in the other half of the pyrite crystal. The recrystallization of pyrite is reported to occur commonly through either pressure-solution and annealing/particle growth at low temperatures and pressures (Lianxing and McClay, 1992).

Cathode luminescence of quartz within the stage 1/2 mineralisation reveals that coarse euhedral quartz crystals are more common than was visually indicated in outcrop or thin section observations. In all sections observed the earliest identifiable quartz generations (often clasts within a later breccia) displays clear oscillatory growth bands. In all cases these are heavily fractured, with (relatively) dark quartz observed within in the fractures.

Within a single veinlet the mineralisation is observed to follow a generalised sequence, with coarse euhedral quartz crystals deposited followed by coarse pyrite in the core of the veinlet. These are then heavily fractured with deposition of Au–Ag (±Cu, Pb) minerals late in the opening sequence, evidenced by their observation within fractures in the early pyrite. The presence of examples of the Au–Ag (±Cu, Pb) minerals within pyrite as primary inclusions, and their presence in multiple generations of stage 2 veinlets, indicates a co-genetic fluid relationship to the pyrite, precluding a separate, much later, introduction of the Au–Ag (±Cu, Pb) minerals into the fractures.

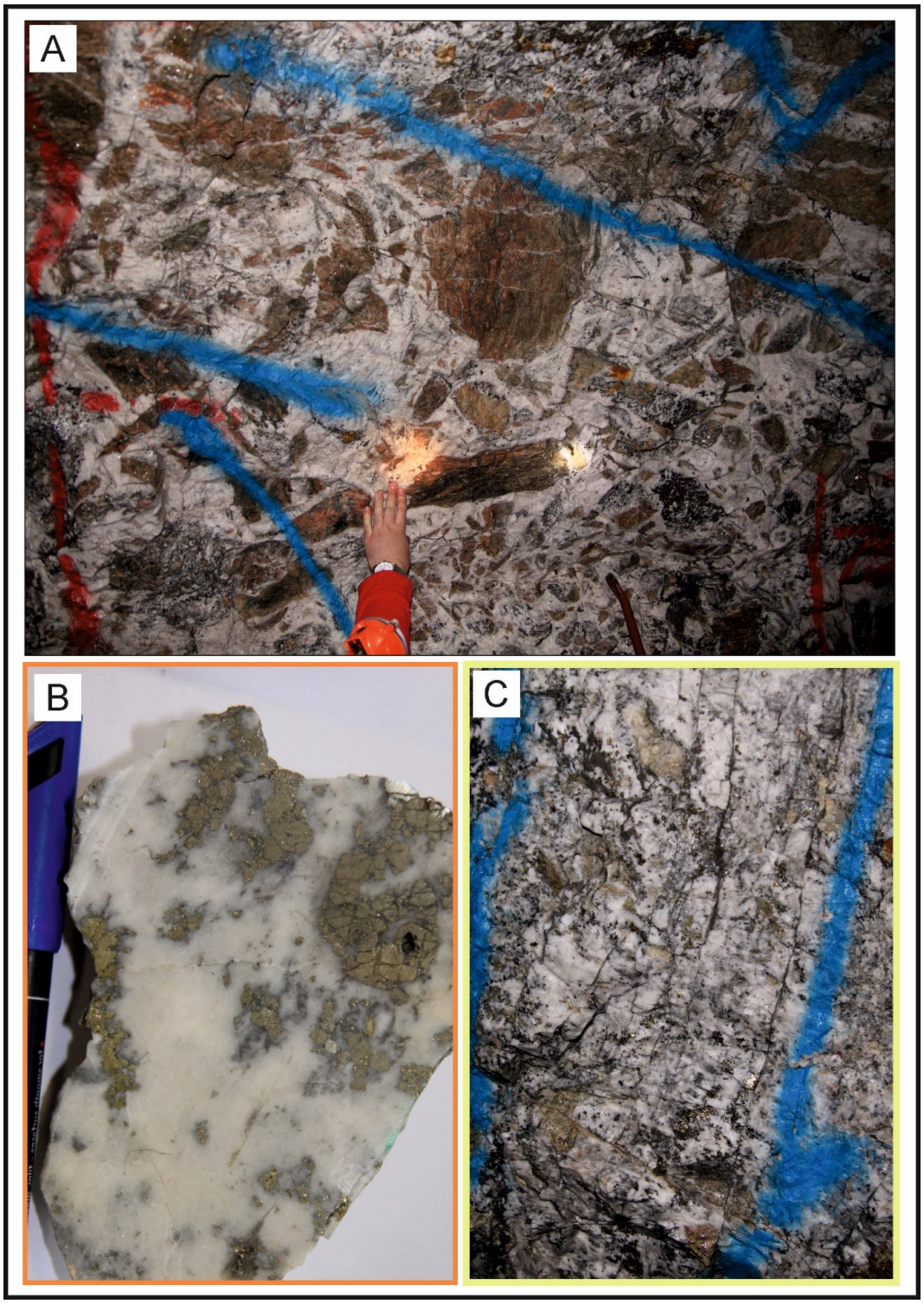

Figure 3.11 – A) Photograph of the Cononish vein showing stage 1 and 2 vein generations forming the cement to brecciated, rotated and altered wall rock in the footwall of the Eas Anie fault (Spence-Jones, 2013). B) Hand specimen of coarse pyrite in the milky white quartz that is distinctive of the early mineralisation (Spence-Jones, 2013). C) Photograph of the Cononish vein showing stage 1 and 2 vein generations forming a complex and chaotic breccia texture with no clear crosscutting veins or comb quartz evident in the outcrop.

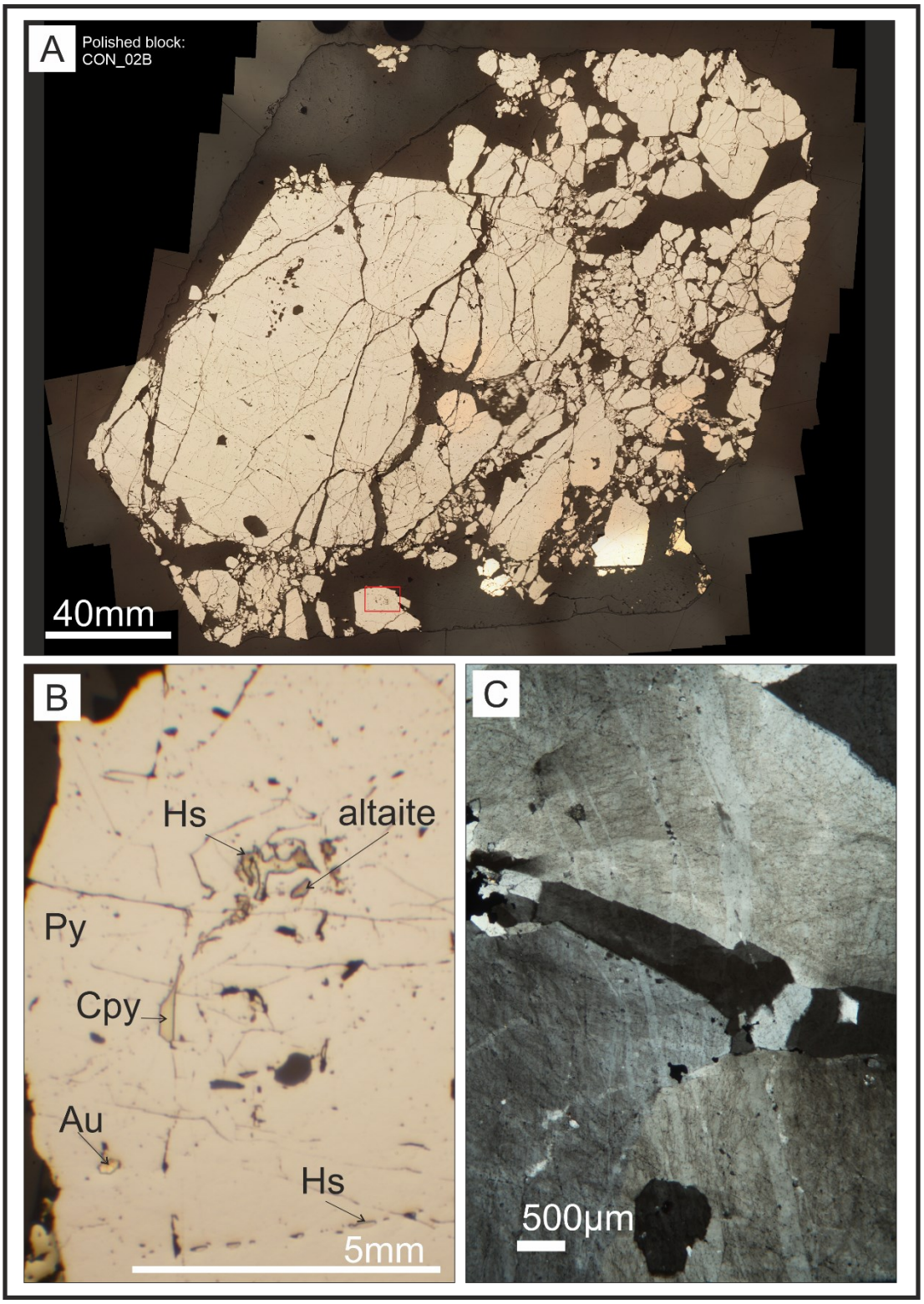

Figure 3.12 – Reflected light images of stage 2 vein material. A) A photo montage of an entire polished block showing coarse fractured early pyrite. B) gold (Au), altaite, hessite (Hs), chalcopyrite (Cpy), assemblages in inclusion within an early coarse pyrite C) Transmitted light XPL image of quartz in thin section CON_CO03 showing stage 1 coarse vein quartz. Different generations of quartz are revealed by differences in the inclusion/fracture density.

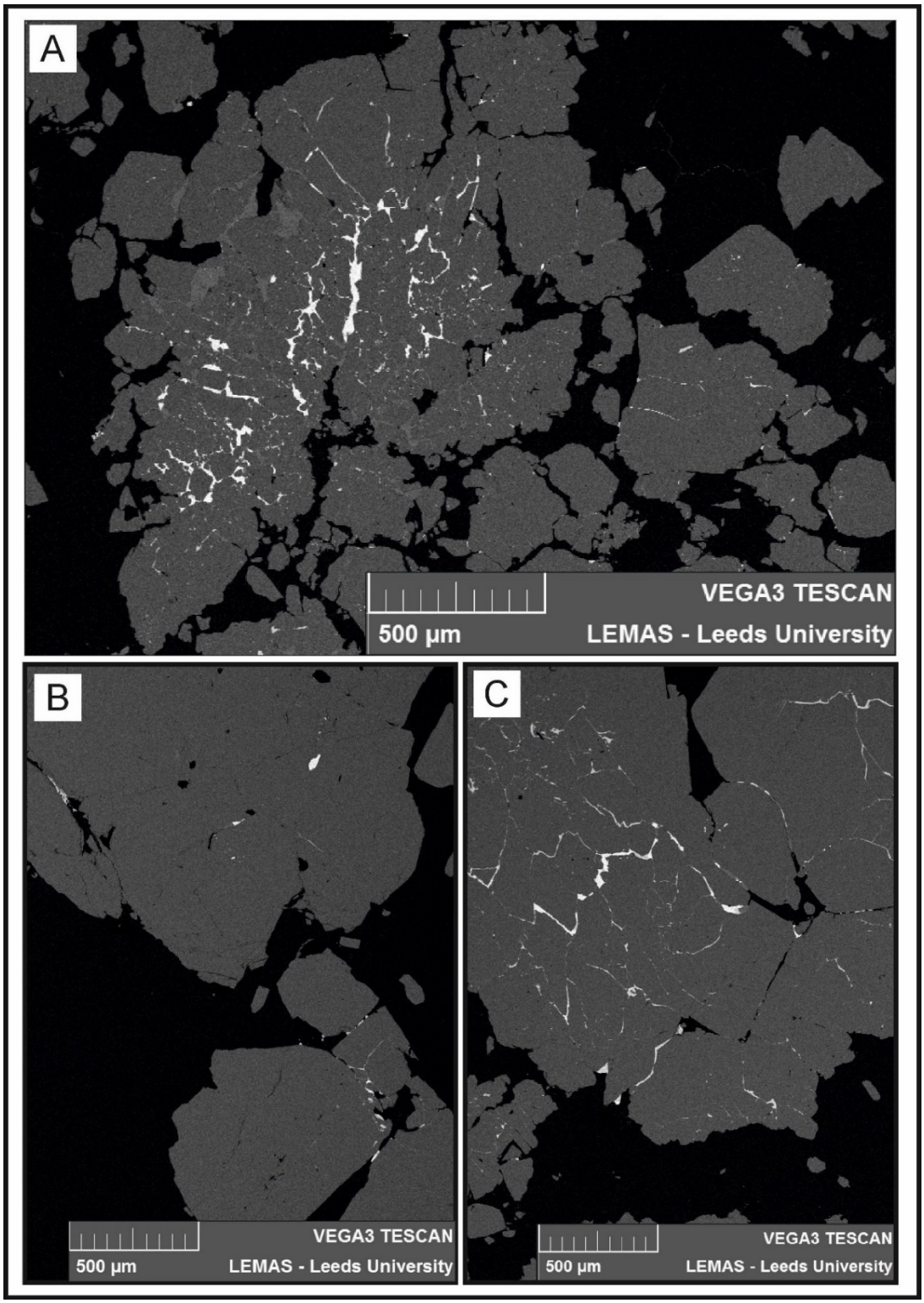

Figure 3.13 – SEM BSE images of TS Sample 1609 showing coarse pyrite crosscut by bright (Galena) veinlets of stage 2 mineralisation.

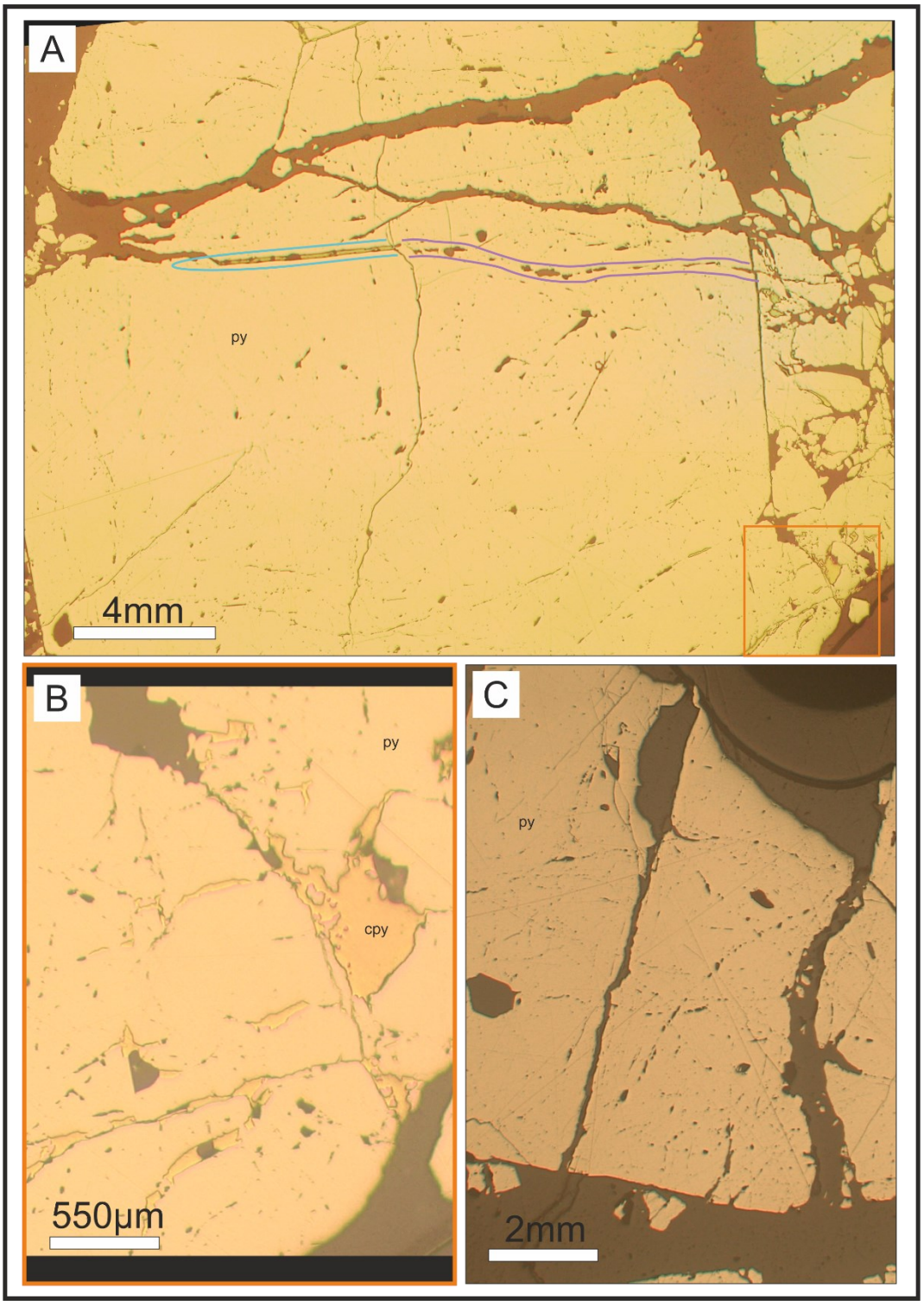

Figure 3.14 – Reflected light photomicrographs of stage 2 coarse pyrite.

A) Coarse pyrite cut by a later hessite galena veinlet which is intact on the left of the image (blue highlight) but appears to be continued as a line of inclusions on the right of the particle. This indicates that the pyrite has recrystallized on the right side of the fracture running down the centre of the particle. B) Enlarged section of image A; showing chalcopyrite in veinlets in the coarse pyrite. C) Additional example, of inclusions trails within the early coarse pyrite.

Stages 3–4 – Evolution of the Au–Ag mineralisation

The vein material formed during Stages 1 and 2 are crosscut and comminuted by later narrow, 0.5–10 cm–wide veinlets of dark grey quartz with sulphides, figures 3.16 and 3.14A. Veins in stages 3 and 4 are distinct as they are both comprised of abundant chalcopyrite and galena. These two sulphides form >50% by volume of the veinlets with subordinate quartz and minor pyrite, sphalerite, calcite, Au–Ag alloys, and rare hessite, figures 3.13, 3.14 and 3.18.

These sulphide rich veins form anastomosing arrays in zones up to half a metre wide, which are best developed in proximity to the observed fault plane of the Eas Anie fault: figures 3.7 and 3.9. Crosscutting relations, figure 3.16, show that earlier veins in these narrow arrays are galena dominated, with only minor chalcopyrite observed, which are interpreted as stage 3. In comparison the later veins (Stage 4) are chalcopyrite dominated assemblages. However, these two distinctions are only general endmembers and veins in these stages are a continuous variation of galena and chalcopyrite rich veinlets which all occupy a consistent structural setting.

Chalcopyrite and galena are observed to be intergrown and have an myrmekitic texture in some thin sections (1604B). The intergrowth shows that rapid crystallisation of both phases simultaneously occurred in the veinlet, figure 3.15. CL imaging of the quartz around the myrmekitic texture reveals it is formed in a vug, with the small amounts of quartz around it showing euhedral forms.

Stage 4 veins are observed to often contain minor calcite and acanthite (Ag2S) as an accessory Ag phase. This marks a distinct difference in comparison to the early veining which contained silver accessories in the form of tellurides (hessite). Whether a particular vein in an individual sample is Stage 3 or 4 is often difficult to decide due to variations in mineralogy along the veins. In practice, the distinction is made on the relative proportions of galena and chalcopyrite and the Au-Ag alloy composition (see section 3.4.1.1.3 for work on the gold alloy compositions).

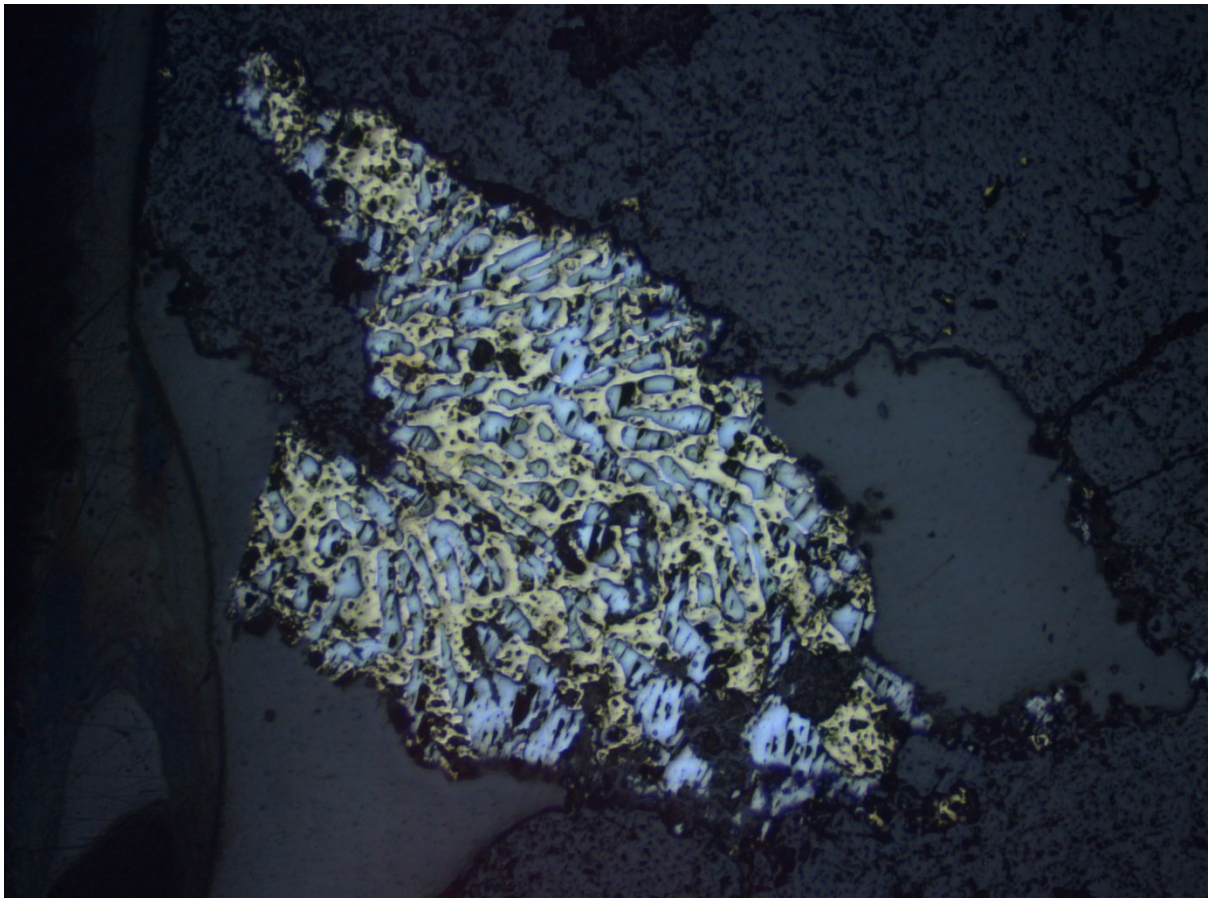

Figure 3.15 – Reflected light image of myrmekitic (intergrowth) texture of chalcopyrite and galena (section 1607B). FOV of image is 16mm.

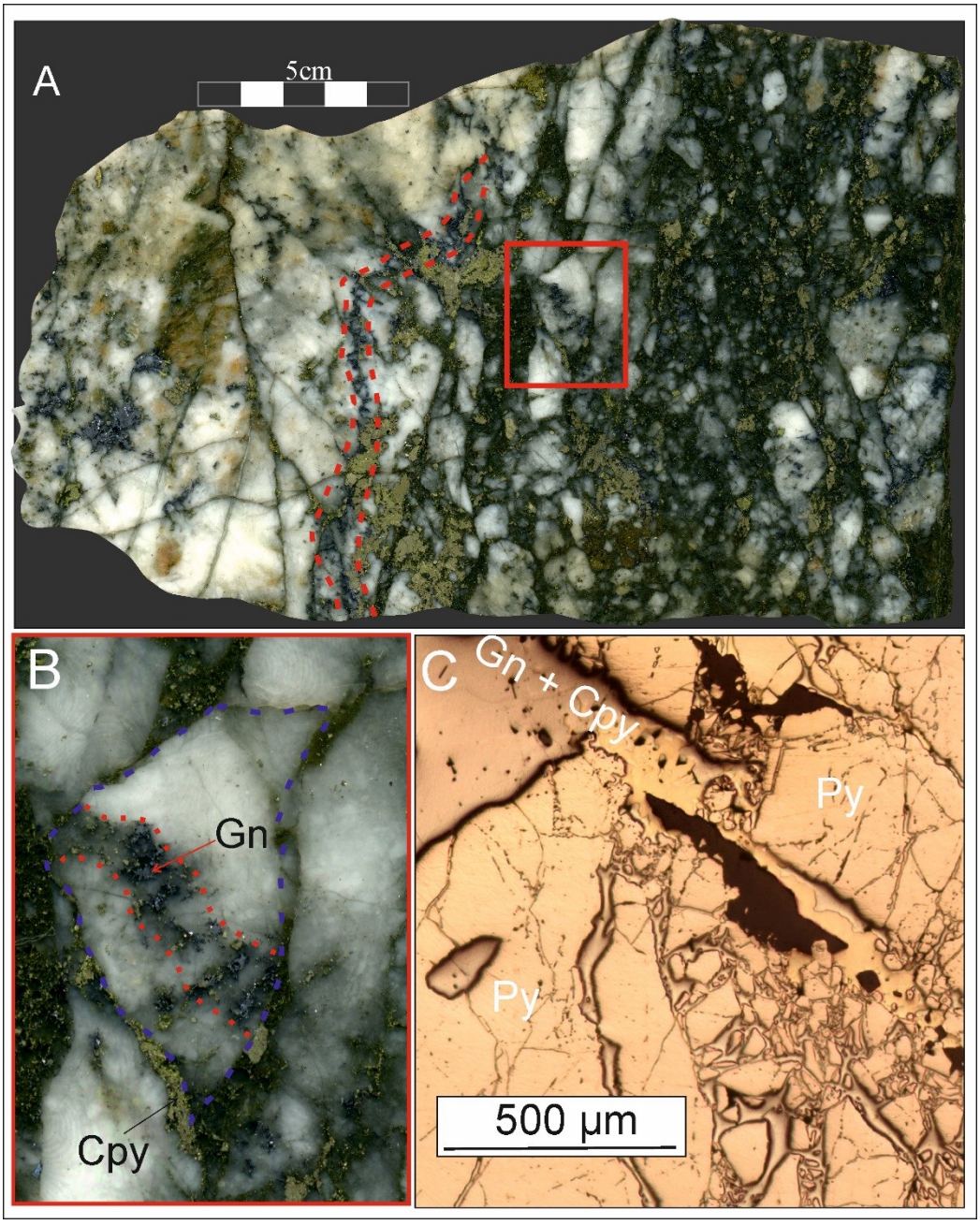

Figure 3.16 – Vein samples showing late stage 3/4 mineralisation. A. Polished hand specimen sample Con_CO03 taken from the footwall of the Eas Anie vein. The right size of the block is the fault plane with late slicken lines and a clay gouge. Early Stage 1/2 quartz is brecciated by multiple crosscutting Stage 3/4 veining, the intensity of fractures and sulphide rich veinlets increases in proximity to the fault structure. The red dashed line marks galena rich veinlets crosscut by later chalcopyrite. B. Area show by the red box in image A. An early generation of galena rich sulphide veining (red) is seen within a clast (blue outline) mantled by later chalcopyrite rich vein material. C) Composite reflected PPL image of sample CON_CO06 showing brittle fracturing and veining of early stage 2 pyrite (Py) by later Stage 3/4 galena (Gn) and chalcopyrite (Cpy).

Stage 5 – Post ore alteration

This stage is only observed in one location underground, referred to as the "666 zone" by miners (Spence-Jones, 2013). At this location, earlier veining from stages 1-4 is strongly altered to magnetite and hematite, and calcite veining is pervasive. The 666 zone is localised to a narrow area in the roof of the adit and appears unrelated to the stage 1-4 mineralising event but rather appears to be a post-ore alteration. The relationship of Stage 5 to the later Pb veining (stage 6) is not known and the earlier placement in the paragenesis is based on the lack of vuggy textures and greater textural and mineralogical similarity to stages 1-4 rather than the brittle vuggy late Pb veining (Spence-Jones, 2013).

Pb-Zn Vein

The late Pb-Zn veining (the B-min of Earls et al. (1992)) clearly crosscuts stages 1-4, often at a different orientation, and comprises predominantly sugary, fragmented, highly vuggy, banded, cockscomb quartz with abundant coarse euhedral galena and yellow sphalerite, figures 3.17 and 3.18. It is temporally separated (determined by cross relationships) from the gold veining (stages 1-4) by a basaltic dyke, figure 3.17 and 3.18 (Earls et al., 1992). No auriferous mineralisation is reported in occurring in the Pb-Zn veins in the literature or found in this study.

The Pb-Zn vein is clearly distinguishable from the A-min quartz in CL and clearly crosscuts the A-min. This was only seen in one thin section which has a late fault/vein on the margin of the section. As no sections of B-Min have been specifically examined, the paragenesis within the Pb-Zn stages cannot be interpreted. However, the B – min is observed to be clearly distinguished from the A-min vein texture. It has clearly defined banded/comb textured un-fractured quartz with growth banding symmetrically building out from the vein margins seen in figure 3.20.

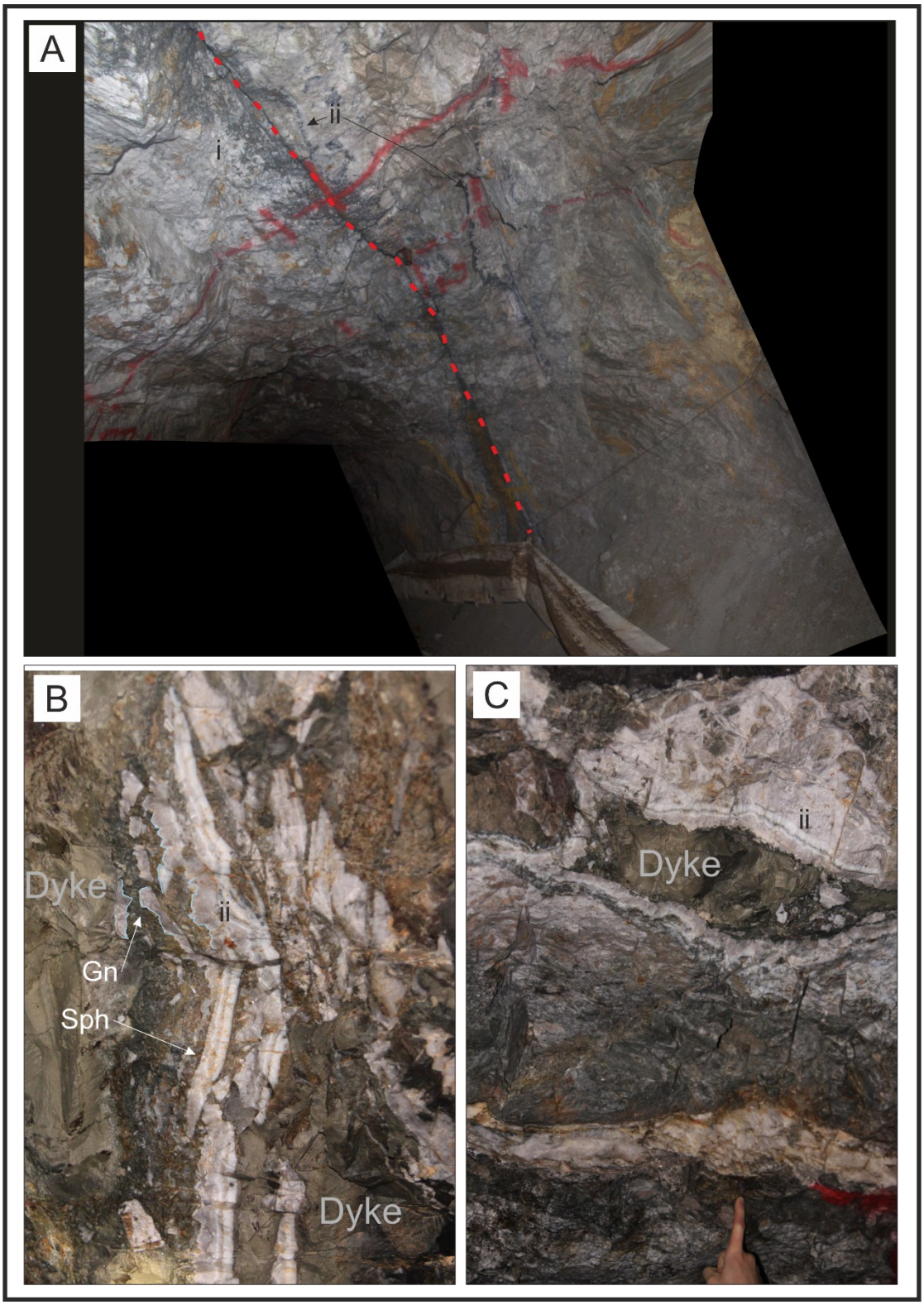

Figure 3.17 – Photographs of the B-Min mineralisation underground. A. Photo of the Eas Anie fault showing the A-min (i) and B-min (ii) veins. B. Galena and sphalerite rich B-min vein showing sugary comb and banded quartz. C. Interaction of the vein and the basalt dyke(s) which crosscuts the A-min an altered clast of dyke is mantled by banded B min.

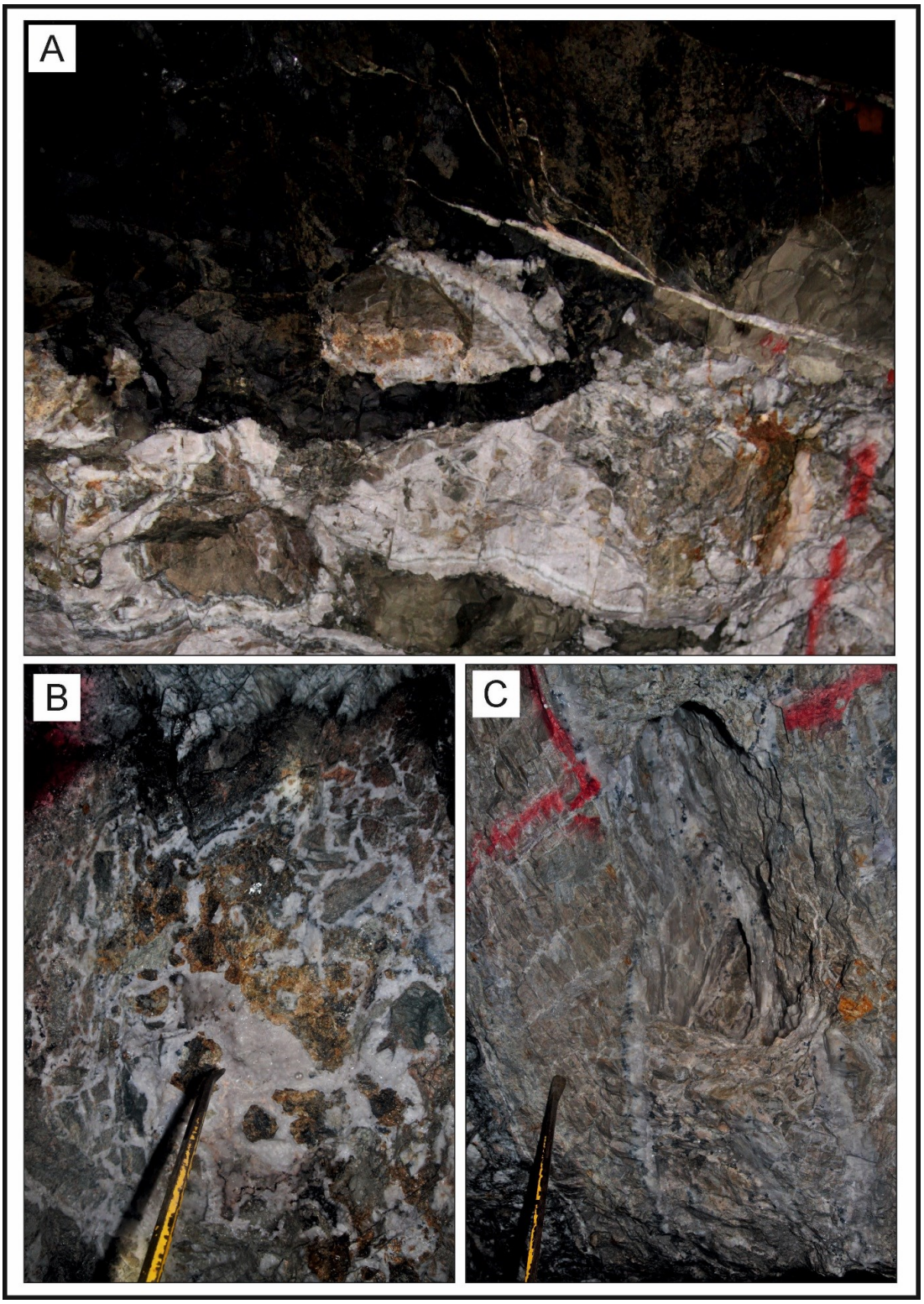

Figure 3.18 – Photographs of the Pb-Zn (B – Min) vein underground. A. interaction of the vein and the basalt dyke(s) which crosscuts the A-min an altered clast of dyke is mantled by banded B min which in turn appears to be crosscut by fresher basalt at the top of the image. B. Coarse sphalerite in the B-Min vein. C. Lookup at the roof where a B-min banded vein with galena at the core exists parallel the Eas Anie fault.

Figure 3.19 – Colour Cathode luminesce image of polish block 03D. Diameter of block is 2.5cm.

Yellow outlines highlight large clasts of early, S1/2, vein in a matrix of S3/4 vein assemblages (which also contains many small clasts of S1/2 vein which are not highlighted). The S3/4 vein has a higher proportion of sulphides and carbonates (red CL colours).

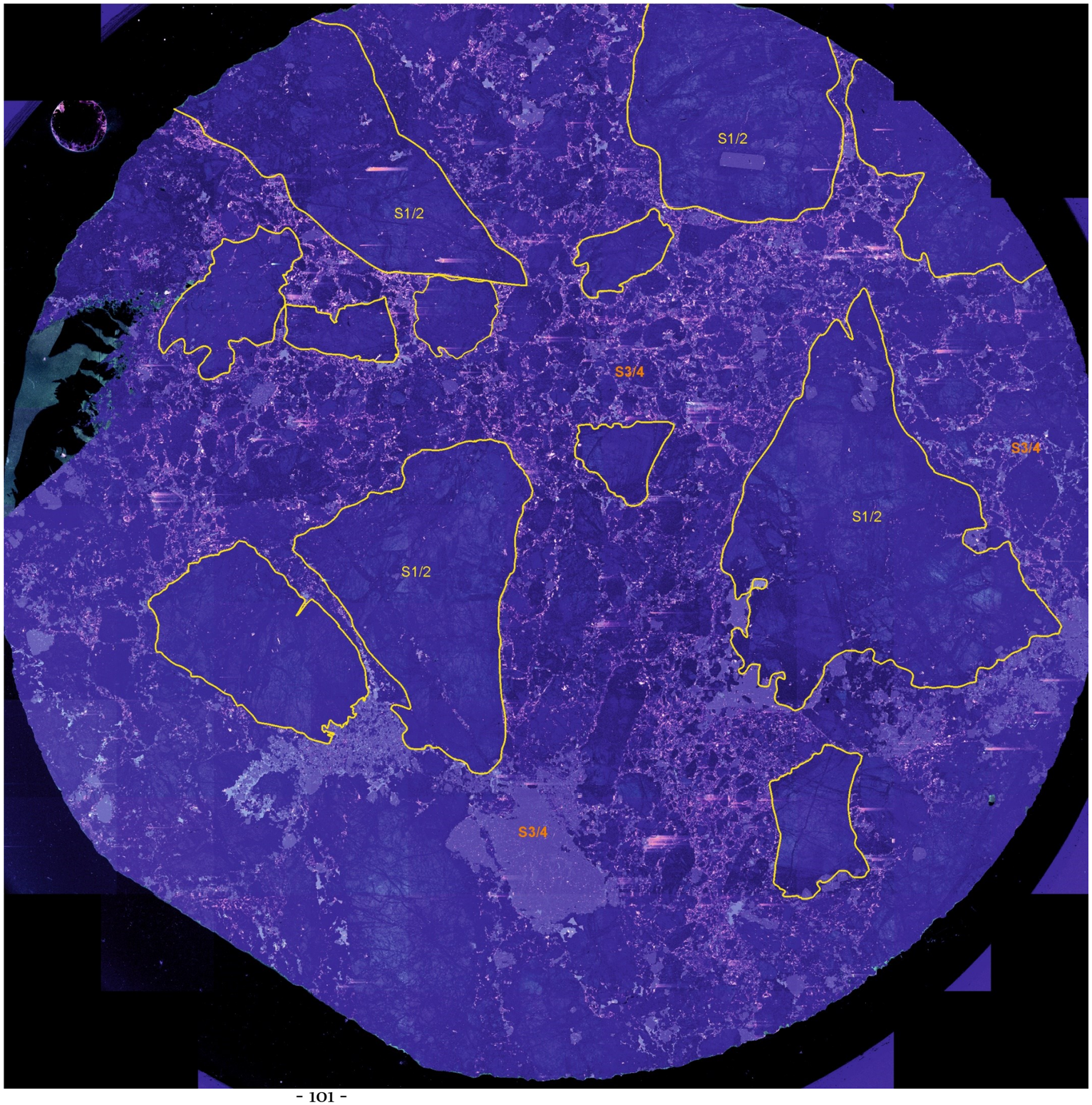

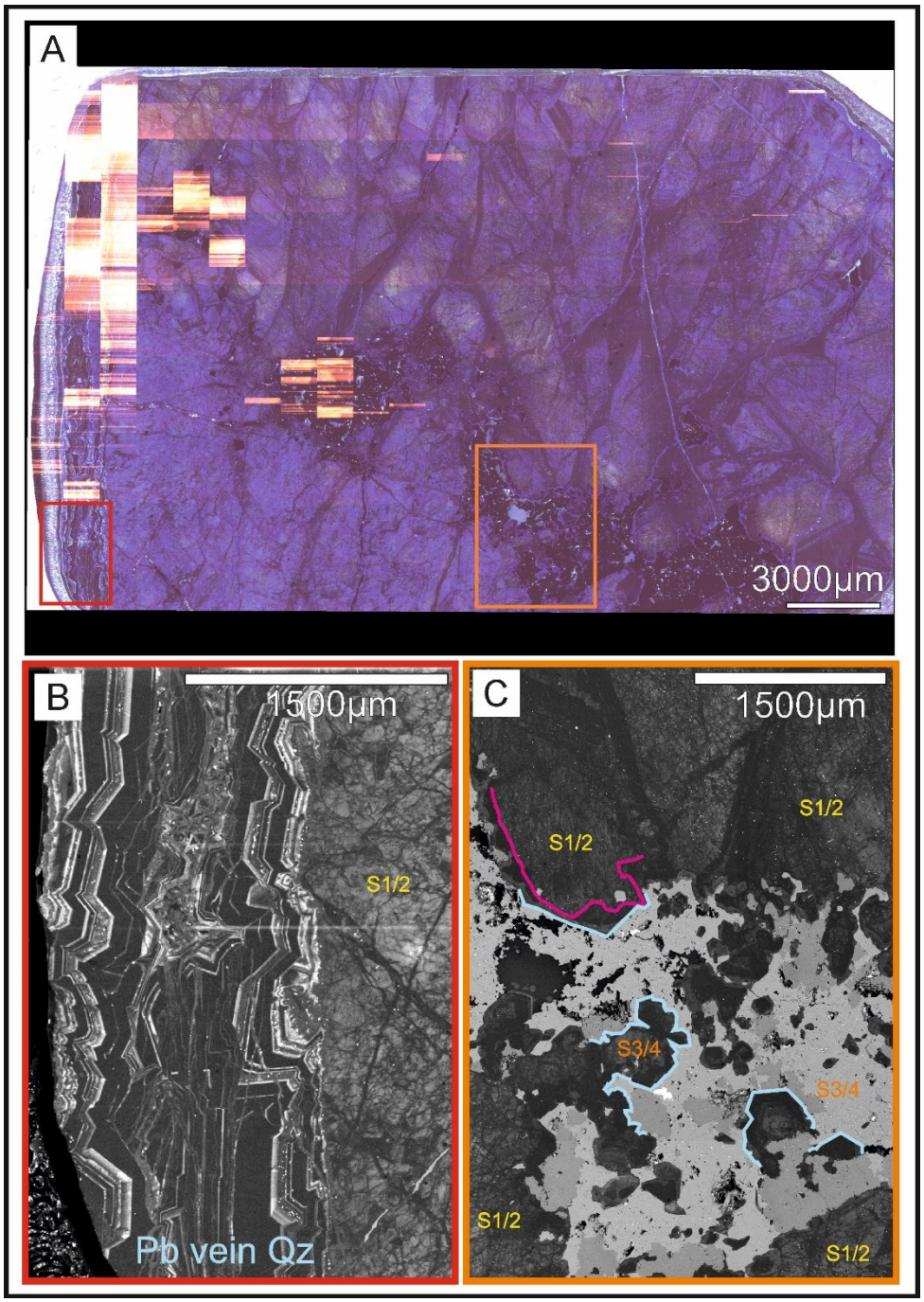

Figure 3.20 – A. Panchromatic CL of the entire thin section 1609B. B. An example of the Late Pb-Zn quartz vein in the Eas Anie fault structure, showing it clearly crosscuts the fractured early Au vein stage 1/2 quartz, which contains banded coxcomb open space filling quartz textures. C. Euhedral quartz with later infilling sulphides in a brecciated quartz. At the top of the picture a brecciated stage 1/2 quartz clast (outlined in purple) on which can be seen an overgrowth of euhedral comb textured stage 3/4 quartz (outlined in light blue). Similar quartz is observed growing into the open space on sulphides at the bottom of the image (highlighted in light blue) and showing almost complete euhedral forms in the centre of the vug, which has been infilled with late sulphides, chalcopyrite dominant.

3.4.1.1.3 Geochemistry

Gold

In situ observations:

The first analysis of the chemistry of gold particles observed in thin sections was conducted during the Masters project of the author (Spence-Jones, 2013). These results are published, combined with PhD observations in Spence-Jones et al. (2018). In the work of Spence-Jones (2013) EDX analysis of the Au and Ag content of 215 gold particles were recorded, along with the major axis length and mineralogical association of the particles. The gold particles' major axes range from 1 to 400 µm, with a median of 15 µm. The median aspect ratio is 2. Some particles are highly elongated along fractures (up to 400 x 5 µm), but the few particles with the largest area (20000-50000 μm^2) are fairly equant with an aspect ratio of 2–5. The composition of the gold ranges from ~10% to ~ 90 wt.% Ag, i.e. from gold to silver rich. This indicates that stable geochemical conditions were not prevalent during the formation of the Cononish deposit.

Spence-Jones (2013) reported the mineralogical association of the gold alloy composition to hessite, chalcopyrite, and galena phases. These three minerals characterise different stages of the paragenesis, and they demonstrate that the gold composition changed markedly through the paragenesis of the auriferous vein (stages 2 to 4 of the paragenesis), with the Ag content of the gold alloy increasing over time; figure 3.21.

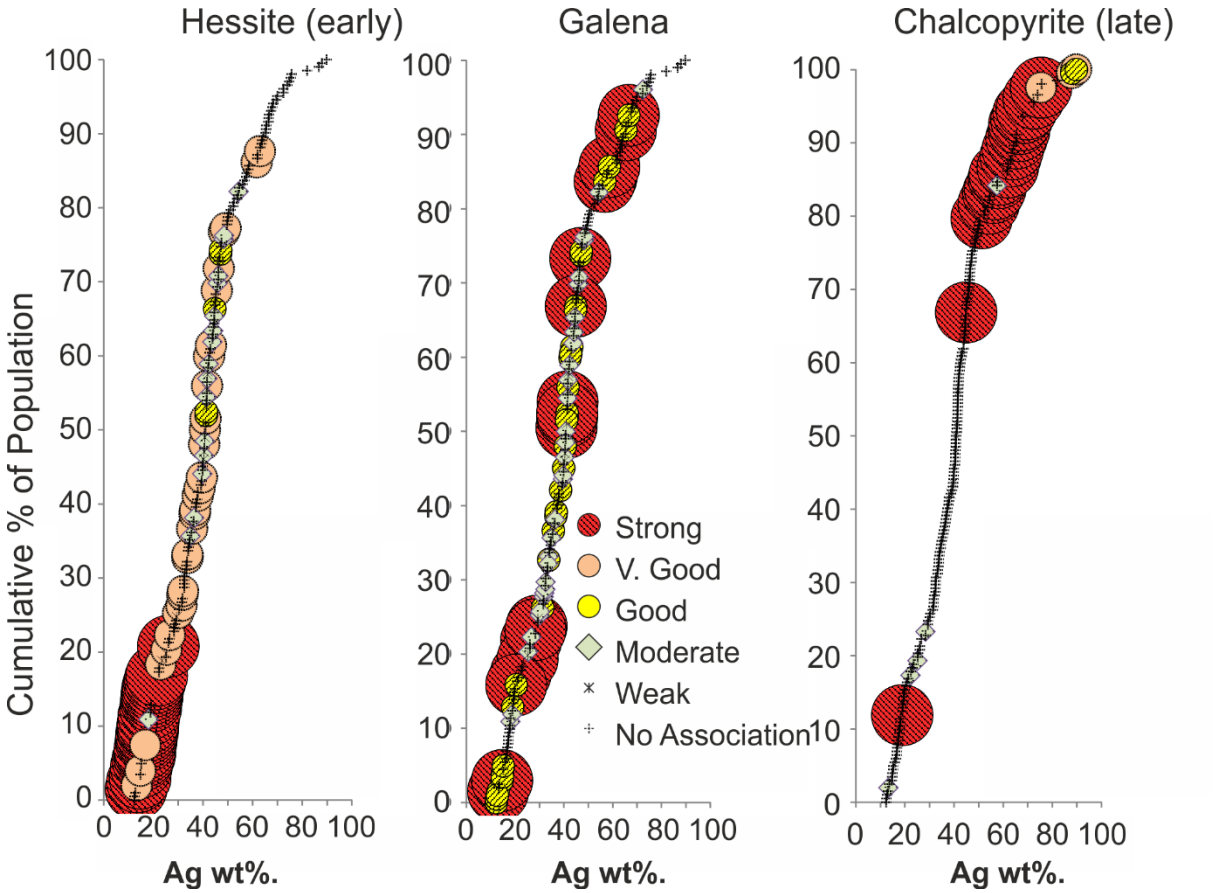

Figure 3.21 – Association of paragenetically constrained minerals to gold of a given composition redrawn from Spence-Jones (2013) data.

The work by Spence-Jones (2013) constrains the gold within the paragenesis, but cannot identify which vein stages, and thus which conditions were fundamental to the formation of the deposit; that is to say: which stage/conditions deposited the largest number/mass of gold particles? To investigate this the composition of gold particles in relation to the vein stages was assessed in an 'unbiased' (bulk) crushed and processed ore sample of the mineralisation, the results are presented in section 3.4.1.2. As the range of gold alloy compositions associated with each stage of the paragenesis has been quantified, the proportion of these specific ranges of gold alloys (as a proportion of the total number of particles within the bulk sample) can be used as a proxy to estimate the proportion of gold deposited in association with the different paragenetic stages within the deposit volume.

Pyrite

Pyrite is present as a mineral ubiquitously within the mineralised vein material. The properties of the pyrite in the different stages were examined in two ways: Firstly, pyrite samples were taken for S-Isotope analysis to investigate possible changes in the fluid source or chemistry between early and late vein stages. Secondly, etching experiments were undertaken to investigate if any textural differences could be observed in different pyrite generations.

S-Isotope analysis

Eleven pyrite S–isotope analyses are given in table 3.3 along with 5 analyses reported in Hill et al. (2013) that were taken from adit samples collected by Spence-Jones (2013). Locations are shown in figure 3.22. These are plotted along with the combined published S–isotope dataset for Cononish in figure 3.23. These results show a range of $\delta^{34}S$ values from -2 to +11.4‰. This reveals a trend of increasing $\delta^{34}S$ through the paragenetic sequence. Two samples could relate to either Stage 3 or 4 as they show mineralogical and textural features of both stages. These were plotted as Stage 3.5. The sample from Hill et al. (2013) with a $\delta^{34}S$ of -2‰, which was not paragenetically constrained in this study, is assumed to belong to Stage 2 and gives a lower value for this stage. If it is included in the statistics, the mean and standard deviation for Stage 2 would be +0.7±1.8‰. To avoid bias in the results, the position of the samples in the paragenesis was determined during sampling before analysis was undertaken.

Table 3.3 – Sulphur isotope results. *Data from Spence-Jones (2013) reported in Hill et al. (2013) assigned to the revised paragenesis here.

Sample	Description	$\delta^{34}S$ (‰)	Stage sampled
CO02a	Stage 2 coarse pyrite in white massive stage 1 quartz vein.	1.3	2
CO02b	Stage 2 coarse pyrite in white massive stage 1 quartz vein.	1.7	2
CO02*	Stage 2 coarse pyrite in white massive stage 1 quartz vein.	1.8	2
	Mean and standard deviation	1.6±0.3	
CO14a*	Sheared stage 3 vein with pyrite, minor Gal > Cpy present.	4.7	3
CO05.2c	Coarse pyrite crosscutting stage 1 and 2, Gal > Cpy.	6.6	3
CO05.2a	Coarse pyrite crosscutting stage 1 and 2, Gal > Cpy.	6.7	3
CO05.2b	Coarse pyrite crosscutting stage 1 and 2, Gal > Cpy.	6.7	3
CO14b*	Stage 3 vein with pyrite crosscutting stage 1 and 2, minor Gal > Cpy.	7.2	3
CO06c	Pyrite veinlet in sulphide rich quartz crosscutting stage 1 and 2.	8.5	3
	Mean and standard deviation	6.7±1.2	
CO06a	Coarse pyrite in stage 3/4 vein (Gal ≈ Cpy).	8.2	3/4
CO06b	Coarse pyrite in stage 3/4 vein (Gal ≈ Cpy).	8.3	3/4
	Mean and standard deviation	8.3±0.1	
CO05.1	Coarse pyrite in veinlet hosting Cpy > Gal.	8.3	4
CO05*	Coarse pyrite from narrow sulphide rich shear hosting Cpy > Gal.	8.9	4
CO03c*	Pyritic veinlet hosting abundant Cpy > Gal.	11.0	4
CO03a	Pyrite veinlet hosting abundant Cpy > Gal.	11.2	4
CO03b	Pyrite veinlet hosting abundant Cpy > Gal.	11.4	4
	Mean and standard deviation	10.2±1.4	

.

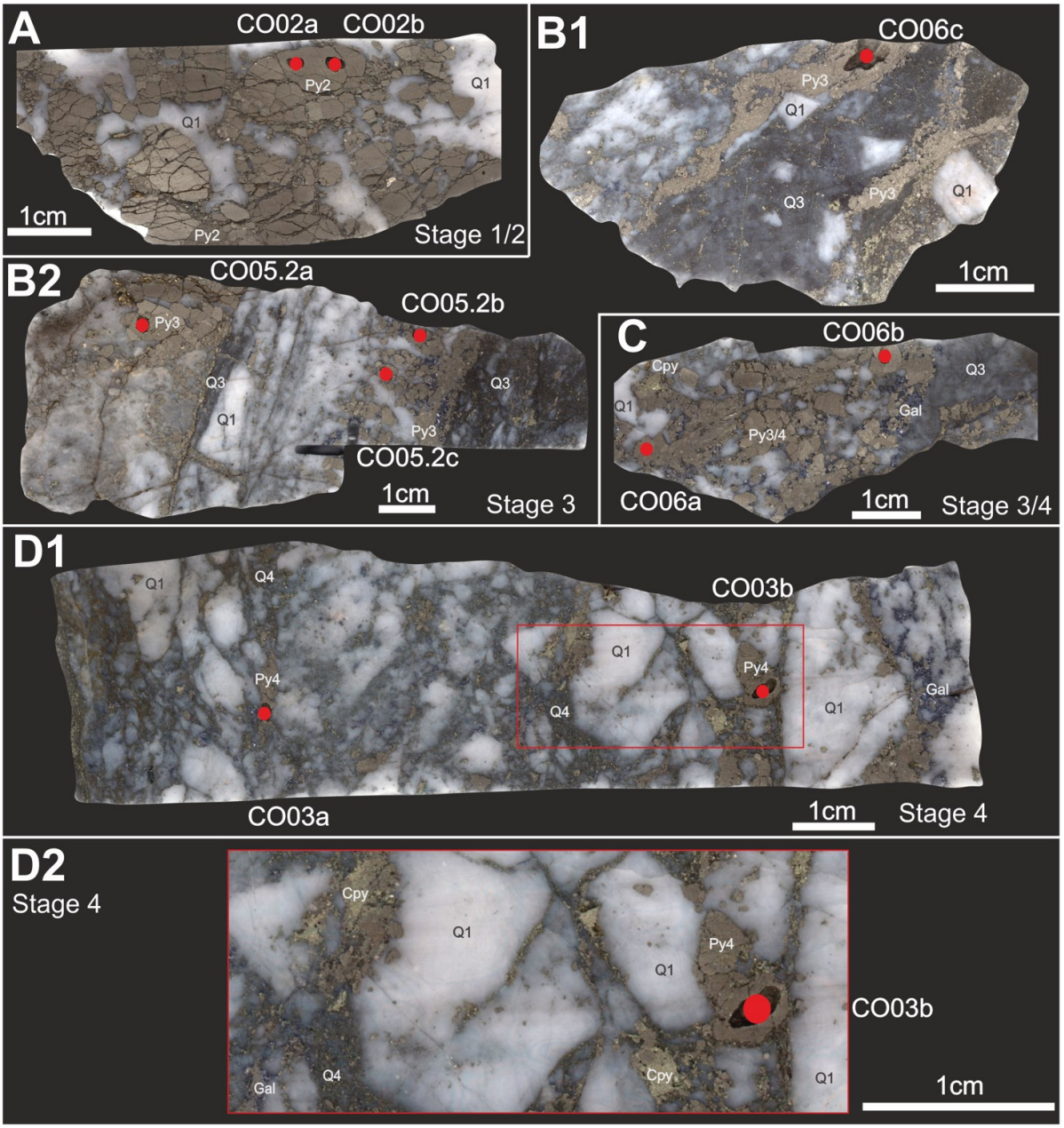

Figure 3.22 – Scans of polished slabs showing the location of drilled sulphur isotope samples (red circles) and the interpreted stage of the pyrite sampled. A. Early Stage 1 milky quartz with coarse pyrite of stage 2. B1. Stage 3 pyritic veinlets with trace galena and chalcopyrite on the margins of a dark pyritic quartz vein brecciating stage 1 quartz. B2. Coarse pyrite crosscutting the margin of a dark pyritic quartz vein crosscutting massive stage 1 quartz. C. Coarse Stage 3/4 pyrite crosscutting stage 1 quartz with approximately equal proportions of coarse galena and chalcopyrite. D1. Multiple coarse Stage 4 pyrite (with coarse chalcopyrite and minor galena) and pyritic quartz veins cross cutting/brecciating Stage 1 quartz. D2. An enlarged proportion (red box in D1) showing the coeval intergrowths of pyrite and chalcopyrite.

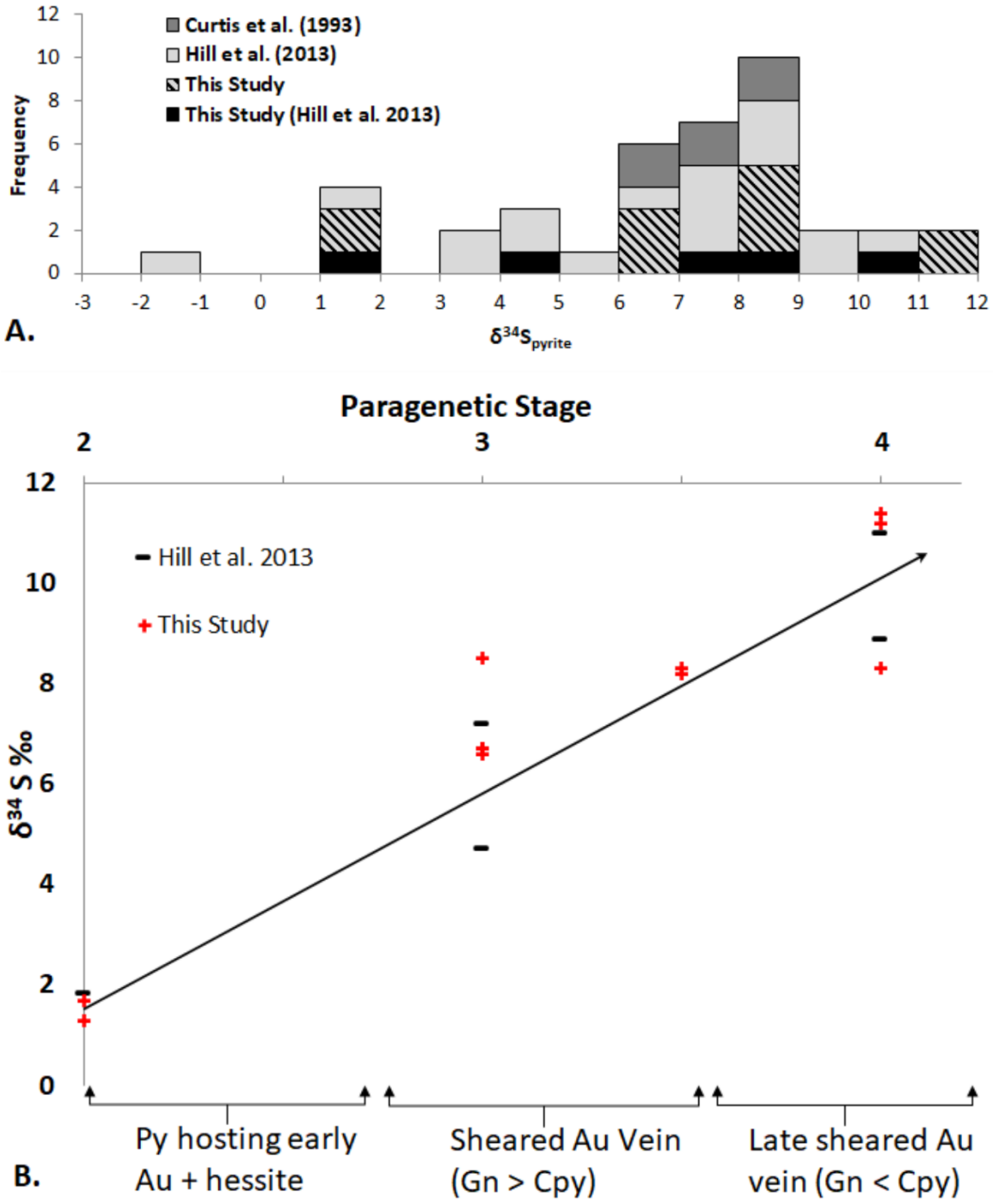

Figure 3.23 – A. Histogram of compiled pyrite $\delta^{34}S$ for the Cononish deposit. Hill et al. (2013) light grey data points are Cononish ore samples not petrogenetically constrained. The black coloured data Hill et al. (2013) points are petrogenetically constrained (those plotted on part B). B.Pyrite $\delta^{34}S$ plotted by interpreted paragenetic stage the pyrite was sampled from. A clear increase is seen from less than 2 ‰ $\delta^{34}S$ to greater than 10 ‰ $\delta^{34}S$.

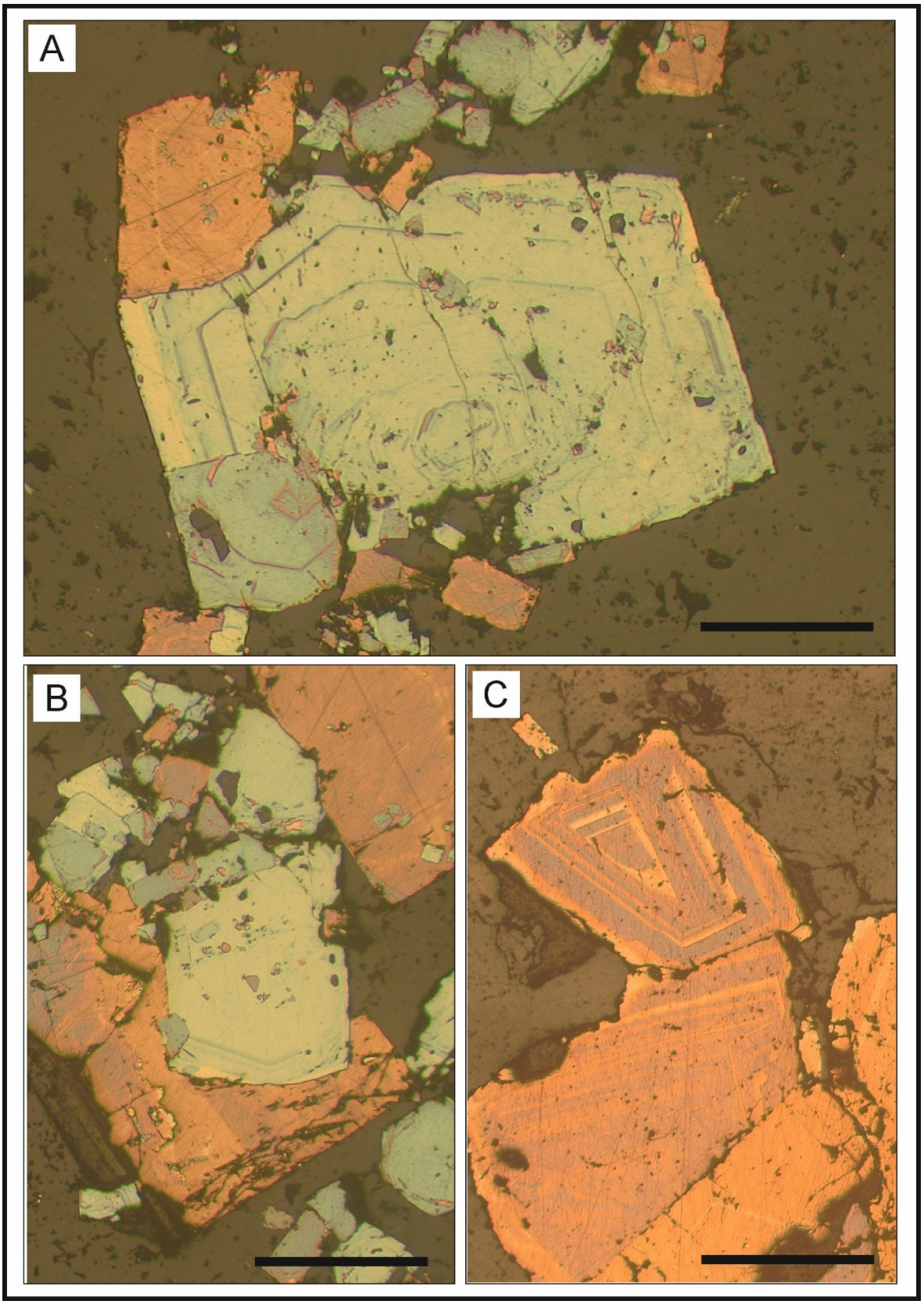

Figure 3.24 – Reflected PPL photomicrographs of pyrite in polished blocks that had the surfaces left exposed to the atmosphere for approximately 2 years. Black bars are 2mm in length.

Pyrite textures (etching experimental results)

A test experimental study was undertaken to evaluate whether an etching solution would be a practical method to examine the growth zoning and internal textures of pyrite particles taken from the Cononish ore. If textures could be revealed by etching then these could be compared for the different paragenetic stages.

Polished blocks of Cononish ore containing pyrite were exposed to potassium permanganate sulphuric acid solution. The samples were exposed to the solution for increasing time increments but no differential or consistent etch was seen to be developed in the pyrite. However, some zoning textures were observed in polished blocks left exposed to the air in a drawer for approximately 2 years. Images of the developed textures are show in figure 3.24.

3.4.1.2 Bulk processed ore, gold gravity concentrate sub-sample

To investigate the properties of gold particles within the deposit, a sub-sample of gold particles taken from the gravity concentration shaking table from the Scotgold ore processing plant at the mine was obtained. This represents the coarse fraction of the gold particles, that are liberated by ore processing to produce doré bars. At the time of sampling, Scotgold Resources were processing stockpiled ore which was mined when the exploration adits were driven. As such this ore was the best available representative sample of the ore system as no targeted stoping of ore was conducted during driving of the exploration adit. Therefore, no particular area of the ore system could be considered over represented or prejudiced to produce the ore feed for the plant.

The sample obtained from the gravity concentration shaking table contained fine gold (25µm +) along with larger particles of galena and heavy ore phases (tellurides). Due to the small size of individual gold particles individual mounting of particles was not practical for most of the sample. The three largest gold particles (each approximately 500 µm in diameter) were picked out and mounted individually in a 35mm resin block with the rest of the sample dump mounted (as a powder) within a 35mm resin block and sectioned for analysis.

A BSE map of the 35mm block was generated by collating interval images across the entire sample, see figure 3.25. A significant proportion of the gold particles show heterogeneity, observed by variations in greyscale within them

indicating multiple depositional events formed the particles. Ideally a statistical analysis would have been conducted using grey scale BSE automated image analysis to count and measure the population of gold particles. However, there is such a broad range of BSE Gray scale brightness from gold particles due to the range in Au-Ag ratios of the gold particles, that this precluded discrimination of the gold particles from galena using grey scale values. Instead, analysis of the population of gold particles was done using morphology (and cubic cleavages) by EDX analysis on the SEM and using reflected light microscope system on the microprobe.

The 3 largest particles, mounted separately also display compositional heterogeneity within the particles. Both sharp and gradational transitions between different compositions were observed within a single particle, figure 3.25 (B & C). Microprobe analysis of the compositions of the gold shows large compositional differences (40+ Ag wt% differences) across heterogeneous zones. The gold appears to have formed from multiple generations of gold deposition having different chemistry with the later crosscutting (and mantling) generations of gold being comparatively silver rich. This observation supports the interpretations based on in situ microscopy that gold evolved to become silver rich over time (Spence-Jones, 2013).

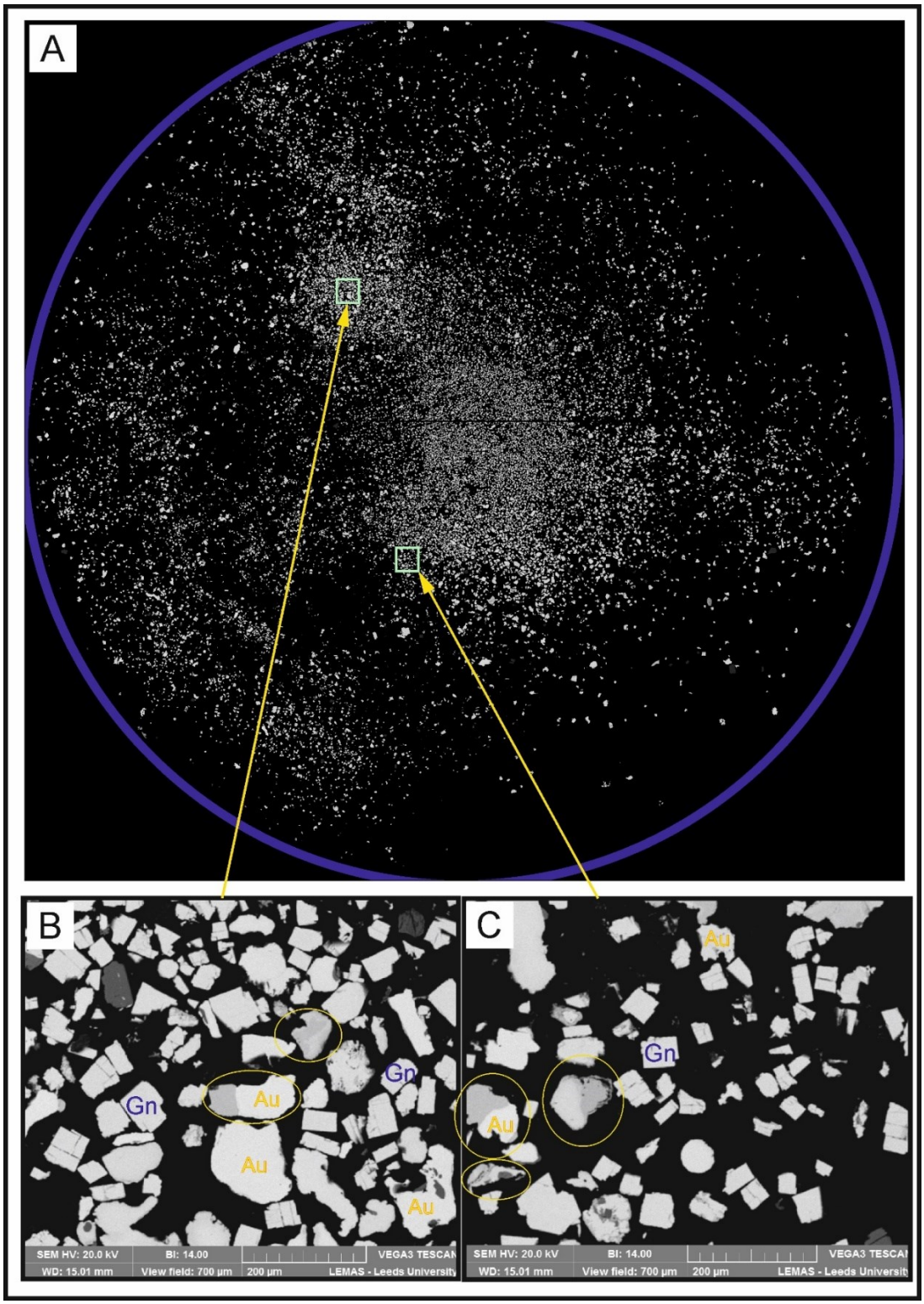

Figure 3.25 – BSE images of the mounted gold gravity concentrate powder. A. Composite image of the polished block containing the dump mounted concentrate powder (block diameter 2.5cm). B & C. Detailed images showing gold particles with both heterogenous and homogeneous alloy contents, along with the abundant co-concentrated galena (Gn) particles.

To investigate the range of compositions within the processed bulk ore sub-sample a total of 427 gold particle were analysed on the microprobe at the University of Leeds to investigate the population of compositions within the sample, figures 3.26 and 3.27. Where gold particles contained multiple compositions, such as in figures 3.35 B and C, they were investigated and the 'core' composition was measured. This core composition was used for the purposes of assigning a composition to each particle for gold signature evaluation. The compositions are shown alongside the population of particles from Spence-Jones (2013) in figure 3.26, allowing comparison of the bulk sample with the gold observed in paragenetically constrained thin section samples obtain in the MGeol project. The results show differences between the population from the bulk sample mine concentrate and the population of gold observed in the thin section samples. The median gold particle composition is of 25.8 %wt Ag in the bulk mine concentrate vs 40.8%wt Ag for the in-situ gold in the thin section samples.

The difference in the populations indicate significant over representation of higher silver composition gold particles in the thin section population. The mine concentrate sample, with a median of 25.8 %wt Ag, indicates that 50% of the gold has a lower silver content than 25.8 %wt Ag. Considering the link between the compositions of gold and the paragenesis identified by (Spence-Jones, 2013), gold below approximately 25% has a very strong association with tellurides, specifically hessite, in the early (stage 2) vein assemblages. Therefore, it is clear that the majority of the gold is deposited early in the paragenesis and has a very strong telluride association. This is supported by a very strong correlation between tellurium concentration and gold grades in Scotgold assay data (Pers. Com).

The presence of internal heterogenicity within the gold particles in the gold gravity concentrate is noted. Internal alloy heterogeneity occurs as two areas of clearly differing composition with a sharp boundary and/or, as thin well-defined 'tracks' that are relatively rich in Ag. These tracks often have diffuse variations within them, figures 3.28. These features indicate that variation occurred in the conditions that control the gold and silver content during deposit formation, becoming progressively Ag rich over time (Chapman et al., 2021). This supports the interpretation of the evolution discussed in relation to the paragenesis. Microprobe investigation into the compositional differences in the late Ag rich (darker in BSE imaging) shows that very large compositional differences can occur over very short distances in the gold particles (>40 Wt%. Ag).

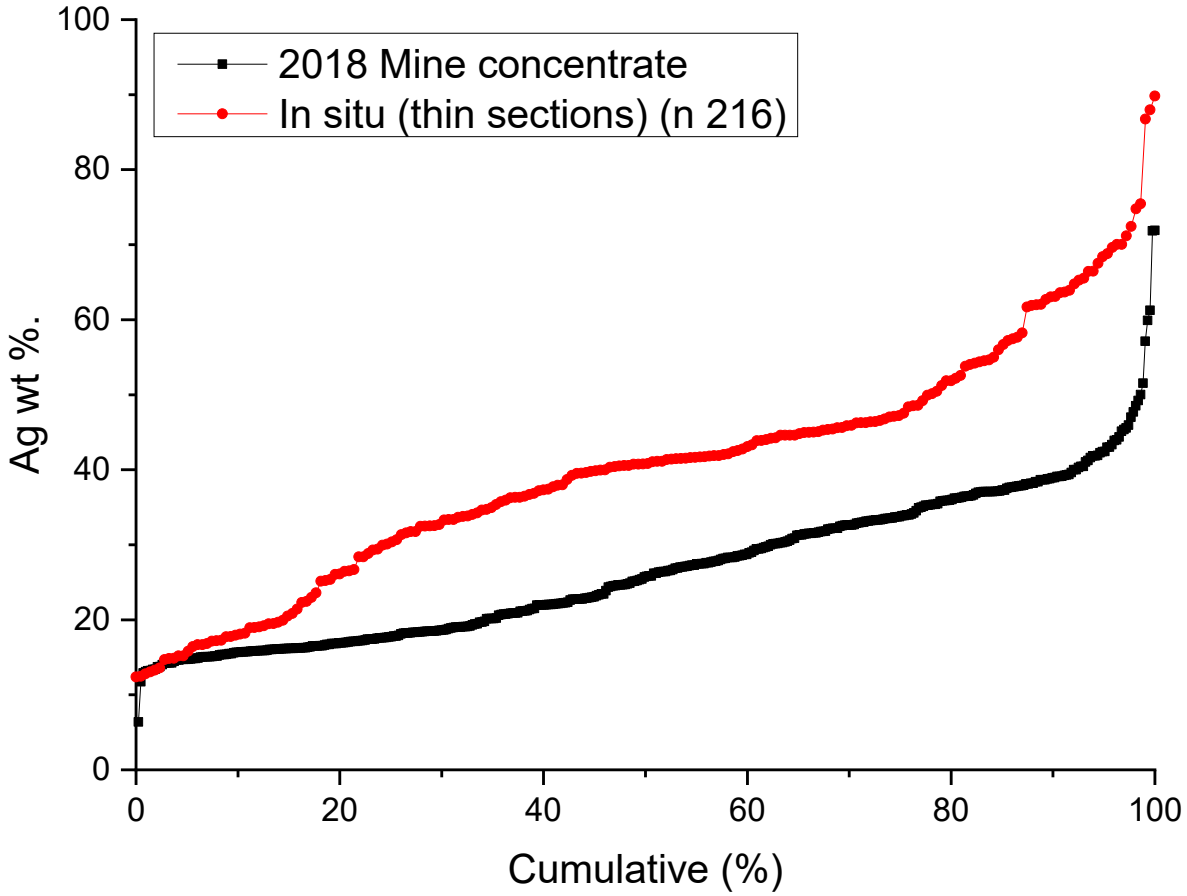

Figure 3.26 – Cumulative frequency distributions of silver in the core of gold particles in the mine concentrate sample vs previously observed in thin section samples (Spence-Jones, 2013).

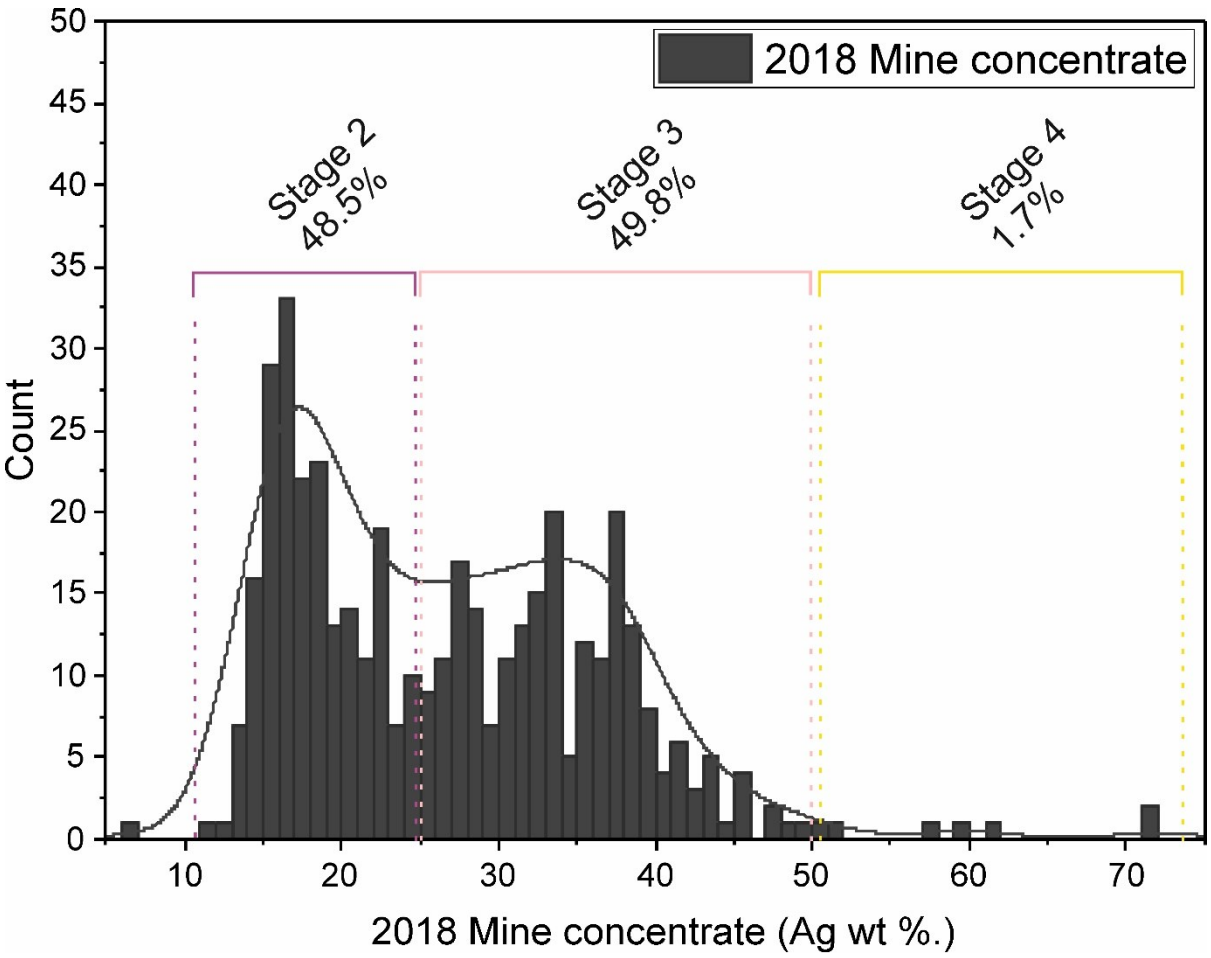

Figure 3.27 – Histogram (1 Ag wt%. Bins) of the core gold particles alloy compositions, recovered from the shaking table concentrate. The proportions within compositional brackets determined from the mineralogical work paragenetic work and gold compositions of Spence-Jones (2013). A smooth curve was produced using a kernel estimation algorithm in Origin pro software (Scott's rule used for bandwidth estimation, scaled to 80% maximum).

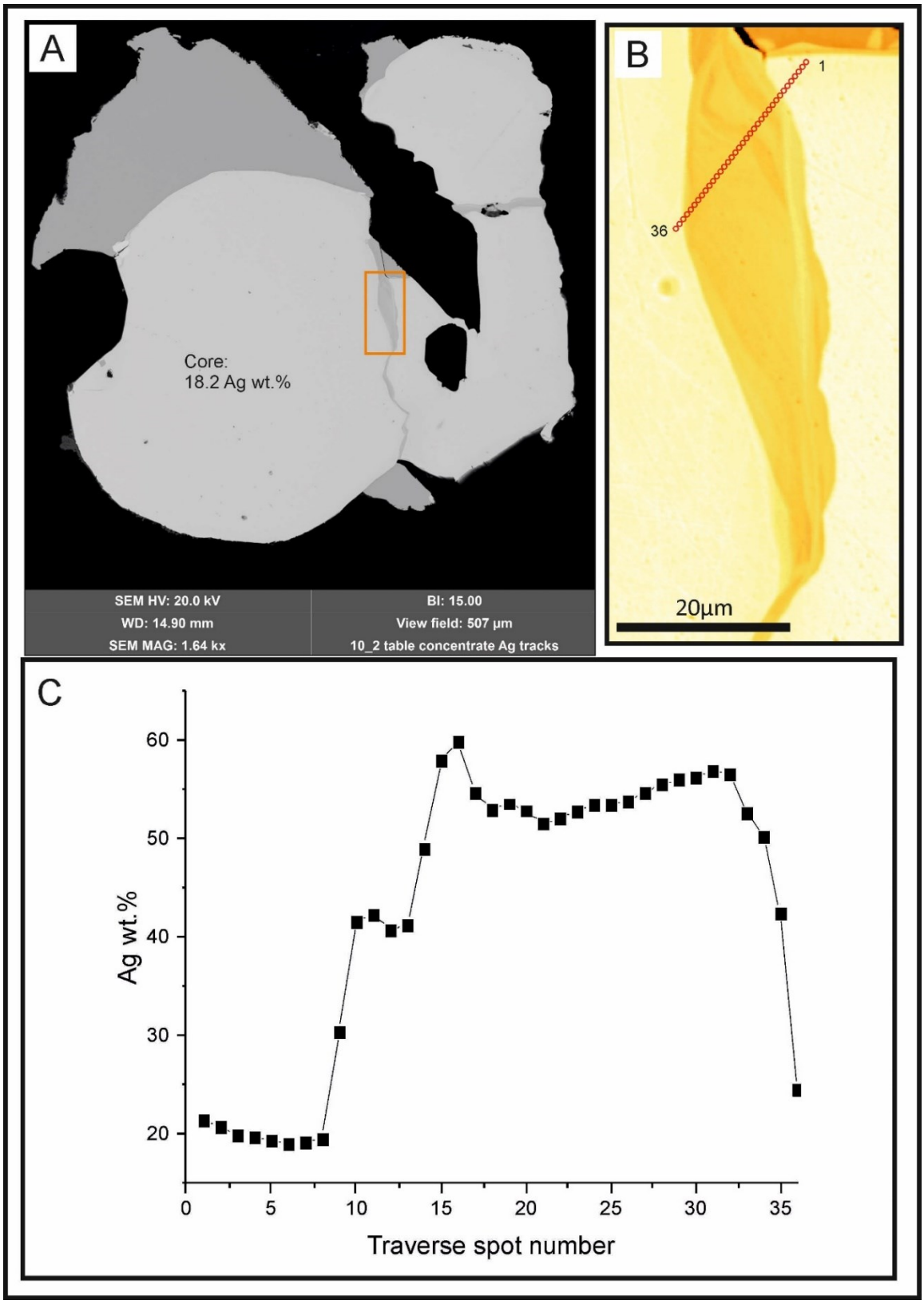

Figure 3.28 – A 36 spot microprobe traverse to investigate the alloy compositional data from a large heterogeneous gold particle taken from the gold gravity concentrate sample. A. image of the particle showing location of false colour image B, showing location of the traverse. C. the alloy compositions from the analysis sites along the traverse.

3.5 Discussion

The mineralogy and textures of the auriferous vein at the core of the Cononish deposit changed temporally during the development of the vein array. The developed paragenesis indicates that the early gold is strongly associated with tellurium minerals in vuggy quartz veins, while the late gold is associated with chalcopyrite in narrow sheared structures. The gold particles in the veins within these arrays show a compositional progression with the silver proportion increasing progressively through the paragenesis.

For the first time the proportion of gold which was formed during specific stages of vein development is estimated on a deposit scale. The results show that the early auriferous stages of the paragenesis are responsible for the most of the gold endowment, with a strong initial peak in abundance followed by a long-skewed tail indicating that progressively less gold is added by each subsequent generation of veinlets within the Eas Anie Structure.

The results show that the Cononish gold vein is formed from multiple generations of fluid flow which have deposited an evolving sequence of mineral assemblages that include the economic gold and silver phases. This evolving sequence is shown by the paragenetic model, figure 3.8. Measurements of the composition of gold-silver alloys show that the composition of the gold and associated mineral assemblages developed significantly through time as the deposit was forming.

The outcomes, implications, and conclusions drawn from the observations presented here are discussed in detail below in the context of the current published literature on the Cononish deposit, ore processes, and genetic models. The discussion is split into three sections: Initially, the textural observations are presented in the context of existing studies. Following that in a section on mineralogy, the new advances and understandings of the chemistry, and the key ore stages (evolution of the Au-Ag composition and sulphur sources are discussed in detail). To conclude, there is a discussion on ‘higher level’ interpretations of possible fluid sources, processes, and a new synthesised genetic model.

3.5.1 Textural Observations

The conclusion that the early (stage 2 and 3) auriferous vein stages are key allows greater focus on the significance of textures in these vein stages. The

variable thickness of the early auriferous vein, the rotated clasts of wall-rock, along with the observed coarse euhedral comb textures of the early quartz pyrite vein generations, indicate that the vein minerals were deposited into an open fluid filled space. Thus, structural controls on the vein dilation and opening of accommodation space infilled with euhedral comb-quartz, is a likely key to the identification of high-grade ore structures and zones within the deposit. This remains untested in the published literature with no significant structural study existing in the public domain.

The significance of the comb textures was initially underestimated and it was the CL analysis which revealed that much of the milky white quartz forming the 'core' vein has relic euhedral crystal growths. Comb quartz textures are often seen preserved within clasts in a brecciated fractured multigenerational quartz vein in CL, see figures 3.19 and 3.20.

The observation of the open space-filling textures indicates that the hydrostatic pressure of the ore forming fluids exceeded lithostatic pressures locally within the Eas Anie structure during the formation of the early mineralisation. This allowed the development of coarse pyrite blebs, which are observed to infill comb quartz, indicating that they formed post quartz in the order of deposition of individual veinlets.

To explore the significance of the open space-filling textures, the textures of the Eas Anie auriferous vein are compared with published descriptions of the giant-quartz-breccia vein in the Tyndrum area by Tanner (2012). This comparison shows that many parallels can be drawn. Tanner (2012) documented that the regional veins have cockade and vuggy textures and reports that as the damaged zone is approached, the veining increases and brecciates the country rock progressively. He inferred that these breccia's formed due to high fluid pressure exploiting pre-existing minor faults which show minor displacements of up to a few meters and minor post-quartz breccia movement. At the margins of the damaged zones of the breccia's, non-rotated clasts of the wall rock are observed, figure 3.29 (4), and become separated by increasingly thicker and more complex networks of quartz veins towards the centre of the damage zone. This results in the wall rock brecciated into ever smaller angular fragments. This can be clearly seen in the reddened altered clasts in the photograph of the exposure of the Eas Anie vein underground, figure 3.29B, when compared to Tanner's (2012) general model of the features, figure 3.29A. The numbers used in Tanner's (2012) figure have been placed on the same features in the photograph for clarification.

In the core of the quartz breccia's, documented by Tanner (2012), massive quartz is observed around matrix supported angular clasts These do not commonly show the same clear vuggy and cockade textures but contain fully cemented textures described by Tanner (2012) as a 'cryptic' cockade textures, figure 3.29 (7). In some places in the core of the breccia, the quartz contains very few wall rock clasts, figure 3.29 (8), and in other places clasts identical to those present in the inner damage zone are observed, figure 3.29 (9). In one area a late fault defined by highly polished slickenside and cataclasite is reported on the margin of the breccia body, figure 3.29 (11). These features are also all observed in the Eas Anie vein photograph.

One additional feature not reported by Tanner (2012) in the regional quartz breccia, but observed at Cononish, is that one margin of the quartz breccia is a sulphide mineralised quartz vein, figure 3.29 (12). Angular clasts of this mineralised quartz (with sulphides) are observed within the later quartz breccia vein, figure 3.29 (13). This late quartz is not ubiquitously observed on such a scale as shown in the photograph in figure 3.29.

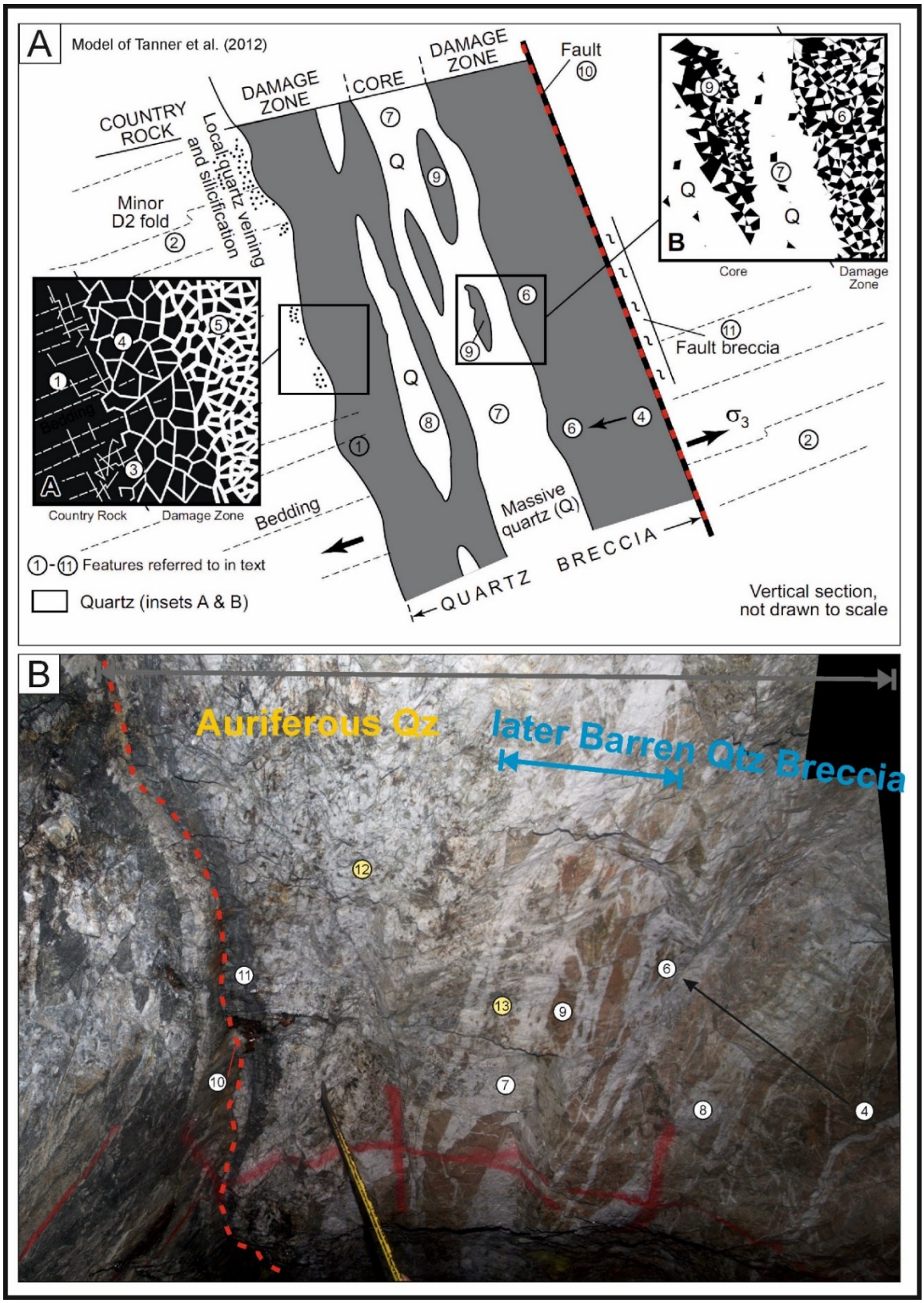

Figure 3.29 – Comparison of the general model showing the features of the Giant Quartz Breccia veins in the Tyndrum area published by Tanner (2012) (top) vs the vein seen in the back of the adit in the Cononish Mine. The numbers used by Tanner (2012) on his figures have been placed on the same features seen underground and are referred to in the text.

It appears that an additional late quartz breccia event occurred after the auriferous quartz vein formation at Cononish, and that this displays features comparable to the large 'barren' quartz breccia bodies, such as the barren vein and mother vein, in the Tyndrum area. This was predicted by Tanner (2012) who stated in his work "…the Cononish set all appear to terminate just before, or against, through-going veins/faults [specifically the mother vein] belonging to other sets and it seems most likely that they pre-dated the other vein sets but had some influence on their spatial development." He based this assumption on the orientation of the Eas Anie (Cononish) vein/fault

If the late quartz breccia formed alongside the other giant quartz breccia bodies in the Tyndrum area, then this presents a conundrum as they appear to be constrained in age by crosscutting dykes belonging to intrusive suites dated to have formed before the age of dated material reported as belonging to the Cononish auriferous vein, see age data presented in figure 3.2. The above interpretation is contradicted in parts by Treagus et al. (1999) who interpreted that the auriferous and mother veins both formed similarly, as echelon vein fragments within dilating transtensional fault zones, with components of left lateral shear. However, the rotation of early vein fragments predicted in this classic shear model is not seen underground at Cononish and the echelon segmentation of the Mother Vein is not supported by (Tanner, 2012).

The early phases (stage 1-2) show comb textures forming most of the width of the vein and are crosscut by later phases (stages 3-4) which are observed as thinner veinlets along fractures and in areas of cataclasis of the early veins. The concentration of these later veinlets around the observed fault plane along with the brecciated, cataclastic, and sheared nature of the late veins contrast with the texture of the early veins. These differences, in both composition (discussed below) and textures can be taken to indicate a change in the mineralising system between the early and late veining.

This change from dilatational, hydrostatic fluid pressures greater than the local lithostatic pressure, to later shearing within the auriferous gold vein which is then followed by a possible later separate dilatational quartz breccia is supported by the structural studies. These report that following early transpressional normal faulting, the later movements observed on the regional structures and veins (both of the mother vein and Eas Anie fault), show left lateral shear motions (Treagus et al., 1999, Tanner, 2012, Tanner, 2014). The magnitude of the total motion accommodated by the Eas Anie fault is

estimated, based on the displacement of the host lithologies, to be between 5 to 9 meters, dependent on the proportions of normal and strike-slip motion (Treagus et al., 1999).

3.5.2 Mineralogy

The mineralogy and paragenesis presented in the results is supported by the descriptions of the Cononish deposit in published studies (Earls et al., 1992, Curtis et al., 1993, Treagus et al., 1999), though here it has been investigated in considerably greater detail. The detailed paragenesis of the veins has never been described and linked to mineral chemistry and stable isotope data. Furthermore, the genesis of the deposit remains contentious, with either magmatic or metamorphic fluids (±meteoric) hypothesised to have formed the deposit (Craw and Chamberlain, 1996, Pattrick et al., 1988, Curtis et al., 1993).

The assemblages identified in the different stages of the paragenesis can be used to constrain the relative Sulphide(S) and Telluride(Te) fugacity when combined with thermodynamic studies of the stability of minerals in the S-Te-metal system (Afifi et al., 1988). This has been performed for the early and late mineralisation and is drawn on figure 3.30.

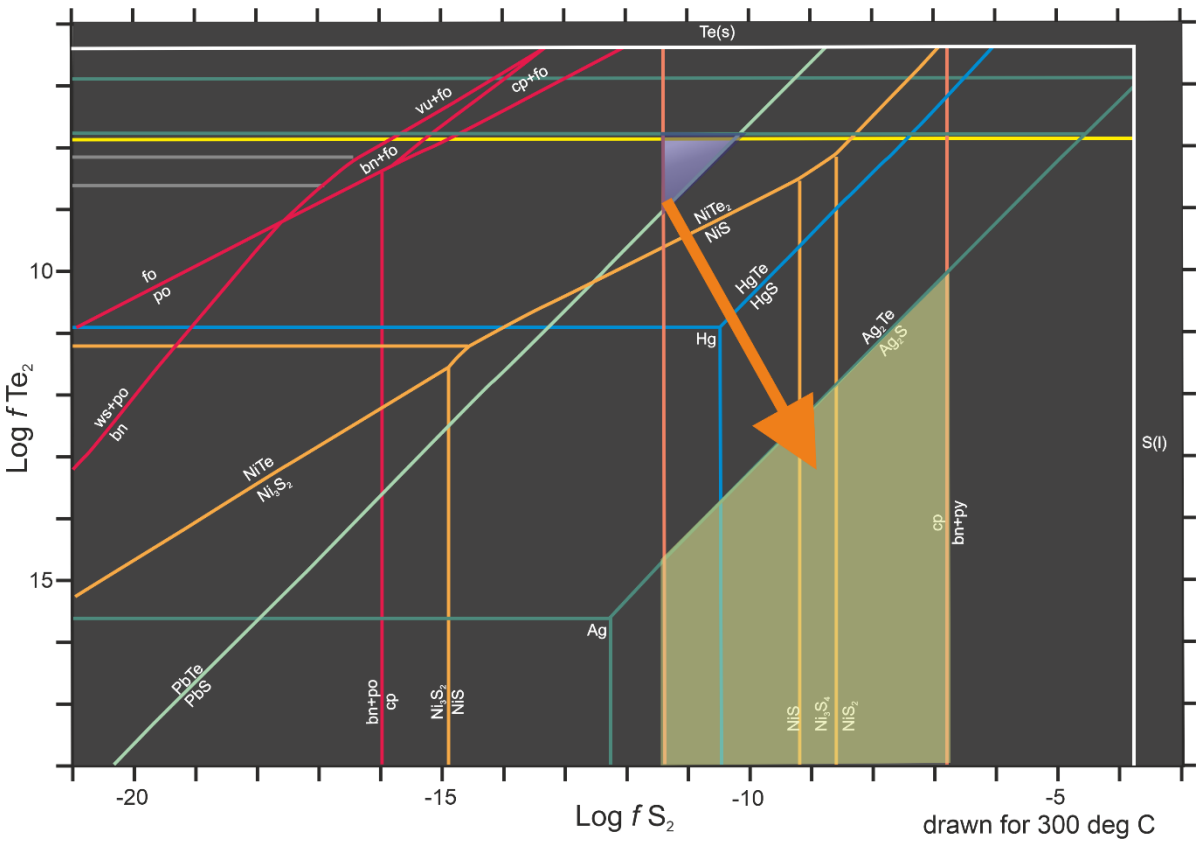

Figure 3.30 – Fugacity diagram showing key stability fields of Sulphides and Tellurides redrawn after (Afifi et al., 1988). Blue area shows the field for the early stage 1/2 assemblage, and yellow zone shows the later stage 3/4 assemblage. Therefore, the orange arrow shows the inferred progression of the Cononish fluid in respect to Te and S fugacity.

3.5.2.1 Evolution of Gold–Silver alloy composition

The wide range of compositions found in gold (Au) particles in the Cononish ore, from 10 to 90% silver (Ag), is a significant observation. This must be considered when making interpretations about the processes that formed the deposit. In a hydrothermal system, Au-Ag alloy compositions are controlled through the ratio of chemical activities *a*Ag/*a*Au (Gammons and Williams-Jones, 1995, Afifi et al., 1988). Where an additional Ag phase such as Ag_2S or Ag_2Te is saturated, the activity of Ag will be buffered by any additional Ag bearing phases (Gammons and Williams-Jones, 1995).

Three possible Ag sinks are observed in the ore; metallic gold alloys, hessite (AgTe2), and galena. Two of these phases contain stoichiometric concentrations of Ag, whereas the galena accommodates Ag as a trace in its lattice. Galena does this through coupled substitution with Sb or Bi (Renock and Becker, 2011). These elements are low in Cononish ores, ~1 ppm and <30 ppm respectively. Therefore, the Ag content in galena is expected to be minor,

and not a significant contributor to Ag grades and thus is not an important buffering phase for Ag (Scotgold Resources, Pers. Com.) So, in the case of coexistence of Au-Ag alloy with hessite, as in the case of the Cononish deposit, the Au-Ag alloy Ag-content is controlled through the reaction (Gammons and Williams-Jones, 1995):

$$Ag_{alloy} + \frac{1}{4}Te_{2(g)} = \frac{1}{2}Ag_2Te_{(s)}$$

Equation 3.1

And

$$aAg_{alloy} = K_{eq1}^{-1}.a_{Te_2}^{-0.25}$$

Equation 3.2

(Where *K* is the equilibrium constant of the reaction in equation 3.1.)

Thus, the composition of Au-Ag alloy in equilibrium with an Ag_2Te saturated fluid will be dependent on the activity of Te_2 in the system. If the activity of tellurium in the ore fluid is high, then hessite will precipitate, removing Ag available to the Au-Ag alloy and therefore the activity of Ag (*a*Ag) in the ore fluid will be suppressed. This will produce Au-rich Au-Ag alloy as the buffered ratio of *a*Ag/*a*Au will be high. At Cononish in the earliest auriferous vein (Stage 2), hessite is abundant along with Au–rich alloy; 90–75% Au (figure 3.27). In Stages 3 and 4, the abundance of hessite decreases, and is absent in late Stage 4 mineralisation, and here associated Au–Ag alloy particles have higher silver contents; 10%–75% Au (figure 3.27). In late Stage 4 veinlets, acanthite (Ag_2S) occurs instead of hessite. It is interpreted that high *a*Te_2 in the early fluid controlled the composition of the Au–Ag alloy and a progressive decrease in *a*Te_2 over time led to the deposition of progressively more Ag–rich alloy until *a*Te_2 decreased sufficiently in late Stage 4 that acanthite was deposited. This shows that tellurium was not available as a ligand, or the conditions changes such that S became a stable phase. The acanthite would have a buffering effect (with a similar mechanism to the hessite) on the silver activity in this last generation of gold alloy deposition. The decrease in galena abundance from

Stage 3 to 4 could also act to increase Ag content in the Au-Ag alloy, but since the Ag content of galena is low, this effect is interpreted as negligible.

The relationship between alloy composition and Te fugacity has been quantified as a function of temperature by Afifi et al. (1988), who shows that the fugacity of Te in a system is related to the mole fraction of Ag (X_{Ag}) in the alloy by:

$$\log f_{Te_2} = \left[\frac{1}{4.576T}\right].\left[\Delta G_T^{\circ}(Ag_2Te) - 18.302.T.Log\ X_{Ag} + 4\left(1 - X_{Ag}\right)^2.(5650 - 1600\left(1 - X_{Ag}\right) - 1.375T)\right]$$

Equation 3.3

(Assuming unit activity of Ag_2Te in hessite and ideal mixing of Au and Ag in the alloy)

This shows that to reduce Te activity with time *via* temperature change, a temperature *rise* would have been required which would seem unlikely given the limited range of fluid inclusion temperatures of 290-340°C (Curtis et al., 1993). The fluid inclusion temperatures are measured from quartz, which the paragenesis shows is predominantly earlier than the Au mineralisation, so are not considered to be fully reliable or representative. In conclusion the data more likely indicate a change in the fluid external to the deposit volume, and thus a change in the source of the fluid or fluid pathway, and/or pathway processes is required as a possible explanation.

3.5.2.2 Sulphur sources

The evolution in $\delta^{34}S$ pyrite from early pyrite with $\delta^{34}S$ of -2 to 2‰ towards a late-stage pyrite with values up to +11.4‰ represents a significant, and statistically robust, shift in the sulphur isotope composition of the fluid. This is interpreted as a change of the sulphur source. Hill et al. (2013) examined the $\delta^{34}S$ of the local stratigraphy and discussed potential sulphur sources for the Au-Ag mineralisation at Cononish. They demonstrated that it is possible to produce the full range of S–isotope values at Cononish, either by mixing of sulphur from different units in the local stratigraphy, or by mixing of magmatic sulphur with metasedimentary derived sulphur with $\delta^{34}S \geq +12$‰ from the Ben Eagach Schist SEDEX–bearing stratigraphic units. Hill et al. (2013) advocated the latter scenario, given the timing of the mineralisation. The age of the

Cononish Au-bearing veins of ~407 Ma (Rice et al. (2012) is identical, within error, to the Inner Starav Granite U-Pb zircon dated at 407±2 Ma (Appleby, 2007) and 408 ± 0.5 Ma (Neilson et al., 2009), the youngest portion of the Etive Pluton Complex situated 15 km to the NW across the Ericht-Laidon Fault. In addition, the δ34S of the early pyrite at Cononish is almost identical to that of sulphides from the Etive granite which average +2.1‰ (Lowry et al., 2005), and to the Sron Garbh appinite–diorite body (+1.0 to +4.8‰) that lies ~5 km to the northeast (Hill et al., 2013). Curtis et al. (1993) suggested magmatic fluid input based on fluid oxygen and hydrogen isotope ratios derived from measurements on quartz. Furthermore, the mineralisation formed >60 Ma later than peak metamorphism at ~470 Ma (Stephenson et al., 2013), so it is difficult to argue that it formed from regional metamorphic fluids, even acknowledging a “deeper-later” model for metamorphic fluid release which, at most, delays fluid release from depth by 50 Ma (Stüwe, 1998). Additional methods such as lead or boron Isotopes studies of the ore/fluids may offer a method for testing these theories by are outside the scope of this study.

The paragenetically constrained pyrite $\delta^{34}S$ data extend the mixing scenario proposed by Hill et al. (2013), now showing that the range of data can be interpreted as early magmatic sulphur progressively mixing over time with metasedimentary sulphur. The latter could be explained by metasedimentary sulphur being released by contact metamorphism and/or greater degrees of fluid-rock interaction during the evolution of the system. The source of the metasedimentary sulphide in this model must be the Easdale Subgroup; specifically, the highest $\delta^{34}S$ values reached can only be explained by sulphur being sourced from Ben Eagach Schist SEDEX sulphides which range up to +28‰, average +20‰ (Moles et al., 2014). The Easdale Subgroup is stratigraphically above the host rocks of the Cononish deposit; however, it is inferred to underlie the deposit on the opposing limb of the Beinn Chuirn Anticline (Hill et al., 2013). To produce the same trend of increasing $\delta^{34}S$ values over time from a purely metasedimentary-sourced hydrothermal system, without magmatic fluid involvement, would require sourcing of fluids from different (yet possibly adjacent) metasedimentary reservoirs within the Easdale Subgroup that range from -15 to +28‰ (Hill et al., 2013). Furthermore, it would necessitate changing sulphur sources or fluid pathways through the metasedimentary sequence during deposit formation with later fluid somehow becoming isolated from the initial sulphur source. Whilst not impossible, we suggest that this option seems rather more contrived given the timing of the mineralisation.

3.5.3 A updated genetic model for the deposit

The decrease in tellurium activity coupled with an increase in $\delta^{34}S$ through the formation of the Au-Ag vein suggest a low $\delta^{34}S$ (averaging +1.6‰, but possibly as low as -2‰). Te+Au+Ag enriched initial ore fluid evolved towards a high $\delta^{34}S$ (≥11‰), low Te, Pb+Cu–bearing fluid. The low $\delta^{34}S$ source is interpreted here as a magmatic pulse of fluid, as advocated by Hill et al. (2013) and Curtis et al. (1993), and this implies that the Te is also most likely of magmatic origin.

The earliest Au-Ag-Te mineralisation is hypothesised to represent the introduction of significant volumes of magmatic fluid into brittle structures. It is suggested that this magmatic fluid ascended rapidly, and out of chemical equilibrium with the Dalradian metamorphic pile through brittle fractures from a blind intrusive crystallising at depth (as suggested by a gravity low that extends beneath the area from the Etive pluton complex (Hill et al., 2013)). The evolution away from the strongly Te saturated initial fluid and increase in $\delta^{34}S$ is interpreted as a waning of magmatic fluid input and regaining of geochemical equilibrium with the Dalradian metasediments by the fluids ascending within the fault.

The alternative explanation of the tellurium-$\delta^{34}S$ evolution with time, is that both early and late fluids were sourced from the Dalradian metasedimentary pile, but that different parts of the stratigraphy released fluids at different times. Associations of gold and tellurium are well known in some orogenic gold districts, for example the Ashanti district (Oberthur et al., 1997) where there is little evidence of a magmatic fluid input, so in these cases Te may be sourced from metasedimentary or metaigneous units (or simply strongly concentrated on precipitation by specific physicochemical gradients in these systems). Pitcairn et al. (2015) demonstrate that carbonaceous shales from the Easdale Subgroup contain early diagenetic pyrite enriched in both Au and Te and could represent a viable source-rock for the mineralisation. However, if the early low-$\delta^{34}S$, high Te+Au fluid at Cononish was sourced from the Dalradian metasediments then, on the basis of its sulphur isotope signature, it would need to come from other formations in the Easdale Subgroup such as the Ben Lawers Schist, or a restricted subset of the diagenetic sulfides of the Ben Eagach schist (Hill et al., 2013) – units very close to those supplying the late high-$\delta^{34}S$ signature. This would require a highly specific contact-metamorphically sourced scenario to enable the origin and evolution of these fluids from adjacent units.

3.6 Conclusions

This study has elucidated the variability of gold mineralisation within the Cononish deposit, and the controls on this variability, through investigation of paragenetically constrained gold alloy chemistry. These results have been combined to develop a refined model for the formation of the deposit and investigate the fundamental ore forming processes.

The results show that the Cononish Au-Ag deposit formed as the result of an initial pulse of fluid that had a low–$\delta^{34}S$ (~1‰), and deposited significant Te+Au+Ag mineralisation which forms much of the mineralisation (>30% of the deposit). This early fluid evolved towards a high–$\delta^{34}S$ (≥11‰), low Te, Pb+Cu bearing fluid, with the veins becoming progressively less significant to the gold endowment of the deposit over time. The low $\delta^{34}S$ source is interpreted here as a magmatic pulse of fluid with evolution away from the strongly Te–saturated initial fluid. This is interpreted as a waning of magmatic fluid input and regaining of geochemical equilibrium within the Dalradian metasediments. Whilst not all examples of high Te-enrichment in orogenic gold deposits can be attributed to a magmatic fluid input, in some orogenic Au deposits it would seem that high Te is a signature of magmatic fluid input. The identification of specific pulses of Te enrichment during formation is an additional tool towards discrimination of a subclass of orogenic gold deposits that have formed through distal or otherwise cryptic magmatic processes.

kk

References

AFIFI, A. M., KELLY, W. C. & ESSENE, E. J. 1988. Phase relations among tellurides, sulfides, and oxides; I, Thermochemical data and calculated equilibria. *Economic Geology,* 83**,** 377-394.

BONS, P. D., ELBURG, M. A. & GOMEZ-RIVAS, E. 2012. A review of the formation of tectonic veins and their microstructures. *Journal of Structural Geology,* 43**,** 33-62.

CHAPMAN, R. J., BANKS, D. A., STYLES, M. T., WALSHAW, R. D., PIAZOLO, S., MORGAN, D. J., GRIMSHAW, M. R., SPENCE-JONES, C. P., MATTHEWS, T. J. & BOROVINSKAYA, O. 2021. Chemical and physical heterogeneity within native gold: implications for the design of gold particle studies. *Mineralium Deposita*.

CHEW, D. M., DALY, J. S., MAGNA, T., PAGE, L. M., KIRKLAND, C. L., WHITEHOUSE, M. J. & LAM, R. 2010. Timing of ophiolite obduction in the Grampian orogen. *Geological Society of America Bulletin,* 122**,** 1787-1799.

COX, S. F. & RUMING, K. 2004. The St Ives mesothermal gold system, Western Australia - a case of golden aftershocks? *Journal of Structural Geology,* 26**,** 1109-1125.

CRAW, D. & CHAMBERLAIN, C. P. 1996. Meteoric incursion and oxygen fronts in the Dalradian metamorphic belt, southwest Scotland: A new hypothesis for regional gold mobility. *Mineralium Deposita,* 31**,** 365-373.

CURTIS, S. F., PATTRICK, R. A. D., JENKIN, G. R. T., FALLICK, A. E., BOYCE, A. J. & TREAGUS, J. E. 1993. Fluid Inclusion and Stable Isotope Study of Fault-Related Mineralization in Tyndrum Area, Scotland. *Transactions of the Institution of Mining and Metallurgy Section B-Applied Earth Science,* 102**,** B39-B47.

EARLS, G., PATTERSON, R. T. G., CLIFFORD, J. A. & MELDRUM, A. H. 1992. The Geology of the Cononish Gold Silver Deposit, Grampian Highlands of Scotland. *In:* BOWDEN, A. A. (ed.) *The Irish Minerals Industry 1980-1990.* Irish Association for Economic Geology.

GAMMONS, C. H. & WILLIAMS-JONES, A. E. 1995. Hydrothermal Geochemistry of Electrum - Thermodynamic Constraints. *Economic Geology and the Bulletin of the Society of Economic Geologists,* 90**,** 420-432. GOLDFARB, R. J., GROVES, D. I. & GARDOLL, S. 2001. Orogenic gold and geologic time: a global synthesis. *Ore Geology Reviews,* 18**,** 1-75.

GROVES, D. I., GOLDFARB, R. J., ROBERT, F. & HART, C. J. R. 2003. Gold deposits in metamorphic belts: Overview of current understanding, outstanding problems, future research, and exploration significance. *Economic Geology and the Bulletin of the Society of Economic Geologists,* 98**,** 1-29.

GÖTZE, J. 2009. Chemistry, textures and physical properties of quartz - geological interpretation and technical application. *Mineralogical Magazine,* 73**,** 645-671.

HILL, N. J., JENKIN, G. R. T., BOYCE, A. J., SANGSTER, C. J. S., CATTERALL, D. J., HOLWELL, D. A., NADEN, J. & RICE, C. M. 2013. How the Neoproterozoic S-isotope record illuminates the genesis of vein gold systems: an example from the Dalradian Supergroup in Scotland. *Geological Society, London, Special Publications,* 393**,** 213-247.

KAMILLI, R. J. 1998. Paragenesis. Geochemistry. Dordrecht: Springer Netherlands.

JÉBRAK, M. 1997. Hydrothermal breccias in vein-type ore deposits: A review of mechanisms, morphology and size distribution. *Ore Geology Reviews,* 12**,** 111-134.

LARGE, R. & MASLENNIKOV, V. 2020. Invisible Gold Paragenesis and Geochemistry in Pyrite from Orogenic and Sediment-Hosted Gold Deposits. *Minerals,* 10**,** 339.

LOWRY, D., BOYCE, A. J., FALLICK, A. E., STEPHENS, W. E. & GRASSINEAU, N. V. 2005. Terrane and basement discrimination in northern Britain using sulphur isotopes and mineralogy of ore deposits. *In:* MCDONALD, I., BOYCE, A. J., BUTLER, I. B.,

HERRINGTON, R. J. & POLYA, D. A. (eds.) *Mineral Deposits and Earth Evolution.* Bath: Geological Soc Publishing House.
LIANXING, G. & MCCLAY, K. R. 1992. Pyrite deformation in stratiform lead-zinc deposits of the Canadian Cordillera. *Mineralium Deposita,* 27**,** 169-181.
MOLES, N. R., BOYCE, A. J. & FALLICK, A. E. 2014. Abundant sulphate in the Neoproterozoic ocean: implications of constant 34S of barite in the Aberfeldy SEDEX deposits, Scottish Dalradian. *Geological Society, London, Special Publications,* 393**,** 189-212.
MUELLER, A. G. & GROVES, D. I. 1991. The classification of Western Australian greenstone-hosted gold deposits according to wallrock-alteration mineral assemblages. *Ore Geology Reviews,* 6**,** 291-331.
NEILSON, J. C., KOKELAAR, B. P. & CROWLEY, Q. G. 2009. Timing, relations and cause of plutonic and volcanic activity of the Siluro-Devonian post-collision magmatic episode in the Grampian Terrane, Scotland. *Journal of the Geological Society,* 166**,** 545-561.
OBERTHUR, T., WEISER, T., AMANOR, J. A. & CHRYSSOULIS, S. L. 1997. Mineralogical siting and distribution of gold in quartz veins and sulfide ores of the Ashanti mine and other deposits in the Ashanti belt of Ghana: Genetic implications. *Mineralium Deposita,* 32**,** 2-15.
ROONEY, A.D., CHEW, D.M., SELBY, D., 2011. Re-Os geochronology of the Neoproterozoic-Cambrian Dalradian Supergroup of Scotland and Ireland: Implications for Neoproterozoic stratigraphy, glaciations and Re-Os systematics. Precambrian Research 185, 202-214.
PATTRICK, R. A. D., BOYCE, A. & MACINTYRE, R. M. 1988. Gold-Silver vein mineralization at Tyndrum, Scotland. *Mineralogy and Petrology,* 38**,** 61-76.
PATTRICK, R. A. D., BOYCE, A. & MACINTYRE, R. M. 1988. Gold-Silver vein mineralization at Tyndrum, Scotland. *Mineralogy and Petrology,* 38**,** 61-76.
PHILLIPS, G. N. & POWELL, R. 2015. A practical classification of gold deposits, with a theoretical basis. *Ore Geology Reviews,* 65, Part 3**,** 568-573.
PITCAIRN, I. K., SKELTON, A. D. L. & WOHLGEMUTH-UEBERWASSER, C. C. 2015. Mobility of gold during metamorphism of the Dalradian in Scotland. *Lithos,* 233**,** 69-88.
RENOCK, D. & BECKER, U. 2011. A first principles study of coupled substitution in galena. *Ore Geology Reviews,* 42**,** 71-83.
RICE, C. M., MARK, D. F., SELBY, D. & HILL, N. J. 2012. Dating vein-hosted Au deposits in the Caledonides of N. Britain. Mineral Deposit Studies Groups meeting abstracts. *Transactions of the Institute of Mining and Metallurgy (Section B: Applied Earth Science),* 121**,** 199–200.
ROBERT, F. & POULSEN, K. H. 1997. World-class Archaean gold deposits in Canada: An overview. *Australian Journal of Earth Sciences,* 44**,** 329-351.
SCOTGOLD RESOURCES LIMITED 2015. Cononish Gold Project Study Update and JORC 2012 Ore Reserve Estimate. ASX Announcements [Online] Available at: http://www.asx.com.au/asx/statistics/displayAnnouncement.do?display=pdf&idsId=01628298.
SPENCE-JONES, C. 2013. *Metallurgical Investigation of the Ore at the Cononish Gold Mine, Scotland.* MGeol Masters, Univeristy of Leicester.
SPENCE-JONES, C. P., JENKIN, G. R. T., BOYCE, A. J., HILL, N. J. & SANGSTER, C. J. S. 2018. Tellurium, magmatic fluids and orogenic gold: An early magmatic fluid pulse at Cononish gold deposit, Scotland. *Ore Geology Reviews*.
STEPHENSON, D., MENDUM, J. R., FETTES, D. J. & LESLIE, A. G. 2013. The Dalradian rocks of Scotland: an introduction. *Proceedings of the Geologists Association,* 124**,** 3-82.
STEPHENSON, D., MENDUM, J. R., FETTES, D. J., SMITH, C. G., GOULD, D., TANNER, P. W. G. & SMITH, R. A. 2013b. The Dalradian rocks of the north-east Grampian Highlands of Scotland. *Proceedings of the Geologists' Association,* 124**,** 318-392.

TANNER, P. W. G. 2012. The giant quartz-breccia veins of the Tyndrum-Dalmally area, Grampian Highlands, Scotland: their geometry, origin and relationship to the Cononish gold-silver deposit. *Earth and Environmental Science Transactions of the Royal Society of Edinburgh,* 103**,** 51-76.

TANNER, P. W. G. 2014. Structural controls and origin of gold–silver mineralization in the Grampian Terrane of Scotland and Ireland. *Geological Magazine,* 151**,** 1072-1094.

TANNER, P. W. G. & THOMAS, P. R. 2010. Major nappe-like D2 folds in the Dalradian rocks of the Beinn Udlaidh area, Central Highlands, Scotland. *Earth and Environmental Science Transactions of the Royal Society of Edinburgh,* 100**,** 371-389.

TREAGUS, J. E., PATTRICK, R. A. D. & CURTIS, S. F. 1999. Movement and mineralization in the Tyndrum Fault Zone, Scotland and its regional significance. *Journal of the Geological Society,* 156**,** 591-604.

VEARNCOMBE, J. R. 1993. Quartz vein morphology and implications for formation depth and classification of Archaean gold-vein deposits. *Ore Geology Reviews,* 8**,** 407-424.

WERTICH, V., LEICHMANN, J., DOSBABA, M. & GÖTZE, J. 2018. Multi-Stage Evolution of Gold-Bearing Hydrothermal Quartz Veins at the Mokrsko Gold Deposit (Czech Republic) Based on Cathodoluminescence, Spectroscopic, and Trace Elements Analyses. *Minerals,* 8**,** 335.

YARDLEY, B. 1996. Earthquakes with gold linings. *Nature,* 382**,** 210-211.

Chapter 4 Cononish Mine Detrital Gold Study

Summary

This chapter examines the relationship between the composition of primary gold mineralisation within a lode gold deposit and the composition of detrital gold particles eroded from it into fluvial deposits. The aim of the study is to investigate if the study of detrital gold particles can provide novel information about the nature of a gold deposit and the mineralisation within a study area.

Detrital gold particles collected from Eas Annie burn which drains the Cononish deposit were collected and the distribution of gold alloy compositions determined. The results show that the distribution of gold alloy compositions is different from the population obtained from the mine (bulk ore) samples. The results demonstrates that the composition of gold particles may be spatially variable within the Cononish ore deposit and provides information on the proportions of different generations of mineralisation, observed in the hard rock mineralogy reported in chapter 3.

This study demonstrates that the collection and compositional analysis of detrital gold particles is a practical method for obtaining characterisations of the gold alloys within a known deposit. It provides foundational evidence to support the conceptual idea that detrital gold populations can be used as a proxy for the overall population of the gold within a deposit. However, it is important to consider the surficial processes such as the erosional and transport processes when using detrital gold populations before using the in gold alloy distributions to evaluate the physiochemical evolution of the mineralising conditions present in different source volumes of the deposit. For example, at Cononish Glacial erosion needed to be considered for its impact on the detrital populations especially those further downstream/ not proximal to the Cononish mine. Further research is needed to examine gold signatures in different volumes with a single deposit/system and to further develop comparisons between deposits which could lead to detrital signatures being a effective tool for regional exploration enabling the identification of favourable styles mineralisation based on the detrital gold signature.

4.1 Introduction

The composition of gold particles in different gold deposits has previously been obtained from thin sections (e.g. (Spence-Jones, 2013, Townley et al., 2003, Liu and Beaudoin, 2021)), through separation from crushed samples/ore (e.g. (Mackenzie and Craw, 2005, Chapman and Mortensen, 2016)) and in detrital placer deposits (e.g. (Chapman et al., 2010 and Chapman et al. 2021)). The composition of gold in a deposit is controlled by the

physiochemical parameters (the temperatures, pressures and fluid compositions, see chapter 1) (Gammons and Williams-Jones, 1995a, Chudnenko and Palyanova, 2016, Pal'yanova, 2008, Pal'yanova and Kolonin, 2004, Pal'yanova et al., 2005). Differences in the range and distribution of Au-Ag alloys compositions when comparing different gold deposit styles were noted early in gold mineralogy studies, see reviews by Fisher (1945) and later by Morrison et al. (1991) and (Chapman et al., 2021).

While the differences in compositional signature between deposit classes has had considerable attention in the literature, the variability of gold particle compositions within parts of individual deposits has received less attention. This is despite documented variability in physiochemical conditions spatially and temporally within individual deposits which are known to effect compositions of gold particles (Bozzolo et al., 2007, Gammons and Barnes, 1989, Gammons and Williams-Jones, 1995b, Chudnenko and Pal'yanova, 2013, Gammons and Williams-Jones, 1995a, Ozoliņš et al., 1998, Afifi et al., 1988, Pal'yanova, 2008, Guisbiers et al., 2016). Studying the populations of gold particles in a single deposit is beneficial as it can provide data on the mineralising conditions, which if the samples are appropriately selected could elucidate variability in the deposit/system, both spatially and temporally. This is something that many studies do not include and instead simply report electrum (without compositional data) in paragenetic studies. Without understanding variability of gold alloy compositions within individual deposits, comparisons of the gold signature between different deposits may be flawed and result in inaccurate or incorrect classifications, especially if the gold signatures are based on a limited number of analyses. Therefore, obtaining deposit scale characterisations of gold particles represents a possible tool to refine classifications, reducing ambiguity, and providing insights into the variability of mineralising processes within individual deposits.

Insights into the composition of gold particles within a deposit can be gained by comparing the composition of detrital gold and that sourced from the in-situ sampling of gold systems, for example the Cononish ore study presented in chapter 3. However, studies assessing the compositions of gold particles within a deposit are challenging because in order to obtain representative sample sizes, bulk sampling is required which destroys the mineralogical, spatial and temporal context of the gold particles, (see discussion in chapter 3).

The Cononish gold mine is an ideal study site due to its accessible, well-studied and characterised mineralisation (examined in detail in chapter 3) and the presence of detrital gold in a small, low order drainages which traverse the deposit. These are factors which rarely coincide. In addition to the logistical suitability of the Cononish mine, the gold

mineralisation has a wide range of gold compositions (0 to 60 %wt Ag in the gold alloy), observed within an established paragenetic sequence (Spence-Jones, 2013, Spence-Jones et al., 2018). The relationship of gold composition and vein stage at the Cononish deposit is systematic, with gold particles in veins evolving to have more silver in the alloy over time, figure 4.1. This makes relating the gold compositions measured in the detrital samples to individual vein stages (observed within thin sections) simpler because differences in compositions between the different stages are dramatic. Because gold alloy compositions can be related to paragenetic stages, the proportions of gold particles (within specified compositional ranges) in the detrital populations can be compared with each other, thereby allowing the relative proportions of the gold particles formed within each stage of the paragenesis to be estimated for the (eroded) source vein material. The relationship of gold alloy composition to paragenetic stages conducted using a mill concentrate (processed) ore sample in chapter 3 will be compared to the results obtained from detrital samples from the Cononish area in this chapter. This assesses the uses of detrital gold as a tool for characterisation of ore systems.

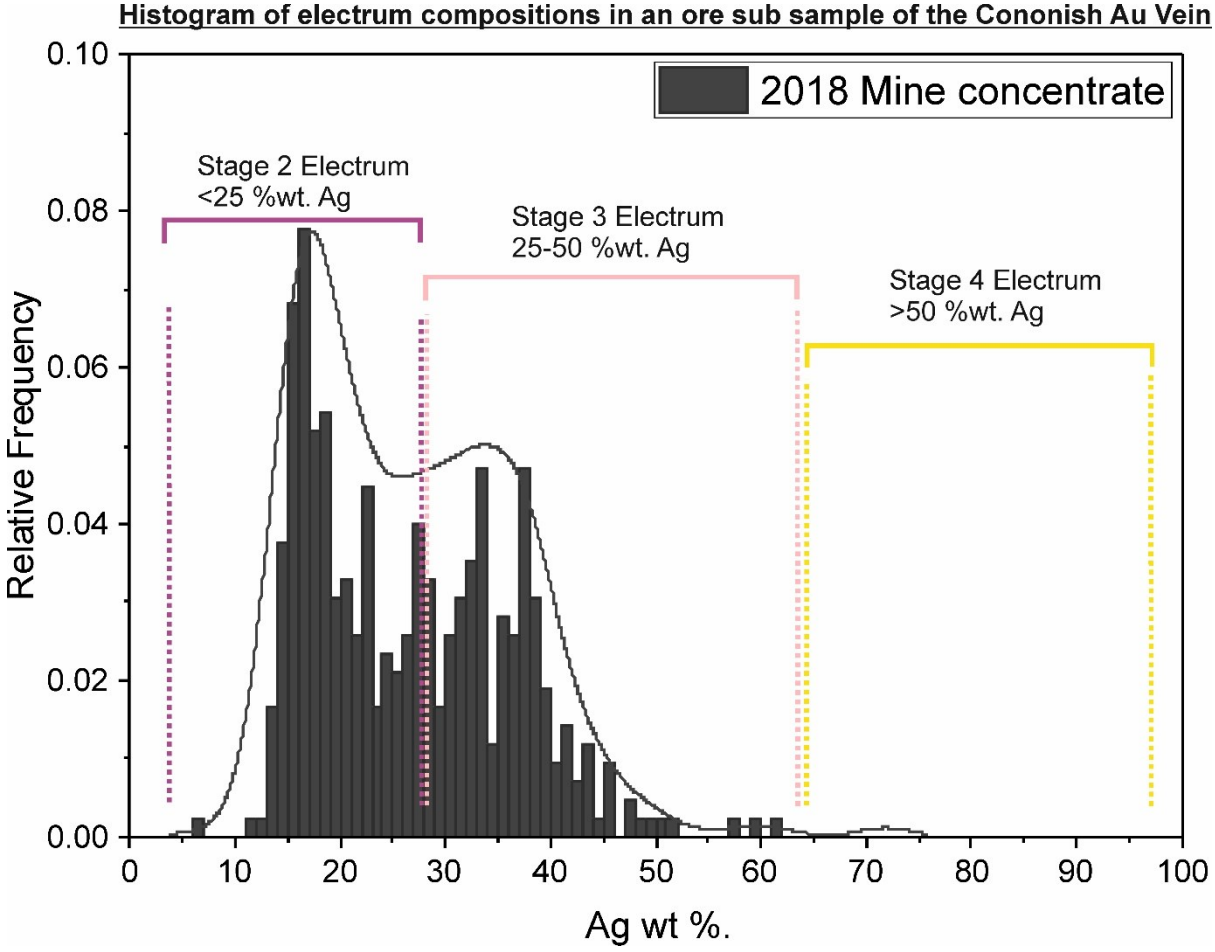

Figure 4.1 – Histogram (1 Ag wt%. Bins) of gold particles recovered from the shaking table concentrate of an ore sample taken from the 400m level of the Cononish mine. The plot shows the proportions of particles within compositional brackets defined by the paragenetic work and gold compositions reported by Spence-Jones (2013). A smooth empirical distributional curve was produced using a kernel estimation algorithm in Origin pro software (with Scott's rule used for bandwidth estimation, scaled to 80% maximum).

Improved understanding of the relationships between the composition of detrital gold populations and the geochemical properties of the mineralisation within lode systems has the potential to benefit evaluation of targets during exploration. The presence of detrital gold in a drainage during exploration indicates that there is a hard rock source of gold upstream. However, this source of gold may not be an economic mineralised system, being sourced from a small or lower grade vein(s). If differences in the compositional signature of the detrital gold population can be used to determine the possible economic potential of the hard rock source, this would be valuable information for exploration programs. A well-developed methodology for appraising detrital gold signatures could allow for improved targeting of an exploration program with more efficient focusing of resources.

In a survey of gold discovery exploration methods Brown and Vearncombe (2014) report that gold panning (which was grouped with stream sediment sampling) is an inferior contributor to discoveries compared to soil (regolith) and rock chip sampling. If stream sediments and panning are undertaken, they are used at a very early stage in exploration programs and are followed by geochemistry surveys (soil and rock chip geochemistry) along with correlated geophysical observations, before being used to evaluate targets for drill rig sampling. The reason that techniques other than gold panning (for example assays on stream sediments) have become the norm in the exploration industry is because they offer independent quantified appraisals of each sample site. For example, the chemical concentration of pathfinder elements in soil samples provides numerical data which can be used comparatively to quantify and compare the prospectivity of areas for a specific (target) style of mineralisation. In contrast to other techniques the number of gold particles recovered when gold panning does not provide independent appraisals between two sites. The amount of gold collected is a function of the grade within a hard rock source, size/morphology of the gold particles, distance to the source, hydrology of the drainage, geomorphology/sedimentology of the sample site, collection methodology, and skill/time invested by the sampler, see chapter 2.

While some variables which influence detrital gold abundance can be controlled to produce more reliable comparisons, others such as geology, hydrology and sedimentology of the sample site cannot be controlled. This means that if abundance and morphology observations are to provide useful data, the nature of each sample site must be evaluated alongside the gold sample obtained from it. Therefore, gold panning remains a technique used by prospectors (experienced individuals who conduct sampling and evaluation of areas personally), and not commonly by large teams in exploration companies.

Studies examining the properties of the gold particles could provide information beneficial to exploration and provide information useful for appraising detrital gold occurrences. For, example in the Cononish area the composition of gold in the drainages around the known deposit can be compared to the composition of gold in other drainages containing detrital gold to evaluate if they are prospective. If the exploration model is to find another deposit of the same style as the Cononish deposit, then detrital gold populations which are similar can be identified and targeted as priorities for follow up exploration.

4.2 Methods

The sample site from the Eas Anie Burn was selected to maximise the number of detrital gold particles collected, table 4.1 and figures 4.2 and 4.3. The site was located on the inside bend of the stream where the river flow is slower so more particles are deposited, figure 4.3. This sample site is referred to as the Eas Anie Burn 2 and the gold particles were collected using the panning and sluicing methods of (Leake et al., 1995). Particles were mounted with the long axis vertical to simplify sectioning by allowing a greater depth tolerance for the amount of material removed during polishing. Once sectioned the maximum size of each of the particles in the 2D section plane (which should equal approximately the intermediate axis length of the particle) was recorded to allow for investigation (correlation) to their composition, and other measurements, such as their physical properties, morphology, inclusions, chemistry and alloy composition.

The size of the gold particles before mounting varied from ~4 mm to ~100 µm. The distribution of the maximum size observed in the 2d sectioned plane is seen to have a pseudo log-normal distribution, see figure 4.6 in which a log normal distributional curve (dashed line) is shown for comparison. The abundance of very fine gold (sub ~200µm) can be considered to be affected by the sampling issues, specifically that the collection and visual identification of such small particles requires special care and focus in sampling. Given the abundance of larger particles the finesse required for collection of such small particles, down to ~50µm, would have been counterproductive given the time available. Above a size of 200µm, at which visual identification is easy, particle abundance is observed to decrease with increasing particle size. This is in agreement with studies of particle sizes of ore samples which showed similar trends between particle size and abundance (Dominy et al., 2008).

In addition to the samples collected during this research, 3 other detrital gold sample populations exist which were collected by Dr Robert Chapman (University of Leeds) prior to this project, see table 4.1. The locations are shown on figures 4.2 and 4.3. The composition of the gold in each sample population was measured at the University of Leeds by Dr Chapman and are these plotted and compared to the Eas Anie Burn 2 sample, collected during this research, in table 4.1 and figure 4.3.

Table 4.1 – Detrital gold sample details

Population_ID	Source	No_Au particles	No_Au Analysis	Lat_WGS84	Long_WGS84	BNG GR
Calliche_1	Uni Leeds collection	91	110	56° 33' 02.4"N	04° 37' 35.5"W	NN 38642 42942
Cononish_1	Uni Leeds collection	29	29	56° 24' 23.5"N	04° 46' 22.8"W	NN 28992 27261
Cononish_2	Uni Leeds collection	60	67	56° 25' 09.7"N	04° 43' 46.1"W	NN 31735 28581
Crom Alt _1	Uni Leeds collection	53	54	56° 26' 57.8"N	04° 42' 26.0"W	NN 33238 31867
Eas Anie Burn_1	Uni Leeds collection	26	27	56° 25' 07.0"N	04° 45' 22.9"W	NN 30073 28563
Eas Anie Burn_2	This study	279	507	56° 25' 08.4"N	04° 45' 56.9"W	NN 29492 28630
River Lochy_1	This study	135	135	56° 24' 38.6"N	04° 51' 10.3"W	NN 24088 27925

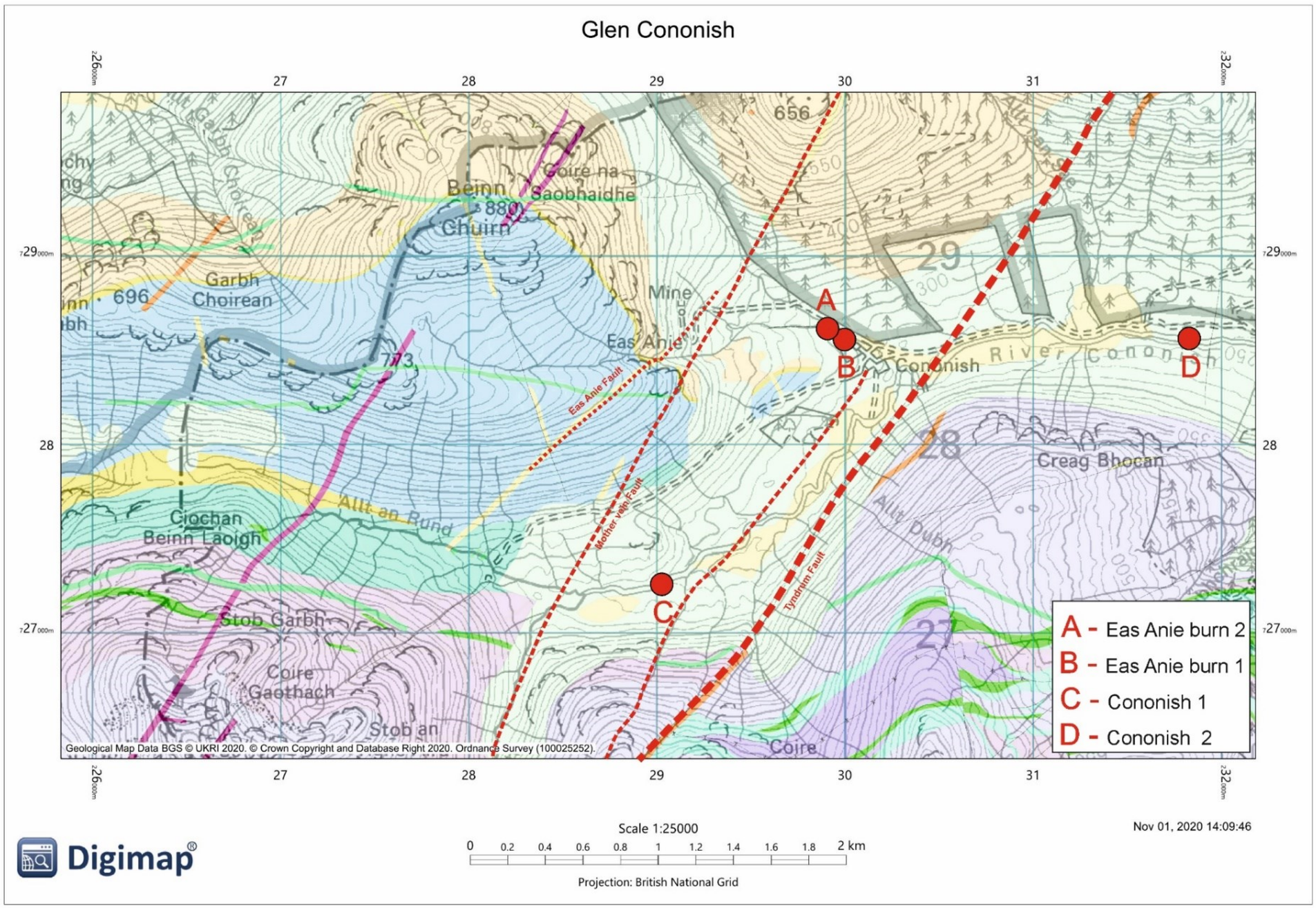

Figure 4.2 – Geological map showing location of detrital gold samples & the location of the Tyndrum fault. See figure 3.1 for a larger scale overview of the regional geology.

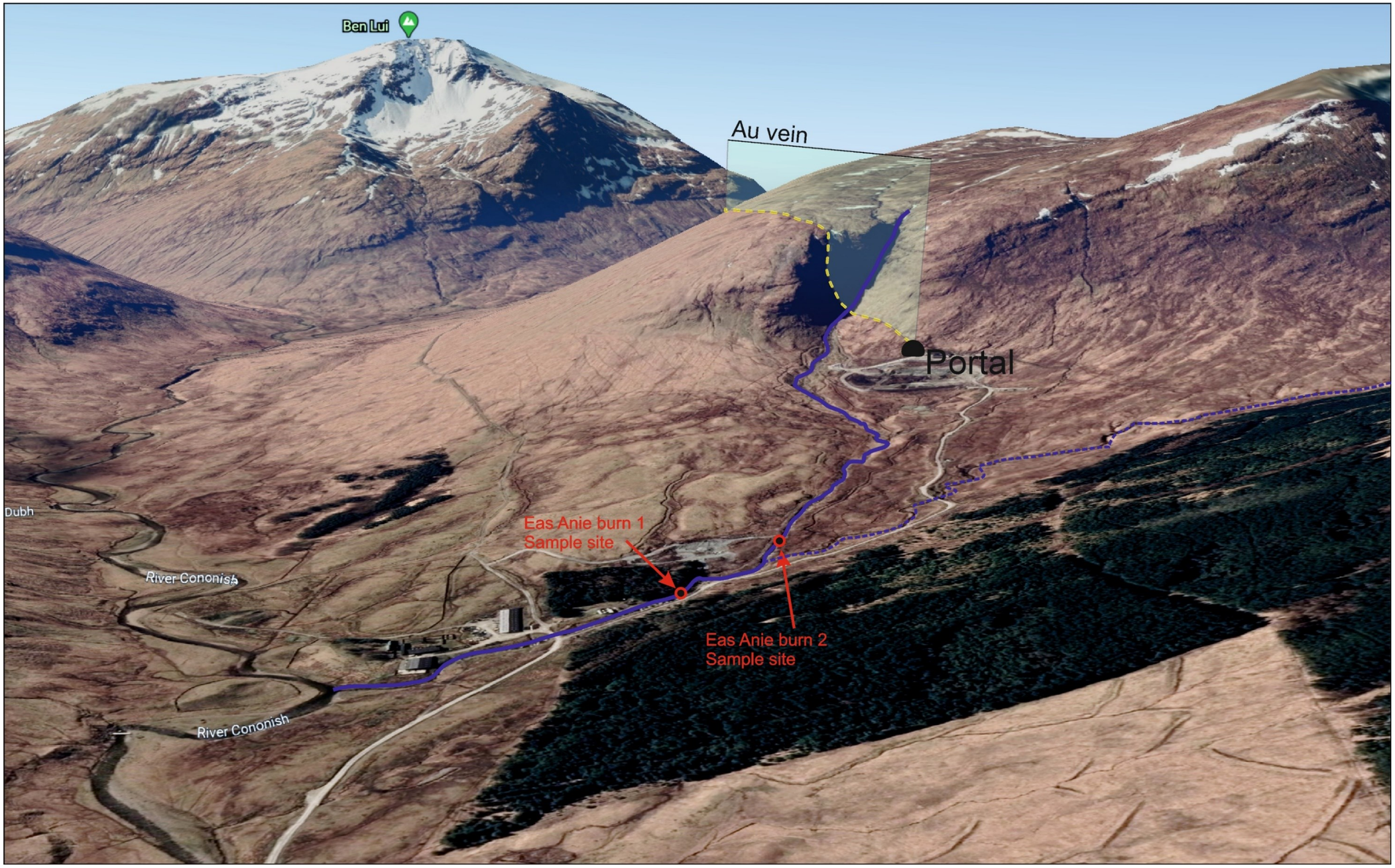

Figure 4.3 – Google earth image of Cononish mine site looking south west towards Ben Lui, showing location of the vein and the detrital gold sample sites.

4.3 Results

4.3.1 Detrital Gold samples

The sample of 279 gold particles from the Eas Anie Burn 2 site (figure 4.4) collected by the author represents the largest available sample and allows examination in detail of the properties of gold in the catchment. The following section presents detailed analysis of this sample.

4.3.1.1 Size and morphology of the gold in Eas Anie Burn

The unmounted gold particles sampled from the Eas Anie Burn ranged from 30 microns to 3mm (figure 4.6) and had rough irregular forms with primary crystal imprints, and composite particles containing attached silicates (predominantly quartz). In many cases gold particles appear to have had minimal morphological modification, with irregular and subspherical shape particles which have rough surfaces or rounded protrusions observed on the surfaces of the particles figure 4.5A-C. Some particles contain external attachments of quartz, figure 4.5C. These morphologies reflect the original morphology of the gold particle as very little flattening and rounding of the particles is observed to have occurred. Studies of morphological changes of gold particles indicate that these morphologies indicate short transport distances (Townley et al., 2003, Crawford, 2007, Wrighton, 2013).

Figure 4.4 – Photographs from the mine site at Cononish looking back down the glen. The red arrow marks the location of detrital gold sample Eas Anie Burn 2.

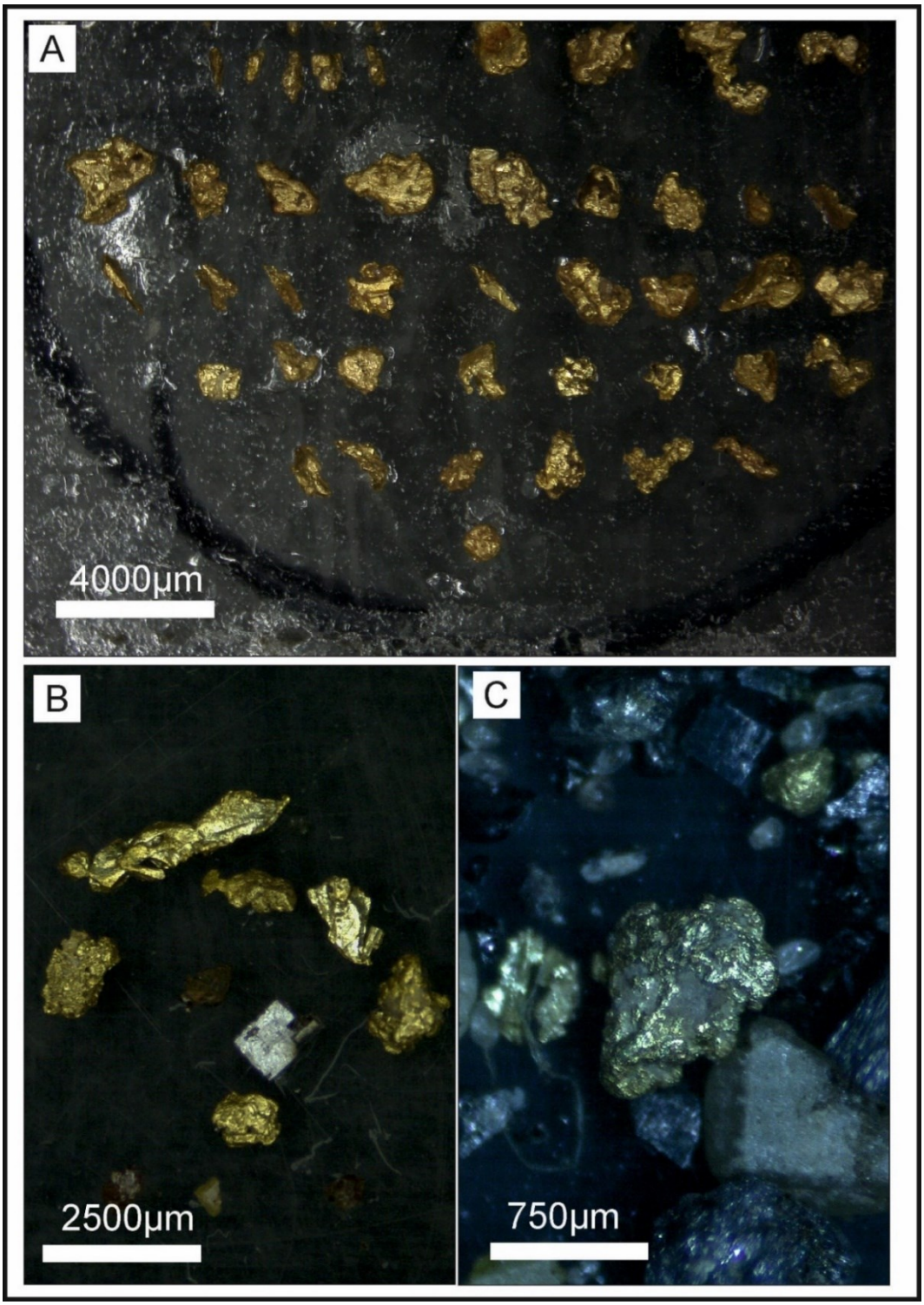

Figure 4.5 – Photographs of the detrital gold sampled from the Eas Anie Burn showing the general morphology of the particles. A – mounted gold particles showing rounded sub spherical forms. B – Elongate irregular shaped particle (top) with rough particles that shown sharp protrusion with minimal rounding. Note also a duller co-collected pyrite cube in the centre of the image. C – Rounded sub-spherical gold particle with attached quartz.

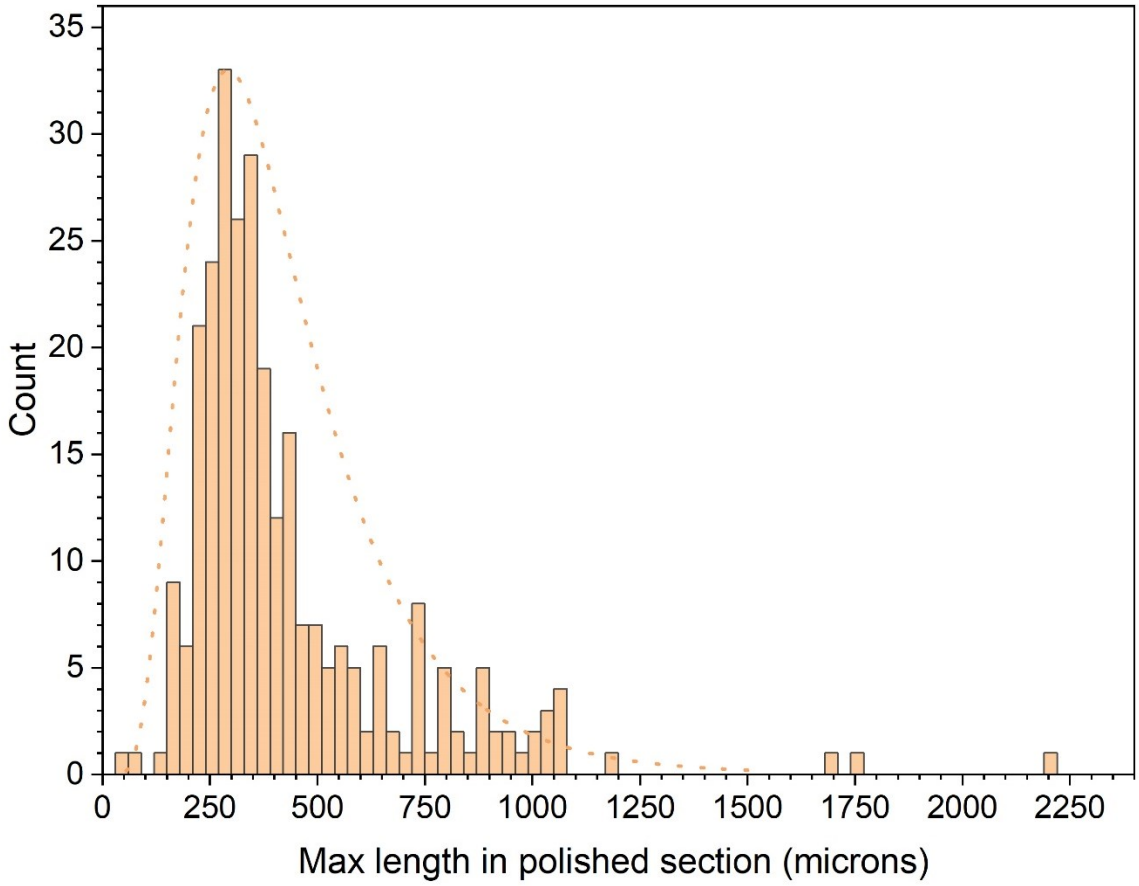

Figure 4.6 – Distribution of the maximum dimension measured for sectioned gold particles, observed in the 2D surface of the polished blocks with a log-normal curve fitted to the data for comparison against.

4.3.1.2 Associated minerals and inclusions in gold

The gold particles sampled and sectioned have additional minerals contained within and attached to them. The most common minerals were silicates, principally quartz but other metal bearing minerals were also seen. These were recorded to compare inclusions with the minerals documented in the Cononish paragenesis (Spence-Jones, 2013).

A total of 76 out of the total of 279 gold particles were observed to contain sulphides or telluride minerals (or both). Figure 4.7 shows the number of particles observed to contain each ore mineral species. Sulphides are more common than tellurides with pyrite observed within 59 gold particles. Hessite is the second most abundant mineral observed.

The minerals pyrite, chalcopyrite, galena, altaite and hessite observed within the detrital gold, have all been found in studies of the vein and are presented as the main vein forming

components (with Quartz) in the interpreted paragenesis. This result indicates that the detrital gold is comparable with the mineralogy of the Eas Anie gold vein, reaffirming the Eas Anie gold vein as the probable source of the gold particles. The mineral Sylvanite ($(Ag,Au)Te_2$) has not been reported in previous mineralogy studies but is considered compatible with the Eas Anie vein because phase diagrams show sylvanite coexists with low stiver gold alloys (>12%wt. Ag) in systems which are documented to have a high abundance of hessite and accessory telluride phases (Afifi et al. 1988).

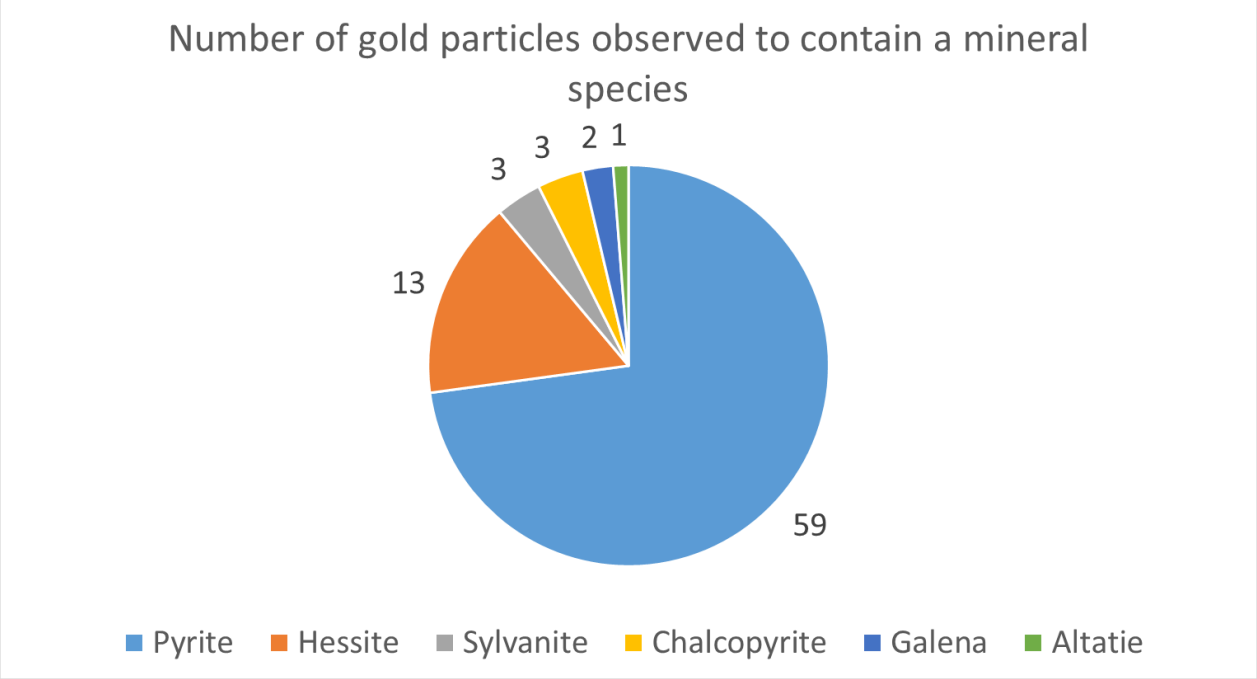

Figure 4.7 – Pie Chart showing abundance of ore minerals as inclusions in the detrital gold sample Eas Anie Burn 2 sample.

4.3.1.3 Chemistry of the gold particles

10% of the population of gold particles examined are not compositionally homogeneous. Most of the heterogeneity observed is porous banding along particle margins or within internal fractures. These bands have lower silver content than the core of the gold particles, see figure 4.8. These are consistent with rim textures observed in placer studies literature resulting from modification by processes in the surficial environment (Groen et al., 1990, Melchiorre et al., 2018, Hough et al., 2007).

The rim textures observed included both porous zones, indicative of volume reduction produced by selective Ag leaching from the alloy, and non-porous gold rich zones/veinlets formed by deposition of Au rich material (Hough et al., 2007, Chapman et al., 2021) These

are common features observed in detrital gold particles formed during surficial transport and are not considered as primary features of the gold within the hard rock ore system (Hough et al., 2009, Hough et al., 2007, Melchiorre et al., 2018, Chapman et al., 2021).

In addition to the typical rims (Au precipitation and Ag depletion processes) observed on the outside of the particles, are internal heterogeneities in the Ag/Au ratio which record Ag enrichment relative to the 'core' of the particle. These are not strongly spatially associated to the surface of the gold particles, show minor or no porosity and can be observed to have diffuse boundaries with gradients in composition. These are consistent with features reported by (Chapman et al., 2021) and are interpreted as primary features of the gold particles, an interpretation supported by the observation of similar textures in the hard rock sourced gold particles (see chapter 3).

Figure 4.8 (p.146) – Placer gold particle heterogeneous Au/Ag alloy textures from the Eas Anie Burn 2 sample. Images A and B – sharp and distinct Au richer tracks (veinlets) following particle boundaries. C and D – Complex banded (oscillatory) Ag rich zones along fractures and particle boundaries. E – Diffuse and gradual (Ag rich) variation between sub particles F – Sharp Ag rich tracks along particle boundaries.

A

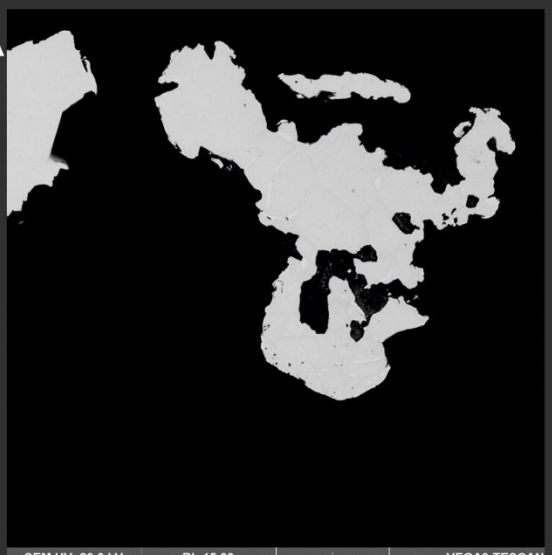

SEM HV: 20.0 kV	BI: 15.00		VEGA3 TESCAN
WD: 14.83 mm	View field: 950 µm	200 µm	LEMAS - Leeds University

B

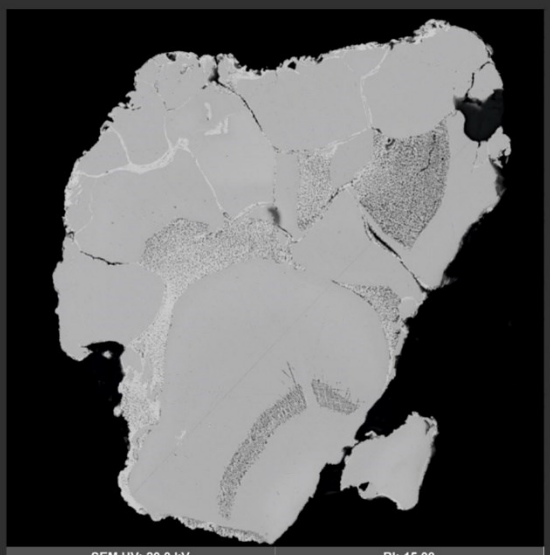

SEM HV: 20.0 kV	BI: 15.00
WD: 15.00 mm	View field: 189 µm
SEM MAG: 2.20 kx	1_2 high res

C

SEM HV: 20.0 kV	BI: 15.00
WD: 15.00 mm	View field: 350 µm
SEM MAG: 1.97 kx	3_7

D

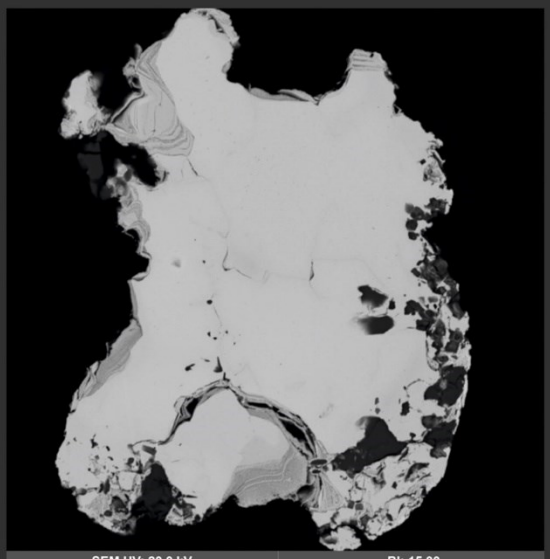

SEM HV: 20.0 kV	BI: 15.00
WD: 14.90 mm	View field: 222 µm
SEM MAG: 2.49 kx	6_2

E

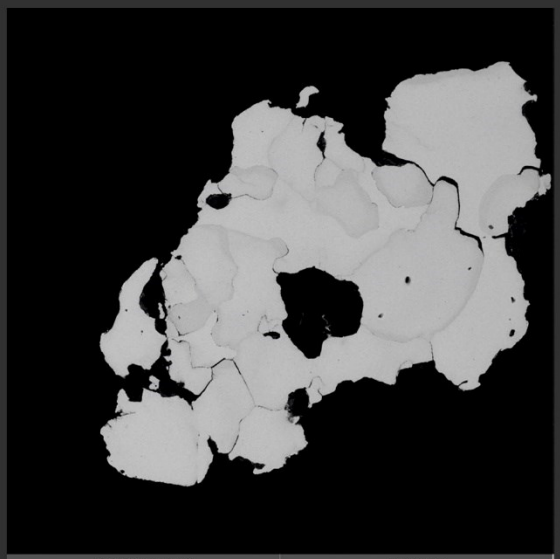

SEM HV: 20.0 kV	BI: 10.00
WD: 15.00 mm	View field: 1.88 mm
SEM MAG: 184 x	4_5

F

SEM HV: 20.0 kV	BI: 15.00
WD: 14.83 mm	View field: 772 µm
SEM MAG: 717 x	2_1

Most of the gold particles were observed to be homogeneous with respect to silver. However, where this was not the case the particles consist principally of a single 'main' homogeneous alloy which is crosscut by volumetrically minor heterogeneous zones. The main alloy of each gold particle collected was measured with care taken to avoid minor heterogeneous areas when collecting data.

The compositional signature of the main gold alloy of the collected particles is shown in figure 4.9, and is a continuous distribution between 0 to 54.1 wt% Ag with a median of value of 27.6 wt% Ag. The compositional distribution is not normally distributed and in addition to the principal peak in abundance at 30 wt% Ag, a minor secondary peak is seen in composition at around 15 wt% Ag, figure 4.10. No systematic relationship exists between the size of the particle and the composition, indicating that size is independent of composition, figure 4.11. Furthermore, no relationship appears to exist between the included minerals and the composition of the host gold particle. Data for the rarer mineral inclusions cannot be assessed as they are not common enough to allow analysis, figure 4.12.

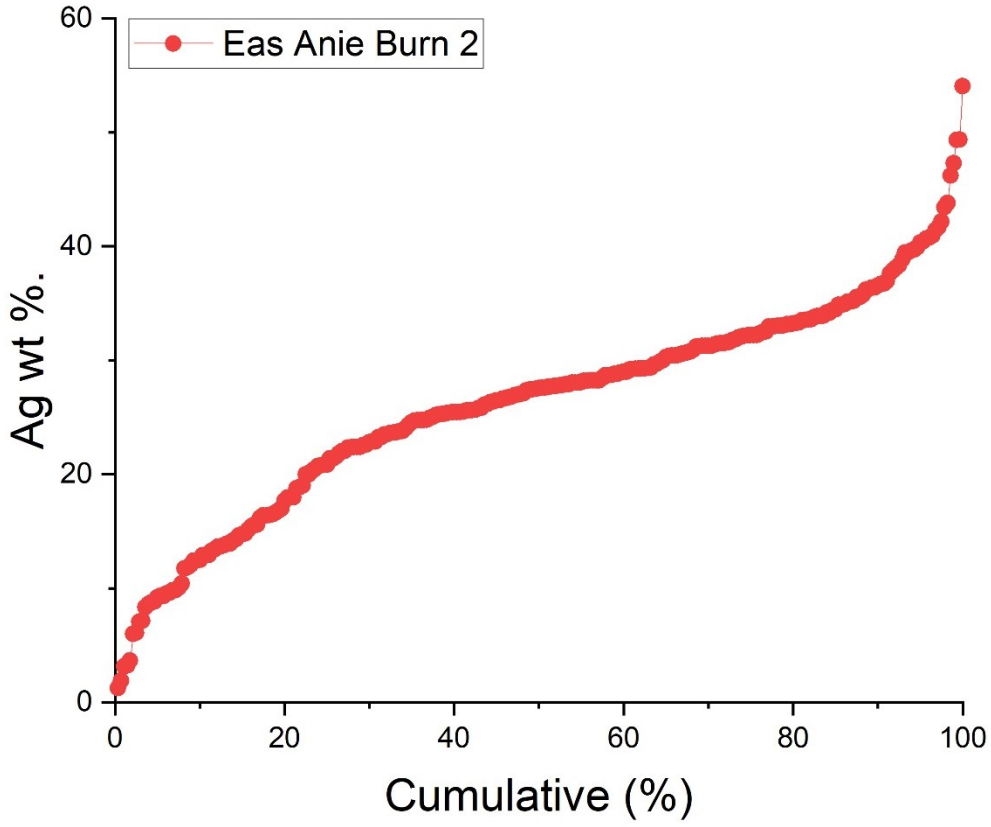

Figure 4.9 – Cumulative frequency plot of gold particle alloy composition Ag wt%. of the Eas Anie Burn 2 sample showing the distribution of the placer population.

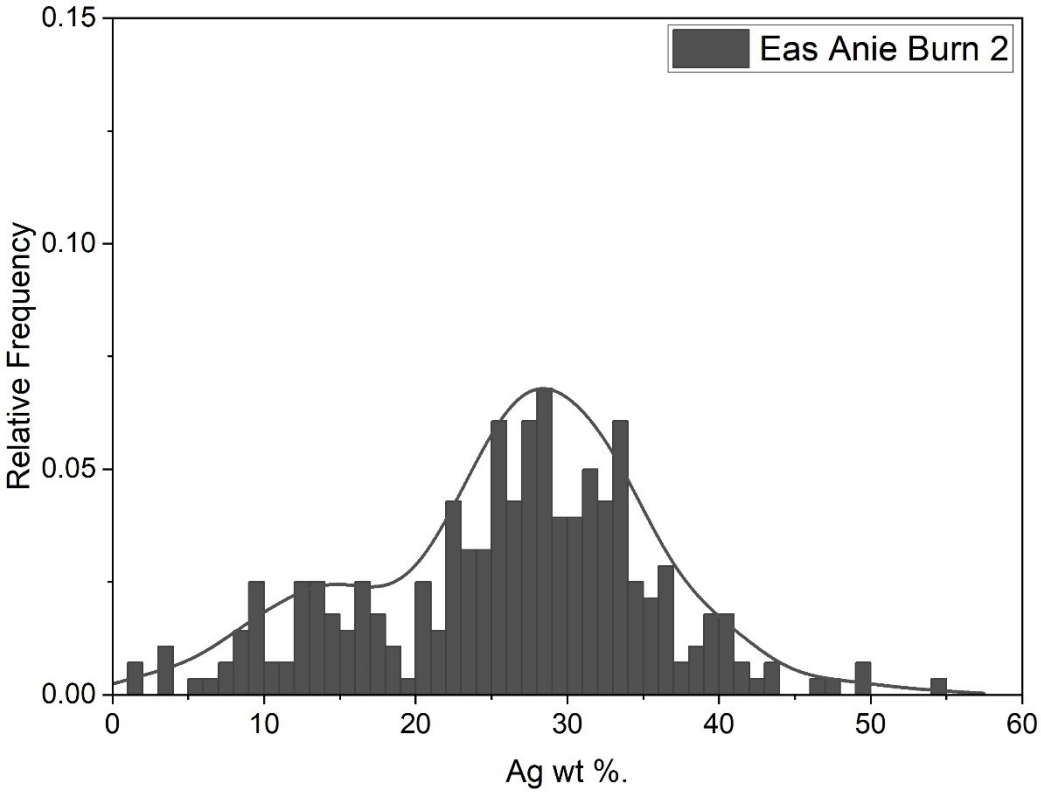

Figure 4.10 – Histogram plot of gold particle alloy composition Ag wt%. of the Eas Anie Burn 2 sample showing the distribution of the placer population with a smoothed kernel distributional curve fitted to the data.

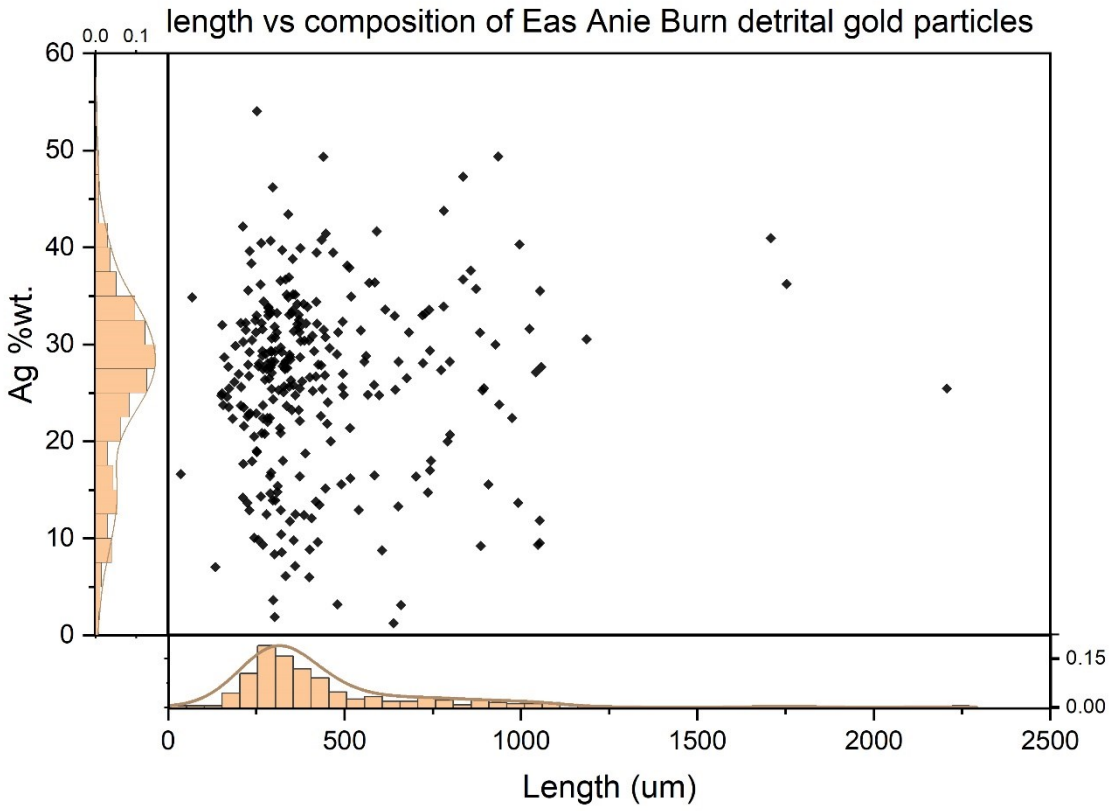

Figure 4.11 – Gold particle length (μm) plotted vs the alloy composition (Ag wt%.) for the Eas Anie Burn 2 sample. Histograms along the axis are plotted using relative frequency as for bin height, with kernel smoothed distribution curve fitted to the data. The data shows no systematic trends appear to exist between particle size of the gold and alloy composition.

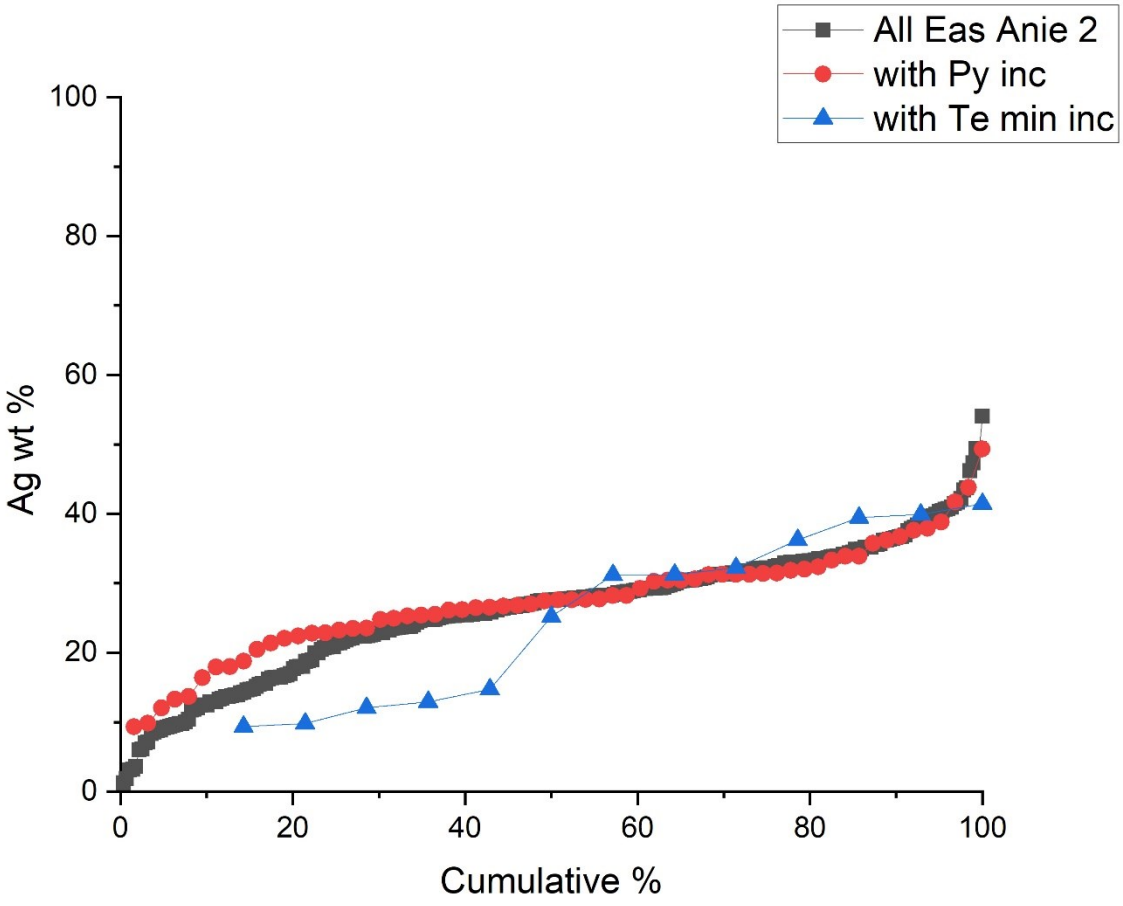

Figure 4.12 – Gold alloy composition plotted (Ag wt%.) for subpopulations of gold particles observed to host the two most common inclusions, pyrite and hessite. Hessite is observed in gold over a wide range of comparisons and although the number of gold particles is limited no correlation to specific compositions are evident, the small step likely due to the small sample number.

Comparison of the two samples available from the Eas Anie Burn, graphically and using a Kolmogorov-Smirnov test demonstrates that the compositional signatures of the two samples are not significantly different (using a 0.05 significance level), figure 4.13 and table 4.2. This is expected as the samples were taken from sites less than 150m apart, although they were collected by different samplers. Because the Eas Anie Burn 2 sample is an order of magnitude larger than the Eas Anie Burn 1 sample, it will be used to represent the Burn in the following analysis and discussions.

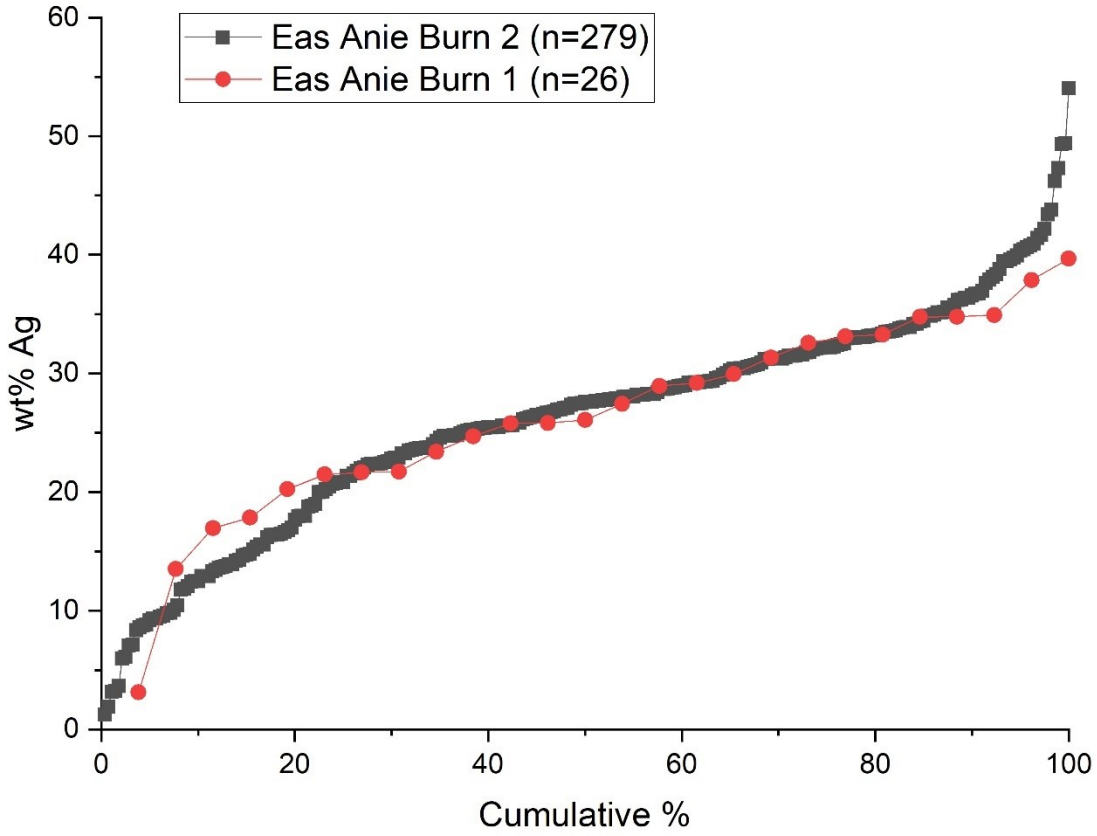

Figure 4.13 – Cumulative frequency plot of the compositional signature of the two samples obtained from Eas Anie Burn.

4.4 Analysis and Discussion

To examine the relationship between the detrital gold population and the in-situ mineralisation the samples taken from Eas Anie Burn were compared with the data obtained from the mineralogical study of the Cononish gold mine (Chapter 3).

Comparing the compositional signature from the detrital population in Eas Anie Burn to the compositional signature obtained from the bulk mine concentrate, figure 4.14, it can be seen that they have different distributions. The distribution of compositions in the mine concentrate has a strongly skewed distribution around a peak at 18 wt% Ag, see discussion in chapter 3, whereas the Eas Anie Burn distribution shows a more symmetrical distribution around a higher central peak (~29 wt% Ag).

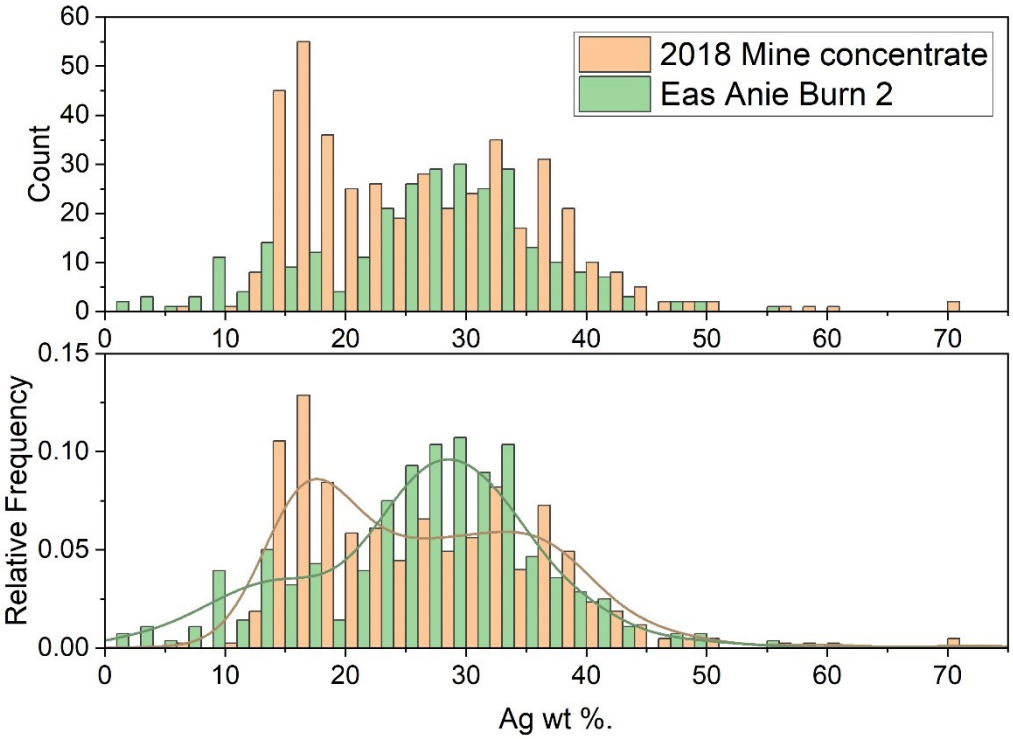

Figure 4.14– Two Histograms showing the distribution of alloy compositions in the detrital Eas Anie Burn 2 sample and the subsampled ore concentrate. The relative frequency histogram with smooth (Scott bandwidth algorithm) kernel density curves which empirically estimate the probability density distribution, shows that a specific range of compositions between ~ 13 to 20 %wt Ag are more prevalent in the mine concentrate sample.

The differences observed between the two populations are statistically significant and need to be explained geologically. Because the two distributions are so different it indicates that the gold particles in the Eas Anie Burn were formed during conditions which were significantly different to those in the mine ore concentrate population. Because of these differences it must be demonstrated that the Eas Anie Burn samples were sourced from the Cononish mine.

The strongest argument for direct sourcing of the Eas Anie gold from the Cononish deposit is the fact that the samples were taken only a few hundred meters away from the vein. In addition, Eas Anie Burn flows over a waterfall which has incised a gorge where the vein is seen in outcrop. It must however be noted that the Glen Cononish valley is a glacial landform and therefore some glacial transport of material may have occurred. For this work the influence of glacial transport is assumed negatable due to the very close proximity of the detrital sample to an actively eroding hard rock source. However, the erosion of the

vein and material above the current land surface due to glacial action would be significant that this may have dispersed vein material down the valley to a larger extent that would be expected to occur fluvially.

There is further evidence supporting that the Eas Anie Burn gold is sourced from the Eas Anie gold vein found within the Cononish Mine in the assemblage of minerals observed as inclusions within the detrital gold. The recorded inclusion mineral assemblage (pyrite + chalcopyrite + galena + altaite + hessite) corresponds to the reported ore mineralogy of the auriferous veins. The only exception is the inclusion of the gold silver telluride mineral, Sylvanite ($(Ag,Au)Te_2$), which has not been observed in sections from the Cononish deposit. The ternary stability diagrams of the Au-Ag-Te system presented by Afifi et al. (1988) indicate that gold with a silver composition of less than 10 wt% electrum would coexist with Sylvanite (in the temperature range estimated for the Cononish Au vein). This is supported by the composition of the two gold particles which contain Sylvanite, which have compositions of 9.8 and 9.2 %wt. Ag. Because the population of gold particles obtained from processed ore, presented in chapter 3, contained gold particles with a silver content as low as 6.3 %wt. Ag, the presence of gold alloy coexisting with Sylvanite is predicted within the Cononish deposit. The independent observation of Sylvanite in the detrital population confirms this prediction and it is therefore compatible with the known properties of Eas Anie Vein mineralisation. Thus, all the inclusion mineralogy supports the direct sourcing of Eas Anie Burn gold particles from the Eas Anie Vein, as expected due to the spatial proximity.

Considering the detrital population, the possibility exists that the difference could be produced by the addition of gold particles from a second, separate unknown auriferous system. This is always a possibility for detrital gold populations, given the allochthonous nature of gold placers, however there is no evidence for a separate source in the catchment of the Eas Anie Burn. No auriferous mineralisation has been documented or discovered outside of the Eas Anie fault during the exploration and resource development drilling on the property which has been extensive over a 50-year period. In addition, the strong structural control on the mineralisation, which restricts it to the damage zone around the fault, means that the mineralised volume can be predictably interpreted. Therefore, the difference in the ore and detrital samples is considered to result from differences in the mineralisation within the distinctly different ore volumes that the samples represent.

Accepting that the direct sourcing of Eas Anie Burn gold particles is from the Eas Anie Vein, the mismatched distribution of compositions between the detrital population and bulk ore population is likely to be due to the samples being sourced from different volumes of

rock, eroded volume vs residual in situ volume. As both populations of gold particles are sourced from a single auriferous vein system, they must be reconcilable geologically. Considering this, the differences between the detrital and ore samples indicate that within the auriferous vein the physiochemical parameters which control gold alloy composition had different evolutions/variations in the different volumes. As the temporal evolution of the in situ auriferous vein is known (see the paragenesis in chapter 3), and the volumes of material which produced the two different populations are definable, insights into the genesis of the auriferous vein systems can be obtained through understanding of the relationship between the two volumes that the gold particles have been obtained from.

One important initial consideration in the comparison between gold signatures, is that the mine ore and detrital samples have been collected using different methods which have different inherent bias across the size range of particles collected. Decreasing abundance with increasing size is present in both ore thin sections and detrital samples but the size ranges are different with limited overlap, figure 4.15. This is because in detrital sampling, small gold particles of <200um are too small to be easily recovered by hand panning, used for this sample, while larger coarse gold particles are rare in thin section.

The abundance of gold particles of increasing sizes approximates to a log linear model which is in keeping with generalised models of crystal size distributions presented by Marsh (1988), who states that a log linear distribution is predicted/expected from basic modelling on the nucleation and growth of crystals. Importantly, when the compositions are correlated to the sizes of the gold particle, figure 4.16, no systematic relationship is observed. As such it can be concluded that the size of the particles can be discounted when considering alloy compositional data.

The rock which was processed to obtain the gold particles extracted from the ore sample was taken from the exploration adit, a single drift approximately 4m wide. In comparison the exact rock which was eroded to produce the detrital gold is unknown but can be assumed to be the volume of rock eroded from above the current land surface. The difference in the volumes is therefore significant with the mine ore population being very tightly constrained and the eroded material being un-constrainable.

The processed ore (bulk ore) gold sample was subsampled from ore extracted from along the 400ml adit. The adit follows the vein structure and the volume of material therefore represents the ‘high grade’ core of the deposit taken from a section mined along the strike of the vein. Therefore, the bulk sample does not include distal mineralisation (>2m away from the vein) in the footwall/hanging wall on either side of the vein and was taken from a narrow (4m) vertical range of vein material. This is considered the most likely reason for

the difference in the compositional populations observed between the bulk sample and the detrital gold sample. Lateral and vertical differences in the mineralisation are explored in the following paragraphs in order to constrain the likely source of the differences as precisely as possible given the current knowledge of the mineralisation in the deposit.

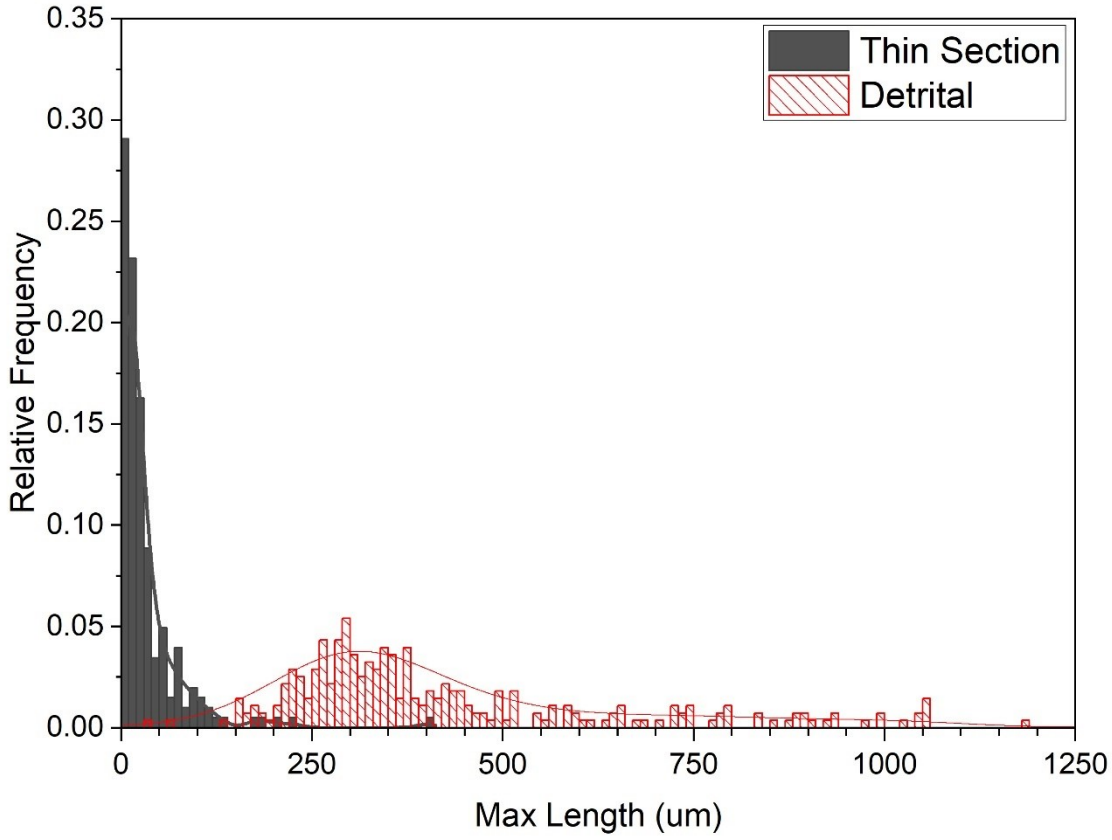

Figure 4.15 – Relative frequency histogram showing the proportions max length of gold particles observed in thin section and in the detrital sample.

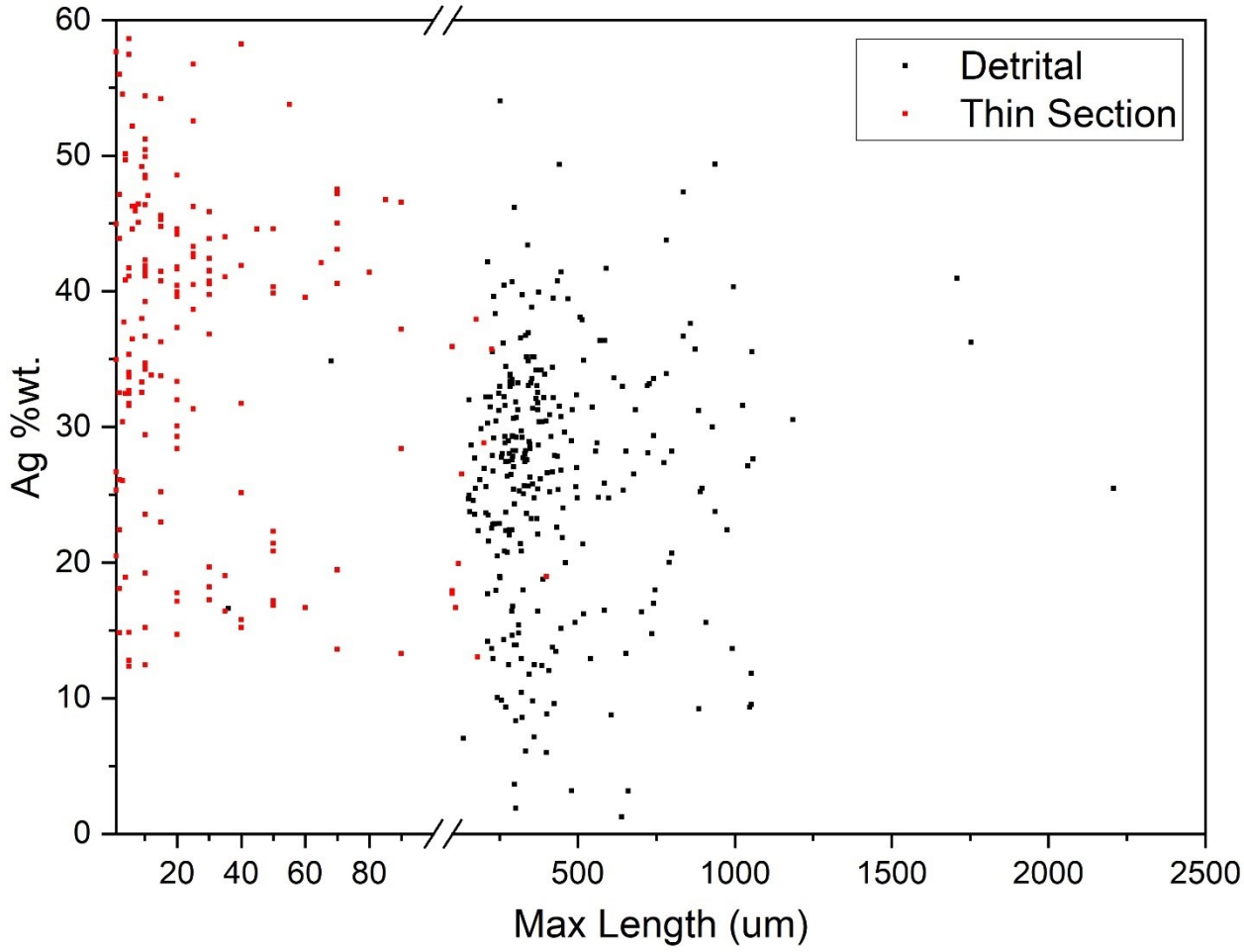

Figure 4.16 – Scatter plot of max length vs Ag % concentration of gold particles in both thin section and the detrital gold samples. Note the break on the x axis at 100µm, where the scale changes to facilitate comparison of the different size ranges of the sample populations.

There are three possible reasons why the different compositional signatures observed in the ore gold samples are unlikely to be due to lateral variations, into the hanging or footwall. Firstly, the material taken from the adit was taken from a width which exceeded the mineralised vein width, it therefore it does include variable amounts of dilution in the form of altered hanging and footwall host lithologies, up to a few meters from the main vein structure. Secondary alteration around the vein known to be limited and only extends up to maximum of 15m's from the Eas Anie fault (into the psammites which show the most developed alteration halo) (Earls et al., 1992) this indicates that permeability of the ore fluids into the host lithologies is limited, occurring only within the damage zone around the faults. The observation by Earls et al. (1992) that alteration is greatest in the most competent host lithologies, psammites, supports that the alteration halo extent is structurally controlled by fractures/damage zone around the fault. Thirdly, variography

conducted on drillhole assays in narrow vein gold systems generally have limited grade continuity perpendicular to the plane of the vein (Samal et al., 2011). Considering this, alongside commercial deposit modelling commissioned by the company, which states that the rock laterally surrounding the adit does not contain significant gold grades (Scotgold Resources Limited, 2015), lateral variations are unlikely to be the reason for the compositional differences observed between the samples.

Therefore, vertical variation within the gold vein is likely to be the cause of the difference in the signature in the compositional signatures of the gold samples. It is known that within orogenic gold vein systems, lateral variations along strike are minor and on the scale of centimetres to tens of metres, whereas vertical zonation is reported occurring over hundreds of metres (Groves, 1993, Goldfarb and Groves, 2015, Groves et al., 1998, Groves et al., 2003).

4.4.1 Reconciliation of the two different gold alloy compositional signatures with a single genetic model for the gold mineralisation at the Cononish mine.

The previous mineralogical analysis of the Cononish deposit in Chapter 3, looked at the gold signatures of individual stages of the paragenesis, and related them related to a bulk sample of gold particles obtained from the processing plant. That study concluded that the early generations of the auriferous mineralisation formed the majority of the gold particles. This conclusion was based on the observations within the exploration adit (Mine level; 400mL), and the ore removed from it. While the observations stand alone, the interpretations based on them, including the new genetic model, must be re-evaluated in the light of the different distribution of gold compositions observed in the detrital gold population.

The distribution obtained from the adit showed that the greatest abundance of gold was associated with early silver poor vein generations, with later generations responsible for progressively smaller proportions of the gold particles in the bulk ore sample. This is interpreted as a magmatic pulse, followed by the magmatic fluid mixing progressively with crustal fluids/lithologies (Spence-Jones et al., 2018). In contrast the populations obtained from the detrital sediment show a much more symmetrical distribution around the median composition of 27.6 %wt.Ag, see figure 4.14.

The difference must be due to differences in the source of the particles in the two populations, as discussed above. Given this: is it possible that the two populations are compatible with the proposed model of a magmatic pulse?

Orogenic gold systems are highly complex with many chemical and physical factors influencing the formation of the ore. Theoretical (reactive transport) models are currently not sophisticated enough to model all the complex processes and interplays of all the variables at the scale of an entire orogenic gold system, as significant numbers of unknowns preclude this. However more simple experimental observations and modelling of fluids propagating in fractures can provide insights into the dynamics of fluid migration and mineralisation.

Experimental studies of fluid pulses introduced into fracture networks have been conducted using radiometric tracers (Reimus et al., 2003). These provide empirical data on the migration of fluids in the crust and the interplay of fluid-rock exchange in the chemical components of fluids over time. The observed concentration profile (of the measured element in solution) over time at a point in a fracture network was examined by Reimus et al. (2003) and they observed that the concentration of an element is dependent on porosity, diffusivity and absorptivity of that element. Measured responses show log normal distributional concentration profiles over time for non-absorbing elements and flatter curves for absorbing elements.

Considering the elements within the Cononish deposit in the context of the work of Reimus et al. (2003) the primary economic elements; Au, Ag and Te, can reasonable be assumed to be non-absorbing. This implies that no exchange with a 'reservoir' of the specific element exists in the host lithologies, at least initially, as the host lithologies do not contain elevated Au, Ag or Te in assay. If such an exchange with a reservoir had occurred, it would moderate concentration in the fluids thereby producing a buffering effect and reducing peak concentrations within a fluid pulse. Accepting that Au, Ag and Te are non-absorbing means that the predicted concentration would follow the log normal concentration gradient over time.

Comparing the non-absorbing models of Reimus et al. (2003) with the compositional signature of gold from the adit, the observed progression in mineralisation fits with the proposed genetic model. It explains the observed decreases in Te fugacity over time through the paragenesis which was previously examined in chapter 3. Given the evidence that a pulse of fluid is genetically important to the mineralisation within the adit, an assessment of whether this model is compatible with the detrital gold compositional signature must be made. To do this a conceptual model is considered in which the temperature and pressure of the mineralising fluids are changed in relation to height in the system. The justification for changing these parameters is that they have been empirically shown to vary with height in orogenic gold systems. Mernagh et al. (2004) used fluid

inclusion micro thermometry to define a temperature gradient of (up to) 100°C/Km in the veins within the Mount Charlotte deposit, Kalgoorlie. Furthermore, the work and models of Sibson et al. (1988) indicate that pressure fluctuations in active faults are likely to be significant and cyclical rapid pressure drops linked to fault movement may be a key trigger for depositional events.

The proposed model is that temperature (and/or pressure) decreased with height, on a scale of 100's of meters, in the vein figure 4.18. The thermodynamic models of gold alloy composition indicate that a decrease in the pressure and temperature conditions (PT) results in a non-linear increase in the Ag concentration of the gold alloy in a pure Au-Ag system (Gammons and Williams-Jones, 1995). In the Au-Ag-Te system, which represents the Cononish mineralisation, (Afifi et al., 1988) report that the concentration of Ag in the gold alloy also increases with decreasing temperatures at a constant Te fugacity. However, because Te fugacity also is dependent on the temperature of the system, an exact relationship between temperature, pressure and the concentration of Ag in the gold alloy is not possible for the Cononish system given the available constraints but we can identify a trend consistent with both lowering T and Te fugacity (Grundler et al., 2013, Afifi et al., 1988).

Therefore, if decreasing PT conditions were present at higher levels, this would shift the alloy compositions of gold to higher silver contents, which is observed in the Eas Anie Burn detrital population when compared to the adit ore sample. This assumption is however impossible to test as the vein which produced the detrital population has been sourced from eroded vein material. Considering the shape of the distribution, addition of volumes of vein material for a range of height in the system (with each increase in height resulting in alloy compositions shifted to higher silver values) could result in an overall distribution different to that observed when sampling that vein at a specific height. A conceptual example of this is shown graphically in figure 4.17 to illustrate how vertical variations in the vein could alter the detrital population.

Figure 4.17 – Long section of the Cononish deposit showing variation in grade volumes that the gold compositional populations (right) are sourced from. Modified after Earls et al. (1992)

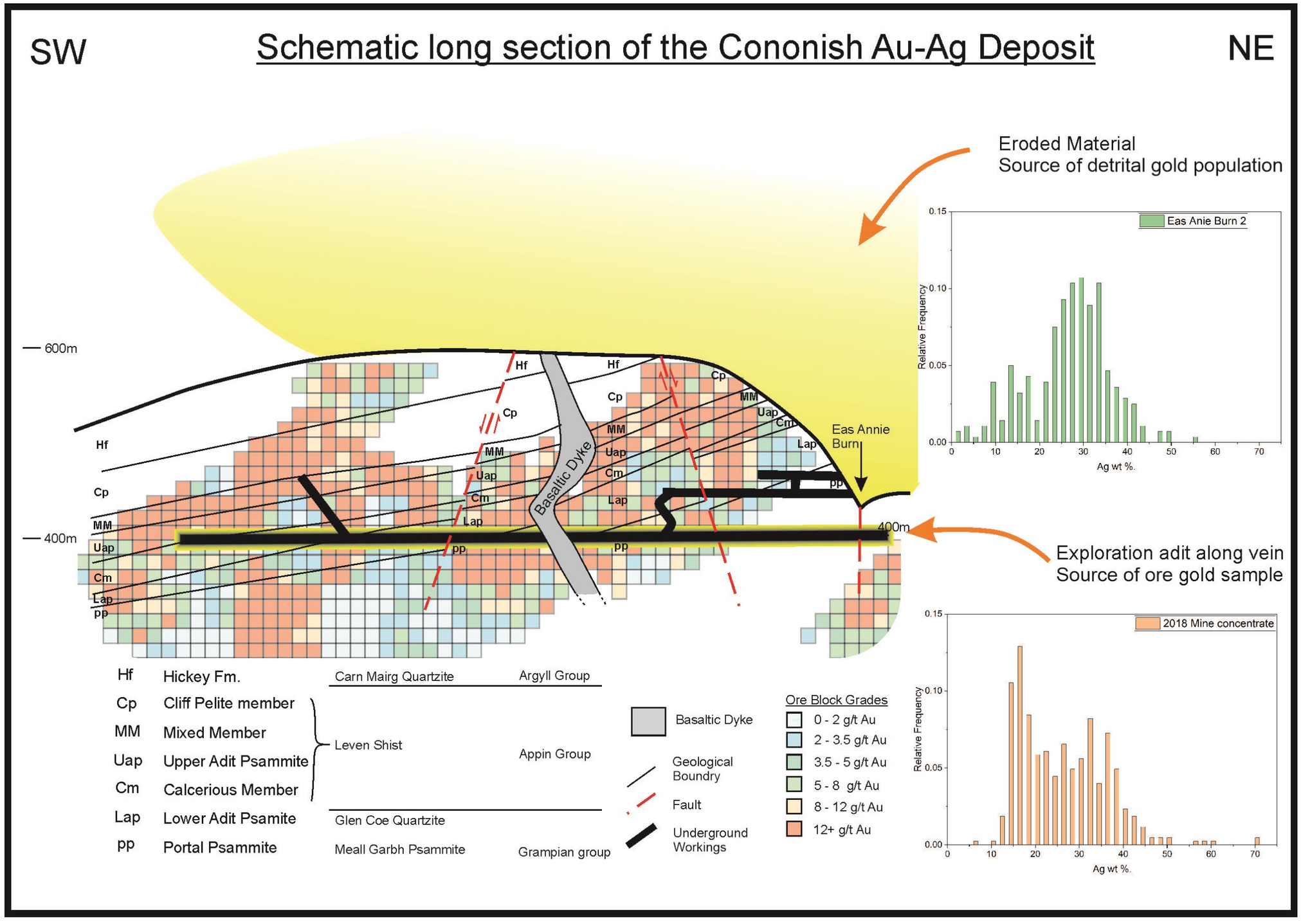

Conceptual model to explain different gold populations observed at the Cononish mine

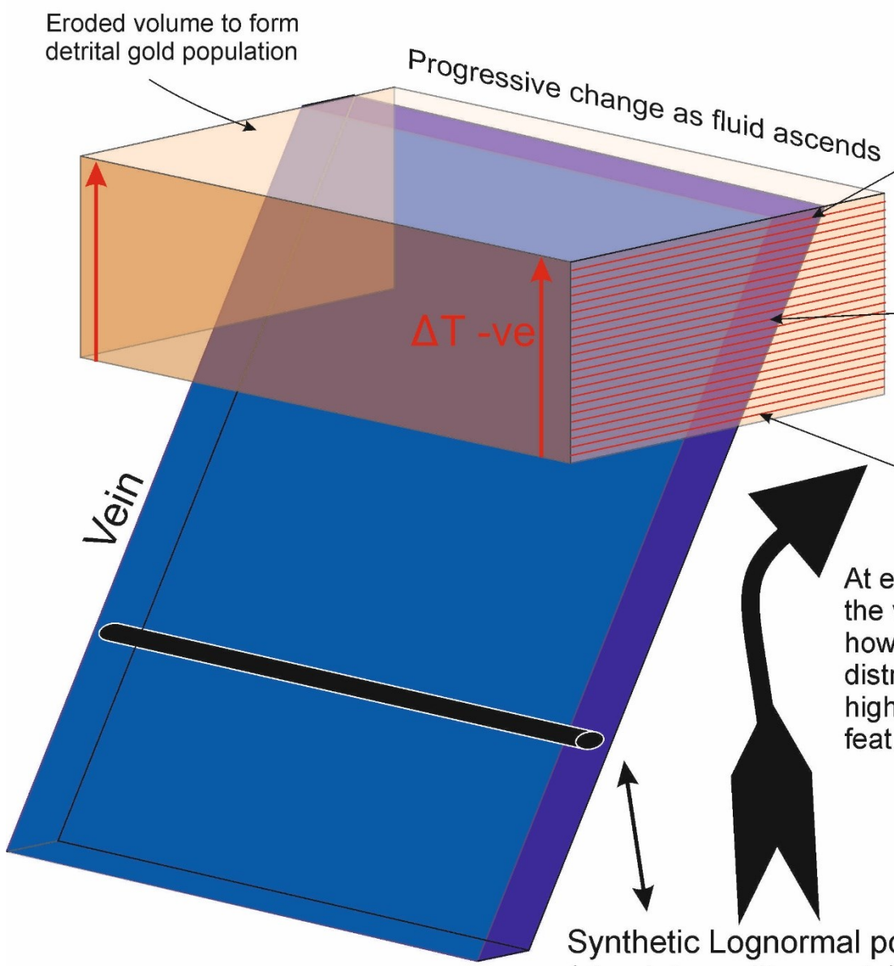

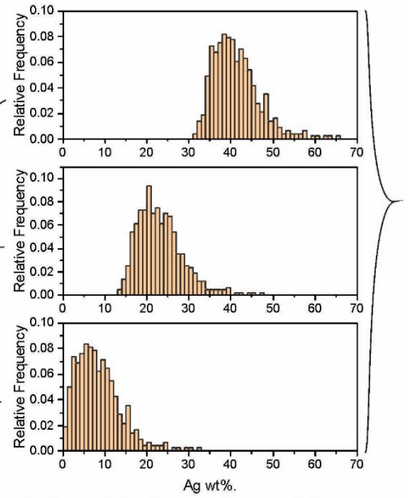

At each height plane the gold population in the vein has a log normal distribution, however with increasing height the distributions are progressively translated to higher Ag values. (retaining all other features of the distribution)

Detrital population proposed model

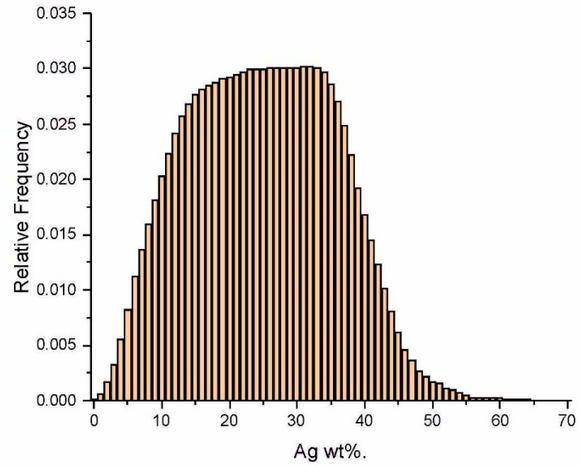

The detrital population is eroded from multiple height levels. Combining them into a overall population results a different distribution uncomparable to the population at one height.

By changing the translation and amplitudes of log-normal distributions any apparent total distribution could be generated.

Synthetic Lognormal population (simulates adit sample)

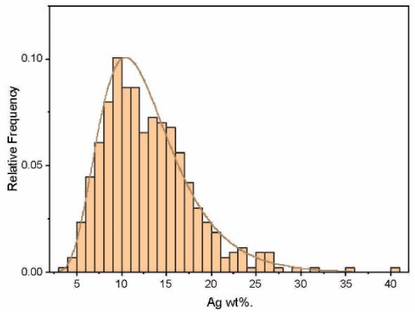

For example, two translation 'groups' results produces a complex overall population (similar to the real data)

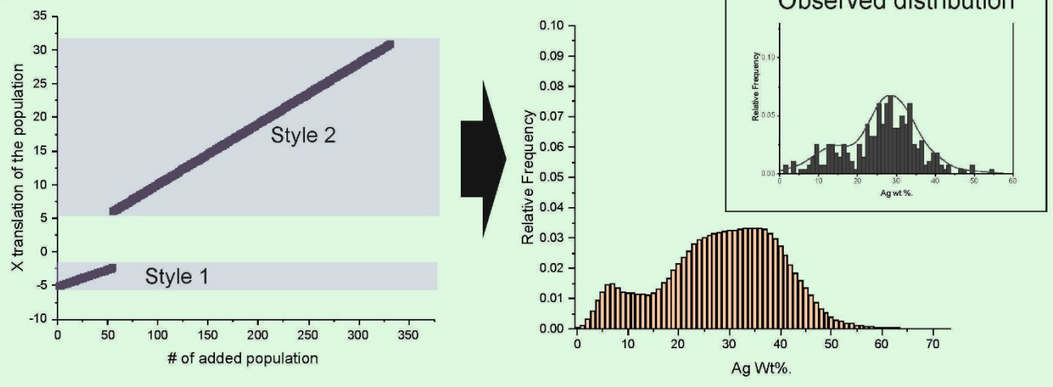

Figure 4.18 – Conceptual model for the Cononish gold mineralisation to explain the different gold compositional populations. It shows a theoretical example for a log normal distribution of the mineralisation that is translated to higher Ag values with increasing height. The multiple populations and different levels are then combined into proportions to replicate the empirical data.

4.4.2 Comparison between the Cononish Detrital compositional signature and regional samples.

In this section detrital gold signatures from selected localities in the wider Tyndrum area are compared. This comparison is undertaken to investigate the geographical extent of the Cononish (Eas Anie) signature and to contrast the gold compositional signature of other locations to assess if they may contain a similar 'style' gold system to the Eas Anie vein.

To investigate the spatial extent of the Eas Anie compositional signature within Glen Cononish two additional detrital sample locations, figures 4.2 and 4.3, were examined from the Cononish River (Cononish 1 and 2). The River Cononish 1 sample was taken upstream of the Eas Anie Burn confluence and the River Cononish sample 2 was taken downstream. Both these sample sites contain populations which are significantly different from the Eas Anie Burn samples, see matrix of P values from K-S testing, see table 4.2, and figure 4.19.

The upstream River Cononish sample, Cononish 1, consists of a significantly different, more gold rich, population of gold particles compared to the population in the Eas Anie Burn. This result is expected as no significant mineralisation within the Eas Anie fault is reported along the strike to the south within in the large U-shaped Glen Cononish valley. Therefore, it is unlikely gold particles sourced from the deposit volume are present at the upstream sample site. However, as gold particles exist within the drainage, some unknown source mineralisation must be present up valley from the sample location.

The location and character of the mineralisation upstream in the higher reaches of the Glen Cononish is unknown. The mineralisation in the River Cononish 1 gold particles is very different to the other samples derived from the Eas Anie vein at the Cononish deposit, however the very small sample size of only 29 particles makes reliable interpretation challenging. Given the presence of the regional Tyndrum fault (figure 4.2), which is speculated to have acted as a major conduit for fluids within a large part of Glen Cononish, it is considered likely that a portion of gold particles may be associated with the main Tyndrum fault or other associated splays, see figure 4.2 (Tanner, 2014, Tanner, 2012).

Table 4.2 – K-S P values for sample pairs in the Cononish area, coloured from highest (green) to lowest p values (red). A low p value indicates that the difference observed between the samples is improbable to replicate from duel sampling a single population.

K-S P value	Eas Anie Burn 1	Eas Anie Burn 2	Cononish 1	Cononish 2
Eas Anie Burn 1				
Eas Anie Burn 2	0.86733			
Cononish 1	0.00857	0.00003		
Cononish 2	0.27826	0.02667	0.00002	

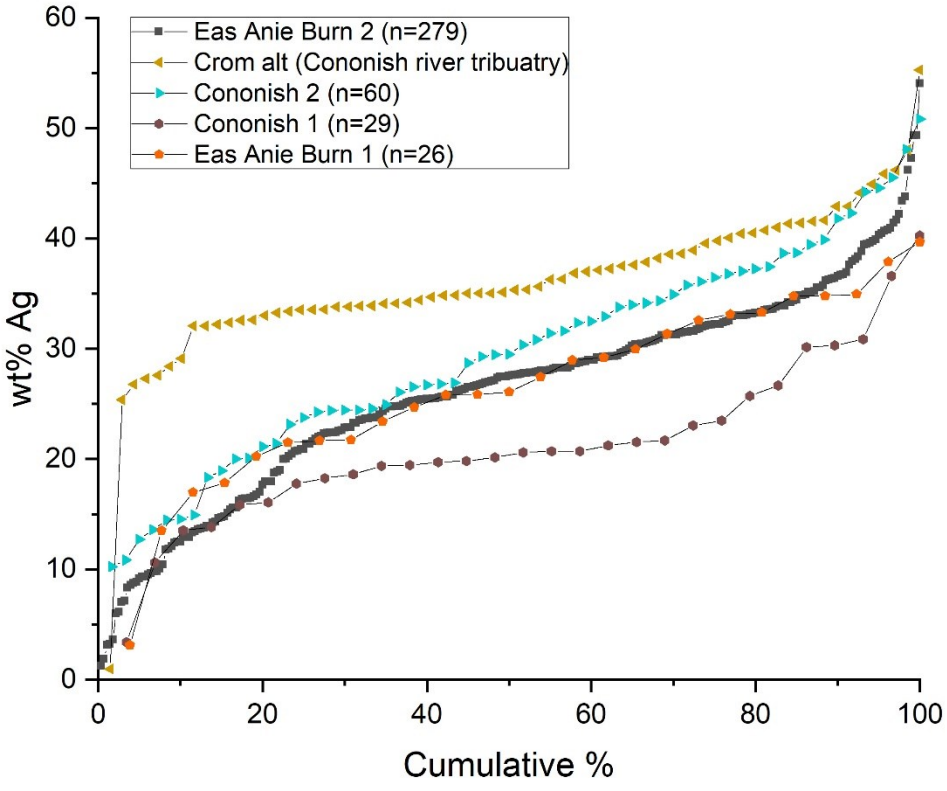

Figure 4.19 – Cumulative frequency plot of Ag composition of gold particles in Glen Cononish. Including a sample population from Crom alt.

Downstream from the Eas Anie Burn confluence, the River Cononish 2 sample has an observed compositional distribution which is more silver rich than the Eas Anie Burn populations. It is significantly different from the larger Eas Anie Burn sample 2 but the K-S result indicates it is not significantly different from the smaller Eas Anie Burn 1 sample. The latter result is due to the similarity between the population of the down steam River Cononish 2 sample and the population in Eas Anie Burn 1. This is expected as a portion of the gold population in the Coronish River 2 sample will have been sourced from the mine area via Eas Anie Burn. The samples from Cononish River 2 & Eas Anie Burn 1 are sufficiently similar that only two large sample sizes would give the resolution to distinguish more subtle differences in composition. These observations highlight the issues with small sample sizes as they produce larger uncertainty when comparing populations and cannot be separated in a statistically robust manner due to the potential for large variance inherent in a small population size, see chapter 2.

The comparison of samples from Glen Cononish River 2 & Eas Anie Burn, table 4.2 and figures 4.18 and 4.19, indicates that the two populations are local to the source rocks and the populations are modified with increasing transport distances due to additional gold particles from multiple sources. First order drainages with large sample populations are likely to produce the best populational characterisations of detrital gold particles. Samples from larger drainages with large catchments provide more challenging populations to analyse due to the increased possibility that they contain particles from multiple sources, potentially containing overlapping compositional ranges.

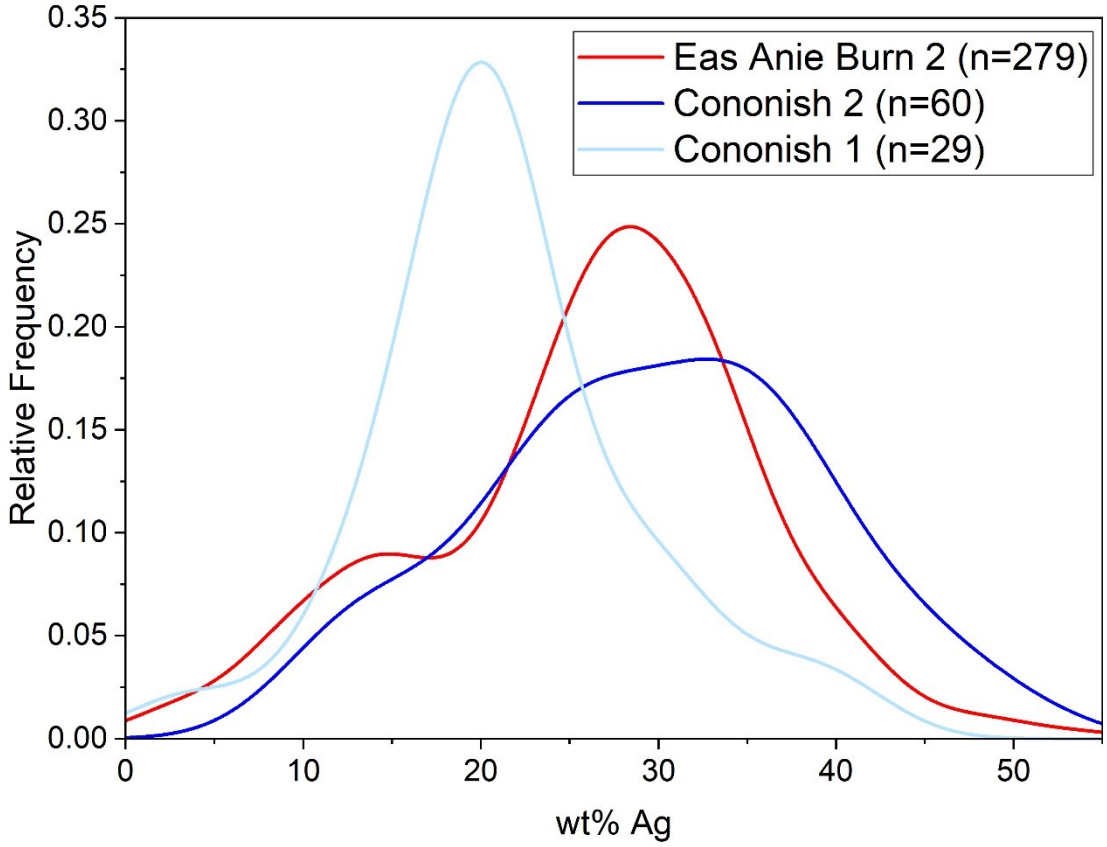

Figure 4.20 – Relative frequency histogram comparing the distributions of the Cononish area samples

The comparison of alloy compositional signatures conducted between the Eas Anie Burn 2 sample and 4 regional samples was conducted. The results are shown in figures 4.19, 4.20 and 4.21 and it can be seen that differences in the shapes of the distributions are observed. When interpreting these diagrams, they are considered a representation of the general mineralisation conditions for a 'system', such that a difference in the peak of composition indicates differences in the principal mineralising conditions.

For example, the distributions of silver composition of two of the populations, Lyon Tributary (Alt Meurain Burn) and Calliche, figure 4.21, have strongly positive skewed distributions with median silver compositions which re lower than the Eas Anie 2 population. they are significantly lower which indicates a different conditions predominated, when compared to the Eas Anie mineralisation, for the majority of the detrital gold particles in these samples. If these samples are hypothesised to be formed as part of a hypothesised 'Eas Anie mineralisation event' with similar fluids and processes to the Eas Anie vein you could predict that early Au rich vein stages predominated in these samples. However, because these two samples include a long

‘silver tail’ but a wide range of gold compositions, as therefore conditions existed in the catchments.

The Crom Alt Burn data, figure 4.21, is very different to the other sample sites as it has a very narrow, high amplitude peak, at a higher silver compared to the Eas Anie Burn 2 gold signature. This narrow high amplitude peak indicates that stable gold precipitation conditions existed within the catchment of the detrital sample. One interpretation of such a narrow high amplitude peak is that the gold particles are derived from a simple single ‘stage’ vein which deposed gold without conditions changing over time/space. If this interpretation is valid such a narrow high amplitude peak would be considered a less attractive potential exploration target as it is likely to be from a narrow/ smaller vein with no or limited mineralisation over a significant vertical extent.

The most attractive exploration target from the detrital samples, considering the gold signature of the Eas Anie detrital population, is the River Lochy sample, figure 4.21. This sample show a very similar distribution to the Eas Anie Burn sample which potentially indicates that the source of the gold particles may be from a mineralising system consistent with that of the Cononish vein. However, it is important to note that the Lochy is a large low order drainage with many tributaries and a large catchment area. Therefore, although the River Lochy sample displays similarities to the Cononish mine samples, the auriferous veins may be hosted in a distributed array or multiple structures. The mineralisation within the Lochy River catchment may therefore lack the economic potential of the Eas Anie vein where the mineralising system is hosted in a single structure. To quantify the potential for economic mineralisation within the Lochy River catchment requires further work to explain the similarities in the gold population to the Eas Anie Vein system.

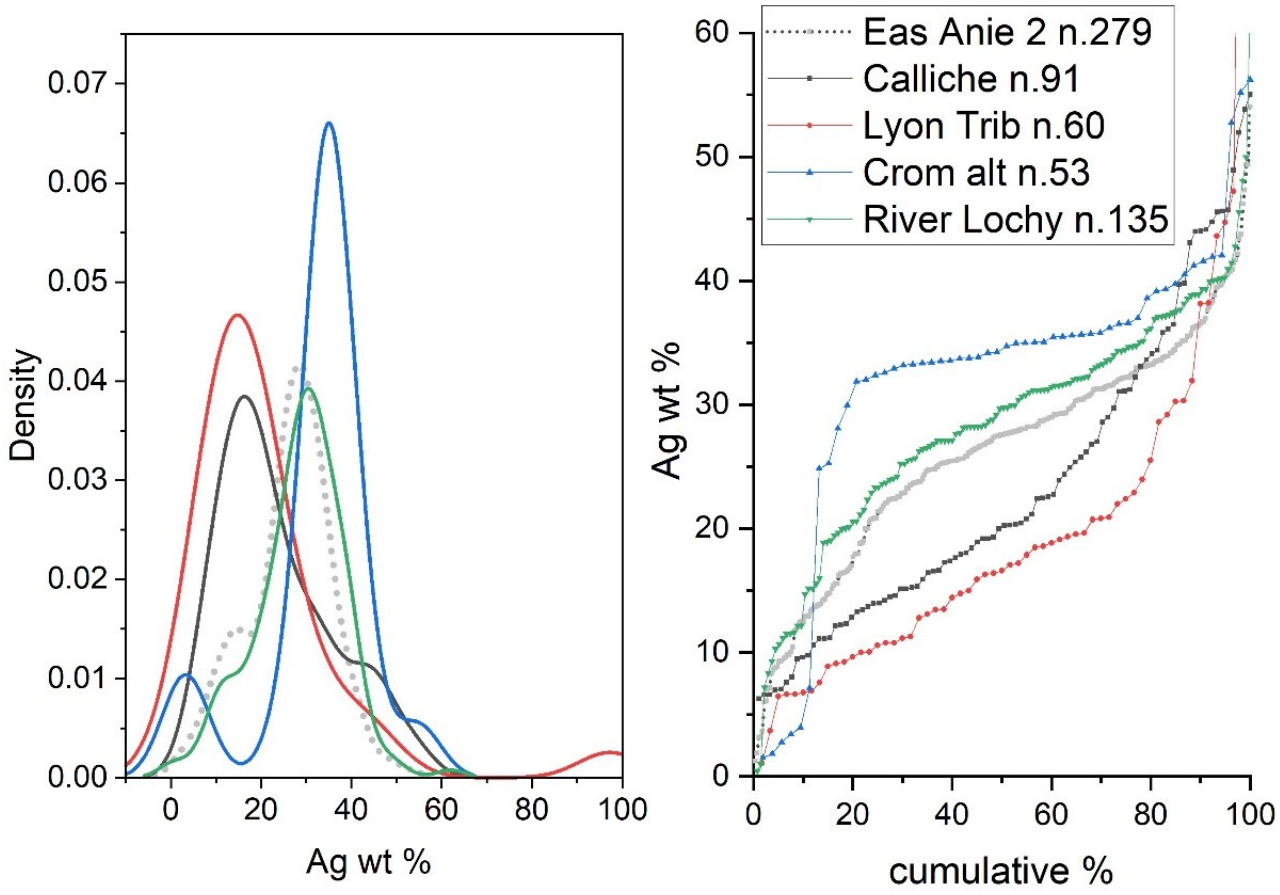

Figure 4.21 – Tyndrum area detrital gold sample comparisons, distribution density histogram and cumulative frequency plots. See table 4.1 for sample locations.

4.5 Conclusions

The gold samples studied from the Cononish project, presented in chapters 3 and 4, demonstrate that comparing the compositional signature of gold particles taken from ore with those from detrital populations is not straightforward. The results obtained from the Cononish mine illustrate that differences in the physiochemical evolution of the mineralising conditions, present in the different source volumes of vein, can alter the gold signatures. This makes linking signatures from lode and detrital sources complex. The Cononish study does however provide an opportunity to better understand auriferous mineralisation.

The composition of the population of detrital gold in the Eas Anie Burn is distinct from the other occurrences in the area proximal to the Cononish Mine. This result

demonstrates that gold formed within mineralising systems, which are known to form economic deposits, can be differentiated from gold populations sourced from other mineralisation/occurrences.

A further significant finding in this research conducted at the Cononish deposit is that in the mineralisation there is no correlation between the alloy composition and size of gold particles. The investigation of relationships between composition and gold particle size completed on gold in thin sections from ore and that in detrital particles, indicates that the size distributions of the gold particles is decoupled from the composition of the alloy within the Cononish deposit. This finding is assumed to be due to the dynamics of crystal growth.

The results suggest that gold compositional signatures obtained from detrital sampling should not be compared with gold signatures sourced from other methods, such as ore material, as has been done previously in studies by Knight et al. (1999) and (Chapman and Mortensen, 2016) and others. This is because, as shown in this study, equivalence cannot be assumed between ore/lode and detrital gold particle populations due to potential differences in the physiochemical evolution of the mineralising conditions of the different populations. Furthermore, in studies where gold signatures between deposits are compared, ideally gold signatures from well-constrained detrital populations demonstrated to be only from a specific deposit should be sought, before comparing detrital signatures with other deposits.

Finally, the correlation between detrital gold particles and those observed in thin sections through gold alloy compositions provides a novel tool for assessing the economic importance of assemblages observed in thin section on a whole deposit/ system scale. For the Cononish deposit, this shows that the majority of the gold mineralization is deposited in assemblages associated with the early and middle stages of the paragenesis and that the late stages observed in thin section have a more minor importance on the endowment of the system.

References

AFIFI, A. M., KELLY, W. C. & ESSENE, E. J. 1988. Phase relations among tellurides, sulfides, and oxides; I, Thermochemical data and calculated equilibria. *Economic Geology,* 83**,** 377-394.

BOZZOLO, G., GARCÉS, J. E. & DERRY, G. N. 2007. Atomistic modeling of segregation and bulk ordering in Ag–Au alloys. *Surface Science,* 601**,** 2038-2046.

BROWN, L. & VEARNCOMBE, J. 2014. Critical analysis of successful gold exploration methods. *Applied Earth Science,* 123**,** 18-24.

CHAPMAN, R., BANKS, D. A. & SPENCE-JONES, C. 2017. Detrital gold as a deposit-specific indicator mineral, British Columbia: analysis CHAPMAN, R. J., BANKS, D. A., STYLES, M. T., WALSHAW, R. D., PIAZOLO, S., MORGAN, D. J., GRIMSHAW, M. R., SPENCE-JONES, C. P., MATTHEWS, T. J. & BOROVINSKAYA, O. 2021. Chemical and physical heterogeneity within native gold: implications for the design of gold particle studies. *Mineralium Deposita*.

CHAPMAN, R. J., BANKS, D. A., STYLES, M. T., WALSHAW, R. D., PIAZOLO, S., MORGAN, D. J., GRIMSHAW, M. R., SPENCE-JONES, C. P., MATTHEWS, T. J. & BOROVINSKAYA, O. 2021. Chemical and physical heterogeneity within native gold: implications for the design of gold particle studies. *Mineralium Deposita*.

CHAPMAN, R. J., MORTENSEN, J. K., CRAWFORD, E. C. & LEBARGE, W. 2010. Microchemical Studies of Placer and Lode Gold in the Klondike District, Yukon, Canada: 1. Evidence for a Small, Gold-Rich, Orogenic Hydrothermal System in the Bonanza and Eldorado Creek Area. *Economic Geology,* 105**,** 1369-1392.

CHAPMAN, R. J. & MORTENSEN, J. K. 2016. Characterization of Gold Mineralization in the Northern Cariboo Gold District, British Columbia, Canada, Through Integration of Compositional Studies of Lode and Detrital Gold with Historical Placer Production: A Template for Evaluation of Orogenic Gold. *Economic Geology,* 111**,** 1321-1345.

CHUDNENKO, K. & PAL'YANOVA, G. 2013. Thermodynamic properties of Ag–Au–Hg solid solutions. *Thermochimica Acta,* 572**,** 65-70.

CHUDNENKO, K. V. & PALYANOVA, G. A. 2016. Thermodynamic modeling of native formation of Au–Ag–Cu–Hg solid solutions. *Applied Geochemistry,* 66**,** 88-100.

CRAWFORD, E. C. 2007. *Klondike placer gold : new tools for examining morphology, composition and crystallinity* by laser-ablation inductively coupled plasma–mass spectrometry. *Geoscience BC Summary of Activities 2016.* Geoscience BC.

DOMINY, S., XIE, Y. & PLATTEN, I. 2008. Characterisation of in-situ gold particle size and distribution for sampling protocol optimisation. *Proc. 9th Int. Cong. on 'Applied mineralogy***,** 175-185.

EARLS, G., PATTERSON, R. T. G., CLIFFORD, J. A. & MELDRUM, A. H. 1992. The Geology of the Cononish Gold Silver Deposit, Grampian Highlands of Scotland. *In:* BOWDEN, A. A. (ed.) *The Irish Minerals Industry 1980-1990.* Irish Association for Economic Geology.

FISHER, N. H. 1945. The fineness of gold, with special reference to the Morobe gold field, New Guinea. *Economic Geology,* 40**,** 449-495.

GAMMONS, C. H. & BARNES, H. L. 1989. The solubility of Ag2S in near-neutral aqueous sulfide solutions at 25 to 300°C. *Geochimica et Cosmochimica Acta,* 53**,** 279-290.

GAMMONS, C. H. & WILLIAMS-JONES, A. E. 1995a. Hydrothermal Geochemistry of Electrum - Thermodynamic Constraints. *Economic Geology and the Bulletin of the Society of Economic Geologists,* 90**,** 420-432.

GAMMONS, C. H. & WILLIAMS-JONES, A. E. 1995b. The solubility of Au□Ag alloy + AgCl in HCl/NaCl solutions at 300°C: New data on the stability of Au (1) chloride complexes in hydrothermal fluids. *Geochimica et Cosmochimica Acta,* 59**,** 3453-3468.

GUISBIERS, G., MENDOZA-CRUZ, R., BAZÁN-DÍAZ, L., VELÁZQUEZ-SALAZAR, J. J., MENDOZA-PEREZ, R., ROBLEDO-TORRES, J. A., RODRIGUEZ-LOPEZ, J.-L., MONTEJANO-CARRIZALES, J. M., WHETTEN, R. L. & JOSÉ-YACAMÁN, M. 2016.

Electrum, the Gold-Silver Alloy, from the Bulk Scale to the Nanoscale: Synthesis, Properties, and Segregation Rules. *ACS nano,* 10**,** 188-198.
GOLDFARB, R. J. & GROVES, D. I. 2015. Orogenic gold: Common or evolving fluid and metal sources through time. *Lithos,* 233**,** 2-26.
GROEN, J. C., CRAIG, J. R. & RIMSTIDT, J. D. 1990. Gold-rich rim formation on electrum grains in placers. *The Canadian Mineralogist,* 28**,** 207-228.
GROVES, D. I. 1993. The crustal continuum model for late-Archaean lode-gold deposits of the Yilgarn Block, Western Australia. *Mineralium Deposita,* 28**,** 366-374.
GROVES, D. I., GOLDFARB, R. J., GEBRE-MARIAM, M., HAGEMANN, S. G. & ROBERT, F. 1998. Orogenic gold deposits: A proposed classification in the context of their crustal distribution and relationship to other gold deposit types. *Ore Geology Reviews,* 13**,** 7-27.
GROVES, D. I., GOLDFARB, R. J., ROBERT, F. & HART, C. J. R. 2003. Gold deposits in metamorphic belts: Overview of current understanding, outstanding problems, future research, and exploration significance. *Economic Geology and the Bulletin of the Society of Economic Geologists,* 98**,** 1-29.
GRUNDLER, P. V., BRUGGER, J., ETSCHMANN, B. E., HELM, L., LIU, W. H., SPRY, P. G., TIAN, Y., TESTEMALE, D. & PRING, A. 2013. Speciation of aqueous tellurium(IV) in hydrothermal solutions and vapors, and the role of oxidized tellurium species in Te transport and gold deposition. *Geochimica Et Cosmochimica Acta,* 120**,** 298-325.
HOUGH, R. M., BUTT, C. R. M. & FISCHER-BÜHNER, J. 2009. The Crystallography, Metallography and Composition of Gold. *Elements,* 5**,** 297-302.
HOUGH, R. M., BUTT, C. R. M., REDDY, S. M. & VERRALL, M. 2007. Gold nuggets: supergene or hypogene? *Australian Journal of Earth Sciences,* 54**,** 959-964.
KNIGHT, J. B., MORTENSEN, J. K. & MORISON, S. R. 1999. Lode and placer gold composition in the Klondike district, Yukon Territory Canada: Implications for the nature and genesis of Klondike placer and lode gold deposits. *Economic Geology and the Bulletin of the Society of Economic Geologists,* 94**,** 649-664.
LEAKE, R. C., CHAPMAN, R. J., BLAND, D. J., CONDLIFFE, E. & STYLES, M. T. 1997. Microchemical characterization of alluvial gold from Scotland. *Transactions of the Institution of Mining and Metallurgy Section B-Applied Earth Science,* 106**,** B85-B98.
LEAKE, R. C., STYLES, M. T., BLAND, D. J., HENNEY, P. J., WETTON, P. D. & NADEN, J. 1995. The interpretation of alluvial gold characteristics as an exploration technique. *British Geological Survey Technical Report WC/95/22*.
LIU, H. & BEAUDOIN, G. 2021. Geochemical signatures in native gold derived from Au-bearing ore deposits. *Ore Geology Reviews,* 132**,** 104066.
MACKENZIE, D. J. & CRAW, D. 2005. The mercury and silver contents of gold in quartz vein deposits, Otago Schist, New Zealand. *New Zealand Journal of Geology and Geophysics,* 48**,** 265-278.
MARSH, B. D. 1988. Crystal size distribution (CSD) in rocks and the kinetics and dynamics of crystallization. *Contributions to Mineralogy and Petrology,* 99**,** 277-291.
MELCHIORRE, E., ORWIN, P., REITH, F., REA, M. A., YAHN, J. & ALLISON, R. 2018. Biological and Geochemical Development of Placer Gold Deposits at Rich Hill, Arizona, USA. *Minerals,* 8**,** 56.
MERNAGH, T. P., HEINRICH, C. A. & MIKUCKI, E. J. 2004. Temperature gradients recorded by fluid inclusions and hydrothermal alteration at the Mount Charlotte gold deposit, Kalgoorlie, Australia. *The Canadian Mineralogist,* 42**,** 1383-1404.
MORRISON, G. W., ROSE, W. J. & JAIRETH, S. 1991. Geological and geochemical controls on the silver content (fineness) of gold in gold-silver deposits. *Ore Geology Reviews,* 6**,** 333-364.
OZOLIŅŠ, V., WOLVERTON, C. & ZUNGER, A. 1998. Cu-Au, Ag-Au, Cu-Ag, and Ni-Au intermetallics: First-principles study of temperature-composition phase diagrams and structures. *Physical Review B,* 57**,** 6427-6443.
PAL'YANOVA, G. 2008. Physicochemical modeling of the coupled behavior of gold and silver in hydrothermal processes: Gold fineness, Au/Ag ratios and their possible implications. *Chemical Geology,* 255**,** 399-413.

PAL'YANOVA, G. A. & KOLONIN, G. R. 2004. Physicochemical features of the behavior of gold and silver in processes of hydrothermal ore formation. *Doklady Earth Sciences,* 394**,** 100-103.

PAL'YANOVA, G. A., SHVAROV, Y. V., SHIRONOSOVA, G. P. & LAPTEV, Y. V. 2005. Methodological approaches to the assessment of gold fineness during thermodynamic modeling of hydrothermal systems. *Geochemistry International,* 43**,** 1247-1251.

REIMUS, P., POHLL, G., MIHEVC, T., CHAPMAN, J., HAGA, M., LYLES, B., KOSINSKI, S., NISWONGER, R. & SANDERS, P. 2003. Testing and parameterizing a conceptual model for solute transport in a fractured granite using multiple tracers in a forced-gradient test. *Water Resources Research,* 39.

SAMAL, A. R., SENGUPTA, R. R. & FIFAREK, R. H. 2011. Modelling spatial anisotropy of gold concentration data using GIS-based interpolated maps and variogram analysis: Implications for structural control of mineralization. *Journal of Earth System Science,* 120**,** 583-593.

SCOTGOLD RESOURCES LIMITED 2015. Cononish Gold Project Study Update and JORC 2012 Ore Reserve Estimate. ASX Announcements [Online] Available at: http://www.asx.com.au/asx/statistics/displayAnnouncement.do?display=pdf&idsId=01628298 .

SIBSON, R. H., ROBERT, F. & POULSEN, K. H. 1988. High-angle reverse faults, fluid-pressure cycling, and mesothermal gold-quartz deposits. *Geology,* 16**,** 551-555.

SPENCE-JONES, C. 2013. *Metallurgical Investigation of the Ore at the Cononish Gold Mine, Scotland.* MGeol Masters, Univeristy of Leicester.

SPENCE-JONES, C. P., JENKIN, G. R. T., BOYCE, A. J., HILL, N. J. & SANGSTER, C. J. S. 2018. Tellurium, magmatic fluids and orogenic gold: An early magmatic fluid pulse at Cononish gold deposit, Scotland. *Ore Geology Reviews*.

TANNER, P. W. G. 2012. The giant quartz-breccia veins of the Tyndrum-Dalmally area, Grampian Highlands, Scotland: their geometry, origin and relationship to the Cononish gold-silver deposit. *Earth and Environmental Science Transactions of the Royal Society of Edinburgh,* 103**,** 51-76.

TANNER, P. W. G. 2014. Structural controls and origin of gold–silver mineralization in the Grampian Terrane of Scotland and Ireland. *Geological Magazine,* 151**,** 1072-1094.

TOWNLEY, B. K., HÉRAIL, G., MAKSAEV, V., PALACIOS, C., PARSEVAL, P. D., SEPULVEDA, F., ORELLANA, R., RIVAS, P. & ULLOA, C. 2003. Gold grain morphology and composition as an exploration tool: application to gold exploration in covered areas. *Geochemistry: Exploration, Environment, Analysis,* 3**,** 29-38.

WRIGHTON, T. M. 2013. *Placer gold microchemical characterization and shape analysis applied as an exploration tool in western Yukon.* Msc, Univeristy of British Columbia.

Chapter 5 Curraghinalt Detrital-Lode study

Summary

This chapter examines the relationship between the composition of primary gold mineralisation within a multi vein lode gold deposit and the composition of detrital gold particles eroded from it into fluvial deposits. In contrast to the previous study conducted at the Cononish mine it utilises limited observations of, and samples from, the in-situ veins. This replicates how a correlative integration of detrital gold analysis can be used at an earlier stage of exploitation of a gold deposit before mining has begun. Gaining the maximum knowledge of a gold deposit immediately before the development of a mine is a critical and a key priority for economic geologists in industry. This chapter provides a realistic example of undertaking a detrital study during the early stages of exploration with the potential to further the understanding of the deposit in a meaningful way for commercial operators.

The results from the Curraghinalt study indicate that the mineralisation was formed in a single continuous system. The results from two detrital samples indicate that minimal differences exist between different veins within the deposit as the gold signatures of the two samples are identical. This provides important information, and constrains on, the nature of the auriferous mineralisation. The identification that a single stage mineralisation event formed the deposit, instead of two events, was not previously identified despite extensive exploration, mining, and several academic studies on the deposit.

5.1 Introduction

The 3-million-ounce Curraghinalt gold deposit discovered in 1983 near the village of Rousky, Northern Ireland, is comprised of an array of quartz carbonate veins hosted by Dalradian rocks (Leuangthong et al., 2018). The measured and indicated resource is stated as 6,343,000 tons of ore grading 15.01g/t Au and the operator, Dalradian Resources, has begun underground drifting in preparation for mining of the deposit (Leuangthong et al., 2018). The Curraghinalt gold deposit is different to the previously examined Cononish mine as the mineralisation is present in a distributed multi-vein array gold system. This provides an opportunity to investigate how multiple detrital samples, along with a limited sample of vein material, can be used to provide information about a large complex vein system.

Whether different gold compositional signatures are present in different areas of the deposit, specifically between different veins, will be tested by analysing multiple detrital gold samples from the Curraghinalt deposit. In addition, a limited mineralogical investigation restricted to a single vein locality, will be undertaken to interpret the

paragenetic stages and to investigate the relationship between the mineralogy of the deposit and the detrital gold. This limited mineralogical study is designed to simulate how limited mineralogical knowledge, such as might be available in the early stages of exploration, can be used alongside detrital sampling to provide valuable information on the nature of the auriferous mineralising system.

5.1.1 District geology

The geology of the region as described by Mitchell (2004) is divided into two terrains by the northwest dipping Omagh thrust. To the north of the thrust the deposit is hosted by Neoproterozoic Dalradian metasediments of the overturned limb of the Sperrin anticline nappe. These form the hanging wall and have been tectonically thrust over Tyrone Igneous Complex and its basement (Tyrone central inlier) which are exposed south of the Omagh thrust (Mitchell, 2004; Hollis et al., 2014).

The Midland Valley Terrane affinity Tyrone Igneous Complex is separated into a suprasubduction zone (SSZ) ophiolite sequence (ca. 484–479 Ma Tyrone Plutonic Group) and a structurally higher volcanic arc/backarc sequence that is known to host VMS style mineralisation (ca. 475–469 Ma Tyrone Volcanic Group). This was accreted shortly after its formation at 470Ma along with the Tyrone Central Inlier, and is thought to represent a rifted microcontinent of Laurentia (Chew et al., 2008, Hollis et al., 2014).

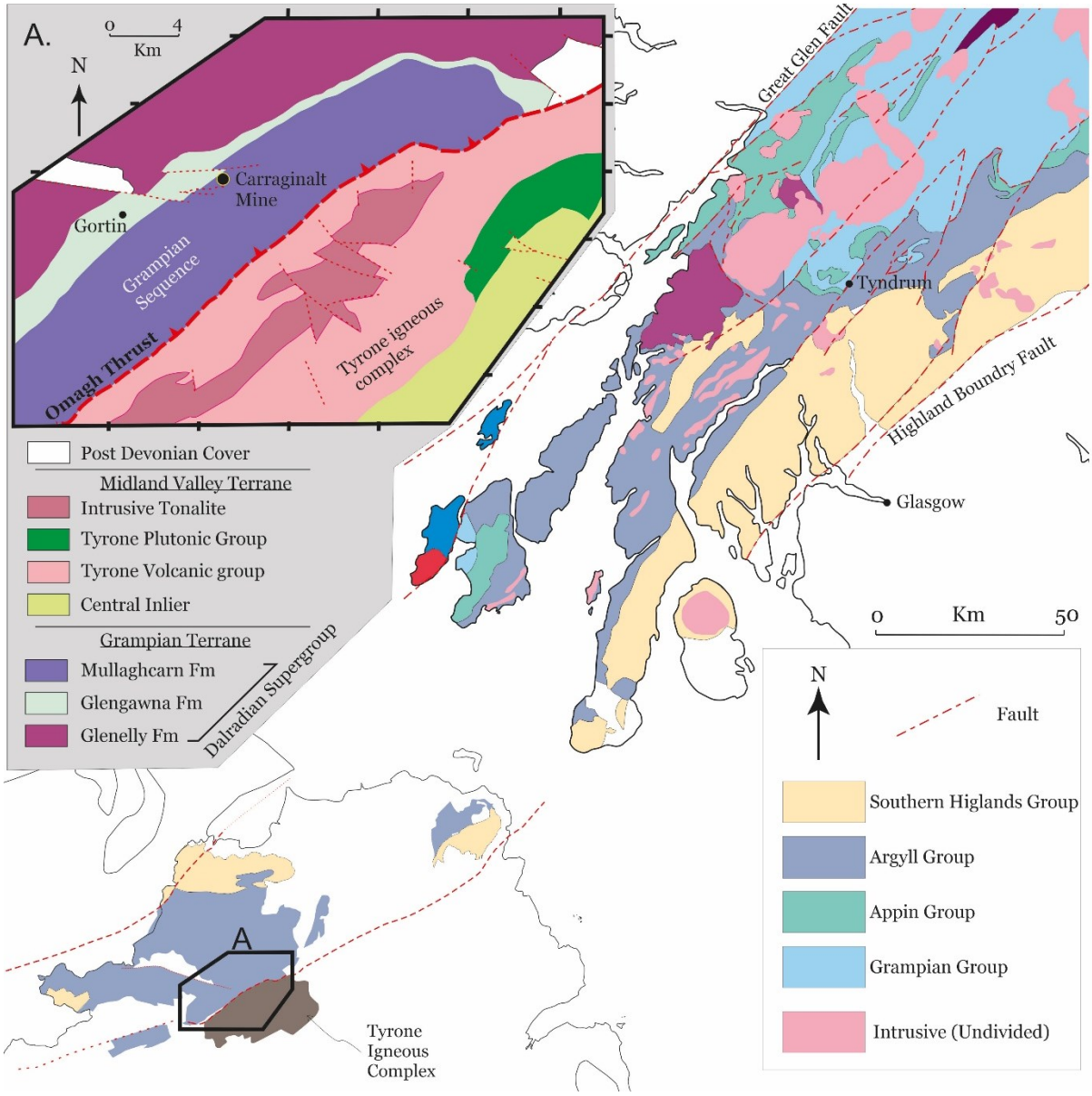

Figure 5.1 – Simplified map of the Grampian Terrane through Scotland and Northern Ireland with an inset showing the local geology around the Curraghinalt mine.

5.1.2 Mineralisation

The deposit has been previously studied by Earls et al. (1989), Wilkinson et al. (1999), Parnell et al. (2000), McCaffrey and Johnston (1996) and Rice et al. (2016) with numerous, publicly available, commercial technical reports (National Instrument 43-101 compliment resource reports). Parnell et al. (2000) has presented a parageneses for the system which has been updated/dated by Rice et al. (2016). Two paragenetic events have been proposed by Rice et al. (2016), Parnell et al. (2000) and Wilkinson et al. (1999) to form the Au Mineralisation. They are an early quartz dominant stage, that appears to have been responsible for introduction of most of the sulphides, and a later quartz + carbonate vein assemblage. These are interpreted as being from two

distinct fluid events which had different fluid sources based on fluid inclusion work of Wilkinson et al. (1999) and Parnell et al. (2000). The most recent 43-101 compliment technical report (Leuangthong et al., 2018) defines the resource of the deposit (see table 5.1) as comprising 21 west-northwest trending sup parallel stacked auriferous quartz-carbonate- sulphide veins.

Table 5.1 – Mineral resource statement for Curraghinalt gold project from Leuangthong et al. (2018)

Resource Category	**Tonnage ('000 t)**	**Grade Au (g/t)**	**Au Metal ('000 oz)**
Measured (M)	34	26.00	28
Indicated (I)	6,309	14.95	3,033
M + I	6,343	15.01	3,061
Inferred	7,722	12.24	3,038

The technical reports on the deposit describe the resource veins as belonging to two structural styles as proposed by Maunula et al. (2014). The two styles are:

- Shear (D) veins – west-northwest trending, steeply dipping, subparallel stacked veins
- Extensional (C) veinlets – arrays of narrow (10's cm thick) steeply dipping extension veins (tension gashes) which are oriented obliquely to the D veins.

All the resource veins are of the D (shear) vein type and are hosted in west-northwesterly trending shear zones which dip 55 to 75 degrees to the northwest and are continuous along the strike. D veins are often laminated, and are typically brecciated veins commonly containing carbonate phases, figure 5.2 (Leuangthong et al., 2018).

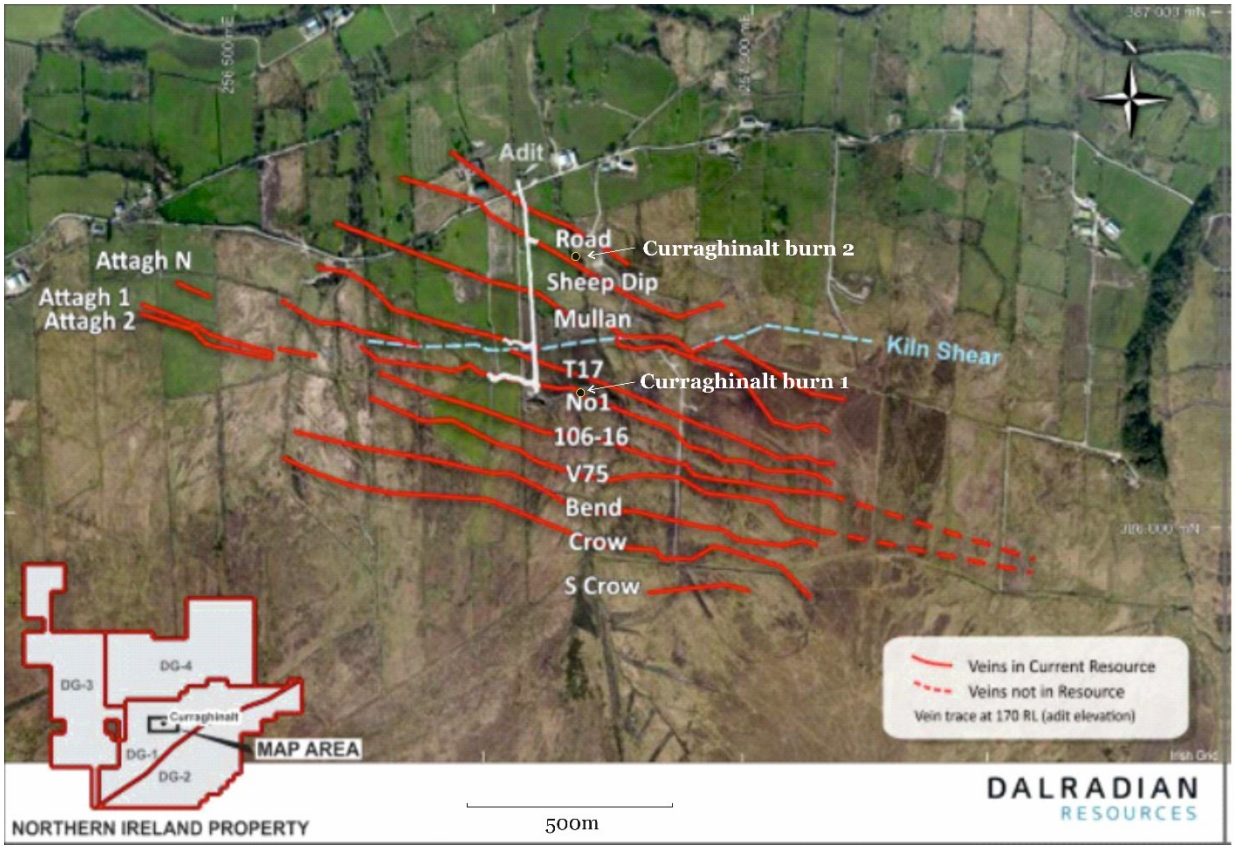

Figure 5.2 – Arial photograph of the Curraghinalt deposit showing the location of the Veins at the level of the adit and the two detrital sample locations (shown in white). Taken from Maunula et al. (2014).

Minor Auriferous quartz veins are reported to also exist between the main modelled veins in the system but have not been included in the deposit resource calculations at present. The 16 individual resource veins have been observed from the surface to depths of 1200m and are up to 3 meters thick, with an average thickness of 0.73m (Couture et al., 2016). Academic studies of the veins have been focused on the main (D) veins, specifically a limited number of veins discovered early in the development of the deposit.

5.2 Methods

In situ samples from the underground workings and detrital gold particles samples used in this work come from field work undertaken at Curraghinalt Mine during the research project. The location of all the samples is shown in tables 5.2 and 5.3. Petrographic sections, both polished block and polished thin sections, were prepared from hand specimens using the facilities at the University of Leeds. Samples were cut to size using diamond lapidary saws and grinding was achieved using Buehler Motopol rotating grinding wheels with 40µm and 10µm diamond-impregnated disks. The 30µm thicknesses of the polished sections was achieved by hand lapping and optical estimation using the birefringence of quartz. Final polishing was performed using the Buehler Automat 250 polishing system with sequentially finer diamond paste and the final finish achieved using 0.5µm diamond suspension or Gamma alumina as needed.

Detrital gold sampling was conducted using sluicing and hand panning methods. Gold particles were examined visually using a binocular microscope and mounted on double sided tape in rows of 5 particles prior to encapsulation in resin blocks. Photographs were taken of selected particles as a reference of the sample and to identify any morphological sub-types. Gold particles of similar size were mounted together on a single block such that the depth of polish exposes the approximate centre of all the particles on the block.

All gold particles were examined by scanning electron microscope, at the University of Leeds, to identify individual mineral inclusions. Once identified the mineralogy was established using the energy dispersive spectroscopy instrument. This study focused on the identification of opaque ‘ore’ mineral inclusions within the gold, typically 2-50 µm in size, as these are used to differentiate between gold deposit styles (Chapman and Mortensen, 2006).

Scanning electron microscopy was conducted using a TESCAN VEGA3 XM (Tungsten source) SEM, equipped with X-max 150 SDD EDS and Aztec 3.3 software and fitted with a TESCAN RGB filtered CL imaging system at the Leeds Electron Microscopy and Spectroscopy Centre (LEMAS) facility. Alloy compositions were determined using EPMA analysis carried out at the University of Leeds on a JEOL JXA8230 EPMA with tungsten source. Analyses were run with an accelerating voltage of 20 kV, beam current of 50 nA and on and off-peak count times of 30s and 15s seconds respectively.

Table 5.2 – Detrital gold samples localities.

Sample ID	Grid Reference	No. of gold particles
Curraghinalt Burn 1	NV 70877 48017	304
Curraghinalt Burn 2	NV 70869 48511	396

Table 5.3 –Location of underground samples used in this study and details of sections made from each location.

Vein Name	Sample number	Location UG ref	Sampled on	X	Y	Z
V75	CSJ_CN_001	End of drift, current blasted face V75 151 south level (left on face)	06/07/2016	257031.80	386153.93	156
V75	CSJ_CN_002	End of drift, current blasted face V75 151 south level (right on face)	06/07/2016	257032.76	386155.29	156
V75	CSJ_CN_003	5.4m east of D92	06/07/2016	257070.14	386131.75	154.97
V75	CSJ_CN_004	8.4m west of D91	06/07/2016	257076.40	386131.08	154.44
V75	CSJ_CN_005	at D90	06/07/2016	257090.36	386125.18	153.87
V75	CSJ_CN_006	V75 170 East level left rib (16m east of D77)	06/07/2016	257110.57	386099.67	173.16
V75	CSJ_CN_007	22m east of D77 lower vein of two, taken bellow crosscuting low angle shear	06/07/2016	257115.81	386096.32	173.16
V75	CSJ_CN_008	V75 Vuggy vein on southen corner of drift /adit intersection.	06/07/2016	257075.93	386119.96	174
106-16	CSJ_CN_009	10.3m east of D66	06/07/2016	257078.76	386193.42	172.81
No. 1	CSJ_CN_010	6.9m West of D72	06/07/2016	257188.64	386239.50	172.76
T17	CSJ_CN_011	T17 vein exposed in north rib of adit aproximatly 10m east of D30	06/07/2016	257020.31	386357.38	170
V75	Photos 110-0044 to 0056	Photos of vein textures in roof at site D93	06/07/2016	257055.56	386139.13	157
Sample site ID	Leeds Sample ID	Number of Standard sections	Number of large format sections	Number of polished blocks		Vein
CSJ_CN_02	67302	1	1			V75
CSJ_CN_03	67303	1				V75
CSJ_CN_04	67304	1	1			V75
CSJ_CN_05	67305	2				V75
CSJ_CN_06	67306	1				V75
CSJ_CN_07	67307	1	1			V75
CSJ_CN_08	67308	1		3		V75
CSJ_CN_10	67309		1			No. 1
CSJ_CN_11	67310	1	1			T17

5.3 Results

5.3.1 Underground vein observations

The resource veins exposed in the underground openings are of variable width and are seen to display a range of textures. The veins examined and sampled (V75, 106-16, No. 1 and T17) are predominantly comprised of quartz-carbonate with highly variable proportions of sulphides, principally pyrite, chalcopyrite and galena. Texturally these veins show laminated textures, comprised of multiple subparallel, mm to 10's cm wide, veinlets, figures 5.3 and 5.4. All the veins observed have evidence of evolving compositions with increasing carbonate observed later in the veinlet sequence in all the veins, evidenced by crosscutting relationships. There is variable brecciation of early phases to produce angular clasts within the laminated vein array occasionally observed to have occurred over multiple generations of mineralisation, figures 5.3 and 5.4.

Subtle differences in the mineralogy, and textures were observed between the different veins most markedly the proportions of carbonate and sulphides in the different veins. For example, the T-17 vein was observed to have minor carbonate in strong contrast to the v75, no1 and 106-16 veins in which pinkish carbonates are abundant. Within individual veins the early and late mineralisation is visually distinct due to different mineralogy. Generally, the early vein material is composed of quartz and sulphides, whereas late veins typically are rich in pinkish brown carbonate cross cutting the earlier quartz veinlets. The late carbonate – quartz veinlets have intergrown textures in places, with euhedral quartz crystals mantled by pink carbonate fill and can be observed crosscutting each other in complex multiple generations of vein opening. This gives a white/pink mottled macroscopic appearance to the vein. In other areas in the late veins the carbonate is massive and they contain little quartz or sulphide mineralisation.

Sulphides are observed within quartz and rarely within the carbonate in the veins. Pyrite is observed as the predominant sulphide and along with chalcopyrite accounts for most of the sulphides. Galena was observed in the T17 and No1 veins but was not observed in the V75 samples. This difference in the veins indicates that the mineralisation is spatially variable on a deposit scale (differing between separate

veins), and potentially also within individual veins. See Figures 5.3 & 5.4 for photographs of the underground exposure of several of these resource veins.

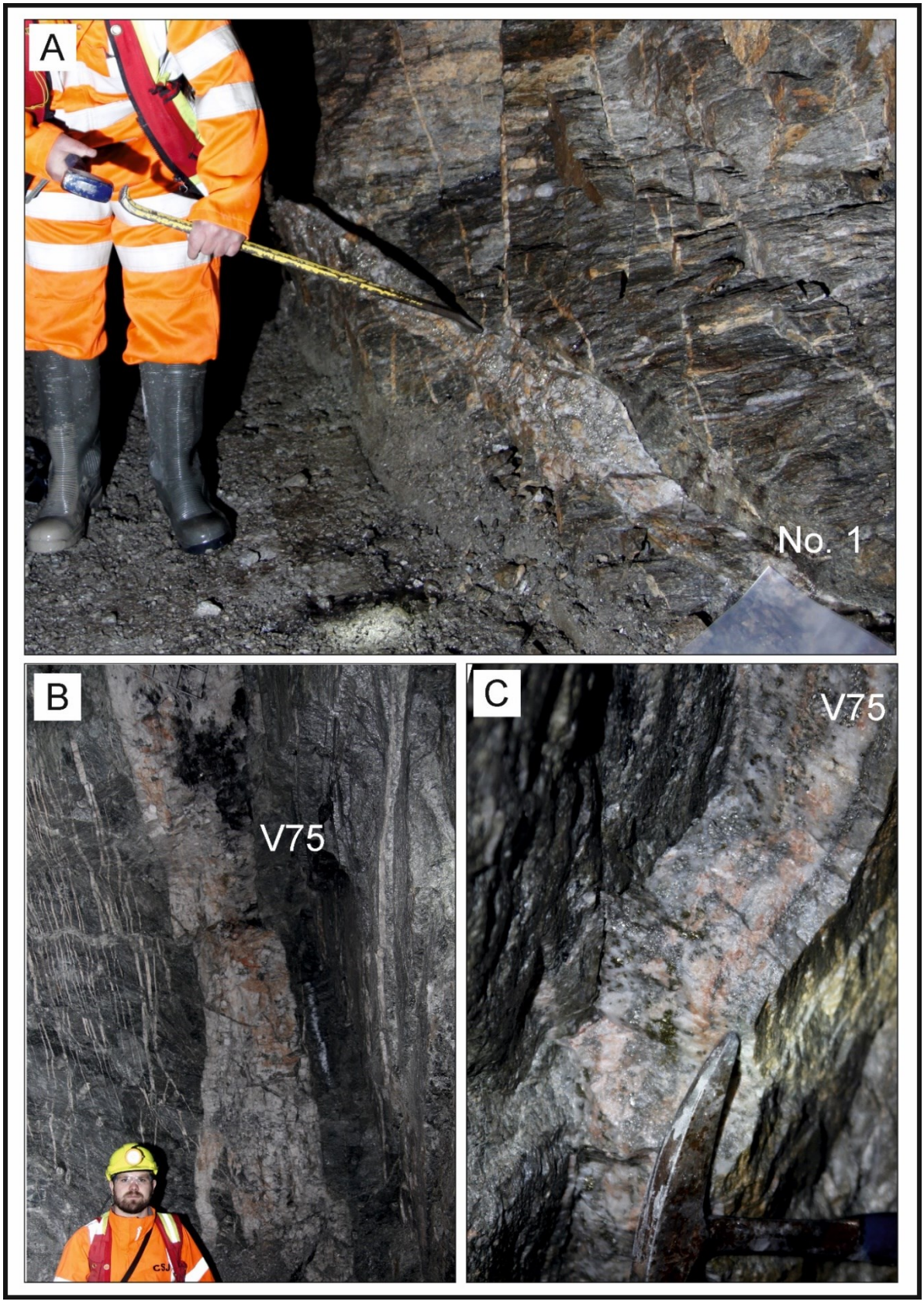

Figure 5.3 – Photographs of the underground exposure of two of the resource veins. Locations are at the following sample sites A) CSJ_CN_010, B) CSJ_CN_002, C) CSJ_CN_006.

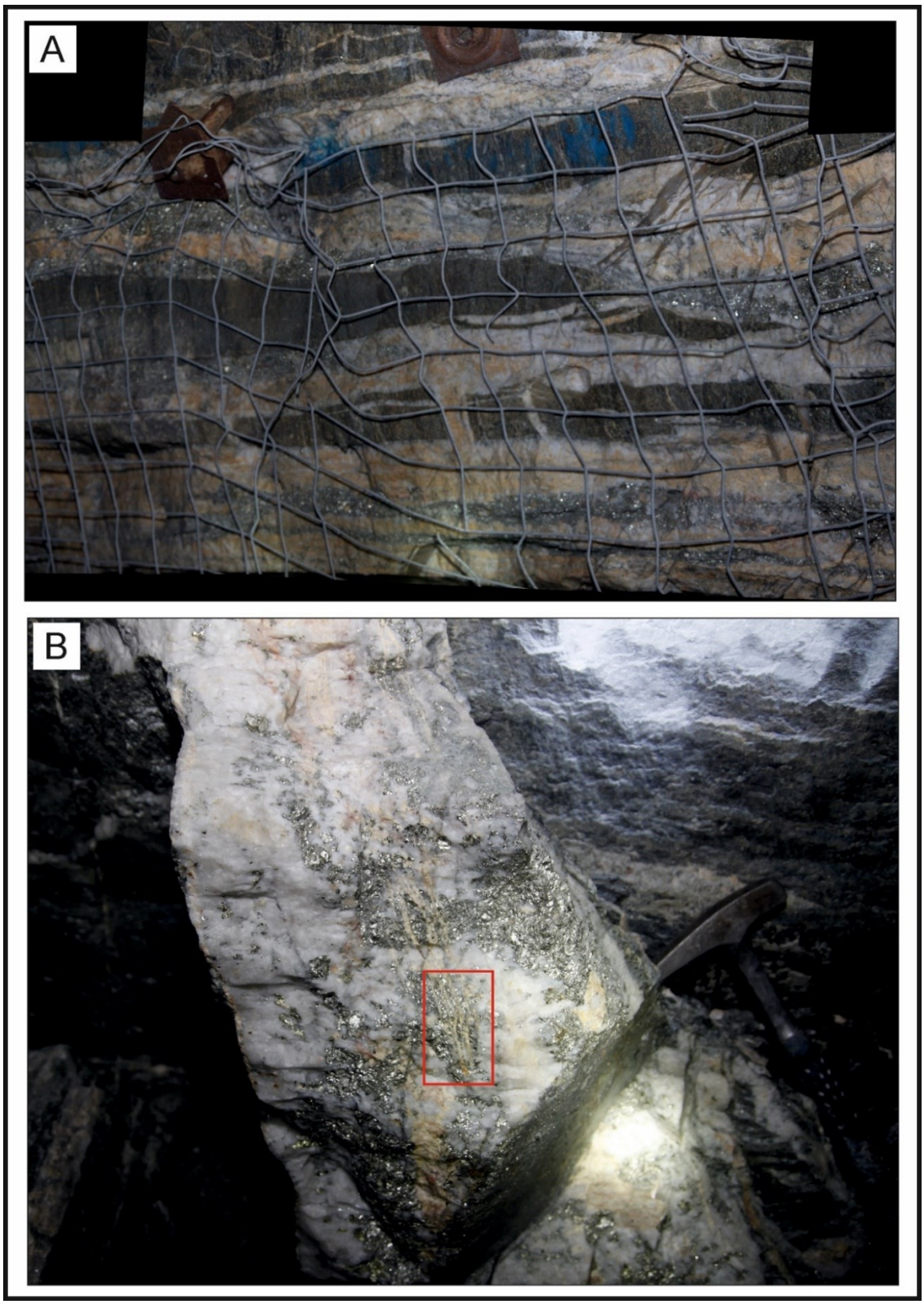

Figure 5.4 – Photographs of the underground exposure of the V75 vein at in the back at site D93 (A) and at sample site CSJ_CN_004 (B). Red box shows approximate location of large format thin section 67304 in photo B. For scale in photo A the rock mesh has a 10cm grid spacing.

5.3.1.1 V75 Vein petrography

The V75 vein is the main vein examined in detail for this study as the driving of drifts for test stoping was ongoing at the time of sampling allowing easy access. The extension of drifts of the V75 vein allowed examination along a significant length of the strike of the vein, and at fresh heading faces it was possible to gain an overall impression of the macroscopic features.

The main resource vein is between 0.75 to 1 m wide and is comprised of an array of anastomosing sub parallel veinlets. However, additional subparallel veins are common in the hanging and footwall alongside the thickest 'main' vein making a complex array of sub parallel mineralisation. The vein has a mottled appearance with patches and bands of a pinkish carbonate in highly variable proportions within it, along with up to 15% sulphides (pyrite and chalcopyrite). The sulphides are principally hosted in the quartz rich generations/ bands within the structure with minor sulphides observed within massive carbonate sections.

Thin sections of the vein examined using cathode luminescence (CL) reveal a complex multigenerational structure within the vein which has been interpreted into a paragenesis to represent the evolution of the mineralogy, figure 5.5. Two distinct vein depositional events are proposed which have differing textural expression in the samples. These have been further are split into subevents to represent early vs late expressions of the continually evolving sequence of the two individual events. The first event is early vein development (stages S1 and S2) consisting of a multigenerational progressive formation of fractured and brecciated euhedral comb quartz and sulphides. The second event consists of a brittle vein development (stages S3 and S4) which fractures earlier stages. The fractures are comprised of high luminescence euhedral, banded comb quartz (S3) associated with and superseded by low luminescence Ca-Mg-Fe Carbonate veinlets (S4), see figures 5.3, 5.6 and 5.7.

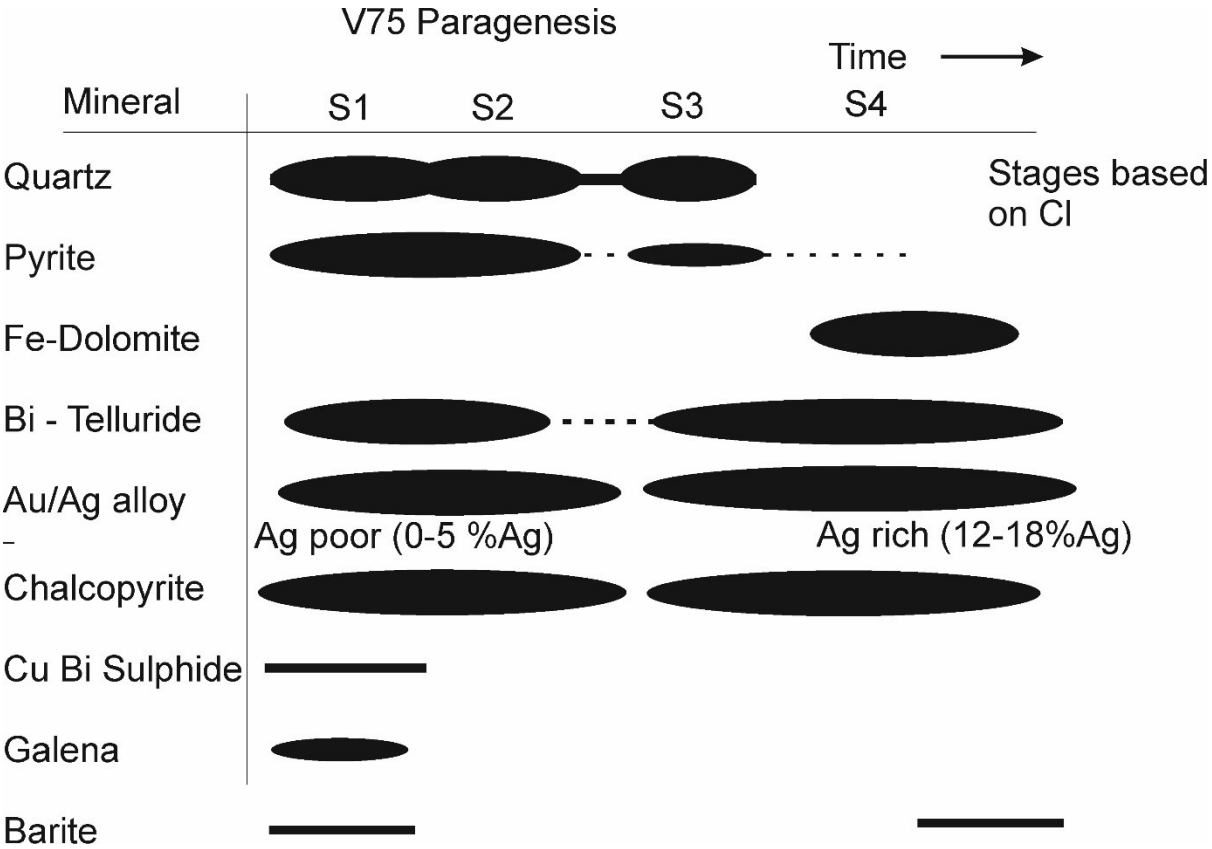

Figure 5.5 – Paragenesis of the V75 Vein obtained from one large format and one standard format thin sections (sample CSJ_CN_004). Stage assemblage relationships were principally determined by CL cross cutting relationships.

Interpreted paragenetic stages

Stage 1

Early quartz - observed to have euhedral growth banding obfuscated by heavy dark fractures giving it a generally dark intensity. In places it is observed to form angular clasts of later vein brecciated development, see figure 5.6.

Stage 2

Early quartz -observed to have euhedral growth banding clearly seen, with only minor obfuscation of the growth textures by dark fractures. It has a much lighter general intensity than stage 1 due to the lower proportion of fractures. This stage forms most of the vein.

Stage 3

Bright intensity growth banded quartz - observed to be found in veinlets which crosscut the early generations with sharp distinct contacts. Growth banding in some parts is distinct, being parallel to the veinlet margin, with growth occurring from the margin

towards the centre of the veinlet. This quartz is principally seen on the margins of the late carbonates, infilling the centre of the late veinlets. It is also seen in veinlets sub parallel to the late carbonate which are composed only of quartz, and in several very small minor veinlets which are crosscut by the late carbonate, as shown in figures 5.6, 5.7 and 5.8.

Stage 4

Non-luminescent Ca-Mg-Fe Carbonates - these infill the centre of the late veinlets and crosscut the stage 3 quartz.

The four stages identified from the CL are the framework from which the paragenesis was interpreted, figures 5.3 and 5.6. Gold mineralisation is associated with sulphides in both the first-generation vein structures (S1/S2) and in the later brittle quartz-carbonate veinlets. In both cases gold alloy is associated with pyrite and minor Bi-tellurides, barite and chalcopyrite. Despite the overall similarities between the two auriferous assemblages they differ, due to the presence of minor galena in the early auriferous assemblage which is absent in the later veinlets.

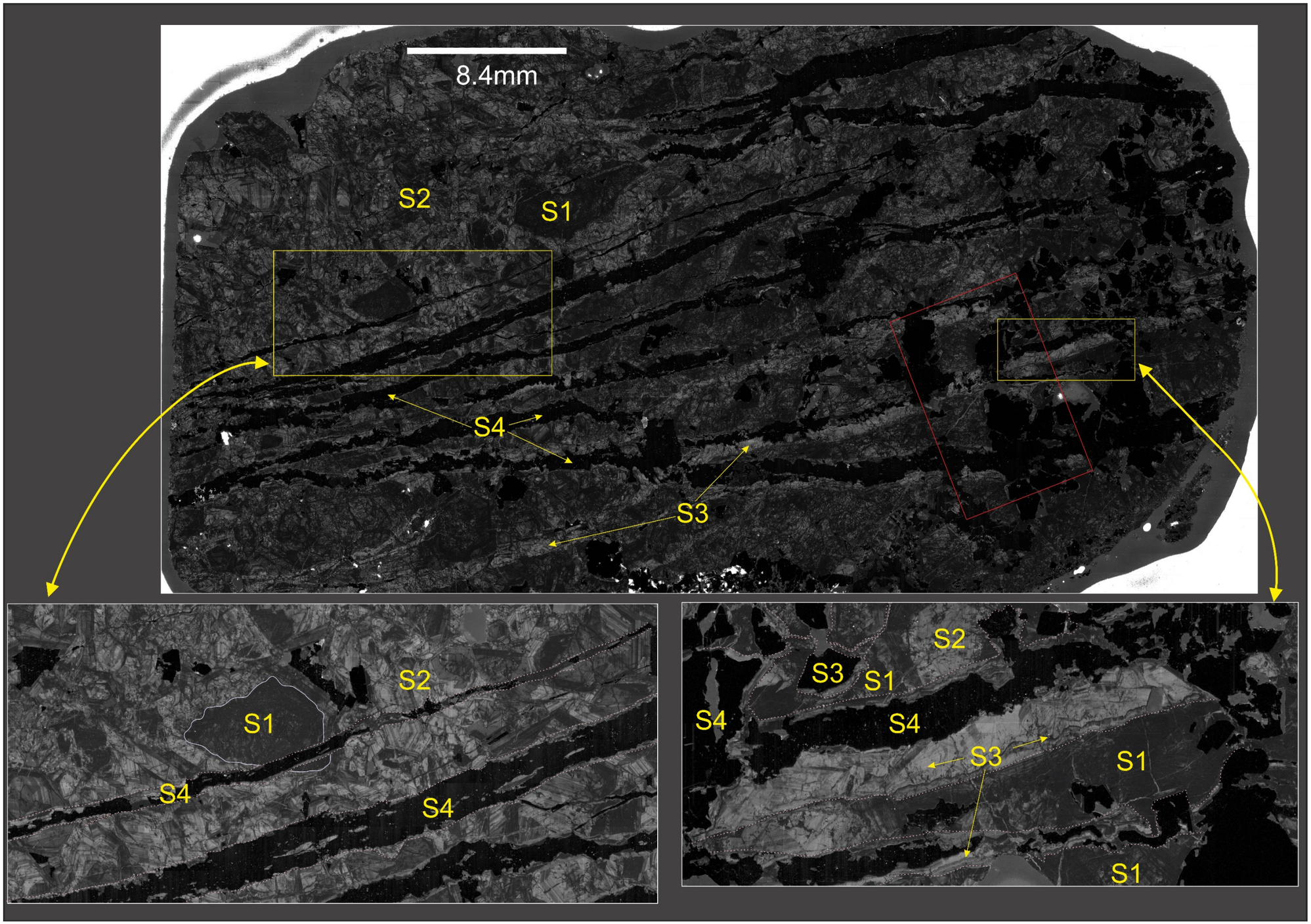

Figure 5.6 – A composite CL image (blue channel) of the whole V75 large thin section annotated to show examples of the 4 CL stages (S1-4) interpreted in the sample. Insets (bottom) show areas where the nature of, and relationship between, the 4 stages can be best observed. The location of the sampled material from which the thin section was cut is shown in figure 5.4(C).

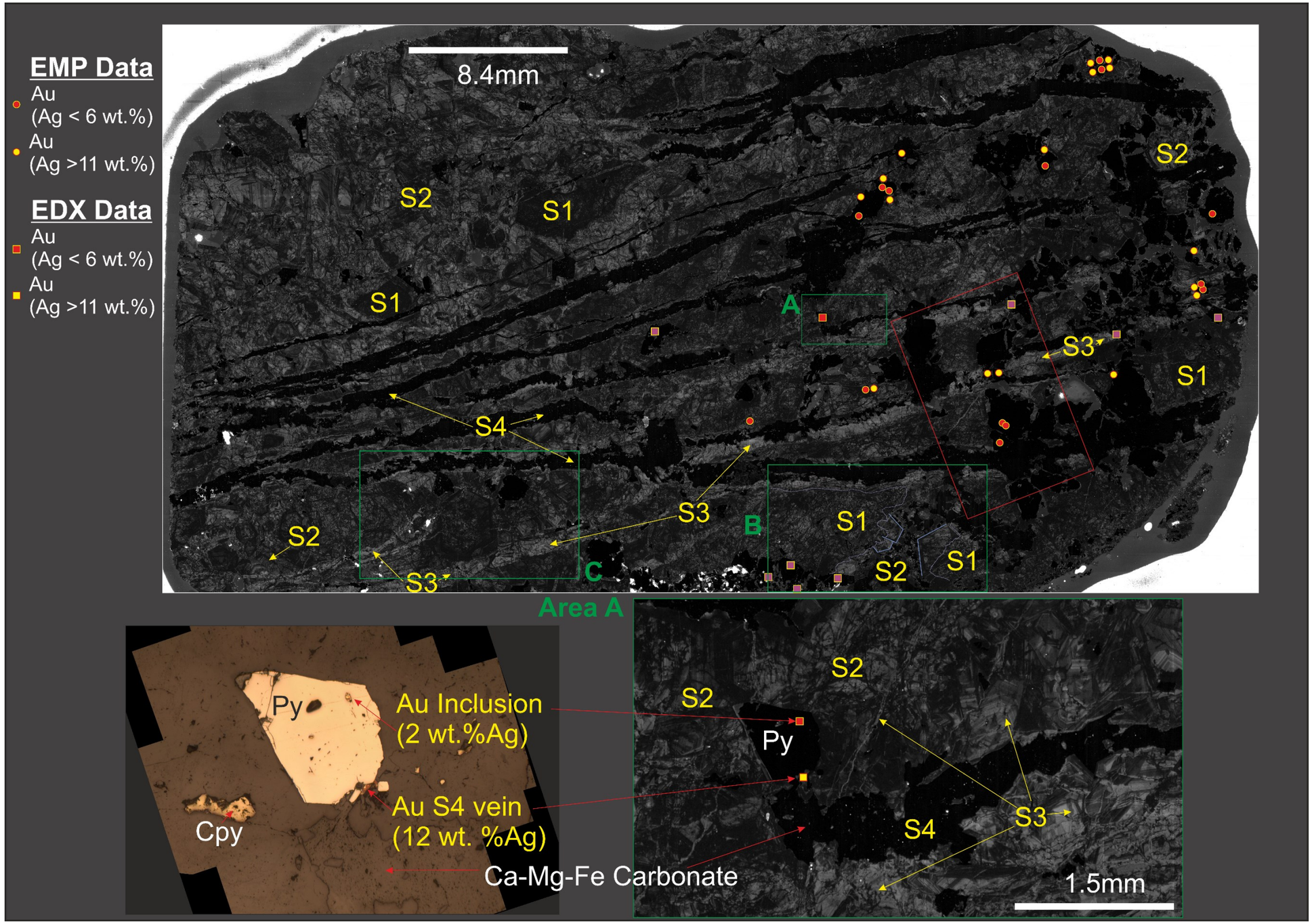

Figure 5.7 –A composite CL image of the whole V75 large thin section annotated to show the location of gold particles associated with the two distinct gold mineralisation events interpreted in the sample. Colours of the gold locational dots indicate their composition. The Insets at the bottom show a detailed view of the green box area A where the nature of, and relationship between, the 2 gold events stages are in close proximity. Sub areas B and C, are shown in more detail in figure 5.8.

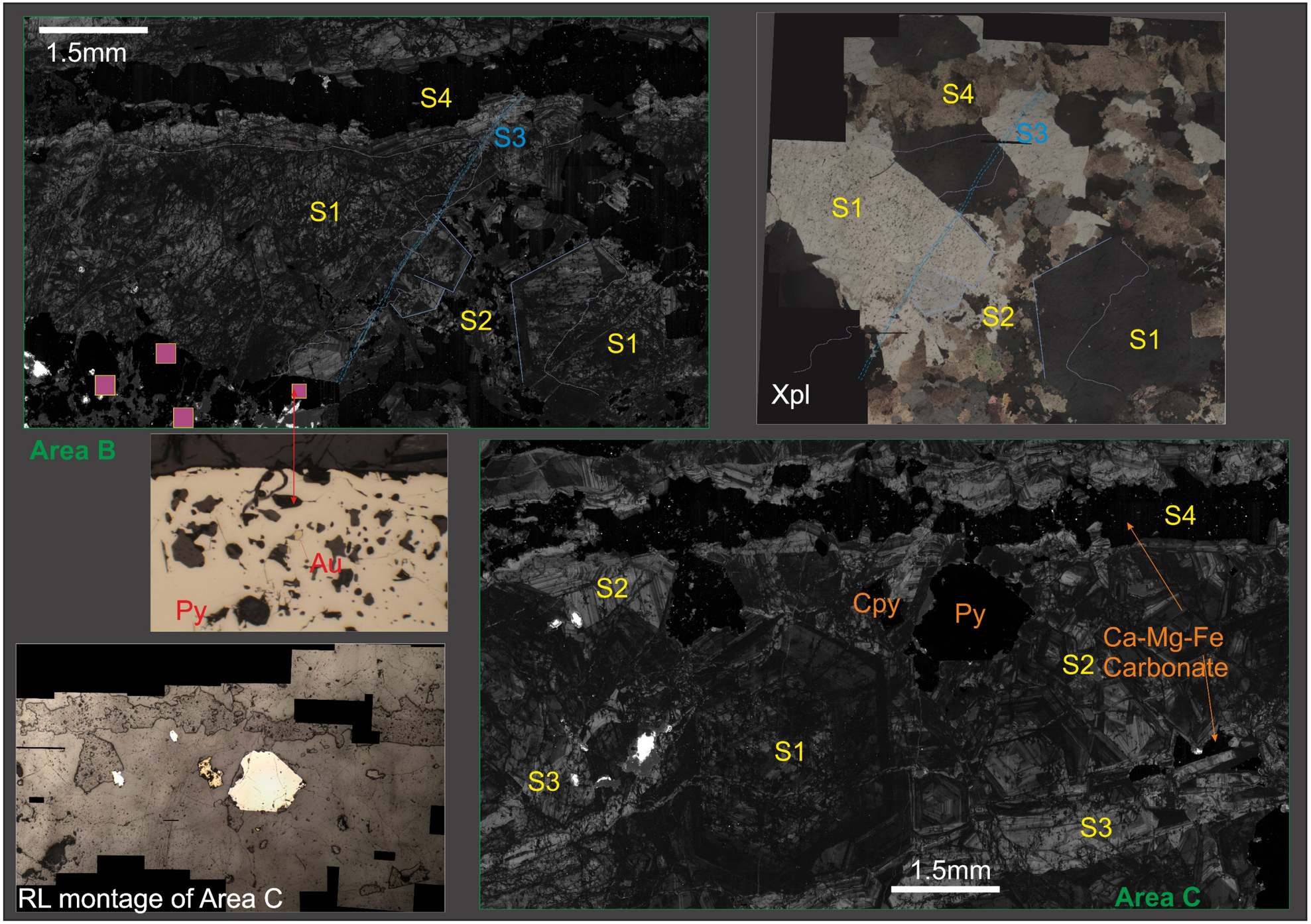

Figure 5.8 – Two detailed sections of Sub areas B and C shown on the composite CL image (figure 5.7). They are annotated to show details of the two distinct gold mineralisation events interpreted in the sample where the nature of, and relationship between, the 2 gold events stages are observed.

The two generations of auriferous assemblages are geochemically distinct. Electron-microprobe-Analysis (EMPA) of the gold alloy shows two distinct compositional populations which do not overlap, figure 5.9. Early gold alloy contained between 3.5 and 5.2 % Ag wt. whereas later gold alloy contained between 11.7 and 17.6 % Ag wt., see figures 5.7 and 5.9. This demonstrates that distinct geochemical conditions formed the two stages of gold mineralisation with no apparent overlap present. This observation of an apparent two stage mineralisation history is in agreement with published accounts of the mineralisation by Parnell et al. (2000) who also described two distinct gold associations.

The position of the gold particles analysed and categorised by silver composition, is shown on the CL images in figure 5.7. There is a strong relationship between the generation of quartz, identified using Cl and the alloy composition of gold particles. The gold particles which are found as inclusions in S1 and S2 quartz and sulphides are consistently low silver (3.5 – 5.2 % Ag wt) whereas the higher silver gold is associated with S3 and S4 veinlets and fractures. In particular the gold in these later stages is observed to be concentrated in areas where S3/4 structures are in contact with earlier sulphides, predominantly pyrite. Examples are shown in figure 5.7 (area A), where both early and late gold of separate compositions are observed in close proximity.

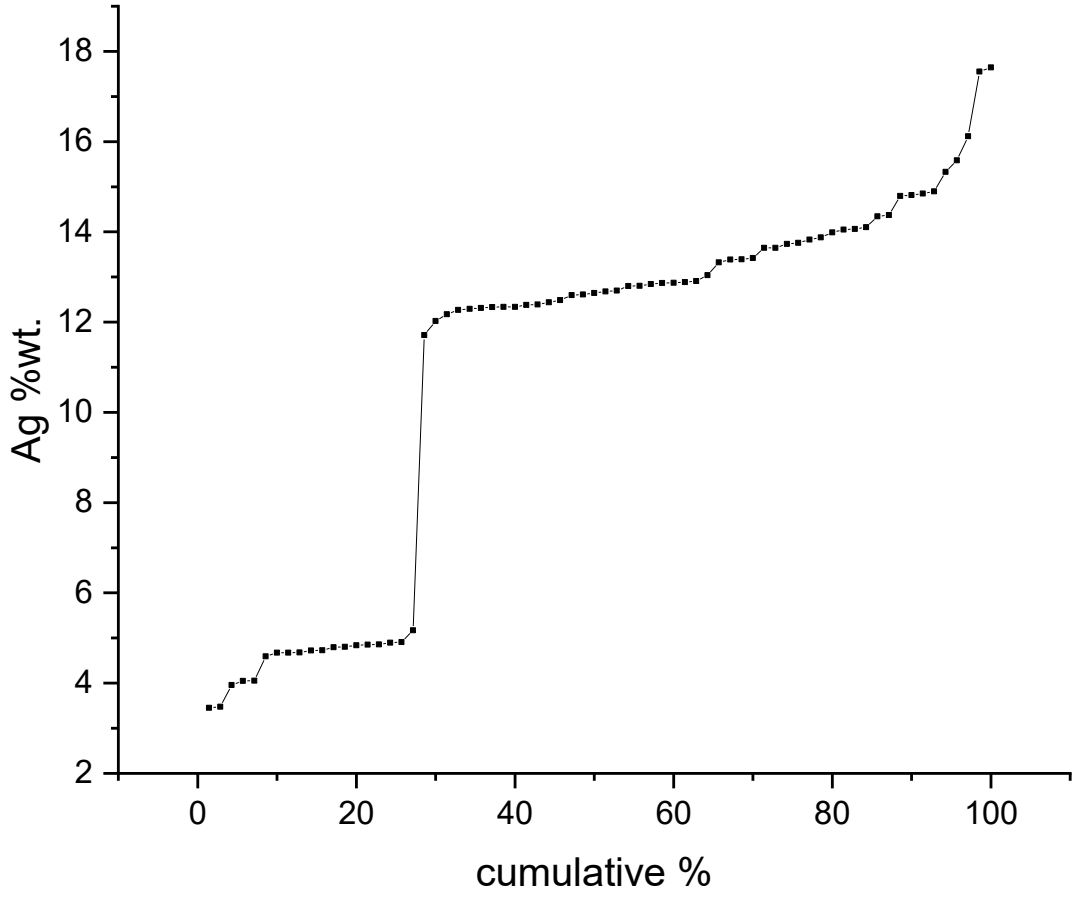

Figure 5.9 – Cumulative frequency plot of EMPA gold alloy silver data from thin section 67304 (n.70). Data shows a clear bimodal distribution and is also plotted as a histogram in figure 5.10.

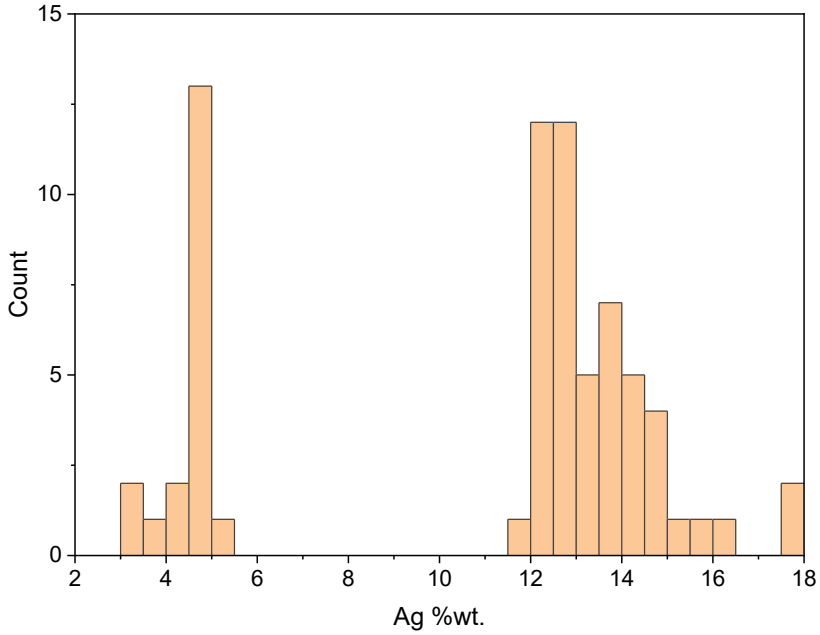

Figure 5.10 – Histogram plot of EMPA gold alloy silver data from thin section 67304 (n.70).

5.3.2 Detrital Gold Results

5.3.2.1 Physical properties of the gold

A total of 304 gold particles were collected at the Curraghinalt Burn 1 site and 396 gold particles from the Burn 2 site. The morphology of the detrital gold particles in the two samples collected from Curraghinalt stream varies from irregular to rounded in shape with some flattened morphologies, figure 5.11. There are no morphological differences apparent between the two samples. The particle size was up to 2mm with no relationship observed between size and morphology. The rough surface texture of the particles along with their shape suggests minimal impacts during a short transport in the fluvial environment.

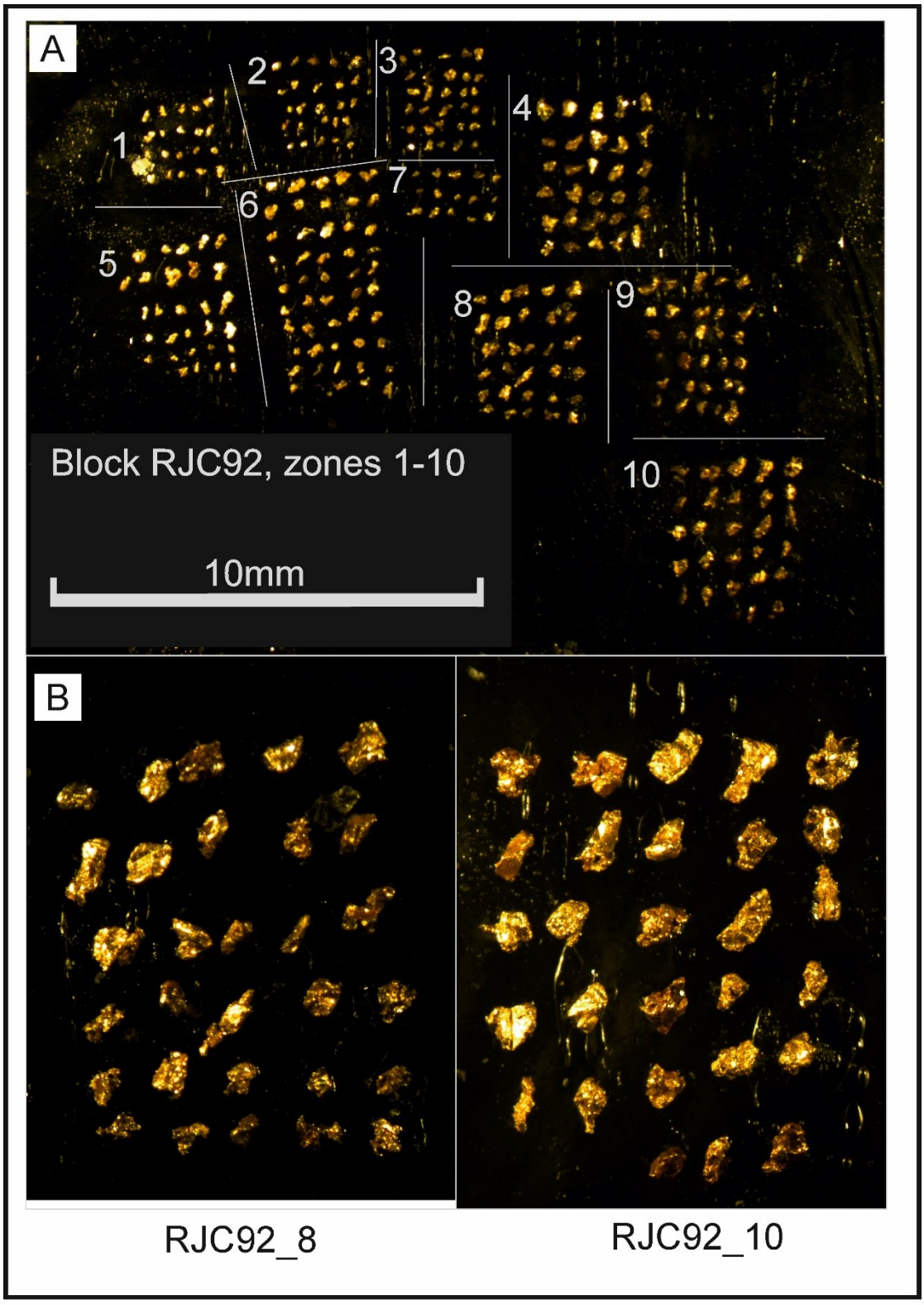

Figure 5.11 – Binocular light microscope images of detrital gold particles mounted before encapsulation in resin for polishing. It shows a selection of gold particles from Curraghinalt Burn 2 showing the irregular rounded forms observed in most gold particles.

5.3.2.2 Composition of the detrital gold particles

The results of electron microprobe analysis (EMPA) of detrital gold particles in the 2 samples are shown in figures 5.12 and 5.13. The plotted distributions (silver content of the alloys) in figure 5.12 show identical distributions and the results of a K-S test confirms that the two distributions are statistically compatible with being subsampled from a single master distribution. As such the two samples can be considered as being sub-sampled from a single master population.

The detrital gold samples show a single alloy distributional curve, figure 5.12, with no evidence of bimodality in the compositions of gold particles or systematic relationship between gold particle size and alloy composition, figure 5.13. No correlation between alloy composition and specific mineral species is present. All the inclusion species observed occurred in gold particles through the complete compositional range as is shown in figure 5.13, where groups of gold particles containing specific inclusions are plotted together and compared against the overall population by silver proportion of the alloy.

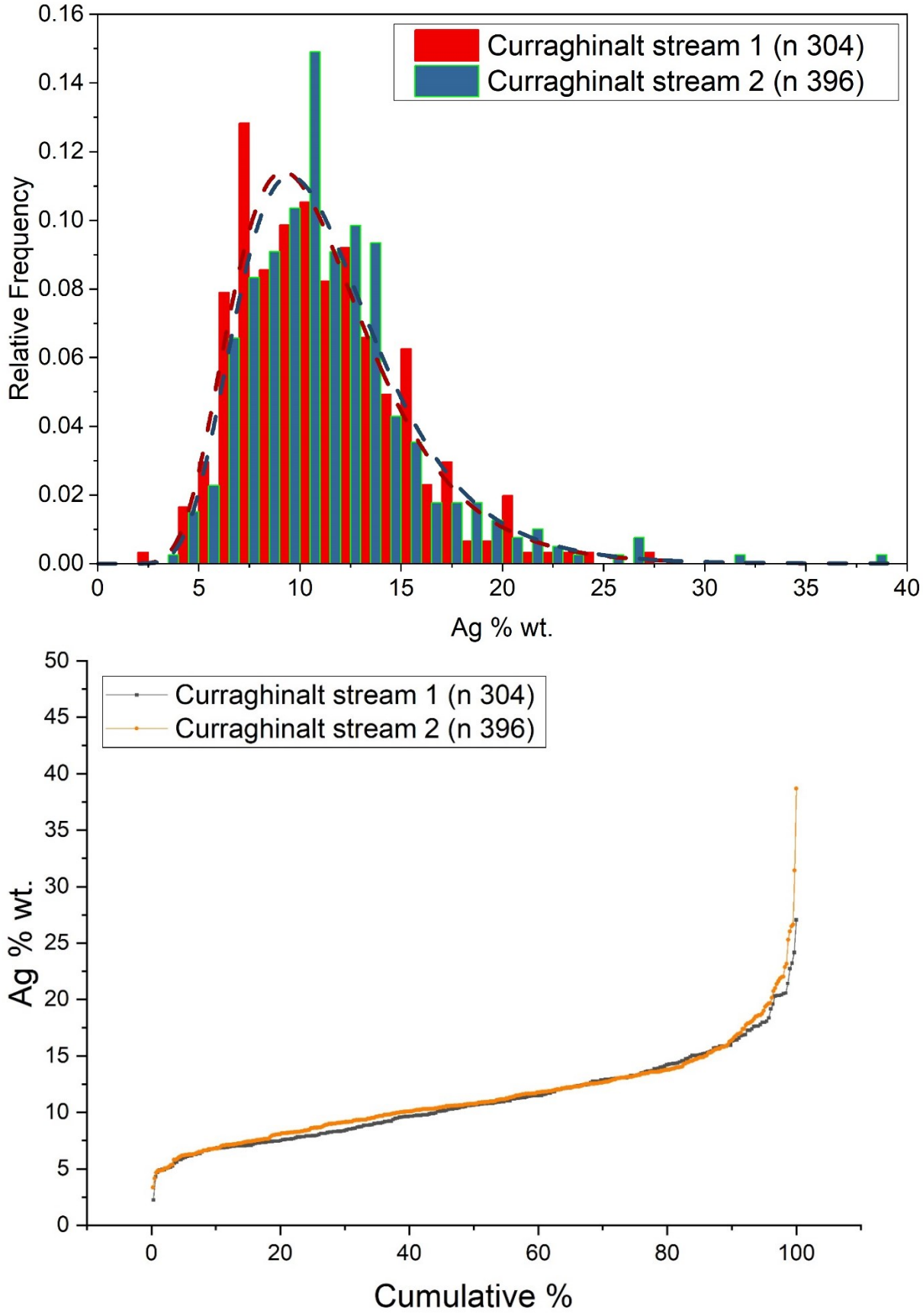

Figure 5.12 – The alloy compositions of the two detrital gold samples from Curraghinalt.

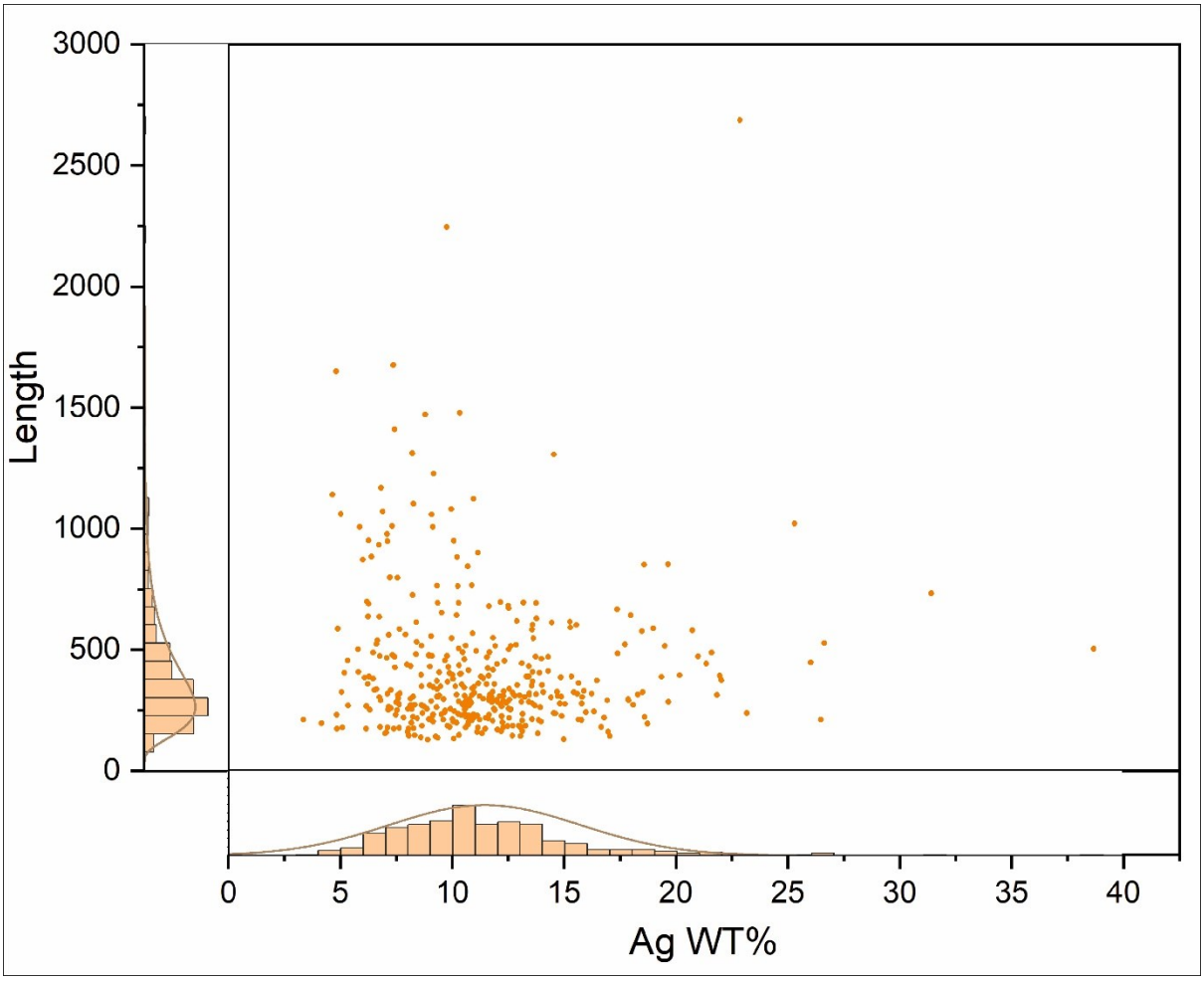

Figure 5.13 – Plot of alloy composition vs length (μm) of the gold particles. The reported length is the longest dimension in the polished section through the gold particle.

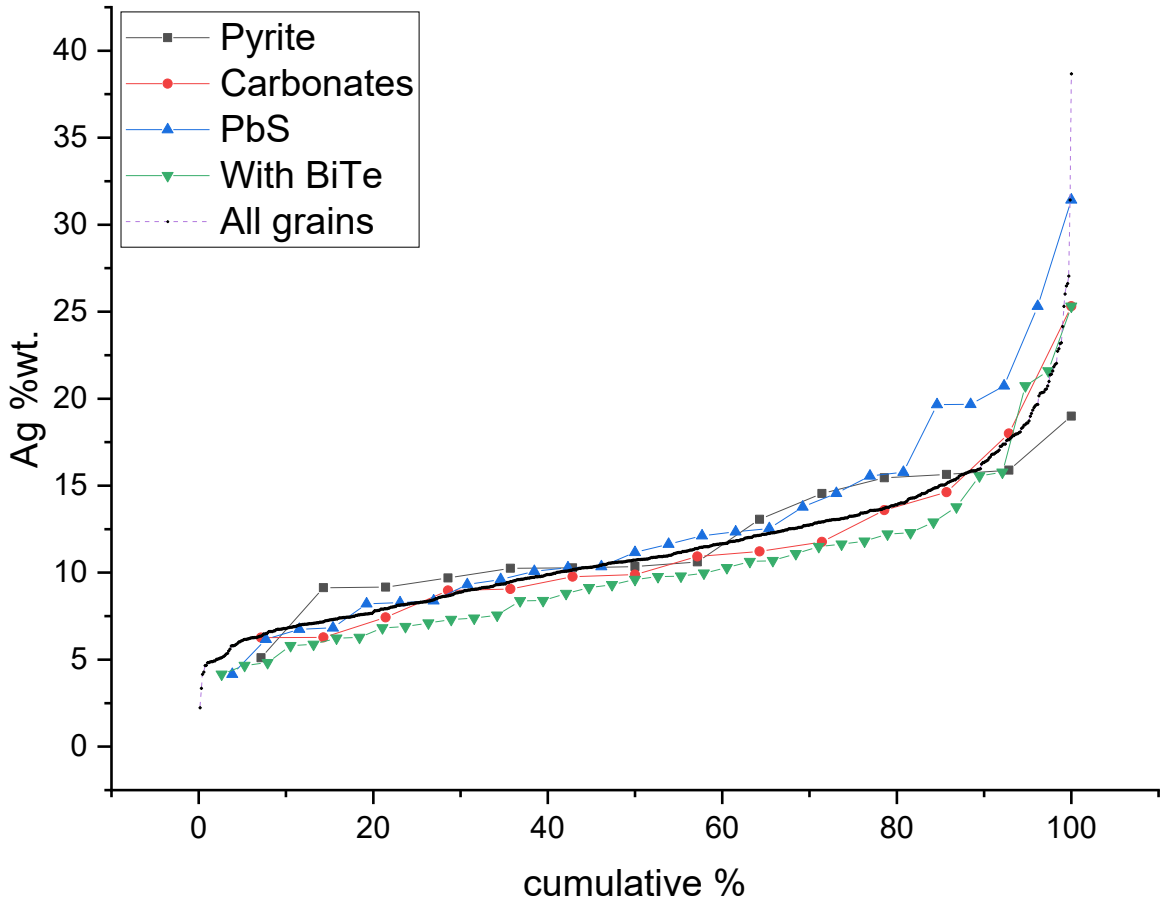

Figure 5.14 – Plot of populations of gold particles containing specific mineral inclusions compared against the overall distribution of particles in the detrital samples.

The detrital gold population analysis reveals that gold particles containing silver between 7 and 13 %wt. form most of the gold. This constrained range of gold alloy composition is considered to be the principal 'window' of physiochemical conditions that produced the Curraghinalt deposit when considering the nature of the auriferous mineralising system at Curraghinalt. A distributional fit test conducted on the largest sample (Curraghinalt Burn sample 2; n. 396) using the OriginPro statistical software indicates that a Lognormal distribution best fits the empirical distribution, see Table 5.4 and Figure 5.15.

Table 5.4 – Distributional fit test using 3 different comparison methods between 4 reference distributions and the empirical alloy data (Ag) from Curraghinalt Burn sample 2. Conducted using the standard tools as part of the OroginPro software. K-S is the Kolmogorov-Smirnov, K-S modified is the Kolmogorov-Smirnov-Lilliefors test and A-D is the Anderson-Darling test for normality.

Distribution	Goodness of Fit tests	Statistics	P-value	Decision at level(5%)
Normal	K-S test	0.0944	0.00166	Reject Normal
	K-S modified test	0.0944	<=0.01	Reject Normal
	A-D test	6.73559	1.58E-16	Reject Normal
Lognormal	K-S test	0.04441	0.41626	Can't reject Lognormal
	K-S modified test	0.04441	0.0565	Can't reject Lognormal
	A-D test	0.69644	0.06851	Can't reject Lognormal
Weibull	K-S modified test	0.10005	<=0.01	Reject Weibull
	A-D test	7.73701	<0.01	Reject Weibull
Gamma	K-S test	0.06635	0.06016	Can't reject Gamma
	K-S modified test	0.05627	0.00578	Reject Gamma
	A-D test	1.28382	<0.005	Reject Gamma

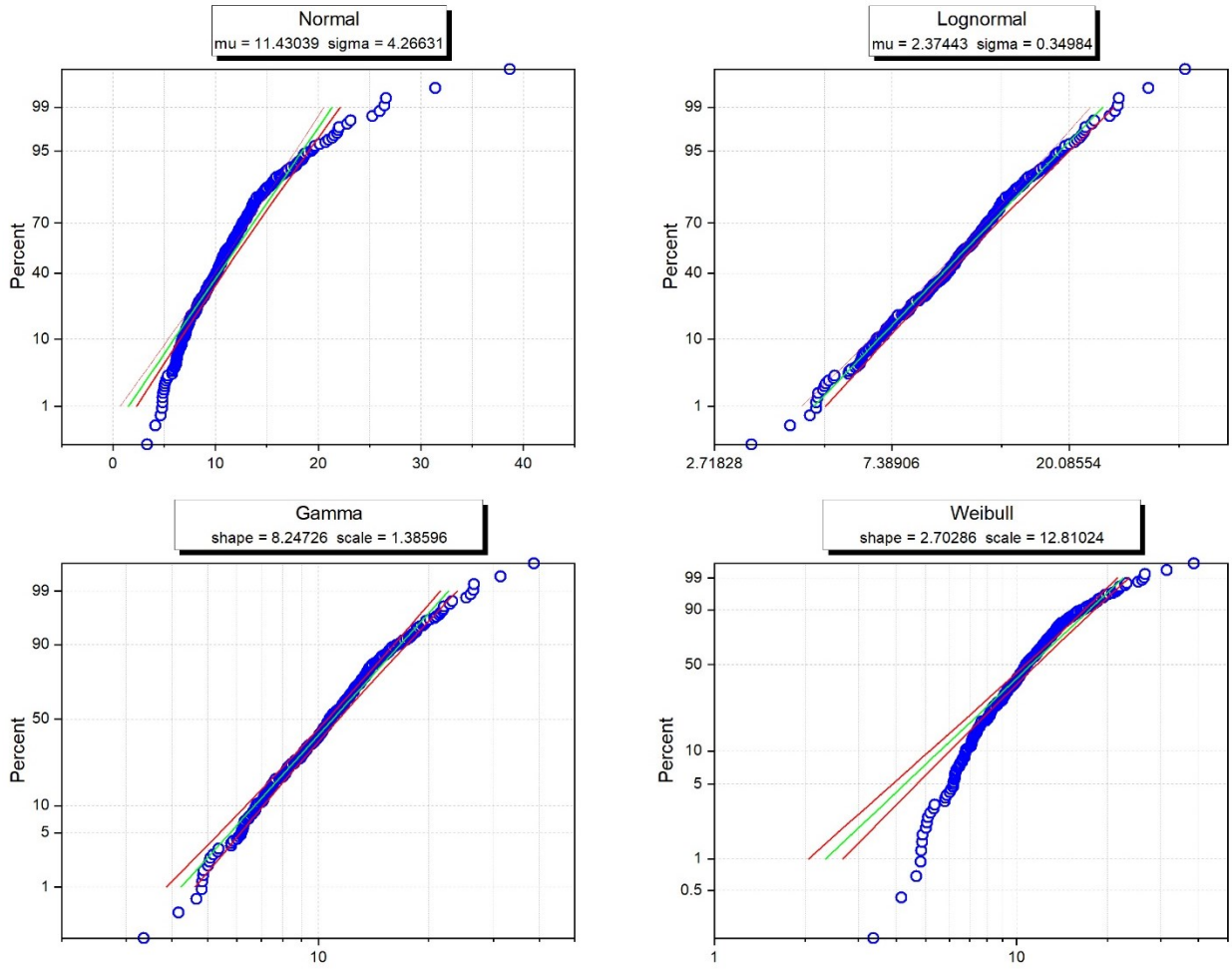

Figure 5.15 – Probability plots of the empirical data against 4 reference distributions showing a good fit of residual values for a log normal distribution.

5.3.2.3 Inclusions

Mineral inclusions, excluding quartz, were present in 32% (98 out of a total 304) of gold particles from Curraghinalt Burn sample 1 and 25% (99 out of a total 396) of gold particles from sample 2, table 5.5. Quartz inclusions were not counted as quartz is ubiquitous in both the vein and the gold particles. The proportions of mineral species observed in the two combined samples is shown in figure 5.16. The 2 samples were combined as analyses of the composition (see below) showed that they were not statistically different.

Table 5.5 – Summary of inclusions found with detrital gold particles

Inclusion type	C'Burn 1 (n=304)	C' Burn 2 (n=396)	Total (n =700)
Bismuth Tellurides Undif.	38	39	77
Galena	27	29	56
Pyrite	27	16	43
Carbonates	10	13	23
Chalcopyrite	4	15	19
Other Sulphides	6	13	19
Misc other	4	9	13
Hessite	5	5	10
Arsenic bearing	5	4	9
(Au,Ag) Tellurides undif.	3	5	8
Total gold particles with an inclusion(s)	98	99	197

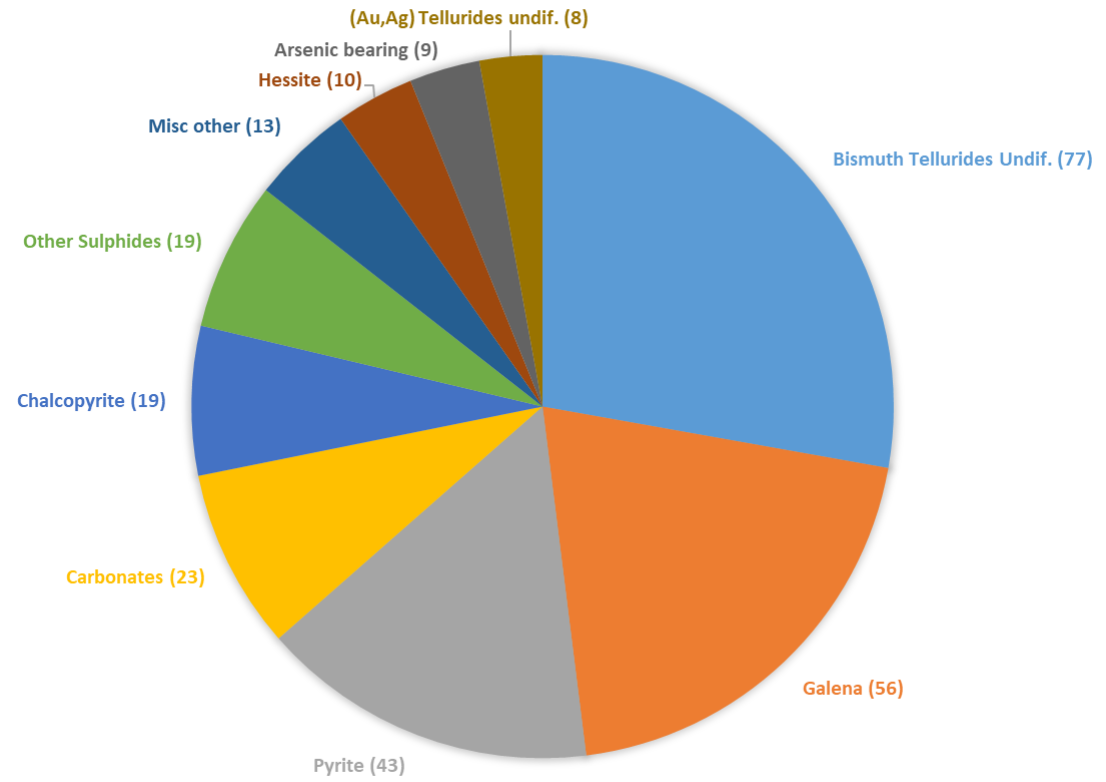

Figure 5.16 – Pie chart showing proportions of mineral species as inclusions within the detrital gold particles from the combined burn 1 and 2 samples.

5.4 Discussion

Comparing the two detrital gold samples, both samples have identical distributions of alloy compositions with the K-S test result indicating no significant difference exists between the two samples. The distance between the two sample localities is 260m and the vein geometry of the deposit means that the downstream detrital gold sample (Curraghinalt Burn 2) includes gold particles from 3 additional resource veins (T17, Mullan and Sheep Dip) which are not in the catchment of the upstream Burn 1 sample, as they intersect the surface downstream of the Burn 1 sample site. Given the similarity of the gold signatures, alongside the known difference in the number of veins contributing to the detrital populations, it is possible to infer that that the mineralised array of veins in the deposit all have comparable gold signatures. It is possible that though southwards-directed glacial transport might have contributed some material from the northerly veins to the Burn 1, However, given the direct outcropping of the vein in the steam bed it is hard to argue that glacial action could totally mask a significant difference between the veins. The inference that the veins are directly comparable assumes that all the gold veins in the deposit contributed approximately equivalent amounts of gold into the detrital population. It is possible however, that if the 3 additional veins had different gold signatures, but only contributed a minor amount into the detrital population, then different gold signatures would not have been detected.

Examining the characteristics of the alloy compositional distributions of the detrital gold samples, a continuous monomodal distribution is observed in both samples. The statistical distribution testing in figure 5.15 showed that the compositional signatures have a good fit to a log-normal distribution of abundance vs composition. The continuous distribution is interpreted as being an indicator that the gold particles formed within a single system which continually evolved to produce the range of compositions observed. No bimodality is observed that may suggest multiple distinctly different mineralising fluids. This interpretation is supported by the work of Rice et al. (2016) who suggested a single system based on radiometric dating. However, a single system model is at odds with the work of Parnell et al., (2000), and Wilkinson et al. (1999), who advocated that two genetically separate mineralisation events occurred evidenced by two distinct fluid inclusion trends.

The observation that the distribution of alloy composition follows a log-normal distribution is notable, as this is not something reported in other detrital gold studies. The distribution may potentially be a result of the evolution of the

fundamental physiochemical mineralising within the system, however without further study on the depositional controls no qualified conclusions can be drawn.

Considering the results of the mineralogical study of the V-75 vein samples from the mine, the thin section observations infer that the gold mineralisation occurred in two paragenetic events: An early quartz dominant stage that appears to have been responsible for introduction of most of the sulphides, and a later quartz + carbonate vein assemblage which is consistent with the findings of previous petrography studies; Rice et al. (2016), Parnell et al. (2000) and Wilkinson et al. (1999). In the V75 thin section studied, which was not available at the time of the earlier studies, these two events have clearly different gold compositions and result in the stepped gold alloy distribution for the thin section, figure 5.17.

However, notable new petrographic findings have been observed in this study about the assemblages of the two phases requiring reassessment of the interpretations of the veins. The observed mineral assemblages differ from the published descriptions in two significant aspects. Firstly, the V-75 vein samples examined do not appear to contain arsenopyrite, which is noted in the early mineralisation by Parnell et al. (2000). Secondly, and more importantly, is the new finding of bismuth telluride minerals in the carbonate-dominant vein assemblage (stage 3/4), see figure 5.3. This makes the assemblages in the two main vein events more similar than has been previously documented, with arsenopyrite and Ca-Mg-Fe carbonate the only differences between the two events.

The fundamental observation of the nature of the vein, especially the descriptions of the cathode luminescence vein textures described by Wilkinson et al. (1999), are comparable with the observations presented in this study. The stage 1 and 2 quartz are directly comparable with the descriptions of Q1 and Q2 by Wilkinson et al. (1999), however the stage 3 quartz in this study appears to represent both Q3 and Q4. Wilkinson et al. (1999) separated these types of quartz by luminescence but noted “Q 4 is sometimes overgrown by dully luminescent (Q3-type) quartz producing oscillatory zoning textures, possibly indicating alternate precipitation”. It is therefore acceptable to combine Q3 and Q4 into one stage, so the stage 3 quartz in this study is compatible with Wilkinson’s findings.

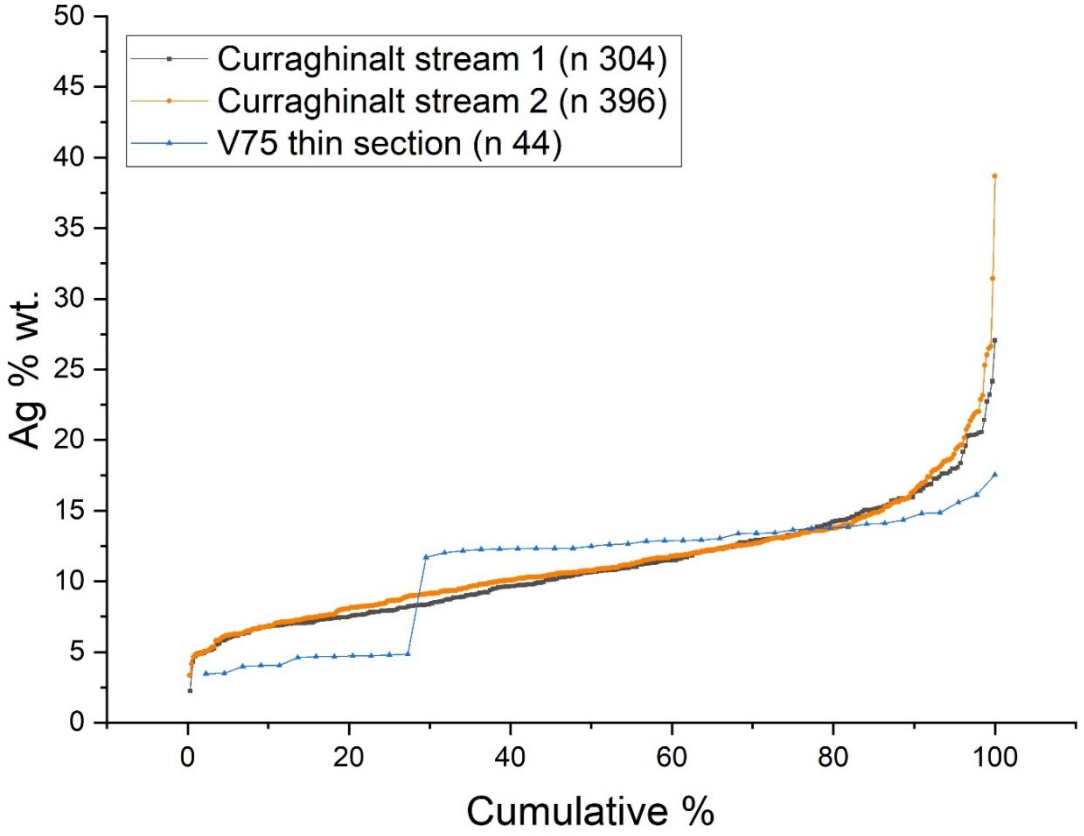

Figure 5.17 – Cumulative frequency plot of the detrital samples compared to the V75 Gold grains observed in situ.

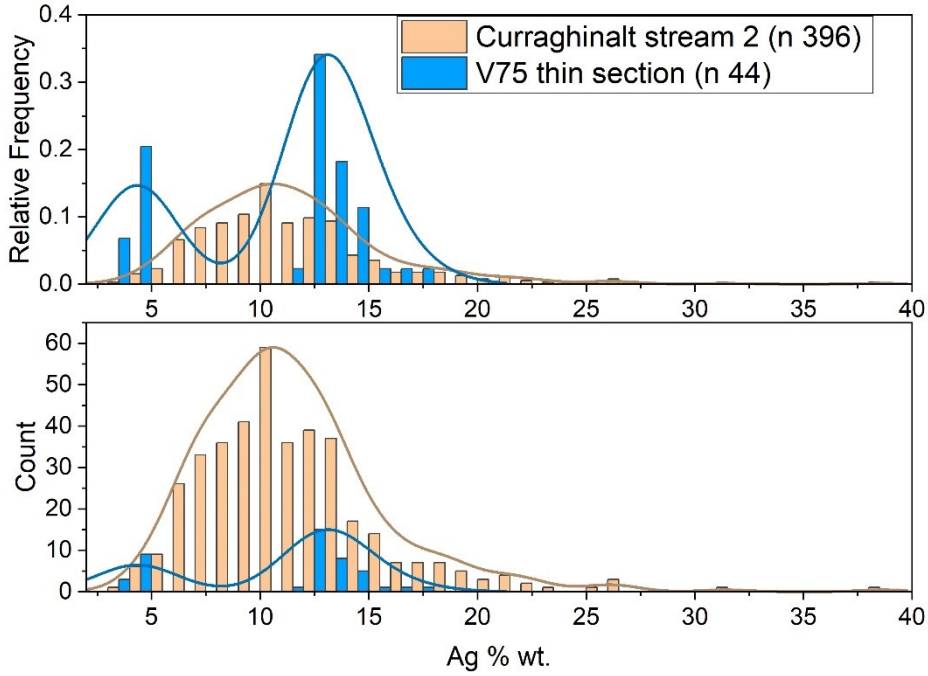

Figure 5.18 – Histogram plot of the gold alloy signature of the detrital sample compared against the gold in the V75 sample.

These two paragenetic events produced distinctly different compositions of gold particles which are associated with different mineral assemblages and textures. Comparison of the alloy signature of the gold particles in the vein thin sections with the detrital gold samples, figures 5.17 and 5.18, shows that the two mineralisation events in the V-75 sample correspond to different parts of the range of alloy compositions observed in the stream.

The V-75 thin section gold stages appear to be two discreet events which straddle the main compositional range identified by the detrital gold sampling. Consideration of the available evidence points to a single system allowing this single sample to be placed within the framework of the Curraghinalt deposits' single auriferous mineralising event. Evidence for a single system is provided by the detrital gold samples and petrographic observations. The detrital gold presents a strong case for a single event because the alloy compositions have a single continuous log normal distribution. Furthermore, the gold particles from the full range of compositions also have consistent assembles of mineral inclusions, see figure 5.14.

Additionally, petrographic evidence further supports a single system hypothesis. Outcrop scale petrographic observations show many discreet cross cutting vein events formed each vein, figure 5.4. Insights from the previous work on the gold particles at the Cononish gold mine (see chapters 3 & 4), suggest that limited ranges of compositions can be observed in individual thin sections, even within a system in which the gold is known to have a wide range of compositions. The presence of only one or two discreet gold depositional events within a single thin section can be applied to the veins in the Curraghinalt deposit as the veinlets observed in outcrop are commonly multiple centimetres width. Interpreting this, the veinlets which are formed are of such a size that only one or two individual 'veinlet' depositional events are present in a single thin section. It would logically follow therefore that on the scale of a single thin section an 'apparent' consistency of compositions in the gold alloy within a thin section would result due to relatively stable local physiochemical controls on gold composition during deposition within a single veinlet deposition event.

The assumption that the eroded veins contain comparable gold resources is impossible to test directly and would be very difficult to assess in the early stages of an exploration program. However, as the Curraghinalt deposit is well advanced with underground development and has had numerous resource estimation studies, further investigation of this assumption is possible.

Information available on the gold resources of the (un-eroded) veins in the deposit provides data on the constancy of grades between different veins.

The summary statistics for 17 resource domains (veins) produced by SRK Consulting are shown in table 5.6. It is important to note that these results are based on fixed length (0.5m) composites of the drill hole assays, ignoring the geology. Therefore, the thickness data reported in table 5.6 does not represent the true vein widths, which would be obtainable from the unpublished drill hole logs. The statistics show that the average gold grade of all the veins is broadly consistent, especially when considering the likelihood of skewing of the calculated means due to the nugget effect. This data broadly supports the assumption that the veins contained approximately equivalent amounts of gold which could be eroded to produce the detrital gold particle population in the Curraghinalt Burn.

Table 5.6 – Uncapped drill core composite samples (snapped to 0.5m lengths) statistics of gold grade (g/t) for each modelled vein structure (domain), from Couture et al. (2016).

Domain	Count	Mean	Std	Min	Max
No.1	438	13.97	18.16	0	137.1
106-16	483	11.83	15.07	0	162.81
V75	259	13.95	16.91	0.02	123.86
Bend	136	7.91	14.69	0	142.6
Crow	190	10.3	15.66	0	123.44
T17	425	18.51	35.34	0	372.7
Mullan	257	11.52	18.85	0	198.43
Sheep Dip	155	12.77	21.22	0	169.38
Road	58	9.66	12.05	0	55.22
Slap Shot	228	8.73	12.89	0	126.89
V55	119	8.63	16.87	0	144.48
Sperrin	129	7.04	10.16	0	69.05
Causeway	180	10.45	23.85	0	294.54
Grizzley	120	10.44	14.76	0	103.21
Slap Shot splay	50	8.16	8.65	0	48.44
Bend Splay	68	11.17	14.81	0	73.75
Total	**3295**	**12.16**	**20.38**	**0**	**372.7**

In current mineralogical studies, the context of observations is achieved by sampling and examining numerous mineralised samples taken from a wide

range of locations. Because of the need for a significant sample size of the mineralisation, impactful mineralogical (or geo-metallurgical) investigations are usually conducted after the initial exploration drilling program, often during the early stages of resource assessment. At this point in the exploration cycle an infill drill program, conducted in order to increase the density of intercepts of the mineralisation, provides an increased sample set which allows for assessments of the representative of different 'styles' of within the deposit. The expansion of drill programs from exploration towards resource definition and infill drilling is a high-risk stage of exploration in which the expenditure increases significantly before a deposit is well defined or important properties of the mineralisation are known (Singer and Kouda, 1999,Carlson, 2019 #1927).

In this study, the mineralogical observations obtained from the V75 vein simulate how knowledge of the nature of the mineralisation is potentially obtainable early on in the exploration process from a focused study of just a few samples. This is achieved by using a parallel detrital gold study to provide a context for the mineralogical sample within the larger auriferous mineralised systems. This could allow mineralogical information to be utilised in decision making at an earlier stage in the exploration cycle of a deposit than would normally be possible. Typically, a detailed study of a single sample of mineralisation would not be advisable as it lacks context and there is no way of quantifying how representative of the mineralisation the sample is. By providing context with a detrital gold study individual samples of mineralisation can be assessed by comparing the alloy composition of gold in a sample to the detrital alloy signature of the deposit.

5.5 Conclusions

This study of the mineralisation at the Curraghinalt mine demonstrates the benefits of combining detrital gold studies with a single hard rock sample. This would be especially beneficial in cases where a mineralising system is not well understood (or limited samples are available) because it is in an early stage of exploration. As demonstrated the detrital gold samples allow gold particles observed in thin sections to be placed in a wider context of the whole mineralising system. The specific findings of the Curraghinalt study indicate that the mineralisation was formed in a single continuous system. This was not previously well defined despite extensive exploration, mining, and several academic studies on the deposit.

References

CHAPMAN, R. J. & MORTENSEN, J. K. 2006. Application of microchemical characterization of placer gold grains to exploration for epithermal gold mineralization in regions of poor exposure. *Journal of Geochemical Exploration,* 91**,** 1-26.

CHEW, D. M., FLOWERDEW, M. J., PAGE, L. M., CROWLEY, Q. G., DALY, J. S., COOPER, M. & WHITEHOUSE, M. J. 2008. The tectonothermal evolution and provenance of the Tyrone Central Inlier, Ireland: Grampian imbrication of an outboard Laurentian microcontinent? *Journal of the Geological Society,* 165**,** 675-685.

COUTURE, J. F., LEUANGTHONG, O. & FREUDIGMANN, S. 2016. Technical Report for the Norhten Ireland Gold Project, Norhten Ireland. by SRK Resources Inc. for Dalradian Resources Inc.

EARLS, G., CLIFFORD, J. & MELDRUM, A. 1989. Curraghinalt gold deposit, County Tyrone, Northern Ireland. *Appl. Earth Sci.(Trans. Inst. Min. Metall. B),* 98**,** B50-51.

HOLLIS, S. P., ROBERTS, S., EARLS, G., HERRINGTON, R., COOPER, M. R., PIERCEY, S. J., ARCHIBALD, S. M. & MOLONEY, M. 2014. Petrochemistry and hydrothermal alteration within the Tyrone Igneous Complex, Northern Ireland: implications for VMS mineralization in the British and Irish Caledonides. *Mineralium Deposita,* 49**,** 575-593.

LEUANGTHONG, O., CHARTIER, D., MACHUCA, D. & FREUDIGMANN, S. 2018. Technical Report for the Curraghinalt Gold Project, Northern Ireland. *SRK Consulting (Canada) Inc. report for Dalradian Resources Inc.*

MAUNULA, T., HENNESSEY, T., FOO, B., DAMJANOVIC, B., VILLENEUVE, A. & JACOBS, C. 2014. Curraghinalt Gold Deposit, Northern Ireland.: Dalradian Resorces Inc.

MCCAFFREY, K. J. W. & JOHNSTON, J. D. 1996. Fractal analysis of a mineralised vein deposit: Curraghinalt gold deposit, County Tyrone. *Mineralium Deposita,* 31**,** 52-58.

MITCHELL, W. I. 2004. The Geology of Northern Ireland : our natural foundation. 2nd ed, Belfast, Geological Survey of Northern Ireland.

PARNELL, J., EARLS, G., WILKINSON, J. J., HUTTON, D. H. W., BOYCE, A. J., FALLICK, A. E., ELLAM, R. M., GLEESON, S. A., MOLES, N. R., CAREY, P. F., LEGG, I. & CAREY, P. F. 2000. Regional Fluid Flow and Gold Mineralization in the Dalradian of the Sperrin Mountains, Northern Ireland. *Economic Geology,* 95**,** 1389-1416.

RICE, C. M., MARK, D. F., SELBY, D., NEILSON, J. E. & DAVIDHEISER-KROLL, B. 2016. Age and Geologic Setting of Quartz Vein-Hosted Gold Mineralization at Curraghinalt, Northern Ireland: Implications for Genesis and Classification. *Economic Geology,* 111**,** 127-150.

SINGER, D. A. & KOUDA, R. 1999. Examining Risk in Mineral Exploration. *Natural Resources Research,* 8**,** 111-122.

WILKINSON, J., BOYCE, A., EARLS, G. & FALLICK, A. 1999. Gold remobilization by low-temperature brines; evidence from the Curraghinalt gold deposit, Northern Ireland. *Economic Geology,* 94**,** 289-296.

Chapter 6. A district scale placer gold study of the Atlin Gold Camp, British Columbia.

Summary

A study examining the placer in the Atlin gold camp was undertaken to apply the previously developed knowledge and methods to an area which has significant economical placer gold production, but where the hard rock origin of the gold particles is unknown. This chapter presents an example of what can be learnt from detrital gold samples when no access to exposed mineralisation is available. It also demonstrates how an exploratory statistical approach to a large detrital dataset can provide information on the nature of auriferous mineralisation which could help focus exploration to locate the hard rock sources of the gold particles.

In this chapter the geographical extents of gold signatures in the Atlin gold camp are examined. Through application of basic principles governing the deposition of gold in veins, the signatures are evaluated to reveal that a large-scale fluid dominated auriferous mineralising system is responsible for the gold endowment. These discoveries allow hypotheses on the source of the detrital gold to be evaluated. It was found that the previously favoured theory of sourcing from Listwanite deposits is unlikely to be correct. This chapter therefore demonstrates how a detrital gold study can test assumptions and provide information to evaluate mineralisation on a camp scale before the hard rock sources are identified.

6.1 Introduction

The Atlin gold camp is a 30km^2 area, east of Lake Atlin in northern British Columbia, Canada (Figure 1) and has produced in excess of 1 million ounces of placer gold derived from unknown lode sources (Ash, 2004). The production statistics for the Atlin area, published up until 1949 indicate that the total production up to that date was 607,994 ounces, with an average fineness of 813 (81.3 wt. % Au) (Holland, 1950). Holland (1950) records the production from individual creeks, with additional information on the gold fineness for some of the more significant placer creeks (see table 6.1).

In the Atlin area the hard rock sources of the placer gold remain unknown despite extensive placer mining and protracted mineral exploration. Study of the Atlin gold camp also provides an additional opportunity to apply the methodologies developed in this thesis to demonstrate how they can be used to further debate and speculation on the unknown source(s) of the placer gold in the region. In particular it tests the hypothesis that the large gold endowment of the Atlin placer gold is due to erosion of veins formed within listwanite units, which that are known to be related to gold mineralisation in other districts, in the Atlin area.

Detrital gold is ubiquitous, occurring in all major drainages within the camp, table 6.1 and figure 6.5. In addition to the large number of economic gold bearing drainages in the camp, the area is known for producing significant numbers of large (>30 oz) nuggets. The largest weighed 84oz and was discovered on Spruce Creek in 1899 (Levson and Blyth, 1993, Mihalynuk et al., 2017). However, despite 100 years of placer mining, only two hard rock gold deposits have been identified in the camp; the Imperial Mine (operated 1899-1902) and a modern (JORC compliant) resource at the Yellowjacket property (Marud, 1989, McIvor, 1989).

Gold production in the Atlin area started on Pine Creek in 1898, with operations rapidly expanding, as miners bound for the Klondike were drawn to Atlin (Cairnes, 1913, Aitken, 1959). Early exploration, based on presence/relative abundance of gold in drainages, was highly successful in the identification of the geographic extent of the gold camp, and led to large mining operations in many of the creeks.

Previous studies of detrital gold in the Atlin camp comprise an unpublished project examining the properties of gold particles from placer deposits which was partially reported as an abstract for the Gold 86 conference (Ballantyne and MacKinnon, 1986), and two papers which explored the significance of minerals externally attached to a small number of large nuggets, Sack and Mihalynuk (2003) and Mihalynuk et al. (2011). The only compositional comparisons of gold from different creeks within the Camp remains the bulk assay records from mining operations published by Holland (1950). This general lack of information has contributed to the publication of numerous, untested speculations on the nature of the unknown hard rock source(s) of the detrital gold. The current theory presented in the literature is that the gold particles are sourced from listwanite altered ultramafic units (Ash and Arksey, 1989, Ash et al., 2001).

Table 6.1 – Gold fineness (Au in the alloy,as parts per thousand) after Holland (1950) for the main economic drainages in the Atlin area pre-1950's.

Mining area	Weight of gold tested (oz)	Fineness range (n)	Average fineness	Total production (oz)
Boulder Creek	6,911	743-794 (6)	774	61,719
McKee Creek	1,764	831-834 (4)	833	44,019
O'Donnell River	248	805-807 (6)	806	6,455
Pine Creek	467	806-818 (1)	812	129,181
Ruby Creek	1,616	800-808 (5)	805	55,338
Spruce Creek	35,115	809-890 (26)	841.75	254,858
Squaw Creek	276	834 (1)	834	3,257
Wright Creek	1,016	802-814 (6)	806	13,698

In the Atlin area, the lack of suitable lode discoveries that could provide a source for the placer gold led Aitken (1959) to conclude that the known low-grade lodes are the roots of more substantive lodes, now completely eroded to form the placer. However, the discovery of visible lode gold in veins hosted within argillaceous metasediments in 2015 has reinvigorated exploration for hard rock sources within the camp (Mihalynuk et al., 2017). These new veins have been suggested by Mihalynuk et al. (2017) to be representative of the nature of the unknown source for the Atlin gold. Currently, a genetic link between hard rock gold occurrences and the detrital placer gold is untested. Since there are only partial descriptions of large detrital nuggets available for comparison with gold from the new lode gold discoveries, along with a lack of published studies examining a significant number of detrital gold particles from the Atlin area, the chemical and physical properties of the abundant detrital placer gold are difficult to related to hard rock mineralisation (Sack and Mihalynuk, 2003, Mihalynuk et al., 2011). The present study addresses these gaps through the collection and analysis of a large number of detrital placer gold particles from the Atlin area and applies the methodology developed in the studies described in previous chapters to this area of economic importance.

This work presents the results of a study of gold particles collected from 15 localities which, analysed, and interpreted the compositional and morphological characteristics of 849 detrital gold particles, together with the smaller numbers of gold particles available from bedrock sources within the Atlin camp. These results are discussed in the context of existing published literature in order to place constraints on the location and nature of in situ mineralization in the Atlin camp.

6.1.1 Geological Background

Mapping of the Atlin area was first conducted by Aitken (1959) at the1:250,000 scale, with later mapping by Bloodgood et al (1989) at 1;50,000 and Ash (2004) at the 1;25,000 scale. Figures 6.1 is simplified compilation based on both data sets. Bedrock in the Atlin camp is comprised of tectonised Carboniferous and early Jurassic metamorphosed oceanic crust and associated sediments of the Cache Creek terrane. The complexity of the Atlin area, along with a lack of small-scale mapping necessitates a review of the larger scale tectonic assemblage of the region around Atlin, the development of which has been the focus of much of the work on the area.

Geological mapping shows Atlin is located on the central western margin of the northern Cache Creek terrane, figure 6.1. The Cache Creek terrane comprises Upper Triassic to early Jurassic subduction-related accretionary complexes with slices of obducted dismembered basement assemblages sandwiched between two magmatic arcs; Quesnellia to the east, and Stikinia to the west (Mihalynuk and Lowe, 2018, English et al., 2001). The paleo geographic reconstructions of how the Cache Creek terrane became enclosed by these arcs are complex because of the interpretations of the carbonate seamounts which exhibit exotic Namurian age Tethyan fauna (Johnston and Borel, 2007). This indicates that the Cache Creek terrane formed distally from the North American margin, to which it is now accreted (Wang-Shi et al., 1985, Johnston and Borel, 2007, Nelson and Colpron, 2007, McGoldrick et al., 2017, English et al., 2010). The Quesnellia and Stikinia arcs are thought to have initially faced east, and formed above the subducting Cache Creek Ocean in the early Mesozoic (Nelson and Colpron, 2007). The present-day enclosure of the Cache creek terrane is the result of the rotation of the northern Stikinia arc, which progressively enclosed a doubly subducting Cache Creek ocean, figure 6.1) (Dostal et al., 2009, English et al., 2010, Johnston and Borel, 2007, Mihalynuk et al., 1992, Struik et al., 2001, Nelson and Colpron, 2007). Within the Cache Creek terrain near Atlin, both the presence of the undeformed Fourth of July intrusive suite, dated at 172 Ma (Mihalynuk et al., 1992) and the cessation of magmatic activity within the Quesnellia arc around 183Ma (Nelson and Bellefontaine, 1996), indicates that the Stikene and Quesnel terranes had collided prior to 180-170 Ma (Nelson and Colpron, 2007).

The Cache Creek terrane is separated from Stikine to the west by the Whitehorse Trough which is separated from the Cache Creek terrane by the sub vertical Nahlin Fault, figure 6.1 (Aitken, 1959, Bloodgood et al., 1989, Mihalynuk et al., 2001). The Whitehorse trough sediments are interpreted to have been deposited in the Mississippian through to Lower Jurassic within the fore arc basin of the Stikinia arc and have been imbricated and thrust over the Stikinia arc by the King Solomon Thrust.

The sediments within the Whitehorse trough have a Stikinie terrane providence, indicating paleoflow to the east (present day orientation). Within the Whitehorse Trough, the stratigraphically highest units exposed along the Sloko River show possible blueshist derived clasts, indicating a Cache Creek provenance. This observation reveals that exhumation and erosion of the eastern portion of the Cache Creek terrain occurred by 172-170, specifically the French Range which contains outcrops of blueshists Ma (English et al., 2018, Erdmer et al., 2000).

The relationship between sediments in the Whitehorse Trough with those in the Cache Creek terrane indicates that the accretionary complex of the Cache Creek terrane belongs tectonically to the Stikinia arc margin sequence. This contrasts with early interpretations and evidence from portions of the Cache Creek Terrane in southern BC, which indicated that the Cache Creek terrane had a Quesnellian affinity. The assignment of the Cache Creek terrain to the Stikinia Arc margin is supported geochemically by the work of McGoldrick et al. (2017). She demonstrated that the Cache Creek ophiolites formed in a supra subduction zone setting and noted the geochemical similarity of the Late Triassic granitic plutons to the Stuhini arc volcanics of the Stikene terrane (Mihalynuk et al., 1992). This new tectonic re-interpretation of the terranes is presented here as a synthesis of recent work and is shown diagrammatically in figure 6.1. This is consistent with reported observations and analogue modelling of modern fore arc basin and accretionary wedge geometries (Malavieille and Trullenque, 2009).

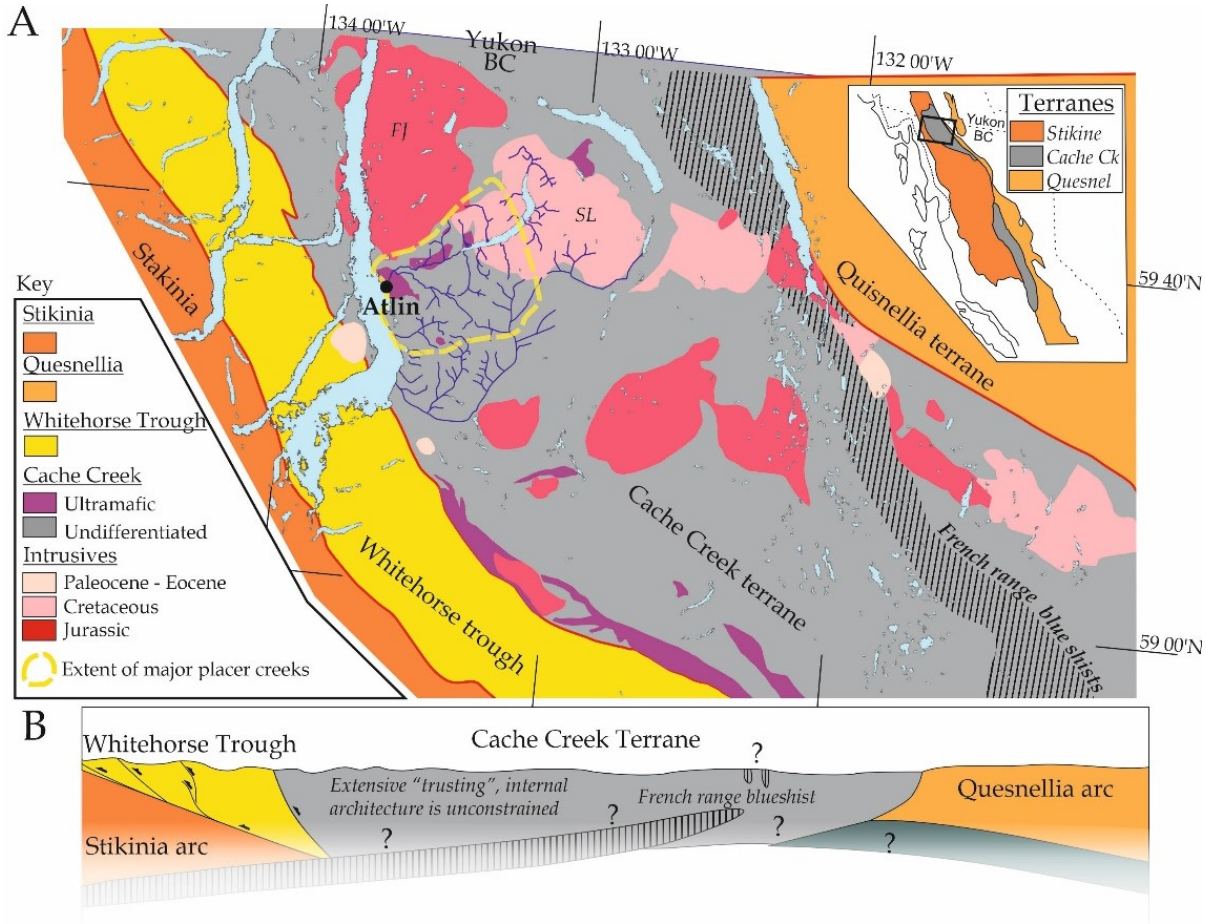

Figure 6.1 – Terrane map of British Columbia and the Yukon (inset top right). A: Simplified tectonic and geological map of the area surrounding Atlin after Bloodgood et al. (1989), Mihalynuk and Lowe (2018), Lowe and Anderson (2018). B: Conceptual sketch cross section of the architecture of the terrane as proposed and detailed in the text. The section has been drawn without internal structures shown within the Cache Creek terrane, as large areas of the terrane have undefined or poorly constrained structural interpretations.

The stratigraphy of the Cache Creek terrane was reviewed by Monger (1975) who consolidated terms across the terrane and discussed in detail the difficulties in assigning formal rock-stratigraphic nomenclature. The stratigraphy in the Atlin area is complicated due to the discontinuous and lensoidal nature of the units. The specific nature of the depositional and tectonic processes is not clear in many cases due to a lack of continuous outcrop. (Monger, 1975, Mihalynuk and Lowe, 2018, English et al., 2018). To address these problems Monger (1975) divided the terrane into 5 formations during the mapping of the area and identified three broad structural and lithostathographic facies belts which have gradational poorly defined boundaries. Around Atlin the sequence predominantly consists of rocks belonging to the southwestern and central facies belts of the Cache Creek terrane. The following

detailed presentation and review of the geology is focused only on the geology of Atlin gold camp.

The bedrock in Atlin gold camp area, figure 6.1 is comprised of mafic extrusive rocks of the Nakina Formation with associated ultramafic bodies which are overlain by and intercalated with the Kedahda Formation, due to extensive thrusting and tectonism. The Kedahda Formation is dominated by variable cherty argillite sequences with lenses of rarer volcanic and carbonate units.

The Nakina formation is exposed in the western parts of the camp and has been mapped (1:2500 scale) by Ash and Arksey (1989) and further investigated and studied geochemically, as a CO_2 sequestration analogue and in the context of the gold mineralisation (Bloodgood et al., 1989, Hansen et al., 2005, Hansen, 2005, Ash and Arksey, 1989, Ash et al., 2001, English et al., 2001). In this area ultramafic units of altered harzburgite with minor dunite lenses form a klippen, tectonically thrust over more typical Nakina formation meta-basalts.

The ultramafic rocks exposed in the Atlin camp are extensively altered by carbonic fluids such that Serpentine + olivine + brucite assemblages are altered to form a progressive ‘zoned listwanites’ assemblages around the fluid pathways. These assemblages are characterised by the following mineral assemblages; serpentine + magnesite distal to the fluid pathways, through an intermediate magnesite + talc alteration, and to a pervasive magnesite + quartz alteration assemblage close to fluid pathways (Bloodgood et al., 1989, Hansen et al., 2005, Hansen, 2005, Ash and Arksey, 1989, Ash et al., 2001).

The meta-basalt and dolerites of the Nakina formation are up to 1000ft thick and are typically massive but in places are recorded as showing flow banding and pillow structures (Ash, 2004, Monger, 1975). In thin sections, taken just south of the gold camp on Monarch Mountain Monger (1975) reports that they consist of a matrix of zoisite altered ‘saussuritic’ feldspar with variable amounts of interstitial diopsidic augite, chlorite, opaques, and rare prehite-pumpellyite. Some basaltic units contain scattered amygdales of chlorite and carbonate, and clino-zoisite. These rocks have been metamorphosed to a maximum of prehnite-pumpellyite facies, with conditions indicating shallow burial and metamorphism post formation.

In the east of the camp the bedrock is a poorly constrained faulted sequence of thinly bedded chert, cherty pelite and pelites with ‘pods’ of interbedded volcanics, greywacke or limestone locally. These are mapped as the Kedahda formation on a terrane scale. The Kedahda represents a significant thickness forming the main component of the central facies belt of the Cache Creek terrane. Thinly bedded to massive limestones

occur as lenses within the unit. Fossil assemblages constrain the limestones deposition as occurring in the Mississippian and Permian. The contact between the Nakina formation and Kadahda formation is reported as conformable and gradational. The Cache Creek sequence is cut by the middle Jurassic (Fourth of July) and late Cretaceous (Surprise Lake) batholiths in the northwest and east of the camp respectively (Bloodgood et al., 1989).

Surficial deposits cover the area, with thin colluvium and morainal veneers present on the summits and hillsides (above 1100m elevation) and thick sequences in the valleys. The surficial deposits have been studied by several researchers and the findings are summarised below (Levson and Blyth, 2001, Levson and Blyth, 1993, Aitken, 1959, Sack and Mihalynuk, 2003). In the valleys and low-lying areas, a thick sequence of Tertiary and Pleistocene cover is observed. The surficial deposits in the area result from the glacial history of the area and the last glaciation is reported to largely obscure evidence of previous events (Levson and Blyth, 1993, Levson and Blyth, 2001). During peak glaciation ice was present across almost the entire area and prograding deltaic sequences in the creeks surrounding both the Atlin and Pine Creek valleys indicate that they were dammed by ice, figures 6.2 and 6.3. Till deposition in most areas during the glaciation was followed by extensive glacial erosion in the valleys creating unconformable channel systems which are the host to the placer gold resources (Levson and Blyth, 1993).

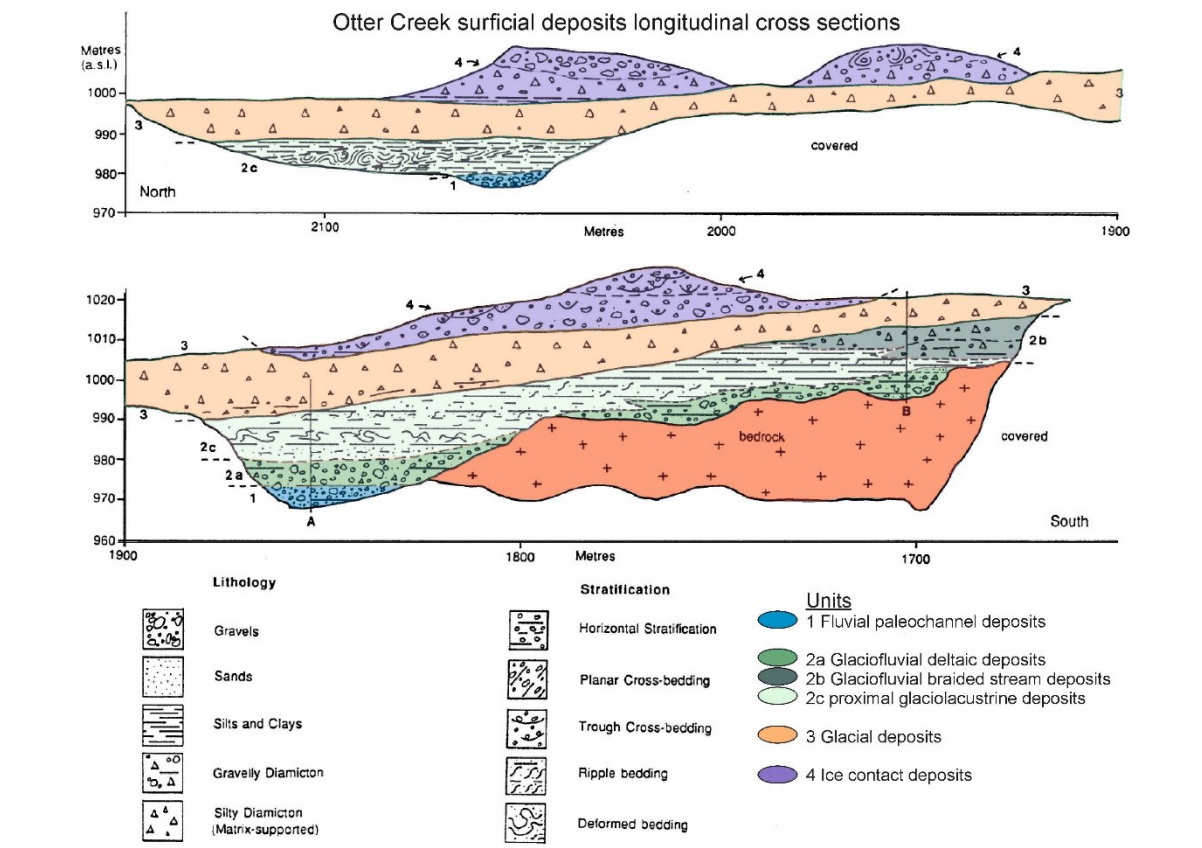

Figure 6.2 – Sections showing the surficial sediments in the upper otter creek mine mapped by Levson and Blyth (2001). The richest placer gold resources are reported in the fluvial paleochannel units, where not eroded by later events.

Figure 6.3 – Steeply dipping deltaic forest gravels (unit 2a on figure 6.2), exposed in cliff section in a historical Lower Otter creek mine. They are overlain by till and fluvioglacial gravels with erosional surfaces highlighted by the blue and green lines.

Figure 6.4 – Surficial gravel deposits in a placer pit on Ruby Creek. Paleochannel fluvial gravels are overlain by columnar jointed Pleistocene basaltic flows and later surficial deposits including deltaic fluvial fans and glacial sediments.

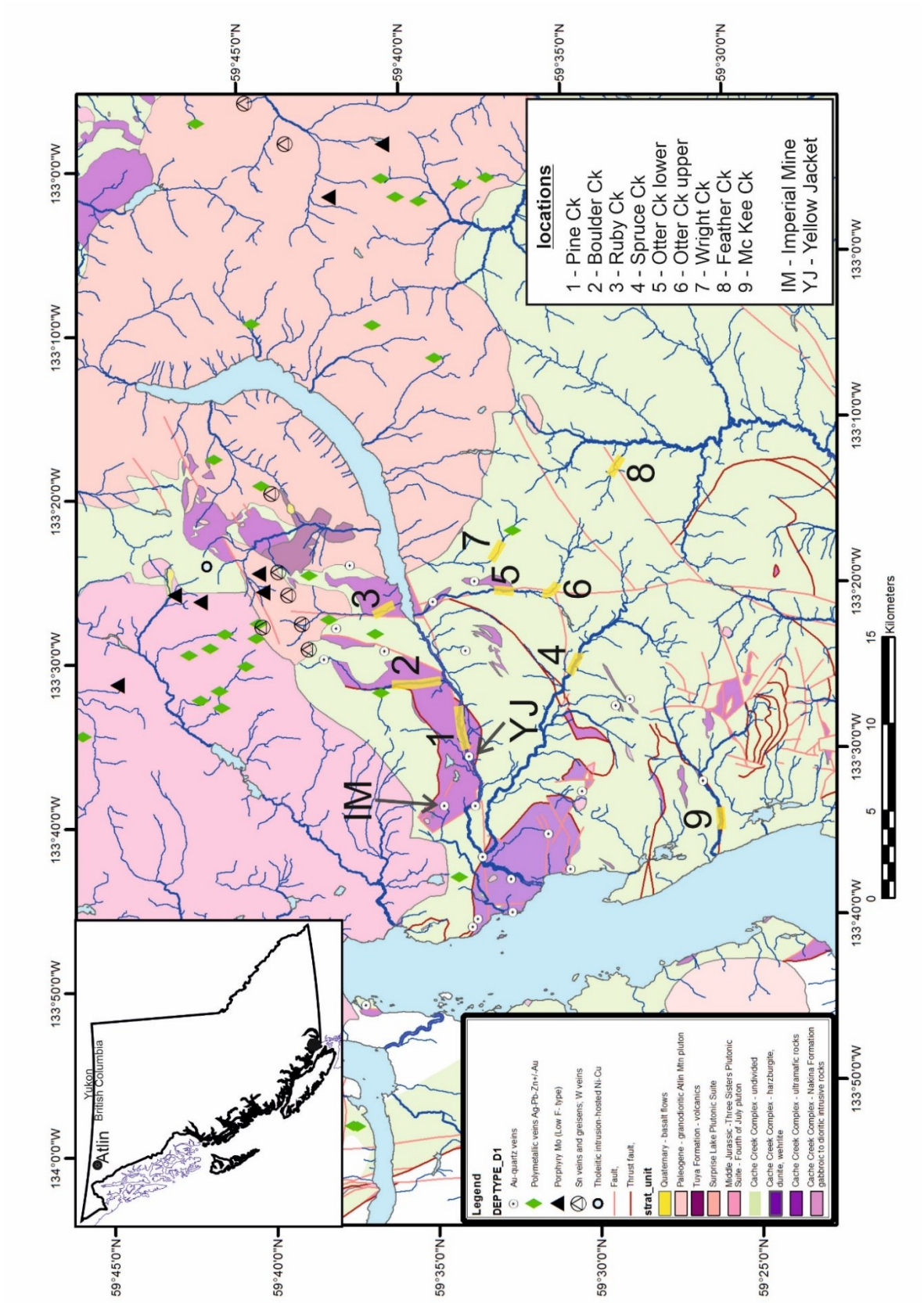

Figure 6.5 – Simplified geological map of the Atlin placer camp showing drainages and sample locations (yellow highlighting of stream lengths) modified after Bloodgood et al. (1989), Mihalynuk and Lowe (2018) ,and Lowe and Anderson (2018).

6.1.2 Mineralisation

In situ Mineralization

There are 21 bedrock-hosted gold occurrences listed within the Atlin Camp. Two of these occurrences, the Imperial Mine and Yellowjacket deposit have been advanced commercially and warrant summary. In addition to the gold showings there are polymetallic Ag-Pb-Zn+/-Au veins reported at the Ruffner mine, and a porphyry style molybdenum mineralisation associated with the batholiths at the Adnac deposit (Kirby, 2009, Bloodgood et al., 1989). Despite concerted efforts, no in situ mineralization has been identified that could be considered a plausible source for the abundant detrital gold produced by the placer mining operations.

The Imperial Mine was active between 1899 and 1902, and the vein is described by Cairnes (1913) as being 2-3 feet wide striking 070, with a dip of between 50° to 60°. The vein comprises multiple vein generations and is hosted in a finely textured rock that ranges from a hornblende-diorite to a hornblende-diorite porphyrite (Cairnes, 1913). The veins consist of rose-coloured quartz exhibiting comb-structures with minor galena, chalcopyrite, pyrite, malachite, and rare native gold. Assays on a sample of the ore sent to the BC geological survey contained 26.47 g/t Ag and 27.1 g/t Au (Aitken, 1959, Cairnes, 1913).

The hard rock Yellowjacket prospect has a reported resource of 184,000 tonnes, at a grade of 4.4g/t (McIvor, 1989). The resource drilling reports only list gold assays, with the amount of silver within the deposit unknown (Ronning, 1986, Marud, 1989, McIvor, 1989). It was discovered during exploration drilling in the 1980s and is a mineralised sequence of deformed, highly altered listwanite, ultramafics, and mafics within the Pine Creek fault zone (Mihalynuk et al., 2017, Ronning, 1986, Marud, 1989, McIvor, 1989).

Placer Resources

The principal commercial focus is placer gold operations with no hard rock mining operational at present. The sedimentology of the placer deposits in Atlin are detailed by Levson and Blyth (1993). The richest gold bearing gravels are reported to be high energy, fluvial palaeochannels of Paleogene and Early Pleistocene age, observed to lie directly upon bedrock. These fluvial paleochannel deposits, where present, are overlain by a sequence of Quaternary sediments up to 30m thick, comprising gravel, sand, silt, and diamicton. The large accumulated thickness of sediments was due to glacial damming of the main drainage valleys. The larger placer operations excavate open pits to reach the basal paleochannel gravels, figure 6.6. This aggradation has

protected the early fluvial gravels from later erosion and deposition of Holocene tills. The richest deposits are known to be the paleochannels (such as those presently mined on Otter Creek, Boulder Creek, and Ruby Creek) however local reworking of gravels, due to local erosion of the sequence, has resulted in sediments throughout the sequence being mined.

Figure 6.6 – Placer operations in Upper Otter Creek in 2015 showing the broad glaciated terrain typical of the valleys in the gold camp.

Figure 6.7 – View of Boulder Creek placer mines, Photograph taken across Lake Superior in 2016.

Sack and Mihalynuk (2003) examined the nature of the gold and associated minerals in placer deposits of the Atlin area. They identified the morphology of the detrital gold as irregular and rough, indicating proximal sourcing of the gold. In addition, thorite and cassiterite were observed attached to the outside of placer gold nuggets from Feather Creek. These features were presented as evidence of a genetic link between the gold mineralization and the Surprise Lake batholith, which is known to be enriched in thorium and base metals, and is located proximal to Feather Creek (Sack and Mihalynuk, 2003). In a follow up study, Mihalynuk et al. (2011) examined minerals attached to nuggets from Otter, Boulder, and Snake Creeks. In these cases, lithic attachments were chert and argilite of the Kedahda formations, representing the bedrock underlying the Creeks which indicates that the sources are local (Mihalynuk et al., 2011).

6.2 Methodology

Samples of detrital gold particles from the Atlin camp were provided by commercial placer miners or collected by the authors using the using the methods of Leake et al. (1997), during visits to the Atlin area, see table 6.2.

Table 6.2 – Details of the samples collected and analysed in this study. Subscript indicates source; [1] – Commercial miner donation. [2] – Donated by Fiona Devine to the University of Leeds collection. [3] – Collected in the field.

	Map #	Sample name	No. of particles
Placer Samples	6	Otter Ck A[3]	63
	6	Otter Ck B[1]	132
	6	Otter Ck C[1]	100
	7	Wright Ck[2]	9
	4	Boulder Ck A[3]	94
	4	Boulder Ck B[2]	27
	3	Pine Ck[3]	27
	?	Quartz Ck[3]	100
	5	Ruby Ck A[3]	37
	5	Ruby Ck B[2]	54
	2	Spruce Ck[1]	79
	8	Feather Ck[3]	40
	7	Wright Ck[3]	83
	1	McKee Ck[2]	3
		Total	849
Lode samples	6	Otter CK 2015 LODE[1]	1
		Yellow Jacket mine[3]	3
		Total	4

Gold particles were examined visually using a binocular microscope and mounted on double sided tape in rows of 5 particles prior to encapsulation in resin blocks. Photographs were taken of selected particles as a reference of the sample and to identify any morphological sub-types. Gold particles of similar size were mounted together on a single block such that the depth of polish exposes the approximate centre of all the particles on the block.

All gold particles were examined by scanning electron microscope, at the University of Leeds, to identify individual mineral inclusions. Once identified the mineralogy was

established using the energy dispersive spectroscopy instrument. This study focused on the identification of opaque ‘ore’ mineral inclusions within the gold, typically 2-50 µm in size, as these are used to differentiate between gold deposit styles (Chapman and Mortensen, 2006).

Alloy compositions were determined using EPMA analysis carried out at the University of Leeds on a JEOL JXA8230 EPMA with tungsten source. Analyses were run with an accelerating voltage of 20 kV, beam current of 50 nA and on and off-peak count times of 30s and 15s seconds respectively. Additional major and minor trace element analysis was conducted on selected sample populations using a Agilent 7500c quadrupolemass spectrometer combined with aGeolas laser ablation system (LA-ICP-MS) at the University of Leeds, see Banks et al. (2017) for the details of the method. The method used takes care to avoid any inclusions revealed on the polished surface during the ablation. Subsequent processing of the time dependent signal generates elemental analyses with lower detection limits than possible using EPMA.

In the LA-ICP-MS analysis the London Bullion Market Association Reference Standard AuRM2 was used as the primary standard for Ag, Al, As, Bi, Cr, Cu, Fe, Mn, Ni, Pb, Pd, Pt, Rh, Sb, Se, Sn, Te and Zn with the additional elements calibrated against the NIST 610. The Ag/Au ratio used in the final quantification used a set of Au-Ag wires, NIST standard 481. The NIST standard 481 80:20 (Au/Ag, wt.%) wire standard was used for quantification and despite the difference in matrix and in the concentration of both elements gave a calibration that was almost identical to that obtained using NIST 610. The calibration for Hg was established using the USGS synthetic sulphide standard MASS-1 as Hg is not present in NIST or the AuRM2 standard. In this instance the calibration was based on using Ag as the internal standard element as there is no Au in MASS-1 and manual extraction of the counts per second ratio for Hg/Ag from the output to use with the Hg/Ag wt/wt ratio of the standard.

6.3 Results

6.3.1 Examination of lode gold occurrences

The potential to characterize in situ mineralization was limited by the lack of exposure however ongoing placer mining sometimes reveals new occurrences in the open pits, and such an opportunity arose during the 2016 field season. The following section documents the samples obtained from examination of the vein discovery, along with examination of a placer nugget with attached rock that was recovered from the same mining operation in the 2016 season.

The site of the gold vein discovered on Otter Creek in 2016 has been described in detail by Mihalynuk et al. (2017). The vein was discovered by one of the local metal detectorists who routinely examine mined areas for nuggets which are rejected by the processing plant classification systems. The vein had been removed by the placer miners before any detailed observations were made, and only vein fragments remained.

A small 1cm sized fragment of the in situ find was donated to this study. It is observed to contain a thin ~4mm milky white quartz vein which has abundant visible gold infilling fractures in the quartz. The vein sample is bounded by a veneer of dark grey phyllitic mudstone showing a strong cleavage parallel to the vein, figure 6.15. The gold appears concentrated on the boundary between the quartz and the host rock.

In addition to the observation of the vein fragments, a placer nugget containing bed rock material was donated by Decoors mining to the study. The large placer nugget shown in figure 6.8 and is 32x28x7mm and comprises a substantial amount of visible gold in factures through a quartz vein with two areas of attached bedrock (sized 13x9x3mm and 9x7x2mm) on one face of the nugget. The bedrock is dark grey, impure psammite comprised primarily of fine sand sized quartz with a mud matrix. Around the quartz, muscovite mica and apatite alteration are present, (figure 6.8) The composition of the placer nugget and the bedrock vein fragment were analysed to be 23.7 %wt (EDX) and 21.7 %wt (EMPA) silver respectively.

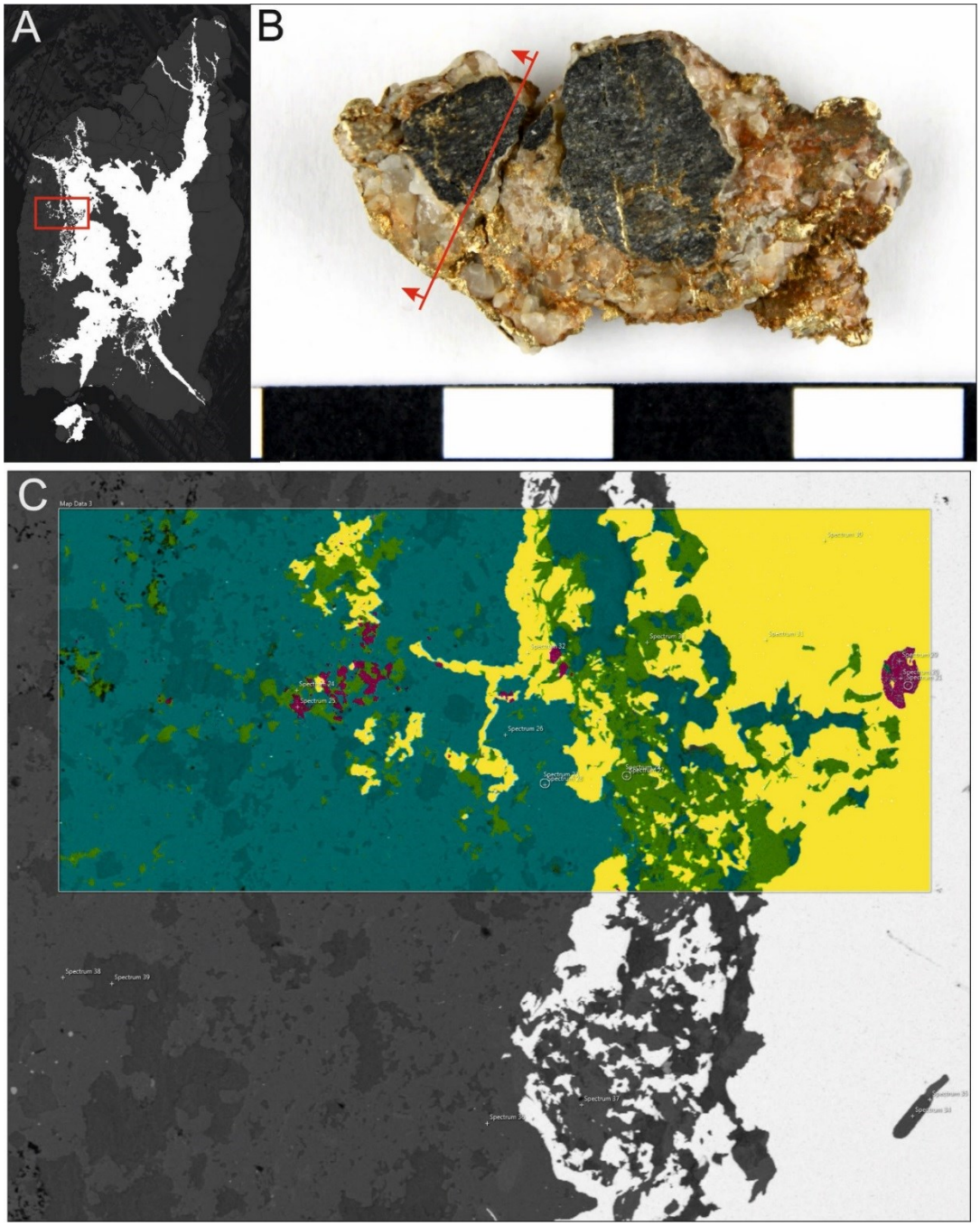

Figure 6.8 – A. BSE montage image of polished block cut from the Otter Creek placer nugget B. Photograph of the donated placer nugget before sectioning to investigate the gold composition and lithological attachments (red line in B shows location of the face of the polish block). C. BSE image with EDX phase map overlaid showing the interface between the host rock and the gold. On the map yellow indicates gold alloy, teal is quartz, green is muscovite and purple is apatite.

6.3.2 Placer Gold Sampling

A total of 812 gold particles collected from 12 locations within the Atlin area were sampled to characterise the composition of detrital gold from eight drainage systems

which host economically viable placer resources. The drainage samples are shown in figure 6.5, and their locations encompass the geographic extent of commercial mining operations existing within the Atlin gold camp, see figure 6.2 and table 6.2. This study has drawn upon both materials collected in the 2016 season and samples previously donated to Leeds University by Fionnuala Devine and subsequently mounted and analysed by Dr Rob Chapman, indicated in table 6.2.

6.3.2.1 Gold Particle Morphologies

The samples collected in 2016 were mounted by the author using the same procedure to facilitate comparison. Detrital gold collected from all the sample sites exhibited a range of morphologies, examples of which are shown in figure 6.8. Where single populations of particles exhibited clear morphological subgroups, these were mounted separately to evaluate the potential influence of multiple sources.

Examining the samples collected in 2016, shown in figure 6.9 and 6.10, a range of morphologies were observed from hackly, angular particles with mineral attachments to flattened platy particles. Spruce Creek was observed to have the largest range of morphologies, with both endmember morphologies existing in a single sample, images C, G and I in figure 6.10. The remaining 2016 samples contained a less extreme range of gold particle morphologies, with the median observed morphology being a smooth rounded oblate spheroid, examples of which are shown in plates C and E of figure 6.9. The range of gold particle morphologies observed are compatible with fluvial transport, where the particles become progressively flattened with increasing deformation (Knight et al., 1999, McCready et al., 2003).

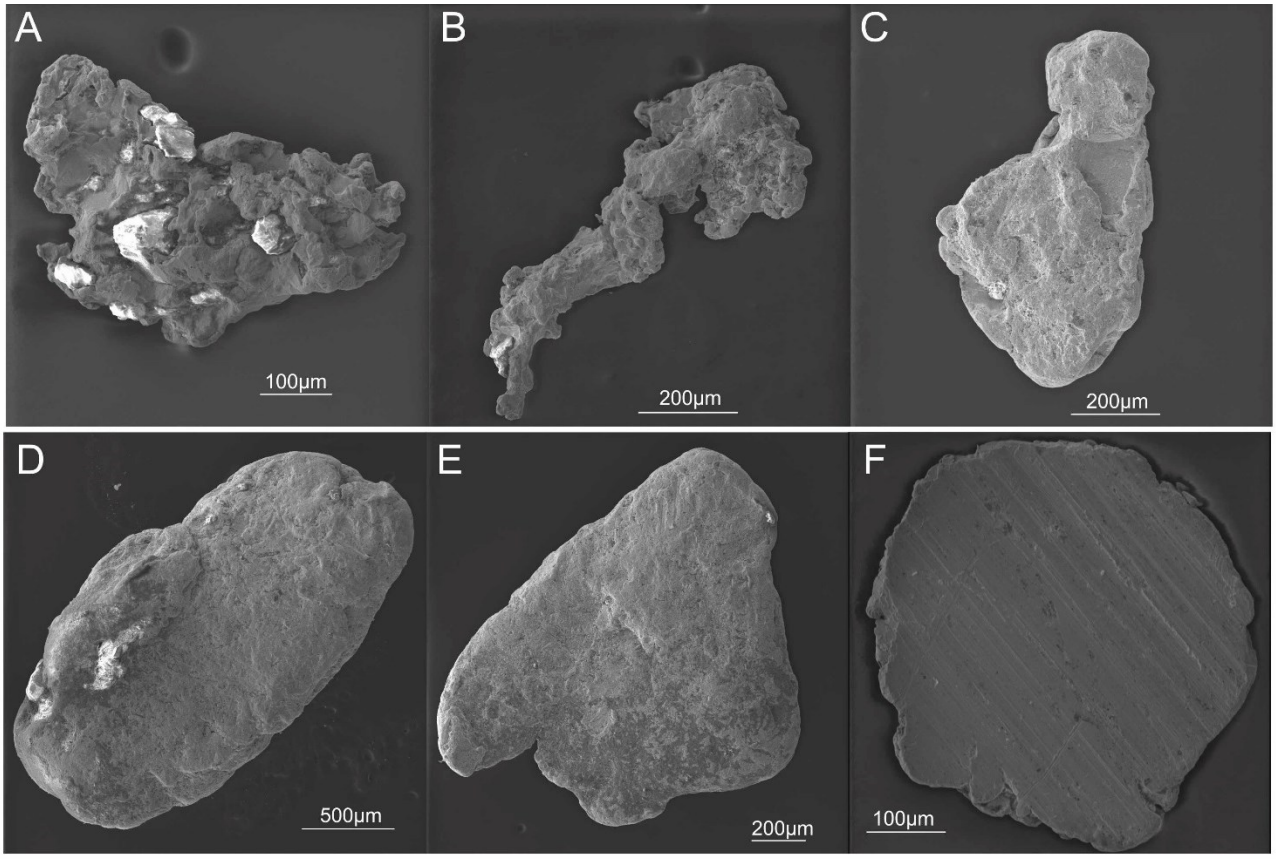

Figure 6.9 – SEM SE images of gold particles, illustrating the general range of gold particle morphologies observed from Spruce Ck (A, B, F) and Otter Ck (C, D, E). Fig 4 A-C shows equant particles with hackly and rough surface textures. Fig. 4A has attachments of quartz, which indicates proximal sourcing. Fig. 4D-F illustrates progressively flattened forms with tool marks.

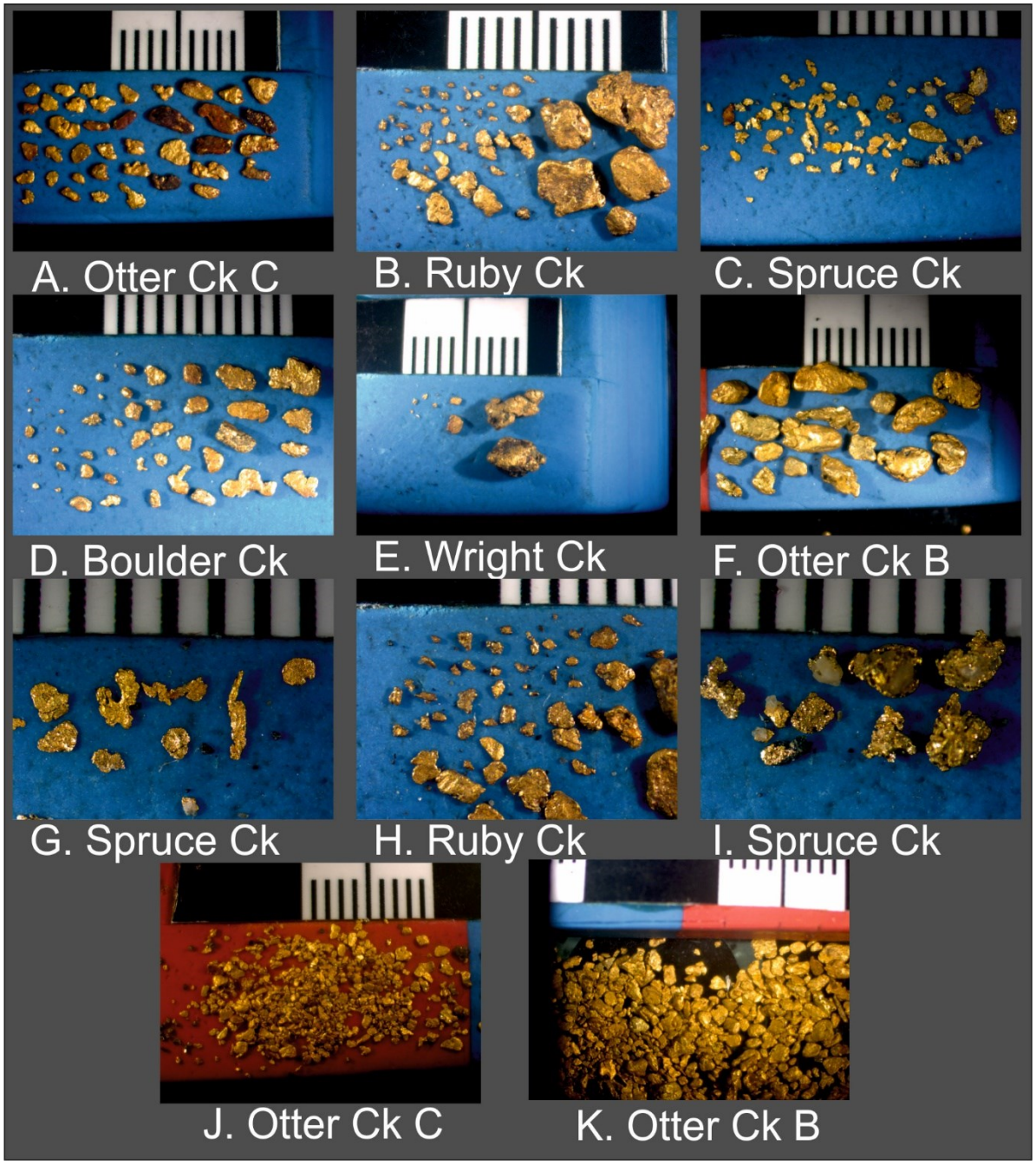

Figure 6.10 – Images of gold particles from different drainages in the Atlin gold camp showing the range of size and morphology of the samples.

6.3.2.2 Gold Composition

All the gold particles in the sample populations were analysed to determine the major element composition (gold and silver proportions) using an electron microprobe. Descriptive statistical parameters of silver compositions of each sample population are shown in table 6.3, and the data is plotted visually on figure 6.11 and 6.12.

Table 6.3 – Tables listing the silver composition (wt%,) values of simple statistical measures by sample for the Atlin gold camp.

Sample	N total	Mean	Standard Deviation	SE of mean	Lower 95% CI of Mean	Upper 95% CI of Mean
Ruby Ck B	54	22.1	8.9	1.2	19.6	24.5
Wright Ck A	81	19.5	8.7	1.0	17.5	21.4
Wright Ck B	8	20.2	5.5	1.9	15.6	24.7
Ruby Ck A	31	22.8	8.0	1.4	19.9	25.8
Quartz Ck	98	21.3	9.1	0.9	19.4	23.1
Pine Ck	26	19.7	8.4	1.6	16.3	23.1
Otter Ck C	109	19.6	8.9	0.9	18.0	21.3
Otter Ck B	132	19.1	7.2	0.6	17.8	20.3
Otter Ck A	63	19.9	8.9	1.1	17.7	22.2
Spruce Ck	76	19.9	10.5	1.2	17.5	22.3
Feather Ck	40	16.9	6.1	1.0	14.9	18.8
Boulder Ck B	27	21.4	6.9	1.3	18.6	24.1
Boulder Ck A	89	20.8	6.4	0.7	19.5	22.2

Sample	Minimum	1st Quartile (Q1)	Median	3rd Quartile (Q3)	Maximum	Interquartile Range (Q3 - Q1)	Range (Maximum - Minimum)
Ruby Ck B	4.9	17.7	20.5	25.9	45.7	8.2	40.7
Wright Ck A	0.6	14.8	19.5	25.0	39.3	10.1	38.6
Wright Ck B	11.2	16.9	20.7	23.2	28.8	6.4	17.6
Ruby Ck A	9.1	18.6	21.2	28.0	49.1	9.4	40.0
Quartz Ck	2.3	15.1	21.5	26.4	43.6	11.4	41.3
Pine Ck	0.3	14.5	20.4	25.4	37.0	10.9	36.7
Otter Ck C	0.3	13.0	19.0	24.9	41.4	11.9	41.2
Otter Ck B	2.0	15.9	20.0	23.0	41.0	7.1	39.0
Otter Ck A	1.3	14.1	22.0	24.8	44.5	10.7	43.2
Spruce Ck	0.2	12.5	18.8	25.6	46.5	13.1	46.3
Feather Ck	6.4	12.0	15.7	22.3	29.2	10.3	22.8
Boulder Ck B	3.2	18.3	21.6	23.2	38.0	5.0	34.8
Boulder Ck A	3.5	18.3	21.1	24.4	40.7	6.1	37.2

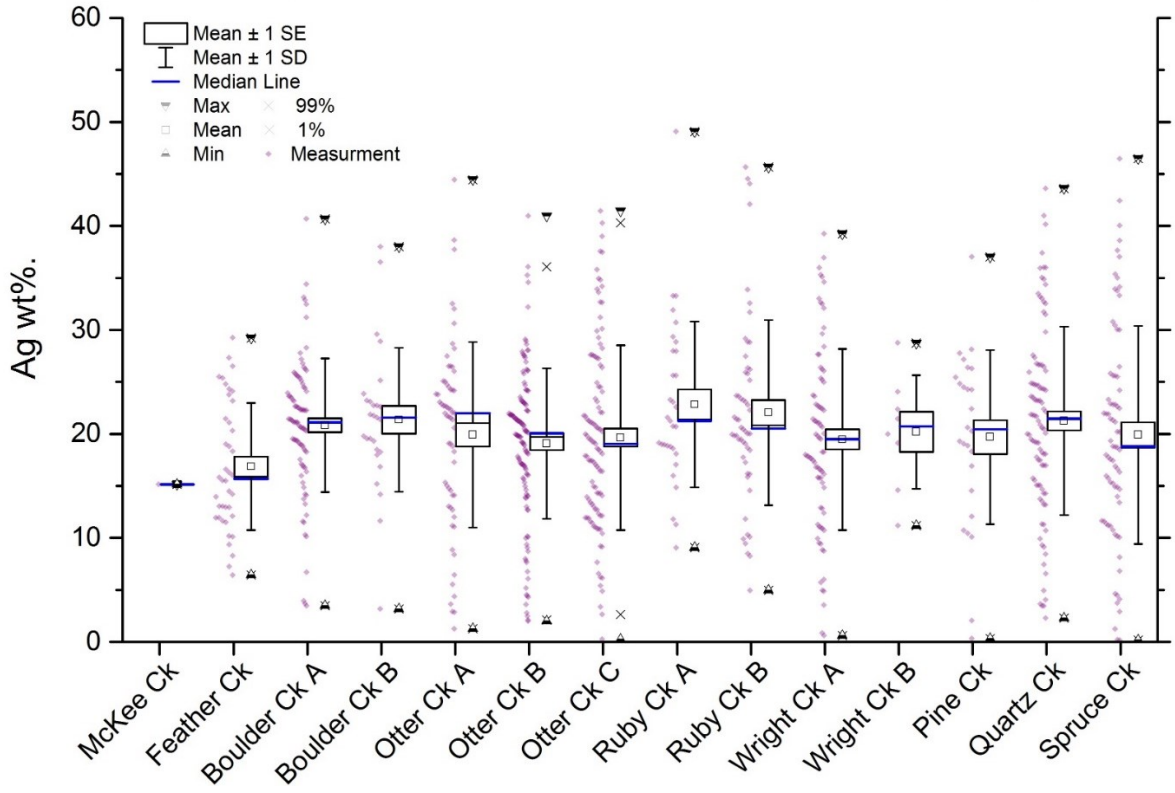

Figure 6.11 – Box plots with Ag composition of the individual gold particles shown for each sample site (purple dots) from each sample site. The values of the parameters used to construct the plot are shown in table 6.3, with the exception of mc Kee creek which has an insufficient sample size.

The populations from the Atlin Camp are found to have similar populations in respect to the silver composition of the gold particles, with the exception of Feather creek that has some distinctions from the other samples, see the map of figure 6.2. The mean and median values are similar with all the samples medians between 18.8 and 22 % wt Ag, again with the exception of the Feather creek at 15.7 % wt Ag. The results of Kolmogorov–Smirnov (K-S) tests, table 6.4, demonstrates that Feather creek samples are significantly different from the main Atlin distribution observed in most of the drainages, figure 6.11 and 6.13.

To evaluate whether or not the gold in the drainages could be sourced from a common population, statistical investigations of the dataset were undertaken, using Origin Pro 9.1 software. Figure 6.11 presents descriptive statistics (see table 6.3 for values) for each drainage, showing the mean, median, standard deviation (SD) and standard error (SE) of the mean. The standard error is defined as $(SE) = SD/\sqrt{n}$, where n is the sample size, and SD is the standard deviation. The standard error is beneficial, as it represents a measure of the statistical accuracy of the mean of the sample, which is theoretically equal to the standard deviation of the distribution of means that would be obtained from many random samples of size.

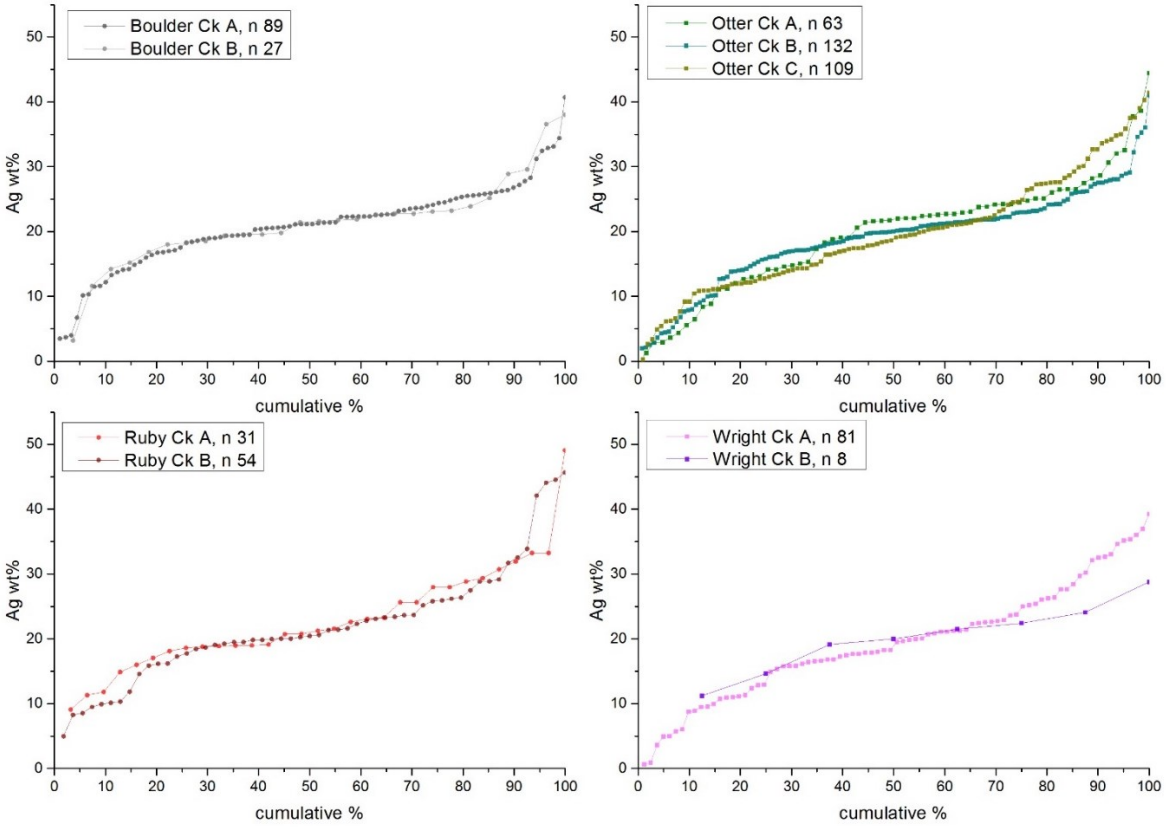

Figure 6.12 – Cumulative frequency plots of silver composition for the four drainages showing reproducibility of the silver distributions where multiple samples have been taken.

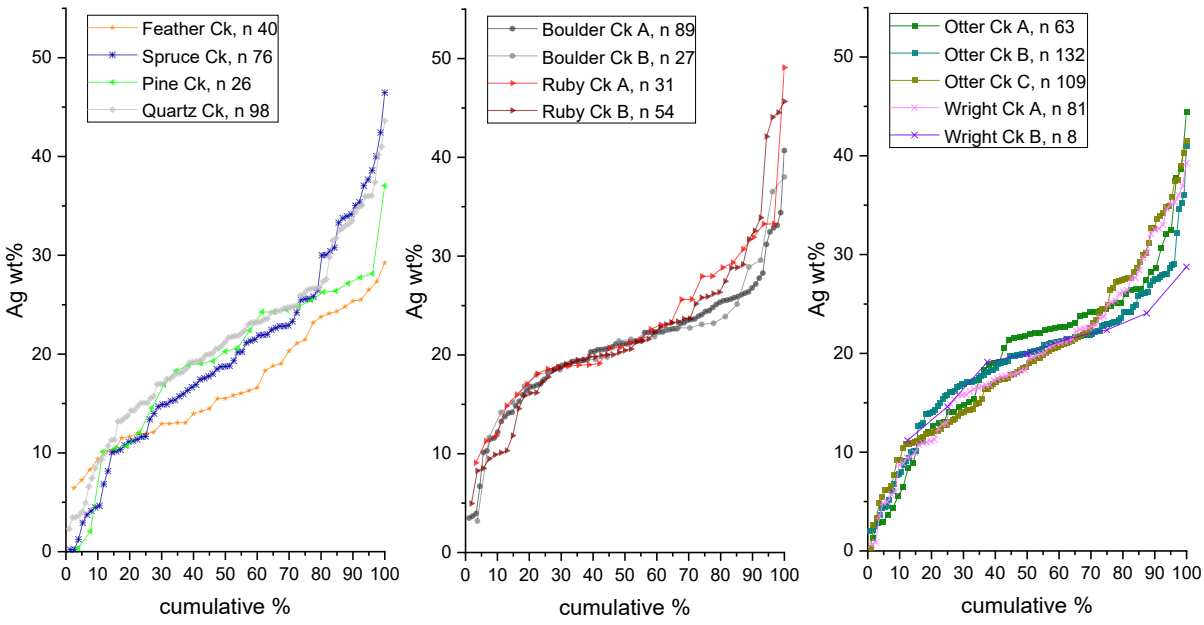

Figure 6.13 – Cumulative plots of the silver distributions of all the Atlin detrital gold Samples.

Table 6.4 – Matrix of K-S pairs results showing the obtained P-values. Values coloured red indicate that the samples are statistically diffent using a 0.05 confidence limit.

K-S	Boulder Ck A	Boulder Ck B	Spruce Ck	Otter Ck A	Otter Ck B	Otter Ck C	Pine Ck	Quartz Ck	Roby Ck A	Ruby Ck B	Wright Ck A	Wright Ck B	Feather Ck
Boulder Ck A													
Boulder Ck B	0.957												
Spruce Ck	0.019	0.050											
Otter Ck A	0.235	0.352	0.369										
Otter Ck B	0.058	0.419	0.091	0.047									
Otter Ck C	0.014	0.061	0.905	0.043	0.230								
Pine Ck	0.579	0.382	0.553	0.711	0.112	0.521							
Quartz Ck	0.262	0.400	0.364	0.741	0.011	0.116	0.718						
Roby Ck A	0.214	0.484	0.070	0.284	0.169	0.053	0.463	0.494					
Ruby Ck B	0.658	0.812	0.085	0.354	0.289	0.052	0.775	0.753	0.958				
Wright Ck A	0.009	0.092	0.914	0.098	0.452	0.810	0.438	0.209	0.053	0.050			
Wright Ck B	0.990	0.987	0.614	0.903	0.964	0.630	0.563	0.694	0.816	0.938	0.689		
Feather Ck	0.000	0.002	0.138	0.016	0.003	0.089	0.048	0.004	0.001	0.002	0.051	0.149	

The results of repeat sampling, figure 6.12, indicate that the gold particles in the different locations within each drainage are derived from a single population, and can therefore be combined to generate a composite sample representative of the drainage. In addition, this result implies that where only a single sample taken in a drainage that sample is representative of that drainage.

Examination of the plots and descriptive statistics, table 6.3 and figure 6.13, reveals that the drainages all have non-normal monomodal distributions, with a strong central peak, indicated by small interquartile ranges (Q1-Q3) between ~7 to 13 wt% Ag around a narrow range of mean values, 19.1 – 22.8 wt% Ag (excluding, Feather Creek 16.9 wt% Ag) and median values, 18.8-22.0 wt% Ag (excluding, Feather Creek 15.7 wt% Ag). This is clear on the cumulative frequency plots, because the plots clearly follow a consistent trend between the 25-75% ranges.

However, there are some differences in the gold alloy signatures between different drainages. The differences between drainages are specifically in the high/low silver Ag parts of the sample populations. Comparing the two individual Boulder Creek samples and three individual Otter Creek samples, which are the best sampled drainages, a visual difference in the distributions is observed, figure 6.14. Examining the distributional plots of the samples, from Boulder creek and Otter Creek, the spread in the distributions within a single drainage is smaller than the difference observed between the drainages. However, K-S testing shows that the samples are not significantly different and the observed differences are compatible with the variation expected if the populations were samples from a single master population. It is therefore concluded that while the data indicates differences, these cannot be demonstrated as statistically significant without sampling a larger number of gold particles, as the probability that the difference is caused by sub sampling remains.

Considering the other drainages in the context of the low silver results described above; Ruby Creek, located next to Boulder Creek, has a similar distribution to the Boulder Creek population while the other drainages appear to follow the low silver component of the distributions found in the Otter Creek sample populations, figure 6.14. This supports the unproven inference that a minor local modification of the mineralisation in the north of the camp, on the northern shore of Lake Superior, vs the rest of the Atlin district, see figure 6.5.

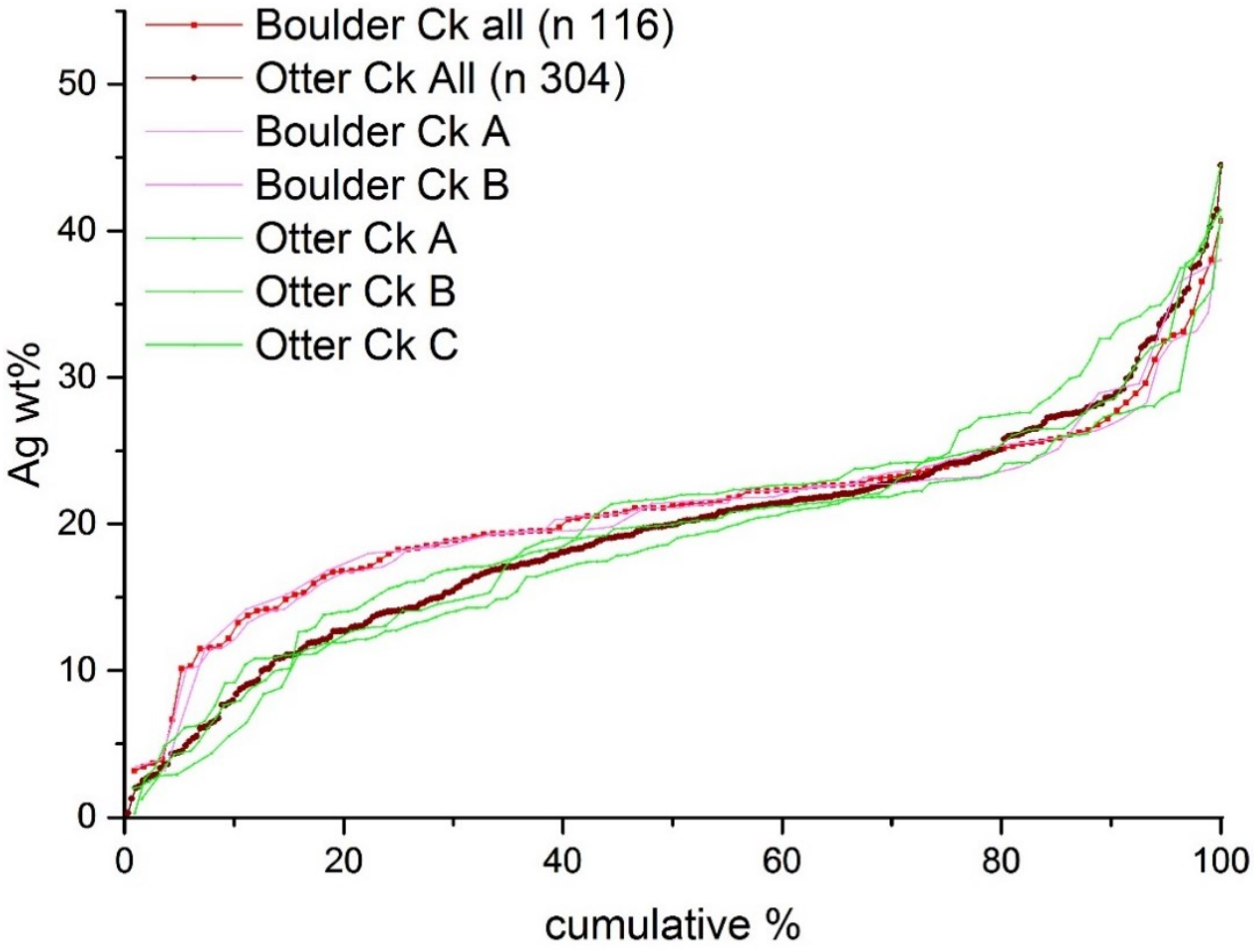

Figure 6.14 – Comparison of the distributions of gold of different silver composition

6.3.2.3 Laser ablation analysis of gold particles compositions

To investigate if additional elements in the gold alloy would provide further information to assist in characterization of gold populations, 117 gold particles from 6 different drainages across the camp were analysed using a LA-ICP-MS system. The laser ablation system provides much lower detection limits than was available using an EMPA by ablating the sample and processing it through a mass spectrometer, a typical ablation pit is shown in figure 6.15.

The LA-ICP-MS analysis found that only 5 elements, Au, Ag, Cu, Sb and Hg were observed above the detection limits in the majority of the particles (>85%), as shown in figure 6.16 and 6.17. These 5 elements commonly appeared to be in the gold alloy, indicated by a consistent ratio to Au during the analysis. This was in contrast to the other elements analysed for, which are recorded above detection in small proportions <35%, of the gold particles. Often these additional elements occurred with up to 21 other elements together in a single grain, as shown by the numbers of elements observed plotted as a histogram in figure 6.17.

Figure 6.15 – Secondary electron image of the site of a LA-ICP-MS analysis. The presence of multiple rims shows where the gold condensed (or melted instead of vaporising) at the edge of the pit. The pulsed nature of the laser has produced multiple levels of condensed gold in the pit which show that a single laser pulse has removed multiple microns depth of material from the base of the pit.

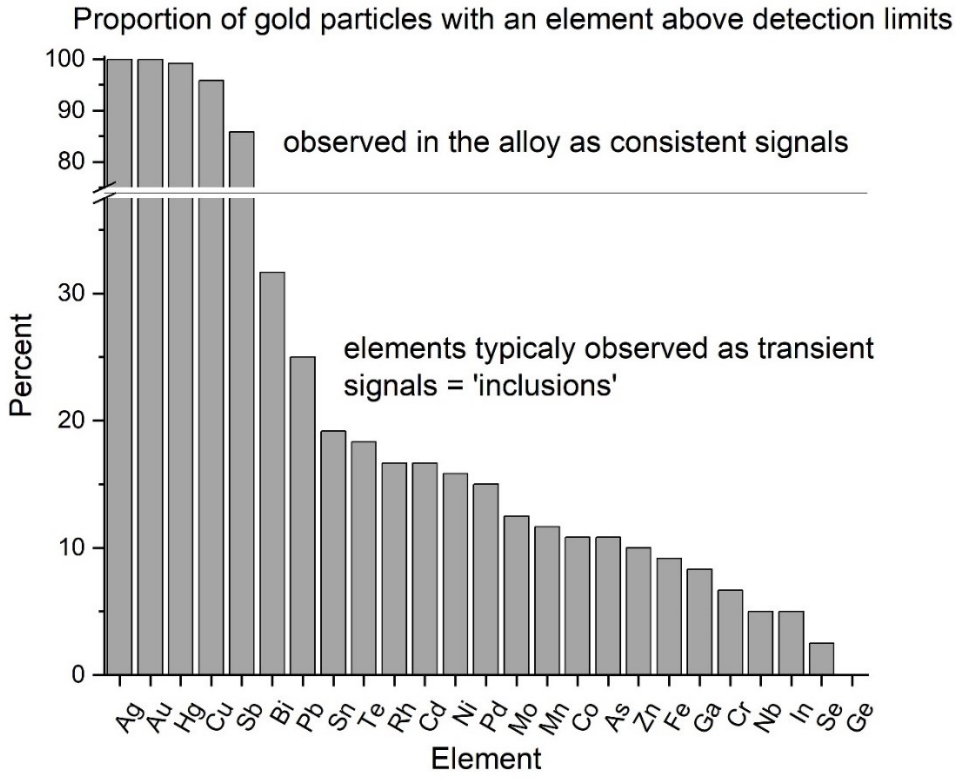

Figure 6.16 – Proportion of gold particles (n=117) from the Atlin camp which had an element above the detection limit of the LA-ICP-MS system.

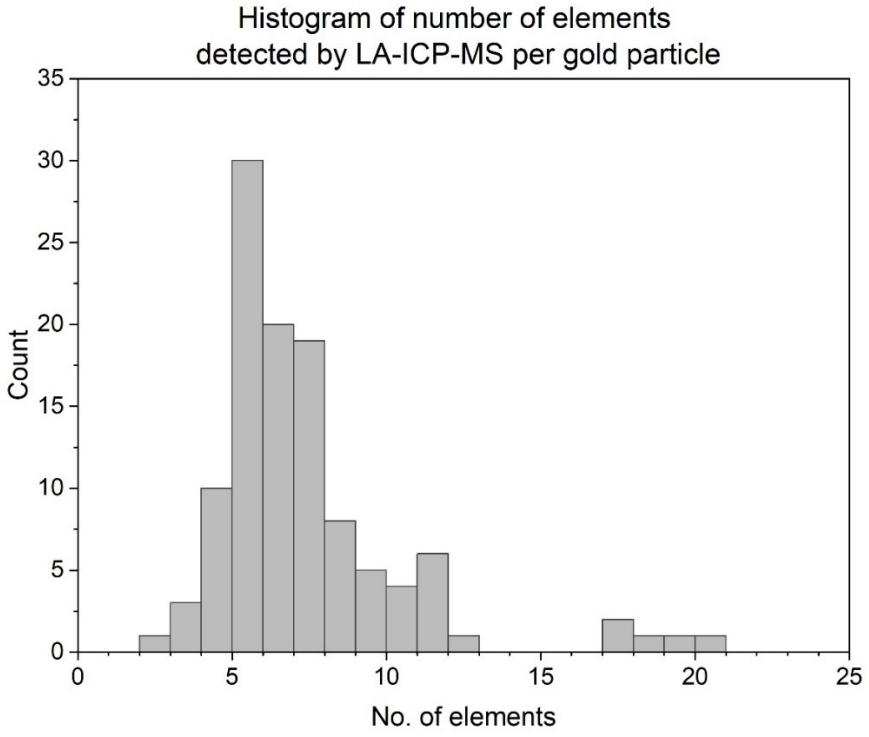

Figure 6.17 – Histogram showing the number of gold particles vs the number of elements above detection on the LA-ICP-MS for the Atlin area (n=117).

The reason these additional elements often appear together is that they are being hosted as exotic mineral phases in the gold alloy. The evidence for this interpretation is that the elements have transient signals, not constantly related to the Au counts, during the ablation of the gold grain. An example of this is shown in figure 6.18 where the counts for Au Ag Cu approximately co-vary over time whereas the counts for Fe (both 56 and 57) along with Hg are observed to have a distinct spike a in the second half of the ablation, indicating heterogeneity or a potential exotic mineral phase.

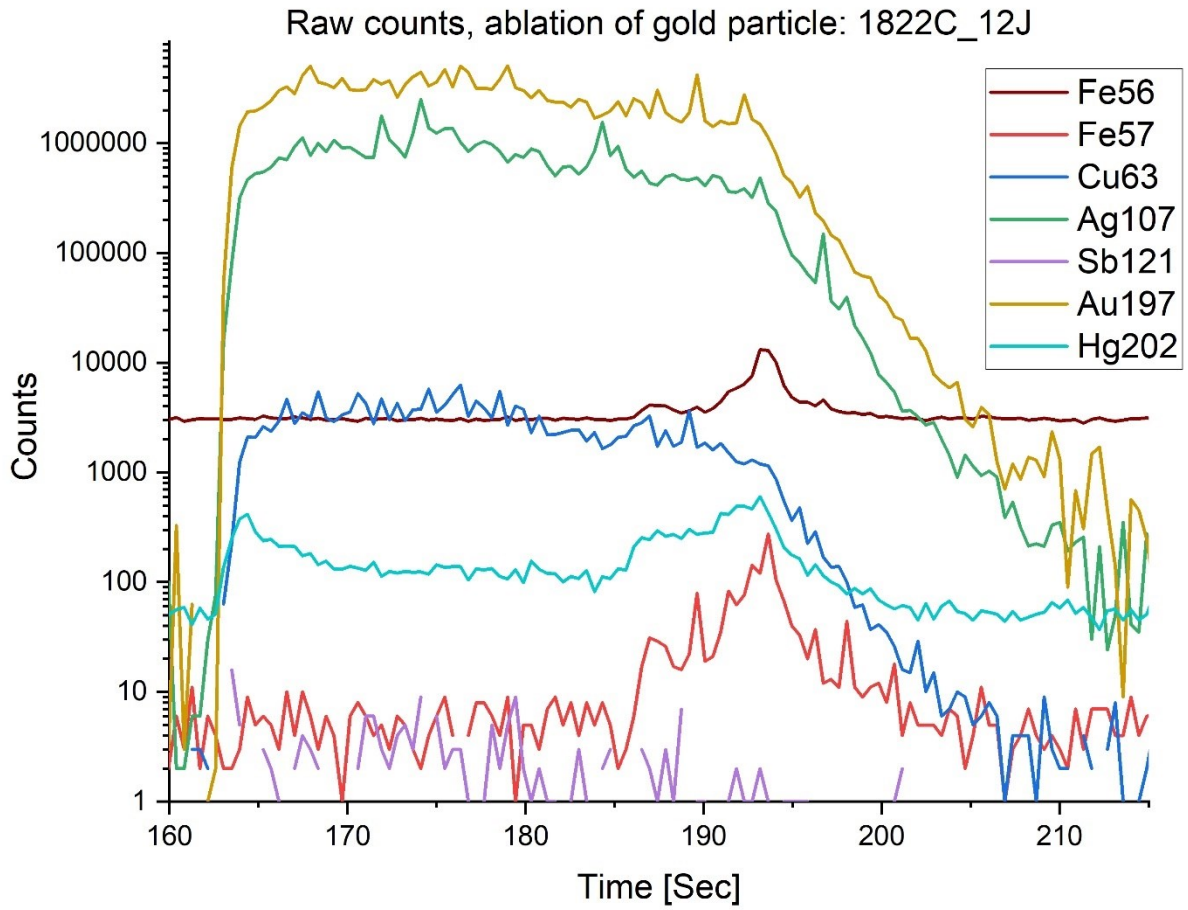

Figure 6.18 – Element counts recorded over the time period of a single laser ablation, gold particle from Feather Creek: 1822_12J. The Fe56 and Fe57 counts are not stable, in relation to the reference line (Au) over the period of ablation.

No clear correlations are observed between any of the three additional alloy hosted elements, Cu, Sb and Hg, and the major components of the gold particles (Ag/Ag), see scatter plot in figure 6.19. Examination of the distributions of individual additional alloy hosted elements for individual drainages was undertaken, see cumulative frequency plots in figure 6.19. Given the sample size of these sample populations all the distributions are consistent with the analysis based on only the Ag component. Specifically the gold samples are consistent with being sampled from a single master distribution.

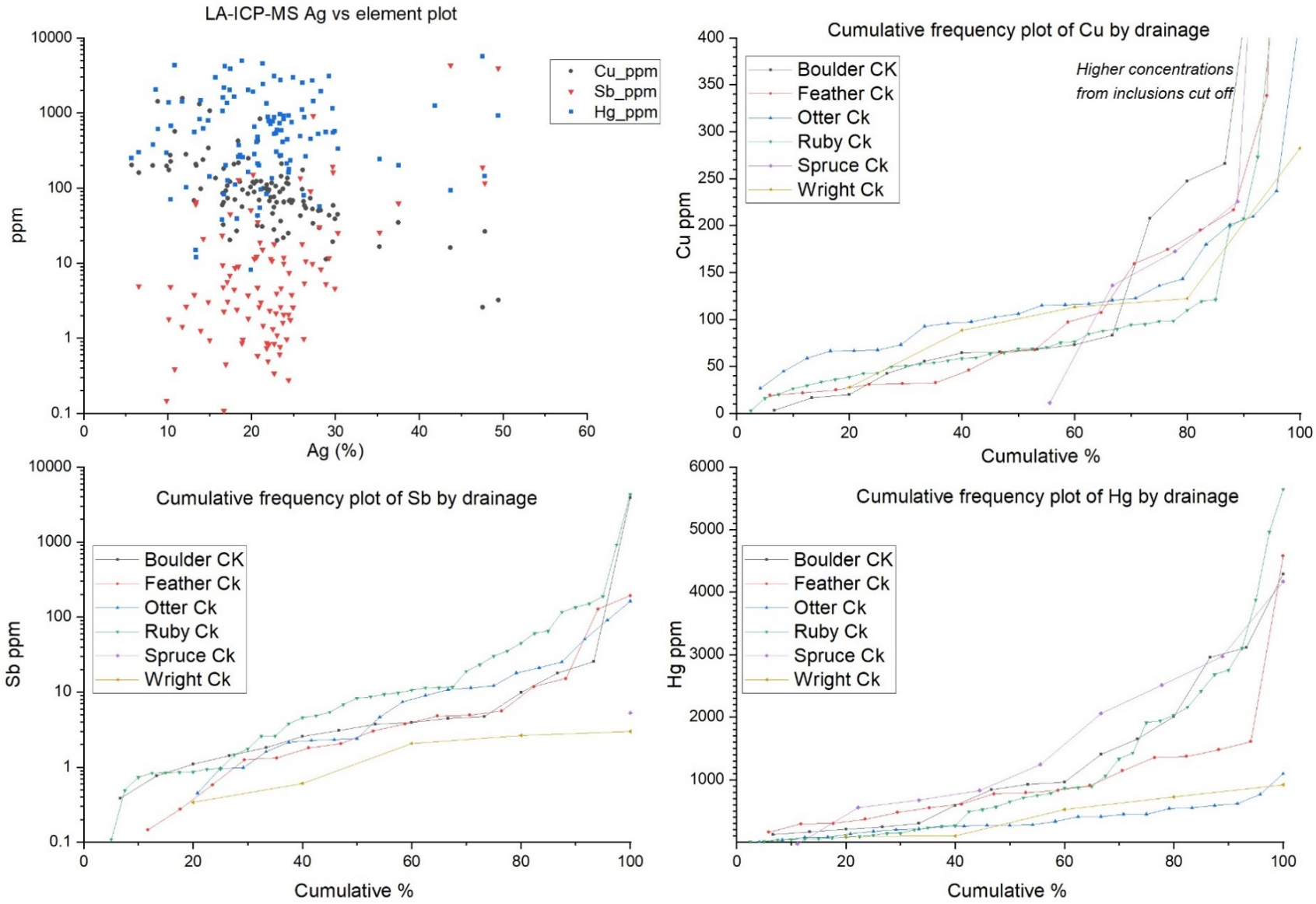

Figure 6.19 – Scatter plot of Sb, Cu and Hg vs Ag alongside cumulative frequency plots for individual elements grouped into populations for each drainage. No systematic relationship exists between Sb, Hg and Ag. A negative correlation is observed between the Cu and Ag, however this is a general feature of AuAgCu alloys and Cu does not differ between individual drainages.

6.3.2.4 Inclusions in detrital gold particles

Examination of the detrital gold particles using Scanning electron microscopy was conducted to examine 2-D homogeneity of the gold silver alloy, prior to EMPA analysis, and to identify inclusions/external mineral attachments which could provide additional data on the original hard rock source of the gold. Inclusions within the particle were divided into two categories, opaque 'ore mineral' phases and translucent mineral phases. These were treated differently with different methodologies applied to the two groups and each is discussed separately below.

At least one opaque mineral inclusion was observed in 10 percent of the detrital gold particles from the Atlin area. Figure 6.20 shows the number of inclusions observed plotted against the total number of gold particles, by drainage, demonstrating that all drainages have a consistent proportion of inclusions observed in the gold particles.

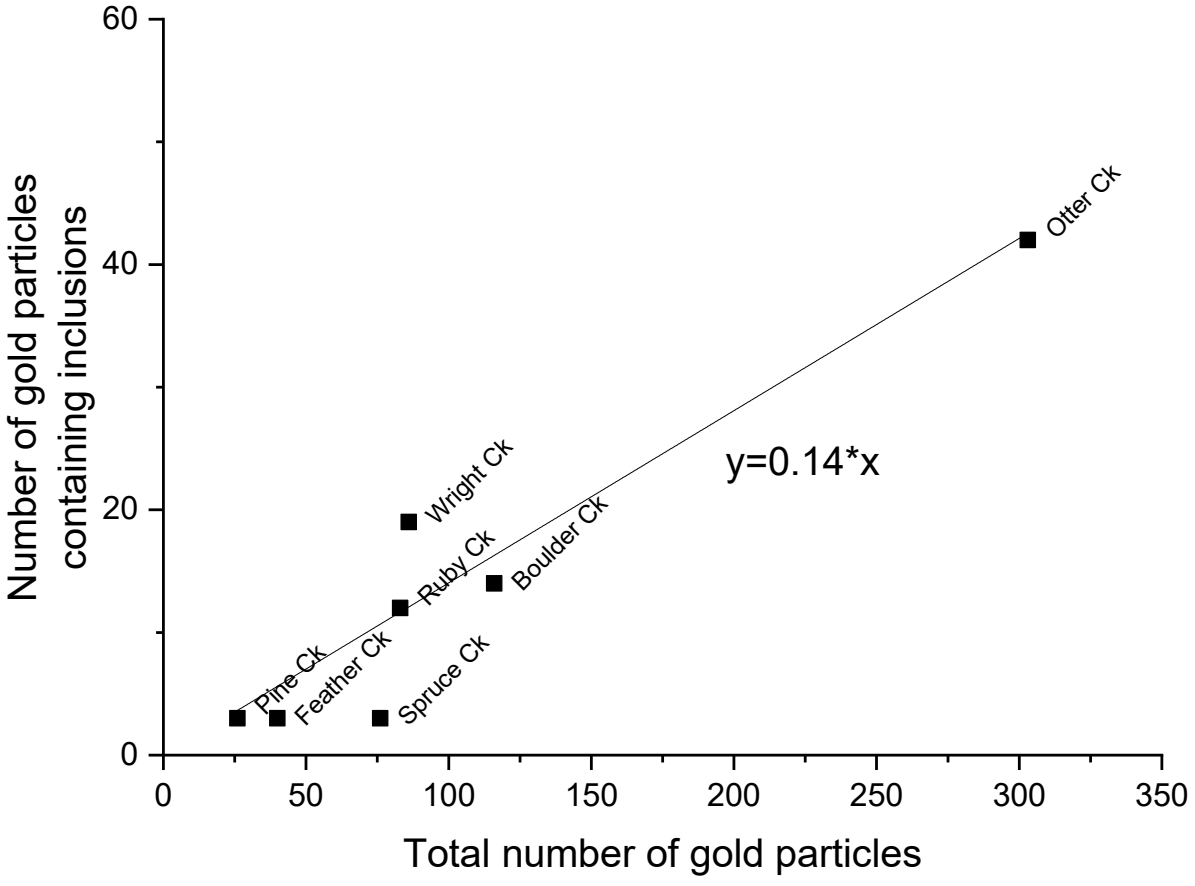

Figure 6.20 – Abundance of particles that have opaque inclusions present vs total population of particles from different drainages.

The Opaque minerals observed range between 5-300 μm in size and often had subhedral, rounded forms, see figure 6.21. The presence of any mineral within the gold was counted as 1 occurrence of the mineral, regardless of how many of that mineral were observed in the gold particle. The most commonly observed minerals were (Fe, Ni) sulphides and sulpharsenides specifically pyrite, pyrrhotite, arsenopyrite, gersdorffite (±Co), and pentlandite. In addition to the Fe and Ni bearing minerals, base metal sulphides such as, sphalerite, chalcopyrite and galena were observed along with Au, Ag Bi and Hg tellurides. Finally, an unidentified Pb-Cu sulphosalt and a Ni sulphosalt (containing minor Sb) were recorded in gold from the Otter, Ruby and Spruce Creek samples.

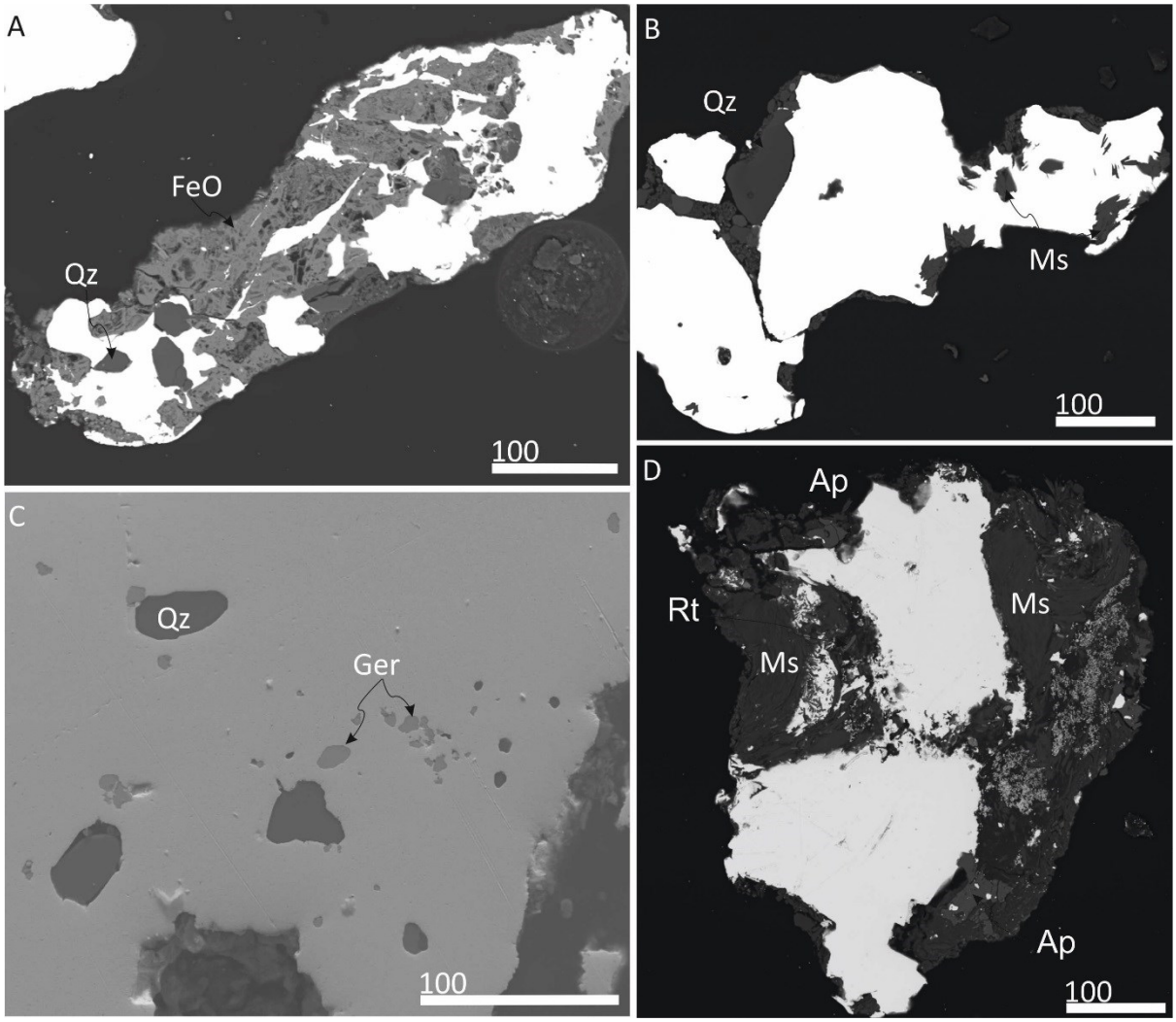

Figure 6.21 – BSE images of 3 gold particles (A-C) and a sample from the 2015 bedrock discovery on Otter Creek (D) showing examples of the attached and included minerals observed. A – Hackly gold with external attachments and inclusions of iron oxide (FeO) and quartz (Qz), from Spruce Creek. B – Gold particle with large, fractured attachment of quartz and euhedral inclusions of muscovite (Ms), from Spruce Creek. C – Abundant inclusions of gersdorffite (Ger) and Quartz, from Otter Creek. D – Section of fragment of composite bedrock/vein with visible gold from the Otter Creek 2015 discovery showing similar textures to the placer samples. Complex mineral attachments observed to contain; pyrite, chalcopyrite, K feldspar, rutile (Rt), Apatite (Ap), Zircon.

EDX analyses of mineral species is semi-quantitative, which does not provide accurate stoichiometry. Because of this the metals and anions present in inclusions are considered as present or absent when reporting elemental signature for an inclusion using the methodology of Chapman (2010). The data is presented in table 6.5 (and figure 6.22), which shows the number of gold particles that contained a mineral (or multiple minerals) incorporating that element. This data allows for a simple comparison of the metal or anion assemblage through the calculation of both a separate metal and anion 'score', which is the percentage of a specific element from total number of elements observed in a drainage. This has the benefit of allowing comparison between different sample sizes and allows the general character of the ore system, to be compared.

Metal scores are shown in table 6.5 and figure 6.22 for grouped drainages. The data shows no subdivisions of the drainages can be made based solely on the types of inclusions present. The comparison of inclusions in samples with a small number of gold particles (<30) is difficult as the inclusions observed are likely to be unrepresentative, due to exponentially decreasing chances of sampling rare inclusions with decreasing sample sizes. However, despite limitations created by using smaller sample sizes the inclusion dataset appears broadly consistent for the different drainages and this reinforces the consistencies between drainages observed in the compositional data.

Table 6.5 (A) – Counts of inclusions analysed which contained a specific metal grouped by drainage, used to calculate the values shown in figure 6.22.

Creeks	Fe	Ni	Bi	Cu	Pb	Co	Ag	Au	Hg	Zn	Total
Boulder Ck	8	3	0	0	1	1	1	0	0	0	14
Otter Ck	25	7	0	6	1	0	0	1	1	1	42
Pine Ck	2	0	0	1	0	0	0	0	0	0	3
Quartz Ck	11	3	0	2	1	1	0	0	0	1	19
Ruby Ck	6	3	0	1	0	1	0	0	0	1	12
Spruce Ck	1	1	0	1	0	0	0	0	0	0	3
Wright Ck	9	0	0	5	4	0	1	0	0	0	19
Feather Ck	2	0	0	0	1	0	0	0	0	0	3
All	64	17	0	16	8	3	2	1	1	3	115

Table 6.5 (B) – Counts of inclusions analysed which contained a specific anion grouped by drainage, used to calculate the values shown in figure 6.22.

Creeks	As	Sb	S	Te	Total
Boulder Ck	3	0	10	1	14
Otter Ck	6	1	28	1	36
Pine Ck	0	0	2	0	2
Quartz Ck	3	0	12	0	15
Ruby Ck	2	0	8	0	10
Spruce Ck	1	1	3	0	5
Wright Ck	1	2	10	0	13
Feather Ck	1	0	3	0	4
All	17	4	76	2	99

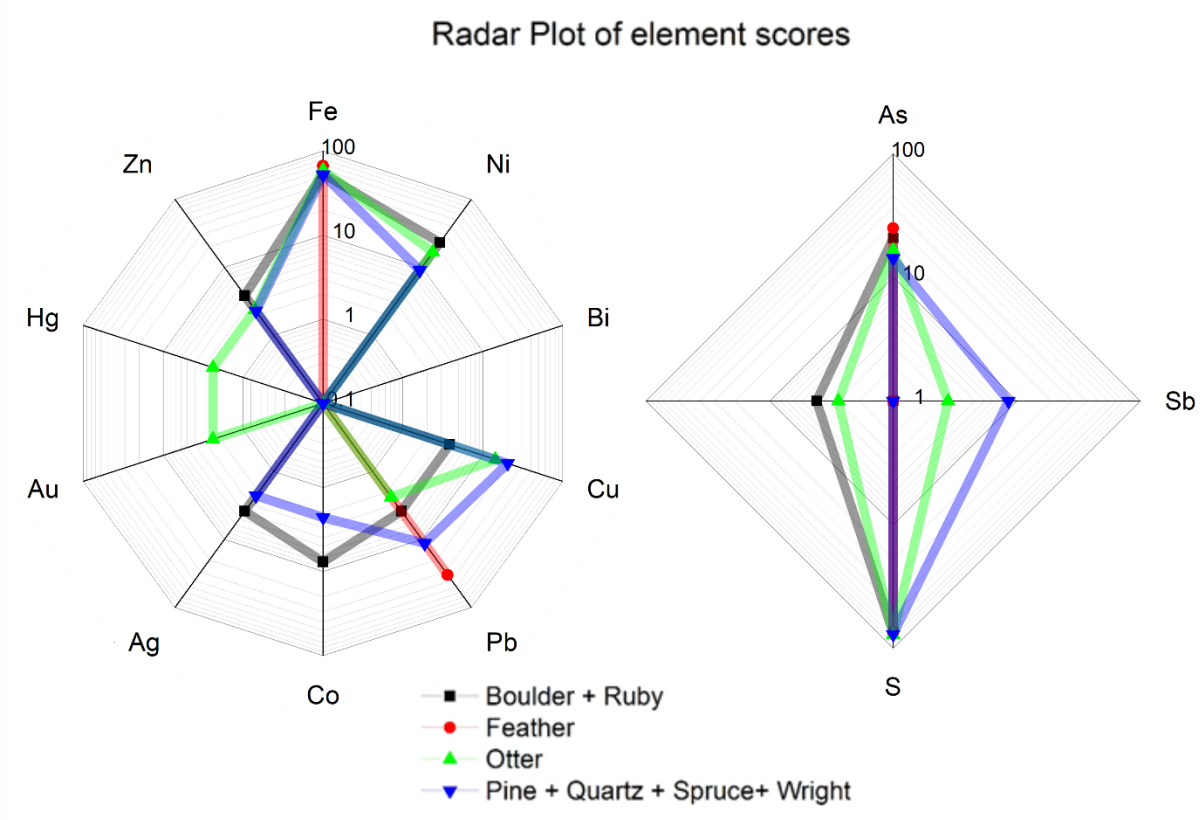

Figure 6.22 – Log plots showing the proportions of metals (left) and anions (right) observed within ore inclusions in grouped drainages. Minor differences are observed in the values for the data, with Co and Hg notable. Values shown are percent of total metals (or anions) allowing comparison between samples of different sizes.

In addition to the opaque minerals many of the particles were observed to have transparent minerals attached to the surface or within sectioned particles. The assemblages and textures observed in these transparent mineral attachments/ inclusions are complex, with (commonly weathered) polymineralic attachments often observed in larger equant gold particles, figure 6.21. In some cases, these silicate attachments/inclusions make up a significant proportion of the gold particle by area, >20%. The abundance of such transparent mineral attachments (and/or inclusions) presents a challenge for statistical analysis and recording, as they are far more common and numerous than the opaque inclusions. Due to this, transparent minerals were not recorded in a systematic way, as was conducted for opaque phases, as this was not practicable given the resources available.

Although not robustly recorded in this study transparent mineral assemblages have the potential to provide additional information on the providence of the gold in the same way as opaque minerals have been used in other studies (Chapman et al., 2021). To investigate this an analysis of a subset of 87 gold particles, observed to contain attachments/inclusions of transparent minerals within gold particles, was undertaken using a SEM. The particles were imaged, and individual phases identified using EDX spectroscopy. The results give a general impression as to the nature of the complex lithic assemblages.

The most common minerals observed within the gold were quartz, muscovite, carbonates (calcite and/or dolomite) and plagioclase feldspars (albite), often as monomineralic euhedral inclusions, figure 6.21. In addition to monomineralic inclusions, transparent minerals occurred within complex polymineralic, ‘lithic’, inclusions. Limited examinations of the complex ‘lithic’ assemblages was undertaken to investigate the possibility of quantifying mineral assemblage’s indicative of specific lithologies. The minerals observed in polymineralic assemblages were; feldspars (range of Na/Ca compositions), iron oxides, chlorites, clinozoiesite/epidote, pumpellyite, potassium feldspar, dolomite, calcite, titanium oxides, kaolinite (+ a range of unidentified clay minerals), amphiboles, pyroxenes, zircon, apatite, talc, serpentinite and olivine.

Whilst the list of minerals observed was extensive, no obvious correlative link to a specific lithology is documented in the Atlin area. It is noted however, that minerals which would indicate an ultramafic association (i.e. olivine/ serpentinite/ talc) host were rare, occurring in less than 2% of the 87 gold particles examined as a preliminary study. No inclusions that would clearly indicate an altered ultramafic listwanite association, specifically brucite or magnesite, were observed.

6.4 Discussion

The analysis of 849 detrital gold particles demonstrates that the populations of detrital gold particles in different drainages within the Atlin placer camp (excluding Feather creek which is considered separately) are indistinguishable on the basis of form, composition, and attached minerals. The gold has a wide range of alloy compositions, 0 to 45%wt. Ag, and analysis of the distributions reveal that the most common composition observed is around 21%wt. Ag.

The only possible differences from the rest of the camp (excluding Feather creek) were observed between the northern drainages, Ruby and Boulder Creeks which have higher proportions of low silver gold particles. However, the differences in the proportions are small, within the expected error indicated by the statistical investigation. They could be explained by random chance producing a similar variation in the samples in these 2 northern drainages. However, it cannot be definitely stated that the differences are not significant as they may be a result of local influence on the mineralisation. Further sampling would be required to investigate if the differences are repeatable and therefore represent a real difference in the gold populations. In all other respects the compositional profiles of gold particles from different drainages within the Atlin camp appear to be consistent.

The similarity of the gold alloy distributions in the different drainages was an unexpected result of the study. Published camp scale detrital gold studies in the literature reported larger, and in some cases considerable variation in gold alloy distributions observed in different drainages or even within a single drainage (Chapman et al., 2000, Chapman and Mortensen, 2006, Chapman et al., 2010). Studies on two gold camps in the Cordillera, Cariboo gold district (Chapman et al., 2011) and Klondike gold fields {Knight et al., 1999b, Chapman and Mortensen, 2010) both report multiple localised placer gold (compositional) signatures which are geographically constrained to small (up to several kilometres wide) areas within the gold district. No published studies have documented consistency in gold signatures on the 12Km+ scale that is documented here for the Atlin gold camp.

The similarity of the gold alloy compositional signatures from the Atlin camp drainages indicates that all the Atlin gold was most likely formed within a single mineralising ‘system’. This is because the range of geochemical conditions the gold alloy formed in must be comparable to produce consistent gold signatures. Given the wide geographic area, a single ‘deposit’ or vein source for all the gold is impossible and multiple sources must exist (Ash, 2004, Mihalynuk et al., 2017). The inference that multiple deposits/veins must exist is supported by reports of large nuggets recovered

from a wide range of the drainages across the Atlin area, as large, 30+ ounce. Gold nuggets of this size are unlikely travel significant distances even in high energy environments.

A single mineralising system, which could produce consistent proportions of gold at variable alloy compositions in multiple comparable veins distributed over a large 20+km^2 area, has not been previously inferred or identified. The Atlin camp gold appears to be uniquely consistent with respect to the gold compositional distributions and because the processes that control gold alloy compositions are known some inferences/insights into the nature and genesis of the mineralisation can be made. Alloy composition of gold is known to be dependent on the physiochemical conditions of the system it formed within (Gammons and Williams-Jones, 1995). The local geology, such as host lithology, has not had any impact on the physiochemical parameters known to control gold alloy compositions during the precipitation and deposition of the gold particles (specifically, the Eh, pH, and activity/speciation of S, Au and Ag within the ore fluids (Chudnenko and Pal'yanova, 2013, Pal'yanova and Kolonin, 2007)). It can therefore be deduced that the auriferous ore fluids gold precipitation mechanism is host rock independent of host lithologies during precipitation of the mineralisation. This indicates that minimal chemical alteration may create around the auriferous veins during the mineralisation event because chemical reactions with the host lithologies are not critical to gold precipitation. This is a fundamental observation with dramatic implications for the nature of the mineralisation and may explain why the hard rock ore veins have been so elusive to traditional exploration efforts so far.

If the local lithologies played a minimal role in the saturation and precipitation of gold particles, then the logical conclusion is that changes in the temperature and pressure are the key controlling factors that resulted in saturating the ore fluid and depositing the gold particles. Saturation and precipitation of gold in response to reducing pressures and temperatures is suggested by Sibson et al. (1988) and others to be a principal control of gold ore formation in mesothermal environments and has been identified as key to the formation of porphyry-epithermal deposits (Sillitoe, 1997). The fluid which transported the gold must be sourced from significantly deeper in the crust equilibrating with, and potentially altering, the crustal sequence during ascent (whilst retaining the ability to transport Au) before deposition was triggered by reduced solubility at lower temperatures/pressures higher in the sequence to form the Atlin mineralisation.

The interpretation that the Atlin camp formed from a single event contradicts the limited published studies on the known hard rock gold occurrences which have identified

multiple possible mineralisation ‘types’ in the Atlin area. The most recent work by Mihalynuk et al. (2017) proposed that the discovery of visible gold within shale hosted veins represented a new alternative source for the placer gold. This is distinct from the historical inferences the gold mineralisation was strongly associated to listwanite alteration of ultramafic units thought to be the main source of placer gold (Bloodgood et al., 1989, Hansen, 2005, Ash et al., 2001). Results from this study indicate that there should be no such distinction made based on host lithology for veins in the Atlin camp. All gold occurrences are related genetically and thus individual placers are part of a wider mineralising system.

The possibility that one style of mineralisation, either listwanite or shale hosted, is an insignificant contributor to the detrital gold population can tested by examination of the inclusions within the gold particles. It is noted that transparent inclusion assemblages which could indicate an ultramafic host were extremely rare in the particles examined. This could indicate that gold within listwanites provided an insignificant proportion of the Atlin gold. However, examination of the opaque mineral inclusions show that a significant proportion of nickel is present in the ore systems that deposited the gold, as evidenced by the presence of the nickel bearing mineral gersdorffite as inclusions within the gold alloys, table 6.5. This is unusual as nickel bearing phases are not commonly reported to this degree in detrital gold populations, in hydrothermal gold systems or in orogenic terranes (Chapman et al., 2021). An obvious source of nickel in the Atlin area could be fluid interactions with ultramafic or mafic lithologies, which could have occurred separately to the deposition, or sourcing, of the gold (Ash et al., 2001). Therefore, the evidence supports that the mineralising fluid has interacted with ultramafic rock but the precipitation of the gold mineralisation appears independent of a host rock chemistry due to pervasiveness of the mineralization across a wide area.

Another theory for the mineralisation in the Atlin camps is that it is related to the large, mineralised batholiths in the area. Sack and Mihalynuk (2003) suggested the batholiths as the source of the mineralising gold bearing fluids that produced the gold population in Feather Creek. This was partly based on observed external attachments of cassiterite, something that has not been observed elsewhere in the Atlin area. The gold signature of detrital gold in Feather Creek is similar to the other populations, but our work demonstrates it to be statistically different from the rest of the Atlin area, see figure 6.13 and table 6.4. While a batholithic source of the fluids is possible and could explain the unique population of gold particles in Feather Creek, data in this study indicates that the Feather Creek gold signature is distinct form the rest of the drainages. Therefore, the evidence of a batholithic fluid source should not be applied to other drainages in the rest of the camp without independent evidence in those

drainages. Considering the possibility of a batholithic fluid source, because our results show no spatial variation within the Atlin gold camp area, a proximal batholith as a source of auriferous fluids is regarded as unlikely. This is because fluids realised from an intrusion would be expected to undergo significant changes spatially, due to cooling and reactions associated with contact metamorphism in the aureole, as seen in the study of gold from the Cononish mine (chapter 3 and 4) and in many other intrusion related gold systems (Sillitoe and Thompson, 1998).

6.5 Conclusion

In conclusion, this study examining 849 detrital gold particles from the Atlin gold camp, indicates that all detrital gold (excluding Feather Creek) formed within a single mineralising system before erosion into the drainages. The results show that the gold occurrences within the camp may be related genetically as part of a wider system and has implications for the interpretation of the metallogeny of the Atlin area and northern Cache Creek Terrane.

The application of known physiochemical perimeters that control gold alloy compositions to detrital gold populations, as demonstrated in this study of the Atlin gold camp, can significantly advance the knowledge of mineralisation that can exists in an area. The ability to test hypothesis using information obtained from detrital studies can significantly aid exploration to developing targeting strategies and sampling programs tailored to a specific area. For example, in the Atlin area the interpretation that the Atlin gold formed as part of a single large gold mineralising system has commercial implications for mineral exploration. The results indicate that mineralisation is not constrained to specific ‘prospective’ lithologies, as was suggested previously (Sack and Mihalynuk, 2003, Mihalynuk et al., 2011, Mihalynuk et al., 2017, Ash et al., 2001, Bloodgood et al., 1989). Therefore, exploration should focus on improving knowledge and understanding of the structural controls of the ore fluids in the camp to identify potential deposits.

The results from the Atlin camp demonstrate how detrital gold studies can be conducted to provide information on the auriferous mineralisation in an area without well-defined or understood hard rock occurrences. The uses of statistical tests on the gold signatures (alloy compositions) of detrital samples provides a robust way to define the extent and nature of populations of gold particles. Once signatures are robustly established, examination of the nature of the identified gold signatures can be undertaken and by applying knowledge of the controls of gold alloy composition, insights into and constraints on the potential hard rock sources can be obtained.

References

AITKEN, J. D. 1959. *Atlin map area, British Columbia*, 1:253,440.

ASH, C. 2004. Geology of the Atlin area, northwest British Columbia. *BC Ministry of Energy, Mines and Petroleum Resources, BC Geological survey, Geoscience map 2004-4*.

ASH, C. H., MACDONALD, R. W. & REYNOLDS, P. 2001. *Relationship between ophiolites and gold-quartz veins in the North American Cordillera*, British Columbia, Ministry of Energy and Mines.

BALLANTYNE, S. B. & MACKINNON, H. F. Gold in the Atlin terran, British Columbia. *In:* CHATER, A. M., ed. Gold 86, 1986 Toronto, Ontario. Geological Association of Cannada Mineral Deposits Division.

BANKS, D., CHAPMAN, R. J. & SPENCE-JONES, C. 2017. Trace Element Quan. *AME Roundup 2017.* Vancover, BC.

BLOODGOOD, M. A., REES, C. J. & LEFEBURE, D. V. 1989. Geology of the Atlin Area (NTS 104N/11W,12E). *In:* MINES, B. M. O. (ed.).

CAIRNES, D. D. 1913. Portions of Atlin District, British Columbia: with special reference to lode mining. *Geological Survey of Canada, Memoir, Geological Series 22,* 37**,** 129.

CHAPMAN, R. J., BANKS, D. A., STYLES, M. T., WALSHAW, R. D., PIAZOLO, S., MORGAN, D. J., GRIMSHAW, M. R., SPENCE-JONES, C. P., MATTHEWS, T. J. & BOROVINSKAYA, O. 2021. Chemical and physical heterogeneity within native gold: implications for the design of gold particle studies. *Mineralium Deposita*.

CHAPMAN, R. J., LEAKE, R. C. & MOLES, N. R. 2000. The use of microchemical analysis of alluvial gold grains in mineral exploration: experiences in Britain and Ireland. *Journal of Geochemical Exploration,* 71**,** 241-268.

CHAPMAN, R. J. & MORTENSEN, J. K. 2006. Application of microchemical characterization of placer gold grains to exploration for epithermal gold mineralization in regions of poor exposure. *Journal of Geochemical Exploration,* 91**,** 1-26.

CHAPMAN, R. J., MORTENSEN, J. K., CRAWFORD, E. C. & LEBARGE, W. 2010. Microchemical Studies of Placer and Lode Gold in the Klondike District, Yukon, Canada: 1. Evidence for a Small, Gold-Rich, Orogenic Hydrothermal System in the Bonanza and Eldorado Creek Area. Economic Geology, 105, 1369-1392.

CHAPMAN, R. J. & MORTENSEN, J. K. 2011. Characterization of placer- and lode-gold grains as an exploration tool in east-central British Columbia (parts of NTS 093A, B, G, H). *Geoscience BC Summary of Activities 2010.* Geoscience BC.

CHAPMAN, R. J. & MORTENSEN, J. K. 2016. Characterization of Gold Mineralization in the Northern Cariboo Gold District, British Columbia, Canada, Through Integration of Compositional Studies of Lode and Detrital Gold with Historical Placer Production: A Template for Evaluation of Orogenic Gold. *Economic Geology,* 111**,** 1321-1345.

CHAPMAN, R. J., MORTENSEN, J. K., CRAWFORD, E. C. & LEBARGE, W. 2010. Microchemical Studies of Placer and Lode Gold in the Klondike District, Yukon, Canada: 1. Evidence for a Small, Gold-Rich, Orogenic Hydrothermal System in the Bonanza and Eldorado Creek Area. *Economic Geology,* 105**,** 1369-1392.

CHUDNENKO, K. & PAL'YANOVA, G. 2013. Thermodynamic properties of Ag–Au–Hg solid solutions. *Thermochimica Acta,* 572**,** 65-70.

CAIRNES, D. D. 1913. Portions of Atlin District, British Columbia: with special reference to lode mining. *Geological Survey of Canada, Memoir, Geological Series 22,* 37**,** 129.

DOSTAL, J., KEPPIE, J. D. & FERRI, F. 2009. Extrusion of high-pressure Cache Creek rocks into the Triassic Stikinia–Quesnellia arc of the Canadian Cordillera: implications for terrane analysis of ancient orogens and palaeogeography. *Geological Society, London, Special Publications,* 327**,** 71-87.

ENGLISH, J., MIHALYNUK, M., JOHNSTON, S. & A. DEVINE, F. 2001. *Atlin TGI Part III: Geology and Petrochemistry of Mafic Rocks Within the Northern Cache Creek Terrane and Tectonic Implications*.

ENGLISH, J., MIHALYNUK, M., JOHNSTON, S., ORCHARD, M., FOWLER, M. & LEONARD, L. 2018. *Atlin TGI, Part VI: Early to Middle Jurassic Sedimentation, Deformation and a Preliminary Assessment of Hydrocarbon Potential, Central Whitehorse Trough and Northern Cache Creek Terrane*.

ENGLISH, J. M., MIHALYNUK, M. G. & JOHNSTON, S. T. 2010. Geochemistry of the northern Cache Creek terrane and implications for accretionary processes in the Canadian Cordillera. *Canadian Journal of Earth Sciences,* 47**,** 13-34.

ERDMER, P., GHENT, E. D., MIHALYNUK, M. & CORDEY, F. 2000. *Coherent blueschist terrane, French range, British Columbia; Lithoprobe Slave/Northern Cordillera*.

GAMMONS, C. H. & WILLIAMS-JONES, A. E. 1995. Hydrothermal Geochemistry of Electrum - Thermodynamic Constraints. *Economic Geology and the Bulletin of the Society of Economic Geologists,* 90**,** 420-432.

GOLDFARB, R. J. & GROVES, D. I. 2015. Orogenic gold: Common or evolving fluid and metal sources through time. *Lithos,* 233**,** 2-26.

GROVES, D. I., GOLDFARB, R. J., GEBRE-MARIAM, M., HAGEMANN, S. G. & ROBERT, F. 1998. Orogenic gold deposits: A proposed classification in the context of their crustal distribution and relationship to other gold deposit types. *Ore Geology Reviews,* 13**,** 7-27.

HANSEN, L. D. 2005. *Geologic setting of listwanite, Atlin, BC: Implications for carbon dioxide sequestration and lode-gold mineralization.* University of British Columbia.

HANSEN, L. D., DIPPLE, G. M., GORDON, T. M. & KELLETT, D. A. 2005. CARBONATED SERPENTINITE (LISTWANITE) AT ATLIN, BRITISH COLUMBIA: A GEOLOGICAL ANALOGUE TO CARBON DIOXIDE SEQUESTRATION. *The Canadian Mineralogist,* 43**,** 225-239.

HOLLAND, S. S. 1950. Placer Gold Production of British Columbia.

JOHNSTON, S. & BOREL, G. D. 2007. *The odyssey of the Cache Creek terrane, Canadian Cordillera: Implications for accretionary orogens, tectonic setting of Panthalassa, the Pacific superwell, and break-up of Pangea*.

KIRBY, C. 2009. *Ruby Creek Molybdenum Project in Northern British Columbia, Canada. Adanac Molybdenum Corporation 43-101 Report.*

KNIGHT, J. B., MORISON, S. R. & MORTENSEN, J. K. 1999. The relationship between placer gold particle shape, rimming, and distance of fluvial transport as exemplified by gold from the Klondike district, Yukon Territory Canada. *Economic Geology and the Bulletin of the Society of Economic Geologists,* 94**,** 635-648.

KNIGHT, J. B., MORTENSEN, J. K. & MORISON, S. R. 1999b. Lode and placer gold composition in the Klondike district, Yukon Territory Canada: Implications for the nature and genesis of Klondike placer and lode gold deposits. Economic Geology and the Bulletin of the Society of Economic Geologists, 94, 649-664.

LEAKE, R. C., CHAPMAN, R. J., BLAND, D. J., CONDLIFFE, E. & STYLES, M. T. 1997. Microchemical characterization of alluvial gold from Scotland. *Transactions of the Institution of Mining and Metallurgy Section B-Applied Earth Science,* 106**,** B85-B98.

LEVSON, V. M. & BLYTH, H. 1993. Applications of Quaternary geology to placer deposit investigations in glaciated areas; a case study, Atlin, British Columbia. *Quaternary International,* 20**,** 93-105.

LEVSON, V. M. & BLYTH, H. 2001. Formation and preservation of a Tertiary to Pleistocene fluvial gold placer in northwest British Columbia. *Quaternary International,* 82**,** 33-50.

LOWE, C. & ANDERSON, R. G. 2018. *Preliminary interpretations of new aeromagnetic data for the Atlin map area, British Columbia*.

MARUD, D. E. S., PHILLIP J. 1989. Diamond Drilling and Geophysical Report on the Yellowjacket Group. *In:* MINES, B. M. O. (ed.). MALAVIEILLE, J. & TRULLENQUE, G. 2009. Consequences of continental subduction on forearc basin and accretionary wedge deformation in SE Taiwan: Insights from analogue modeling. *Tectonophysics,* 466**,** 377-394.

MARUD, D. E. S., PHILLIP J. 1989. Diamond Drilling and Geophysical Report on the Yellowjacket Group. *In:* MINES, B. M. O. (ed.).

MCGOLDRICK, S., ZAGOREVSKI, A. & CANIL, D. 2017. *Geochemistry of volcanic and plutonic rocks from the Nahlin ophiolite with implications for a Permo-Triassic arc in the Cache Creek terrane, northwestern British Columbia*.

MCCREADY, A. J., PARNELL, J. & CASTRO, L. 2003. Crystalline Placer Gold from the Rio Neuquen,Argentina: Implications for the Gold Budget in Placer Gold Formation. *Economic Geology,* 98**,** 623-633.

MCIVOR, D. F. 1989. Geophysical Survey Programs on the Yellowjacket North Property, North Summary Report: Geological Mapping, Lithogeochemical Sampling and and South Claim Groups. *In:* MINES, B. M. O. (ed.).

MCIVOR, D. F. 1989. Geophysical Survey Programs on the Yellowjacket North Property, North Summary Report: Geological Mapping, Lithogeochemical Sampling and and South Claim Groups. *In:* MINES, B. M. O. (ed.).

MIHALYNUK, M., JOHNSTON, S., LOWE, C., CORDEY, F., ENGLISH, J., A. M. DEVINE, F., LARSON, K. & MERRAN, Y. 2001. *Atlin TGI Part II: Preliminary Results from the Atlin Targeted Geoscience Initiative, Nakina Area, Northwest British Columbia*.

MIHALYNUK, M. & LOWE, C. 2018. *Atlin TGI, Part I: An Introduction to the Atlin Targeted Geoscience Initiative*.

MIHALYNUK, M. G., AMBROSE, T. K., DEVINE, F. A. M. & JOHNSTON, S. T. 2011. Atlin Placer Gold Nuggets Containing Mineral and Rock Matter: Implications for Lode Gold Exploration. *BC Ministry of Mines; Geological Fieldwork 2010*.

MIHALYNUK, M. G., SMITH, M. T., GABITES, J. E., RUNKLE, D. & LEFEBURE, D. 1992. Age of emplacement and basement character of the Cache Creek terrane as constrained by new isotopic and geochemical data. *Canadian Journal of Earth Sciences,* 29**,** 2463-2477.

MIHALYNUK, M. G., ZAGOREVSKI, A., DEVINE, F. A. M. & HUMPHREY, E. 2017. A new lode gold discovery at Otter Creek: Another source for the Atlin Placers. *BC Ministry of Mines; Geological Fieldwork 2016*.

MONGER, J. W. H. 1975. *Upper Paleozoic rocks of the Atlin terrane, northwestern British Columbia and south-central Yukon / J. W. H. Monger,* Ottawa, Dept. of Energy, Mines and Resources : available from Information Canada.

PAL'YANOVA, G. A. & KOLONIN, G. R. 2007. Geochemical mobility of Au and Ag during hydrothermal transfer and precipitation: Thermodynamic simulation. *Geochemistry International,* 45**,** 744-757.

PITCAIRN, I. K., TEAGLE, D. A. H., CRAW, D., OLIVO, G. R., KERRICH, R. & BREWER, T. S. 2006. Sources of metals and fluids in orogenic gold deposits: Insights from the Otago and Alpine schists, New Zealand. *Economic Geology,* 101**,** 1525-1546.

NELSON, J. & COLPRON, M. 2007. Tectonics and metallogeny of the British Columbia, Yukon and Alaskan Cordillera, 1.8 Ga to the present. *In:* GOODFELLOW, W. D. (ed.) *Mineral Deposits of Canada: A Synthesis of Major Deposit-Types, District Metallogeny, the Evolution of Geological Provinces, and Exploration Methods.* Geological Association of Canada.

NELSON, J. L. & BELLEFONTAINE, K. A. 1996. The geology and mineral deposits of north-central Quesnellia; Tezzeron Lake to Discovery Creek, central British Columbia. *British Columbia Ministry of Energy, Mines and Petroleum Resources,* Bulletin 99**,** 112.

RONNING, P. A. 1986. Diamond Drilling and Geophysical Report on the Yellowjacket Property. *In:* MINES, B. M. O. (ed.).

SACK, P. J. & MIHALYNUK, M. G. 2003. Proximal gold cassiterite nuggets and composition of the Feather Creek placer gravels: clues to a lode source near Atlin, BC. *In:* BC MINISTRY OF ENERGY, M. A. P. R., BRITISH COLUMBIA GEOLOGICAL SURVEY (ed.).

SIBSON, R. H., ROBERT, F. & POULSEN, K. H. 1988. High-angle reverse faults, fluid-pressure cycling, and mesothermal gold-quartz deposits. *Geology,* 16**,** 551-555.

SILLITOE, R. H. 1997. Characteristics and controls of the largest porphyry copper-gold and epithermal gold deposits in the circum-Pacific region. *Australian Journal of Earth Sciences,* 44**,** 373-388.

SILLITOE, R. H. & THOMPSON, J. F. H. 1998. Intrusion–Related Vein Gold Deposits: Types, Tectono-Magmatic Settings and Difficulties of Distinction from Orogenic Gold Deposits. Resource Geology, 48, 237-250.

STRUIK, L. C., SCHIARIZZA, P., ORCHARD, M. J., CORDEY, F., SANO, H., MACINTYRE, D. G., LAPIERRE, H. & TARDY, M. 2001. Imbricate architecture of the upper Paleozoic to Jurassic oceanic Cache Creek Terrane, central British Columbia. *Canadian Journal of Earth Sciences,* 38**,** 495-514.

WANG-SHI, W., STEVENS, C. H. & BAMBER, E. W. 1985. New Carboniferous and Permian Tethyan and Boreal Corals from Northwestern British Columbia, Canada. *Journal of Paleontology,* 59**,** 1489-1504.

Chapter 7 Discussion and Conclusions

The detrital gold and mineralogical studies of deposits presented in this work demonstrate that detrital gold samples can provide fresh insights into the auriferous systems that they are sourced from. Detrital populations, which contain a large number of gold particles, provide the best representative samples of gold particles from a deposit. When detrital sampling is combined with traditional mineralogical studies, this can provide information on the larger mineralising system which was not previously obtainable. Detrital gold studies have the potential to be used to classify and compare different auriferous deposits. This study demonstrates that detrital gold samples can be even more beneficial when paragenetically constrained gold particle data is available for an individual deposit, thereby allowing gold signatures on a deposit scale to be related to vein paragenetic assemblages.

The two mine studies undertaken at the Cononish and Curraghinalt mines examined the alloy composition of individual gold particles obtained from different veins and linked them to the detrital gold populations eroded from the deposits. Both studies demonstrate that silver concentration of the gold particles in thin sections can be related to parts of the vein paragenesis. Because gold composition is conserved into the detrital environment, comparison between gold particles in the detrital population and in situ allows evaluation of how prevalent the vein material sampled in thin section is on a deposit scale.

The adopted methodology allows small-scale in situ observations (such as hand specimens or thin sections) to be related and interpreted in the context of the wider mineralisation. This has the potential to address many problems inherent in current deposit studies such as difficulties obtaining representative samples of the mineralisation on a deposit scale. The observation that gold systems are complex ,and the physiochemical parameters that control gold composition are variable, is expected as many studies report evolving ore fluids within systems. Examples of deposit types for which this is applicable are: orogenic (LaFlamme et al., 2018, Groves and Vearncombe, 1990, Uemoto et al., 2002, Groves et al., 2003), Carlin type (Blamey et al., 2017) intrusion-related Au (Stephens et al., 2004, Hart and Goldfarb, 2005, Hart, 2007), epithermal (Heinrich, 2005, Smith et al., 2017, Canet et al., 2011) and porphyry (Sillitoe, 2010, Allan et al., 2011).

How representative a collected vein sample is, is currently dependent on the experience of the sampling geologist, the amount of the mineralisation, and how much data on the deposit is available to be examined and studied. This is problematic as access to the vein before mining has commenced will naturally be limited and often restricted to drill core samples which makes identification of large-scale textures and

variations within vein hosted mineralisation difficult to identify without extensive experience.

Currently it is challenging to quantify how representative of the wider mineralisation a section of drill core is. The most reliable method is comparison of observations, drill logs and assay data of the sample to the wider deposit dataset. One issue with this approach is that assays are destructive tests, with a half or quarter of sawn core destroyed during the testing process. The remaining portion of core to be examined may or may not contain comparable mineralisation to the destroyed portion. The thin section data from both the Cononish and Curraghinalt mines in this study showed that only one or two generations of mineralisation are observed in an area the size of a single thin section, with different generations observed in thin sections taken from a single hand specimen. This is problematic as there may be a discrepancy between an assay of drill core (often taken over 25cm or larger lengths) and the observations in a thin section of only be ~5cm in size.

The difficulty of obtaining representative samples of ore systems is well studied and in industry extensive efforts have been made to reduce uncertainty when estimating resources and modelling deposits. Industry standards and codes, such as the Australasian Code for Reporting of Exploration Results, Mineral Resources and Ore Reserves (JORC) and the Canadian Institute of Mining Metallurgy and Petroleum (CIM): National Instrument 43-101 standard, have been developed to promote best practice and reduce uncertainty (JORC, 2012, CIM, 2014). These codes address deposit analysis and modelling but significantly less attention has been focused on the question of how representative academic studies of a deposit may be. The question of whether the results published from economic geological studies are reproducible is a contentious issue. Because individual studies vary widely in the sampling strategy and focus, review papers which aim to collate, synthesise and interpret data from published studies have the potential to include and even magnify uncertainties or errors (Barnes and Latypov, 2016, Baker, 2016, Munafò and Davey Smith, 2018).

This difficulty in collating data is clear in the extensive literature focused on developing classifications for orogenic gold systems which has numerous competing classification criteria based on a variety of criteria, such as fluid inclusion data, structural style, mineralogy, geochemistry, setting. If deposit studies do not include information on the context of observations within the wider mineralising system, then comparisons which seek to contrast differences between deposits will be hampered.

In both mine site studies undertaken as part of this research, the silver content of the gold alloys increases over time. This is an observation which is consistent with published observations in other auriferous systems. This appears to hold for epithermal (Carrillo Rosúa et al., 2002, Zoheir and Moritz, 2014) and orogenic systems (Uemoto et al., 2002, Spence-Jones et al., 2018), but the data of Palacios et al. (2001) indicates that this trend may not apply to porphyry systems. However, the work of Palacios et al. (2001) is not presented in a paragenetic reference frame as samples were taken from different spatially separated lithologies and so differences may be due to host rock or spatial changes in the mineralising conditions. Considering the available data, it is concluded that in the majority of individual hydrothermal systems the silver content increases within time. Considering this as a working hypothesis for orogenic and epithermal gold systems, this is consistent with what would be expected to occur according to thermodynamic models. This is because decreasing temperature/pressure increases the proportion of silver in gold alloys deposited from the mineralising fluids (Gammons and Williams-Jones, 1995).

If the gold alloy signature progressively changes over time in auriferous vein systems towards higher silver proportions, then analysis of detrital populations has the potential to be a comparative tool to investigate the mineralisation. This is because the proportion of gold of different compositions can be assessed. For example, in this study, differences in the shape of the distributions are seen when the data from the three study locations is compared. Comparing the study areas, the Curraghinalt mine is the largest deposit studied and it shows the tightest distribution of compositions and log-normal distribution of alloy compositions when compared to Cononish and Atlin, table 7.1, figures 7.1 and 7.2. Cononish and Atlin have very similar ranges of composition however the peak abundance of compositions is very different with Cononish being the silver richest system.

Table 7.1 – Comparison between the properties of the studied systems and the nature of their detrital gold signatures. [1] from Treagus et al. (1999) .[2] from Rice et al. (2016).

	Cononish	*Curraghinalt*	*Atlin*
Age	410±14 Ma[1]	462.7–452.8 Ma[2]	Unknown
Host Terrain	Grampian	Grampian	Cache Creek
Deposit style	Single vein	Vein array	Unknown (multiple distributed veins probable)
Host lithologies	Metasediments (amphibolite facies)	Metasediments (upper greenschist facies)	Metasediments and volcanic accretionary complex (prehnite-pumpellyite facies)
Range of gold signature	Wide	Tight	Moderate
Spatial variability of gold signature	Variable within the deposit	Consistent on a deposit scale	Consistent on a camp scale

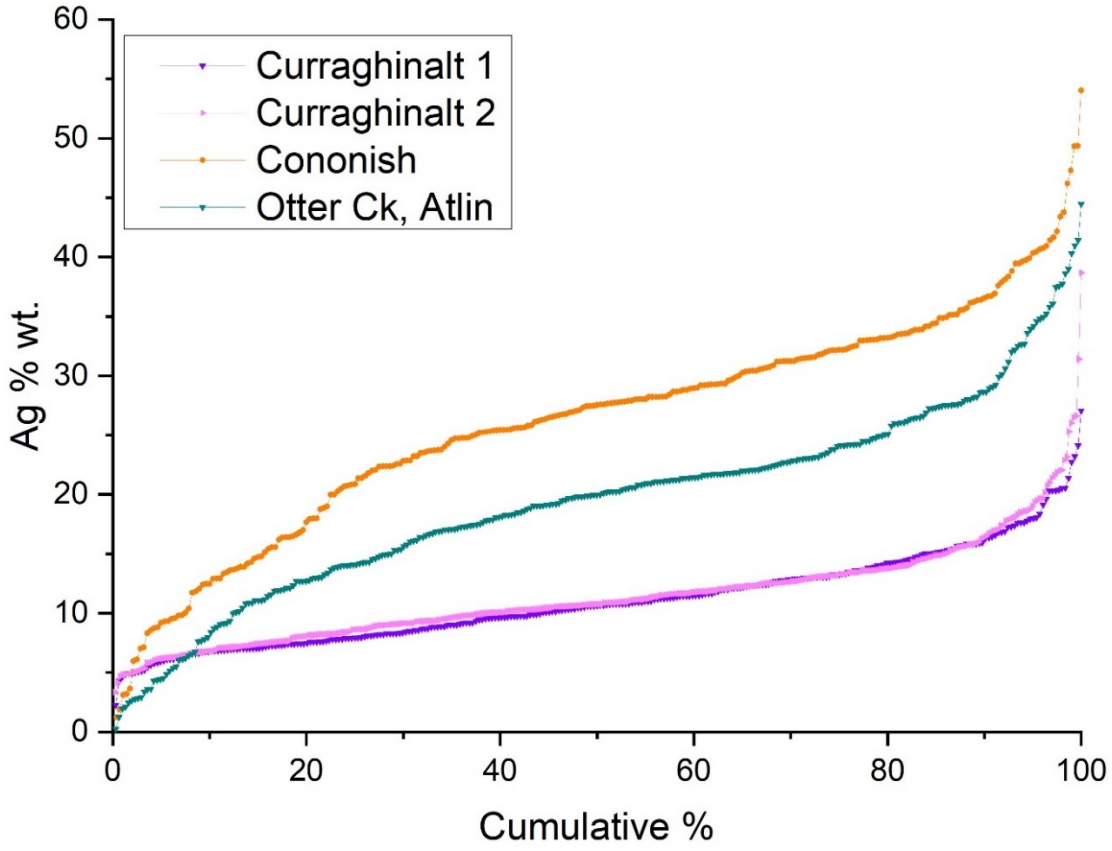

Figure 7.1 – Cumulative frequency plot comparing the gold signatures of detrital gold from the three different areas studied in the project.

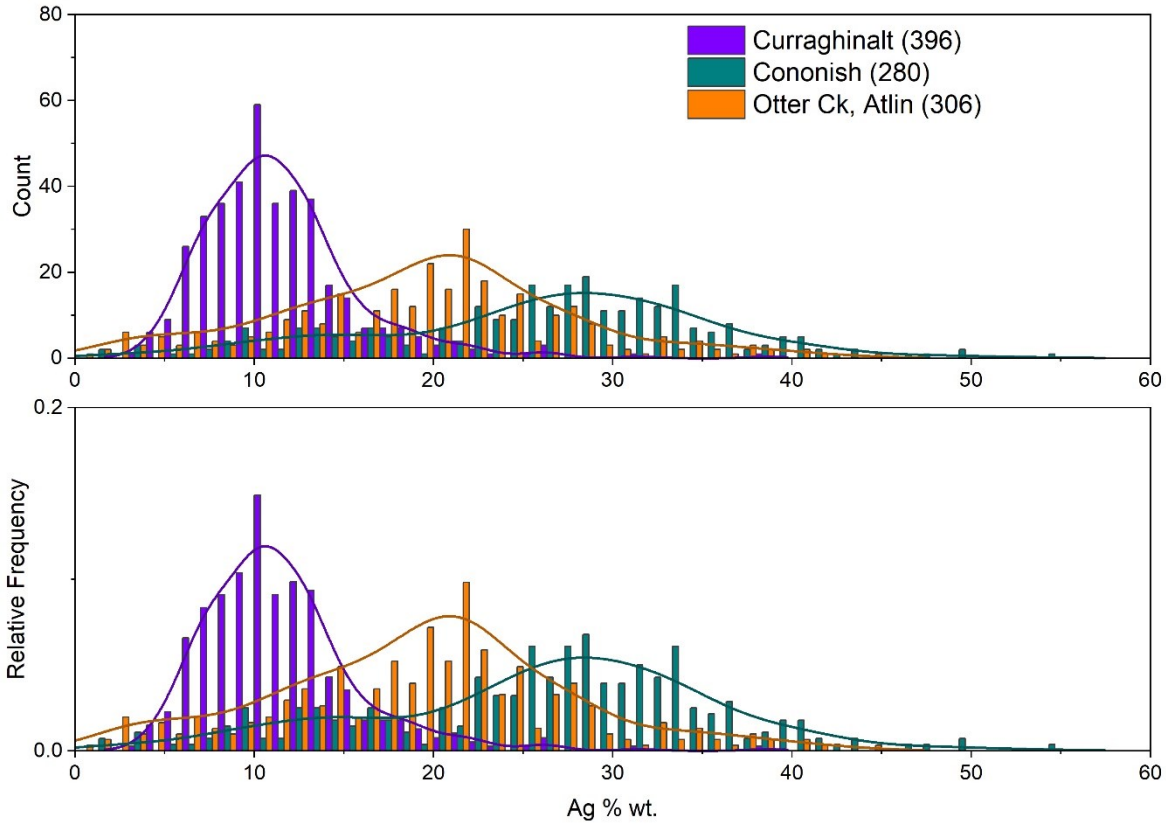

Figure 7.2 – Histogram comparison of the three study areas gold signatures.

Comparing the three areas studied here to the detrital gold populations of Chapman et al. (2021), figure 7.3, it can be seen that the three populations are comparable to the other phanerozoic orogenic populations. While the differences between the systems are clear, it is not possible to definitely state the reasons for the observed differences. It can be speculated that the amplitude of the peak in abundance could reflect the stability of conditions during alloy precipitation. This would fit the data because the gold signature which has the widest range of alloy compositions is the Cononish mine which formed from a magmatic fluid pulse that was not in equilibrium with the host rocks (Spence-Jones et al. 2018). The unstable nature of the Cononish system is evidenced by the evolving paragenesis and the presence of strong alteration of the host lithologies around the mineralisation.

Further support of the link between deposit formation processes is the gold signature at the Curraghinalt mine, which has the largest defined gold resource of any of the deposits studied. The Curraghinalt vein system has the tightest and smallest range of alloy compositions of the studied deposits. This is despite a spaced array of veins indicating relatively stable conditions of gold deposition in the system. The lack of a strong chemical alteration halo at the Curraghinalt deposit provides an additional

indication which supports the inference that the mineralising system in the deposit in relatively stable, compared to other auriferous deposits.

Published work comparing between orogenic gold deposits clearly states that significant difference alteration is observed between different orogenic deposits (Groves et al., 2003). However, limited correlation between alteration and deposit grade/tonnage can be gleaned from published accounts, and most of the comparative accounts in publications are made between different 'styles' of orogenic gold deposit in different geological settings (Mortensen et al. 2021). Numerous problems exist with relating alteration directly to gold endowment, most significantly is that alteration is decoupled from gold precipitation, spatially and/or temporally in these deposits. Furthermore, many published accounts do not commonly compare and contrast the alteration around mineralised and unmineralized faults/structures in a district. This means that assessments as to the extent of alteration and its potential as a good indicator of grade are fraught with problems.

Considering factors that control the deposition of gold particles, and their compositions, are complex, gold signatures/alloy compositional distributions might provide an insight into the processes. If further investigations are able to relate the form of the alloy distribution to the nature of the mineralising system, this would allow detrital gold compositional signatures to be used as more efficient tools to understand and exploit auriferous resources. This could be archive by further work sampling detrital populations from known deposits and comparing and contrasting between distributions statistical.

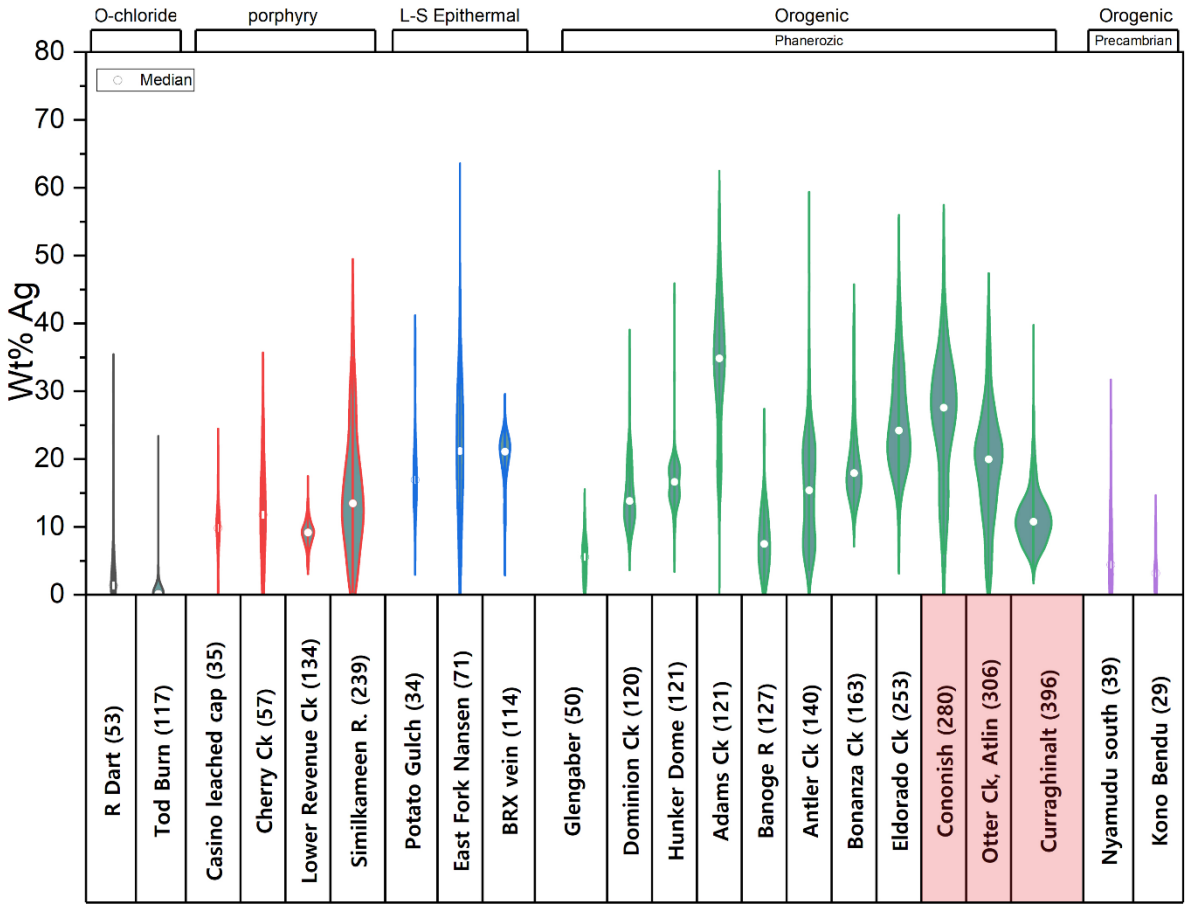

Figure 7.3 – Comparison of this studies' gold signatures (highlighted red) to other deposits.

Conclusion

This work addressed the disconnect between detrital gold studies and traditional mineralogical studies of auriferous ore deposits. It provides data enabling assumptions to be tested of how comparable detrital populations are to those obtained directly from the ore. The conclusions of such studies undertaken at two mines, is that ore samples and detrital gold particles are not equivalent because they are sourced from different volumes of mineralised material. Detrital populations are regarded as superior representative samples of the mineralisation as they are the residual lags resultant from the erosion of a huge volume of material.

The results presented in this study demonstrate that by analysing samples from detrital populations alongside others taken from in situ mineralisation, comparisons between them provide valuable insights into the mineralisation on both a micro scale while retaining a macro scale context. Further such studies relating ore samples to detrital populations have the potential to quantify aspects of ore genesis, such as changes temporally and spatially of the mineralisation which are currently difficult to quantify and are often speculated about. Ideally a study would be conducted which linked detrital gold samples to gold populations of bulk samples obtained from different locations within an active mine. This would identify spatial differences in the gold systems and relate them to the overall deposit, however this is logistically challenging as mines typically work multiple stopes/locations simultaneously meaning that processing plant bulk feed is a composite of multiple locations.

References

ALLAN, M. M., MORRISON, G. W. & YARDLEY, B. W. D. 2011. Physicochemical Evolution of a Porphyry-Breccia System: A Laser Ablation ICP-MS Study of Fluid Inclusions in the Mount Leyshon Au Deposit, Queensland, Australia. *Economic Geology,* 106**,** 413-436.

BAKER, M. 2016. 1,500 scientists lift the lid on reproducibility. *Nature,* 533**,** 452-454.

BARNES, S. & LATYPOV, R. 2016. 'From Igneous Petrology to Ore Genesis': an Introduction to this Thematic Issue of Journal of Petrology. *Journal of Petrology,* 56**,** 2295-2296.

BLAMEY, N. J. F., CAMPBELL, A. R. & HEIZLER, M. T. 2017. The Hydrothermal Fluid Evolution of Vein Sets at the Pipeline Gold Mine, Nevada. *Minerals,* 7**,** 100.

CANET, C., FRANCO, S. I., PROL-LEDESMA, R. M., GONZÁLEZ-PARTIDA, E. & VILLANUEVA-ESTRADA, R. E. 2011. A model of boiling for fluid inclusion studies: Application to the Bolaños Ag–Au–Pb–Zn epithermal deposit, Western Mexico. *Journal of Geochemical Exploration,* 110**,** 118-125.

CARRILLO ROSÚA, F. J., MORALES RUANO, S. & FENOLL HACH-ALÍ, P. 2002. THE THREE GENERATIONS OF GOLD IN THE PALAI–ISLICA EPITHERMAL DEPOSIT, SOUTHEASTERN SPAIN. *The Canadian Mineralogist,* 40**,** 1465-1481.

CHAPMAN, R. J., BANKS, D. A., STYLES, M. T., WALSHAW, R. D., PIAZOLO, S., MORGAN, D. J., GRIMSHAW, M. R., SPENCE-JONES, C. P., MATTHEWS, T. J. & BOROVINSKAYA, O. 2021. Chemical and physical heterogeneity within native gold: implications for the design of gold particle studies. *Mineralium Deposita*.

CIM 2014. National Instrument 43-101; Definition Standards for Mineral Resources & Mineral Reserves. Quebec: Canadian Institute of Mining, Metallurgy and Petroleum.

GAMMONS, C. H. & WILLIAMS-JONES, A. E. 1995. Hydrothermal Geochemistry of Electrum - Thermodynamic Constraints. *Economic Geology and the Bulletin of the Society of Economic Geologists,* 90**,** 420-432.

GROVES, D. I., GOLDFARB, R. J., ROBERT, F. & HART, C. J. R. 2003. Gold deposits in metamorphic belts: Overview of current understanding, outstanding problems, future research, and exploration significance. *Economic Geology and the Bulletin of the Society of Economic Geologists,* 98**,** 1-29.

GROVES, D. I. & VEARNCOMBE, J. R. 1990. The Scale of Ore-Depositional System - an Important Restraint on Epigenetic Vs Remobilized Syngenetic Origins for Archean Mesothermal Gold Deposits. *Geologische Rundschau,* 79**,** 345-353.

HART, C. & GOLDFARB, R. Distinguishing intrusion-related from orogenic gold systems. New Zealand Minerals Conference Proceedings, 2005. 125-133.

HART, C. J. 2007. Reduced intrusion-related gold systems. *Mineral Deposits of Canada: A synthesis of Major deposit types, district metallogeny, the Evolution of geological provinces, and exploration methods: Geological Association of Canada, Mineral Deposits Division, Special Publication,* 5**,** 95-112.

HEINRICH, C. 2005. The physical and chemical evolution of low-salinity magmatic fluids at the porphyry to epithermal transition: a thermodynamic study. *Mineralium Deposita,* 39**,** 864-889.

JORC 2012. Australasian Code for Reporting of Exploration Results, Mineral Resources and Ore Reserves

(The JORC Code). The Joint Ore Reserves Committee of The Australasian Institute of Mining and Metallurgy, Australian Institute of Geoscientists and Minerals Council of Australia.

LAFLAMME, C., SUGIONO, D., THÉBAUD, N., CARUSO, S., FIORENTINI, M., SELVARAJA, V., JEON, H., VOUTE, F. & MARTIN, L. 2018. Multiple sulfur isotopes monitor fluid evolution of an Archean orogenic gold deposit. *Geochimica et Cosmochimica Acta,* 222**,** 436-446.

Mortensen, J., Craw, D., & MacKenzie, D. (2021). Concepts and Revised Models for Phanerozoic Orogenic Gold Deposits. Geological Society, London, Special Publications, SP516-2021. doi:10.1144/SP516-2021-39

MUNAFÒ, M. R. & DAVEY SMITH, G. 2018. Robust research needs many lines of evidence. *Nature,* 553**,** 399-401.
PALACIOS, C., HERAIL, G., TOWNLEY, B., MAKSAEV, V., SEPULVEDA, F., DE PARSEVAL, P., RIVAS, P., LAHSEN, A. & PARADA, M. A. 2001. The Composition of Gold in the Cerro Casale Gold-Rich Porphyry Deposit, Maricunga Belt, Northern Chile. *The Canadian Mineralogist,* 39**,** 907-915.
SILLITOE, R. H. 2010. Porphyry Copper Systems. *Economic Geology,* 105**,** 3-41.
SMITH, D. J., NADEN, J., JENKIN, G. R. T. & KEITH, M. 2017. Hydrothermal alteration and fluid pH in alkaline-hosted epithermal systems. *Ore Geology Reviews,* 89**,** 772-779.
SPENCE-JONES, C. P., JENKIN, G. R. T., BOYCE, A. J., HILL, N. J. & SANGSTER, C. J. S. 2018. Tellurium, magmatic fluids and orogenic gold: An early magmatic fluid pulse at Cononish gold deposit, Scotland. *Ore Geology Reviews*.
STEPHENS, J. R., MAIR, J. L., OLIVER, N. H. S., HART, C. J. R. & BAKER, T. 2004. Structural and mechanical controls on intrusion-related deposits of the Tombstone Gold Belt, Yukon, Canada, with comparisons to other vein-hosted ore-deposit types. *Journal of Structural Geology,* 26**,** 1025-1041.
UEMOTO, T., RIDLEY, J., MIKUCKI, E., GROVES, D. I. & KUSAKABE, M. 2002. Fluid chemical evolution as a factor in controlling the distribution of gold at the Archean Golden Crown lode gold deposit, Murchison province, western Australia. *Economic Geology and the Bulletin of the Society of Economic Geologists,* 97**,** 1227-1248.
ZOHEIR, B. & MORITZ, R. 2014. Fluid evolution in the El-Sid gold deposit, Eastern Desert, Egypt. *Geological Society, London, Special Publications,* 402.

Appendix A – Data Tables

Cononish Mine Concentrate EMPA Data

ID	Au WT%	Ag WT%	Hg WT%	Cu WT%	Pd WT%	TOTAL
Con_conc_01	80.411	16.953	-0.111	-0.038	0.072	97.287
Con_conc_02	64.872	30.103	-0.202	-0.031	-0.057	94.684
Con_conc_03	74.681	23.067	-0.030	-0.011	0.008	97.715
Con_conc_04	78.676	17.613	-0.110	0.004	0.042	96.225
Con_conc_05	60.016	36.271	-0.066	-0.004	0.010	96.227
Con_conc_06	71.441	27.690	-0.020	-0.025	-0.018	99.068
Con_conc_07	64.209	32.679	-0.074	-0.009	-0.016	96.789
Con_conc_08	71.596	27.267	-0.051	0.000	0.053	98.864
Con_conc_08	71.588	27.276	-0.004	-0.012	0.078	98.926
Con_conc_09	78.496	18.704	-0.192	-0.010	-0.003	96.994
Con_conc_10	79.623	18.204	-0.068	0.075	-0.029	97.805
Con_conc_11	72.201	26.895	-0.171	-0.032	0.059	98.952
Con_conc_12	61.874	36.447	-0.021	-0.024	-0.001	98.275
Con_conc_13	72.668	26.405	-0.164	-0.040	-0.026	98.842
Con_conc_14	79.137	18.651	-0.021	-0.009	0.042	97.801
Con_conc_15	55.524	41.838	-0.118	-0.049	-0.018	97.178
Con_conc_16	52.070	31.654	-0.030	-0.039	0.022	83.676
Con_conc_17	69.656	28.305	-0.078	-0.030	0.021	97.873
Con_conc_18	69.596	28.720	0.049	-0.011	0.034	98.388
Con_conc_19	68.822	29.446	-0.108	-0.004	-0.040	98.115
Con_conc_20	80.881	16.929	-0.145	-0.015	-0.022	97.628
Con_conc_21	77.637	20.164	-0.034	0.003	-0.048	97.722
Con_conc_22	81.116	16.040	-0.108	-0.026	0.012	97.035
Con_conc_23	81.497	16.512	-0.187	0.023	0.008	97.854
Con_conc_24	60.047	37.130	-0.035	-0.005	0.003	97.141
Con_conc_25	80.477	16.704	-0.128	-0.024	-0.048	96.980
Con_conc_26	65.800	32.137	-0.160	-0.025	-0.009	97.742
Con_conc_27	65.483	33.132	-0.051	0.033	0.021	98.618
Con_conc_28	82.341	15.471	0.067	0.018	-0.001	97.897
Con_conc_29	63.211	35.270	-0.131	0.006	-0.009	98.347
Con_conc_30	76.299	21.500	-0.030	0.015	-0.017	97.767
Con_conc_31	60.083	38.196	0.006	0.001	-0.009	98.276
Con_conc_32	66.578	31.313	-0.095	0.019	0.040	97.854
Con_conc_33	83.839	14.771	-0.177	0.026	-0.030	98.429
Con_conc_34	71.755	27.039	0.010	0.008	0.056	98.868
Con_conc_35	82.826	15.064	-0.198	0.019	0.048	97.758
Con_conc_36	70.759	27.015	-0.024	0.004	0.022	97.776
Con_conc_37	82.187	15.855	-0.112	-0.010	-0.041	97.879
Con_conc_38	68.583	29.604	0.025	0.009	0.022	98.244
Con_conc_40	79.436	19.085	-0.039	-0.038	0.050	98.494
Con_conc_41	60.100	37.101	-0.054	-0.037	0.050	97.160

ID	Au WT%	Ag WT%	Hg WT%	Cu WT%	Pd WT%	TOTAL
Con_conc_42	72.726	25.337	-0.105	-0.047	-0.017	97.894
Con_conc_43	48.811	50.022	-0.066	-0.044	0.042	98.766
Con_conc_044	66.513	32.535	-0.046	-0.065	-0.097	98.840
Con_conc_045	77.384	20.801	-0.139	-0.030	-0.022	97.994
Con_conc_046	66.024	32.197	-0.025	-0.038	-0.013	98.145
Con_conc_047	83.764	14.716	-0.080	-0.017	0.015	98.398
Con_conc_048	76.135	22.012	0.018	-0.011	-0.028	98.126
Con_conc_049	77.889	21.224	-0.237	-0.009	0.038	98.904
Con_conc_050	98.555	20.742	-0.118	-0.029	0.004	119.153
Con_conc_051	60.897	37.779	-0.210	-0.045	0.040	98.460
con_conc_52	22.961	71.849	-0.029	-0.017	0.031	94.794
con_conc_53	48.817	48.516	-0.168	0.017	-0.004	97.179
con_conc_54	81.233	17.249	-0.079	-0.023	0.046	98.427
con_conc_55	77.157	18.458	0.017	0.012	-0.005	95.639
con_conc_56	82.509	15.039	0.059	-0.013	0.025	97.619
con_conc_57	67.886	27.140	-0.055	-0.012	-0.013	94.945
con_conc_58	80.384	17.641	-0.025	-0.037	0.076	98.039
con_conc_59	82.062	15.901	-0.107	-0.031	0.033	97.859
con_conc_60	59.649	38.810	-0.048	-0.049	0.015	98.376
con_conc_61	82.030	16.613	0.011	-0.025	-0.015	98.614
con_conc_62	60.367	37.631	-0.012	-0.011	0.014	97.989
con_conc_63	82.971	15.167	0.003	-0.008	0.013	98.147
con_conc_64	73.433	24.348	-0.064	-0.019	-0.023	97.676
con_conc_65	60.150	37.093	-0.057	-0.044	-0.001	97.141
con_conc_66	62.774	35.475	-0.131	-0.009	0.051	98.160
con_conc_67	74.479	23.197	-0.146	-0.003	0.031	97.558
con_conc_68	81.587	15.750	-0.082	-0.029	-0.061	97.164
con_conc_69	64.433	33.699	-0.056	-0.043	0.046	98.079
con_conc_70	61.929	35.839	-0.093	-0.034	0.064	97.705
con_conc_71	65.426	32.463	-0.213	-0.043	0.021	97.654
con_conc_72	67.410	30.278	-0.045	-0.030	0.021	97.634
con_conc_73	59.340	37.514	-0.108	0.035	-0.019	96.763
con_conc_74	59.319	37.844	-0.007	-0.023	0.022	97.156
con_conc_75	49.808	47.716	0.040	-0.036	0.035	97.563
con_conc_76	81.618	16.145	0.035	-0.012	0.013	97.799
con_conc_77	72.507	24.646	-0.219	-0.032	0.011	96.912
con_conc_78	79.036	19.017	0.063	0.080	-0.002	98.194
con_conc_79	69.951	28.288	0.007	0.062	-0.036	98.272
con_conc_80	84.291	13.405	0.115	0.085	0.017	97.913
con_conc_81	59.001	39.348	0.022	0.157	-0.032	98.496
con_conc_82	64.100	33.897	0.037	0.064	-0.028	98.070
con_conc_83	75.153	22.954	0.016	0.052	0.027	98.202
Con_conc_84	66.323	32.643	0.012	0.053	-0.022	99.010
Con_conc__001	61.512	35.881	0.287	0.033	-0.007	97.706
Con_conc__002	48.680	49.233	0.027	0.033	0.008	97.982
Con_conc__003	75.102	23.434	0.029	0.061	-0.008	98.619
Con_conc__004	82.841	16.171	0.014	0.057	0.004	99.087
Con_conc__005	67.133	31.516	0.027	0.044	0.011	98.731

ID	Au WT%	Ag WT%	Hg WT%	Cu WT%	Pd WT%	TOTAL
Con_conc__006	74.475	24.706	-0.011	0.067	-0.024	99.212
Con_conc__007	61.939	37.914	-0.113	0.035	0.000	99.775
Con_conc__008	73.474	24.685	0.055	0.052	0.019	98.286
Con_conc__009	59.732	39.117	0.007	0.010	-0.037	98.828
Con_conc__010	66.631	30.612	0.021	0.055	-0.029	97.289
Con_conc__011	56.707	42.273	0.066	0.035	-0.028	99.053
Con_conc__012	39.970	57.137	-0.076	0.043	0.026	97.100
Con_conc__013	80.447	17.742	0.001	0.056	0.025	98.270
Con_conc__014	81.469	16.397	0.047	0.061	-0.009	97.965
Con_conc__015	80.894	17.109	-0.043	0.049	0.003	98.012
Con_conc__016	84.630	14.011	0.061	0.072	-0.018	98.756
Con_conc__017	68.785	29.498	0.127	0.068	-0.022	98.456
Con_conc__018	81.388	17.401	0.083	0.052	0.025	98.948
Con_conc__019	78.351	20.864	0.050	0.059	-0.016	99.307
Con_conc__020	83.393	15.359	0.030	0.074	0.000	98.856
Con_conc__021	55.871	43.020	0.027	0.033	0.084	99.035
Con_conc__022	65.127	33.986	0.016	0.044	0.058	99.230
Con_conc__023	56.260	41.841	0.014	0.047	0.062	98.223
Con_conc__024	68.908	30.158	0.059	0.043	0.073	99.241
Con_conc__025	45.734	51.537	-0.011	0.055	0.044	97.358
Con_conc__026	73.886	24.885	0.119	0.074	-0.012	98.952
Con_conc__027	74.178	23.869	0.006	0.054	0.039	98.147
Con_conc__028	70.669	26.676	0.055	0.054	-0.020	97.433
Con_conc__029	85.564	13.230	0.034	0.078	0.007	98.913
Con_conc__030	62.853	36.196	0.144	0.049	-0.003	99.240
Con_conc__031	66.106	32.178	0.046	0.030	-0.021	98.340
Con_conc__032	80.979	18.106	0.010	0.062	0.061	99.218
Con_conc__033	64.121	33.964	0.335	0.054	-0.052	98.423
Con_conc__034	70.386	27.603	0.005	0.054	-0.006	98.041
Con_conc__035	82.619	16.237	0.150	0.063	-0.013	99.056
Con_conc__036	66.412	31.794	0.060	0.062	-0.031	98.298
Con_conc__037	70.631	28.358	0.051	0.108	0.094	99.242
Con_conc__038	54.599	45.956	-0.050	0.051	-0.006	100.549
Con_conc__039	82.919	15.800	0.004	0.067	-0.051	98.739
Con_conc__040	53.941	45.129	-0.025	0.067	0.003	99.114
Con_conc__041	64.660	34.104	-0.133	0.080	-0.014	98.696
Con_conc__042	60.227	39.253	0.034	0.052	-0.052	99.514
Con_conc__043	65.077	34.229	-0.047	0.062	-0.022	99.300
Con_conc__044	65.810	33.533	0.072	0.052	0.041	99.508
Con_conc__045	58.004	41.612	0.042	0.042	0.032	99.733
Con_conc__046	64.645	33.749	-0.113	0.051	0.026	98.357
Con_conc__047	72.898	25.856	0.113	0.061	0.038	98.965
Con_conc__048	77.449	21.941	0.179	0.070	0.033	99.672
Con_conc__049	82.127	16.721	-0.051	0.087	0.072	98.956
Con_conc__050	81.233	17.698	-0.050	0.075	-0.005	98.951
Con_conc__051	83.475	14.848	0.080	0.081	-0.060	98.423
Con_conc__052	80.787	17.399	0.000	0.065	0.038	98.289
Con_conc__053	72.622	26.187	-0.063	0.064	0.002	98.811

ID	Au WT%	Ag WT%	Hg WT%	Cu WT%	Pd WT%	TOTAL
Con_conc__054	58.579	40.444	-0.040	0.034	0.006	99.023
Con_conc__055	77.067	22.185	0.034	0.045	-0.018	99.313
Con_conc__056	80.275	18.583	-0.040	0.051	-0.011	98.858
Con_conc__057	80.105	18.497	0.108	0.068	-0.038	98.738
Con_conc__058	77.793	20.901	0.073	0.072	0.078	98.918
Con_conc__059	62.381	36.470	0.035	0.036	0.029	98.952
Con_conc__060	80.979	18.256	0.055	0.065	0.010	99.365
Con_conc__061	68.111	31.246	-0.002	0.083	0.044	99.483
Con_conc__062	60.601	38.108	0.014	0.038	-0.025	98.737
Con_conc__063	80.688	15.479	0.022	0.062	0.037	96.288
Con_conc__064	85.833	13.185	0.029	0.076	0.026	99.148
Con_conc__065	82.377	16.493	-0.036	0.055	0.036	98.925
Con_conc__066	69.863	28.495	0.044	0.055	0.008	98.465
Con_conc__067	63.223	36.038	-0.024	0.035	-0.017	99.255
Con_conc__068	84.122	15.370	0.053	0.079	-0.009	99.615
Con_conc__069	74.524	25.419	-0.067	0.042	-0.019	99.900
Con_conc__070	77.210	21.489	0.064	0.054	0.003	98.820
Con_conc__071	66.183	33.221	0.020	0.046	-0.041	99.428
Con_conc__072	67.494	31.589	0.009	0.030	-0.032	99.090
Con_conc__073	77.382	22.167	-0.026	0.050	0.035	99.607
Con_conc__074	72.407	27.467	0.087	0.062	0.003	100.025
Con_conc__075	80.519	18.234	0.149	0.055	0.008	98.964
Con_conc__076	62.853	36.324	-0.011	0.059	-0.043	99.182
Con_conc__077	60.644	37.274	0.099	0.038	0.038	98.093
Con_conc__078	61.779	36.837	-0.001	0.049	-0.015	98.649
Con_conc__079	76.297	22.754	-0.070	0.066	0.039	99.087
Con_conc__080	65.063	33.508	-0.029	0.049	-0.052	98.538
Con_conc__081	64.247	35.377	0.092	0.069	-0.034	99.752
Con_conc__082	75.920	23.001	0.129	0.047	0.052	99.149
Con_conc__083	83.054	15.843	0.029	0.077	-0.036	98.968
Con_conc__084	61.551	38.670	-0.078	0.063	0.004	100.209
Con_conc__085	76.360	22.337	0.185	0.064	-0.064	98.881
Con_conc__086	60.119	38.961	0.002	0.045	0.008	99.134
Con_conc__087	80.670	18.318	0.093	0.060	0.033	99.174
Con_conc__088	60.872	38.667	-0.090	0.034	-0.022	99.461
Con_conc__089	68.603	29.433	-0.019	0.041	0.083	98.140
Con_conc__090	73.286	25.698	-0.051	0.055	0.039	99.027
Con_conc__091	85.815	13.089	0.037	0.065	-0.015	98.991
Con_conc__092	91.762	6.386	-0.098	0.102	0.066	98.218
Con_conc__093	82.215	17.307	0.060	0.068	-0.002	99.648
Con_conc__094	80.670	18.907	0.038	0.070	-0.037	99.650
Con_conc__095	65.997	33.318	-0.062	0.065	-0.041	99.277
Con_conc__096	73.523	25.835	0.021	0.061	0.074	99.513
Con_conc__097	54.268	43.333	0.054	0.042	0.000	97.697
Con_conc__098	54.667	43.000	0.082	0.031	0.034	97.814
Con_conc__099	80.227	18.333	0.020	0.110	0.002	98.692
Con_conc__100	73.355	25.775	0.119	0.078	0.006	99.332
Con_conc__101	61.886	35.952	0.132	0.044	-0.008	98.006

ID	Au WT%	Ag WT%	Hg WT%	Cu WT%	Pd WT%	TOTAL
Con_conc__102	76.231	22.727	0.018	0.080	-0.032	99.024
Con_conc__103	71.326	27.806	0.114	0.049	0.060	99.356
Con_conc__104	84.958	14.636	-0.016	0.079	0.000	99.657
Con_conc__105	61.351	37.737	0.037	0.040	0.017	99.183
Con_conc__106	62.485	36.201	0.103	0.052	-0.020	98.821
Con_conc__107	63.262	35.334	-0.058	0.027	0.063	98.627
Con_conc__108	68.819	30.462	-0.069	0.039	0.038	99.288
Con_conc__109	84.183	15.023	-0.087	0.074	-0.032	99.162
Con_conc__110	51.832	47.008	-0.011	0.072	0.037	98.937
Con_conc__111	61.331	38.095	0.106	0.047	-0.004	99.575
Con_conc__112	72.331	26.183	-0.034	0.038	0.056	98.573
Con_conc__113	62.815	37.078	-0.021	0.033	0.034	99.939
Con_conc__114	83.369	15.739	0.048	0.057	0.035	99.249
Con_conc__115	81.755	17.419	-0.065	0.079	-0.018	99.170
Con_conc__116	82.880	16.111	0.171	0.167	-0.039	99.290
Con_conc__117	62.287	36.520	0.018	0.010	-0.008	98.828
Con_conc__118	56.841	41.228	-0.009	0.048	0.019	98.127
Con_conc__119	53.377	45.554	-0.052	0.028	0.005	98.912
Con_conc__120	83.410	15.318	-0.041	0.047	-0.023	98.710
Con_conc__121	75.702	23.455	0.067	0.045	-0.036	99.232
Con_conc__122	72.034	27.445	0.062	0.066	-0.074	99.533
Con_conc__123	70.092	28.922	0.043	0.038	-0.059	99.035
Con_conc__124	68.484	30.177	-0.055	0.037	-0.002	98.642
Con_conc__125	84.029	15.645	0.084	0.064	-0.017	99.806
Con_conc__126	81.511	16.534	0.110	0.056	0.017	98.228
Con_conc__127	66.127	33.484	0.014	0.030	-0.001	99.654
Con_conc__128	63.792	35.896	0.044	0.052	-0.015	99.769
Con_conc__129	64.283	34.908	0.022	0.040	0.008	99.260
Con_conc__130	71.484	27.464	-0.007	0.063	-0.050	98.954
Con_conc__131	69.094	29.800	0.055	0.045	-0.006	98.988
Con_conc__132	77.543	22.268	0.007	0.066	0.024	99.908
Con_conc__133	62.311	37.084	0.059	0.042	0.052	99.549
Con_conc__134	60.782	38.928	0.011	0.061	0.049	99.831
Con_conc__135	80.664	18.600	0.134	0.059	0.009	99.465
Con_conc__136	73.412	26.416	0.017	0.049	0.015	99.908
Con_conc__137	68.965	30.881	0.092	0.060	0.030	100.029
Con_conc__138	68.641	28.592	0.021	0.045	-0.012	97.287
Con_conc__139	65.756	33.162	0.189	0.054	0.028	99.190
Con_conc__140	75.889	22.732	0.023	0.063	-0.032	98.675
Con_conc__141	67.697	31.429	0.057	0.068	-0.082	99.169
Con_conc__142	72.227	27.584	-0.032	0.057	-0.086	99.750
Con_conc__143	71.988	26.549	0.129	0.056	-0.039	98.682
Con_conc__144	84.690	15.721	0.074	0.086	-0.001	100.570
Con_conc__145	59.893	39.304	-0.012	0.071	0.068	99.324
Con_conc__146	64.090	35.803	0.043	0.059	0.011	100.007
Con_conc__147	83.797	14.890	0.071	0.094	-0.050	98.803
Con_conc__148	80.888	17.580	0.167	0.102	0.011	98.747
Con_conc__149	78.062	21.116	-0.105	0.098	-0.031	99.141

ID	Au WT%	Ag WT%	Hg WT%	Cu WT%	Pd WT%	TOTAL
Con_conc__150	84.338	15.149	0.064	0.088	-0.011	99.628
Con_conc__153	78.622	20.701	0.036	0.056	0.012	99.426
Con_conc__154	59.322	39.993	0.040	0.027	-0.015	99.366
Con_conc__155	69.196	30.381	0.048	0.046	-0.066	99.605
Con_conc__156	67.016	33.235	0.048	0.034	0.010	100.343
Con_conc__157	85.558	13.711	-0.045	0.062	0.020	99.306
Con_conc__158	82.774	16.502	-0.005	0.066	-0.029	99.307
Con_conc__159	36.857	61.266	0.032	0.046	-0.014	98.186
Con_conc__160	73.329	26.336	0.047	0.069	0.014	99.796
Con_conc__161	70.607	28.991	0.057	0.067	0.037	99.760
Con_conc__162	76.508	22.758	-0.030	0.061	-0.044	99.252
Con_conc__163	58.659	40.286	0.050	0.036	-0.013	99.017
Con_conc__164	70.968	28.546	0.102	0.049	-0.058	99.607
Con_conc__165	73.178	26.434	0.137	0.055	-0.002	99.802
Con_conc__166	25.385	71.918	0.081	0.027	0.000	97.412
Con_conc__167	69.284	29.711	0.081	0.039	0.038	99.153
Con_conc__168	70.578	28.702	0.131	0.060	-0.005	99.466
Con_conc__169	70.626	29.236	0.028	0.043	0.023	99.955
Con_conc__170	74.095	25.135	0.083	0.059	-0.008	99.366
Con_conc__171	65.206	34.991	-0.059	0.045	0.003	100.186
Con_conc__172	64.006	35.130	0.073	0.035	0.026	99.269
Con_conc__173	81.648	18.527	0.072	0.055	0.007	100.310
Con_conc__174	72.219	26.867	-0.016	0.048	0.022	99.140
Con_conc__175	61.025	38.401	-0.008	0.041	0.016	99.474
Con_conc__176	66.277	32.616	0.010	0.052	0.014	98.969
Con_conc__177	85.132	14.209	0.036	0.063	-0.032	99.409
Con_conc__178	79.789	19.652	-0.001	0.049	-0.026	99.463
Con_conc__179	66.596	32.617	0.032	0.062	0.018	99.325
Con_conc__180	81.738	17.126	0.070	0.066	-0.007	98.993
Con_conc__181	61.175	37.175	0.050	0.037	0.043	98.479
Con_conc__182	74.863	24.448	0.034	0.062	-0.011	99.396
Con_conc__183	67.668	31.813	0.013	0.053	-0.003	99.543
Con_conc__184	84.314	14.245	0.091	0.078	-0.026	98.702
Con_conc__185	60.127	38.667	0.020	0.039	0.022	98.875
Con_conc__186	85.216	14.238	0.057	0.066	0.030	99.607
Con_conc__187	84.561	15.075	-0.064	0.061	-0.038	99.595
Con_conc__188	61.562	38.780	0.027	0.041	-0.028	100.381
Con_conc__189	71.432	28.030	-0.003	0.048	0.005	99.512
Con_conc__190	58.209	41.026	0.011	0.035	0.028	99.308
Con_conc__191	62.511	36.476	0.016	0.027	-0.011	99.020
Con_conc__192	83.019	16.823	0.055	0.063	-0.012	99.947
Con_conc__193	55.564	43.906	0.000	0.041	0.018	99.529
Con_conc__194	65.460	33.848	-0.011	0.059	-0.047	99.309
Con_conc__195	83.819	15.842	-0.021	0.053	0.023	99.716
Con_conc__196	71.694	27.769	0.120	0.049	0.009	99.641
Con_conc__197	82.922	15.384	-0.011	0.074	0.007	98.376
Con_conc__198	62.936	37.070	0.092	0.026	-0.009	100.114
Con_conc__199	77.721	20.915	0.039	0.054	-0.010	98.719

ID	Au WT%	Ag WT%	Hg WT%	Cu WT%	Pd WT%	TOTAL
Con_conc__200	77.899	22.038	-0.019	0.055	-0.028	99.945
Con_conc__201	80.733	18.342	0.075	0.056	0.027	99.234
Con_conc__203	84.269	14.849	-0.053	0.080	-0.030	99.115
Con_conc__204	66.540	33.312	-0.015	0.070	-0.002	99.905
Con_conc__205	84.117	15.064	0.020	0.079	0.025	99.304
Con_conc__206	82.389	17.434	0.059	0.084	-0.017	99.948
Con_conc__207	66.660	32.620	0.068	0.057	0.011	99.415
Con_conc__208	75.543	24.777	0.042	0.083	-0.008	100.436
Con_conc__209	66.149	32.970	0.092	0.082	-0.016	99.275
Con_conc__210	56.777	41.912	0.020	0.131	-0.010	98.829
Con_conc__211	60.218	38.394	0.011	0.141	0.006	98.770
Con_conc__212	73.794	24.526	0.067	0.056	-0.001	98.442
Con_conc__213	69.725	30.251	0.009	0.098	-0.046	100.037
Con_conc__214	80.215	19.317	0.021	0.089	-0.021	99.622
Con_conc__215	67.057	31.760	-0.017	0.058	-0.017	98.841
Con_conc__216	70.886	28.171	0.045	0.077	-0.005	99.174
Con_conc__217	85.597	12.896	0.074	0.070	0.068	98.704
Con_conc__218	67.632	32.203	-0.029	0.065	-0.006	99.864
Con_conc__219	72.073	27.207	-0.037	0.057	0.005	99.306
Con_conc__220	84.146	14.726	-0.082	0.069	-0.003	98.856
Con_conc__221	81.181	18.453	0.072	0.073	0.017	99.796
Con_conc__222	74.567	24.629	0.002	0.062	-0.032	99.229
Con_conc__223	66.788	32.066	0.050	0.047	0.037	98.988
Con_conc__224	86.959	11.737	0.046	0.109	-0.037	98.814
Con_conc__225	78.432	21.358	0.126	0.062	0.002	99.981
Con_conc__226	73.990	25.225	0.142	0.062	0.021	99.439
Con_conc__227	76.186	22.726	-0.016	0.070	0.001	98.967
Con_conc__228	79.791	19.171	-0.021	0.080	0.021	99.041
Con_conc__229	66.410	32.924	0.023	0.051	-0.008	99.400
Con_conc__230	77.621	22.081	-0.060	0.065	0.001	99.707
Con_conc__231	81.832	17.541	0.040	0.074	-0.018	99.469
Con_conc__232	78.801	18.972	0.024	0.040	0.002	97.839
Con_conc__233	82.476	17.044	-0.012	0.056	0.043	99.608
Con_conc__234	78.112	20.617	-0.014	0.046	0.021	98.781
Con_conc__235	84.191	14.462	0.148	0.074	-0.036	98.840
Con_conc__236	67.733	31.588	0.024	0.062	-0.018	99.390
Con_conc__237	81.388	16.105	0.037	0.082	0.027	97.639
Con_conc__238	81.932	19.034	0.053	0.059	-0.009	101.069
Con_conc__239	60.396	37.081	-0.006	0.040	-0.035	97.475
Con_conc__240	77.634	22.127	0.034	0.069	-0.003	99.862
Con_conc__241	83.994	16.532	0.081	0.047	0.028	100.681
Con_conc__242	80.810	18.433	0.031	0.066	-0.018	99.322
Con_conc__243	68.790	31.527	0.073	0.053	0.000	100.444
Con_conc__244	65.888	34.546	-0.058	0.031	0.037	100.443
Con_conc__245	62.115	37.025	-0.061	0.051	0.001	99.131
Con_conc__246	66.293	33.555	-0.037	0.044	-0.014	99.842
Con_conc__247	82.761	16.033	0.042	0.066	-0.035	98.866
Con_conc__248	67.647	30.816	-0.066	0.051	-0.023	98.424

ID	Au WT%	Ag WT%	Hg WT%	Cu WT%	Pd WT%	TOTAL
Con_conc__249	63.773	37.277	0.020	0.063	0.026	101.159
Con_conc__250	65.366	33.708	-0.056	0.038	-0.006	99.050
Con_conc__251	72.463	27.484	0.028	0.062	0.014	100.051
Con_conc__252	84.317	14.717	0.016	0.092	0.022	99.164
Con_conc__253	82.833	16.181	-0.023	0.065	0.012	99.068
Con_conc__254	83.723	15.666	0.004	0.100	0.007	99.499
Con_conc__255	80.358	18.811	-0.015	0.067	-0.049	99.171
Con_conc__256	79.897	19.473	0.000	0.060	0.043	99.472
Con_conc__257	76.939	21.974	0.008	0.060	0.047	99.028
Con_conc__258	82.495	16.240	0.009	0.065	-0.052	98.757
Con_conc__259	82.601	17.221	-0.001	0.080	0.016	99.918
Con_conc__260	85.533	13.760	0.076	0.101	0.018	99.487
Con_conc__261	84.067	16.106	-0.025	0.094	-0.011	100.231
Con_conc__262	78.652	21.175	0.025	0.095	0.027	99.974
Con_conc__263	79.709	20.121	-0.043	0.074	0.055	99.917
Con_conc__264	82.756	15.110	0.098	0.064	0.002	98.030
Con_conc__265	79.129	20.169	0.005	0.084	-0.025	99.361
Con_conc__266	81.455	17.917	0.003	0.076	0.061	99.510
Con_conc__267	79.882	19.429	0.091	0.102	-0.025	99.479
Con_conc__268	60.174	39.101	0.066	0.055	-0.003	99.394
Con_conc__269	83.788	16.077	0.128	0.092	0.007	100.091
Con_conc__270	78.491	21.146	-0.011	0.058	0.024	99.708
Con_conc__271	85.891	13.383	0.057	0.077	0.031	99.439
Con_conc__272	82.642	16.910	0.051	0.094	0.035	99.732
Con_conc__273	60.249	39.626	-0.018	0.080	0.005	99.941
Con_conc__274	84.797	14.645	0.039	0.104	0.020	99.606
Con_conc__275	83.544	15.888	0.010	0.092	0.040	99.575
Con_conc__276	81.602	17.808	0.076	0.088	-0.051	99.523
Con_conc__277	78.026	21.978	-0.015	0.065	0.025	100.079
Con_conc__278	82.014	17.576	0.054	0.075	0.022	99.741
Con_conc__279	83.266	16.160	-0.005	0.109	0.034	99.563
Con_conc__280	80.134	19.024	0.042	0.085	-0.015	99.270
Con_conc__281	64.539	35.376	-0.012	0.077	-0.015	99.965
Con_conc__282	79.824	19.081	0.058	0.090	-0.064	98.989
Con_conc__283	67.427	33.016	0.033	0.086	-0.029	100.534
Con_conc__284	78.053	22.889	-0.035	0.071	-0.022	100.955
Con_conc__285	82.326	17.815	0.015	0.070	0.063	100.289
Con_conc__286	85.127	14.262	0.046	0.078	0.022	99.536
Con_conc__287	83.680	15.589	0.033	0.076	0.005	99.384
Con_conc__288	83.261	16.240	0.057	0.080	0.029	99.666
Con_conc__289	81.613	17.167	0.032	0.074	0.005	98.891
Con_conc__290	76.353	23.316	0.090	0.069	-0.020	99.809
Con_conc__291	69.134	30.001	0.006	0.065	0.018	99.225
Con_conc__292	67.009	33.398	0.112	0.061	-0.007	100.573
Con_conc__293	82.666	16.813	0.072	0.047	0.021	99.621
Con_conc__294	76.793	22.866	0.020	0.052	-0.012	99.720
Con_conc__295	77.246	22.617	0.028	0.061	0.020	99.972
Con_conc__296	79.639	19.773	-0.051	0.210	0.029	99.600

ID	Au WT%	Ag WT%	Hg WT%	Cu WT%	Pd WT%	TOTAL
Con_conc__297	72.505	27.897	0.056	0.045	-0.022	100.481
Con_conc__298	77.643	21.987	-0.031	0.049	0.014	99.663
Con_conc__299	79.302	20.236	-0.026	0.053	-0.028	99.538
Con_conc__300	77.286	22.037	0.050	0.063	-0.013	99.424
Con_conc__301	75.090	24.541	0.055	0.075	0.008	99.770
Con_conc__302	78.793	19.116	0.126	0.056	-0.005	98.086
Con_conc__303	72.149	28.163	0.040	0.057	-0.019	100.389
Con_conc__304	58.080	40.459	0.214	0.057	0.013	98.822
Con_conc__305	63.011	36.632	-0.033	0.055	0.007	99.672
Con_conc__306	55.285	42.422	0.548	0.048	0.008	98.311
Con_conc__307	62.049	38.184	0.005	0.073	-0.024	100.287
Con_conc__308	67.557	31.322	0.022	0.065	0.030	98.996
Con_conc__309	81.155	18.418	0.083	0.073	-0.027	99.703
Con_conc__310	74.205	25.121	0.116	0.060	0.037	99.540
Con_conc__311	62.305	37.653	0.001	0.051	0.014	100.024
Con_conc__312	73.342	27.113	-0.009	0.069	0.002	100.515
Con_conc__313	82.980	16.264	-0.017	0.071	-0.018	99.280
Con_conc__314	82.218	15.893	-0.004	0.078	0.001	98.187
Con_conc__315	78.209	20.759	0.058	0.059	-0.054	99.030
Con_conc__316	73.652	26.572	0.008	0.053	0.018	100.303
Con_conc__317	80.420	18.457	0.048	0.098	-0.019	99.004
Con_conc__318	56.774	42.402	-0.068	0.044	-0.023	99.130
Con_conc__319	66.405	32.859	-0.017	0.045	-0.010	99.282
Con_conc__320	65.816	33.337	0.169	0.051	0.062	99.434
Con_conc__321	82.550	16.830	0.074	0.087	-0.022	99.518
Con_conc__322	83.253	16.198	-0.021	0.055	0.025	99.510
Con_conc__323	83.283	16.258	-0.007	0.058	0.016	99.608
Con_conc__324	83.839	14.754	0.030	0.074	0.012	98.709
Con_conc__325	83.204	15.947	0.080	0.066	0.036	99.333
Con_conc__326	57.958	40.000	0.065	0.038	0.026	98.086
Con_conc__327	82.625	17.092	0.027	0.090	-0.014	99.820
Con_conc__328	64.180	35.254	0.009	0.027	0.025	99.495
Con_conc__329	70.543	28.308	0.069	0.049	-0.007	98.962
Con_conc__330	83.741	15.706	-0.004	0.054	0.058	99.555
Con_conc__331	80.180	18.376	0.016	0.061	0.029	98.661
Con_conc__332	68.320	31.460	0.064	0.059	-0.004	99.898
Con_conc__333	77.714	22.248	0.127	0.063	-0.011	100.140
Con_conc__334	59.588	37.870	0.003	0.035	0.008	97.503
Con_conc__335	78.735	20.907	0.035	0.056	-0.028	99.705
Con_conc__336	80.390	19.693	0.060	0.046	0.017	100.205
Con_conc__337	82.598	16.971	-0.007	0.051	-0.006	99.607
Con_conc__338	80.515	18.228	0.025	0.065	-0.016	98.817
Con_conc__339	55.398	44.358	0.031	0.042	-0.003	99.826
Con_conc__340	82.549	16.328	0.062	0.064	-0.016	98.987
Con_conc__341	79.536	20.174	-0.041	0.056	0.013	99.738
Con_conc__342	39.003	59.913	0.037	0.031	-0.002	98.982
Con_conc__343	62.857	37.002	0.020	0.030	-0.030	99.879
Con_conc__344	52.945	45.375	0.079	0.027	0.005	98.432

ID	Au WT%	Ag WT%	Hg WT%	Cu WT%	Pd WT%	TOTAL
Con_conc__345	54.951	43.992	0.004	0.052	-0.029	98.970
Con_conc__346	58.286	39.095	0.013	0.034	-0.030	97.397

Cononish Area Detrital EMPA Data

Block	Grain ID	Sample	Traverse?	Au WT%	Ag WT%	Hg WT%	Cu WT%	Total
RJC 97	RJC97 1 1	Eas Annie Burn 2		72.07	27.65	0.00	0.07	99.79
RJC 97	RJC97 1 2	Eas Annie Burn 2		87.66	11.85	0.10	0.13	99.74
RJC 97	RJC97 1 3	Eas Annie Burn 2		57.70	40.94	0.06	0.08	98.77
RJC 97	RJC97 1 4	Eas Annie Burn 2		62.17	36.24	0.09	0.09	98.60
RJC 97	RJC97 1 5	Eas Annie Burn 2		74.12	25.45	0.11	0.08	99.76
RJC 97	RJC97 2 1	Eas Annie Burn 2		74.10	25.25	0.10	0.08	99.53
RJC 97	RJC97 2 2	Eas Annie Burn 2		68.98	30.00	0.19	0.09	99.26
RJC 97	RJC97 2 3	Eas Annie Burn 2		76.61	23.78	0.17	0.11	100.68
RJC 97	RJC97 2 4	Eas Annie Burn 2		84.31	15.57	0.08	0.12	100.09
RJC 97	RJC97 2 5	Eas Annie Burn 2		86.74	12.92	0.07	0.08	99.81
RJC 97	RJC97 2 6	Eas Annie Burn 2		48.56	49.38	0.21	0.08	98.22
RJC 97	RJC97 2 7	Eas Annie Burn 2		89.90	9.20	0.32	0.17	99.59
RJC 97	RJC97 2 8	Eas Annie Burn 2		90.33	9.52	0.13	0.10	100.08
RJC 97	RJC97 2 9	Eas Annie Burn 2		59.43	40.33	0.13	0.08	99.96
RJC 97	RJC97 2 10 core	Eas Annie Burn 2		69.00	30.54	0.07	0.08	99.68
RJC 97	RJC97 2 10 tract	Eas Annie Burn 2		75.51	20.26	0.08	0.06	95.92
RJC 97	RJC97 2 11	Eas Annie Burn 2		68.35	31.21	0.17	0.09	99.81
RJC 97	RJC97 2 12 core	Eas Annie Burn 2		84.32	16.38	0.20	0.14	101.04
RJC 97	RJC97 2 12 trail dark	Eas Annie Burn 2	T	69.48	30.41	0.10	0.08	100.07
RJC 97	RJC97 2 12 trail margin inter	Eas Annie Burn 2	T	68.88	31.12	0.14	0.09	100.23
RJC 97	RJC97 2 12 trav	Eas Annie Burn 2	T	83.94	16.72	0.20	0.11	100.96
RJC 97	RJC97 2 12 trav	Eas Annie Burn 2	T	83.77	16.76	0.11	0.12	100.76
RJC 97	RJC97 2 12 trav	Eas Annie Burn 2	T	83.79	16.52	0.16	0.11	100.57

Block	Grain ID	Sample	Traverse?	Au WT%	Ag WT%	Hg WT%	Cu WT%	Total
RJC 97	RJC97 2 12 trav	Eas Annie Burn 2	T	83.97	16.59	0.15	0.11	100.82
RJC 97	RJC97 2 12 trav	Eas Annie Burn 2	T	83.87	16.48	0.10	0.12	100.57
RJC 97	RJC97 2 12 trav	Eas Annie Burn 2	T	50.58	47.55	0.14	0.10	98.36
RJC 97	RJC97 2 12 trav	Eas Annie Burn 2	T	69.40	30.81	0.13	0.08	100.43
RJC 97	RJC97 2 12 trav	Eas Annie Burn 2	T	69.22	30.71	0.05	0.11	100.09
RJC 97	RJC97 2 12 trav	Eas Annie Burn 2	T	69.03	30.38	0.07	0.12	99.60
RJC 97	RJC97 2 12 trav	Eas Annie Burn 2	T	68.78	31.03	0.09	0.11	100.00
RJC 97	RJC97 2 12 trav	Eas Annie Burn 2	T	76.84	23.65	0.13	0.12	100.73
RJC 97	RJC97 2 12 trav	Eas Annie Burn 2	T	82.40	18.26	0.15	0.12	100.93
RJC 97	RJC97 2 12 trav	Eas Annie Burn 2	T	82.92	17.30	0.17	0.12	100.51
RJC 97	RJC97 2 12 trav	Eas Annie Burn 2	T	83.90	17.07	0.11	0.15	101.22
RJC 97	RJC97 2 12 trav	Eas Annie Burn 2	T	83.46	17.09	0.10	0.14	100.80
RJC 97	RJC97 2 12 trav	Eas Annie Burn 2	T	84.05	16.71	0.07	0.13	100.96
RJC 97	RJC97 2 12 trav	Eas Annie Burn 2	T	84.30	16.56	0.09	0.14	101.10
RJC 97	RJC97 2 13	Eas Annie Burn 2		80.10	20.01	0.10	0.15	100.35
RJC 97	RJC97 2 14	Eas Annie Burn 2		91.18	8.75	0.27	0.23	100.42
RJC 97	RJC97 2 15	Eas Annie Burn 2		66.25	33.17	0.12	0.07	99.60
RJC 98	RJC98 1 1	Eas Annie Burn 2		72.02	28.06	0.07	0.07	100.22
RJC 98	RJC98 1 2	Eas Annie Burn 2		63.26	36.71	0.00	0.07	100.04
RJC 98	RJC98 1 3	Eas Annie Burn 2		82.22	17.98	0.01	0.11	100.32
RJC 98	RJC98 1 4 Core	Eas Annie Burn 2		68.66	31.26	0.06	0.10	100.08
RJC 98	RJC98 1 5	Eas Annie Burn 2		73.20	27.13	0.11	0.14	100.58
RJC 98	RJC98 1 6	Eas Annie Burn 2		74.21	26.53	0.21	0.13	101.07
RJC 98	RJC98 1 7	Eas Annie Burn 2		54.95	43.78	0.04	0.15	98.91
RJC 98	RJC98 1 8	Eas Annie Burn 2		65.97	33.91	0.06	0.10	100.04
RJC 98	RJC98 1 9	Eas Annie Burn 2		86.19	14.73	0.18	0.12	101.22
RJC 98	RJC98 1 10	Eas Annie Burn 2		64.30	35.74	0.11	0.09	100.24
RJC 98	RJC98 1 11	Eas Annie Burn 2		75.23	25.32	0.17	0.09	100.81

Block	Grain ID	Sample	Traverse?	Au WT%	Ag WT%	Hg WT%	Cu WT%	Total
RJC 98	RJC98 1 12	Eas Annie Burn 2		62.45	37.62	0.08	0.09	100.24
RJC 98	RJC98 1 13	Eas Annie Burn 2		91.62	9.32	0.13	0.12	101.20
RJC 98	RJC98 1 14	Eas Annie Burn 2		51.70	47.30	0.13	0.07	99.21
RJC 98	RJC98 1 15	Eas Annie Burn 2		72.86	27.35	0.20	0.06	100.46
RJC 98	RJC98 1 16	Eas Annie Burn 2		68.84	31.60	0.08	0.06	100.58
RJC 98	RJC98 1 17	Eas Annie Burn 2		64.17	35.54	0.15	0.09	99.95
RJC 98	RJC98 1 18	Eas Annie Burn 2		98.73	1.25	0.20	0.61	100.78
RJC 98	RJC98 1 19	Eas Annie Burn 2		67.15	33.03	0.15	0.08	100.41
RJC 98	RJC98 1 20	Eas Annie Burn 2		78.06	22.39	0.11	0.07	100.63
RJC 98	RJC98 1 21	Eas Annie Burn 2		97.41	3.15	0.28	0.13	100.96
RJC 98	RJC98 1 22	Eas Annie Burn 2		83.59	17.00	0.20	0.11	100.90
RJC 98	RJC98 1 23	Eas Annie Burn 2		75.06	25.49	0.19	0.14	100.88
RJC 98	RJC98 1 24	Eas Annie Burn 2		66.35	33.61	0.06	0.05	100.06
RJC 98	RJC98 1 25	Eas Annie Burn 2		71.69	28.22	0.11	0.08	100.10
RJC 98	RJC98 1 26	Eas Annie Burn 2		62.31	37.90	0.06	0.08	100.34
RJC 98	RJC98 1 27	Eas Annie Burn 2		79.28	20.70	0.11	0.14	100.22
RJC 98	RJC98 1 28	Eas Annie Burn 2		86.88	13.66	0.24	0.10	100.88
RJC 98	RJC98 1 29	Eas Annie Burn 2		70.96	28.98	0.11	0.06	100.11
RJC 98	RJC98 1 30	Eas Annie Burn 2		60.99	38.12	0.00	0.06	99.17
RJC 98	RJC98 1 31	Eas Annie Burn 2		65.93	33.58	0.15	0.07	99.72
RJC 100	RJC100 1 1	Eas Annie Burn 2		72.58	27.74	0.04	0.16	100.52
RJC 100	RJC100 1 2 Core	Eas Annie Burn 2		44.63	54.05	0.01	0.10	98.79
RJC 101	RJC100 1 2 trav 1	Eas Annie Burn 2	T	92.37	3.78	0.08	0.11	96.34
RJC 102	RJC100 1 2 trav 1	Eas Annie Burn 2	T	94.06	3.50	0.03	0.12	97.71
RJC 103	RJC100 1 2 trav 1	Eas Annie Burn 2	T	92.92	4.05	0.12	0.12	97.20
RJC 104	RJC100 1 2 trav 1	Eas Annie Burn 2	T	91.89	5.54	0.00	0.12	97.54
RJC 105	RJC100 1 2 trav 1	Eas Annie Burn 2	T	91.95	4.77	0.12	0.10	96.94
RJC 106	RJC100 1 2 trav 1	Eas Annie Burn 2	T	91.18	4.24	0.05	0.13	95.61

Block	Grain ID	Sample	Traverse?	Au WT%	Ag WT%	Hg WT%	Cu WT%	Total
RJC 107	RJC100 1 2 trav 1	Eas Annie Burn 2	T	90.37	3.90	0.18	0.13	94.58
RJC 108	RJC100 1 2 trav 1	Eas Annie Burn 2	T	91.58	3.65	0.10	0.13	95.46
RJC 109	RJC100 1 2 trav 1	Eas Annie Burn 2	T	90.87	3.27	0.08	0.10	94.32
RJC 110	RJC100 1 2 trav 1	Eas Annie Burn 2	T	88.83	3.74	0.10	0.13	92.80
RJC 111	RJC100 1 2 trav 1	Eas Annie Burn 2	T	89.17	4.23	0.08	0.12	93.61
RJC 112	RJC100 1 2 trav 1	Eas Annie Burn 2	T	87.25	6.58	0.03	0.13	93.99
RJC 113	RJC100 1 2 trav 1	Eas Annie Burn 2	T	77.64	14.97	0.00	0.10	92.71
RJC 114	RJC100 1 2 trav 1	Eas Annie Burn 2	T	60.09	37.46	0.08	0.10	97.73
RJC 115	RJC100 1 2 trav 1	Eas Annie Burn 2	T	47.39	52.25	0.10	0.10	99.83
RJC 116	RJC100 1 2 trav 1	Eas Annie Burn 2	T	48.11	51.25	0.02	0.11	99.48
RJC 117	RJC100 1 2 trav 1	Eas Annie Burn 2	T	50.00	49.46	0.09	0.11	99.66
RJC 118	RJC100 1 2 trav 1	Eas Annie Burn 2	T	50.29	49.24	0.06	0.09	99.68
RJC 119	RJC100 1 2 trav 1	Eas Annie Burn 2	T	50.22	49.45	0.13	0.11	99.90
RJC 120	RJC100 1 2 trav 1	Eas Annie Burn 2	T	49.13	50.22	0.09	0.09	99.54
RJC 121	RJC100 1 2 trav 1	Eas Annie Burn 2	T	48.12	51.28	0.16	0.10	99.67
RJC 122	RJC100 1 2 trav 1	Eas Annie Burn 2	T	47.31	51.85	0.16	0.10	99.42
RJC 123	RJC100 1 2 trav 1	Eas Annie Burn 2	T	47.13	51.79	0.12	0.08	99.12
RJC 124	RJC100 1 2 trav 1	Eas Annie Burn 2	T	47.24	52.05	0.04	0.11	99.45
RJC 125	RJC100 1 2 trav 1	Eas Annie Burn 2	T	47.28	52.07	0.19	0.09	99.64
RJC 126	RJC100 1 2 trav 1	Eas Annie Burn 2	T	47.45	51.76	0.17	0.08	99.47
RJC 127	RJC100 1 2 trav 1	Eas Annie Burn 2	T	47.52	51.68	0.17	0.10	99.47
RJC 128	RJC100 1 2 trav 1	Eas Annie Burn 2	T	47.80	51.48	0.09	0.09	99.46
RJC 129	RJC100 1 2 trav 1	Eas Annie Burn 2	T	48.29	50.58	0.13	0.08	99.07
RJC 130	RJC100 1 2 trav 1	Eas Annie Burn 2	T	48.91	50.42	0.17	0.11	99.61
RJC 131	RJC100 1 2 trav 1	Eas Annie Burn 2	T	49.18	50.07	0.19	0.10	99.54
RJC 132	RJC100 1 2 trav 1	Eas Annie Burn 2	T	49.72	49.79	0.19	0.10	99.80
RJC 133	RJC100 1 2 trav 1	Eas Annie Burn 2	T	49.81	49.63	0.25	0.09	99.78
RJC 134	RJC100 1 2 trav 1	Eas Annie Burn 2	T	79.92	21.47	0.05	0.12	101.56

Block	Grain ID	Sample	Traverse?	Au WT%	Ag WT%	Hg WT%	Cu WT%	Total
RJC 135	RJC100 1 2 trav 1	Eas Annie Burn 2	T	90.75	7.39	0.00	0.12	98.25
RJC 136	RJC100 1 2 trav 1	Eas Annie Burn 2	T	79.94	24.26	0.11	0.12	104.44
RJC 137	RJC100 1 2 trav 1	Eas Annie Burn 2	T	52.95	47.61	0.06	0.09	100.72
RJC 138	RJC100 1 2 trav 1	Eas Annie Burn 2	T	50.27	49.68	0.04	0.09	100.08
RJC 139	RJC100 1 3	Eas Annie Burn 2		59.40	40.68	0.08	0.10	100.26
RJC 100	RJC100 1 4	Eas Annie Burn 2		70.04	30.43	0.28	0.14	100.90
RJC 100	RJC100 1 5	Eas Annie Burn 2		74.75	25.47	0.15	0.13	100.49
RJC 100	RJC100 1 6	Eas Annie Burn 2		83.32	17.69	0.20	0.12	101.33
RJC 100	RJC100 1 7	Eas Annie Burn 2		96.85	3.64	0.13	0.26	100.89
RJC 100	RJC100 1 8	Eas Annie Burn 2		68.06	32.18	0.12	0.12	100.47
RJC 100	RJC100 1 9	Eas Annie Burn 2		72.53	28.25	0.10	0.13	101.02
RJC 100	RJC100 1 10	Eas Annie Burn 2		71.63	29.26	0.11	0.11	101.11
RJC 100	RJC100 1 11	Eas Annie Burn 2		90.84	9.83	0.21	0.12	101.00
RJC 100	RJC100 1 12	Eas Annie Burn 2		74.91	25.81	0.05	0.14	100.91
RJC 100	RJC100 1 13	Eas Annie Burn 2		77.87	23.24	0.18	0.13	101.42
RJC 100	RJC100 1 14	Eas Annie Burn 2		69.16	31.38	0.21	0.12	100.87
RJC 100	RJC100 1 15	Eas Annie Burn 2		69.70	30.91	0.16	0.14	100.91
RJC 100	RJC100 1 16 core	Eas Annie Burn 2		74.48	26.67	0.11	0.14	101.41
RJC 100	RJC100 1 17	Eas Annie Burn 2		92.70	8.57	0.14	0.15	101.55
RJC 100	RJC100 1 18	Eas Annie Burn 2		79.84	20.77	0.17	0.11	100.88
RJC 100	RJC100 1 19	Eas Annie Burn 2		69.92	31.23	0.03	0.14	101.32
RJC 100	RJC100 1 20	Eas Annie Burn 2		91.02	10.05	0.08	0.17	101.33
RJC 100	RJC100 1 21	Eas Annie Burn 2		68.78	31.56	0.07	0.09	100.49
RJC 100	RJC100 1 22	Eas Annie Burn 2		71.87	29.00	0.00	0.09	100.95
RJC 100	RJC100 1 23	Eas Annie Burn 2		72.25	28.25	0.07	0.13	100.70
RJC 100	RJC100 1 24	Eas Annie Burn 2		76.05	24.33	0.01	0.10	100.48
RJC 100	RJC100 1 25	Eas Annie Burn 2		71.29	29.22	0.06	0.10	100.67
RJC 100	RJC100 1 26	Eas Annie Burn 2		72.93	27.69	0.11	0.09	100.82

Block	Grain ID	Sample	Traverse?	Au WT%	Ag WT%	Hg WT%	Cu WT%	Total
RJC 100	RJC100 1 27	Eas Annie Burn 2		86.70	14.20	0.16	0.08	101.13
RJC 100	RJC100 1 28	Eas Annie Burn 2		78.91	21.57	0.13	0.12	100.72
RJC 100	RJC100 1 29	Eas Annie Burn 2		90.25	10.42	0.19	0.17	101.03
RJC 100	RJC100 1 30	Eas Annie Burn 2		78.11	22.37	0.24	0.12	100.84
RJC 100	RJC100 2 1	Eas Annie Burn 2		65.32	35.15	0.10	0.10	100.67
RJC 100	RJC100 2 2	Eas Annie Burn 2		71.73	29.34	0.07	0.12	101.26
RJC 100	RJC100 2 3	Eas Annie Burn 2		61.65	38.37	0.09	0.07	100.18
RJC 100	RJC100 2 4	Eas Annie Burn 2		68.37	31.83	0.03	0.08	100.31
RJC 100	RJC100 2 5	Eas Annie Burn 2		71.79	29.28	0.13	0.14	101.34
RJC 100	RJC100 2 6	Eas Annie Burn 2		87.00	14.31	0.27	0.10	101.68
RJC 100	RJC100 2 7	Eas Annie Burn 2		61.19	38.83	0.04	0.09	100.14
RJC 100	RJC100 2 8	Eas Annie Burn 2		82.33	18.88	0.17	0.11	101.48
RJC 100	RJC100 2 9	Eas Annie Burn 2		76.46	24.72	0.16	0.09	101.44
RJC 100	RJC100 2 10	Eas Annie Burn 2		74.61	26.49	0.11	0.11	101.32
RJC 100	RJC100 2 11	Eas Annie Burn 2		76.89	23.50	0.23	0.11	100.73
RJC 100	RJC100 2 12 Core	Eas Annie Burn 2		67.81	33.18	0.15	0.13	101.26
RJC 100	RJC100 2 12 trans	Eas Annie Burn 2	T	68.08	33.92	0.07	0.09	102.16
RJC 100	RJC100 2 12 trans	Eas Annie Burn 2	T	68.60	33.06	0.02	0.09	101.76
RJC 100	RJC100 2 12 trans	Eas Annie Burn 2	T	74.01	3.30	0.21	0.10	77.63
RJC 100	RJC100 2 12 trans	Eas Annie Burn 2	T	76.41	2.94	0.19	0.09	79.64
RJC 100	RJC100 2 12 trans	Eas Annie Burn 2	T	70.90	20.57	0.05	0.11	91.63
RJC 100	RJC100 2 12 trans	Eas Annie Burn 2	T	72.70	19.91	0.19	0.06	92.86
RJC 100	RJC100 2 12 trans	Eas Annie Burn 2	T	74.17	3.99	0.15	0.10	78.41
RJC 100	RJC100 2 12 trans	Eas Annie Burn 2	T	75.14	3.35	0.10	0.08	78.67
RJC 100	RJC100 2 12 trans	Eas Annie Burn 2	T	73.19	2.97	0.15	0.08	76.39
RJC 100	RJC100 2 12 trans	Eas Annie Burn 2	T	74.98	3.70	0.18	0.08	78.95
RJC 100	RJC100 2 12 trans	Eas Annie Burn 2	T	75.59	4.00	0.14	0.13	79.85
RJC 100	RJC100 2 12 trans	Eas Annie Burn 2	T	72.51	2.94	0.08	0.04	75.57

Block	Grain ID	Sample	Traverse?	Au WT%	Ag WT%	Hg WT%	Cu WT%	Total
RJC 100	RJC100 2 12 trans	Eas Annie Burn 2	T	75.18	3.48	0.06	0.03	78.75
RJC 100	RJC100 2 12 trans	Eas Annie Burn 2	T	76.91	5.36	0.04	0.08	82.39
RJC 100	RJC100 2 12 trans	Eas Annie Burn 2	T	68.27	4.07	0.11	0.07	72.52
RJC 100	RJC100 2 12 trans	Eas Annie Burn 2	T	76.02	12.02	0.15	0.11	88.29
RJC 100	RJC100 2 12 trans	Eas Annie Burn 2	T	46.32	54.31	0.07	0.06	100.76
RJC 100	RJC100 2 12 trans	Eas Annie Burn 2	T	71.97	22.02	0.11	0.05	94.15
RJC 100	RJC100 2 12 trans	Eas Annie Burn 2	T	80.38	3.99	0.10	0.05	84.53
RJC 100	RJC100 2 12 trans	Eas Annie Burn 2	T	78.41	3.55	0.04	0.03	82.03
RJC 100	RJC100 2 12 trans	Eas Annie Burn 2	T	65.03	31.90	0.03	0.08	97.05
RJC 100	RJC100 2 12 trans	Eas Annie Burn 2	T	63.88	32.35	0.15	0.05	96.43
RJC 100	RJC100 2 12 trans	Eas Annie Burn 2	T	83.48	3.41	0.01	0.04	86.94
RJC 100	RJC100 2 12 trans	Eas Annie Burn 2	T	51.11	48.36	0.04	0.10	99.61
RJC 100	RJC100 2 12 trans	Eas Annie Burn 2	T	58.13	42.90	0.06	0.07	101.16
RJC 100	RJC100 2 12 trans	Eas Annie Burn 2	T	59.10	41.53	0.13	0.07	100.83
RJC 100	RJC100 2 12 trans	Eas Annie Burn 2	T	60.16	40.47	0.08	0.06	100.77
RJC 100	RJC100 2 12 trans	Eas Annie Burn 2	T	60.72	40.30	0.11	0.07	101.20
RJC 100	RJC100 2 12 trans	Eas Annie Burn 2	T	59.16	41.87	0.11	0.06	101.20
RJC 100	RJC100 2 12 trans	Eas Annie Burn 2	T	58.28	43.01	0.03	0.05	101.38
RJC 100	RJC100 2 12 trans	Eas Annie Burn 2	T	56.91	43.90	0.00	0.03	100.84
RJC 100	RJC100 2 12 trans	Eas Annie Burn 2	T	55.39	45.49	0.17	0.03	101.08
RJC 100	RJC100 2 12 trans	Eas Annie Burn 2	T	54.29	47.09	0.11	0.03	101.52
RJC 100	RJC100 2 12 trans	Eas Annie Burn 2	T	51.08	49.78	0.01	0.03	100.89
RJC 100	RJC100 2 13	Eas Annie Burn 2		78.51	22.54	0.14	0.11	101.30
RJC 100	RJC100 2 14	Eas Annie Burn 2		89.68	11.75	0.15	0.15	101.73
RJC 100	RJC100 2 15	Eas Annie Burn 2		62.63	6.11	0.00	0.07	68.82
RJC 100	RJC100 2 16	Eas Annie Burn 2		59.16	40.45	0.00	0.10	99.71
RJC 100	RJC100 2 17	Eas Annie Burn 2		76.26	24.58	0.04	0.13	101.01
RJC 100	RJC100 2 18	Eas Annie Burn 2		65.92	34.38	0.09	0.14	100.54

Block	Grain ID	Sample	Traverse?	Au WT%	Ag WT%	Hg WT%	Cu WT%	Total
RJC 100	RJC100 2 19	Eas Annie Burn 2		59.92	39.93	0.21	0.08	100.15
RJC 100	RJC100 2 20	Eas Annie Burn 2		71.31	28.83	0.05	0.09	100.28
RJC 100	RJC100 2 21	Eas Annie Burn 2		75.73	25.06	0.04	0.10	100.94
RJC 100	RJC100 2 22	Eas Annie Burn 2		73.65	26.93	0.17	0.11	100.87
RJC 100	RJC100 2 23	Eas Annie Burn 2		78.38	22.41	0.18	0.10	101.07
RJC 100	RJC100 2 24	Eas Annie Burn 2		86.17	14.62	0.28	0.24	101.32
RJC 100	RJC100 2 25	Eas Annie Burn 2		80.53	20.47	0.16	0.11	101.26
RJC 100	RJC100 2 26	Eas Annie Burn 2		71.35	29.31	0.08	0.09	100.82
RJC 100	RJC100 2 27	Eas Annie Burn 2		73.05	27.76	0.17	0.08	101.05
RJC 100	RJC100 2 28	Eas Annie Burn 2		68.32	32.21	0.13	0.11	100.77
RJC 100	RJC100 2 29	Eas Annie Burn 2		77.42	22.88	0.15	0.10	100.55
RJC 100	RJC100 2 30	Eas Annie Burn 2		88.32	12.91	0.26	0.13	101.62
RJC 100	RJC100 3 1	Eas Annie Burn 2		70.55	30.41	0.06	0.07	101.09
RJC 100	RJC100 3 2	Eas Annie Burn 2		76.76	24.03	0.12	0.11	101.03
RJC 100	RJC100 3 3	Eas Annie Burn 2		68.15	32.22	0.08	0.10	100.56
RJC 100	RJC100 3 4 core	Eas Annie Burn 2		79.11	22.08	0.05	0.13	101.37
RJC 100	RJC100 3 5	Eas Annie Burn 2		67.20	33.25	0.20	0.09	100.74
RJC 100	RJC100 3 6	Eas Annie Burn 2		66.84	33.54	0.07	0.08	100.52
RJC 100	RJC100 3 7	Eas Annie Burn 2		72.56	28.03	0.15	0.11	100.85
RJC 100	RJC100 3 8 core	Eas Annie Burn 2		74.19	26.37	0.13	0.11	100.80
RJC 100	RJC100 3 8 trans 1	Eas Annie Burn 2	T	72.06	28.66	0.12	0.08	100.91
RJC 100	RJC100 3 8 trans 1	Eas Annie Burn 2	T	72.56	28.70	0.18	0.09	101.53
RJC 100	RJC100 3 8 trans 1	Eas Annie Burn 2	T	72.41	28.61	0.18	0.09	101.29
RJC 100	RJC100 3 8 trans 1	Eas Annie Burn 2	T	72.21	29.14	0.10	0.08	101.53
RJC 100	RJC100 3 8 trans 1	Eas Annie Burn 2	T	71.17	29.48	0.13	0.11	100.89
RJC 100	RJC100 3 8 trans 1	Eas Annie Burn 2	T	71.74	29.78	0.15	0.10	101.78
RJC 100	RJC100 3 8 trans 1	Eas Annie Burn 2	T	71.12	30.02	0.20	0.09	101.42
RJC 100	RJC100 3 8 trans 1	Eas Annie Burn 2	T	71.75	29.80	0.04	0.11	101.70

Block	Grain ID	Sample	Traverse?	Au WT%	Ag WT%	Hg WT%	Cu WT%	Total
RJC 100	RJC100 3 8 trans 1	Eas Annie Burn 2	T	71.65	29.10	0.11	0.13	100.98
RJC 100	RJC100 3 8 trans 1	Eas Annie Burn 2	T	72.21	28.99	0.15	0.09	101.44
RJC 100	RJC100 3 8 trans 1	Eas Annie Burn 2	T	71.54	29.45	0.11	0.09	101.20
RJC 100	RJC100 3 8 trans 1	Eas Annie Burn 2	T	71.30	29.87	0.10	0.10	101.36
RJC 100	RJC100 3 8 trans 1	Eas Annie Burn 2	T	70.25	31.29	0.15	0.07	101.77
RJC 100	RJC100 3 8 trans 1	Eas Annie Burn 2	T	63.02	38.92	0.16	0.09	102.18
RJC 100	RJC100 3 8 trans 1	Eas Annie Burn 2	T	61.02	41.06	0.10	0.09	102.27
RJC 100	RJC100 3 8 trans 1	Eas Annie Burn 2	T	60.76	41.78	0.14	0.07	102.75
RJC 100	RJC100 3 8 trans 1	Eas Annie Burn 2	T	62.52	39.82	0.05	0.06	102.44
RJC 100	RJC100 3 8 trans 1	Eas Annie Burn 2	T	63.90	38.25	0.04	0.07	102.25
RJC 100	RJC100 3 8 trans 1	Eas Annie Burn 2	T	65.16	37.37	0.08	0.05	102.65
RJC 100	RJC100 3 8 trans 1	Eas Annie Burn 2	T	55.72	43.92	0.03	0.10	99.76
RJC 100	RJC100 3 8 trans 1	Eas Annie Burn 2	T	59.74	31.89	0.00	0.04	91.67
RJC 100	RJC100 3 8 trans 1	Eas Annie Burn 2	T	63.10	25.54	0.00	0.06	88.70
RJC 100	RJC100 3 8 trans 1	Eas Annie Burn 2	T	67.03	33.45	0.08	0.09	100.66
RJC 100	RJC100 3 8 trans 1	Eas Annie Burn 2	T	67.30	32.98	0.20	0.09	100.57
RJC 100	RJC100 3 8 trans 1	Eas Annie Burn 2	T	67.97	32.02	0.05	0.10	100.14
RJC 100	RJC100 3 8 trans 1	Eas Annie Burn 2	T	68.25	32.21	0.19	0.08	100.73
RJC 100	RJC100 3 8 trans 1	Eas Annie Burn 2	T	69.67	30.71	0.15	0.08	100.62
RJC 100	RJC100 3 8 trans 1	Eas Annie Burn 2	T	70.25	30.44	0.18	0.10	100.97
RJC 100	RJC100 3 8 trans 1	Eas Annie Burn 2	T	69.82	30.62	0.20	0.10	100.74
RJC 100	RJC100 3 9	Eas Annie Burn 2		60.74	39.63	0.11	0.10	100.57
RJC 100	RJC100 3 10	Eas Annie Burn 2		72.98	27.61	0.16	0.12	100.86
RJC 100	RJC100 3 11	Eas Annie Burn 2		85.28	15.41	0.16	0.14	100.99
RJC 100	RJC100 3 12	Eas Annie Burn 2		71.58	28.93	0.10	0.10	100.72
RJC 100	RJC100 3 13	Eas Annie Burn 2		66.21	34.17	0.13	0.11	100.61
RJC 100	RJC100 3 14	Eas Annie Burn 2		76.18	24.76	0.11	0.11	101.17
RJC 100	RJC100 3 15	Eas Annie Burn 2		75.65	25.39	0.12	0.12	101.27

Block	Grain ID	Sample	Traverse?	Au WT%	Ag WT%	Hg WT%	Cu WT%	Total
RJC 100	RJC100 3 16	Eas Annie Burn 2		75.47	25.28	0.11	0.10	100.96
RJC 100	RJC100 3 17	Eas Annie Burn 2		68.33	32.08	0.03	0.08	100.51
RJC 100	RJC100 3 18	Eas Annie Burn 2		64.91	35.56	0.01	0.08	100.55
RJC 100	RJC100 3 19	Eas Annie Burn 2		78.97	22.39	0.15	0.13	101.63
RJC 100	RJC100 3 20	Eas Annie Burn 2		68.71	31.47	0.11	0.11	100.40
RJC 100	RJC100 3 21	Eas Annie Burn 2		60.68	39.48	0.09	0.08	100.32
RJC 100	RJC100 3 22	Eas Annie Burn 2		63.58	36.94	0.17	0.08	100.76
RJC 100	RJC100 3 23	Eas Annie Burn 2		72.46	28.04	0.15	0.13	100.78
RJC 100	RJC100 3 24	Eas Annie Burn 2		82.03	18.99	0.22	0.09	101.34
RJC 100	RJC100 3 25	Eas Annie Burn 2		75.03	25.62	0.06	0.11	100.82
RJC 100	RJC100 3 26	Eas Annie Burn 2		75.51	25.41	0.16	0.09	101.18
RJC 100	RJC100 3 27	Eas Annie Burn 2		72.94	27.06	0.19	0.13	100.32
RJC 100	RJC100 3 28	Eas Annie Burn 2		88.36	12.47	0.17	0.10	101.10
RJC 100	RJC100 3 29	Eas Annie Burn 2		78.39	22.82	0.16	0.07	101.44
RJC 100	RJC100 3 30	Eas Annie Burn 2		69.45	30.28	0.12	0.10	99.95
RJC 100	RJC100 3 8 trans	Eas Annie Burn 2	T	66.19	20.92	0.00	0.05	87.16
RJC 100	RJC100 3 8 trans	Eas Annie Burn 2	T	66.81	20.41	0.00	0.05	87.27
RJC 100	RJC100 3 8 trans	Eas Annie Burn 2	T	67.66	18.48	0.00	0.03	86.18
RJC 100	RJC100 3 8 trans	Eas Annie Burn 2	T	66.93	18.58	0.00	0.04	85.55
RJC 100	RJC100 3 8 trans	Eas Annie Burn 2	T	64.76	22.48	0.00	0.04	87.28
RJC 100	RJC100 3 8 trans	Eas Annie Burn 2	T	66.29	19.28	0.00	0.03	85.60
RJC 100	RJC100 3 8 trans	Eas Annie Burn 2	T	67.58	17.64	0.00	0.03	85.24
RJC 100	RJC100 3 8 trans	Eas Annie Burn 2	T	68.16	15.80	0.00	0.04	84.00
RJC 100	RJC100 3 8 trans	Eas Annie Burn 2	T	67.43	16.11	0.00	0.04	83.58
RJC 100	RJC100 3 8 trans	Eas Annie Burn 2	T	67.93	15.25	0.00	0.03	83.21
RJC 100	RJC100 3 8 trans	Eas Annie Burn 2	T	66.70	15.44	0.00	0.03	82.18
RJC 100	RJC100 3 8 trans	Eas Annie Burn 2	T	68.28	13.69	0.00	0.03	82.00
RJC 100	RJC100 4 1 core	Eas Annie Burn 2		53.20	46.20	0.11	0.07	99.58

Block	Grain ID	Sample	Traverse?	Au WT%	Ag WT%	Hg WT%	Cu WT%	Total
RJC 100	RJC100 4 1 trans	Eas Annie Burn 2	T	55.92	44.07	0.03	0.08	100.11
RJC 100	RJC100 4 1 trans	Eas Annie Burn 2	T	56.27	43.71	0.13	0.05	100.16
RJC 100	RJC100 4 1 trans	Eas Annie Burn 2	T	56.89	43.56	0.09	0.06	100.60
RJC 100	RJC100 4 1 trans	Eas Annie Burn 2	T	56.86	42.92	0.11	0.06	99.96
RJC 100	RJC100 4 1 trans	Eas Annie Burn 2	T	57.35	42.58	0.05	0.06	100.04
RJC 100	RJC100 4 1 trans	Eas Annie Burn 2	T	56.29	43.68	0.13	0.07	100.18
RJC 100	RJC100 4 1 trans	Eas Annie Burn 2	T	53.90	45.65	0.07	0.07	99.68
RJC 100	RJC100 4 1 trans	Eas Annie Burn 2	T	51.58	48.14	0.10	0.06	99.88
RJC 100	RJC100 4 1 trans	Eas Annie Burn 2	T	51.11	47.97	0.08	0.07	99.23
RJC 100	RJC100 4 1 trans	Eas Annie Burn 2	T	51.74	47.67	0.04	0.09	99.54
RJC 100	RJC100 4 1 trans	Eas Annie Burn 2	T	51.87	47.96	0.15	0.06	100.04
RJC 100	RJC100 4 1 trans	Eas Annie Burn 2	T	52.99	47.15	0.03	0.05	100.22
RJC 100	RJC100 4 1 trans	Eas Annie Burn 2	T	62.47	38.74	0.09	0.09	101.38
RJC 100	RJC100 4 1 trans	Eas Annie Burn 2	T	63.03	37.67	0.06	0.07	100.82
RJC 100	RJC100 4 1 trans	Eas Annie Burn 2	T	64.30	36.52	0.03	0.06	100.91
RJC 100	RJC100 4 1 trans	Eas Annie Burn 2	T	65.33	35.61	0.18	0.06	101.17
RJC 100	RJC100 4 1 trans	Eas Annie Burn 2	T	68.72	32.06	0.10	0.06	100.94
RJC 100	RJC100 4 1 trans	Eas Annie Burn 2	T	68.34	32.43	0.12	0.08	100.97
RJC 100	RJC100 4 1 trans	Eas Annie Burn 2	T	64.84	35.57	0.06	0.08	100.56
RJC 100	RJC100 4 1 trans	Eas Annie Burn 2	T	52.39	46.71	0.16	0.08	99.35
RJC 100	RJC100 4 1 trans	Eas Annie Burn 2	T	46.91	52.59	0.09	0.07	99.67
RJC 100	RJC100 4 1 trans	Eas Annie Burn 2	T	50.73	49.08	0.08	0.07	99.97
RJC 100	RJC100 4 1 trans	Eas Annie Burn 2	T	52.02	47.78	0.17	0.06	100.04
RJC 100	RJC100 4 1 trans	Eas Annie Burn 2	T	54.62	45.77	0.01	0.09	100.48
RJC 100	RJC100 4 1 trans	Eas Annie Burn 2	T	54.16	45.28	0.10	0.10	99.64
RJC 100	RJC100 4 1 trans	Eas Annie Burn 2	T	54.23	45.41	0.23	0.08	99.96
RJC 100	RJC100 4 1 trans	Eas Annie Burn 2	T	54.15	45.72	0.02	0.08	99.97
RJC 100	RJC100 4 1 trans	Eas Annie Burn 2	T	53.91	45.86	0.03	0.10	99.90

Block	Grain ID	Sample	Traverse?	Au WT%	Ag WT%	Hg WT%	Cu WT%	Total
RJC 100	RJC100 4 1 trans	Eas Annie Burn 2	T	53.76	46.18	0.07	0.08	100.09
RJC 100	RJC100 4 1 trans	Eas Annie Burn 2	T	53.42	45.98	0.09	0.09	99.58
RJC 100	RJC100 4 1 trans	Eas Annie Burn 2	T	53.43	46.02	0.10	0.08	99.63
RJC 100	RJC100 4 1 trans	Eas Annie Burn 2	T	53.63	46.20	0.15	0.08	100.07
RJC 100	RJC100 4 1 trans	Eas Annie Burn 2	T	53.61	45.99	0.12	0.07	99.78
RJC 100	RJC100 4 1 trans	Eas Annie Burn 2	T	53.64	46.27	0.07	0.07	100.06
RJC 100	RJC100 4 1 trans	Eas Annie Burn 2	T	53.47	46.32	0.08	0.06	99.93
RJC 100	RJC100 4 1 trans	Eas Annie Burn 2	T	53.42	45.91	0.13	0.07	99.53
RJC 100	RJC100 4 2	Eas Annie Burn 2		75.05	25.62	0.17	0.11	100.96
RJC 100	RJC100 4 3	Eas Annie Burn 2		84.57	16.42	0.15	0.09	101.23
RJC 100	RJC100 4 4	Eas Annie Burn 2		69.88	30.43	0.07	0.12	100.50
RJC 100	RJC100 4 5	Eas Annie Burn 2		72.32	28.05	0.11	0.10	100.58
RJC 100	RJC100 4 6	Eas Annie Burn 2		73.06	27.60	0.14	0.12	100.91
RJC 100	RJC100 4 7 core	Eas Annie Burn 2		70.64	30.37	0.16	0.06	101.24
RJC 100	RJC100 4 7 trav	Eas Annie Burn 2	T	70.74	30.34	0.09	0.07	101.24
RJC 100	RJC100 4 7 trav	Eas Annie Burn 2	T	70.57	29.89	0.09	0.09	100.63
RJC 100	RJC100 4 7 trav	Eas Annie Burn 2	T	70.60	30.12	0.10	0.08	100.90
RJC 100	RJC100 4 7 trav	Eas Annie Burn 2	T	70.18	29.84	0.13	0.08	100.23
RJC 100	RJC100 4 7 trav	Eas Annie Burn 2	T	70.54	30.18	0.06	0.11	100.90
RJC 100	RJC100 4 7 trav	Eas Annie Burn 2	T	70.42	30.20	0.10	0.10	100.82
RJC 100	RJC100 4 7 trav	Eas Annie Burn 2	T	70.38	30.24	0.17	0.07	100.85
RJC 100	RJC100 4 7 trav	Eas Annie Burn 2	T	70.03	30.65	0.09	0.08	100.84
RJC 100	RJC100 4 7 trav	Eas Annie Burn 2	T	69.04	31.65	0.03	0.07	100.79
RJC 100	RJC100 4 7 trav	Eas Annie Burn 2	T	60.56	39.22	0.08	0.07	99.94
RJC 100	RJC100 4 7 trav	Eas Annie Burn 2	T	45.94	53.40	0.02	0.06	99.42
RJC 100	RJC100 4 7 trav	Eas Annie Burn 2	T	44.87	54.28	0.08	0.07	99.30
RJC 100	RJC100 4 7 trav	Eas Annie Burn 2	T	44.19	54.90	0.04	0.09	99.21
RJC 100	RJC100 4 7 trav	Eas Annie Burn 2	T	45.80	53.32	0.03	0.06	99.20

Block	Grain ID	Sample	Traverse?	Au WT%	Ag WT%	Hg WT%	Cu WT%	Total
RJC 100	RJC100 4 7 trav	Eas Annie Burn 2	T	62.11	38.71	0.16	0.07	101.05
RJC 100	RJC100 4 7 trav	Eas Annie Burn 2	T	68.34	32.28	0.05	0.08	100.75
RJC 100	RJC100 4 7 trav	Eas Annie Burn 2	T	69.13	31.40	0.07	0.10	100.70
RJC 100	RJC100 4 7 trav	Eas Annie Burn 2	T	69.50	30.66	0.13	0.08	100.37
RJC 100	RJC100 4 7 trav	Eas Annie Burn 2	T	70.07	30.47	0.06	0.08	100.69
RJC 100	RJC100 4 7 trav	Eas Annie Burn 2	T	70.18	30.18	0.02	0.07	100.44
RJC 100	RJC100 4 7 trav	Eas Annie Burn 2	T	70.09	29.99	0.12	0.08	100.28
RJC 100	RJC100 4 7 trav	Eas Annie Burn 2	T	70.68	30.20	0.10	0.06	101.04
RJC 100	RJC100 4 7 trav	Eas Annie Burn 2	T	70.74	29.88	0.10	0.07	100.79
RJC 100	RJC100 4 8	Eas Annie Burn 2		71.49	29.20	0.24	0.08	101.00
RJC 100	RJC100 4 9	Eas Annie Burn 2		86.75	14.79	0.22	0.11	101.87
RJC 100	RJC100 4 10	Eas Annie Burn 2		78.05	22.33	0.16	0.10	100.64
RJC 100	RJC100 4 11	Eas Annie Burn 2		82.88	17.95	0.03	0.10	100.96
RJC 100	RJC100 4 12	Eas Annie Burn 2		66.79	33.87	0.10	0.08	100.84
RJC 100	RJC100 4 13	Eas Annie Burn 2		87.37	13.64	0.03	0.08	101.12
RJC 100	RJC100 4 14	Eas Annie Burn 2		63.88	36.56	0.14	0.09	100.67
RJC 100	RJC100 4 15	Eas Annie Burn 2		59.07	40.77	0.06	0.11	100.00
RJC 100	RJC100 4 16	Eas Annie Burn 2		77.55	23.24	0.08	0.09	100.95
RJC 100	RJC100 4 17	Eas Annie Burn 2		91.70	9.35	0.12	0.11	101.28
RJC 100	RJC100 4 18	Eas Annie Burn 2		76.60	23.64	0.19	0.09	100.53
RJC 100	RJC100 4 19	Eas Annie Burn 2		72.35	28.23	0.05	0.09	100.72
RJC 100	RJC100 4 20	Eas Annie Burn 2		64.17	36.18	0.15	0.07	100.57
RJC 100	RJC100 4 21	Eas Annie Burn 2		72.35	28.73	0.13	0.06	101.27
RJC 100	RJC100 4 22	Eas Annie Burn 2		73.26	27.44	0.18	0.10	100.98
RJC 100	RJC100 4 23	Eas Annie Burn 2		74.68	26.11	0.18	0.07	101.05
RJC 100	RJC100 4 24	Eas Annie Burn 2		74.25	26.75	0.13	0.11	101.24
RJC 100	RJC100 4 25	Eas Annie Burn 2		68.78	32.15	0.08	0.11	101.12
RJC 100	RJC100 4 26	Eas Annie Burn 2		69.92	30.62	0.06	0.11	100.71

Block	Grain ID	Sample	Traverse?	Au WT%	Ag WT%	Hg WT%	Cu WT%	Total
RJC 100	RJC100 4 27	Eas Annie Burn 2		73.77	27.48	0.14	0.08	101.47
RJC 100	RJC100 4 28	Eas Annie Burn 2		66.69	33.34	0.14	0.09	100.27
RJC 100	RJC100 4 29	Eas Annie Burn 2		72.32	28.43	0.14	0.08	100.97
RJC 100	RJC100 4 30	Eas Annie Burn 2		67.56	32.96	0.10	0.05	100.67
RJC 100	RJC100 5 1	Eas Annie Burn 2		69.55	31.49	0.03	0.09	101.16
RJC 100	RJC100 5 3	Eas Annie Burn 2		67.47	32.97	0.09	0.07	100.61
RJC 100	RJC100 5 4	Eas Annie Burn 2		71.46	29.87	0.14	0.07	101.54
RJC 100	RJC100 5 5	Eas Annie Burn 2		68.33	32.00	0.14	0.08	100.56
RJC 100	RJC100 5 6	Eas Annie Burn 2		56.32	43.41	0.11	0.07	99.91
RJC 100	RJC100 5 7	Eas Annie Burn 2		93.98	7.04	0.31	0.16	101.50
RJC 100	RJC100 5 8	Eas Annie Burn 2		76.97	23.75	0.08	0.07	100.86
RJC 100	RJC100 5 9	Eas Annie Burn 2		77.17	23.54	0.14	0.06	100.91
RJC 100	RJC100 5 10	Eas Annie Burn 2		72.82	27.82	0.14	0.09	100.88
RJC 100	RJC100 5 11	Eas Annie Burn 2		58.10	42.18	0.00	0.07	100.34
RJC 100	RJC100 5 12	Eas Annie Burn 2		76.03	24.95	0.07	0.09	101.14
RJC 100	RJC100 5 13 core	Eas Annie Burn 2		69.01	31.52	0.08	0.08	100.68
RJC 100	RJC100 5 14	Eas Annie Burn 2		71.58	29.27	0.11	0.09	101.05
RJC 100	RJC100 5 15	Eas Annie Burn 2		67.97	32.48	0.17	0.07	100.69
RJC 100	RJC100 5 16	Eas Annie Burn 2		87.14	13.90	0.14	0.09	101.27
RJC 100	RJC100 5 18	Eas Annie Burn 2		88.10	12.92	0.19	0.11	101.32
RJC 100	RJC100 5 19	Eas Annie Burn 2		71.73	28.67	0.04	0.10	100.54
RJC 100	RJC100 5 20	Eas Annie Burn 2		65.60	34.86	0.07	0.06	100.58
RJC 100	RJC100 5 21	Eas Annie Burn 2		78.43	22.86	0.06	0.05	101.40
RJC 100	RJC100 5 23	Eas Annie Burn 2		77.08	23.67	0.16	0.07	100.98
RJC 100	RJC100 5 24	Eas Annie Burn 2		68.51	32.21	0.12	0.06	100.89
RJC 100	RJC100 5 25	Eas Annie Burn 2		84.00	16.79	0.09	0.10	100.98
RJC 100	RJC100 5 26	Eas Annie Burn 2		71.89	27.90	0.16	0.06	100.01
RJC 99	RJC99 1 1	Eas Annie Burn 2		83.73	16.63	0.04	0.08	100.48

Block	Grain ID	Sample	Traverse?	Au WT%	Ag WT%	Hg WT%	Cu WT%	Total
RJC 99	RJC99 1 2	Eas Annie Burn 2		69.20	31.25	0.13	0.07	100.65
RJC 99	RJC99 1 3 core	Eas Annie Burn 2		78.16	22.59	0.08	0.07	100.90
RJC 99	RJC99 1 3 trav	Eas Annie Burn 2	T	74.42	26.46	0.04	0.07	100.98
RJC 99	RJC99 1 3 trav	Eas Annie Burn 2	T	74.66	25.92	0.00	0.08	100.66
RJC 99	RJC99 1 3 trav	Eas Annie Burn 2	T	74.73	25.66	0.08	0.08	100.55
RJC 99	RJC99 1 3 trav	Eas Annie Burn 2	T	75.11	25.35	0.12	0.07	100.66
RJC 99	RJC99 1 3 trav	Eas Annie Burn 2	T	75.71	25.17	0.02	0.08	100.98
RJC 99	RJC99 1 3 trav	Eas Annie Burn 2	T	75.61	24.77	0.06	0.08	100.52
RJC 99	RJC99 1 3 trav	Eas Annie Burn 2	T	74.85	24.73	0.15	0.09	99.81
RJC 99	RJC99 1 3 trav	Eas Annie Burn 2	T	75.96	24.92	0.01	0.09	100.98
RJC 99	RJC99 1 3 trav	Eas Annie Burn 2	T	75.68	24.77	0.05	0.08	100.58
RJC 99	RJC99 1 3 trav	Eas Annie Burn 2	T	75.12	24.43	0.17	0.11	99.83
RJC 99	RJC99 1 3 trav	Eas Annie Burn 2	T	75.59	24.50	0.08	0.09	100.27
RJC 99	RJC99 1 3 trav	Eas Annie Burn 2	T	76.22	24.59	0.15	0.10	101.05
RJC 99	RJC99 1 3 trav	Eas Annie Burn 2	T	75.98	24.36	0.07	0.09	100.50
RJC 99	RJC99 1 3 trav	Eas Annie Burn 2	T	76.18	24.56	0.12	0.07	100.93
RJC 99	RJC99 1 3 trav	Eas Annie Burn 2	T	75.94	24.22	0.12	0.06	100.35
RJC 99	RJC99 1 3 trav	Eas Annie Burn 2	T	76.63	24.17	0.10	0.08	100.99
RJC 99	RJC99 1 3 trav	Eas Annie Burn 2	T	76.46	23.97	0.04	0.06	100.53
RJC 99	RJC99 1 3 trav	Eas Annie Burn 2	T	76.80	24.38	0.06	0.07	101.31
RJC 99	RJC99 1 4	Eas Annie Burn 2		64.08	36.36	0.15	0.07	100.66
RJC 99	RJC99 1 5	Eas Annie Burn 2		72.26	28.22	0.15	0.07	100.70
RJC 99	RJC99 1 6	Eas Annie Burn 2		65.30	34.94	0.07	0.08	100.39
RJC 99	RJC99 1 7	Eas Annie Burn 2		88.62	12.48	0.21	0.08	101.38
RJC 99	RJC99 1 8	Eas Annie Burn 2		75.93	24.77	0.04	0.07	100.81
RJC 99	RJC99 1 9	Eas Annie Burn 2		74.08	25.83	0.20	0.07	100.19
RJC 99	RJC99 1 10	Eas Annie Burn 2		49.75	49.34	0.09	0.03	99.21
RJC 99	RJC99 1 11	Eas Annie Burn 2		68.76	31.77	0.04	0.05	100.62

Block	Grain ID	Sample	Traverse?	Au WT%	Ag WT%	Hg WT%	Cu WT%	Total
RJC 99	RJC99 1 12	Eas Annie Burn 2		58.14	41.68	0.06	0.07	99.93
RJC 99	RJC99 1 13	Eas Annie Burn 2		72.39	28.23	0.13	0.06	100.81
RJC 99	RJC99 1 14	Eas Annie Burn 2		85.15	15.57	0.23	0.08	101.03
RJC 99	RJC99 1 15	Eas Annie Burn 2		72.43	27.83	0.16	0.08	100.50
RJC 99	RJC99 1 16	Eas Annie Burn 2		89.01	12.06	0.09	0.12	101.29
RJC 99	RJC99 1 17	Eas Annie Burn 2		79.63	21.38	0.11	0.06	101.17
RJC 99	RJC99 1 18	Eas Annie Burn 2		69.15	31.26	0.16	0.06	100.62
RJC 99	RJC99 1 19	Eas Annie Burn 2		96.75	3.20	0.20	0.09	100.24
RJC 99	RJC99 1 20	Eas Annie Burn 2		71.28	28.68	0.05	0.08	100.09
RJC 99	RJC99 1 21	Eas Annie Burn 2		80.49	19.98	0.13	0.06	100.67
RJC 99	RJC99 1 22	Eas Annie Burn 2		67.31	33.22	0.09	0.05	100.67
RJC 99	RJC99 1 23	Eas Annie Burn 2		81.88	18.76	0.21	0.09	100.94
RJC 99	RJC99 1 24	Eas Annie Burn 2		87.63	13.31	0.08	0.08	101.11
RJC 99	RJC99 1 25	Eas Annie Burn 2		70.86	29.37	0.14	0.05	100.42
RJC 99	RJC99 1 26	Eas Annie Burn 2		63.46	36.39	0.14	0.05	100.05
RJC 99	RJC99 1 27	Eas Annie Burn 2		74.92	25.45	0.12	0.05	100.53
RJC 99	RJC99 1 28	Eas Annie Burn 2		75.77	24.75	0.11	0.06	100.69
RJC 99	RJC99 1 29	Eas Annie Burn 2		87.40	13.45	0.19	0.10	101.14
RJC 99	RJC99 1 30	Eas Annie Burn 2		74.48	26.19	0.15	0.06	100.88
RJC 99	RJC99 2 1	Eas Annie Burn 2		79.22	21.81	0.18	0.04	101.25
RJC 99	RJC99 2 2	Eas Annie Burn 2		66.03	34.18	0.07	0.06	100.34
RJC 99	RJC99 2 3	Eas Annie Burn 2		74.05	26.31	0.09	0.06	100.52
RJC 99	RJC99 2 4	Eas Annie Burn 2		68.96	31.26	0.17	0.06	100.45
RJC 99	RJC99 2 5	Eas Annie Burn 2		70.74	29.61	0.08	0.04	100.48
RJC 99	RJC99 2 6	Eas Annie Burn 2		60.38	39.46	0.11	0.06	100.00
RJC 99	RJC99 2 7	Eas Annie Burn 2		66.52	33.00	0.22	0.06	99.79
RJC 99	RJC99 2 8	Eas Annie Burn 2		84.19	16.48	0.15	0.09	100.91
RJC 99	RJC99 2 9	Eas Annie Burn 2		65.25	34.85	0.12	0.07	100.30

Block	Grain ID	Sample	Traverse?	Au WT%	Ag WT%	Hg WT%	Cu WT%	Total
RJC 99	RJC99 2 10	Eas Annie Burn 2		67.56	32.53	0.12	0.05	100.26
RJC 99	RJC99 2 11	Eas Annie Burn 2		66.37	33.78	0.12	0.07	100.34
RJC 99	RJC99 2 12	Eas Annie Burn 2		78.70	22.02	0.13	0.08	100.93
RJC 99	RJC99 2 13	Eas Annie Burn 2		98.30	1.89	0.12	0.11	100.42
RJC 99	RJC99 2 14	Eas Annie Burn 2		72.98	27.45	0.11	0.06	100.60
RJC 99	RJC99 2 15	Eas Annie Burn 2		66.62	33.89	0.15	0.05	100.72
RJC 99	RJC99 2 16	Eas Annie Burn 2		60.52	39.74	0.04	0.04	100.34
RJC 99	RJC99 2 17	Eas Annie Burn 2		84.22	16.40	0.26	0.12	101.01
RJC 99	RJC99 2 18	Eas Annie Burn 2		74.51	25.66	0.08	0.12	100.36
RJC 99	RJC99 2 19	Eas Annie Burn 2		64.79	35.19	0.11	0.10	100.19
RJC 99	RJC99 2 20	Eas Annie Burn 2		79.74	20.85	0.20	0.05	100.84
RJC 99	RJC99 2 21	Eas Annie Burn 2		67.26	33.07	0.11	0.06	100.50
RJC 99	RJC99 2 22	Eas Annie Burn 2		82.68	17.98	0.16	0.07	100.89
RJC 99	RJC99 2 23	Eas Annie Burn 2		90.84	9.61	0.23	0.08	100.76
RJC 99	RJC99 2 24	Eas Annie Burn 2		75.41	25.19	0.21	0.07	100.88
RJC 99	RJC99 2 25	Eas Annie Burn 2		93.37	7.15	0.20	0.13	100.85
RJC 99	RJC99 2 26	Eas Annie Burn 2		69.74	30.77	0.03	0.11	100.66
RJC 99	RJC99 2 27	Eas Annie Burn 2		73.80	26.80	0.08	0.09	100.77
RJC 99	RJC99 2 28	Eas Annie Burn 2		66.60	33.49	0.07	0.06	100.22
RJC 99	RJC99 2 29	Eas Annie Burn 2		77.03	23.71	0.20	0.06	101.01
RJC 99	RJC99 2 30	Eas Annie Burn 2		67.01	33.03	0.08	0.07	100.19
RJC 99	RJC99 3 1	Eas Annie Burn 2		83.97	16.19	0.15	0.04	100.36
RJC 99	RJC99 3 2	Eas Annie Burn 2		68.35	32.37	0.11	0.06	100.89
RJC 99	RJC99 3 3	Eas Annie Burn 2		90.72	9.80	0.13	0.06	100.71
RJC 99	RJC99 3 4	Eas Annie Burn 2		91.68	8.83	0.19	0.06	100.77
RJC 99	RJC99 3 5	Eas Annie Burn 2		94.33	6.00	0.05	0.11	100.49
RJC 99	RJC99 3 6	Eas Annie Burn 2		72.58	27.91	0.07	0.08	100.65
RJC 99	RJC99 3 7	Eas Annie Burn 2		87.89	12.41	0.11	0.08	100.49

Block	Grain ID	Sample	Traverse?	Au WT%	Ag WT%	Hg WT%	Cu WT%	Total
RJC 99	RJC99 3 8	Eas Annie Burn 2		65.54	34.45	0.15	0.08	100.22
RJC 99	RJC99 3 9	Eas Annie Burn 2		73.19	27.57	0.12	0.06	100.93
RJC 99	RJC99 3 10 core	Eas Annie Burn 2		63.45	36.72	0.14	0.05	100.36
RJC 99	RJC99 3 10 trans	Eas Annie Burn 2	T	50.87	47.51	0.01	0.04	98.43
RJC 99	RJC99 3 10 trans	Eas Annie Burn 2	T	51.13	47.79	0.11	0.04	99.06
RJC 99	RJC99 3 10 trans	Eas Annie Burn 2	T	51.64	47.70	0.08	0.02	99.44
RJC 99	RJC99 3 10 trans	Eas Annie Burn 2	T	51.72	47.41	0.08	0.02	99.24
RJC 99	RJC99 3 10 trans	Eas Annie Burn 2	T	51.83	47.04	0.08	0.05	99.00
RJC 99	RJC99 3 10 trans	Eas Annie Burn 2	T	52.23	46.74	0.10	0.05	99.12
RJC 99	RJC99 3 10 trans	Eas Annie Burn 2	T	52.07	46.60	0.10	0.05	98.83
RJC 99	RJC99 3 10 trans	Eas Annie Burn 2	T	52.09	46.54	0.08	0.06	98.77
RJC 99	RJC99 3 10 trans	Eas Annie Burn 2	T	52.50	46.64	0.08	0.04	99.26
RJC 99	RJC99 3 10 trans	Eas Annie Burn 2	T	52.48	46.47	0.00	0.04	98.99
RJC 99	RJC99 3 10 trans	Eas Annie Burn 2	T	52.78	46.49	0.08	0.05	99.40
RJC 99	RJC99 3 10 trans	Eas Annie Burn 2	T	52.99	46.50	0.06	0.04	99.60
RJC 99	RJC99 3 10 trans	Eas Annie Burn 2	T	53.32	46.61	0.12	0.04	100.09
RJC 99	RJC99 3 10 trans	Eas Annie Burn 2	T	53.10	46.36	0.06	0.06	99.59
RJC 99	RJC99 3 10 trans	Eas Annie Burn 2	T	53.14	46.21	0.00	0.04	99.39
RJC 99	RJC99 3 10 trans	Eas Annie Burn 2	T	53.23	45.98	0.07	0.05	99.33
RJC 99	RJC99 3 10 trans	Eas Annie Burn 2	T	53.16	46.16	0.05	0.04	99.42
RJC 99	RJC99 3 10 trans	Eas Annie Burn 2	T	53.42	46.17	0.09	0.04	99.71
RJC 99	RJC99 3 11	Eas Annie Burn 2		79.53	21.38	0.03	0.06	100.99
RJC 99	RJC99 3 12	Eas Annie Burn 2		85.54	15.13	0.07	0.05	100.80
RJC 99	RJC99 3 13 core	Eas Annie Burn 2		70.96	29.70	0.14	0.05	100.85
RJC 99	RJC99 3 14 core	Eas Annie Burn 2		79.33	20.85	0.12	0.07	100.37
RJC 99	RJC99 3 15	Eas Annie Burn 2		69.83	30.69	0.16	0.04	100.72
RJC 99	RJC99 3 16	Eas Annie Burn 2		74.09	26.61	0.06	0.04	100.80
RJC 99	RJC99 3 17	Eas Annie Burn 2		91.99	8.35	0.13	0.10	100.57

Block	Grain ID	Sample	Traverse?	Au WT%	Ag WT%	Hg WT%	Cu WT%	Total
RJC 99	RJC99 3 18	Eas Annie Burn 2		73.30	26.98	0.00	0.04	100.32
RJC 99	RJC99 3 19	Eas Annie Burn 2		75.63	24.79	0.10	0.06	100.59
RJC 99	RJC99 3 20	Eas Annie Burn 2		86.49	13.77	0.18	0.10	100.54
RJC 99	RJC99 3 21	Eas Annie Burn 2		58.39	41.42	0.08	0.05	99.95
RJC 99	RJC99 3 22	Eas Annie Burn 2		64.52	35.16	0.11	0.05	99.84
RJC 99	RJC99 3 23	Eas Annie Burn 2		74.92	25.58	0.24	0.04	100.78
RJC 99	RJC99 3 24	Eas Annie Burn 2		71.57	28.81	0.03	0.04	100.45
RJC 99	RJC99 3 25	Eas Annie Burn 2		87.24	13.92	0.03	0.06	101.25
RJC 98	RJC98 2 1 core	River Locky 2018		74.64	25.71	0.08	0.08	100.51
RJC 98	RJC98 2 1 trav	River Locky 2018	T	70.51	29.21	0.06	0.06	99.84
RJC 98	RJC98 2 1 trav	River Locky 2018	T	70.66	29.21	0.20	0.04	100.11
RJC 98	RJC98 2 1 trav	River Locky 2018	T	67.00	32.88	0.19	0.06	100.13
RJC 98	RJC98 2 1 trav	River Locky 2018	T	56.79	42.03	0.17	0.05	99.04
RJC 98	RJC98 2 1 trav	River Locky 2018	T	55.99	43.00	0.15	0.05	99.19
RJC 98	RJC98 2 1 trav	River Locky 2018	T	55.09	43.53	0.20	0.06	98.89
RJC 98	RJC98 2 1 trav	River Locky 2018	T	54.46	44.41	0.18	0.07	99.12
RJC 98	RJC98 2 1 trav	River Locky 2018	T	53.65	45.27	0.02	0.05	99.00
RJC 98	RJC98 2 1 trav	River Locky 2018	T	52.64	45.92	0.06	0.05	98.68
RJC 98	RJC98 2 1 trav	River Locky 2018	T	50.73	47.34	0.10	0.04	98.21
RJC 98	RJC98 2 1 trav	River Locky 2018	T	51.88	46.71	0.08	0.05	98.72
RJC 98	RJC98 2 1 trav	River Locky 2018	T	49.04	49.80	0.21	0.06	99.10
RJC 98	RJC98 2 1 trav	River Locky 2018	T	48.45	49.99	0.08	0.09	98.61
RJC 98	RJC98 2 1 trav	River Locky 2018	T	48.62	50.45	0.10	0.06	99.22
RJC 98	RJC98 2 1 trav	River Locky 2018	T	47.11	51.80	0.09	0.06	99.05
RJC 98	RJC98 2 1 trav	River Locky 2018	T	64.38	36.78	0.02	0.08	101.26
RJC 98	RJC98 2 1 trav	River Locky 2018	T	73.94	26.19	0.23	0.09	100.46
RJC 98	RJC98 2 1 trav	River Locky 2018	T	74.02	26.21	0.21	0.08	100.53
RJC 98	RJC98 2 1 trav	River Locky 2018	T	74.14	26.51	0.07	0.06	100.78

Block	Grain ID	Sample	Traverse?	Au WT%	Ag WT%	Hg WT%	Cu WT%	Total
RJC 98	RJC98 2 1 trav	River Locky 2018	T	74.58	25.98	0.13	0.07	100.76
RJC 98	RJC98 2 1 trav	River Locky 2018	T	74.93	26.24	0.10	0.06	101.33
RJC 98	RJC98 2 1 trav	River Locky 2018	T	75.17	25.55	0.00	0.07	100.78
RJC 98	RJC98 2 1 trav	River Locky 2018	T	75.06	25.42	0.18	0.07	100.72
RJC 98	RJC98 2 1 trav	River Locky 2018	T	75.46	25.58	0.16	0.06	101.26
RJC 98	RJC98 2 1 trav	River Locky 2018	T	75.27	25.58	0.14	0.07	101.07
RJC 98	RJC98 2 1 trav	River Locky 2018	T	74.51	25.23	0.13	0.04	99.92
RJC 98	RJC98 2 1 trav	River Locky 2018	T	74.74	25.54	0.13	0.05	100.46
RJC 98	RJC98 2 1 trav	River Locky 2018	T	74.59	26.06	0.19	0.07	100.92
RJC 98	RJC98 2 1 trav	River Locky 2018	T	74.27	25.93	0.18	0.06	100.44
RJC 100	RJC100 7 2	River Locky 2018		66.02	33.54	0.09	0.07	99.73
RJC 100	RJC100 7 3	River Locky 2018		72.41	28.12	0.19	0.07	100.79
RJC 100	RJC100 7 4	River Locky 2018		72.40	28.35	0.10	0.06	100.92
RJC 100	RJC100 7 5	River Locky 2018		73.40	27.75	0.18	0.07	101.39
RJC 100	RJC100 7 6	River Locky 2018		62.88	37.12	0.08	0.08	100.16
RJC 100	RJC100 7 7	River Locky 2018		66.44	34.35	0.11	0.09	101.00
RJC 100	RJC100 7 8	River Locky 2018		59.88	40.07	0.08	0.07	100.10
RJC 100	RJC100 7 9	River Locky 2018		81.67	18.86	0.10	0.08	100.72
RJC 100	RJC100 7 10	River Locky 2018		70.56	29.78	0.06	0.07	100.47
RJC 100	RJC100 7 11	River Locky 2018		68.95	31.24	0.11	0.06	100.36
RJC 100	RJC100 7 12	River Locky 2018		85.73	15.59	0.15	0.10	101.57
RJC 100	RJC100 7 13	River Locky 2018		65.73	34.66	0.10	0.05	100.54
RJC 100	RJC100 7 14	River Locky 2018		81.44	19.05	0.11	0.07	100.67
RJC 100	RJC100 7 15	River Locky 2018		72.05	28.81	0.16	0.06	101.08
RJC 100	RJC100 7 16	River Locky 2018		64.65	35.16	0.10	0.06	99.97
RJC 100	RJC100 7 17	River Locky 2018		68.27	32.23	0.03	0.06	100.58
RJC 100	RJC100 7 18	River Locky 2018		74.26	26.43	0.12	0.05	100.86
RJC 100	RJC100 7 19	River Locky 2018		74.17	26.65	0.00	0.09	100.90

Block	Grain ID	Sample	Traverse?	Au WT%	Ag WT%	Hg WT%	Cu WT%	Total
RJC 100	RJC100 7 20 core	River Locky 2018		62.86	37.09	0.15	0.07	100.17
RJC 100	RJC100 7 21	River Locky 2018		68.95	31.72	0.03	0.06	100.76
RJC 100	RJC100 7 22	River Locky 2018		73.04	27.11	0.06	0.08	100.29
RJC 100	RJC100 7 23	River Locky 2018		71.34	29.22	0.08	0.08	100.72
RJC 100	RJC100 7 24 core	River Locky 2018		72.25	28.26	0.16	0.09	100.76
RJC 100	RJC100 7 24 trans	River Locky 2018	T	73.02	27.83	0.09	0.06	100.99
RJC 100	RJC100 7 24 trans	River Locky 2018	T	72.95	27.39	0.06	0.05	100.45
RJC 100	RJC100 7 24 trans	River Locky 2018	T	72.88	27.63	0.17	0.06	100.73
RJC 100	RJC100 7 24 trans	River Locky 2018	T	73.27	28.02	0.12	0.07	101.48
RJC 100	RJC100 7 24 trans	River Locky 2018	T	72.88	27.89	0.13	0.06	100.96
RJC 100	RJC100 7 24 trans	River Locky 2018	T	72.64	28.21	0.13	0.07	101.05
RJC 100	RJC100 7 24 trans	River Locky 2018	T	71.93	28.73	0.18	0.08	100.92
RJC 100	RJC100 7 24 trans	River Locky 2018	T	71.55	29.38	0.06	0.06	101.05
RJC 100	RJC100 7 24 trans	River Locky 2018	T	70.42	30.00	0.00	0.06	100.48
RJC 100	RJC100 7 24 trans	River Locky 2018	T	69.78	30.92	0.01	0.07	100.77
RJC 100	RJC100 7 24 trans	River Locky 2018	T	69.11	31.06	0.15	0.05	100.38
RJC 100	RJC100 7 24 trans	River Locky 2018	T	71.30	28.09	0.20	0.08	99.67
RJC 100	RJC100 7 24 trans	River Locky 2018	T	78.92	21.62	0.15	0.07	100.76
RJC 100	RJC100 7 24 trans	River Locky 2018	T	83.48	17.18	0.17	0.06	100.89
RJC 100	RJC100 7 24 trans	River Locky 2018	T	78.54	22.33	0.12	0.06	101.04
RJC 100	RJC100 7 24 trans	River Locky 2018	T	71.54	28.60	0.12	0.05	100.31
RJC 100	RJC100 7 24 trans	River Locky 2018	T	70.44	30.32	0.13	0.06	100.95
RJC 100	RJC100 7 24 trans	River Locky 2018	T	70.51	30.04	0.04	0.05	100.65
RJC 100	RJC100 7 24 trans	River Locky 2018	T	70.63	29.46	0.11	0.07	100.27
RJC 100	RJC100 7 24 trans	River Locky 2018	T	71.71	29.35	0.16	0.05	101.27
RJC 100	RJC100 7 24 trans	River Locky 2018	T	72.27	29.00	0.07	0.04	101.38
RJC 100	RJC100 7 24 trans	River Locky 2018	T	72.37	28.49	0.08	0.03	100.97
RJC 100	RJC100 7 24 trans	River Locky 2018	T	72.93	28.46	0.14	0.04	101.56

Block	Grain ID	Sample	Traverse?	Au WT%	Ag WT%	Hg WT%	Cu WT%	Total
RJC 100	RJC100 7 24 trans	River Locky 2018	T	72.90	28.10	0.10	0.04	101.15
RJC 100	RJC100 7 24 trans	River Locky 2018	T	73.45	27.75	0.09	0.03	101.31
RJC 100	RJC100 7 25	River Locky 2018		69.17	31.55	0.17	0.07	100.96
RJC 100	RJC100 7 26	River Locky 2018		69.28	31.19	0.10	0.06	100.64
RJC 100	RJC100 7 27	River Locky 2018		62.85	37.66	0.04	0.05	100.59
RJC 100	RJC100 7 28	River Locky 2018		65.27	35.07	0.09	0.07	100.49
RJC 100	RJC100 7 29	River Locky 2018		72.57	28.70	0.16	0.05	101.49
RJC 100	RJC100 7 30	River Locky 2018		74.27	26.53	0.06	0.05	100.91
RJC 100	RJC100 8 1	River Locky 2018		69.68	31.00	0.00	0.08	100.76
RJC 100	RJC100 8 2	River Locky 2018		66.49	34.35	0.09	0.07	101.00
RJC 100	RJC100 8 3	River Locky 2018		60.81	39.35	0.08	0.06	100.30
RJC 100	RJC100 8 4 core	River Locky 2018		73.68	27.12	0.12	0.08	101.00
RJC 100	RJC100 8 4 core to rim trav	River Locky 2018	T	63.84	36.15	0.23	0.09	100.31
RJC 100	RJC100 8 4 core to rim trav	River Locky 2018	T	63.69	36.44	0.15	0.06	100.34
RJC 100	RJC100 8 4 core to rim trav	River Locky 2018	T	64.01	35.78	0.12	0.08	100.00
RJC 100	RJC100 8 4 core to rim trav	River Locky 2018	T	63.85	36.34	0.13	0.10	100.42
RJC 100	RJC100 8 4 core to rim trav	River Locky 2018	T	63.90	36.42	0.04	0.10	100.47
RJC 100	RJC100 8 4 core to rim trav	River Locky 2018	T	63.98	36.27	0.06	0.09	100.40
RJC 100	RJC100 8 4 core to rim trav	River Locky 2018	T	63.95	36.29	0.02	0.08	100.35
RJC 100	RJC100 8 4 core to rim trav	River Locky 2018	T	64.02	36.39	0.10	0.08	100.60
RJC 100	RJC100 8 4 core to rim trav	River Locky 2018	T	64.56	35.93	0.14	0.09	100.71

Block	Grain ID	Sample	Traverse?	Au WT%	Ag WT%	Hg WT%	Cu WT%	Total
RJC 100	RJC100 8 4 core to rim trav	River Locky 2018	T	64.19	36.35	0.11	0.09	100.75
RJC 100	RJC100 8 4 core to rim trav	River Locky 2018	T	64.30	36.41	0.11	0.08	100.91
RJC 100	RJC100 8 4 core to rim trav	River Locky 2018	T	64.54	36.03	0.02	0.10	100.69
RJC 100	RJC100 8 4 core to rim trav	River Locky 2018	T	64.02	36.24	0.07	0.10	100.44
RJC 100	RJC100 8 4 core to rim trav	River Locky 2018	T	64.38	36.00	0.07	0.10	100.55
RJC 100	RJC100 8 4 core to rim trav	River Locky 2018	T	64.08	36.59	0.25	0.09	101.02
RJC 100	RJC100 8 4 core to rim trav	River Locky 2018	T	63.83	36.38	0.15	0.07	100.43
RJC 100	RJC100 8 4 core to rim trav	River Locky 2018	T	63.90	36.54	0.07	0.06	100.58
RJC 100	RJC100 8 4 core to rim trav	River Locky 2018	T	64.17	36.60	0.06	0.08	100.91
RJC 100	RJC100 8 4 core to rim trav	River Locky 2018	T	64.05	36.21	0.06	0.09	100.41
RJC 100	RJC100 8 4 core to rim trav	River Locky 2018	T	64.60	36.41	0.07	0.10	101.17
RJC 100	RJC100 8 4 core to rim trav	River Locky 2018	T	64.27	36.21	0.05	0.08	100.60
RJC 100	RJC100 8 4 core to rim trav	River Locky 2018	T	64.27	36.25	0.18	0.07	100.77
RJC 100	RJC100 8 4 core to rim trav	River Locky 2018	T	64.00	36.04	0.18	0.09	100.31
RJC 100	RJC100 8 4 core to rim trav	River Locky 2018	T	64.12	36.20	0.10	0.10	100.52

Block	Grain ID	Sample	Traverse?	Au WT%	Ag WT%	Hg WT%	Cu WT%	Total
RJC 100	RJC100 8 4 core to rim trav	River Locky 2018	T	64.15	36.42	0.12	0.10	100.78
RJC 100	RJC100 8 4 core to rim trav	River Locky 2018	T	64.84	35.79	0.18	0.10	100.91
RJC 100	RJC100 8 4 core to rim trav	River Locky 2018	T	64.11	36.08	0.10	0.08	100.37
RJC 100	RJC100 8 4 core to rim trav	River Locky 2018	T	64.55	35.88	0.15	0.11	100.69
RJC 100	RJC100 8 4 core to rim trav	River Locky 2018	T	64.61	36.49	0.16	0.07	101.34
RJC 100	RJC100 8 4 core to rim trav	River Locky 2018	T	64.36	35.93	0.03	0.09	100.41
RJC 100	RJC100 8 4 core to rim trav	River Locky 2018	T	64.25	36.35	0.31	0.06	100.96
RJC 100	RJC100 8 4 core to rim trav	River Locky 2018	T	64.34	36.11	0.09	0.08	100.61
RJC 100	RJC100 8 4 core to rim trav	River Locky 2018	T	64.41	35.95	0.10	0.11	100.57
RJC 100	RJC100 8 4 core to rim trav	River Locky 2018	T	64.39	36.11	0.20	0.09	100.80
RJC 100	RJC100 8 4 core to rim trav	River Locky 2018	T	64.29	36.41	0.03	0.07	100.80
RJC 100	RJC100 8 4 core to rim trav	River Locky 2018	T	64.18	36.41	0.14	0.08	100.81
RJC 100	RJC100 8 4 core to rim trav	River Locky 2018	T	64.10	36.43	0.06	0.07	100.66
RJC 100	RJC100 8 4 core to rim trav	River Locky 2018	T	64.15	36.31	0.12	0.09	100.67
RJC 100	RJC100 8 4 core to rim trav	River Locky 2018	T	64.34	36.36	0.08	0.08	100.85

Block	Grain ID	Sample	Traverse?	Au WT%	Ag WT%	Hg WT%	Cu WT%	Total
RJC 100	RJC100 8 4 core to rim trav	River Locky 2018	T	64.35	36.09	0.15	0.08	100.67
RJC 100	RJC100 8 4 core to rim trav	River Locky 2018	T	64.16	36.49	0.08	0.07	100.81
RJC 100	RJC100 8 4 core to rim trav	River Locky 2018	T	64.46	36.10	0.18	0.07	100.81
RJC 100	RJC100 8 4 core to rim trav	River Locky 2018	T	64.41	36.14	0.18	0.10	100.83
RJC 100	RJC100 8 4 core to rim trav	River Locky 2018	T	64.20	36.28	0.12	0.08	100.68
RJC 100	RJC100 8 4 core to rim trav	River Locky 2018	T	64.34	36.39	0.04	0.08	100.85
RJC 100	RJC100 8 4 core to rim trav	River Locky 2018	T	64.09	36.42	0.08	0.07	100.66
RJC 100	RJC100 8 4 core to rim trav	River Locky 2018	T	64.02	36.40	0.07	0.07	100.56
RJC 100	RJC100 8 4 core to rim trav	River Locky 2018	T	64.27	36.30	0.00	0.09	100.65
RJC 100	RJC100 8 4 core to rim trav	River Locky 2018	T	64.46	36.10	0.26	0.08	100.91
RJC 100	RJC100 8 4 core to rim trav	River Locky 2018	T	64.21	36.24	0.16	0.08	100.69
RJC 100	RJC100 8 4 core to rim trav	River Locky 2018	T	64.25	36.15	0.14	0.09	100.63
RJC 100	RJC100 8 4 core to rim trav	River Locky 2018	T	64.42	36.28	0.11	0.10	100.91
RJC 100	RJC100 8 4 core to rim trav	River Locky 2018	T	64.21	36.17	0.21	0.07	100.66
RJC 100	RJC100 8 4 core to rim trav	River Locky 2018	T	64.07	36.46	0.12	0.07	100.71

Block	Grain ID	Sample	Traverse?	Au WT%	Ag WT%	Hg WT%	Cu WT%	Total
RJC 100	RJC100 8 4 core to rim trav	River Locky 2018	T	64.47	36.45	0.05	0.08	101.05
RJC 100	RJC100 8 4 core to rim trav	River Locky 2018	T	64.43	35.95	0.09	0.09	100.57
RJC 100	RJC100 8 4 core to rim trav	River Locky 2018	T	64.36	36.01	0.13	0.09	100.59
RJC 100	RJC100 8 4 core to rim trav	River Locky 2018	T	64.19	36.08	0.15	0.09	100.52
RJC 100	RJC100 8 4 core to rim trav	River Locky 2018	T	64.08	36.14	0.16	0.09	100.47
RJC 100	RJC100 8 4 core to rim trav	River Locky 2018	T	64.10	36.15	0.13	0.07	100.46
RJC 100	RJC100 8 5	River Locky 2018		72.36	28.21	0.21	0.09	100.88
RJC 100	RJC100 8 6	River Locky 2018		59.47	40.93	0.07	0.06	100.52
RJC 100	RJC100 8 7	River Locky 2018		64.14	35.95	0.11	0.08	100.27
RJC 100	RJC100 8 8	River Locky 2018		88.73	12.18	0.28	0.10	101.29
RJC 100	RJC100 8 9	River Locky 2018		68.70	31.53	0.14	0.09	100.46
RJC 100	RJC100 8 10	River Locky 2018		100.50	0.44	0.31	0.09	101.34
RJC 100	RJC100 8 11	River Locky 2018		77.45	23.33	0.14	0.06	100.97
RJC 100	RJC100 8 12	River Locky 2018		73.71	27.10	0.17	0.09	101.07
RJC 100	RJC100 8 13	River Locky 2018		68.81	31.45	0.12	0.08	100.46
RJC 100	RJC100 8 14 core 1 long dark	River Locky 2018		59.76	39.93	0.22	0.08	99.98
RJC 100	RJC100 8 14 core 2 bright	River Locky 2018		92.14	9.29	0.30	0.10	101.83
RJC 100	RJC100 8 15	River Locky 2018		79.56	21.14	0.15	0.13	100.99
RJC 100	RJC100 8 16	River Locky 2018		76.86	24.22	0.05	0.07	101.20
RJC 100	RJC100 8 17	River Locky 2018		73.67	26.86	0.04	0.08	100.65
RJC 100	RJC100 8 18	River Locky 2018		61.97	38.91	0.17	0.09	101.15

Block	Grain ID	Sample	Traverse?	Au WT%	Ag WT%	Hg WT%	Cu WT%	Total
RJC 100	RJC100 8 19	River Locky 2018		85.52	15.16	0.06	0.08	100.82
RJC 100	RJC100 8 20	River Locky 2018		61.19	38.80	0.13	0.09	100.21
RJC 100	RJC100 8 21	River Locky 2018		70.06	30.41	0.14	0.08	100.70
RJC 100	RJC100 8 22	River Locky 2018		77.60	22.89	0.20	0.08	100.77
RJC 100	RJC100 8 23	River Locky 2018		66.99	33.28	0.08	0.03	100.37
RJC 100	RJC100 8 24	River Locky 2018		65.94	34.47	0.03	0.07	100.52
RJC 100	RJC100 8 25	River Locky 2018		61.68	38.56	0.16	0.07	100.47
RJC 100	RJC100 8 26	River Locky 2018		86.77	14.69	0.09	0.10	101.66
RJC 100	RJC100 8 27	River Locky 2018		69.82	30.79	0.13	0.06	100.81
RJC 100	RJC100 8 28	River Locky 2018		58.85	41.46	0.12	0.07	100.50
RJC 100	RJC100 8 29	River Locky 2018		72.08	28.25	0.14	0.10	100.57
RJC 100	RJC100 8 30	River Locky 2018		54.13	45.54	0.03	0.10	99.80
RJC 100	RJC100 9 1	River Locky ROB 18		80.10	20.55	0.14	0.11	100.89
RJC 100	RJC100 9 2	River Locky ROB 18		90.50	10.29	0.03	0.17	100.99
RJC 100	RJC100 9 3	River Locky ROB 18		73.29	28.22	0.10	0.10	101.72
RJC 100	RJC100 9 4	River Locky ROB 18		70.17	30.67	0.14	0.10	101.09
RJC 100	RJC100 9 5	River Locky ROB 18		68.50	32.05	0.12	0.09	100.76
RJC 100	RJC100 9 6 core	River Locky ROB 18		75.79	25.49	0.10	0.08	101.46
RJC 100	RJC100 9 6 trans	River Locky ROB 18	T	76.45	4.35	0.30	0.08	81.17
RJC 100	RJC100 9 6 trans	River Locky ROB 18	T	77.41	4.27	0.36	0.07	82.11
RJC 100	RJC100 9 6 trans	River Locky ROB 18	T	85.15	4.47	0.27	0.04	89.93

Block	Grain ID	Sample	Traverse?	Au WT%	Ag WT%	Hg WT%	Cu WT%	Total
RJC 100	RJC100 9 6 trans	River Locky ROB 18	T	89.15	4.49	0.21	0.07	93.92
RJC 100	RJC100 9 6 trans	River Locky ROB 18	T	89.80	4.38	0.22	0.08	94.48
RJC 100	RJC100 9 6 trans	River Locky ROB 18	T	90.79	4.53	0.26	0.06	95.64
RJC 100	RJC100 9 6 trans	River Locky ROB 18	T	91.21	4.54	0.19	0.08	96.03
RJC 100	RJC100 9 6 trans	River Locky ROB 18	T	91.76	4.60	0.24	0.05	96.65
RJC 100	RJC100 9 6 trans	River Locky ROB 18	T	92.31	4.67	0.23	0.06	97.28
RJC 100	RJC100 9 6 trans	River Locky ROB 18	T	93.09	4.60	0.15	0.05	97.90
RJC 100	RJC100 9 6 trans	River Locky ROB 18	T	93.91	4.59	0.30	0.07	98.87
RJC 100	RJC100 9 6 trans	River Locky ROB 18	T	94.03	4.56	0.27	0.05	98.91
RJC 100	RJC100 9 6 trans	River Locky ROB 18	T	94.04	4.79	0.15	0.07	99.05
RJC 100	RJC100 9 6 trans	River Locky ROB 18	T	95.05	4.64	0.19	0.06	99.94
RJC 100	RJC100 9 6 trans	River Locky ROB 18	T	94.83	4.72	0.19	0.08	99.83
RJC 100	RJC100 9 6 trans	River Locky ROB 18	T	95.00	4.83	0.21	0.08	100.12
RJC 100	RJC100 9 6 trans	River Locky ROB 18	T	95.32	4.66	0.26	0.07	100.31
RJC 100	RJC100 9 6 trans	River Locky ROB 18	T	95.15	4.73	0.22	0.10	100.20

Block	Grain ID	Sample	Traverse?	Au WT%	Ag WT%	Hg WT%	Cu WT%	Total
RJC 100	RJC100 9 6 trans	River Locky ROB 18	T	95.10	5.00	0.28	0.10	100.49
RJC 100	RJC100 9 6 trans	River Locky ROB 18	T	95.52	4.78	0.16	0.09	100.55
RJC 100	RJC100 9 6 trans	River Locky ROB 18	T	95.38	4.77	0.26	0.10	100.52
RJC 100	RJC100 9 6 trans	River Locky ROB 18	T	95.87	4.78	0.24	0.10	100.98
RJC 100	RJC100 9 6 trans	River Locky ROB 18	T	96.28	4.81	0.23	0.09	101.41
RJC 100	RJC100 9 6 trans	River Locky ROB 18	T	96.03	4.84	0.16	0.10	101.13
RJC 100	RJC100 9 6 trans	River Locky ROB 18	T	96.09	4.80	0.09	0.10	101.08
RJC 100	RJC100 9 6 trans	River Locky ROB 18	T	96.80	4.83	0.17	0.09	101.89
RJC 100	RJC100 9 6 trans	River Locky ROB 18	T	95.99	4.96	0.21	0.10	101.26
RJC 100	RJC100 9 6 trans	River Locky ROB 18	T	96.05	5.01	0.15	0.09	101.30
RJC 100	RJC100 9 6 trans	River Locky ROB 18	T	96.11	4.78	0.25	0.09	101.23
RJC 100	RJC100 9 6 trans	River Locky ROB 18	T	96.45	4.92	0.26	0.10	101.72
RJC 100	RJC100 9 6 trans	River Locky ROB 18	T	96.47	4.96	0.28	0.10	101.80
RJC 100	RJC100 9 6 trans	River Locky ROB 18	T	96.49	4.85	0.28	0.09	101.70
RJC 100	RJC100 9 6 trans	River Locky ROB 18	T	96.86	4.95	0.24	0.09	102.13

Block	Grain ID	Sample	Traverse?	Au WT%	Ag WT%	Hg WT%	Cu WT%	Total
RJC 100	RJC100 9 6 trans	River Locky ROB 18	T	96.79	5.01	0.34	0.09	102.24
RJC 100	RJC100 9 6 trans	River Locky ROB 18	T	96.61	5.04	0.34	0.10	102.09
RJC 100	RJC100 9 6 trans	River Locky ROB 18	T	96.69	4.98	0.23	0.12	102.02
RJC 100	RJC100 9 6 trans	River Locky ROB 18	T	96.75	4.99	0.16	0.08	101.99
RJC 100	RJC100 9 6 trans	River Locky ROB 18	T	95.93	4.94	0.19	0.11	101.17
RJC 100	RJC100 9 6 trans	River Locky ROB 18	T	96.27	4.98	0.19	0.08	101.51
RJC 100	RJC100 9 6 trans	River Locky ROB 18	T	95.45	4.80	0.29	0.10	100.65
RJC 100	RJC100 9 6 trans	River Locky ROB 18	T	95.19	4.78	0.19	0.08	100.25
RJC 100	RJC100 9 6 trans	River Locky ROB 18	T	95.76	4.73	0.27	0.08	100.84
RJC 100	RJC100 9 6 trans	River Locky ROB 18	T	95.60	4.61	0.25	0.10	100.56
RJC 100	RJC100 9 6 trans	River Locky ROB 18	T	95.49	4.89	0.21	0.09	100.68
RJC 100	RJC100 9 6 trans	River Locky ROB 18	T	95.86	4.66	0.27	0.08	100.87
RJC 100	RJC100 9 6 trans	River Locky ROB 18	T	96.11	4.56	0.27	0.09	101.03
RJC 100	RJC100 9 6 trans	River Locky ROB 18	T	96.05	4.53	0.21	0.11	100.90
RJC 100	RJC100 9 6 trans	River Locky ROB 18	T	95.23	4.30	0.27	0.10	99.89

Block	Grain ID	Sample	Traverse?	Au WT%	Ag WT%	Hg WT%	Cu WT%	Total
RJC 100	RJC100 9 6 trans	River Locky ROB 18	T	94.95	4.27	0.21	0.10	99.53
RJC 100	RJC100 9 6 trans	River Locky ROB 18	T	93.98	4.39	0.38	0.10	98.86
RJC 100	RJC100 9 6 trans	River Locky ROB 18	T	93.55	4.28	0.28	0.12	98.23
RJC 100	RJC100 9 6 trans	River Locky ROB 18	T	92.63	4.25	0.30	0.15	97.33
RJC 100	RJC100 9 6 trans	River Locky ROB 18	T	92.37	4.23	0.15	0.14	96.89
RJC 100	RJC100 9 6 trans	River Locky ROB 18	T	91.78	4.29	0.34	0.15	96.56
RJC 100	RJC100 9 6 trans	River Locky ROB 18	T	92.67	4.17	0.27	0.14	97.25
RJC 100	RJC100 9 6 trans	River Locky ROB 18	T	91.91	4.16	0.23	0.14	96.44
RJC 100	RJC100 9 6 trans	River Locky ROB 18	T	91.82	4.10	0.22	0.12	96.27
RJC 100	RJC100 9 6 trans	River Locky ROB 18	T	91.93	4.16	0.23	0.13	96.45
RJC 100	RJC100 9 6 trans	River Locky ROB 18	T	91.67	4.21	0.13	0.14	96.16
RJC 100	RJC100 9 6 trans	River Locky ROB 18	T	92.42	4.14	0.23	0.14	96.93
RJC 100	RJC100 9 6 trans	River Locky ROB 18	T	91.76	4.25	0.23	0.15	96.40
RJC 100	RJC100 9 6 trans	River Locky ROB 18	T	91.95	4.19	0.20	0.14	96.49
RJC 100	RJC100 9 6 trans	River Locky ROB 18	T	93.36	4.18	0.18	0.12	97.84

Block	Grain ID	Sample	Traverse?	Au WT%	Ag WT%	Hg WT%	Cu WT%	Total
RJC 100	RJC100 9 6 trans	River Locky ROB 18	T	92.71	4.21	0.29	0.15	97.36
RJC 100	RJC100 9 6 trans	River Locky ROB 18	T	92.93	4.06	0.21	0.13	97.34
RJC 100	RJC100 9 6 trans	River Locky ROB 18	T	93.01	4.20	0.29	0.12	97.62
RJC 100	RJC100 9 6 trans	River Locky ROB 18	T	93.81	4.11	0.23	0.14	98.29
RJC 100	RJC100 9 6 trans	River Locky ROB 18	T	93.15	4.18	0.25	0.14	97.71
RJC 100	RJC100 9 6 trans	River Locky ROB 18	T	93.50	4.05	0.22	0.11	97.89
RJC 100	RJC100 9 6 trans	River Locky ROB 18	T	93.51	4.16	0.22	0.12	98.02
RJC 100	RJC100 9 6 trans	River Locky ROB 18	T	93.53	4.09	0.34	0.11	98.08
RJC 100	RJC100 9 6 trans	River Locky ROB 18	T	93.85	4.01	0.35	0.11	98.32
RJC 100	RJC100 9 6 trans	River Locky ROB 18	T	93.84	4.04	0.08	0.13	98.09
RJC 100	RJC100 9 6 trans	River Locky ROB 18	T	93.84	4.17	0.29	0.11	98.41
RJC 100	RJC100 9 6 trans	River Locky ROB 18	T	93.85	4.24	0.13	0.11	98.33
RJC 100	RJC100 9 6 trans	River Locky ROB 18	T	93.89	4.15	0.14	0.14	98.32
RJC 100	RJC100 9 6 trans	River Locky ROB 18	T	94.23	4.03	0.14	0.11	98.52
RJC 100	RJC100 9 6 trans	River Locky ROB 18	T	93.98	4.14	0.17	0.12	98.41

Block	Grain ID	Sample	Traverse?	Au WT%	Ag WT%	Hg WT%	Cu WT%	Total
RJC 100	RJC100 9 6 trans	River Locky ROB 18	T	94.35	4.15	0.19	0.11	98.80
RJC 100	RJC100 9 6 trans	River Locky ROB 18	T	94.22	4.14	0.26	0.11	98.73
RJC 100	RJC100 9 6 trans	River Locky ROB 18	T	93.94	4.13	0.22	0.10	98.39
RJC 100	RJC100 9 6 trans	River Locky ROB 18	T	93.82	4.34	0.14	0.12	98.41
RJC 100	RJC100 9 6 trans	River Locky ROB 18	T	93.84	4.24	0.11	0.11	98.31
RJC 100	RJC100 9 6 trans	River Locky ROB 18	T	94.20	4.23	0.17	0.12	98.71
RJC 100	RJC100 9 6 trans	River Locky ROB 18	T	94.09	4.24	0.19	0.12	98.64
RJC 100	RJC100 9 6 trans	River Locky ROB 18	T	94.49	4.30	0.05	0.12	98.97
RJC 100	RJC100 9 6 trans	River Locky ROB 18	T	93.65	4.47	0.26	0.11	98.48
RJC 100	RJC100 9 6 trans	River Locky ROB 18	T	93.99	4.46	0.21	0.12	98.78
RJC 100	RJC100 9 7	River Locky ROB 18		92.65	8.34	0.27	0.16	101.42
RJC 100	RJC100 9 8	River Locky ROB 18		57.50	42.76	0.10	0.09	100.45
RJC 100	RJC100 9 9	River Locky ROB 18		64.23	36.17	0.06	0.08	100.53
RJC 100	RJC100 9 10	River Locky ROB 18		88.74	12.16	0.12	0.14	101.15
RJC 100	RJC100 9 11	River Locky ROB 18		51.76	48.06	0.05	0.07	99.93

Block	Grain ID	Sample	Traverse?	Au WT%	Ag WT%	Hg WT%	Cu WT%	Total
RJC 100	RJC100 9 12	River Locky ROB 18		75.44	25.61	0.06	0.09	101.19
RJC 100	RJC100 9 13	River Locky ROB 18		93.29	7.20	0.23	0.13	100.85
RJC 100	RJC100 9 14	River Locky ROB 18		66.77	34.00	0.23	0.10	101.10
RJC 100	RJC100 9 15	River Locky ROB 18		77.18	23.94	0.15	0.07	101.34
RJC 100	RJC100 9 16	River Locky ROB 18		80.62	20.60	0.17	0.08	101.48
RJC 100	RJC100 9 17	River Locky ROB 18		80.19	21.54	0.20	0.08	102.01
RJC 100	RJC100 9 18	River Locky ROB 18		61.04	39.36	0.06	0.09	100.54
RJC 100	RJC100 9 19	River Locky ROB 18		66.16	34.69	0.03	0.11	101.00
RJC 100	RJC100 9 20	River Locky ROB 18		81.36	19.97	0.15	0.13	101.61
RJC 100	RJC100 9 21	River Locky ROB 18		90.24	10.71	0.14	0.11	101.20
RJC 100	RJC100 9 22	River Locky ROB 18		74.71	26.26	0.20	0.09	101.25
RJC 100	RJC100 9 23	River Locky ROB 18		62.14	38.18	0.07	0.10	100.50
RJC 100	RJC100 9 24	River Locky ROB 18		89.07	11.52	0.41	0.10	101.10
RJC 100	RJC100 6 1	River Locky 2018		68.89	31.17	0.22	0.10	100.38
RJC 100	RJC100 6 2 core	River Locky 2018		68.12	32.12	0.17	0.06	100.48
RJC 100	RJC100 6 3	River Locky 2018		77.39	23.29	0.12	0.07	100.87
RJC 100	RJC100 6 4	River Locky 2018		84.84	16.01	0.19	0.09	101.14

Block	Grain ID	Sample	Traverse?	Au WT%	Ag WT%	Hg WT%	Cu WT%	Total
RJC 100	RJC100 6 5 core	River Locky 2018		62.33	37.53	0.16	0.08	100.10
RJC 99	RJC99 5 1	River Locky 2018		60.25	40.18	0.08	0.04	100.56
RJC 99	RJC99 5 2	River Locky 2018		67.61	33.01	0.23	0.07	100.92
RJC 99	RJC99 5 3	River Locky 2018		89.36	11.15	0.24	0.06	100.82
RJC 99	RJC99 5 4	River Locky 2018		81.52	19.46	0.14	0.07	101.20
RJC 99	RJC99 5 5	River Locky 2018		68.65	31.60	0.06	0.02	100.33
RJC 99	RJC99 5 6	River Locky 2018		71.05	29.78	0.09	0.06	100.98
RJC 99	RJC99 5 7	River Locky 2018		59.88	40.03	0.02	0.06	99.98
RJC 99	RJC99 5 8	River Locky 2018		69.23	31.20	0.14	0.06	100.63
RJC 99	RJC99 5 9	River Locky 2018		89.29	11.49	0.19	0.09	101.07
RJC 99	RJC99 5 10	River Locky 2018		68.23	32.14	0.07	0.05	100.49
RJC 99	RJC99 5 11	River Locky 2018		70.78	29.99	0.18	0.02	100.97
RJC 99	RJC99 5 12	River Locky 2018		49.30	49.99	0.00	0.04	99.33
RJC 99	RJC99 5 13	River Locky 2018		65.87	34.75	0.13	0.09	100.83
RJC 99	RJC99 5 14	River Locky 2018		77.03	23.61	0.15	0.05	100.84
RJC 99	RJC99 5 15	River Locky 2018		81.90	18.93	0.07	0.08	100.97
RJC 99	RJC99 4 1	River Locky 2018		80.79	20.03	0.05	0.07	100.94
RJC 99	RJC99 4 2	River Locky 2018		72.83	28.23	0.10	0.06	101.23
RJC 99	RJC99 4 3	River Locky 2018		70.24	29.96	0.06	0.06	100.32
RJC 99	RJC99 4 4	River Locky 2018		99.35	1.00	0.16	0.08	100.58
RJC 99	RJC99 4 5	River Locky 2018		63.39	37.16	0.05	0.05	100.65
RJC 99	RJC99 4 6	River Locky 2018		68.44	32.27	0.16	0.06	100.93
RJC 99	RJC99 4 7	River Locky 2018		60.72	38.91	0.03	0.07	99.73
RJC 99	RJC99 4 8	River Locky 2018		81.38	19.65	0.15	0.08	101.27
RJC 99	RJC99 4 9	River Locky 2018		73.50	27.14	0.15	0.05	100.84
RJC 99	RJC99 4 10	River Locky 2018		76.91	23.72	0.13	0.05	100.81
RJC 99	RJC99 4 11	River Locky 2018		70.87	29.67	0.11	0.08	100.73
RJC 99	RJC99 4 12 core	River Locky 2018		36.18	61.96	0.05	0.03	98.23

Block	Grain ID	Sample	Traverse?	Au WT%	Ag WT%	Hg WT%	Cu WT%	Total
RJC 99	RJC99 4 12 trav	River Locky 2018	T	33.99	63.81	0.07	0.04	97.91
RJC 99	RJC99 4 12 trav	River Locky 2018	T	34.18	63.57	0.10	0.02	97.87
RJC 99	RJC99 4 12 trav	River Locky 2018	T	34.02	63.29	0.07	0.02	97.40
RJC 99	RJC99 4 12 trav	River Locky 2018	T	34.07	63.39	0.06	0.02	97.55
RJC 99	RJC99 4 12 trav	River Locky 2018	T	34.27	63.46	0.00	0.03	97.76
RJC 99	RJC99 4 12 trav	River Locky 2018	T	34.16	63.13	0.11	0.03	97.42
RJC 99	RJC99 4 12 trav	River Locky 2018	T	34.69	62.21	0.10	0.00	97.00
RJC 99	RJC99 4 12 trav	River Locky 2018	T	34.52	62.70	0.14	0.02	97.38
RJC 99	RJC99 4 12 trav	River Locky 2018	T	34.69	62.50	0.11	0.04	97.34
RJC 99	RJC99 4 12 trav	River Locky 2018	T	34.21	62.95	0.08	0.03	97.27
RJC 99	RJC99 4 12 trav	River Locky 2018	T	35.01	61.81	0.08	0.03	96.93
RJC 99	RJC99 4 12 trav	River Locky 2018	T	34.67	62.38	0.05	0.02	97.12
RJC 99	RJC99 4 12 trav	River Locky 2018	T	34.79	62.15	0.14	0.01	97.08
RJC 99	RJC99 4 12 trav	River Locky 2018	T	34.97	62.23	0.04	0.00	97.24
RJC 99	RJC99 4 12 trav	River Locky 2018	T	34.78	62.52	0.03	0.00	97.33
RJC 99	RJC99 4 12 trav	River Locky 2018	T	34.83	62.47	0.17	0.02	97.49
RJC 99	RJC99 4 12 trav	River Locky 2018	T	34.46	62.45	0.09	0.01	97.02
RJC 99	RJC99 4 12 trav	River Locky 2018	T	34.74	62.90	0.09	0.00	97.73
RJC 99	RJC99 4 12 trav	River Locky 2018	T	34.68	62.80	0.15	0.02	97.65
RJC 99	RJC99 4 12 trav	River Locky 2018	T	34.58	62.83	0.04	0.01	97.46
RJC 99	RJC99 4 12 trav	River Locky 2018	T	35.07	61.86	0.17	0.01	97.11
RJC 99	RJC99 4 12 trav	River Locky 2018	T	34.92	62.17	0.10	0.03	97.21
RJC 99	RJC99 4 12 trav	River Locky 2018	T	34.63	62.59	0.05	0.01	97.28
RJC 99	RJC99 4 12 trav	River Locky 2018	T	34.77	62.09	0.10	0.01	96.98
RJC 99	RJC99 4 12 trav	River Locky 2018	T	34.98	62.21	0.11	0.01	97.31
RJC 99	RJC99 4 12 trav	River Locky 2018	T	35.15	62.14	0.11	0.02	97.42
RJC 99	RJC99 4 12 trav	River Locky 2018	T	35.47	61.78	0.16	0.01	97.41
RJC 99	RJC99 4 12 trav	River Locky 2018	T	35.31	62.25	0.13	0.01	97.70

Block	Grain ID	Sample	Traverse?	Au WT%	Ag WT%	Hg WT%	Cu WT%	Total
RJC 99	RJC99 4 12 trav	River Locky 2018	T	35.48	61.95	0.18	0.01	97.63
RJC 99	RJC99 4 12 trav	River Locky 2018	T	34.89	62.36	0.10	0.02	97.37
RJC 99	RJC99 4 12 trav	River Locky 2018	T	34.59	62.94	0.03	0.01	97.57
RJC 99	RJC99 4 12 trav	River Locky 2018	T	35.40	61.95	0.14	0.00	97.49
RJC 99	RJC99 4 12 trav	River Locky 2018	T	34.93	62.34	0.17	0.02	97.47
RJC 99	RJC99 4 12 trav	River Locky 2018	T	35.30	62.29	0.19	0.01	97.80
RJC 99	RJC99 4 12 trav	River Locky 2018	T	35.15	62.16	0.17	0.01	97.49
RJC 99	RJC99 4 12 trav	River Locky 2018	T	35.21	61.83	0.05	0.01	97.11
RJC 99	RJC99 4 12 trav	River Locky 2018	T	35.10	62.10	0.06	0.01	97.27
RJC 99	RJC99 4 12 trav	River Locky 2018	T	35.47	61.51	0.18	0.00	97.16
RJC 99	RJC99 4 12 trav	River Locky 2018	T	35.50	61.49	0.14	0.01	97.14
RJC 99	RJC99 4 12 trav	River Locky 2018	T	35.23	62.12	0.00	0.01	97.37
RJC 99	RJC99 4 12 trav	River Locky 2018	T	35.11	62.64	0.19	0.01	97.95
RJC 99	RJC99 4 12 trav	River Locky 2018	T	34.77	62.65	0.13	0.01	97.55
RJC 99	RJC99 4 12 trav	River Locky 2018	T	35.06	61.93	0.10	0.02	97.11
RJC 99	RJC99 4 12 trav	River Locky 2018	T	35.30	62.00	0.01	0.03	97.33
RJC 99	RJC99 4 12 trav	River Locky 2018	T	35.18	62.10	0.13	0.00	97.41
RJC 99	RJC99 4 12 trav	River Locky 2018	T	35.69	61.33	0.14	0.00	97.17
RJC 99	RJC99 4 12 trav	River Locky 2018	T	35.13	61.87	0.19	0.01	97.21
RJC 99	RJC99 4 12 trav	River Locky 2018	T	35.24	62.15	0.14	0.02	97.55
RJC 99	RJC99 4 12 trav	River Locky 2018	T	35.82	61.11	0.08	0.00	97.01
RJC 99	RJC99 4 12 trav	River Locky 2018	T	35.17	61.61	0.14	0.01	96.94
RJC 99	RJC99 4 12 trav	River Locky 2018	T	35.12	61.99	0.16	0.01	97.28
RJC 99	RJC99 4 12 trav	River Locky 2018	T	35.36	61.83	0.10	0.01	97.30
RJC 99	RJC99 4 12 trav	River Locky 2018	T	35.42	61.67	0.18	0.04	97.31
RJC 99	RJC99 4 12 trav	River Locky 2018	T	35.42	61.98	0.10	0.01	97.51
RJC 99	RJC99 4 12 trav	River Locky 2018	T	35.57	61.42	0.14	0.00	97.13
RJC 99	RJC99 4 12 trav	River Locky 2018	T	35.38	61.74	0.05	0.01	97.18

Block	Grain ID	Sample	Traverse?	Au WT%	Ag WT%	Hg WT%	Cu WT%	Total
RJC 99	RJC99 4 12 trav	River Locky 2018	T	35.04	62.14	0.14	0.00	97.31
RJC 99	RJC99 4 12 trav	River Locky 2018	T	35.29	62.63	0.03	0.01	97.96
RJC 99	RJC99 4 12 trav	River Locky 2018	T	35.64	61.07	0.05	0.02	96.78
RJC 99	RJC99 4 12 trav	River Locky 2018	T	34.67	62.83	0.09	0.03	97.62
RJC 99	RJC99 4 13	River Locky 2018		72.81	27.67	0.13	0.08	100.69
RJC 99	RJC99 4 14	River Locky 2018		75.05	25.24	0.13	0.05	100.47
RJC 99	RJC99 4 15	River Locky 2018		67.36	32.80	0.19	0.05	100.41
RJC 99	RJC99 4 16	River Locky 2018		76.36	24.02	0.06	0.08	100.52
RJC 99	RJC99 4 17	River Locky 2018		67.08	33.18	0.11	0.06	100.43
RJC 99	RJC99 4 18	River Locky 2018		68.79	31.17	0.16	0.05	100.17
RJC 99	RJC99 4 19	River Locky 2018		63.69	36.92	0.11	0.03	100.76
RJC 99	RJC99 4 20	River Locky 2018		89.33	11.60	0.10	0.09	101.12
RJC 99	RJC99 4 21	River Locky 2018		85.72	15.16	0.11	0.07	101.06
RJC 99	RJC99 4 22	River Locky 2018		73.40	27.08	0.12	0.06	100.67
RJC 99	RJC99 4 23	River Locky 2018		75.59	25.23	0.07	0.03	100.92
RJC 99	RJC99 4 24	River Locky 2018		60.14	40.23	0.06	0.03	100.46
RJC 99	RJC99 4 25	River Locky 2018		80.10	20.13	0.08	0.07	100.37
RJC 99	RJC99 4 26	River Locky 2018		62.28	37.42	0.09	0.08	99.87
RJC 99	RJC99 4 27	River Locky 2018		62.68	37.27	0.03	0.05	100.03
RJC 99	RJC99 4 28	River Locky 2018		66.98	33.67	0.08	0.08	100.81
RJC 99	RJC99 4 29	River Locky 2018		78.27	22.32	0.13	0.06	100.78
RJC 99	RJC99 4 30	River Locky 2018		68.36	31.78	0.17	0.04	100.35

Curraghinalt v75 Thin section (67304)

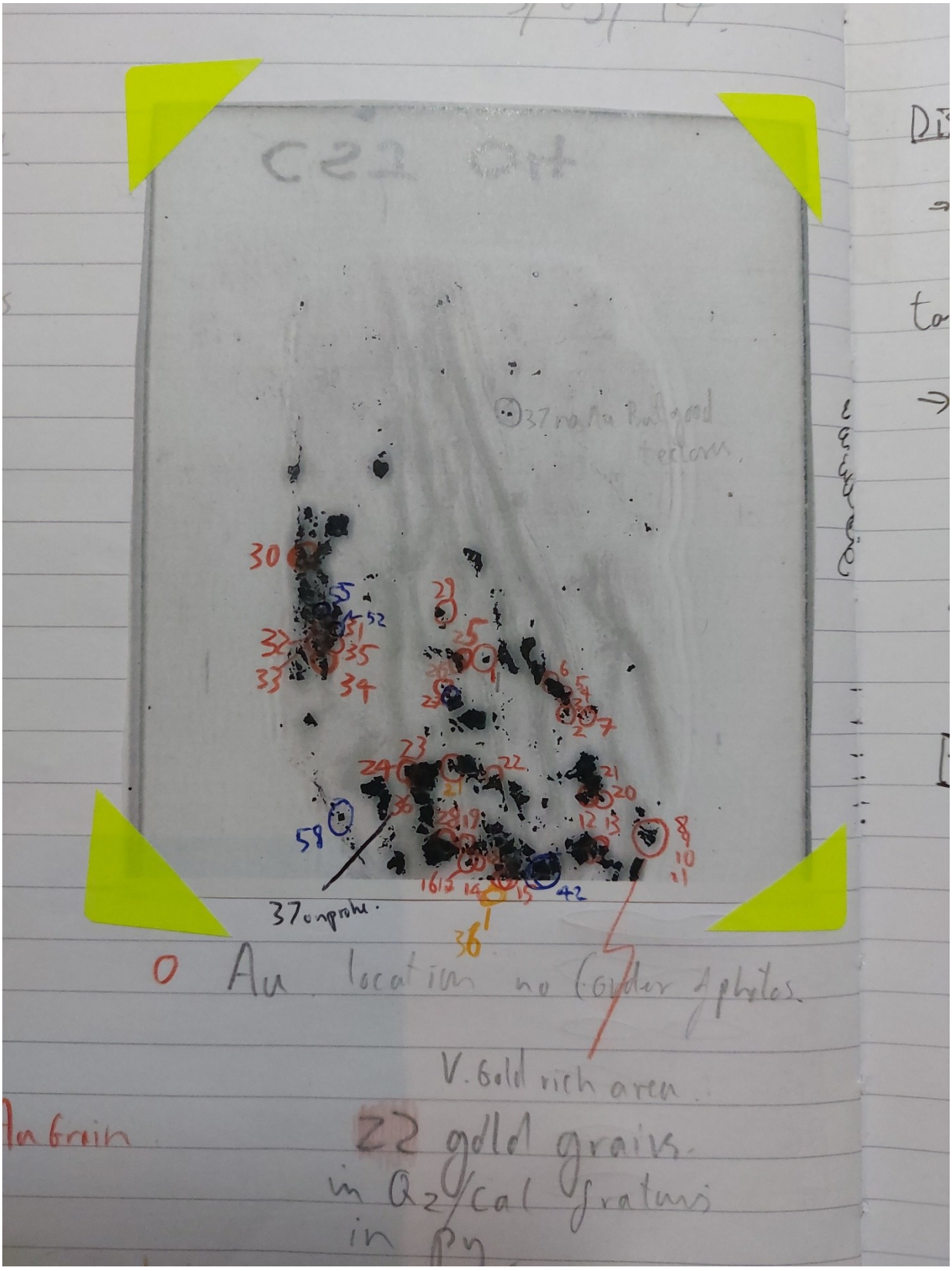

EMPA data V75 thin section

site ID	NUMBER	Au WT%	Ag WT %	Hg WT%	Cu WT%	TOTAL
Au 4 inc py smaller	14.00	95.58	3.45	0.09	0.07	99.20
Au 4 inc py larger	13.00	96.11	3.48	0.22	0.11	99.91
Au 1 inc py	9.00	95.58	3.96	0.17	0.06	99.78
Au 8 sub 1 qz	19.00	96.09	4.05	0.13	0.11	100.38
Au 36/37 inc py	47.00	78.70	4.05	0.00	0.00	82.76
Au 27	50.00	93.93	4.59	0.07	0.08	98.67
Au 27	50.00	94.12	4.68	0.23	0.05	99.07
Au 3 inc py	12.00	95.61	4.68	0.22	0.12	100.62
Au 12 inc py round	29.00	93.74	4.68	0.23	0.05	98.70
Au 18 inc py	44.00	93.55	4.72	0.19	0.05	98.52
Au 8 sub 6	24.00	95.78	4.73	0.28	0.05	100.84
Au 12 inc py round	29.00	94.34	4.79	0.10	0.05	99.29
Au 8 sub 3	21.00	95.54	4.80	0.18	0.06	100.58
Au 24	46.00	91.36	4.84	0.01	0.08	96.28
Au 18 inc py	44.00	92.19	4.85	0.22	0.04	97.30
Au 6 inc py	16.00	90.47	4.86	0.14	0.11	95.59
Au 6 inc py	16.00	90.82	4.90	0.28	0.07	96.07
Au 6 inc py	16.00	90.45	4.91	0.33	0.09	95.78
Au 36/37 inc py	47.00	94.97	5.17	0.05	0.05	100.24
Au 1 rim py	8.00	88.52	11.71	0.40	0.00	100.64
Au 8 sub 2	20.00	87.40	12.03	0.40	0.02	99.84
Au 8 sub 8	26.00	85.37	12.18	0.26	0.01	97.81
Au 21 secondary std	51.00	88.20	12.27	0.40	0.00	100.88
Au 28	45.00	87.46	12.29	0.35	0.01	100.11
Au36 sub 7 north in qz	42.00	86.28	12.31	0.24	0.02	98.85
Au 8 sub 5	23.00	87.96	12.33	0.32	0.03	100.64
Au 21 secondry std	4.00	87.27	12.34	0.23	0.00	99.84

Au 2 between 2 py	10.00	85.80	12.34	0.26	0.03	98.43
Au 21 secondary std	51.00	87.74	12.38	0.39	0.01	100.52
Au 21 secondry std	4.00	87.37	12.39	0.34	0.02	100.12
Au 21 secondry std	4.00	86.94	12.44	0.38	0.02	99.78
Au 21 sub au 3	7.00	84.10	12.49	0.29	0.03	96.92
Au 21 secondary std	51.00	87.51	12.60	0.37	0.00	100.47
Au 7 inc py	18.00	87.01	12.61	0.34	0.02	99.98
Au 2 north Au bleb	11.00	85.90	12.65	0.28	0.01	98.84
Au 2 north Au bleb	11.00	86.66	12.68	0.41	0.02	99.76
Au36 sub 7 north in qz	42.00	86.23	12.70	0.30	0.02	99.25
site ID	NUMBER	Au WT%	Ag WT %	Hg WT%	Cu WT%	TOTAL
Au 21 secondary std	51.00	86.67	12.80	0.32	0.02	99.80
Au 2 between 2 py	10.00	86.39	12.80	0.32	0.02	99.53
Au 21 sub au 2	6.00	86.98	12.84	0.38	0.02	100.22
Au 15 thin in fracture	34.00	68.57	12.87	0.00	0.00	81.44
Au 21 sub au 3	7.00	86.12	12.87	0.29	0.02	99.31
Au 8 sub 7	25.00	86.79	12.89	0.29	0.02	99.98
Au 21 secondry std	3.00	87.91	12.91	0.40	0.01	101.23
Au 21 sub au 1	5.00	87.09	13.04	0.52	0.02	100.66
Au 21 secondry std	4.00	86.68	13.32	0.26	0.03	100.29
Au36 sub 6	41.00	84.84	13.39	0.43	0.06	98.72
Au 5 frac py	15.00	84.46	13.39	0.34	0.02	98.21
Au 8 sub 9	28.00	86.82	13.42	0.36	0.01	100.61
Au36 sub 8 west in py margin	43.00	87.26	13.64	0.31	0.03	101.25
Au36 sub 6	41.00	84.57	13.65	0.34	0.07	98.63
Au36 sub 4	39.00	85.27	13.73	0.36	0.03	99.39
Au 15	33.00	83.21	13.76	0.13	0.09	97.18
Au36 sub 2	37.00	83.45	13.83	0.33	0.10	97.70

Au36 sub 8 west in py margin	43.00	87.37	13.88	0.29	0.03	101.56
Au 15	33.00	83.44	13.99	0.35	0.09	97.86
Au36 sub 5	40.00	83.33	14.05	0.45	0.04	97.88
Au 21 secondary std	51.00	87.00	14.06	0.31	0.00	101.38
Au 8 sub 8 south	27.00	84.47	14.10	0.36	0.03	98.97
Au 12 on vein margin	30.00	81.49	14.34	0.19	0.03	96.05
Au 12 on vein margin	30.00	81.98	14.37	0.29	0.01	96.65
Au 15 thin in fracture	34.00	81.72	14.80	0.34	0.01	96.87
Au 35	49.00	84.08	14.82	0.33	0.10	99.33
Au36 sub 1	36.00	81.85	14.85	0.34	0.10	97.15
Au36 sub 1	36.00	81.69	14.90	0.36	0.12	97.06
Au 15 thin in fracture	34.00	81.10	15.33	0.44	0.02	96.89
Au36 sub 3	38.00	81.17	15.58	0.33	0.05	97.14
Au 8 sub 4	22.00	84.15	16.12	0.30	0.01	100.58
Au 14 thin in fracture	35.00	80.88	17.55	0.28	0.01	98.72
Au 14 thin in fracture	35.00	81.22	17.64	0.34	0.02	99.22

site ID	NUMBER	Au WT%	Ag WT%	Hg WT%	Cu WT%	TOTAL
Au 4 inc py smaller	14.00	95.58	3.45	0.09	0.07	99.20
Au 4 inc py larger	13.00	96.11	3.48	0.22	0.11	99.91
Au 1 inc py	9.00	95.58	3.96	0.17	0.06	99.78
Au 8 sub 1 qz	19.00	96.09	4.05	0.13	0.11	100.38
Au 36/37 inc py	47.00	78.70	4.05	0.00	0.00	82.76
Au 27	50.00	93.93	4.59	0.07	0.08	98.67
Au 27	50.00	94.12	4.68	0.23	0.05	99.07
Au 3 inc py	12.00	95.61	4.68	0.22	0.12	100.62
Au 12 inc py round	29.00	93.74	4.68	0.23	0.05	98.70
Au 18 inc py	44.00	93.55	4.72	0.19	0.05	98.52
Au 8 sub 6	24.00	95.78	4.73	0.28	0.05	100.84
Au 12 inc py round	29.00	94.34	4.79	0.10	0.05	99.29
Au 8 sub 3	21.00	95.54	4.80	0.18	0.06	100.58
Au 24	46.00	91.36	4.84	0.01	0.08	96.28
Au 18 inc py	44.00	92.19	4.85	0.22	0.04	97.30
Au 6 inc py	16.00	90.47	4.86	0.14	0.11	95.59
Au 6 inc py	16.00	90.82	4.90	0.28	0.07	96.07

Au 6 inc py	16.00	90.45	4.91	0.33	0.09	95.78
Au 36/37 inc py	47.00	94.97	5.17	0.05	0.05	100.24
Au 1 rim py	8.00	88.52	11.71	0.40	0.00	100.64
Au 8 sub 2	20.00	87.40	12.03	0.40	0.02	99.84
Au 8 sub 8	26.00	85.37	12.18	0.26	0.01	97.81
Au 21 secondary std	51.00	88.20	12.27	0.40	0.00	100.88
Au 28	45.00	87.46	12.29	0.35	0.01	100.11
Au36 sub 7 north in qz	42.00	86.28	12.31	0.24	0.02	98.85
Au 8 sub 5	23.00	87.96	12.33	0.32	0.03	100.64
Au 21 secondry std	4.00	87.27	12.34	0.23	0.00	99.84
Au 2 between 2 py	10.00	85.80	12.34	0.26	0.03	98.43
Au 21 secondary std	51.00	87.74	12.38	0.39	0.01	100.52
Au 21 secondry std	4.00	87.37	12.39	0.34	0.02	100.12
Au 21 secondry std	4.00	86.94	12.44	0.38	0.02	99.78
Au 21 sub au 3	7.00	84.10	12.49	0.29	0.03	96.92
Au 21 secondary std	51.00	87.51	12.60	0.37	0.00	100.47
Au 7 inc py	18.00	87.01	12.61	0.34	0.02	99.98
Au 2 north Au bleb	11.00	85.90	12.65	0.28	0.01	98.84
Au 2 north Au bleb	11.00	86.66	12.68	0.41	0.02	99.76
Au36 sub 7 north in qz	42.00	86.23	12.70	0.30	0.02	99.25
Au 21 secondary std	51.00	86.67	12.80	0.32	0.02	99.80
Au 2 between 2 py	10.00	86.39	12.80	0.32	0.02	99.53
Au 21 sub au 2	6.00	86.98	12.84	0.38	0.02	100.22
Au 15 thin in fracture	34.00	68.57	12.87	0.00	0.00	81.44
Au 21 sub au 3	7.00	86.12	12.87	0.29	0.02	99.31
Au 8 sub 7	25.00	86.79	12.89	0.29	0.02	99.98
Au 21 secondry std	3.00	87.91	12.91	0.40	0.01	101.23
Au 21 sub au 1	5.00	87.09	13.04	0.52	0.02	100.66
Au 21 secondry std	4.00	86.68	13.32	0.26	0.03	100.29
Au36 sub 6	41.00	84.84	13.39	0.43	0.06	98.72
Au 5 frac py	15.00	84.46	13.39	0.34	0.02	98.21
Au 8 sub 9	28.00	86.82	13.42	0.36	0.01	100.61
Au36 sub 8 west in py margin	43.00	87.26	13.64	0.31	0.03	101.25
Au36 sub 6	41.00	84.57	13.65	0.34	0.07	98.63
Au36 sub 4	39.00	85.27	13.73	0.36	0.03	99.39
Au 15	33.00	83.21	13.76	0.13	0.09	97.18
Au36 sub 2	37.00	83.45	13.83	0.33	0.10	97.70

Au36 sub 8 west in py margin	43.00	87.37	13.88	0.29	0.03	101.56
Au 15	33.00	83.44	13.99	0.35	0.09	97.86
Au36 sub 5	40.00	83.33	14.05	0.45	0.04	97.88
Au 21 secondary std	51.00	87.00	14.06	0.31	0.00	101.38
Au 8 sub 8 south	27.00	84.47	14.10	0.36	0.03	98.97
Au 12 on vein margin	30.00	81.49	14.34	0.19	0.03	96.05
Au 12 on vein margin	30.00	81.98	14.37	0.29	0.01	96.65
Au 15 thin in fracture	34.00	81.72	14.80	0.34	0.01	96.87
Au 35	49.00	84.08	14.82	0.33	0.10	99.33
Au36 sub 1	36.00	81.85	14.85	0.34	0.10	97.15
Au36 sub 1	36.00	81.69	14.90	0.36	0.12	97.06
Au 15 thin in fracture	34.00	81.10	15.33	0.44	0.02	96.89
Au36 sub 3	38.00	81.17	15.58	0.33	0.05	97.14
Au 8 sub 4	22.00	84.15	16.12	0.30	0.01	100.58
Au 14 thin in fracture	35.00	80.88	17.55	0.28	0.01	98.72
Au 14 thin in fracture	35.00	81.22	17.64	0.34	0.02	99.22

Curraghinalt Detrital EMPA Data

Block	Grain ID	Creek	Au WT%	Ag WT%	Hg WT%	Cu WT%	TOTAL
RJC 90	1_1	Curraghinalt Burn	90.06	9.07	0.26	0.03	99.43
RJC 90	1_2	Curraghinalt Burn	90.18	8.80	0.26	0.08	99.32
RJC 90	1_3	Curraghinalt Burn	89.24	9.77	0.67	0.02	99.70
RJC 90	1_4	Curraghinalt Burn	91.44	7.38	0.55	0.03	99.40
RJC 90	1_5	Curraghinalt Burn	86.22	4.67	0.27	0.09	91.24
RJC 90	1_6	Curraghinalt Burn	88.41	9.17	0.19	0.05	97.82
RJC 90	1_7	Curraghinalt Burn	93.19	6.02	0.16	0.08	99.45
RJC 90	1_8	Curraghinalt Burn	91.89	6.90	0.27	0.06	99.12
RJC 90	1_9	Curraghinalt Burn	91.40	7.43	0.25	0.05	99.13
RJC 90	1_10	Curraghinalt Burn	84.66	10.96	3.84	0.04	99.50
RJC 90	1_11	Curraghinalt Burn	91.63	7.12	0.42	0.06	99.23
RJC 90	1_12	Curraghinalt Burn	90.82	9.14	0.11	0.05	100.12
RJC 90	1_13	Curraghinalt Burn	74.27	25.31	0.66	0.01	100.24
RJC 90	1_14	Curraghinalt Burn	88.79	10.22	0.43	0.03	99.48
RJC 90	1_15	Curraghinalt Burn	92.26	5.87	0.40	0.08	98.61
RJC 90	1_16	Curraghinalt Burn	90.10	7.31	0.39	0.03	97.83
RJC 90	1_17	Curraghinalt Burn	91.75	7.55	0.16	0.08	99.54
RJC 90	1_18	Curraghinalt Burn	82.10	17.38	0.18	0.01	99.67
RJC 90	1_19	Curraghinalt Burn	90.10	9.31	0.36	0.04	99.82
RJC 90	1_20	Curraghinalt Burn	92.50	6.40	0.25	0.04	99.20
RJC 90	2_1	Curraghinalt Burn	94.66	5.02	0.19	0.08	99.95
RJC 90	2_2	Curraghinalt Burn	91.54	7.10	0.27	0.07	98.98
RJC 90	4_1	Curraghinalt Burn	90.41	6.82	0.22	0.06	97.50
RJC 90	4_2	Curraghinalt Burn	90.51	8.27	0.33	0.08	99.19
RJC 90	4_3	Curraghinalt Burn	84.24	14.56	0.32	0.03	99.15
RJC 90	4_4	Curraghinalt Burn	88.58	9.97	0.19	0.03	98.77
RJC 90	4_5	Curraghinalt Burn	94.25	4.82	0.33	0.08	99.48
RJC 90	4_6	Curraghinalt Burn	83.77	15.26	0.23	0.04	99.30
RJC 90	4_7	Curraghinalt Burn	89.29	10.35	0.16	0.05	99.85
RJC 90	4_8	Curraghinalt Burn	87.32	10.70	0.22	0.03	98.27
RJC 90	4_9	Curraghinalt Burn	93.03	6.73	0.33	0.08	100.18
RJC 90	4_10	Curraghinalt Burn	93.49	6.26	0.16	0.07	99.99
RJC 90	3_1	Curraghinalt Burn	76.04	22.87	0.10	0.00	99.02
RJC 90	3_2	Curraghinalt Burn	90.36	8.22	0.23	0.05	98.86
RJC 91	1_1	Curraghinalt Burn	81.03	18.59	0.26	0.02	99.90
RJC 91	1_2	Curraghinalt Burn	86.86	12.16	0.33	0.03	99.39
RJC 91	1_3	Curraghinalt Burn	90.59	8.24	0.29	0.05	99.16
RJC 91	1_4	Curraghinalt Burn	88.60	10.07	0.14	0.02	98.83
RJC 91	1_5	Curraghinalt Burn	88.31	10.20	0.27	0.03	98.82
RJC 91	1_6	Curraghinalt Burn	90.02	7.93	0.10	0.08	98.13
RJC 91	1_7	Curraghinalt Burn	85.04	13.77	0.56	0.05	99.42
RJC 91	1_8	Curraghinalt Burn	83.23	15.56	0.41	0.01	99.22
RJC 91	1_9	Curraghinalt Burn	87.72	11.16	0.33	0.03	99.24
RJC 91	1_10	Curraghinalt Burn	86.38	12.62	0.25	0.03	99.28
RJC 91	2_1	Curraghinalt Burn	90.06	8.42	0.31	0.03	98.82

Block	Grain ID	Creek	Au WT%	Ag WT%	Hg WT%	Cu WT%	TOTAL
RJC 91	2_2	Curraghinalt Burn	85.82	13.20	0.59	0.04	99.65
RJC 91	2_3	Curraghinalt Burn	89.22	9.69	0.09	0.05	99.06
RJC 91	2_4	Curraghinalt Burn	93.32	5.81	0.29	0.05	99.48
RJC 91	2_5	Curraghinalt Burn	86.68	12.34	0.45	0.03	99.50
RJC 91	2_6	Curraghinalt Burn	83.65	15.59	0.33	0.01	99.58
RJC 91	2_7	Curraghinalt Burn	89.33	9.88	0.30	0.05	99.56
RJC 91	2_8	Curraghinalt Burn	88.69	10.31	0.35	0.04	99.38
RJC 91	2_9	Curraghinalt Burn	89.80	8.65	0.38	0.04	98.86
RJC 91	2_10	Curraghinalt Burn	84.41	14.62	0.18	0.02	99.24
RJC 91	2_11	Curraghinalt Burn	85.78	13.32	0.58	0.01	99.70
RJC 91	2_12	Curraghinalt Burn	86.99	12.02	0.20	0.02	99.24
RJC 91	2_13	Curraghinalt Burn	91.29	7.43	0.23	0.05	99.00
RJC 91	2_14	Curraghinalt Burn	88.94	9.63	0.28	0.02	98.86
RJC 91	2_15	Curraghinalt Burn	86.68	10.47	0.69	0.02	97.86
RJC 91	2_16	Curraghinalt Burn	92.80	5.19	0.29	0.09	98.36
RJC 91	2_17	Curraghinalt Burn	88.05	10.15	0.11	0.01	98.33
RJC 91	2_18	Curraghinalt Burn	87.27	11.66	0.19	0.03	99.15
RJC 91	2_19	Curraghinalt Burn	92.15	6.53	0.28	0.07	99.03
RJC 91	2_20	Curraghinalt Burn	86.88	12.53	0.08	0.02	99.51
RJC 91	2_21	Curraghinalt Burn	79.57	19.00	0.21	0.01	98.79
RJC 91	2_22	Curraghinalt Burn	67.98	31.42	0.21	0.00	99.61
RJC 91	2_23	Curraghinalt Burn	89.64	9.06	0.17	0.04	98.90
RJC 91	2_24	Curraghinalt Burn	88.00	10.92	0.16	0.02	99.10
RJC 91	2_25	Curraghinalt Burn	84.40	13.77	0.95	0.02	99.13
RJC 91	3_1	Curraghinalt Burn	80.96	17.99	0.30	0.02	99.26
RJC 91	3_2	Curraghinalt Burn	92.07	6.27	0.19	0.08	98.62
RJC 91	3_3	Curraghinalt Burn	88.97	9.01	0.25	0.03	98.26
RJC 91	3_4	Curraghinalt Burn	86.32	12.90	0.19	0.01	99.41
RJC 91	3_5	Curraghinalt Burn	90.85	7.22	0.39	0.04	98.50
RJC 91	3_6	Curraghinalt Burn	91.48	6.65	0.09	0.06	98.28
RJC 91	3_7	Curraghinalt Burn	80.32	18.48	0.44	0.01	99.24
RJC 91	3_8	Curraghinalt Burn	87.28	11.84	0.15	0.02	99.29
RJC 91	3_9	Curraghinalt Burn	91.28	6.75	0.26	0.05	98.33
RJC 91	3_10	Curraghinalt Burn	91.35	7.34	0.36	0.04	99.09
RJC 91	4_1	Curraghinalt Burn	84.23	14.30	0.45	0.04	99.02
RJC 91	4_2	Curraghinalt Burn	88.55	9.98	0.38	0.00	98.91
RJC 91	4_3	Curraghinalt Burn	88.46	9.54	0.40	0.01	98.42
RJC 91	4_4	Curraghinalt Burn	84.97	12.54	0.25	0.03	97.79
RJC 91	4_5	Curraghinalt Burn	90.07	7.17	0.28	0.06	97.58
RJC 91	4_6	Curraghinalt Burn	72.02	26.62	0.35	0.03	99.03
RJC 91	4_7	Curraghinalt Burn	85.94	12.52	0.31	0.02	98.80
RJC 91	5_1	Curraghinalt Burn	89.73	9.36	0.31	0.04	99.43
RJC 91	5_2	Curraghinalt Burn	85.71	10.29	0.17	0.04	96.21
RJC 91	5_3	Curraghinalt Burn	86.17	11.93	0.27	0.02	98.39
RJC 91	5_4	Curraghinalt Burn	83.16	15.28	0.21	0.00	98.65
RJC 91	5_5	Curraghinalt Burn	89.18	7.07	0.43	0.07	96.76
RJC 91	5_6	Curraghinalt Burn	88.17	9.78	0.22	0.05	98.21
RJC 91	5_7	Curraghinalt Burn	86.87	8.98	0.12	0.05	96.01

Block	Grain ID	Creek	Au WT%	Ag WT%	Hg WT%	Cu WT%	TOTAL
RJC 91	5_8	Curraghinalt Burn	87.22	10.25	0.42	0.04	97.93
RJC 91	5_9	Curraghinalt Burn	89.49	8.40	0.07	0.05	98.01
RJC 91	5_10	Curraghinalt Burn	77.57	20.73	0.60	0.02	98.92
RJC 91	5_11	Curraghinalt Burn	91.78	4.89	0.23	0.07	96.97
RJC 91	5_12	Curraghinalt Burn	83.23	14.46	0.34	0.02	98.05
RJC 91	5_13	Curraghinalt Burn	87.95	10.37	0.34	0.04	98.70
RJC 91	5_14	Curraghinalt Burn	89.68	8.39	0.29	0.06	98.42
RJC 91	5_15	Curraghinalt Burn	79.13	19.66	0.62	0.02	99.42
RJC 91	6_1	Curraghinalt Burn	91.74	5.36	0.13	0.07	97.30
RJC 91	6_2	Curraghinalt Burn	84.01	13.60	0.23	0.02	97.87
RJC 91	6_3	Curraghinalt Burn	82.79	15.64	0.29	0.01	98.74
RJC 91	6_4	Curraghinalt Burn	75.69	21.00	1.24	0.01	97.93
RJC 91	6_5	Curraghinalt Burn	89.04	8.64	0.40	0.08	98.15
RJC 91	6_6	Curraghinalt Burn	89.11	6.48	0.21	0.07	95.87
RJC 91	6_7	Curraghinalt Burn	91.77	6.20	0.77	0.08	98.82
RJC 91	6_8	Curraghinalt Burn	87.62	10.74	0.37	0.05	98.78
RJC 91	6_9	Curraghinalt Burn	84.66	13.60	0.38	0.08	98.72
RJC 91	6_10	Curraghinalt Burn	87.68	10.88	0.11	0.04	98.71
RJC 91	6_11	Curraghinalt Burn	88.59	8.97	0.17	0.04	97.77
RJC 91	6_12	Curraghinalt Burn	91.85	5.80	0.27	0.09	98.01
RJC 92	1_1	Curraghinalt Burn	87.50	11.76	0.45	0.07	99.79
RJC 92	1_2	Curraghinalt Burn	84.07	14.55	0.22	0.06	98.89
RJC 92	1_3	Curraghinalt Burn	87.12	10.88	0.41	0.05	98.46
RJC 92	1_4	Curraghinalt Burn	86.00	7.83	0.33	0.07	94.22
RJC 92	1_5	Curraghinalt Burn	85.19	10.61	0.22	0.01	96.04
RJC 92	1_6	Curraghinalt Burn	87.70	11.49	0.10	0.09	99.39
RJC 92	1_7	Curraghinalt Burn	87.06	8.06	0.29	0.09	95.50
RJC 92	1_8	Curraghinalt Burn	86.82	10.93	0.31	0.05	98.11
RJC 92	1_9	Curraghinalt Burn	91.75	7.12	0.22	0.08	99.17
RJC 92	1_10	Curraghinalt Burn	87.03	12.12	0.44	0.04	99.63
RJC 92	1_11	Curraghinalt Burn	83.80	15.00	0.18	0.08	99.06
RJC 92	1_12	Curraghinalt Burn	88.16	9.15	0.26	0.09	97.67
RJC 92	1_13	Curraghinalt Burn	86.79	12.29	0.16	0.05	99.30
RJC 92	1_15	Curraghinalt Burn	81.20	16.98	0.99	0.04	99.21
RJC 92	1_16	Curraghinalt Burn	53.08	3.35	0.16	0.04	56.63
RJC 92	1_17	Curraghinalt Burn	72.83	26.48	1.07	0.04	100.42
RJC 92	1_18	Curraghinalt Burn	88.84	7.64	0.21	0.08	96.77
RJC 92	1_19	Curraghinalt Burn	86.92	10.77	0.17	0.01	97.87
RJC 92	1_20	Curraghinalt Burn	82.51	15.04	0.23	0.03	97.81
RJC 92	2_1	Curraghinalt Burn	81.75	13.29	0.17	0.04	95.24
RJC 92	2_2	Curraghinalt Burn	83.49	12.14	0.31	0.06	96.00
RJC 92	2_3	Curraghinalt Burn					
RJC 92	2_4	Curraghinalt Burn	86.69	11.50	0.17	0.04	98.40
RJC 92	2_5	Curraghinalt Burn	89.98	9.35	0.15	0.08	99.56
RJC 92	2_6	Curraghinalt Burn	88.40	7.07	0.28	0.02	95.76
RJC 92	2_7	Curraghinalt Burn	88.79	9.60	0.14	0.01	98.55
RJC 92	2_8	Curraghinalt Burn	85.98	12.41	0.37	0.05	98.82
RJC 92	2_9	Curraghinalt Burn	93.74	4.16	0.16	0.07	98.14

Block	Grain ID	Creek	Au WT%	Ag WT%	Hg WT%	Cu WT%	TOTAL
RJC 92	2_10	Curraghinalt Burn	85.93	10.75	0.20	0.05	96.93
RJC 92	2_11	Curraghinalt Burn	84.27	12.70	0.28	0.05	97.30
RJC 92	2_12	Curraghinalt Burn	83.86	11.80	0.19	0.01	95.86
RJC 92	2_13	Curraghinalt Burn	86.64	7.26	0.12	0.03	94.05
RJC 92	2_14	Curraghinalt Burn	87.39	8.66	0.32	0.09	96.46
RJC 92	2_15	Curraghinalt Burn	80.61	16.34	0.76	0.02	97.74
RJC 92	2_16	Curraghinalt Burn	90.77	8.17	0.26	0.05	99.25
RJC 92	2_17	Curraghinalt Burn	89.48	8.02	0.22	0.05	97.77
RJC 92	2_18	Curraghinalt Burn	87.87	9.26	0.31	0.02	97.46
RJC 92	2_19	Curraghinalt Burn	75.64	23.17	1.15	0.02	99.98
RJC 92	2_20	Curraghinalt Burn	81.69	11.61	0.11	0.03	93.44
RJC 92	2_21	Curraghinalt Burn	89.64	8.05	0.28	0.06	98.03
RJC 92	2_22	Curraghinalt Burn	87.30	8.33	0.09	0.04	95.76
RJC 92	2_23	Curraghinalt Burn	86.12	13.07	0.25	0.04	99.48
RJC 92	2_24	Curraghinalt Burn	85.68	10.32	0.17	0.04	96.20
RJC 92	2_25	Curraghinalt Burn	92.37	4.86	0.31	0.04	97.58
RJC 92	3_1	Curraghinalt Burn	86.27	12.20	0.17	0.03	98.67
RJC 92	3_2	Curraghinalt Burn	85.79	13.14	0.19	0.02	99.15
RJC 92	3_3	Curraghinalt Burn	89.73	8.27	0.31	0.05	98.37
RJC 92	3_4	Curraghinalt Burn	87.81	11.16	0.07	0.01	99.05
RJC 92	3_5	Curraghinalt Burn	82.61	15.90	0.96	0.02	99.49
RJC 92	3_6	Curraghinalt Burn	83.78	14.73	0.24	0.02	98.77
RJC 92	3_7	Curraghinalt Burn	88.92	10.07	0.07	0.02	99.08
RJC 92	3_8	Curraghinalt Burn	85.94	11.34	0.43	0.04	97.74
RJC 92	3_9	Curraghinalt Burn	88.88	8.26	0.22	0.04	97.40
RJC 92	3_10	Curraghinalt Burn	85.17	12.63	0.40	0.03	98.22
RJC 92	3_11	Curraghinalt Burn	80.15	18.09	0.51	0.01	98.75
RJC 92	3_12	Curraghinalt Burn	87.73	11.30	0.23	0.06	99.33
RJC 92	3_13	Curraghinalt Burn	83.70	14.83	0.78	0.02	99.33
RJC 92	3_14	Curraghinalt Burn	86.75	8.03	0.17	0.03	94.98
RJC 92	3_15	Curraghinalt Burn	85.72	10.76	0.33	0.04	96.84
RJC 92	3_16	Curraghinalt Burn	83.20	15.64	0.14	0.02	99.00
RJC 92	3_17	Curraghinalt Burn	87.19	8.74	0.17	0.04	96.14
RJC 92	3_18	Curraghinalt Burn	77.09	22.03	0.54	0.03	99.69
RJC 92	3_19	Curraghinalt Burn	88.08	8.92	0.12	0.03	97.16
RJC 92	3_20	Curraghinalt Burn	85.86	12.47	0.20	0.04	98.56
RJC 92	3_21	Curraghinalt Burn	84.65	12.54	0.17	0.02	97.38
RJC 92	3_22	Curraghinalt Burn	89.60	8.21	0.31	0.07	98.19
RJC 92	3_23	Curraghinalt Burn	84.28	13.27	0.55	0.04	98.13
RJC 92	3_24	Curraghinalt Burn	88.16	10.09	0.22	0.08	98.55
RJC 92	3_25	Curraghinalt Burn	83.62	11.88	0.62	0.05	96.16
RJC 92	3_26	Curraghinalt Burn	89.77	8.97	0.23	0.05	99.03
RJC 92	3_27	Curraghinalt Burn	84.43	12.76	0.31	0.02	97.52
RJC 92	3_28	Curraghinalt Burn	86.98	12.04	0.29	0.05	99.36
RJC 92	3_29	Curraghinalt Burn	88.27	8.44	0.13	0.03	96.87
RJC 92	3_30	Curraghinalt Burn	87.26	11.23	0.34	0.03	98.86
RJC 92	4_1	Curraghinalt Burn	84.17	13.64	0.65	0.02	98.48
RJC 92	4_2	Curraghinalt Burn	84.43	14.30	0.69	0.03	99.45

Block	Grain ID	Creek	Au WT%	Ag WT%	Hg WT%	Cu WT%	TOTAL
RJC 92	4_3	Curraghinalt Burn	85.96	13.74	0.19	0.02	99.91
RJC 92	4_4	Curraghinalt Burn	86.48	12.86	0.40	0.04	99.77
RJC 92	4_5	Curraghinalt Burn	86.31	12.93	0.11	0.01	99.36
RJC 92	4_6	Curraghinalt Burn	69.84	18.52	0.05	0.02	88.42
RJC 92	4_7	Curraghinalt Burn	73.32	26.02	0.21	0.00	99.54
RJC 92	4_8	Curraghinalt Burn	92.78	5.33	0.25	0.05	98.41
RJC 92	4_9	Curraghinalt Burn	89.68	9.44	0.31	0.06	99.48
RJC 92	4_10	Curraghinalt Burn	88.01	11.60	0.23	0.03	99.88
RJC 92	4_11	Curraghinalt Burn	88.45	9.80	0.40	0.04	98.69
RJC 92	4_12	Curraghinalt Burn	87.62	10.61	0.12	0.02	98.37
RJC 92	4_13	Curraghinalt Burn	86.07	11.22	0.14	0.04	97.47
RJC 92	4_14	Curraghinalt Burn	91.54	6.74	0.64	0.03	98.95
RJC 92	4_15	Curraghinalt Burn	87.32	10.39	0.29	0.04	98.04
RJC 92	4_16	Curraghinalt Burn	86.85	10.57	0.09	0.05	97.56
RJC 92	4_17	Curraghinalt Burn	88.82	9.83	0.53	0.00	99.18
RJC 92	4_18	Curraghinalt Burn	87.98	10.56	0.22	0.05	98.81
RJC 92	4_19	Curraghinalt Burn	86.42	7.60	0.16	0.05	94.22
RJC 92	4_20	Curraghinalt Burn	86.17	13.25	0.35	0.03	99.79
RJC 92	4_21	Curraghinalt Burn	90.31	8.62	0.10	0.07	99.11
RJC 92	4_22	Curraghinalt Burn	84.80	13.90	0.38	0.02	99.11
RJC 92	4_23	Curraghinalt Burn	88.96	7.65	0.20	0.05	96.87
RJC 92	4_24	Curraghinalt Burn	91.84	7.26	0.34	0.04	99.47
RJC 92	4_25	Curraghinalt Burn	92.88	6.09	0.33	0.06	99.36
RJC 92	4_26	Curraghinalt Burn	85.15	14.06	0.51	0.03	99.75
RJC 92	4_27	Curraghinalt Burn	83.19	15.34	0.14	0.03	98.69
RJC 92	4_28	Curraghinalt Burn	90.12	7.12	0.15	0.03	97.44
RJC 92	4_29	Curraghinalt Burn	91.15	7.98	0.41	0.03	99.56
RJC 92	4_30	Curraghinalt Burn	86.79	11.84	0.39	0.03	99.04
RJC 92	5_1	Curraghinalt Burn	80.22	17.89	0.67	0.02	98.80
RJC 92	5_2	Curraghinalt Burn	83.94	13.97	0.27	0.04	98.23
RJC 92	5_3	Curraghinalt Burn	87.86	10.62	0.49	0.03	99.00
RJC 92	5_4	Curraghinalt Burn	86.26	9.34	0.27	0.07	95.94
RJC 92	5_5	Curraghinalt Burn	83.89	14.02	0.24	0.03	98.17
RJC 92	5_6	Curraghinalt Burn	78.47	19.35	1.14	0.04	99.00
RJC 92	5_7	Curraghinalt Burn	84.13	10.28	0.33	0.06	94.80
RJC 92	5_8	Curraghinalt Burn	85.85	11.09	0.50	0.03	97.47
RJC 92	5_9	Curraghinalt Burn	84.44	13.60	0.18	0.02	98.24
RJC 92	5_10	Curraghinalt Burn	89.75	6.30	0.16	0.05	96.26
RJC 92	5_11	Curraghinalt Burn	85.66	13.10	0.27	0.04	99.07
RJC 92	5_12	Curraghinalt Burn	86.70	10.05	0.30	0.02	97.08
RJC 92	5_13	Curraghinalt Burn	82.83	13.59	0.36	0.02	96.80
RJC 92	5_14	Curraghinalt Burn	89.24	7.58	0.29	0.06	97.17
RJC 92	5_15	Curraghinalt Burn	81.15	17.73	0.28	0.03	99.20
RJC 92	5_16	Curraghinalt Burn	86.29	11.81	0.18	0.05	98.33
RJC 92	5_17	Curraghinalt Burn	84.57	14.88	0.45	0.02	99.93
RJC 92	5_18	Curraghinalt Burn	90.72	8.18	0.25	0.09	99.23
RJC 92	5_19	Curraghinalt Burn	88.26	7.00	0.19	0.07	95.52
RJC 92	5_20	Curraghinalt Burn	90.27	8.15	0.19	0.02	98.63

Block	Grain ID	Creek	Au WT%	Ag WT%	Hg WT%	Cu WT%	TOTAL
RJC 92	5_21	Curraghinalt Burn	87.15	12.21	0.27	0.03	99.66
RJC 92	5_22	Curraghinalt Burn	84.15	13.83	0.28	0.03	98.30
RJC 92	5_23	Curraghinalt Burn	91.64	5.10	0.08	0.10	96.91
RJC 92	5_24	Curraghinalt Burn	89.30	7.40	0.14	0.04	96.88
RJC 92	5_25	Curraghinalt Burn	87.07	6.19	0.27	0.06	93.59
RJC 92	5_26	Curraghinalt Burn	85.60	10.57	0.41	0.05	96.63
RJC 92	5_27	Curraghinalt Burn	78.91	16.80	0.26	0.04	96.00
RJC 92	5_28	Curraghinalt Burn	88.41	10.72	0.17	0.04	99.33
RJC 92	5_29	Curraghinalt Burn	89.24	8.60	0.12	0.03	97.99
RJC 92	6_1	Curraghinalt Burn	85.21	13.71	0.67	0.03	99.61
RJC 92	6_2	Curraghinalt Burn	84.65	14.01	0.56	0.02	99.23
RJC 92	6_3	Curraghinalt Burn	85.58	13.02	0.39	0.05	99.03
RJC 92	6_4	Curraghinalt Burn	89.33	9.44	0.45	0.02	99.24
RJC 92	6_5	Curraghinalt Burn	86.98	11.17	0.26	0.03	98.43
RJC 92	6_6	Curraghinalt Burn	92.18	4.83	0.23	0.02	97.26
RJC 92	6_7	Curraghinalt Burn	84.07	10.67	0.25	0.03	95.02
RJC 92	6_8	Curraghinalt Burn	89.16	8.67	0.28	0.03	98.14
RJC 92	6_9	Curraghinalt Burn	90.74	8.26	0.31	0.05	99.35
RJC 92	6_10	Curraghinalt Burn	85.29	13.58	0.41	0.04	99.33
RJC 92	6_11	Curraghinalt Burn	84.78	13.76	0.28	0.01	98.83
RJC 92	6_12	Curraghinalt Burn	88.40	9.10	0.17	0.06	97.73
RJC 92	6_14	Curraghinalt Burn	80.78	18.61	0.43	0.01	99.83
RJC 92	6_15	Curraghinalt Burn	87.97	10.48	0.33	0.04	98.82
RJC 92	6_16	Curraghinalt Burn	89.10	9.90	0.24	0.03	99.27
RJC 92	6_17	Curraghinalt Burn	83.79	13.43	0.65	0.02	97.88
RJC 92	6_18	Curraghinalt Burn	86.69	11.53	0.34	0.02	98.58
RJC 92	6_19	Curraghinalt Burn	87.03	11.64	0.36	0.04	99.06
RJC 92	6_20	Curraghinalt Burn	86.09	12.57	0.22	0.02	98.90
RJC 92	6_21	Curraghinalt Burn	90.77	7.63	0.27	0.08	98.74
RJC 92	6_22	Curraghinalt Burn	85.75	10.95	0.47	0.05	97.22
RJC 92	6_23	Curraghinalt Burn	91.99	6.17	0.11	0.09	98.36
RJC 92	6_24	Curraghinalt Burn	87.61	9.31	0.27	0.00	97.19
RJC 92	6_25	Curraghinalt Burn	84.34	12.70	0.54	0.03	97.61
RJC 92	6_26	Curraghinalt Burn	86.56	11.11	0.27	0.04	97.99
RJC 92	6_27	Curraghinalt Burn	90.48	7.50	0.25	0.05	98.27
RJC 92	6_28	Curraghinalt Burn	82.23	12.54	0.33	0.04	95.14
RJC 92	6_29	Curraghinalt Burn	84.47	14.90	0.50	0.02	99.89
RJC 92	6_30	Curraghinalt Burn	89.19	8.64	0.45	0.08	98.36
RJC 92	6_31	Curraghinalt Burn	85.89	12.56	0.20	0.02	98.68
RJC 92	6_32	Curraghinalt Burn	92.14	7.55	0.27	0.05	100.00
RJC 92	6_33	Curraghinalt Burn	85.38	13.15	0.19	0.02	98.74
RJC 92	6_34	Curraghinalt Burn	85.30	10.76	0.16	0.08	96.30
RJC 92	6_35	Curraghinalt Burn	82.15	14.70	0.41	0.02	97.28
RJC 92	6_36	Curraghinalt Burn	84.21	12.72	0.95	0.02	97.89
RJC 92	6_37	Curraghinalt Burn	80.24	15.83	0.87	0.01	96.95
RJC 92	6_38	Curraghinalt Burn	86.31	10.02	0.36	0.04	96.73
RJC 92	6_39	Curraghinalt Burn	82.97	15.80	0.24	0.01	99.02
RJC 92	6_40	Curraghinalt Burn	91.33	7.18	0.15	0.04	98.70

Block	Grain ID	Creek	Au WT%	Ag WT%	Hg WT%	Cu WT%	TOTAL
RJC 92	6_41	Curraghinalt Burn	85.61	11.65	0.22	0.06	97.54
RJC 92	6_42	Curraghinalt Burn	86.27	10.43	1.19	0.01	97.91
RJC 92	6_43	Curraghinalt Burn	86.30	11.66	0.12	0.01	98.10
RJC 92	6_44	Curraghinalt Burn	86.58	12.31	0.38	0.02	99.29
RJC 92	6_45	Curraghinalt Burn	87.25	10.63	0.16	0.07	98.11
RJC 92	6_46	Curraghinalt Burn	87.94	10.73	0.18	0.01	98.85
RJC 92	6_47	Curraghinalt Burn					
RJC 92	6_48	Curraghinalt Burn	91.22	6.80	0.25	0.05	98.32
RJC 92	6_49	Curraghinalt Burn	87.54	11.13	0.11	0.03	98.82
RJC 92	6_50	Curraghinalt Burn	86.62	10.99	0.23	0.05	97.89
RJC 92	7_1	Curraghinalt Burn	83.66	15.78	0.35	0.03	99.81
RJC 92	7_2	Curraghinalt Burn	80.91	17.06	0.78	0.04	98.78
RJC 92	7_3	Curraghinalt Burn	90.05	9.16	0.20	0.02	99.43
RJC 92	7_4	Curraghinalt Burn	88.09	6.79	0.15	0.04	95.07
RJC 92	7_5	Curraghinalt Burn	91.15	7.48	0.16	0.06	98.85
RJC 92	7_6	Curraghinalt Burn	84.55	13.07	0.12	0.02	97.76
RJC 92	7_7	Curraghinalt Burn	86.01	13.15	0.12	0.00	99.28
RJC 92	7_8	Curraghinalt Burn	87.61	9.06	0.24	0.04	96.96
RJC 92	7_9	Curraghinalt Burn	88.99	10.31	0.02	0.02	99.34
RJC 92	7_10	Curraghinalt Burn	83.76	13.88	0.15	0.02	97.80
RJC 92	7_11	Curraghinalt Burn	85.51	13.56	0.25	0.00	99.32
RJC 92	7_12	Curraghinalt Burn	86.55	12.03	0.18	0.04	98.80
RJC 92	7_13	Curraghinalt Burn	89.03	10.20	0.19	0.02	99.43
RJC 92	7_14	Curraghinalt Burn	84.97	13.04	0.33	0.01	98.36
RJC 92	7_15	Curraghinalt Burn	87.45	12.26	0.30	0.02	100.03
RJC 92	8_1	Curraghinalt Burn	86.43	11.77	0.33	0.03	98.56
RJC 92	8_2	Curraghinalt Burn	89.28	9.49	0.20	0.01	98.98
RJC 92	8_3	Curraghinalt Burn	89.97	9.80	0.14	0.01	99.92
RJC 92	8_4	Curraghinalt Burn	81.21	16.24	0.28	0.01	97.74
RJC 92	8_5	Curraghinalt Burn	86.91	11.81	0.22	0.02	98.96
RJC 92	8_6	Curraghinalt Burn	80.78	16.93	0.27	0.04	98.03
RJC 92	8_7	Curraghinalt Burn	84.30	11.64	0.25	0.05	96.23
RJC 92	8_8	Curraghinalt Burn	91.73	6.62	0.06	0.06	98.47
RJC 92	8_9	Curraghinalt Burn	88.59	9.35	0.21	0.04	98.19
RJC 92	8_10	Curraghinalt Burn	87.99	10.64	0.26	0.01	98.90
RJC 92	8_11	Curraghinalt Burn	87.38	9.14	0.23	0.05	96.80
RJC 92	8_12	Curraghinalt Burn	86.18	11.89	0.56	0.03	98.66
RJC 92	8_13	Curraghinalt Burn	91.00	8.33	0.12	0.01	99.46
RJC 92	8_14	Curraghinalt Burn	88.29	10.88	0.36	0.03	99.56
RJC 92	8_15	Curraghinalt Burn	84.00	12.21	0.29	0.05	96.56
RJC 92	8_16	Curraghinalt Burn	85.83	13.44	0.26	0.02	99.54
RJC 92	8_17	Curraghinalt Burn	85.36	13.95	0.29	0.01	99.61
RJC 92	8_18	Curraghinalt Burn	87.47	6.63	0.25	0.06	94.40
RJC 92	8_19	Curraghinalt Burn	87.16	12.30	0.33	0.02	99.81
RJC 92	8_20	Curraghinalt Burn	87.70	10.96	0.19	0.05	98.91
RJC 92	8_21	Curraghinalt Burn	87.00	12.21	0.46	0.03	99.70
RJC 92	8_22	Curraghinalt Burn	80.21	16.66	1.23	0.02	98.12
RJC 92	8_23	Curraghinalt Burn	89.20	10.43	0.26	0.01	99.91

Block	Grain ID	Creek	Au WT%	Ag WT%	Hg WT%	Cu WT%	TOTAL
RJC 92	8_24	Curraghinalt Burn	85.01	13.00	0.41	0.04	98.46
RJC 92	8_25	Curraghinalt Burn	80.53	18.73	0.21	0.01	99.47
RJC 92	8_26	Curraghinalt Burn	91.94	6.23	0.22	0.08	98.48
RJC 92	8_27	Curraghinalt Burn	89.03	10.08	0.12	0.03	99.26
RJC 92	8_28	Curraghinalt Burn	87.65	9.69	0.61	0.07	98.01
RJC 92	8_29	Curraghinalt Burn	85.85	11.39	0.32	0.03	97.58
RJC 92	8_30	Curraghinalt Burn	86.08	12.29	0.24	0.04	98.65
RJC 92	9_1	Curraghinalt Burn	88.52	9.67	0.25	0.04	98.49
RJC 92	9_2	Curraghinalt Burn	88.22	10.01	0.31	0.05	98.59
RJC 92	9_3	Curraghinalt Burn	89.08	9.30	0.17	0.06	98.62
RJC 92	9_4	Curraghinalt Burn	90.73	9.01	0.20	0.03	99.96
RJC 92	9_5	Curraghinalt Burn	89.46	8.89	0.27	0.02	98.63
RJC 92	9_6	Curraghinalt Burn	78.67	18.29	0.58	0.02	97.57
RJC 92	9_7	Curraghinalt Burn	90.61	6.32	0.16	0.24	97.32
RJC 92	9_8	Curraghinalt Burn	89.84	7.16	0.25	0.03	97.28
RJC 92	9_9	Curraghinalt Burn	84.73	14.42	0.45	0.00	99.60
RJC 92	9_10	Curraghinalt Burn	86.25	10.87	0.29	0.04	97.45
RJC 92	9_11	Curraghinalt Burn	88.21	10.90	0.43	0.03	99.56
RJC 92	9_12	Curraghinalt Burn	90.38	8.15	0.28	0.03	98.84
RJC 92	9_13	Curraghinalt Burn	84.41	13.43	0.39	0.05	98.29
RJC 92	9_14	Curraghinalt Burn	84.93	13.46	0.16	0.03	98.58
RJC 92	9_15	Curraghinalt Burn	81.09	17.87	1.17	0.02	100.14
RJC 92	9_16	Curraghinalt Burn	82.35	15.98	0.11	0.01	98.45
RJC 92	9_17	Curraghinalt Burn	76.45	21.97	0.33	0.00	98.75
RJC 92	9_18	Curraghinalt Burn	83.38	15.45	0.37	0.01	99.22
RJC 92	9_19	Curraghinalt Burn	87.22	11.90	0.15	0.03	99.30
RJC 92	9_20	Curraghinalt Burn	93.95	5.06	0.16	0.05	99.23
RJC 92	9_21	Curraghinalt Burn	86.44	12.81	0.30	0.03	99.58
RJC 92	9_22	Curraghinalt Burn	88.43	10.59	0.23	0.03	99.28
RJC 92	9_23	Curraghinalt Burn	89.20	10.29	0.52	0.02	100.04
RJC 92	9_24	Curraghinalt Burn	86.52	11.39	0.59	0.02	98.53
RJC 92	9_25	Curraghinalt Burn	77.21	21.84	0.86	0.02	99.94
RJC 92	9_26	Curraghinalt Burn	87.27	11.69	0.54	0.01	99.51
RJC 92	9_27	Curraghinalt Burn	87.56	10.04	0.39	0.07	98.05
RJC 92	9_28	Curraghinalt Burn	87.68	10.21	0.34	0.04	98.26
RJC 92	9_29	Curraghinalt Burn	89.43	9.52	0.11	0.04	99.10
RJC 92	9_30	Curraghinalt Burn	91.85	6.76	0.16	0.07	98.84
RJC 92	10_1	Curraghinalt Burn	83.05	14.87	0.35	0.02	98.28
RJC 92	10_2	Curraghinalt Burn	81.87	17.40	0.20	0.00	99.46
RJC 92	10_3	Curraghinalt Burn	57.56	38.67	2.91	0.00	99.14
RJC 92	10_4	Curraghinalt Burn	86.07	13.58	0.47	0.03	100.16
RJC 92	10_5	Curraghinalt Burn	86.39	13.12	0.23	0.02	99.77
RJC 92	10_6	Curraghinalt Burn	86.44	12.53	0.54	0.03	99.53
RJC 92	10_7	Curraghinalt Burn	82.45	6.26	0.16	0.05	88.93
RJC 92	10_8	Curraghinalt Burn	88.60	10.55	0.17	0.02	99.35
RJC 92	10_9	Curraghinalt Burn	91.15	7.66	0.29	0.04	99.15
RJC 92	10_10	Curraghinalt Burn	77.68	21.60	0.35	0.01	99.63
RJC 92	10_11	Curraghinalt Burn	91.26	6.48	0.11	0.06	97.92

Block	Grain ID	Creek	Au WT%	Ag WT%	Hg WT%	Cu WT%	TOTAL
RJC 92	10_12	Curraghinalt Burn	87.11	12.01	0.16	0.02	99.29
RJC 92	10_13	Curraghinalt Burn	78.37	19.67	1.96	0.02	100.02
RJC 92	10_14	Curraghinalt Burn	79.74	20.16	0.28	0.02	100.21
RJC 92	10_15	Curraghinalt Burn	87.58	11.56	0.18	0.04	99.35
RJC 92	10_16	Curraghinalt Burn	82.36	10.30	0.22	0.05	92.92
RJC 92	10_17	Curraghinalt Burn	89.94	9.32	0.19	0.04	99.48
RJC 92	10_18	Curraghinalt Burn	88.59	7.46	0.12	0.11	96.28
RJC 92	10_19	Curraghinalt Burn	86.28	12.61	0.23	0.03	99.15
RJC 92	10_20	Curraghinalt Burn	89.36	8.15	0.30	0.04	97.84
RJC 92	10_21	Curraghinalt Burn	80.16	19.50	0.63	0.02	100.30
RJC 92	10_22	Curraghinalt Burn	82.31	16.48	0.76	0.04	99.60
RJC 92	10_23	Curraghinalt Burn	86.91	10.55	0.21	0.04	97.71
RJC 92	10_24	Curraghinalt Burn	77.02	21.37	1.09	0.04	99.51
RJC 92	10_25	Curraghinalt Burn	86.40	9.16	0.28	0.06	95.90
RJC 92	10_26	Curraghinalt Burn	85.27	13.46	0.23	0.03	98.99
RJC 92	10_27	Curraghinalt Burn	86.87	11.67	0.13	0.03	98.70
RJC 92	10_28	Curraghinalt Burn	89.78	9.92	0.30	0.04	100.04
RJC 92	10_29	Curraghinalt Burn					
RJC 92	10_30	Curraghinalt Burn					
RJC 92	10_31	Curraghinalt Burn					
RJC 92	10_32	Curraghinalt Burn					
RJC 92	10_33	Curraghinalt Burn					
RJC 99	6_1	Curraghinalt Burn Rob 2016	90.41	9.71	0.52	0.11	100.75
RJC 99	6_2	Curraghinalt Burn Rob 2016	84.95	15.21	0.14	0.04	100.34
RJC 99	6_3	Curraghinalt Burn Rob 2016	90.14	9.86	0.23	0.11	100.34
RJC 99	6_4	Curraghinalt Burn Rob 2016	89.53	10.81	0.60	0.09	101.02
RJC 99	6_5	Curraghinalt Burn Rob 2016	92.13	8.37	0.00	0.08	100.58
RJC 99	6_6	Curraghinalt Burn Rob 2016	89.61	10.60	0.20	0.08	100.49
RJC 99	6_7	Curraghinalt Burn Rob 2016	85.82	14.30	0.39	0.11	100.63
RJC 99	6_8	Curraghinalt Burn Rob 2016	90.02	10.14	0.30	0.06	100.52
RJC 99	6_9	Curraghinalt Burn Rob 2016	84.07	16.39	0.40	0.08	100.94
RJC 99	6_10	Curraghinalt Burn Rob 2016	92.67	7.81	0.09	0.09	100.66
RJC 99	6_11	Curraghinalt Burn Rob 2016	87.09	13.06	0.45	0.05	100.65
RJC 99	6_12	Curraghinalt Burn Rob 2016	89.64	10.79	0.51	0.09	101.03
RJC 99	6_13	Curraghinalt Burn Rob 2016	89.24	10.79	0.26	0.05	100.34
RJC 99	6_14	Curraghinalt Burn Rob 2016	90.04	10.72	0.54	0.08	101.38
RJC 99	6_15	Curraghinalt Burn Rob 2016	89.47	11.32	0.18	0.07	101.04
RJC 99	6_16	Curraghinalt Burn Rob 2016	90.14	10.62	0.17	0.08	101.00
RJC 99	6_17	Curraghinalt Burn Rob 2016	85.84	14.55	0.38	0.06	100.84

Block	Grain ID	Creek	Au WT%	Ag WT%	Hg WT%	Cu WT%	TOTAL
RJC 99	6_18	Curraghinalt Burn Rob 2016	93.42	7.50	0.19	0.11	101.22
RJC 99	6_19	Curraghinalt Burn Rob 2016	94.02	6.37	0.27	0.15	100.81
RJC 99	6_20	Curraghinalt Burn Rob 2016	91.52	9.05	0.31	0.07	100.96
RJC 99	6_21	Curraghinalt Burn Rob 2016	91.58	8.12	0.23	0.11	100.04
RJC 99	6_22	Curraghinalt Burn Rob 2016	91.19	9.67	0.36	0.10	101.32
RJC 99	6_23	Curraghinalt Burn Rob 2016	86.13	14.22	0.31	0.05	100.71
RJC 99	6_24	Curraghinalt Burn Rob 2016	87.42	12.93	0.30	0.10	100.75
RJC 99	6_25	Curraghinalt Burn Rob 2016	85.50	14.78	0.90	0.04	101.22
RJC 99	6_26	Curraghinalt Burn Rob 2016	94.16	6.85	0.31	0.11	101.43
RJC 99	6_27	Curraghinalt Burn Rob 2016	91.07	9.04	0.24	0.10	100.45
RJC 99	6_28	Curraghinalt Burn Rob 2016	88.18	11.84	0.35	0.07	100.44
RJC 99	6_29	Curraghinalt Burn Rob 2016	86.18	13.31	0.60	0.08	100.16
RJC 99	6_30	Curraghinalt Burn Rob 2016	90.83	9.65	0.38	0.12	100.99
RJC 99	7_1	Curraghinalt Burn Rob 2016	88.02	12.39	0.80	0.06	101.27
RJC 99	7_2	Curraghinalt Burn Rob 2016	87.70	12.86	0.68	0.11	101.35
RJC 99	7_3	Curraghinalt Burn Rob 2016	95.19	4.29	0.00	0.10	99.58
RJC 99	7_4	Curraghinalt Burn Rob 2016	92.07	8.31	0.32	0.12	100.83
RJC 99	7_5	Curraghinalt Burn Rob 2016	85.79	14.74	0.52	0.06	101.11
RJC 99	7_6	Curraghinalt Burn Rob 2016	92.94	7.45	0.14	0.11	100.64
RJC 99	7_7	Curraghinalt Burn Rob 2016	90.56	9.91	0.32	0.09	100.87
RJC 99	7_8	Curraghinalt Burn Rob 2016	84.94	15.04	0.22	0.11	100.29
RJC 99	7_9	Curraghinalt Burn Rob 2016	80.21	20.56	0.73	0.06	101.57
RJC 99	7_10	Curraghinalt Burn Rob 2016	81.79	17.64	1.34	0.06	100.83
RJC 99	7_11	Curraghinalt Burn Rob 2016	91.96	8.45	0.35	0.13	100.89
RJC 99	7_12	Curraghinalt Burn Rob 2016	87.17	13.47	0.41	0.09	101.14
RJC 99	7_13	Curraghinalt Burn Rob 2016	87.07	13.25	0.25	0.08	100.66
RJC 99	7_14	Curraghinalt Burn Rob 2016	90.35	10.32	0.24	0.13	101.04
RJC 99	7_15	Curraghinalt Burn Rob 2016	81.35	17.79	1.19	0.05	100.39
RJC 99	7_16	Curraghinalt Burn Rob 2016	93.67	6.26	0.25	0.15	100.33
RJC 99	7_17	Curraghinalt Burn Rob 2016	89.00	11.68	0.27	0.12	101.07
RJC 99	7_18	Curraghinalt Burn Rob 2016	90.23	9.94	0.34	0.09	100.62

Block	Grain ID	Creek	Au WT%	Ag WT%	Hg WT%	Cu WT%	TOTAL
RJC 99	7_19	Curraghinalt Burn Rob 2016	93.67	6.85	0.27	0.15	100.94
RJC 99	7_20	Curraghinalt Burn Rob 2016	92.91	7.60	0.35	0.11	100.97
RJC 99	7_21	Curraghinalt Burn Rob 2016	88.15	12.01	0.31	0.07	100.56
RJC 99	7_22	Curraghinalt Burn Rob 2016	89.23	10.92	0.23	0.06	100.44
RJC 99	7_23	Curraghinalt Burn Rob 2016	89.29	11.31	0.20	0.05	100.84
RJC 99	7_24	Curraghinalt Burn Rob 2016	92.49	8.73	0.26	0.08	101.55
RJC 99	7_25	Curraghinalt Burn Rob 2016	92.76	7.82	0.23	0.10	100.91
RJC 99	7_26	Curraghinalt Burn Rob 2016	92.53	7.90	0.29	0.06	100.78
RJC 99	7_27	Curraghinalt Burn Rob 2016	90.14	10.48	0.16	0.11	100.88
RJC 99	7_28	Curraghinalt Burn Rob 2016	90.07	10.93	0.29	0.08	101.38
RJC 99	7_29	Curraghinalt Burn Rob 2016	86.58	13.85	0.49	0.05	100.96
RJC 99	7_30	Curraghinalt Burn Rob 2016	86.37	14.01	0.24	0.05	100.67
RJC 99	8_1	Curraghinalt Burn Rob 2016	87.63	12.95	0.23	0.08	100.89
RJC 99	8_2	Curraghinalt Burn Rob 2016	80.39	19.16	1.23	0.06	100.84
RJC 99	8_3	Curraghinalt Burn Rob 2016	84.96	15.86	0.08	0.05	100.95
RJC 99	8_4	Curraghinalt Burn Rob 2016	85.44	15.13	0.20	0.07	100.83
RJC 99	8_5	Curraghinalt Burn Rob 2016	94.40	5.84	0.27	0.15	100.65
RJC 99	8_6	Curraghinalt Burn Rob 2016	83.76	15.93	0.71	0.05	100.46
RJC 99	8_7	Curraghinalt Burn Rob 2016	91.19	9.56	0.48	0.08	101.30
RJC 99	8_8	Curraghinalt Burn Rob 2016	92.06	8.24	0.65	0.12	101.06
RJC 99	8_9	Curraghinalt Burn Rob 2016	93.05	7.58	0.27	0.09	100.98
RJC 99	8_10	Curraghinalt Burn Rob 2016	87.68	12.37	0.20	0.06	100.31
RJC 99	8_11	Curraghinalt Burn Rob 2016	94.60	6.11	0.28	0.13	101.12
RJC 99	8_12	Curraghinalt Burn Rob 2016	81.18	17.26	2.79	0.06	101.29
RJC 99	8_13	Curraghinalt Burn Rob 2016	89.20	10.95	0.51	0.09	100.75
RJC 99	8_14	Curraghinalt Burn Rob 2016	92.51	8.14	0.31	0.13	101.09
RJC 99	8_15	Curraghinalt Burn Rob 2016	92.70	8.51	0.12	0.07	101.40
RJC 99	8_16	Curraghinalt Burn Rob 2016	93.47	7.43	0.33	0.11	101.34
RJC 99	8_17	Curraghinalt Burn Rob 2016	92.86	7.40	0.12	0.11	100.49
RJC 99	8_18	Curraghinalt Burn Rob 2016	88.68	12.35	0.18	0.07	101.29
RJC 99	8_19	Curraghinalt Burn Rob 2016	89.77	10.68	0.51	0.06	101.02

Block	Grain ID	Creek	Au WT%	Ag WT%	Hg WT%	Cu WT%	TOTAL
RJC 99	8_20	Curraghinalt Burn Rob 2016	91.00	9.36	0.20	0.09	100.64
RJC 99	8_21	Curraghinalt Burn Rob 2016	91.52	9.04	0.51	0.10	101.16
RJC 99	8_22	Curraghinalt Burn Rob 2016	90.86	9.77	0.28	0.09	101.00
RJC 99	8_23	Curraghinalt Burn Rob 2016	95.75	5.10	0.14	0.18	101.16
RJC 99	8_24	Curraghinalt Burn Rob 2016	80.57	19.59	0.63	0.04	100.84
RJC 99	8_25	Curraghinalt Burn Rob 2016	87.20	13.26	0.47	0.06	100.99
RJC 99	9_1	Curraghinalt Burn Rob 2016	87.54	12.98	0.38	0.06	100.96
RJC 99	9_2	Curraghinalt Burn Rob 2016	87.52	13.03	0.22	0.08	100.84
RJC 99	9_3	Curraghinalt Burn Rob 2016	88.19	12.26	0.45	0.08	100.98
RJC 99	9_4	Curraghinalt Burn Rob 2016	91.55	8.85	0.29	0.13	100.82
RJC 99	9_5	Curraghinalt Burn Rob 2016	88.61	11.63	0.54	0.10	100.88
RJC 99	9_6	Curraghinalt Burn Rob 2016	88.47	12.24	0.19	0.05	100.95
RJC 99	9_7	Curraghinalt Burn Rob 2016	87.66	13.51	0.13	0.09	101.38
RJC 99	9_8	Curraghinalt Burn Rob 2016	85.94	14.36	0.11	0.08	100.49
RJC 99	9_9	Curraghinalt Burn Rob 2016	91.28	8.89	0.16	0.09	100.42
RJC 99	9_10	Curraghinalt Burn Rob 2016	94.01	6.03	0.23	0.08	100.36
RJC 99	9_11	Curraghinalt Burn Rob 2016	91.91	7.96	0.85	0.09	100.82
RJC 99	9_12	Curraghinalt Burn Rob 2016	88.62	12.46	0.03	0.06	101.17
RJC 99	9_13	Curraghinalt Burn Rob 2016	90.13	10.78	0.56	0.06	101.53
RJC 99	9_14	Curraghinalt Burn Rob 2016	89.19	11.18	0.55	0.07	100.98
RJC 99	9_15	Curraghinalt Burn Rob 2016	92.09	8.24	0.37	0.10	100.80
RJC 97	3_1	Curraghinalt Burn Rob 2016	71.92	27.05	0.67	0.12	99.76
RJC 97	3_2	Curraghinalt Burn Rob 2016	90.07	9.58	0.36	0.16	100.17
RJC 97	3_3	Curraghinalt Burn Rob 2016	97.65	2.24	0.14	0.27	100.30
RJC 97	3_4	Curraghinalt Burn Rob 2016	93.12	7.03	0.30	0.17	100.61
RJC 97	3_5	Curraghinalt Burn Rob 2016	91.92	7.91	0.23	0.20	100.25
RJC 97	3_6	Curraghinalt Burn Rob 2016	91.25	9.10	0.24	0.14	100.73
RJC 97	3_7	Curraghinalt Burn Rob 2016	86.95	13.33	0.33	0.16	100.77
RJC 97	3_8	Curraghinalt Burn Rob 2016					
RJC 97	4_1	Curraghinalt Burn Rob 2016	76.43	23.22	0.86	0.12	100.63
RJC 97	4_2	Curraghinalt Burn Rob 2016	85.61	14.26	0.40	0.19	100.46

Block	Grain ID	Creek	Au WT%	Ag WT%	Hg WT%	Cu WT%	TOTAL
RJC 97	4_3	Curraghinalt Burn Rob 2016	92.18	6.92	0.49	0.23	99.82
RJC 97	4_4	Curraghinalt Burn Rob 2016	89.00	10.78	0.27	0.19	100.24
RJC 97	4_5	Curraghinalt Burn Rob 2016	78.39	21.41	0.23	0.12	100.15
RJC 97	4_6	Curraghinalt Burn Rob 2016	79.62	20.39	0.10	0.14	100.25
RJC 97	4_7	Curraghinalt Burn Rob 2016	82.02	17.97	0.18	0.15	100.33
RJC 97	4_8	Curraghinalt Burn Rob 2016	90.45	9.46	0.26	0.20	100.37
RJC 97	4_9	Curraghinalt Burn Rob 2016	90.11	10.11	0.31	0.16	100.70
RJC 97	4_10	Curraghinalt Burn Rob 2016	93.91	5.61	0.21	0.28	100.01
RJC 97	4_11	Curraghinalt Burn Rob 2016	92.06	7.61	0.21	0.24	100.12
RJC 97	4_12	Curraghinalt Burn Rob 2016	91.25	8.84	0.22	0.25	100.56
RJC 97	4_13	Curraghinalt Burn Rob 2016	89.41	10.52	0.17	0.19	100.29
RJC 97	4_14	Curraghinalt Burn Rob 2016	91.58	9.00	0.16	0.15	100.90
RJC 97	4_15	Curraghinalt Burn Rob 2016	94.95	5.03	0.31	0.25	100.54
RJC 97	4_16	Curraghinalt Burn Rob 2016	93.24	6.51	0.26	0.19	100.20
RJC 97	4_17	Curraghinalt Burn Rob 2016	82.82	17.40	0.30	0.14	100.65
RJC 97	4_18	Curraghinalt Burn Rob 2016	94.56	5.15	0.30	0.21	100.21
RJC 97	4_19	Curraghinalt Burn Rob 2016	94.59	5.50	0.22	0.22	100.53
RJC 97	4_20	Curraghinalt Burn Rob 2016	93.39	6.36	0.21	0.18	100.14
RJC 97	4_21	Curraghinalt Burn Rob 2016	92.81	7.04	0.27	0.30	100.43
RJC 97	4_22	Curraghinalt Burn Rob 2016	92.36	7.44	0.10	0.29	100.19
RJC 97	4_23	Curraghinalt Burn Rob 2016	86.11	13.90	0.28	0.16	100.44
RJC 97	4_24	Curraghinalt Burn Rob 2016	75.94	24.15	0.23	0.11	100.43
RJC 97	4_25	Curraghinalt Burn Rob 2016	82.33	16.82	0.97	0.12	100.23
RJC 97	4_26	Curraghinalt Burn Rob 2016	84.26	15.68	0.28	0.14	100.36
RJC 97	4_27	Curraghinalt Burn Rob 2016	85.76	14.28	0.33	0.16	100.54
RJC 97	4_28	Curraghinalt Burn Rob 2016	92.60	6.88	0.32	0.22	100.02
RJC 97	4_29	Curraghinalt Burn Rob 2016	93.22	6.17	0.25	0.27	99.91
RJC 97	4_30	Curraghinalt Burn Rob 2016	88.21	11.47	0.44	0.17	100.28
RJC 97	4_31	Curraghinalt Burn Rob 2016	88.22	11.28	0.18	0.17	99.85
RJC 97	4_32	Curraghinalt Burn Rob 2016	91.37	8.70	0.20	0.13	100.41
RJC 97	4_33	Curraghinalt Burn Rob 2016	84.43	15.31	0.30	0.11	100.16

Block	Grain ID	Creek	Au WT%	Ag WT%	Hg WT%	Cu WT%	TOTAL
RJC98	3_1	Curraghinalt Burn Rob 2016	91.81	7.74	0.20	0.36	100.11
RJC98	3_2	Curraghinalt Burn Rob 2016	83.79	16.43	0.26	0.06	100.54
RJC98	3_3	Curraghinalt Burn Rob 2016	89.52	10.90	0.25	0.18	100.86
RJC98	3_4	Curraghinalt Burn Rob 2016	95.06	5.24	0.11	0.23	100.65
RJC98	3_5	Curraghinalt Burn Rob 2016	92.85	7.25	0.25	0.19	100.53
RJC98	3_6	Curraghinalt Burn Rob 2016	87.48	12.74	0.23	0.14	100.59
RJC98	3_7	Curraghinalt Burn Rob 2016	93.58	7.29	0.31	0.14	101.32
RJC98	3_8	Curraghinalt Burn Rob 2016	91.20	8.89	0.69	0.20	100.97
RJC98	3_9	Curraghinalt Burn Rob 2016	83.58	15.72	1.35	0.06	100.72
RJC98	3_10	Curraghinalt Burn Rob 2016	95.54	4.89	0.22	0.15	100.80
RJC98	3_11	Curraghinalt Burn Rob 2016	93.85	6.74	0.18	0.14	100.91
RJC98	3_12	Curraghinalt Burn Rob 2016	92.11	8.51	0.25	0.19	101.06
RJC98	3_13	Curraghinalt Burn Rob 2016	79.86	20.31	0.45	0.09	100.72
RJC98	3_14	Curraghinalt Burn Rob 2016	86.55	14.01	0.21	0.10	100.87
RJC98	3_15	Curraghinalt Burn Rob 2016	85.28	15.04	0.36	0.14	100.81
RJC98	3_16	Curraghinalt Burn Rob 2016	94.42	6.15	0.13	0.16	100.86
RJC98	3_17	Curraghinalt Burn Rob 2016	81.29	18.37	0.49	0.10	100.25
RJC98	3_18	Curraghinalt Burn Rob 2016	93.32	7.29	0.23	0.22	101.05
RJC98	3_19	Curraghinalt Burn Rob 2016	89.84	10.60	0.12	0.13	100.68
RJC98	3_20	Curraghinalt Burn Rob 2016	91.57	9.18	0.30	0.15	101.19
RJC98	3_21	Curraghinalt Burn Rob 2016	84.45	15.95	0.30	0.09	100.80
RJC98	3_22Missing	Curraghinalt Burn Rob 2016					
RJC98	3_23	Curraghinalt Burn Rob 2016	92.65	7.63	0.33	0.19	100.80
RJC98	3_24	Curraghinalt Burn Rob 2016	93.10	7.08	0.31	0.08	100.58
RJC98	3_25	Curraghinalt Burn Rob 2016	93.56	7.03	0.21	0.18	100.98
RJC98	3_26	Curraghinalt Burn Rob 2016	94.28	6.28	0.22	0.16	100.94
RJC98	3_27	Curraghinalt Burn Rob 2016	92.55	7.85	0.45	0.12	100.97
RJC98	3_28	Curraghinalt Burn Rob 2016	86.93	13.64	0.27	0.16	101.01
RJC98	3_29	Curraghinalt Burn Rob 2016	91.58	8.29	0.28	0.15	100.29
RJC98	3_30	Curraghinalt Burn Rob 2016	85.98	14.34	0.13	0.09	100.54
RJC98	4_1	Curraghinalt Burn Rob 2016	92.30	8.13	0.32	0.13	100.89

Block	Grain ID	Creek	Au WT%	Ag WT%	Hg WT%	Cu WT%	TOTAL
RJC98	4_2	Curraghinalt Burn Rob 2016					
RJC98	4_3	Curraghinalt Burn Rob 2016	91.61	8.85	0.51	0.11	101.09
RJC98	4_4	Curraghinalt Burn Rob 2016	86.52	12.73	1.04	0.08	100.36
RJC98	4_5	Curraghinalt Burn Rob 2016	93.82	6.62	0.24	0.14	100.82
RJC98	4_6	Curraghinalt Burn Rob 2016	89.53	11.50	0.28	0.15	101.47
RJC98	4_7	Curraghinalt Burn Rob 2016	87.59	13.08	0.41	0.11	101.19
RJC98	4_8	Curraghinalt Burn Rob 2016	82.49	18.06	0.35	0.06	100.96
RJC98	4_9	Curraghinalt Burn Rob 2016	87.84	12.76	0.20	0.06	100.86
RJC98	4_10	Curraghinalt Burn Rob 2016	88.11	11.80	0.45	0.16	100.52
RJC98	4_11	Curraghinalt Burn Rob 2016	90.73	9.78	0.25	0.10	100.86
RJC98	4_12	Curraghinalt Burn Rob 2016	84.43	15.86	0.28	0.06	100.62
RJC98	4_13	Curraghinalt Burn Rob 2016	80.00	20.36	0.23	0.11	100.69
RJC98	4_14	Curraghinalt Burn Rob 2016	92.63	7.93	0.18	0.12	100.87
RJC98	4_15	Curraghinalt Burn Rob 2016	89.47	11.01	0.23	0.09	100.79
RJC98	5_1	Curraghinalt Burn Rob 2016	93.37	6.77	0.25	0.16	100.55
RJC98	5_2	Curraghinalt Burn Rob 2016	92.90	7.00	0.15	0.17	100.22
RJC98	5_3	Curraghinalt Burn Rob 2016	92.27	8.19	0.34	0.08	100.88
RJC98	5_4	Curraghinalt Burn Rob 2016	79.63	20.53	0.18	0.07	100.42
RJC98	5_5	Curraghinalt Burn Rob 2016	90.65	9.61	0.21	0.11	100.58
RJC98	6_1	Curraghinalt Burn Rob 2016	95.35	5.94	0.16	0.11	101.56
RJC98	6_2	Curraghinalt Burn Rob 2016	90.54	9.77	0.38	0.13	100.83
RJC98	6_3	Curraghinalt Burn Rob 2016	87.49	13.00	0.65	0.11	101.25
RJC98	6_4	Curraghinalt Burn Rob 2016	90.91	8.57	1.64	0.05	101.16
RJC98	6_5	Curraghinalt Burn Rob 2016	93.94	7.05	0.10	0.16	101.25
RJC98	6_6	Curraghinalt Burn Rob 2016	93.14	6.86	0.22	0.27	100.49
RJC98	6_7	Curraghinalt Burn Rob 2016	85.69	14.46	0.22	0.20	100.58
RJC98	6_8	Curraghinalt Burn Rob 2016	93.19	6.98	0.25	0.15	100.57
RJC98	6_9	Curraghinalt Burn Rob 2016	90.68	10.09	0.18	0.19	101.14
RJC98	6_10	Curraghinalt Burn Rob 2016	83.64	16.89	0.19	0.09	100.81
RJC98	6_11	Curraghinalt Burn Rob 2016	84.98	15.34	0.28	0.15	100.76
RJC98	6_12	Curraghinalt Burn Rob 2016	89.88	10.10	0.46	0.14	100.58

Block	Grain ID	Creek	Au WT%	Ag WT%	Hg WT%	Cu WT%	TOTAL
RJC98	6_13	Curraghinalt Burn Rob 2016	84.98	15.73	0.14	0.13	100.98
RJC98	6_14	Curraghinalt Burn Rob 2016	93.19	7.09	0.37	0.17	100.82
RJC98	6_15	Curraghinalt Burn Rob 2016	90.95	9.63	0.22	0.17	100.97
RJC98	6_16	Curraghinalt Burn Rob 2016	93.58	6.61	0.19	0.19	100.56
RJC98	6_17	Curraghinalt Burn Rob 2016	93.56	6.66	0.21	0.20	100.63
RJC98	6_18	Curraghinalt Burn Rob 2016	93.65	7.04	0.15	0.19	101.04
RJC98	6_19	Curraghinalt Burn Rob 2016	93.43	7.06	0.38	0.11	100.97
RJC98	6_20	Curraghinalt Burn Rob 2016	88.28	12.32	0.36	0.11	101.08
RJC98	7_1	Curraghinalt Burn Rob 2016	87.26	13.11	0.21	0.11	100.70
RJC98	7_2	Curraghinalt Burn Rob 2016	91.19	9.49	0.28	0.15	101.11
RJC98	7_3	Curraghinalt Burn Rob 2016	83.54	16.59	0.27	0.09	100.48
RJC98	7_4	Curraghinalt Burn Rob 2016	95.21	4.94	0.26	0.21	100.62
RJC98	7_5	Curraghinalt Burn Rob 2016	92.86	7.33	0.21	0.14	100.54
RJC98	7_6	Curraghinalt Burn Rob 2016	87.89	12.02	0.77	0.08	100.76
RJC98	7_7	Curraghinalt Burn Rob 2016	86.32	13.58	0.75	0.06	100.72
RJC98	7_8	Curraghinalt Burn Rob 2016	89.60	10.68	0.11	0.13	100.52
RJC98	7_9	Curraghinalt Burn Rob 2016	93.58	6.90	0.43	0.14	101.05
RJC98	7_10	Curraghinalt Burn Rob 2016	92.83	7.34	0.23	0.14	100.55
RJC 100	14_1	Curraghinalt Burn Rob 2016	89.61	11.04	0.25	0.13	101.03
RJC 100	14_2	Curraghinalt Burn Rob 2016	90.62	9.74	0.36	0.08	100.80
RJC 100	14_3	Curraghinalt Burn Rob 2016	85.20	14.58	0.20	0.16	100.14
RJC 100	11_1	Curraghinalt Burn Rob 2016	93.00	7.67	0.26	0.13	101.05
RJC 100	11_2	Curraghinalt Burn Rob 2016	87.74	12.90	0.29	0.09	101.03
RJC 100	11_3	Curraghinalt Burn Rob 2016	83.47	17.28	0.26	0.08	101.09
RJC 100	11_4	Curraghinalt Burn Rob 2016	89.49	11.69	0.22	0.12	101.51
RJC 100	11_5	Curraghinalt Burn Rob 2016	81.99	17.97	0.87	0.08	100.91
RJC 100	11_6	Curraghinalt Burn Rob 2016	92.94	7.91	0.19	0.10	101.14
RJC 100	11_7	Curraghinalt Burn Rob 2016	89.43	10.84	0.40	0.11	100.78
RJC 100	11_8	Curraghinalt Burn Rob 2016	87.86	12.91	0.34	0.12	101.24
RJC 100	11_9	Curraghinalt Burn Rob 2016	84.40	15.85	0.55	0.07	100.87
RJC 100	11_10	Curraghinalt Burn Rob 2016	88.26	12.12	0.25	0.09	100.73

Block	Grain ID	Creek	Au WT%	Ag WT%	Hg WT%	Cu WT%	TOTAL
RJC 100	11_11	Curraghinalt Burn Rob 2016	94.89	5.80	0.35	0.15	101.19
RJC 100	11_12	Curraghinalt Burn Rob 2016	90.06	10.38	0.57	0.08	101.08
RJC 100	11_13	Curraghinalt Burn Rob 2016	85.39	15.86	0.16	0.10	101.51
RJC 100	11_14	Curraghinalt Burn Rob 2016	87.68	12.85	0.19	0.11	100.82
RJC 100	11_15	Curraghinalt Burn Rob 2016	87.11	13.85	0.28	0.09	101.34
RJC 100	11_16	Curraghinalt Burn Rob 2016	95.46	4.93	0.16	0.21	100.76
RJC 100	11_17	Curraghinalt Burn Rob 2016	88.95	11.47	0.09	0.11	100.63
RJC 100	11_18	Curraghinalt Burn Rob 2016	85.67	15.07	0.71	0.11	101.56
RJC 100	11_19	Curraghinalt Burn Rob 2016	89.55	10.66	0.12	0.12	100.45
RJC 100	11_20	Curraghinalt Burn Rob 2016	93.92	7.16	0.17	0.12	101.37
RJC 100	11_21	Curraghinalt Burn Rob 2016	87.66	13.25	0.24	0.11	101.26
RJC 100	11_22	Curraghinalt Burn Rob 2016	89.85	10.49	0.30	0.08	100.72
RJC 100	11_23	Curraghinalt Burn Rob 2016	85.06	15.19	0.31	0.09	100.64
RJC 100	12_1	Curraghinalt Burn Rob 2016	92.40	8.31	0.53	0.12	101.36
RJC 100	12_2	Curraghinalt Burn Rob 2016	89.65	11.02	0.25	0.11	101.02
RJC 100	12_3	Curraghinalt Burn Rob 2016	87.68	12.74	0.55	0.07	101.04
RJC 100	12_4	Curraghinalt Burn Rob 2016	90.43	10.17	0.58	0.13	101.32
RJC 100	12_5	Curraghinalt Burn Rob 2016	93.26	7.32	0.23	0.11	100.93
RJC 100	12_6	Curraghinalt Burn Rob 2016	90.15	10.36	0.29	0.13	100.92
RJC 100	12_7	Curraghinalt Burn Rob 2016	88.31	12.41	0.65	0.06	101.44
RJC 100	12_8	Curraghinalt Burn Rob 2016	86.80	13.69	0.12	0.10	100.71
RJC 100	12_9	Curraghinalt Burn Rob 2016	87.03	13.65	0.43	0.11	101.21
RJC 100	12_10	Curraghinalt Burn Rob 2016	90.29	10.29	0.30	0.11	101.00
RJC 100	12_11	Curraghinalt Burn Rob 2016	90.48	10.28	0.15	0.13	101.04
RJC 100	12_12	Curraghinalt Burn Rob 2016	88.89	11.42	0.44	0.07	100.82
RJC 100	12_13	Curraghinalt Burn Rob 2016	93.00	7.42	0.23	0.12	100.77
RJC 100	12_14	Curraghinalt Burn Rob 2016	93.70	6.95	0.10	0.14	100.89
RJC 100	12_15	Curraghinalt Burn Rob 2016	91.38	9.22	0.22	0.12	100.94
RJC 100	12_16	Curraghinalt Burn Rob 2016	89.12	11.98	0.39	0.10	101.60
RJC 100	12_17	Curraghinalt Burn Rob 2016	88.18	12.15	0.39	0.09	100.81
RJC 100	12_18	Curraghinalt Burn Rob 2016	91.21	9.90	0.03	0.07	101.20

Block	Grain ID	Creek	Au WT%	Ag WT%	Hg WT%	Cu WT%	TOTAL
RJC 100	12_19	Curraghinalt Burn Rob 2016	93.72	6.80	0.26	0.22	101.00
RJC 100	12_20	Curraghinalt Burn Rob 2016	86.77	14.11	0.26	0.09	101.22
RJC 100	12_21	Curraghinalt Burn Rob 2016	79.40	20.35	1.49	0.06	101.31
RJC 100	12_22	Curraghinalt Burn Rob 2016	92.58	7.93	0.16	0.18	100.86
RJC 100	12_23	Curraghinalt Burn Rob 2016	85.84	15.05	0.69	0.11	101.70
RJC 100	12_24	Curraghinalt Burn Rob 2016	91.29	9.21	0.11	0.12	100.73
RJC 100	12_25	Curraghinalt Burn Rob 2016	88.87	11.21	0.17	0.12	100.37
RJC 100	12_26	Curraghinalt Burn Rob 2016	92.23	8.34	0.27	0.15	101.00
RJC 100	12_27	Curraghinalt Burn Rob 2016	87.47	13.06	0.26	0.11	100.89
RJC 100	12_28	Curraghinalt Burn Rob 2016	90.06	10.74	0.19	0.09	101.08
RJC 100	12_29	Curraghinalt Burn Rob 2016	89.10	11.49	0.34	0.09	101.02
RJC 100	12_30	Curraghinalt Burn Rob 2016	89.20	11.38	0.14	0.13	100.85
RJC 100	13_1	Curraghinalt Burn Rob 2016	77.43	22.73	0.23	0.09	100.48
RJC 100	13_2	Curraghinalt Burn Rob 2016	82.53	17.60	0.12	0.09	100.34
RJC 100	13_3	Curraghinalt Burn Rob 2016	84.17	16.33	0.39	0.08	100.97
RJC 100	13_4	Curraghinalt Burn Rob 2016	89.66	10.26	0.22	0.12	100.25
RJC 100	13_5	Curraghinalt Burn Rob 2016	88.82	11.24	0.21	0.18	100.45
RJC 100	13_6	Curraghinalt Burn Rob 2016	92.08	8.04	0.10	0.14	100.37
RJC 100	13_7	Curraghinalt Burn Rob 2016	88.67	12.44	0.32	0.11	101.54
RJC 100	13_8	Curraghinalt Burn Rob 2016	89.70	11.25	0.24	0.07	101.27
RJC 100	13_9	Curraghinalt Burn Rob 2016	90.93	9.62	0.30	0.16	101.01
RJC 100	13_10	Curraghinalt Burn Rob 2016	92.34	8.58	0.25	0.13	101.31
RJC 100	13_11	Curraghinalt Burn Rob 2016	96.21	4.68	0.35	0.18	101.43
RJC 100	13_12	Curraghinalt Burn Rob 2016	92.51	7.83	0.34	0.11	100.79
RJC 100	13_13	Curraghinalt Burn Rob 2016	88.98	12.11	0.27	0.13	101.49
RJC 100	13_14	Curraghinalt Burn Rob 2016	91.98	9.20	0.12	0.07	101.38
RJC 100	13_15	Curraghinalt Burn Rob 2016	90.62	9.74	0.12	0.12	100.60
RJC 100	13_16	Curraghinalt Burn Rob 2016	87.86	12.15	0.64	0.11	100.76
RJC 100	13_17	Curraghinalt Burn Rob 2016	83.65	16.83	0.20	0.11	100.78
RJC 100	13_18	Curraghinalt Burn Rob 2016	84.00	15.42	0.32	0.08	99.82
RJC 100	13_19	Curraghinalt Burn Rob 2016	88.12	12.61	0.35	0.09	101.17

Block	Grain ID	Creek	Au WT%	Ag WT%	Hg WT%	Cu WT%	TOTAL
RJC 100	13_20	Curraghinalt Burn Rob 2016	89.03	11.50	0.31	0.12	100.96
RJC 100	13_21	Curraghinalt Burn Rob 2016	92.87	7.45	0.19	0.18	100.69
RJC 100	13_22	Curraghinalt Burn Rob 2016	91.20	9.72	0.13	0.14	101.20
RJC 100	13_23	Curraghinalt Burn Rob 2016	87.20	13.06	0.52	0.09	100.87
RJC 100	13_24	Curraghinalt Burn Rob 2016	92.60	8.31	0.20	0.19	101.30
RJC 100	13_25	Curraghinalt Burn Rob 2016	91.99	8.70	0.16	0.13	100.98
RJC 100	13_26	Curraghinalt Burn Rob 2016	88.83	11.45	0.39	0.05	100.72
RJC 100	13_27	Curraghinalt Burn Rob 2016	82.46	17.64	0.50	0.08	100.69
RJC 100	13_28	Curraghinalt Burn Rob 2016	88.84	11.58	0.24	0.11	100.77
RJC 100	13_29	Curraghinalt Burn Rob 2016	85.49	14.92	0.33	0.09	100.83
RJC 100	13_30	Curraghinalt Burn Rob 2016	92.75	7.62	0.20	0.16	100.73

Atlin EMPA data

Block	Grain ID	Inclusions	Au WT%	Ag WT%	Cu WT%	Hg WT%	TOTAL
RJC 65	McKee Ck 13.1		83.01	15.01	0.03	0.28	98.33
RJC 65	McKee Ck 13.1		84.06	15.14	0.03	0.32	99.55
RJC 65	McKee Ck 13.1		85.07	13.06	0.02	0.36	98.51
RJC 65	Otter upper .1	holes	71.29	28.64	0.00	0.25	100.17
RJC 65	Otter upper .2	FeO (surfice)	87.76	11.88	0.00	0.17	99.81
RJC 65	Otter upper 10	external?	77.76	22.05	0.01	0.15	99.98
RJC 65	Otter upper 11	Quartz, FeO, Na feldsapr, TiO, Amphinole (actinolite), Olivine? OPX? AlCaAlFeSiO (clinozoiesite/Epidote??), Titanite,	82.97	17.26	0.00	0.15	100.38
RJC 65	Otter upper 12	TiO with V FeO, Kfsp, Qz, TiO, Ca Amphibole?, Ca,Na Plag feldspar, Clinozoiesite/epidote, MgKFe AlSiO (check)	93.05	6.14	0.02	0.26	99.46
RJC 65	Otter upper 13	Qz, Biotite??? MgKFe AlSiO (check), CPX, Chlorite, Na Feldspar, Titanite,	84.36	14.87	0.00	0.41	99.64
RJC 65	Otter upper 14		84.87	14.28	0.03	0.41	99.58
RJC 65	Otter upper 15	FeS, NiFeS/ FeS exsolution textures. Chlorite	86.97	12.74	0.01	0.21	99.93
RJC 65	Otter upper 16	Qz, FeO, Na Feldspar, Talc? Titanite, K spar (with Ba)???	82.32	17.88	0.00	0.24	100.43
RJC 65	Otter upper 17		83.27	16.41	0.00	0.23	99.90
RJC 65	Otter upper 18	Qz, k Feldspar, FeO, TiO	79.12	21.07	0.00	0.27	100.47
RJC 65	Otter upper 19	External gunk	77.93	20.95	0.01	0.45	99.33
RJC 65	Otter upper 20	nb	71.45	27.60	0.00	0.11	99.16
RJC 65	Otter upper 21	FeS, Qz, FeO	74.86	24.50	0.00	0.10	99.46
RJC 65	Otter upper 22	Qz, TiO, Kspar, FeO, Kalonite, MG Al Si O Fe phase ??????, Pargasite Amphibole,	70.35	29.25	0.00	0.16	99.76
RJC 65	Otter upper 23		88.62	11.07	0.00	0.29	99.98
RJC 65	Otter upper 24		60.04	39.00	0.00	0.08	99.12
RJC 65	Otter upper 25		80.96	18.61	0.00	0.26	99.83
RJC 65	Otter upper 26		82.03	17.04	0.00	0.31	99.38
RJC 65	Otter upper 27	MgO????	86.46	12.72	0.00	0.21	99.39
RJC 65	Otter upper 28		91.49	7.65	0.85	0.16	100.15

Block	Grain ID	Inclusions	Au WT%	Ag WT%	Cu WT%	Hg WT%	TOTAL
RJC 65	Otter upper 29		82.79	17.41	0.00	0.21	100.40
RJC 65	Otter upper 3	FeMgCaO Calcite, K spar, Quartz, Cpy	75.06	24.90	0.00	0.35	100.31
RJC 65	Otter upper 30	FeO, Qz, Mg Al SiO Fe phase (CHECK), Chlorite,	57.43	41.44	0.00	0.27	99.15
RJC 65	Otter upper 31	Qz, FeO, + others CHECK	81.75	18.50	0.00	0.16	100.41
RJC 65	Otter upper 32		86.05	13.39	0.00	0.13	99.57
RJC 65	Otter upper 33		78.18	21.75	0.00	0.18	100.11
RJC 65	Otter upper 34		87.05	13.01	0.03	0.13	100.22
RJC 65	Otter upper 35		75.81	24.05	0.00	0.29	100.16
RJC 65	Otter upper 4	mush, external	63.97	35.81	0.09	0.36	100.24
RJC 65	Otter upper 5	CaKMgAlSiO mineral, Carbonate, FeO Feo , Quartz, TiO Chlorite?(check), Kspar, Clinozoesite, Na feldspar	96.31	2.64	0.00	0.45	99.40
RJC 65	Otter upper 6		78.75	21.70	0.01	0.24	100.70
RJC 65	Otter upper 7		82.21	17.43	0.00	0.36	100.01
RJC 65	Otter upper 8	external crap?	82.07	17.46	0.00	0.28	99.82
RJC 65	Otter upper 9	external ?	66.15	33.61	0.00	0.11	99.87
RJC 65	RubyCk 9.1		77.61	21.60	0.00	0.48	99.70
RJC 65	RubyCk 9.10		82.33	17.74	0.00	0.26	100.33
RJC 65	RubyCk 9.11		79.92	19.22	0.08	0.21	99.42
RJC 65	RubyCk 9.12		77.24	22.79	0.00	0.12	100.16
RJC 65	RubyCk 9.13		79.09	20.44	0.00	0.19	99.73
RJC 65	RubyCk 9.14		54.77	44.06	0.00	0.08	98.91
RJC 65	RubyCk 9.15		74.06	26.34	0.03	0.22	100.64
RJC 65	RubyCk 9.16		79.22	20.61	0.00	0.20	100.04
RJC 65	RubyCk 9.17		77.15	22.28	0.00	0.19	99.63
RJC 65	RubyCk 9.18		89.70	8.26	1.60	0.10	99.66
RJC 65	RubyCk 9.19		75.59	23.67	0.01	0.31	99.57
RJC 65	RubyCk 9.2		70.56	29.16	0.00	0.26	99.97
RJC 65	RubyCk 9.20		90.51	9.47	0.02	0.05	100.05
RJC 65	RubyCk 9.3		80.70	18.43	0.00	0.33	99.46
RJC 65	RubyCk 9.4		79.74	20.01	0.00	0.20	99.95

Block	Grain ID	Inclusions	Au WT%	Ag WT%	Cu WT%	Hg WT%	TOTAL
RJC 65	RubyCk 9.5		79.83	19.81	0.00	0.14	99.78
RJC 65	RubyCk 9.6		94.81	4.94	0.02	0.25	100.02
RJC 65	RubyCk 9.7		52.53	45.66	0.00	0.82	99.01
RJC 65	RubyCk 9.8		74.63	25.16	0.00	0.41	100.21
RJC 65	RubyCk 9.9		81.66	18.65	0.03	0.16	100.50
RJC 65	SpruceCk 11.1		69.62	30.77	0.00	0.23	100.61
RJC 65	SpruceCk 11.10		66.08	33.29	0.00	0.17	99.54
RJC 65	SpruceCk 11.11		85.92	14.67	0.01	0.13	100.74
RJC 65	SpruceCk 11.12		79.26	20.21	0.00	0.61	100.08
RJC 65	SpruceCk 11.13		73.24	25.80	0.00	0.35	99.38
RJC 65	SpruceCk 11.14		75.31	22.89	0.00	2.19	100.40
RJC 65	SpruceCk 11.15		85.07	13.98	0.01	0.44	99.50
RJC 65	SpruceCk 11.16		79.03	20.19	0.00	0.33	99.55
RJC 65	SpruceCk 11.17		79.72	18.70	0.00	1.59	100.01
RJC 65	SpruceCk 11.18		78.87	17.75	0.01	3.54	100.17
RJC 65	SpruceCk 11.19		84.10	15.95	0.00	0.21	100.26
RJC 65	SpruceCk 11.2		65.43	33.96	0.00	0.26	99.65
RJC 65	SpruceCk 11.20		96.32	2.91	0.04	0.15	99.41
RJC 65	SpruceCk 11.21		99.06	0.21	0.00	0.11	99.38
RJC 65	SpruceCk 11.22		82.37	17.43	0.00	0.20	100.01
RJC 65	SpruceCk 11.23		88.79	10.06	0.00	0.23	99.09
RJC 65	SpruceCk 11.24		77.29	21.89	0.00	0.12	99.31
RJC 65	SpruceCk 11.25		78.34	21.46	0.00	0.20	100.00
RJC 65	SpruceCk 11.26		98.92	0.18	0.00	0.24	99.34
RJC 65	SpruceCk 11.27		94.73	4.11	0.08	0.27	99.19
RJC 65	SpruceCk 11.28		94.81	4.64	0.02	0.30	99.76
RJC 65	SpruceCk 11.29		94.86	4.47	0.04	0.25	99.61
RJC 65	SpruceCk 11.3		58.85	40.03	0.00	0.04	98.93
RJC 65	SpruceCk 11.30		78.20	21.14	0.00	0.32	99.66
RJC 65	SpruceCk 11.31		77.48	21.99	0.00	0.19	99.66
RJC 65	SpruceCk 11.33		80.74	18.75	0.01	0.36	99.87

Block	Grain ID	Inclusions	Au WT%	Ag WT%	Cu WT%	Hg WT%	TOTAL
RJC 65	SpruceCk 11.34		83.45	15.72	0.01	0.17	99.34
RJC 65	SpruceCk 11.35		76.85	22.45	0.00	0.21	99.52
RJC 65	SpruceCk 11.36		97.64	1.24	0.06	0.92	99.86
RJC 65	SpruceCk 11.37		77.48	21.92	0.01	0.21	99.62
RJC 65	SpruceCk 11.38		87.83	11.61	0.01	0.09	99.54
RJC 65	SpruceCk 11.39		75.84	23.30	0.00	0.49	99.63
RJC 65	SpruceCk 11.4		73.49	25.60	0.00	0.32	99.41
RJC 65	SpruceCk 11.40		88.32	11.20	0.01	0.20	99.73
RJC 65	SpruceCk 11.41		61.45	37.65	0.00	0.21	99.32
RJC 65	SpruceCk 11.42		84.76	14.91	0.00	0.23	99.90
RJC 65	SpruceCk 11.43		82.77	16.32	0.00	0.36	99.45
RJC 65	SpruceCk 11.44		81.28	17.56	0.00	0.19	99.03
RJC 65	SpruceCk 11.45		56.64	42.44	0.00	0.10	99.18
RJC 65	SpruceCk 11.46		57.21	38.60	0.00	3.41	99.22
RJC 65	SpruceCk 11.5		76.70	22.82	0.00	0.44	99.97
RJC 65	SpruceCk 11.6		86.72	13.39	0.00	0.31	100.42
RJC 65	SpruceCk 11.7		65.75	34.14	0.00	0.19	100.08
RJC 65	SpruceCk 11.8		78.29	21.33	0.00	0.32	99.94
RJC 65	SpruceCk 11.9		84.23	15.34	0.00	0.30	99.87
RJC 65	SpruceCk 12.1		83.01	16.65	0.00	0.12	99.78
RJC 65	SpruceCk 12.10		83.84	15.24	0.01	0.28	99.37
RJC 65	SpruceCk 12.11		80.83	19.32	0.00	0.25	100.40
RJC 65	SpruceCk 12.12		73.34	26.46	0.00	0.32	100.12
RJC 65	SpruceCk 12.13		76.19	22.63	0.02	1.33	100.16
RJC 65	SpruceCk 12.14		89.66	10.32	0.03	0.27	100.28
RJC 65	SpruceCk 12.15		68.88	30.04	0.04	0.21	99.18
RJC 65	SpruceCk 12.16		90.29	8.14	0.03	0.29	98.74
RJC 65	SpruceCk 12.17		80.03	18.79	0.02	0.18	99.03
RJC 65	SpruceCk 12.17		79.89	18.88	0.01	0.20	98.98
RJC 65	SpruceCk 12.18		89.30	10.16	0.05	0.38	99.88
RJC 65	SpruceCk 12.19		81.45	17.98	0.02	0.16	99.62

Block	Grain ID	Inclusions	Au WT%	Ag WT%	Cu WT%	Hg WT%	TOTAL
RJC 65	SpruceCk 12.19		97.35	1.89	0.03	0.15	99.42
RJC 65	SpruceCk 12.2		92.96	6.81	0.02	0.18	99.97
RJC 65	SpruceCk 12.20		61.81	37.04	0.08	0.24	99.17
RJC 65	SpruceCk 12.21		63.42	35.37	0.07	0.21	99.08
RJC 65	SpruceCk 12.21		96.41	3.76	0.09	0.04	100.30
RJC 65	SpruceCk 12.3		83.13	14.90	0.00	2.04	100.07
RJC 65	SpruceCk 12.4		88.28	11.36	0.00	0.20	99.84
RJC 65	SpruceCk 12.5		74.40	25.57	0.02	0.13	100.12
RJC 65	SpruceCk 12.6		88.28	11.65	0.04	0.03	100.00
RJC 65	SpruceCk 12.7		83.10	16.89	0.02	0.36	100.36
RJC 65	SpruceCk 12.8		81.28	18.47	0.00	0.25	100.01
RJC 65	SpruceCk 12.9		89.59	11.13	0.03	0.23	100.98
RJC 65	WrightCk 10.1		88.47	11.18	0.02	0.22	99.89
RJC 65	WrightCk 10.2		77.41	22.37	0.00	0.15	99.93
RJC 67	10 Otter upper .1		78.78	21.26	0.00	0.15	100.19
RJC 67	10 Otter upper 10	ext	82.11	18.09	0.00	0.08	100.28
RJC 67	10 Otter upper 11	ext	79.07	20.81	0.02	0.50	100.39
RJC 67	10 Otter upper 12	FeCaMgCo3 complex	76.84	22.52	0.00	0.22	99.59
RJC 67	10 Otter upper 13	ext	80.82	19.05	0.01	0.08	99.96
RJC 67	10 Otter upper 2	ext	78.99	21.40	0.00	0.11	100.50
RJC 67	10 Otter upper 3	External coating sedimentry!	72.43	27.41	0.00	0.19	100.03
RJC 67	10 Otter upper 4	external minerals	79.75	20.43	0.00	0.17	100.36
RJC 67	10 Otter upper 5	FeO coat with primary Dolomite	97.67	0.27	0.56	0.71	99.21
RJC 67	10 Otter upper 6	ext	79.23	20.60	0.02	0.18	100.03
RJC 67	10 Otter upper 7	ext	78.89	20.50	0.00	0.15	99.54
RJC 67	10 Otter upper 8	ext	85.04	14.93	0.03	0.24	100.25
RJC 67	10 Otter upper 9	pentrative FeO extral coat	71.53	27.60	0.00	0.24	99.37
RJC 67	9 Boulder .1	carbonate	76.98	23.20	0.00	0.35	100.53
RJC 67	9 Boulder 2	chlorite	75.98	23.86	0.00	0.19	100.03
RJC 67	9 Boulder 3		81.68	18.25	0.00	0.35	100.29

Block	Grain ID	Inclusions	Au WT%	Ag WT%	Cu WT%	Hg WT%	TOTAL
RJC 67	11 otter nug	ChalcoPyrite, Pyrite KFsp, TiO (rutile), MoS?, Apatite, Zircon, Na feldspar, Pyrite, Chloritoid, Mg Carbonate, ChalcoPyrite, BaAlPO mineral ??, kaolinite, Titanite (possible with some U Zr P phases??)	78.78	21.72	0.00	0.28	100.78
RJC 67	Spruce 12.1		77.42	22.82	0.00	0.15	100.40
RJC 67	Spruce 12.10		51.65	46.46	0.00	0.23	98.34
RJC 67	Spruce 12.2	NiAs + NiAsS	69.06	30.00	0.03	0.13	99.22
RJC 67	Spruce 12.3		68.63	30.42	0.00	0.20	99.25
RJC 67	Spruce 12.4		95.93	3.73	0.05	0.19	99.90
RJC 67	Spruce 12.5	CuSbS	73.65	25.48	0.03	0.16	99.33
RJC 67	Spruce 12.6	FeS	64.59	35.02	0.00	0.14	99.76
RJC 67	Spruce 12.7		88.66	10.76	0.03	0.20	99.65
RJC 67	Spruce 12.8		65.00	33.76	0.00	0.15	98.91
RJC 67	Spruce 12.9		73.87	24.20	0.07	1.95	100.08
RJC 68	BOULDER CK 10.1		83.19	16.84	0.02	0.27	100.33
RJC 68	BOULDER CK 10.2		63.38	36.54	0.24	0.30	100.47
RJC 68	BOULDER CK 10.3		80.81	19.54	0.01	0.51	100.87
RJC 68	BOULDER CK 10.4		79.07	21.40	0.00	0.21	100.68
RJC 68	BOULDER CK 10.5		78.35	21.85	0.01	0.35	100.55
RJC 68	BOULDER CK 10.6		61.68	38.01	0.02	0.10	99.80
RJC 68	BOULDER CK 10.7		70.63	29.59	0.00	0.14	100.35
RJC 68	BOULDER CK 10.8		97.21	3.18	0.03	0.20	100.62
RJC 68	BOULDER CK 10.9		81.46	18.49	0.39	0.42	100.76
RJC 68	OTTER CK 11.1		81.26	19.94	0.03	0.17	101.40
RJC 68	OTTER CK UPPER 11.10		75.25	28.22	0.01	0.30	103.78
RJC 68	OTTER CK UPPER 11.11		77.61	24.53	0.00	0.12	102.25
RJC 68	OTTER CK UPPER 11.12		67.12	34.20	0.03	0.13	101.48
RJC 68	OTTER CK UPPER 11.13		88.66	13.93	0.00	0.25	102.84
RJC 68	OTTER CK UPPER 11.14		90.19	13.68	0.01	0.37	104.26

Block	Grain ID	Inclusions	Au WT%	Ag WT%	Cu WT%	Hg WT%	TOTAL
RJC 68	OTTER CK UPPER 11.14		84.33	19.21	0.00	0.11	103.65
RJC 68	OTTER CK UPPER 11.15		84.49	19.27	0.01	0.16	103.93
RJC 68	OTTER CK UPPER 11.16		66.92	34.95	0.01	0.29	102.18
RJC 68	OTTER CK UPPER 11.16		66.70	34.80	0.02	0.22	101.74
RJC 68	OTTER CK UPPER 11.17		74.50	27.25	0.00	0.22	101.97
RJC 68	OTTER CK UPPER 11.18		90.26	12.14	0.03	0.23	102.66
RJC 68	OTTER CK UPPER 11.19		97.92	5.40	0.04	0.14	103.50
RJC 68	OTTER CK UPPER 11.2		81.65	19.83	0.00	0.60	102.09
RJC 68	OTTER CK UPPER 11.20		65.43	37.47	0.00	0.15	103.05
RJC 68	OTTER CK UPPER 11.21		87.67	14.06	0.02	0.35	102.10
RJC 68	OTTER CK UPPER 11.22		74.91	26.38	0.01	0.12	101.42
RJC 68	OTTER CK UPPER 11.23		81.93	20.24	0.01	0.18	102.36
RJC 68	OTTER CK UPPER 11.24		90.51	11.94	0.00	0.25	102.70
RJC 68	OTTER CK UPPER 11.25		97.06	6.57	0.05	0.15	103.83
RJC 68	OTTER CK UPPER 11.26		82.37	19.48	0.01	0.21	102.06
RJC 68	OTTER CK UPPER 11.27		81.62	21.11	0.02	0.24	102.99
RJC 68	OTTER CK UPPER 11.28		85.55	16.65	0.02	0.31	102.53
RJC 68	OTTER CK UPPER 11.29		91.97	10.85	0.04	0.26	103.12
RJC 68	OTTER CK UPPER 11.3		86.75	15.40	0.02	0.20	102.36
RJC 68	OTTER CK UPPER 11.30		72.94	29.90	0.00	0.18	103.02
RJC 68	OTTER CK UPPER 11.31		90.47	11.09	0.04	0.30	101.89
RJC 68	OTTER CK UPPER 11.32		68.58	32.65	0.01	0.13	101.38

Block	Grain ID	Inclusions	Au WT%	Ag WT%	Cu WT%	Hg WT%	TOTAL
RJC 68	OTTER CK UPPER 11.33		71.61	31.19	0.00	0.15	102.95
RJC 68	OTTER CK UPPER 11.34		82.74	19.54	0.02	0.21	102.52
RJC 68	OTTER CK UPPER 11.35		80.45	22.08	0.00	0.28	102.81
RJC 68	OTTER CK UPPER 11.36		90.54	11.42	0.06	0.33	102.36
RJC 68	OTTER CK UPPER 11.37		84.37	17.84	0.01	0.29	102.52
RJC 68	OTTER CK UPPER 11.38		90.97	10.42	0.59	0.63	102.61
RJC 68	OTTER CK UPPER 11.39		88.32	14.30	0.03	0.11	102.75
RJC 68	OTTER CK UPPER 11.4		71.96	30.11	0.02	0.18	102.27
RJC 68	OTTER CK UPPER 11.40		70.19	32.69	0.00	0.24	103.12
RJC 68	OTTER CK UPPER 11.41		90.52	11.57	0.03	0.21	102.33
RJC 68	OTTER CK UPPER 11.42		93.30	9.15	0.05	0.19	102.69
RJC 68	OTTER CK UPPER 11.43		88.92	13.26	0.02	0.28	102.48
RJC 68	OTTER CK UPPER 11.44		84.50	18.31	0.01	0.12	102.95
RJC 68	OTTER CK UPPER 11.45		74.24	27.29	0.01	0.08	101.62
RJC 68	OTTER CK UPPER 11.46		75.04	26.62	0.02	0.13	101.80
RJC 68	OTTER CK UPPER 11.47		81.86	19.98	0.02	0.32	102.18
RJC 68	OTTER CK UPPER 11.48		60.67	40.29	0.01	0.21	101.19
RJC 68	OTTER CK UPPER 11.49		94.75	6.21	0.50	0.88	102.34
RJC 68	OTTER CK UPPER 11.5		89.18	14.32	0.03	0.15	103.68
RJC 68	OTTER CK UPPER 11.50		89.64	12.33	0.00	0.26	102.23
RJC 68	OTTER CK UPPER 11.51		67.17	33.93	0.03	0.28	101.41
RJC 68	OTTER CK UPPER 11.52		78.43	23.10	0.05	0.20	101.77

Block	Grain ID	Inclusions	Au WT%	Ag WT%	Cu WT%	Hg WT%	TOTAL
RJC 68	OTTER CK UPPER 11.53		97.07	4.89	0.11	0.45	102.51
RJC 68	OTTER CK UPPER 11.54		84.77	16.86	0.03	0.16	101.82
RJC 68	OTTER CK UPPER 11.55		82.51	16.39	0.06	3.66	102.62
RJC 68	OTTER CK UPPER 11.56		73.81	27.51	0.00	0.29	101.61
RJC 68	OTTER CK UPPER 11.57		90.27	11.92	0.02	0.12	102.33
RJC 68	OTTER CK UPPER 11.58		89.90	12.14	0.05	0.12	102.20
RJC 68	OTTER CK UPPER 11.59		89.66	3.36	8.86	0.07	101.95
RJC 68	OTTER CK UPPER 11.6		91.70	9.19	0.03	0.18	101.10
RJC 68	OTTER CK UPPER 11.60		64.33	37.57	0.02	0.05	101.98
RJC 68	OTTER CK UPPER 11.7		91.57	10.88	0.01	0.17	102.62
RJC 68	OTTER CK UPPER 11.8		78.96	23.38	0.01	0.19	102.54
RJC 68	OTTER CK UPPER 11.9		91.69	10.83	0.01	0.22	102.75
RJC 68	RUBY CK 12.1		84.73	15.85	0.02	0.29	100.89
RJC 68	RUBY CK 12.10		73.29	27.46	0.03	0.45	101.22
RJC 68	RUBY CK 12.11		90.74	10.30	0.04	0.22	101.30
RJC 68	RUBY CK 12.12		71.38	28.85	0.01	0.42	100.66
RJC 68	RUBY CK 12.13		71.68	28.81	0.02	0.41	100.92
RJC 68	RUBY CK 12.14		74.87	25.90	0.02	0.20	100.99
RJC 68	RUBY CK 12.15		86.00	14.55	0.09	0.02	100.67
RJC 68	RUBY CK 12.2		77.43	23.24	0.03	0.29	100.99
RJC 68	RUBY CK 12.3	Qz, Amphiole, Clinozoisite, FeO, Epidote,	77.39	23.63	0.04	0.15	101.22
RJC 68	RUBY CK 12.4		77.32	23.37	0.02	0.20	100.90
RJC 68	RUBY CK 12.5		66.45	33.88	0.01	0.09	100.43
RJC 68	RUBY CK 12.6		54.88	44.54	0.01	0.10	99.53
RJC 68	RUBY CK 12.7		91.88	8.50	0.02	0.57	100.97
RJC 68	RUBY CK 12.8		83.75	17.26	0.03	0.17	101.21

Block	Grain ID	Inclusions	Au WT%	Ag WT%	Cu WT%	Hg WT%	TOTAL
RJC 68	RUBY CK 12.9		80.33	19.48	0.02	1.18	101.00
RJC 68	RUBY CK 13.1		79.44	21.34	0.02	0.15	100.94
RJC 68	RUBY CK 13.2		79.34	20.24	0.01	0.39	99.98
RJC 68	RUBY CK 13.3		56.36	42.10	0.01	0.22	98.69
RJC 68	RUBY CK 13.4		74.57	26.19	0.00	0.16	100.93
RJC 68	RUBY CK 13.5		69.08	31.70	0.00	0.18	100.96
RJC 68	RUBY CK 13.6		89.99	10.09	0.61	0.11	100.82
RJC 68	RUBY CK 13.7		81.72	19.95	0.02	0.19	101.88
RJC 68	WRIGHT CK 14.1		76.33	24.05	0.02	0.25	100.65
RJC 68	WRIGHT CK 14.2		85.57	14.59	0.00	0.26	100.42
RJC 68	WRIGHT CK 14.3		72.17	28.75	0.00	0.21	101.13
RJC 68	WRIGHT CK 14.4		81.25	19.12	0.00	0.32	100.68
RJC 70	1.1 RUBY CK	Qz, Apatite, AlKSiO2	87.89	11.81	0.07	0.08	99.84
RJC 70	1.2 RUBY CK		77.63	23.07	0.03	0.31	101.04
RJC 70	1.3 RUBY CK	Qz, Apatite, FeO, CuFeS	74.66	25.79	0.04	0.34	100.82
RJC 70	1.4 RUBY CK	FeS with Ni	84.07	16.13	0.05	0.22	100.47
RJC 70	1.5 RUBY CK	Qz	84.49	16.17	0.02	0.20	100.89
RJC 70	2.1 WRIGHT CK	Qz FeO	79.06	21.45	0.03	0.29	100.84
RJC 70	2.2 WRIGHT CK	Qz FeO	79.99	19.97	0.05	0.07	100.08
RJC 70	2.2 WRIGHT CK		80.70	20.08	0.02	0.13	100.94
RJC 70	3.1 OTTER CK L		84.85	15.63	0.05	0.20	100.74
RJC 70	3.10 OTTER CK L		80.23	19.15	0.04	0.27	99.69
RJC 70	3.11 OTTER CK L		82.95	16.94	0.04	0.14	100.07
RJC 70	3.12 OTTER CK L		77.94	22.25	0.03	0.22	100.44
RJC 70	3.13 OTTER CK L		77.74	22.18	0.02	0.32	100.27
RJC 70	3.14 OTTER CK L		80.34	20.48	0.02	0.16	101.01
RJC 70	3.15 OTTER CK L	FeO, Qz, Na feldsapr, Kfsp, Plag, TiO, Apatite, Monazite,	83.62	16.56	0.04	0.23	100.46
RJC 70	3.16 OTTER CK L		83.23	17.16	0.04	0.15	100.58
RJC 70	3.17 OTTER CK L		71.59	28.04	0.01	0.23	99.86
RJC 70	3.18 OTTER CK L		78.95	21.45	0.01	0.31	100.72

Block	Grain ID	Inclusions	Au WT%	Ag WT%	Cu WT%	Hg WT%	TOTAL
RJC 70	3.19 OTTER CK L	Pyrite, K spar,Quartz (BaAlPO mineral?, Quartz, Clays)	79.11	21.18	0.03	0.12	100.44
RJC 70	3.2 OTTER CK L	AlSiKFe (very small)	86.64	12.68	0.03	0.45	99.79
RJC 70	3.20 OTTER CK L		84.32	16.03	0.04	0.28	100.68
RJC 70	3.21 OTTER CK L		78.71	21.65	0.03	0.20	100.58
RJC 70	3.22 OTTER CK L		73.07	27.54	0.03	0.27	100.92
RJC 70	3.23 OTTER CK L	SiO, FeO, Kfsp, kaolinite, Biotite, Pyrite,	78.87	21.81	0.05	0.29	101.02
RJC 70	3.24 OTTER CK L		74.95	24.93	0.02	0.20	100.09
RJC 70	3.3 OTTER CK L	FeS, Kfs, MgAlCaKFeSiO (possible Omphacite)	93.98	6.07	0.06	0.31	100.42
RJC 70	3.4 OTTER CK L		79.12	20.81	0.03	0.25	100.22
RJC 70	3.5 OTTER CK L	K fsp, Qz, Epidote, Pyrite,	81.63	18.33	0.05	0.22	100.24
RJC 70	3.6 OTTER CK L	Qz, Na Feldspar, K Fsp	84.22	15.76	0.04	0.21	100.23
RJC 70	3.7 OTTER CK L	Qz, Plag Feldspar, K Spar, Chlorite, Titanite, Na feldsapr, Ca-amphibole	78.86	21.42	0.02	0.21	100.52
RJC 70	3.8 OTTER CK L		81.48	19.16	0.04	0.04	100.72
RJC 70	3.9 OTTER CK L		77.57	23.06	0.03	0.12	100.78
RJC 69	1.1 OTTER CK L	FeO, Qz,	79.34	16.73	0.00	0.09	96.17
RJC 69	1.10 OTTER CK L	Calcite, Qz + Ext	73.11	23.54	0.00	0.14	96.80
RJC 69	1.11 OTTER CK L	ext	72.34	24.23	0.00	0.19	96.77
RJC 69	1.12 OTTER CK L	ext	71.08	26.08	0.01	0.31	97.48
RJC 69	1.13 OTTER CK L	ext	75.59	21.18	0.01	0.09	96.88
RJC 69	1.14 OTTER CK L	ext	74.67	21.82	0.03	0.27	96.79
RJC 69	1.15 OTTER CK L	FeO ext	68.60	28.04	0.01	0.21	96.86
RJC 69	1.2 OTTER CK L	Pyrite, Qz, +ext, Na feldspar	78.02	19.88	0.00	0.25	98.15
RJC 69	1.3 OTTER CK L	Phospate, FeO,	78.89	18.27	0.01	0.16	97.33
RJC 69	1.4 OTTER CK L	ext	62.48	34.57	0.00	0.11	97.16
RJC 69	1.5 OTTER CK L	ext	87.18	9.36	0.00	0.23	96.77
RJC 69	1.6 OTTER CK L	ext	65.30	32.19	0.00	0.25	97.74
RJC 69	1.7 OTTER CK L	ext	80.91	16.08	0.01	0.39	97.39
RJC 69	1.8 OTTER CK L	ext	79.68	17.07	0.00	0.35	97.10
RJC 69	1.9 OTTER CK L	Qz, Ext	74.99	21.84	0.00	0.17	97.00
RJC 69	2.1 OTTER CK L	-	76.49	20.25	0.01	0.26	97.01

Block	Grain ID	Inclusions	Au WT%	Ag WT%	Cu WT%	Hg WT%	TOTAL
RJC 69	2.10 OTTER CK L	Kspar, Qz,	76.97	20.87	0.02	0.16	98.02
RJC 69	2.2 OTTER CK L	-	82.06	14.21	0.01	0.49	96.78
RJC 69	2.3 OTTER CK L	-	77.77	20.25	0.00	0.27	98.29
RJC 69	2.4 OTTER CK L	-	61.95	36.07	0.00	0.09	98.11
RJC 69	2.5 OTTER CK L	Na fldspar, Qz,	82.01	16.17	0.01	0.17	98.35
RJC 69	2.6 OTTER CK L	ext	69.28	27.51	0.00	0.46	97.26
RJC 69	2.7 OTTER CK L	ext	78.02	19.23	0.00	0.25	97.50
RJC 69	2.8 OTTER CK L	ext	93.74	2.79	0.11	0.37	97.01
RJC 69	2.9 OTTER CK L	ext	57.75	40.97	0.00	0.07	98.80
RJC 69	3.1 BOULDER CK	Qz, Kfsp, epidote (ClinoZoisite), Chlorite (replacing Biotite), pumpellite, Ca-amphibole	74.72	22.73	0.01	0.27	97.73
RJC 69	3.10 BOULDER CK		72.30	25.14	0.01	0.35	97.80
RJC 69	3.11 BOULDER CK	Albite, Amphibole, Pumpellyite, Chlorite, Ca-amphibole, cordierite	82.91	14.18	0.02	0.13	97.24
RJC 69	3.12 BOULDER CK		73.51	22.62	0.03	0.31	96.47
RJC 69	3.13 BOULDER CK		74.98	21.75	0.00	0.12	96.85
RJC 69	3.14 BOULDER CK		74.06	22.74	0.02	0.32	97.13
RJC 69	3.15 BOULDER CK		75.48	21.57	0.02	0.21	97.27
RJC 69	3.2 BOULDER CK		78.23	19.78	0.01	0.30	98.32
RJC 69	3.3 BOULDER CK	Ca-amphibole, Kfsp, Qz, Tourmaline, Pagioclase feldspar, Chlorite, Alkali feldspar, Ti-magnetite, titanite, Carbonate ??, Serpentine, Biotite	73.86	23.08	0.00	0.32	97.26
RJC 69	3.4 BOULDER CK		78.62	19.31	0.02	0.17	98.12
RJC 69	3.5 BOULDER CK		84.69	11.63	0.02	0.50	96.84
RJC 69	3.6 BOULDER CK	SiO, Alkali feldspar, Muscovite, FeO (Ti magnatie) Mg Ca Fe amphibole, Ilmenite (Mn)	77.68	19.54	0.00	0.21	97.44
RJC 69	3.7 BOULDER CK	Mn rich Illmanite, Qz, Monazite, Mg Ca amphibole , epidote (ClinoZoisite), Biotite	79.14	17.98	0.00	0.19	97.31
RJC 69	3.8 BOULDER CK		68.67	28.90	0.00	0.27	97.84
RJC 69	3.9 BOULDER CK		82.30	15.19	0.00	0.08	97.57
RJC 69	4.1 RUBY CK		78.03	19.81	0.00	0.20	98.05
RJC 69	4.2 RUBY CK	Chlorite (After Biotite), orthopyroxene, Qz, Ca-amphibole, Garnet (Fe rich) ??, Biotite	78.25	19.47	0.02	0.27	98.01
RJC 69	4.3 RUBY CK		76.19	21.40	0.01	0.30	97.90

Block	Grain ID	Inclusions	Au WT%	Ag WT%	Cu WT%	Hg WT%	TOTAL
RJC 69	4.4 RUBY CK	NiAsS Qz, Chlorite, Ni silicate Phase ??	64.97	32.56	0.00	0.20	97.73
RJC 69	4.5 RUBY CK	Epidote, Na feldsapr, Chlorite, Ti phase (Unknown), K feldspar, Qz	86.63	9.89	0.04	0.23	96.80
RJC 69	4.6 RUBY CK		78.39	19.05	0.03	0.37	97.83
RJC 69	4.7 RUBY CK		77.30	20.00	0.03	0.15	97.48
RJC 69	5.1 OTTER CK L	Qz, Ext	80.19	18.07	0.04	0.25	98.55
RJC 69	5.10 OTTER CK L	-	70.57	27.31	0.00	0.22	98.09
RJC 69	5.11 OTTER CK L	Kspar, FeO externals, Qz	77.06	21.68	0.03	0.24	99.00
RJC 69	5.12 OTTER CK L	-	80.19	17.67	0.03	0.13	98.01
RJC 69	5.13 OTTER CK L	-	83.42	14.96	0.01	0.28	98.66
RJC 69	5.14 OTTER CK L	Calcite	89.77	7.99	0.07	0.21	98.04
RJC 69	5.15 OTTER CK L	ZnS (in Qz), Qz, K spar, Ba phosphate, CuFeS,	92.90	4.30	0.07	0.24	97.52
RJC 69	5.16 OTTER CK L	-	78.29	20.12	0.02	0.16	98.59
RJC 69	5.17 OTTER CK L	Inclusions of NiAsS, SbS, NiSbS	91.90	5.19	0.07	0.27	97.43
RJC 69	5.18 OTTER CK L	-	92.47	4.43	0.07	0.39	97.36
RJC 69	5.19 OTTER CK L	-	89.64	7.65	0.07	0.22	97.58
RJC 69	5.2 OTTER CK L	-	73.31	24.68	0.03	0.28	98.30
RJC 69	5.20 OTTER CK L	-	88.49	8.71	0.16	0.30	97.66
RJC 69	5.21 OTTER CK L	-	70.87	26.00	0.01	0.40	97.28
RJC 69	5.22 OTTER CK L	Na feldsapr, Qz, FeO, TiO, ClinoZoisite	84.11	13.88	0.16	0.36	98.50
RJC 69	5.23 OTTER CK L	-	78.93	18.53	0.01	1.10	98.56
RJC 69	5.24 OTTER CK L	-	87.52	10.10	0.01	0.29	97.92
RJC 69	5.25 OTTER CK L	-	76.74	21.38	0.00	0.13	98.26
RJC 69	5.26 OTTER CK L	complex possible external Qz + lots of other	95.24	2.11	0.08	0.26	97.69
RJC 69	5.27 OTTER CK L	FeO, NiAsS,	91.98	4.53	0.08	0.39	96.98
RJC 69	5.28 OTTER CK L	-	77.28	19.96	0.01	0.37	97.62
RJC 69	5.3 OTTER CK L	Qz, Kspar,	90.99	6.76	0.03	0.28	98.06
RJC 69	5.4 OTTER CK L	ext	76.60	20.93	0.00	0.20	97.73
RJC 69	5.5 OTTER CK L	-	86.99	9.97	0.03	0.19	97.18
RJC 69	5.6 OTTER CK L	-	76.13	22.96	0.01	0.42	99.52
RJC 69	5.7 OTTER CK L	-	74.88	22.26	0.02	1.57	98.73

Block	Grain ID	Inclusions	Au WT%	Ag WT%	Cu WT%	Hg WT%	TOTAL
RJC 69	5.8 OTTER CK L	Kspar, Qz,	80.37	17.08	0.00	0.43	97.88
RJC 69	5.9 OTTER CK L	-	78.21	19.76	0.02	0.20	98.21
RJC 69	6.1 OTTER CK L	-	79.28	18.16	0.02	0.30	97.75
RJC 69	6.11 OTTER CK L	ext	69.45	28.92	0.01	0.21	98.58
RJC 69	6.12 OTTER CK L	ext	80.67	17.32	0.01	0.27	98.27
RJC 69	6.13 OTTER CK L	ext	71.10	26.20	0.01	0.17	97.48
RJC 69	6.14 OTTER CK L	ext	72.29	25.79	0.00	0.32	98.41
RJC 69	6.15 OTTER CK L	FeS, Complex FeO on rim (looks semi primary as Au within grain. + Complex other rim minerals	77.29	20.29	0.00	0.16	97.73
RJC 69	6.16 OTTER CK L	Qz, K feldspar, Calcite, FeO, Titanite, Na feldsapr	77.28	21.22	0.01	0.27	98.79
RJC 69	6.17 OTTER CK L	ext	74.87	22.77	0.01	0.50	98.15
RJC 69	6.18 OTTER CK L	FeAsS, Kspar, FeS, Qz, Dolomite, CuFeS	77.97	19.81	0.01	0.23	98.03
RJC 69	6.19 OTTER CK L		74.71	23.34	0.02	0.24	98.31
RJC 69	6.2 OTTER CK L	NiAsS, Qz	83.31	13.81	0.01	0.25	97.39
RJC 69	6.20 OTTER CK L		75.57	21.84	0.01	0.27	97.70
RJC 69	6.21 OTTER CK L		74.36	24.21	0.00	0.23	98.80
RJC 69	6.22 OTTER CK L		77.84	19.70	0.01	0.08	97.63
RJC 69	6.23 OTTER CK L	AuTe2, HgTe	94.72	1.99	0.02	0.32	97.05
RJC 69	6.24 OTTER CK L	FeCuS, FeS, Qz,	93.73	2.47	0.19	0.29	96.69
RJC 69	6.25 OTTER CK L	K feldspar, Na Feld	78.28	18.88	0.02	0.16	97.34
RJC 69	6.25 OTTER CK L		75.70	21.79	0.00	0.16	97.65
RJC 69	6.3 OTTER CK L	Kspar, Qz, (lo confidence not ext)	89.14	7.82	0.09	0.45	97.51
RJC 69	6.4 OTTER CK L	Qz, FeS, Kspar,	74.84	22.88	0.00	0.19	97.92
RJC 69	6.5 OTTER CK L	Qz, FeNiS, FeS, FeO, Alkali feldsapr	86.27	10.15	0.05	0.56	97.03
RJC 69	6.6 OTTER CK L	K feldsapr, Na feldspar, Qz, + others check	68.65	28.60	0.00	0.34	97.60
RJC 69	6.7 OTTER CK L	ext	80.83	17.06	0.00	0.19	98.08
RJC 69	6.8 OTTER CK L	ext	69.84	27.91	0.00	0.18	97.94
RJC 69	6.9 OTTER CK L	6.10 is missing	68.83	29.08	0.01	0.23	98.15
RJC 69	7.10 OTTER CK L	FeNiS, Qz, +complex lithic	76.86	19.91	0.02	0.28	97.06
RJC 69	7.11 OTTER CK L		78.23	19.69	0.03	0.10	98.05

Block	Grain ID	Inclusions	Au WT%	Ag WT%	Cu WT%	Hg WT%	TOTAL
RJC 69	7.12 OTTER CK L		80.23	16.90	0.02	0.12	97.26
RJC 69	7.13 OTTER CK L		73.34	24.17	0.00	0.22	97.74
RJC 69	7.14 OTTER CK L		81.62	15.32	0.02	0.20	97.16
RJC 69	7.15 OTTER CK L		76.46	19.83	0.03	0.29	96.61
RJC 69	7.16 OTTER CK L		76.06	21.48	0.00	0.24	97.78
RJC 69	7.17 OTTER CK L		73.51	23.15	0.00	0.25	96.91
RJC 69	7.18 OTTER CK L		82.39	14.04	0.02	0.18	96.63
RJC 69	7.19 OTTER CK L		73.36	23.15	0.03	0.35	96.88
RJC 69	7.2 OTTER CK L	PbS, PbAgSbS mineral, + Secondary Au/Ag veriations	62.25	35.26	0.00	0.09	97.60
RJC 69	7.20 OTTER CK L		75.60	21.06	0.01	0.25	96.91
RJC 69	7.21 OTTER CK L		79.16	17.53	0.00	0.31	97.01
RJC 69	7.22 OTTER CK L		92.43	3.59	0.06	0.29	96.37
RJC 69	7.23 OTTER CK L		74.79	21.98	0.01	0.22	97.00
RJC 69	7.24 OTTER CK L		81.57	14.62	0.03	0.26	96.48
RJC 69	7.25 OTTER CK L		78.41	17.83	0.04	0.36	96.64
RJC 69	7.26 OTTER CK L		75.41	21.26	0.02	0.12	96.81
RJC 69	7.27 OTTER CK L		69.13	27.70	0.01	0.17	97.01
RJC 69	7.28 OTTER CK L		76.24	20.18	0.05	0.26	96.73
RJC 69	7.29 OTTER CK L		77.45	19.03	0.05	0.45	96.98
RJC 69	7.3 OTTER CK L	Qz, FeS, FeO, + others CHECK	74.15	22.98	0.01	0.56	97.70
RJC 69	7.30 OTTER CK L		72.77	24.15	0.03	0.21	97.16
RJC 69	7.31 OTTER CK L		86.27	9.05	0.04	0.16	95.52
RJC 69	7.4 OTTER CK L	ext	83.58	14.01	0.02	0.29	97.90
RJC 69	7.5 OTTER CK L	Folded grain entrapping material?? Mapped, Qz , Feldsaprs	83.90	12.71	0.04	0.10	96.75
RJC 69	7.6 OTTER CK L	Qz, K feldspar, FeS,	76.45	21.07	0.03	0.22	97.76
RJC 69	7.7 OTTER CK L	Qz, FeS,	70.41	26.91	0.01	0.21	97.54
RJC 69	7.8 OTTER CK L	Qz , Kspar, Na feldspar, FeO,	83.78	12.99	0.02	0.24	97.04
RJC 69	7.9 OTTER CK L		70.76	26.10	0.01	0.18	97.04
wrs 1822C	12A		78.31	21.23	0.00	0.00	99.54
wrs 1822C	12B		72.89	27.76	0.02	0.05	100.72

Block	Grain ID	Inclusions	Au WT%	Ag WT%	Cu WT%	Hg WT%	TOTAL
wrs 1822C	12C		72.15	27.95	0.01	0.00	100.11
wrs 1822C	12D		81.93	18.09	0.03	0.04	100.09
wrs 1822C	12E		70.77	30.70	0.01	0.01	101.50
wrs 1822C	12F DARK		80.02	19.13	0.03	0.00	99.18
wrs 1822C	12G		82.03	18.76	0.03	0.00	100.82
wrs 1822C	12H		85.75	14.85	0.14	0.00	100.74
wrs 1822C	12I		73.33	27.97	0.01	0.00	101.31
wrs 1822C	12J		71.20	29.33	0.02	0.15	100.70
wrs 1822C	12K		79.21	20.69	0.01	0.04	99.95
wrs 1822C	12L		83.04	17.05	0.03	0.00	100.12
wrs 1822C	12M		78.40	21.57	0.01	0.00	99.98
wrs 1822C	12N		79.20	20.73	0.03	0.00	99.96
wrs 1822C	12O	fes2	67.48	33.26	0.01	0.05	100.79
wrs 1822C	12P		74.46	25.62	0.02	0.00	100.10
wrs 1822C	12P DARK		73.44	25.61	0.02	0.00	99.07
wrs 1822C	12Q		90.69	9.07	0.04	0.00	99.80
wrs 1822C	12R		77.63	23.27	0.02	0.00	100.93
wrs 1822C	12S		81.17	18.85	0.03	0.02	100.06
wrs 1822C	12T		88.35	11.28	0.02	0.00	99.65
wrs 1822C	12U		77.55	22.58	0.00	0.00	100.13
wrs 1822C	12V		88.66	11.80	0.16	0.00	100.62
wrs 1822C	12X		77.64	23.04	0.03	0.00	100.71
wrs 1822C	12Y	fes2	83.87	15.97	0.03	0.00	99.87
wrs 1822C	12A		77.65	23.24	0.02	0.00	100.91
wrs 1822C	12B		81.40	18.96	0.03	0.00	100.40
wrs 1822C	12E		99.30	0.38	0.03	0.00	99.71
wrs 1822C	12F		72.33	28.84	0.01	0.00	101.18
wrs 1822C	13A		81.48	19.00	0.01	0.00	100.48
wrs 1822C	13B	FeCoNIAsS	68.81	31.92	0.01	0.00	100.74
wrs 1822C	13C		53.28	49.08	0.00	0.00	102.36
wrs 1822C	13D	ZnS	81.59	18.58	0.01	0.00	100.19

Block	Grain ID	Inclusions	Au WT%	Ag WT%	Cu WT%	Hg WT%	TOTAL
wrs 1822C	12O	fes2	67.48	33.26	0.01	0.05	100.79
wrs 1822C	12Y	fes2	83.87	15.97	0.03	0.00	99.87
wrs 1822C	13B	FeCoNIAsS	68.81	31.92	0.01	0.00	100.74
wrs 1822C	13D	ZnS	81.59	18.58	0.01	0.00	100.19
WRS 1862A	7A		78.78	20.54	0.02	0.00	99.34
WRS 1862A	7B	Apatite, Gersdorffite	75.34	23.64	0.01	0.00	98.98
WRS 1862A	7C		66.21	32.87	0.01	0.14	99.23
WRS 1862A	7D		79.46	18.94	0.01	0.00	98.41
WRS 1862A	7E		76.08	23.26	0.00	0.23	99.57
WRS 1862A	7F	Arsenopyrite	75.27	24.48	0.02	0.00	99.77
WRS 1862A	7G		78.51	20.81	0.00	0.00	99.32
WRS 1862A	7H		72.31	27.77	0.00	0.01	100.09
WRS 1862A	7I		74.15	25.49	0.00	0.04	99.68
WRS 1862A	7J		75.56	23.50	0.01	0.00	99.07
WRS 1862A	7K		82.65	16.97	0.03	0.00	99.64
WRS 1862A	7L		78.44	20.36	0.01	0.00	98.80
WRS 1862A	7M		77.04	22.64	0.00	0.01	99.70
WRS 1862A	7N		76.94	22.32	0.01	0.00	99.27
WRS 1862A	7O		78.39	21.44	0.02	0.00	99.85
WRS 1862A	7P	Pyrite	80.69	19.36	0.01	0.00	100.06
WRS 1862A	7Q		71.20	28.29	0.00	0.12	99.61
WRS 1862B	12A		76.31	23.92	0.01	0.00	100.24
WRS 1862B	12B		76.32	22.33	0.00	0.00	98.66
WRS 1862B	12C		75.26	24.80	0.00	0.00	100.07
WRS 1862B	12D		81.85	16.74	0.01	0.33	98.93
WRS 1862B	12E		84.62	14.20	0.01	0.00	98.83
WRS 1862B	12F		81.72	15.97	0.01	0.27	97.97
WRS 1862B	12G		96.18	3.68	0.10	0.00	99.97
WRS 1862B	12H		77.79	21.39	0.00	0.00	99.18
WRS 1862B	12I		74.12	26.39	0.01	0.00	100.52
WRS 1862B	12J	Pyrite	78.66	21.12	0.01	0.00	99.79

Block	Grain ID	Inclusions	Au WT%	Ag WT%	Cu WT%	Hg WT%	TOTAL
WRS 1862B	12K		77.21	22.64	0.00	0.00	99.85
WRS 1862B	12L		77.24	22.51	0.02	0.00	99.77
WRS 1862B	12M		89.46	10.13	0.12	0.00	99.71
WRS 1862B	12N		67.68	34.41	0.01	0.00	102.09
WRS 1862B	12O		82.77	16.80	0.02	0.00	99.60
WRS 1862B	12P		73.58	26.08	0.00	0.00	99.66
WRS 1862B	12Q		78.26	21.24	0.00	0.00	99.51
WRS 1862B	12R VERY LIGHT		90.10	9.45	0.03	0.00	99.59
WRS 1862B	12R LIGHT		84.83	14.85	0.03	0.00	99.71
WRS 1862B	12R DARK		76.79	23.57	0.00	0.00	100.37
WRS 1862B	12S		79.39	20.60	0.01	0.00	100.00
WRS 1862B	12T		76.66	23.59	0.00	0.00	100.26
WRS 1862B	12U		77.02	22.26	0.01	0.00	99.29
WRS 1862B	12V		83.11	15.31	0.01	0.00	98.42
WRS 1862B	12W		72.31	27.17	0.00	0.00	99.48
WRS 1862B	12X		77.38	23.15	0.02	0.00	100.55
WRS 1862B	12Y		74.39	26.24	0.01	0.00	100.65
WRS 1862B	12Z		67.76	32.45	0.00	0.00	100.21
WRS 1862B	12A1		70.17	30.62	0.01	0.00	100.79
WRS 1862B	12A2		79.46	21.05	0.02	0.02	100.55
WRS 1862D	15A	CaMgFe carb	78.74	21.12	0.02	0.00	99.88
WRS 1862D	15B		78.42	22.56	0.00	0.00	100.98
WRS 1862D	15C	Fe=Ni>CoAsS	79.29	21.12	0.01	0.00	100.42
wrs 1862 C	12A		81.02	19.12	0.01	0.04	100.19
wrs 1862 C	12b		79.09	21.10	0.03	0.07	100.29
wrs 1862 C	12C		95.20	3.95	0.01	0.16	99.33
wrs 1862 C	12D		82.64	17.53	0.00	0.00	100.17
wrs 1862 C	12E		81.76	18.57	0.00	0.00	100.33
wrs 1862 C	12F		81.44	17.09	0.01	0.00	98.54
wrs 1862 C	12G		96.02	3.48	0.07	0.00	99.58
wrs 1862 C	12H/1		78.36	22.27	0.02	0.00	100.64

Block	Grain ID	Inclusions	Au WT%	Ag WT%	Cu WT%	Hg WT%	TOTAL
wrs 1862 C	12H		83.60	16.61	0.01	0.00	100.22
wrs 1862 C	12J		73.99	25.79	0.01	0.00	99.79
wrs 1862 C	12K		80.53	19.52	0.01	0.00	100.07
wrs 1862 C	12L		78.25	22.28	0.01	0.00	100.54
wrs 1862 C	12M	NIFeS2	83.50	14.10	0.00	0.00	97.69
wrs 1862 C	12N	FeS2	86.71	13.26	0.04	0.01	100.02
wrs 1862 C	12O		75.03	25.90	0.00	0.00	100.93
wrs 1862 C	12P		81.23	19.33	0.01	0.00	100.57
wrs 1862 C	12Q		81.01	18.99	0.00	0.00	100.00
wrs 1862 C	12T		87.68	11.59	0.02	0.00	99.28
wrs 1862 C	12 R	Ag Te, PbS	78.67	20.68	0.01	0.00	99.35
wrs 1862 C	12S	FeS2	80.53	18.81	0.00	0.00	99.35
wrs 1862 E	8A		83.00	16.37	0.01	0.10	99.48
wrs 1862 E	8B		79.79	20.52	0.01	0.11	100.42
wrs 1862 E	8C		88.54	11.48	0.00	0.04	100.05
wrs 1862 E	8D		74.52	25.11	0.01	0.17	99.82
wrs 1862 E	8E		80.01	19.46	0.00	0.02	99.49
wrs 1862 E	8F		74.75	25.32	0.01	0.04	100.12
wrs 1862 E	8G		67.11	33.12	0.00	0.13	100.37
wrs 1862 E	8H		69.04	31.19	0.07	0.53	100.82
wrs 1862 E	8I		93.70	6.70	0.05	0.00	100.45
wrs 1862 E	8J		81.02	18.26	0.01	0.00	99.29
wrs 1862 E	8K		73.25	25.64	0.02	0.45	99.36
wrs 1862 E	8L		73.83	26.77	0.00	0.06	100.67
wrs 1862 E	8M		75.63	24.09	0.03	0.11	99.85
wrs 1862 E	8N		75.03	24.40	0.00	0.00	99.43
wrs 1862 E	8O		74.45	25.54	0.20	0.23	100.42
wrs 1862 E	8P		88.83	10.30	0.01	0.95	100.09
wrs 1862 E	8Q		85.92	13.74	0.00	0.00	99.67
wrs 1862 E	8R		81.56	18.39	0.00	0.00	99.94
wrs 1862 E	8S		77.64	22.32	0.11	0.04	100.11

Block	Grain ID	Inclusions	Au WT%	Ag WT%	Cu WT%	Hg WT%	TOTAL
wrs 1862 E	8T		80.63	19.41	0.01	0.17	100.21
wrs 1862 E	8U		79.87	20.30	0.01	0.00	100.18
wrs 1862 E	8V		85.59	12.19	0.02	0.02	97.82
wrs 1862 E	8X		60.35	40.69	0.01	0.00	101.06
wrs 1862 E	8Y		78.96	21.35	0.04	0.04	100.38
WRS 1862D	16A		62.06	37.74	0.02	0.00	99.82
WRS 1862D	16B		77.48	21.98	0.00	0.00	99.46
WRS 1862D	16C		77.50	22.05	0.01	0.00	99.56
WRS 1862D	16D		78.15	21.54	0.02	0.00	99.71
WRS 1862D	16E		87.14	12.69	0.02	0.00	99.85
WRS 1862D	16F		77.02	24.15	0.01	0.00	101.18
WRS 1862D	16G		75.08	24.24	0.01	0.00	99.34
WRS 1862D	16H		84.63	15.32	0.01	0.00	99.97
WRS 1862D	16I		77.38	22.69	0.00	0.00	100.07
WRS 1862D	16J		76.92	22.58	0.00	0.00	99.50
WRS 1862D	16K		82.42	17.27	0.01	0.00	99.71
WRS 1862D	16L		73.48	26.50	0.00	0.02	100.01
WRS 1862D	16M		81.01	19.06	0.00	0.00	100.07
WRS 1862D	16N		56.18	44.45	0.02	0.00	100.66
WRS 1862D	16O		72.74	27.47	0.02	0.00	100.22
WRS 1862D	16P		74.27	25.04	0.01	0.00	99.32
WRS 1862D	16Q		80.60	18.80	0.01	0.00	99.41
WRS 1862D	16R		77.16	21.72	0.02	0.00	98.90
WRS 1862D	16S		77.54	22.04	0.01	0.00	99.59
WRS 1862D	16T	CuFeS2 FeMgCaCO3	73.63	26.02	0.01	0.02	99.68
WRS 1862D	16U	FeAsS	73.20	26.52	0.02	0.03	99.76
WRS 1862D	16V		77.74	22.34	0.01	0.00	100.09
WRS 1862D	16W	FeNiAsS	88.48	11.17	0.02	0.00	99.67
wrs 1862 E	9A		75.55	25.08	0.00	0.01	100.64
wrs 1862 E	9B		94.36	6.44	0.04	0.01	100.85
wrs 1862 E	9C		79.40	21.36	0.00	0.00	100.77

Block	Grain ID	Inclusions	Au WT%	Ag WT%	Cu WT%	Hg WT%	TOTAL
wrs 1862 E	9D		78.10	23.04	0.01	0.03	101.18
wrs 1862 E	9E		95.59	4.36	0.05	0.05	100.05
wrs 1862 E	9K		71.96	28.21	0.02	0.04	100.23
wrs 1862 E	9L	FeS2/PbS	76.49	21.64	0.01	1.52	99.66
wrs 1862 E	9M		68.58	32.52	0.02	0.00	101.12
wrs 1862 E	9N		79.39	20.57	0.01	0.00	99.97
wrs 1862 E	9O		62.71	38.63	0.00	0.00	101.35
wrs 1862 E	9F		81.70	19.08	0.00	0.00	100.78
wrs 1862 E	9G		86.05	12.93	0.03	0.04	99.03
wrs 1862 E	9L		77.41	22.43	0.00	0.08	99.93
wrs 1862 E	9M		76.11	24.21	0.01	0.00	100.33
WRS 1862D	17A		96.10	3.63	0.03	0.00	99.76
WRS 1862D	17B		84.92	13.03	0.02	0.00	97.97
WRS 1862D	17C		68.44	32.03	0.01	0.00	100.48
WRS 1862D	17D		75.72	24.49	0.00	0.00	100.22
WRS 1862D	17E		90.34	8.40	0.00	0.16	98.90
WRS 1862D	17F		76.31	23.83	0.00	0.00	100.14
WRS 1862D	17G	LREE PO4	73.23	26.43	0.02	0.01	99.69
WRS 1862D	17H		74.60	24.75	0.00	0.00	99.36
WRS 1862D	17I	FeS2	93.74	5.54	0.09	0.00	99.37
WRS 1862D	17J	CuFeS2	83.40	15.02	1.18	0.02	99.61
WRS 1862D	17K		71.58	28.66	0.00	0.00	100.24
WRS 1862D	17L		97.82	1.26	0.00	0.00	99.08
WRS 1862D	17M	FeS2	96.18	2.92	0.07	0.00	99.17
WRS 1862D	17N		84.42	14.77	0.00	0.00	99.19
WRS 1862D	17O		87.63	12.01	0.03	0.00	99.67
WRS 1862D	17P		85.59	14.10	0.02	0.00	99.71
WRS 1862D	17Q		68.43	30.61	0.02	0.14	99.20
WRS 1862D	17R		96.61	2.85	0.04	0.00	99.51
WRS 1862D	17S		75.78	22.87	0.00	0.00	98.65
WRS 1862D	17T		88.25	8.85	0.00	0.65	97.75

Block	Grain ID	Inclusions	Au WT%	Ag WT%	Cu WT%	Hg WT%	TOTAL
WRS 1862D	17U		86.28	14.09	0.03	0.00	100.40
WRS 1862D	17V		83.85	14.55	0.01	0.94	99.35
WRS 1862D	17W		77.59	22.70	0.00	0.00	100.29
WRS 1862D	17X		82.04	18.29	0.00	0.00	100.33
WRS 1862D	17Y		76.27	23.78	0.02	0.00	100.08
WRS 1862D	17Z		88.69	11.06	0.02	0.00	99.77
WRS 1862A	1A	CuFeS2 Quartz, FeO, Kspar, (chlorite??)	94.42	3.55	0.93	0.00	98.90
WRS 1862A	1B		63.41	36.94	0.00	0.02	100.37
WRS 1862A	1C	FeS2/Pyrho, AgS,FeS2,FeAgS	79.69	19.61	0.03	0.08	99.41
WRS 1862A	1D	Hessite, Tourmaline, FeO, Plag, Kspar?? Cordierite?? Calcite	80.36	17.24	0.00	0.00	97.60
WRS 1862A	1E		75.72	23.72	0.01	0.00	99.44
WRS 1862A	1F		85.96	12.90	0.02	0.00	98.87
WRS 1862A	1G		65.81	34.62	0.00	0.05	100.49
WRS 1862A	1H	Rutile, Quartz, FeO, Possible Clays (AlSiFe+minor K,Ca), Kfeldspar	78.40	21.24	0.00	0.24	99.88
WRS 1862A	1I	NA Feldspar, Ti bearing FeO, Quartz, Cordorite??? O Al Si Fe minor Mg Ca Ti	79.02	20.66	0.01	0.07	99.76
WRS 1862A	1J		86.29	12.84	0.00	0.18	99.31
WRS 1862C	10A		90.05	8.74	0.04	0.21	99.04
WRS 1862C	10B		82.99	16.79	0.01	0.00	99.79
WRS 1862C	10C		79.38	21.21	0.01	0.00	100.59
WRS 1862C	10D		74.32	25.34	0.00	0.75	100.41
WRS 1862C	10E	CuFeS2	88.81	11.08	0.00	0.00	99.90
WRS 1862C	10F		77.73	22.41	0.02	0.00	100.16
WRS 1862C	10G		78.96	21.06	0.00	0.00	100.03
WRS 1862C	10H		83.42	15.77	0.00	0.00	99.18
WRS 1862C	10I		83.12	15.76	0.02	0.00	98.91
WRS 1862C	10J		70.96	29.63	0.00	0.00	100.60
WRS 1862C	10K		71.58	28.38	0.01	0.12	100.09
WRS 1862C	10L		73.31	26.05	0.00	0.00	99.36
WRS 1862C	10M		76.71	23.61	0.00	0.00	100.31

Block	Grain ID	Inclusions	Au WT%	Ag WT%	Cu WT%	Hg WT%	TOTAL
WRS 1862C	10N		67.28	32.51	0.00	0.00	99.79
WRS 1862C	10O		83.19	15.82	0.01	0.00	99.01
WRS 1862D	10A		74.81	25.19	0.01	0.00	100.01
WRS 1862D	10B		80.07	19.50	0.01	0.00	99.58
WRS 1862D	10C		79.91	19.81	0.02	0.11	99.84
WRS 1862D	10D		89.74	9.52	0.04	0.00	99.30
WRS 1862D	10E		79.02	20.80	0.00	0.00	99.82
WRS 1862D	10F		81.77	17.63	0.01	0.26	99.68
WRS 1862D	10G		82.10	18.00	0.00	0.00	100.09
WRS 1862D	10H		61.43	39.26	0.00	0.00	100.69
WRS 1862D	10I	FeS2	86.06	12.40	0.00	0.12	98.58
WRS 1862D	10J		73.84	26.39	0.00	0.00	100.24
WRS 1862D	10K		93.22	4.95	0.06	0.58	98.81
WRS 1862D	10L		87.10	10.99	0.02	0.93	99.04
WRS 1862D	10M		89.22	9.94	0.03	0.00	99.19
WRS 1862D	10N		90.22	8.84	0.03	0.05	99.14
WRS 1862D	10O	PbS, PbCuSbS, FeS2	93.10	5.72	0.04	0.00	98.86
wrs 1862 E	4A		81.94	16.13	0.00	2.06	100.14
wrs 1862 E	4B		78.57	20.03	0.01	0.56	99.17
wrs 1862 E	4C		68.86	32.64	0.00	0.00	101.50
wrs 1862 E	4D		81.31	17.87	0.01	0.23	99.42
wrs 1862 E	4E		93.80	0.62	5.39	0.00	99.80
wrs 1862 E	4F		98.98	0.86	0.01	0.00	99.84
wrs 1862 E	4G		89.74	9.43	0.02	1.36	100.56
wrs 1862 E	4H		95.04	4.87	0.06	0.45	100.42
wrs 1862 E	4I		77.84	21.44	0.00	0.07	99.36
wrs 1862 E	4I LIGHT		90.53	9.10	0.02	0.09	99.74
wrs 1862 E	4J		65.93	35.11	0.01	0.00	101.05
wrs 1862 E	4K		73.16	27.62	0.00	0.01	100.79
wrs 1862 E	4L		66.26	35.31	0.00	0.01	101.58
wrs 1862 E	4M		66.84	32.11	0.00	1.62	100.56

Block	Grain ID	Inclusions	Au WT%	Ag WT%	Cu WT%	Hg WT%	TOTAL
wrs 1862 E	4N		63.86	35.99	0.01	1.37	101.23
wrs 1862 E	4O LIGHT 1		77.70	22.25	0.01	0.00	99.96
wrs 1862 E	4O DARK3		69.53	31.79	0.01	0.00	101.34
WRS 1862A	2A		82.74	16.62	0.00	0.00	99.36
WRS 1862A	2B	U silicate/CaCO3,PbS+Se	81.24	17.46	0.01	0.00	98.70
WRS 1862A	2C		74.59	24.96	0.02	0.22	99.79
WRS 1862A	2D	FeS2	83.42	16.50	0.00	0.00	99.92
WRS 1862A	2E		67.44	33.01	0.00	0.10	100.55
WRS 1862A	2F		84.51	14.84	0.03	0.00	99.37
WRS 1862A	2G	Pb>Cu SbS, FeS2, CuFeS2	73.27	26.21	0.01	0.00	99.49
WRS 1862A	2H	FeAsS/PbS	80.77	18.26	0.02	0.48	99.52
WRS 1862C	9A		88.51	11.28	0.04	0.00	99.83
WRS 1862C	9B		83.04	16.38	0.00	0.29	99.72
WRS 1862C	9C		87.00	10.92	0.02	0.14	98.08
WRS 1862C	9D		80.33	19.96	0.00	0.00	100.29
WRS 1862C	9E		88.91	10.72	0.06	0.00	99.69
WRS 1862A	3A		78.63	21.05	0.00	0.08	99.76
WRS 1862A	3B		81.28	17.84	0.02	0.00	99.13
WRS 1862A	3C		81.27	17.68	0.01	0.45	99.41
WRS 1862A	3D		83.85	15.31	0.02	0.00	99.18
WRS 1862A	3E	CuFeS2	82.53	16.81	0.00	0.00	99.34
WRS 1862C	8A		82.16	18.26	0.00	0.00	100.43
WRS 1862C	8B		77.98	22.52	0.01	0.25	100.76
WRS 1862C	8C		93.23	6.00	0.07	0.34	99.63
WRS 1862C	8D		77.75	22.74	0.00	0.00	100.49
WRS 1862C	8E		72.47	27.64	0.00	0.00	100.11
WRS 1862C	8F		78.19	22.58	0.00	0.00	100.77
WRS 1862C	8G		69.46	30.20	0.01	0.00	99.68
WRS 1862C	8H		76.07	22.84	0.01	0.00	98.92
WRS 1862D	14A		88.49	10.45	0.06	0.00	99.00
WRS 1862D	14B		87.56	12.06	0.00	0.08	99.71

Block	Grain ID	Inclusions	Au WT%	Ag WT%	Cu WT%	Hg WT%	TOTAL
WRS 1862D	14C		63.43	37.04	0.01	0.07	100.56
WRS 1862D	14D		74.63	24.83	0.01	0.03	99.50
WRS 1862D	14E		74.08	25.43	0.00	0.04	99.55
WRS 1862D	14F	FeS2	88.95	10.10	0.00	0.28	99.33
WRS 1862D	14G		79.54	19.29	0.00	0.00	98.83
WRS 1862D	14H		73.75	26.28	0.01	0.09	100.12
WRS 1862D	14I		78.60	20.28	0.00	0.45	99.33
WRS 1862D	14J		75.63	24.28	0.00	0.02	99.93
WRS 1862D	14K		74.63	24.48	0.00	0.08	99.19
WRS 1862D	14L		88.62	10.72	0.07	0.12	99.53
WRS 1862D	14M		80.41	16.90	0.01	0.15	97.47
WRS 1862D	14N		85.08	14.53	0.00	0.00	99.61
WRS 1862D	14O		97.67	2.05	0.01	0.00	99.74
wrs 1862 E	7B	CuFeS2	73.12	27.16	0.00	0.23	100.50
wrs 1862 E	7C		77.51	22.40	0.01	0.60	100.52
wrs 1862 E	7D		80.69	18.87	0.01	0.38	99.94
wrs 1862 E	7E		81.78	18.31	0.02	0.00	100.11
wrs 1862 E	7F		75.17	24.25	0.01	0.21	99.63
wrs 1862 E	7H		71.35	0.33	0.01	28.66	100.35
wrs 1862 E	7L		71.79	28.12	0.01	0.26	100.18
wrs 1862 E	7M/1		64.42	36.81	0.00	0.08	101.31
wrs 1862 E	7M		79.42	20.61	0.00	0.22	100.24
wrs 1862 E	7P		73.09	27.76	0.00	0.27	101.11
wrs 1862 E	7Q		73.61	26.39	0.01	0.14	100.15
wrs 1862 E	7R		80.23	19.04	0.01	0.37	99.64
WRS 1862A	4A	FeNiAsS	73.05	26.65	0.00	0.00	99.70
WRS 1862A	4B		75.12	24.83	0.00	0.00	99.95
WRS 1862A	4C	FeNiAsS	84.37	15.05	0.02	0.00	99.45
WRS 1862A	4D		79.53	20.48	0.01	0.00	100.02
WRS 1862A	4E	FeS2	74.07	25.93	0.01	0.00	100.00
WRS 1862A	4F		77.46	21.75	0.00	0.00	99.21

Block	Grain ID	Inclusions	Au WT%	Ag WT%	Cu WT%	Hg WT%	TOTAL
WRS 1862A	4G	FeNiAsS+Co	72.43	27.56	0.01	0.00	100.00
WRS 1862A	4H		81.34	17.76	0.00	0.00	99.09
WRS 1862A	4I	ZnS, PbS	84.41	15.04	0.00	0.00	99.45
WRS 1862A	4J	CuFeS2	70.28	29.79	0.00	0.00	100.07
WRS 1862B	10A		83.87	15.06	0.02	0.00	98.94
WRS 1862B	10B		91.79	7.44	0.05	0.00	99.28
WRS 1862B	10C		90.24	8.44	0.01	0.00	98.69
WRS 1862B	10D		77.97	21.85	0.01	0.00	99.83
WRS 1862B	10E		76.06	22.97	0.00	0.00	99.03
WRS 1862B	10F		64.83	36.03	0.02	0.00	100.88
WRS 1862B	10G		75.47	23.20	0.01	0.00	98.68
WRS 1862B	10H		84.72	14.27	0.01	0.00	99.01
WRS 1862B	10I		72.34	24.86	0.01	0.00	97.20
WRS 1862B	10J		77.38	21.83	0.02	0.00	99.23
WRS 1862B	10K		80.00	19.48	0.01	0.00	99.49
WRS 1862B	10L		91.15	4.93	0.10	0.00	96.17
WRS 1862B	10M		77.81	19.24	0.01	0.00	97.06
WRS 1862B	10N		63.79	35.96	0.00	0.00	99.75
WRS 1862B	10O		80.25	19.32	0.01	0.00	99.58
WRS 1862B	10P		74.88	24.38	0.00	0.00	99.26
WRS 1862B	10Q		82.68	16.99	0.03	0.00	99.69
WRS 1862C	11A		91.31	9.12	0.02	0.00	100.44
WRS 1862C	11B		61.33	41.00	0.00	0.00	102.35
WRS 1862C	11C		84.54	13.75	0.03	1.83	100.14
WRS 1862C	11D		93.53	6.57	0.04	0.00	100.14
WRS 1862C	11E		90.30	9.31	0.03	0.00	99.63
WRS 1862C	11F		77.04	23.23	0.00	0.00	100.27
WRS 1862C	11G		79.79	20.07	0.00	0.00	99.86
WRS 1862C	11H	CuFeS2	73.93	26.75	0.01	0.00	100.69
WRS 1862C	11I		74.83	26.62	0.00	0.00	101.45
WRS 1862C	11J		81.91	18.51	0.02	0.10	100.54

Block	Grain ID	Inclusions	Au WT%	Ag WT%	Cu WT%	Hg WT%	TOTAL
WRS 1862C	11K		66.54	34.37	0.00	0.00	100.91
WRS 1862C	11L		81.63	19.17	0.00	0.00	100.80
WRS 1862C	11M		75.90	24.70	0.01	0.00	100.61
WRS 1862C	11N		86.90	13.52	0.03	0.00	100.45
WRS 1862C	11O		88.86	10.71	0.01	0.00	99.59
WRS 1862C	11P		79.67	19.99	0.00	0.00	99.66
WRS 1862C	11Q		69.86	31.73	0.00	0.00	101.60
WRS 1862C	11R		76.41	24.36	0.00	0.00	100.77
WRS 1862C	11S		78.08	22.12	0.00	0.00	100.20
WRS 1862C	11T		94.99	4.05	0.04	0.11	99.19
WRS 1862C	11U		95.66	3.48	0.04	0.00	99.18
WRS 1862C	11V		76.62	23.20	0.00	0.00	99.82
WRS 1862C	11W		73.71	26.44	0.01	0.00	100.15
WRS 1862C	11X		77.72	22.39	0.00	0.00	100.11
WRS 1862C	11Y		61.06	40.17	0.01	0.00	101.23
WRS 1862D	11A		83.72	15.72	0.03	0.00	99.47
WRS 1862D	11B		83.93	15.53	0.01	0.00	99.47
WRS 1862D	11C	pyrrhotite	75.85	24.64	0.00	0.00	100.49
WRS 1862D	11D		76.63	23.30	0.00	0.00	99.93
WRS 1862D	11E		85.93	13.18	0.01	0.00	99.13
WRS 1862D	11F		85.06	14.28	0.01	0.00	99.35
WRS 1862D	11G	pyrite	72.57	27.34	0.01	0.18	100.09
WRS 1862D	11H		82.89	16.96	0.00	0.00	99.85
WRS 1862D	11I		66.61	33.48	0.00	0.02	100.11
WRS 1862D	11J	BaAl silicate	82.47	17.47	0.01	0.00	99.94
WRS 1862D	11K	FeS2	74.14	26.04	0.01	0.00	100.19
WRS 1862D	11L		68.73	31.50	0.00	0.00	100.23
WRS 1862D	11M		96.55	3.46	0.12	0.00	100.13
WRS 1862D	11N		87.43	11.32	0.02	0.00	98.76
WRS 1862D	11O	FeS2	65.47	34.87	0.00	0.14	100.48
WRS 1862D	11P		80.29	19.13	0.02	0.00	99.43

Block	Grain ID	Inclusions	Au WT%	Ag WT%	Cu WT%	Hg WT%	TOTAL
WRS 1862D	11Q		80.17	19.90	0.01	0.00	100.08
WRS 1862D	11R LIGHT		98.16	1.16	0.00	0.00	99.32
WRS 1862D	11R DARK		66.72	33.02	0.00	0.00	99.75
WRS 1862D	11S		76.25	23.52	0.02	0.00	99.78
WRS 1862D	11T	FeS2	74.82	24.18	0.00	0.00	99.00
WRS 1862D	11U		79.10	20.86	0.01	0.00	99.96
WRS 1862D	11V		63.14	37.40	0.00	0.00	100.54
WRS 1862D	11W		85.86	13.20	0.00	0.00	99.07
WRS 1862D	11X	CaTi silicate	93.91	2.30	1.87	0.59	98.66
WRS 1862D	11Y		77.46	21.67	0.00	0.00	99.13
WRS 1862D	11Z		78.27	21.25	0.01	0.00	99.52
WRS 1862D	11A1		67.61	32.54	0.00	0.00	100.15
WRS 1862D	11B1	FeS2	68.38	32.71	0.00	0.00	101.09
WRS 1862D	11C1		81.71	17.48	0.01	0.00	99.20
WRS 1862D	11D1		82.66	16.97	0.01	0.25	99.89
wrs 1862 E	5A		96.11	3.65	0.05	0.01	99.82
wrs 1862 E	5B		67.09	33.19	0.00	0.04	100.32
wrs 1862 E	5C		75.99	24.30	0.04	0.02	100.35
wrs 1862 E	5D		88.50	11.29	0.02	0.19	100.00
wrs 1862 E	5E		64.95	36.01	0.00	0.03	100.99
wrs 1862 E	5F		81.89	18.23	0.00	0.08	100.20
wrs 1862 E	5G LIGHT 1		73.46	23.59	0.02	0.00	97.07
wrs 1862 E	5G DARK 3		43.59	59.40	0.01	0.21	103.21
wrs 1862 E	5H		57.69	43.61	0.01	0.07	101.38
wrs 1862 E	5I		65.79	35.04	0.00	0.00	100.84
wrs 1862 E	5J		81.97	18.07	0.01	0.08	100.13
WRS 1862A	5A		89.28	9.92	0.01	0.00	99.22
WRS 1862A	5B		80.20	18.07	0.02	0.00	98.29
WRS 1862A	5C		84.89	14.67	0.02	0.00	99.58
WRS 1862A	5D		75.14	24.74	0.01	0.00	99.90
WRS 1862A	5E		73.06	26.63	0.00	0.00	99.70

Block	Grain ID	Inclusions	Au WT%	Ag WT%	Cu WT%	Hg WT%	TOTAL
WRS 1862A	5F		79.05	20.58	0.01	0.00	99.64
WRS1862D	13A		71.89	27.84	0.01	0.08	99.81
WRS1862D	13B		75.96	24.60	0.00	0.00	100.57
WRS1862D	13C		73.79	25.40	0.01	0.05	99.25
wrs 1822C	11A		88.27	11.63	0.05	0.00	99.96
wrs 1822C	11B		83.53	16.30	0.02	0.00	99.85
wrs 1822C	11C		74.84	24.79	0.00	0.00	99.63
wrs 1822C	11D		92.46	7.24	0.03	0.00	99.73
wrs 1822C	11E		87.45	12.09	0.04	0.00	99.59
wrs 1822C	11F		81.50	18.33	0.04	0.00	99.87
wrs 1822C	11G		75.70	24.31	0.02	0.00	100.03
wrs 1822C	11H		75.53	25.49	0.02	0.00	101.04
wrs 1822A	18A		92.66	6.42	0.14	0.00	99.22
wrs 1822A	18B		78.52	21.45	0.00	0.00	99.97
wrs 1822A	18C		87.67	11.93	0.04	0.00	99.64
wrs 1822A	18D		84.37	15.48	0.03	0.00	99.88
wrs 1822A	18E		81.72	19.02	0.02	0.00	100.76
wrs 1822A	18F		86.66	13.04	0.07	0.00	99.77
wrs 1822A	18G		90.11	9.35	0.05	0.00	99.51
wrs 1822A	18H		86.90	12.95	0.02	0.00	99.87
wrs 1822A	18I		78.80	21.09	0.03	0.03	99.94
wrs 1822B	16A		85.21	13.95	0.03	0.00	99.20
wrs 1822B	16B		88.78	10.19	0.04	0.00	99.00
wrs 1822B	16C		73.75	26.50	0.01	0.00	100.26
wrs 1822B	16D		83.61	15.81	0.04	0.00	99.46
wrs 1822B	16E		74.61	25.36	0.02	0.00	100.00
wrs 1822B	16F		88.13	11.50	0.04	0.00	99.67
wrs 1822B	16G		86.38	12.94	0.03	0.00	99.35
wrs 1822B	16H		80.56	18.80	0.00	0.00	99.36
wrs 1822B	16J		82.92	16.03	0.03	0.00	98.98
wrs 1822B	16K		84.20	15.51	0.03	0.00	99.73

Block	Grain ID	Inclusions	Au WT%	Ag WT%	Cu WT%	Hg WT%	TOTAL
wrs 1822B	16L		72.64	27.32	0.01	0.00	99.97
wrs 1822B	16M		91.12	8.28	0.04	0.00	99.44
wrs 1822B	16N		85.09	14.20	0.03	0.00	99.33
wrs 1822B	16O		85.83	13.04	0.04	0.00	98.91
wrs 1822B	16P		84.10	14.48	0.02	0.00	98.60
wrs 1822B	16Q		83.05	16.59	0.04	0.00	99.68
wrs 1822B	16R		78.92	20.31	0.02	0.00	99.25
wrs 1822B	16S		86.89	11.94	0.07	0.00	98.90
wrs 1822B	16T		76.44	23.17	0.02	0.00	99.62
wrs 1822B	16U		88.82	10.10	0.04	0.00	98.96
wrs 1822B	16V		70.89	29.24	0.01	0.00	100.14
wrs 1822D	5A		75.97	23.76	0.02	0.00	99.74
wrs 1822D	5B		76.29	24.10	0.01	0.00	100.40

Atlin LA-ICP-MS Data

Full Grain ID	LA Size	Date run	Deposit	S_ppm	Ti_ppm	V_ppm	Cr_ppm	Mn_ppm	Fe_ppm	Co_ppm	Ni_ppm	Cu_ppm
1822C_11D	50	31/08/2016	Feather Ck	124.6626								159.3249
1822C_11B	50	31/08/2016	Feather Ck	111.2583								32.42062
1822C_11C	50	31/08/2016	Feather Ck	103.7765						0.220587		21.74354
1822C_11A	50	31/08/2016	Feather Ck	163.1822								195.1308
1822C_11F	50	31/08/2016	Feather Ck	157.733								216.6807
1822C_11G	50	31/08/2016	Feather Ck	170.7707			1.453446					45.91041
1822C_11H	50	31/08/2016	Feather Ck	91.02329								24.88128
1822A_18B	50	05/09/2016	Feather Ck	175.8447	6.818104	0.328353		19.21403	320.3674	0.154321	0.48691	19.13107
1822A_18D	50	05/09/2016	Feather Ck	123.804							0.523157	107.2412
1822A_18C	50	05/09/2016	Feather Ck	129.4552		0.076072					0.486579	67.63052
1822A_18F	50	05/09/2016	Feather Ck			0.06295					0.953439	338.3802
1822A_18E	50	05/09/2016	Feather Ck								0.715308	31.57629
1822A_18A	50	05/09/2016	Feather Ck									1414.997
1822A_18J	50	05/09/2016	Feather Ck	454.556								30.72069
1822A_18G	50	05/09/2016	Feather Ck	506.7085								64.45361
1822A_18H	50	05/09/2016	Feather Ck	464.1044	5.045515	1.842244		45.7727	1819.422	0.231943	1.613119	174.4936
1822A_18I	50	05/09/2016	Feather Ck	546.6843	11.5211	0.3866		25.53263	345.6993	0.23359	1.20245	97.28884
1822C_12E	50	31/08/2016	Ruby Ck					1.473482		0.011014	0.664384	33.56096
1822C_12A	50	31/08/2016	Ruby Ck									75.33329
1822C_12B	50	31/08/2016	Ruby Ck								0.211544	50.36456
1822C_12C	50	31/08/2016	Ruby Ck		452.0675	7.385853	25.49109	516.3004	12158.99	8.165041	188.6504	18.70801
1822C_12D	50	31/08/2016	Ruby Ck				1.926623				0.353336	31.75788
1822C_12I	50	31/08/2016	Ruby Ck	138.0293								42.60632
1822C_12J	50	31/08/2016	Ruby Ck	104.3348								43.11153
1822C_12G	50	31/08/2016	Ruby Ck	98.49366								20.30504
1822C_12H	50	31/08/2016	Ruby Ck	120.0567								1064.681
1822C_12K	50	31/08/2016	Ruby Ck	92.66247								56.05313
1822C_12F	50	31/08/2016	Ruby Ck	154.4919	8.192342	4.104646	5.130199	30.96413	2743.063	0.970335	18.09598	64.71316

Full Grain ID	LA Size	Date run	Deposit	S_ppm	Ti_ppm	V_ppm	Cr_ppm	Mn_ppm	Fe_ppm	Co_ppm	Ni_ppm	Cu_ppm
1822C_12S	50	31/08/2016	Ruby Ck	259.4447		0.231206						121.0808
1822C_12R	50	31/08/2016	Ruby Ck	230.5803								87.90296
1822C_12V	50	31/08/2016	Ruby Ck	175.6342								98.54283
1822C_13B	50	31/08/2016	Ruby Ck	109.9369								16.10802
1822C_13A	50	31/08/2016	Ruby Ck	2585.828	3.296721	8.678001	52.40974	52.76781	7785.956	447.5618	3478.944	184.9859
1822C_13C	50	31/08/2016	Ruby Ck	124.215	9.023164	0.134907		5.162036	131.0406	0.059177	3.699021	84.70312
RJC65_7,1	50	08/02/2018	Boulder CK									68.27602
RJC65_7,2	50	08/02/2018	Boulder CK									64.34301
RJC65_7,3	50	08/02/2018	Boulder CK									16.46588
RJC65_7,4	50	08/02/2018	Boulder CK								2.562274	83.21255
RJC65_7,5	50	08/02/2018	Boulder CK									65.24951
RJC65_7,6	50	08/02/2018	Boulder CK									266.2944
RJC65_7,7	50	08/02/2018	Boulder CK									247.6567
RJC65_7,8	50	08/02/2018	Boulder CK									55.3048
RJC65_7,9	50	08/02/2018	Boulder CK									20.03259
RJC65_7,10	50	08/02/2018	Boulder CK									207.7565
RJC65_7,11	50	08/02/2018	Boulder CK									73.20877
RJC65_7,11 INCLUSION	50	08/02/2018	Boulder CK			19.55619	983.598	117.8733	27076.32	23.88869	965.2492	106.3292
RJC65_7,12	50	08/02/2018	Boulder CK						5210.703	196.0342	9312.046	2687.263
RJC65_7,13	50	08/02/2018	Boulder CK									1575.185
RJC65_7,14	50	08/02/2018	Boulder CK									563.296
RJC65_7,15	50	08/02/2018	Boulder CK									42.42641
RJC65_7,16	50	08/02/2018	Boulder CK									3.202794
RJC65_10,1	100	08/02/2018	Wright Ck									282.527
RJC65_10,2	50	08/02/2018	Wright Ck									27.66435
RJC65_9,1	50	08/02/2018	Ruby Ck									35.97454
RJC65_9,2	50	08/02/2018	Ruby Ck									29.62271
RJC65_9,3	50	08/02/2018	Ruby Ck									119.1955
RJC65_9,4	50	08/02/2018	Ruby Ck									94.43138
RJC65_9,4?	50	08/02/2018	Ruby Ck									89.59912
RJC65_9,7	50	08/02/2018	Ruby Ck									2.565722

Full Grain ID	LA Size	Date run	Deposit	S_ppm	Ti_ppm	V_ppm	Cr_ppm	Mn_ppm	Fe_ppm	Co_ppm	Ni_ppm	Cu_ppm
RJC65_9,8	50	08/02/2018	Ruby Ck									52.56951
RJC65_9,9	50	08/02/2018	Ruby Ck					91.35457	105.13		1.372978	421.8523
RJC65_9,10	50	08/02/2018	Ruby Ck									94.96838
RJC65_9,11	50	08/02/2018	Ruby Ck									831.4837
RJC65_9,12	50	08/02/2018	Ruby Ck									68.67789
RJC65_9,13	50	08/02/2018	Ruby Ck									97.9553
RJC65_9,14	50	08/02/2018	Ruby Ck									26.27936
RJC65_9,15	50	08/02/2018	Ruby Ck									49.62467
RJC65_9,16	50	08/02/2018	Ruby Ck									76.43721
RJC65_9,17	50	08/02/2018	Ruby Ck					3.249608				63.21976
RJC65_9,17 INCLUSION	50	08/02/2018	Ruby Ck			11.85004	49.25259	3445.767	10977.14	22.53846	238.7522	71.15922
RJC65_9,18	50	08/02/2018	Ruby Ck					3.663411				23317.81
RJC65_9,19	50	08/02/2018	Ruby Ck					4.034422				58.60099
RJC65_9,20	50	08/02/2018	Ruby Ck									273.0754
RJC65_9,21	50	08/02/2018	Ruby Ck									110.0048
RJC65_12,1	25	08/02/2018	Spruce Ck									
RJC65_12,2	25	08/02/2018	Spruce Ck									
RJC65_12,3	25	08/02/2018	Spruce Ck									
RJC65_12,4	25	08/02/2018	Spruce Ck									
RJC65_12,5	50	08/02/2018	Spruce Ck									11.30786
RJC65_12,6	25	08/02/2018	Spruce Ck									225.5688
RJC65_12,7	25	08/02/2018	Spruce Ck									136.2697
RJC65_12,8	25	08/02/2018	Spruce Ck									172.5714
RJC65_12,9	25	08/02/2018	Spruce Ck									1313.176
RJC65_12,10	25	08/02/2018	Spruce Ck									
RJC67_11,2	25	12/02/2018	OC Au vein									198.6514
RJC67_11,1	25	12/02/2018	OC Au vein							1.096027		34.70175
RJC70_1,1	50	12/02/2018	Ruby Ck									207.4843
RJC70_1,1	100	12/02/2018	Ruby Ck									198.8249
RJC70_1,2	50	12/02/2018	Ruby Ck									54.03382
RJC70_1,3	50	12/02/2018	Ruby Ck									38.61467

Full Grain ID	LA Size	Date run	Deposit	S_ppm	Ti_ppm	V_ppm	Cr_ppm	Mn_ppm	Fe_ppm	Co_ppm	Ni_ppm	Cu_ppm
RJC70_1,4	50	12/02/2018	Ruby Ck									59.27121
RJC70_1,5	50	12/02/2018	Ruby Ck									68.80707
RJC70_1,5b	50	12/02/2018	Ruby Ck									70.27207
RJC70_2,1	50	12/02/2018	Wright Ck									113.3099
RJC70_2,1	50	12/02/2018	Wright Ck									88.49368
RJC70_2,2	50	12/02/2018	Wright Ck									122.3118
RJC70_3,1	50	12/02/2018	Otter Ck									423.5494
RJC70_3,2	50	12/02/2018	Otter Ck									236.9107
RJC70_3,3	50	12/02/2018	Otter Ck									200.9443
RJC70_3,4	50	12/02/2018	Otter Ck									136.0633
RJC70_3,5	50	12/02/2018	Otter Ck									122.5023
RJC70_3,6	50	12/02/2018	Otter Ck									92.74235
RJC70_3,7	50	12/02/2018	Otter Ck									97.45759
RJC70_3,8	50	12/02/2018	Otter Ck									114.9449
RJC70_3,9	50	12/02/2018	Otter Ck									66.34974
RJC70_3,10	50	12/02/2018	Otter Ck									66.74137
RJC70_3,11	50	12/02/2018	Otter Ck									102.4969
RJC70_3,12	50	12/02/2018	Otter Ck									67.30555
RJC70_3,13	50	12/02/2018	Otter Ck									95.86441
RJC70_3,14	50	12/02/2018	Otter Ck									115.6847
RJC70_3,15	50	12/02/2018	Otter Ck									26.74804
RJC70_3,16	50	12/02/2018	Otter Ck									120.5364
RJC70_3,17	50	12/02/2018	Otter Ck				13.00338					58.47103
RJC70_3,18	50	12/02/2018	Otter Ck									106.1457
RJC70_3,19	50	12/02/2018	Otter Ck									116.7124
RJC70_3,20	50	12/02/2018	Otter Ck									179.9788
RJC70_3,21	50	12/02/2018	Otter Ck									143.293
RJC70_3,22	50	12/02/2018	Otter Ck									44.68886
RJC70_3,23	50	12/02/2018	Otter Ck									209.4797
RJC70_3,24	50	12/02/2018	Otter Ck									73.13928

Full Grain ID	Zn_ppm	Ga_ppm	Ge_ppm	As_ppm	Se_ppm	Y_ppm	Nb_ppm	Mo_ppm	Rh_ppm	Pd_ppm	Ag_ppm
1822C_11D										0.1743364	65488.7985
1822C_11B											166106.209
1822C_11C								5.87114446			238250.855
1822C_11A									0.01853247	0.49093638	98864.775
1822C_11F											184615.112
1822C_11G								0.11745877			225234.69
1822C_11H											244058.67
1822A_18B	2.14844123			0.86957154		0.04422621	0.00889628	0.21472408			296766.594
1822A_18D									0.02692494		171099.141
1822A_18C										1.69245534	131781.031
1822A_18F									0.04780759	0.09081312	148658.305
1822A_18E								0.07184644			207262.422
1822A_18A											88300.4588
1822A_18J											213139.935
1822A_18G								0.10451846			238515.822
1822A_18H	4.43660485	0.10078478		0.89384123		0.06896332		0.18084186	0.02284067		101497.756
1822A_18I	1.19584299	0.19744505				0.05633262		0.14244476			139491.121
1822C_12E								0.04014416			273532.319
1822C_12A											222955.917
1822C_12B						0.0062666					282656.691
1822C_12C	89.60707	1.56371367		24.8129483		5.91233017	4.12720617	0.50943323			220213.296
1822C_12D								0.05155561			40980
1822C_12I											258287.696
1822C_12J										0.11269664	292454.413
1822C_12G											174304.313
1822C_12H									0.02288906	0.06837674	150189.312

Full Grain ID	Zn_ppm	Ga_ppm	Ge_ppm	As_ppm	Se_ppm	Y_ppm	Nb_ppm	Mo_ppm	Rh_ppm	Pd_ppm	Ag_ppm
1822C_12K	0.44299597										188640.705
1822C_12F	8.19033756	0.25647149		1.22572221		0.64547524	0.11351373	0.18177641			166972.185
1822C_12S	0.44635715							0.05259014			174528.836
1822C_12R				0.29306859					0.01575013		203386.496
1822C_12V										0.09379385	213764.957
1822C_13B				0.59742946						0.05665048	437303.867
1822C_13A	10.995537	0.47109312		6284.04106		2.25965611		0.06890278	0.00935997	0.0505318	288593.357
1822C_13C	2.63920246	0.16327045		0.84421886		0.08721454	0.02337649	0.05951392			165741.596
RJC65_7,1						NA			0.15506129		249511.268
RJC65_7,2						NA					229920.528
RJC65_7,3						NA					352809.302
RJC65_7,4						NA					195987.488
RJC65_7,5						NA					238437.873
RJC65_7,6						NA					233815.535
RJC65_7,7						NA				1.07975387	196052.882
RJC65_7,8						NA					226877.886
RJC65_7,9						NA			0.07314394		230487.367
RJC65_7,10						NA			0.09154448		179310.487
RJC65_7,11						NA				0.81987875	171498.61
RJC65_7,11 INCLUSION	96.4220361	2.87771758		26.7538955		NA	0.3590787			1.16216463	170983.083
RJC65_7,12				17.4203626		NA			0.20917402		171888.3
RJC65_7,13						NA			0.0876525	0.62468204	117530.779
RJC65_7,14						NA				1.02894886	108445.033
RJC65_7,15		0.13305924				NA					207108.195
RJC65_7,16				2.34874507		NA					494326.387
RJC65_10,1						NA					121912.185
RJC65_10,2						NA					226945.864
RJC65_9,1						NA					234819.69

Full Grain ID	Zn_ppm	Ga_ppm	Ge_ppm	As_ppm	Se_ppm	Y_ppm	Nb_ppm	Mo_ppm	Rh_ppm	Pd_ppm	Ag_ppm
RJC65_9,2						NA			0.11837649		280942.865
RJC65_9,3						NA					201818.699
RJC65_9,4						NA					220841.614
RJC65_9,4?						NA			0.0459921		219743.589
RJC65_9,7						NA					475486.397
RJC65_9,8						NA					272603.839
RJC65_9,9						NA				30.5700192	207466.606
RJC65_9,10						NA					189539.856
RJC65_9,11				0.88586475		NA					210067.842
RJC65_9,12						NA				0.52830507	246339.156
RJC65_9,13						NA				2.24425766	218095.454
RJC65_9,14						NA					478207.452
RJC65_9,15						NA					279622.554
RJC65_9,16						NA					227049.521
RJC65_9,17						NA					247798.382
RJC65_9,17 INCLUSION	55.548837	4.27181498		33.8541691	85.6052563	NA	6.27048099	1.00499546			193895.085
RJC65_9,18					36.3604368	NA			0.87476737	4.55055722	90724.4811
RJC65_9,19						NA					263121.516
RJC65_9,20					35.0346779	NA					103195.209
RJC65_9,21						NA			0.14821117		218170.833
RJC65_12,1						NA					170404.743
RJC65_12,2						NA					85980.6392
RJC65_12,3						NA					151178.052
RJC65_12,4						NA					168049.227
RJC65_12,5						NA					288864.74
RJC65_12,6						NA					103918.63
RJC65_12,7						NA					157205.604
RJC65_12,8						NA					260820.452

Full Grain ID	Zn_ppm	Ga_ppm	Ge_ppm	As_ppm	Se_ppm	Y_ppm	Nb_ppm	Mo_ppm	Rh_ppm	Pd_ppm	Ag_ppm
RJC65_12,9						NA					138193.976
RJC65_12,10						NA					418764.248
RJC67_11,2											82296.796
RJC67_11,1											375071.065
RJC70_1,1		0.06403312							0.08638304		133506.87
RJC70_1,1									0.08430378		134153.824
RJC70_1,2											264583.05
RJC70_1,3											299364.188
RJC70_1,4											165115.432
RJC70_1,5											209012.317
RJC70_1,5b											180318.514
RJC70_2,1											243962.766
RJC70_2,1	0.44956919								0.04601744		233514.47
RJC70_2,2											211202.221
RJC70_3,1											184075.85
RJC70_3,2											142416.357
RJC70_3,3											56871.9178
RJC70_3,4											242677.425
RJC70_3,5											206098.05
RJC70_3,6											169466.377
RJC70_3,7											237430.348
RJC70_3,8											203354.637
RJC70_3,9											262132.334
RJC70_3,10											221525.501
RJC70_3,11											198997.136
RJC70_3,12											244829.707
RJC70_3,13											260324.625
RJC70_3,14											224347.216

Full Grain ID	Zn_ppm	Ga_ppm	Ge_ppm	As_ppm	Se_ppm	Y_ppm	Nb_ppm	Mo_ppm	Rh_ppm	Pd_ppm	Ag_ppm
RJC70_3,15											182643.881
RJC70_3,16											186132.503
RJC70_3,17											297253.164
RJC70_3,18											229199.68
RJC70_3,19									0.16850026		241930.371
RJC70_3,20											167026.944
RJC70_3,21											235172.586
RJC70_3,22											303023.296
RJC70_3,23											235816.221
RJC70_3,24											270167.759

Full Grain ID	Cd_ppm	In_ppm	Sn_ppm	Sb_ppm	Te_ppm	La_ppm	W_ppm	Pt_ppm	Au_ppm	Hg_ppm	Pb_ppm	Bi_ppm	Th_ppm	U_ppm
1822C_11D			0.16991179	4.93938614					933921.768	300.021315		0.1406919		
1822C_11B			0.15360265	4.81484259	0.33702957				832135.569	1609.23763				
1822C_11C			0.12023857	2.06273158	0.59636591				760774.801	829.886157	8.41701892	1.64956583		
1822C_11A			0.1000794	0.14697131					900482.492	293.642729		0.02030777		
1822C_11F				128.090072	0.36097735				814511.635	370.351309	0.02614804	0.0111081		
1822C_11G		0.00547412		1.32629102	0.5395975				773769.02	775.967551	0.19927628			
1822C_11H				0.27672631	0.51937057				755664.783	159.846431				
1822A_18B			0.57859845	193.371407	0.55552764	0.03059897	0.10291619		701339.786	1142.84376	8.29200389	2.19251653	0.01371029	0.00838495
1822A_18D				5.61726895					827307.645	1356.00161				
1822A_18C			0.23157343	3.78606045	0.63735879	0.00795262			867461.151	552.224598		1.5893418		
1822A_18F			0.34177218	3.03291843					850207.346	791.304895	0.13469665			
1822A_18E			0.31361906	0.57980886	1.67705826		0.04783636		792225.245	477.163982		0.18121531	0.00591747	
1822A_18A									909676.02	608.524159				
1822A_18J			0.30119942	15.101377					781782.427	4576.41878		0.54070827		
1822A_18G				11.8344776	1.11786121		0.06356327		759993.939	905.659047		0.29717999		
1822A_18H				1.80772306		0.0211877	0.21995923		894576.185	1373.23281	26.1831782	6.29782479	0.03850628	0.02961624
1822A_18I			0.70712001	1.2548994	2.87771505	0.05508429	0.12512975		857982.616	1482.00257	7.27143071	1.7978795	0.03082032	
1822C_12E				919.686891	0.36728277				724081.269	1430.59257		0.01475588		
1822C_12A	0.49471983			11.4307961	0.5916215				776243.136	713.096555				
1822C_12B	0.31275903			8.32551702	0.68845971				715340.213	1943.18671				
1822C_12C	1.39341068	0.03089162	0.90418327	1.66595007	1.60024481	1.15395355	11.0395801	0.03546661	763547.131	2702.725 31	8.05776973	1.32735772	1.94572484	5.39742426

Full Grain ID	Cd_ppm	In_ppm	Sn_ppm	Sb_ppm	Te_ppm	La_ppm	W_ppm	Pt_ppm	Au_ppm	Hg_ppm	Pb_ppm	Bi_ppm	Th_ppm	U_ppm
1822C_12D			0.19504247		0.45048777				864393.76	94591.5051				
1822C_12I				134.55809					740904.737	492.111862	0.10300135	0.15869273		
1822C_12J				11.7317567	0.64789762				704283.36	3102.28912				
1822C_12G				6.83509112					823537.966	2032.08069		0.00616851		
1822C_12H	2.62370796			0.94399032					848479.681	142.583302		0.02656454		
1822C_12K				0.85443635					806249.126	4960.15547				
1822C_12F			0.15204639	0.10964947	1.52907579	0.03857238	0.27684092		827821.505	2162.45942	0.82033697	0.06046499	0.09229803	0.43167351
1822C_12S	0.46874099		0.33307328	44.8228174			0.04720796		821168.437	3875.68756	0.11129236			
1822C_12R				11.5336278					795632.911	650.209813	0.05712491			
1822C_12V				1.46128438					783542.198	2417.06556	0.04683644			
1822C_13B			1.09045631	4346.63643		0.00629091			558128.697	92.7917401	0.05721743	0.15546687		
1822C_13A			0.64017341	26.7090993	4.12786663	0.35933541	0.57500449		688454.885	2012.73063	4.90583758	3.06975438	0.01130359	0.30388302
1822C_13C			0.20076023	9.35099045	0.82690634	0.00998931	0.03441939		832826.333	1059.5637	0.06947631	0.02282522	0.02099687	0.11768973
RJC65_7,1				2.57592719		NA	NA		747459.469	2958.25576			NA	NA
RJC65_7,2				3.9631599		NA	NA		769709.338	301.827916			NA	NA
RJC65_7,3				25.7511694		NA	NA		646905.175	243.166459		0.13947729	NA	NA
RJC65_7,4			1.25455313	3.75634897		NA	NA		803758.24	163.485932			NA	NA
RJC65_7,5	0.61219152			9.99063332		NA	NA		760645.86	840.337761		0.07704475	NA	NA
RJC65_7,6	2.41249081			0.77263882		NA	NA		764954.393	960.041452		0.55128796	NA	NA
RJC65_7,7	1.36781214			1.81965125		NA	NA		801683.206	2011.98821			NA	NA
RJC65_7,8				17.9174134		NA	NA		769935.195	3113.69693			NA	NA
RJC65_7,9				1.09224676		NA	NA		768898.39	592.676498		0.36892294	NA	NA

Full Grain ID	Cd_ppm	In_ppm	Sn_ppm	Sb_ppm	Te_ppm	La_ppm	W_ppm	Pt_ppm	Au_ppm	Hg_ppm	Pb_ppm	Bi_ppm	Th_ppm	U_ppm
RJC65_7,10				4.46245819		NA	NA		818827.458	1649.74436			NA	NA
RJC65_7,11				3.07234079		NA	NA		828297.928	126.360929			NA	NA
RJC65_7,11 INCLUSION		0.09438846		2.42973959		NA	NA		799376.692	186.142807	31.1649429		NA	NA
RJC65_7,12	3.90220889	0.05112406	1.29455014	3335.83941		NA	NA		807085.718	238.650524		22.5677126	NA	NA
RJC65_7,13	10.3128879			1.43228384		NA	NA		879477.55	1404.02807			NA	NA
RJC65_7,14	1.95269259			0.3858203		NA	NA		886699.877	4288.42588			NA	NA
RJC65_7,15	0.35721599			4.69704552		NA	NA		792632.024	212.113555		0.05394707	NA	NA
RJC65_7,16				3931.46118		NA	NA		500811.897	924.125373		0.57763726	NA	NA
RJC65_10,1				2.65557022		NA	NA		877700.575	102.056897			NA	NA
RJC65_10,2				0.33904548		NA	NA		772501.912	524.220252			NA	NA
RJC65_9,1				2.59984412		NA	NA		762389.394	2752.34239			NA	NA
RJC65_9,2		0.05165388	2.61135776	30.1446122		NA	NA		718930.614	56.4748116		7.49705387	NA	NA
RJC65_9,3	0.57487334			150.998729		NA	NA		795997.256	1913.27616			NA	NA
RJC65_9,4	0.4061894			0.84025862		NA	NA		778278.035	784.672839			NA	NA
RJC65_9,4?				0.49299646		NA	NA		779275.11	891.16196			NA	NA
RJC65_9,7				189.031951		NA	NA		518677.158	5644.50923	0.33838822		NA	NA
RJC65_9,8				9.75575477		NA	NA		724651.85	2681.73598	0.2493102		NA	NA
RJC65_9,9				35.3856357	2.31041526	NA	NA		791798.067	42.8374593	3.38361013	1.13015039	NA	NA
RJC65_9,10				0.95225682		NA	NA		810107.387	256.552947	0.28347581		NA	NA
RJC65_9,11	2.37634695		1.36598439	19.0080201		NA	NA		789022.365	53.9294553	0.22961149	0.51403026	NA	NA
RJC65_9,12				1.74703539		NA	NA		753355.039	234.668511	0.18394038		NA	NA
RJC65_9,13				0.86818537		NA	NA		781720.493	82.750646	0.23425709		NA	NA

Full Grain ID	Cd_ppm	In_ppm	Sn_ppm	Sb_ppm	Te_ppm	La_ppm	W_ppm	Pt_ppm	Au_ppm	Hg_ppm	Pb_ppm	Bi_ppm	Th_ppm	U_ppm
RJC65_9,14				116.892104		NA	NA		521505.423	143.394938		0.55857297	NA	NA
RJC65_9,15						NA	NA		719805.793	522.028707			NA	NA
RJC65_9,16				0.84711241		NA	NA		771996.89	876.303737			NA	NA
RJC65_9,17				3.7968128		NA	NA	0.41743155	751381.8	749.134768			NA	NA
RJC65_9,17 INCLUSION			10.199657	4.83115794		NA	NA		790234.596	812.096849	34.2500317	5.62091145	NA	NA
RJC65_9,18	17.231562	0.0476508		50.1520985		NA	NA		885720.622	124.210246			NA	NA
RJC65_9,19				5.44325859		NA	NA		735939.949	868.725888	1.66346808	0.06671869	NA	NA
RJC65_9,20	1.02762832			4.86933002		NA	NA		896420.459	70.3243611			NA	NA
RJC65_9,21	0.89673315			0.73534416		NA	NA		780384.919	1332.46333			NA	NA
RJC65_12,1						NA	NA		829619.334	-24.0775274			NA	NA
RJC65_12,2						NA	NA		911957.77	2061.59076			NA	NA
RJC65_12,3						NA	NA		801545.46	47276.4878			NA	NA
RJC65_12,4						NA	NA		827780.545	4170.22763			NA	NA
RJC65_12,5				5.3066237		NA	NA		710563.627	555.017799			NA	NA
RJC65_12,6						NA	NA		895181.516	674.285264			NA	NA
RJC65_12,7						NA	NA		839685.368	2972.75826			NA	NA
RJC65_12,8						NA	NA		736495.735	2511.24093			NA	NA
RJC65_12,9						NA	NA		859665.635	827.21302			NA	NA
RJC65_12,10						NA	NA		579992.35	1243.40173			NA	NA
RJC67_11,2									917124.885	379.667952			NA	NA
RJC67_11,1				62.4608708					624630.078	200.598359			NA	NA

Full Grain ID	Cd_ppm	In_ppm	Sn_ppm	Sb_ppm	Te_ppm	La_ppm	W_ppm	Pt_ppm	Au_ppm	Hg_ppm	Pb_ppm	Bi_ppm	Th_ppm	U_ppm
RJC70_1,1	0.48030836			60.7608806				0.16300914	866209.025	14.9487609		0.11767715	NA	NA
RJC70_1,1	0.48292872			65.1302033	0.24374307			0.19896579	865569.159	11.9250573		0.12652014	NA	NA
RJC70_1,2				10.690656					735087.146	265.079413			NA	NA
RJC70_1,3				4.56688461					700025.041	567.589102			NA	NA
RJC70_1,4				23.1689375					834764.105	38.0232396			NA	NA
RJC70_1,5				2.59693847					790715.771	200.507994			NA	NA
RJC70_1,5b				8.67201724					819491.681	110.860774			NA	NA
RJC70_2,1				2.07083691					755000.007	921.845772			NA	NA
RJC70_2,1			0.10418689	0.61114086	0.26832216			0.09229181	765669.829	725.541695	0.06931957	0.02513329	NA	NA
RJC70_2,2				2.98294037					788577.245	95.2391146			NA	NA
RJC70_3,1				9.02609419					815232.62	258.954436			NA	NA
RJC70_3,2				21.0899699					856707.576	618.066466			NA	NA
RJC70_3,3									942676.547	250.591122			NA	NA
RJC70_3,4									756739.715	446.796431			NA	NA
RJC70_3,5				12.1352664					793356.181	408.273108	2.8582736		NA	NA
RJC70_3,6				0.4496247					830239.083	201.347882			NA	NA
RJC70_3,7				1.61058526					762058.519	411.494914	0.57000116		NA	NA
RJC70_3,8				11.3985889					796237.918	281.101207			NA	NA
RJC70_3,9				0.98984438					737720.203	80.1234192			NA	NA
RJC70_3,10				2.33680208					777638.572	766.848705			NA	NA
RJC70_3,11				50.6860106					800841.574	8.10689251			NA	NA
RJC70_3,12				7.40931819					754918.543	177.035606			NA	NA

Full Grain ID	Cd_ppm	In_ppm	Sn_ppm	Sb_ppm	Te_ppm	La_ppm	W_ppm	Pt_ppm	Au_ppm	Hg_ppm	Pb_ppm	Bi_ppm	Th_ppm	U_ppm
RJC70_3,13				18.0493117					738463.126	1098.33477			NA	NA
RJC70_3,14				10.816831					775390.925	135.357498			NA	NA
RJC70_3,15				2.39422229					817286.38	38.9611075	1.11943609	0.51605344	NA	NA
RJC70_3,16									813473.185	273.429789		0.34520957	NA	NA
RJC70_3,17				162.164306					701962.652	550.545101			NA	NA
RJC70_3,18				2.14361917					770149.646	542.384709			NA	NA
RJC70_3,19				0.96866504					757739.669	212.110955			NA	NA
RJC70_3,20				2.2661971					832708.349	82.4619973			NA	NA
RJC70_3,21				4.64453945					764406.778	272.698911			NA	NA
RJC70_3,22				25.2866772					696574.74	331.988757			NA	NA
RJC70_3,23									763387.068	587.231178			NA	NA
RJC70_3,24				90.6007813					729219.126	449.375434			NA	NA